

Nuclear Structure and Reactions  
paring in nuclei with Cooper pair transfer

G. Potel and R. A. Broglia

December 5, 2014



# Contents

<b>1</b>	<b>Introduction</b>	<b>11</b>
<b>2</b>	<b>Pairing with transfer</b>	<b>13</b>
2.1	Nuclear Structure in a nutshell . . . . .	13
2.2	Connection between theory and experiment . . . . .	22
2.A	Quantity Parameter . . . . .	25
2.B	Relation between collectivity and correlations . . . . .	28
2.C	Quantity, Pauli principle, closed shells and single particle motion	28
2.D	Cooper pairs . . . . .	28
2.D.1	independent-particle motion . . . . .	28
2.D.2	independent-pair motion . . . . .	34
2.E	Pair vibration two-N spectroscopic amplitudes . . . . .	35
2.E.1	Pair removal mode . . . . .	41
2.E.2	Pair addition mode . . . . .	43
2.F	Halo pair addition mode and pigmy: a new symbiotic elementary mode of nuclear excitation . . . . .	48
2.F.1	Cooper pair binding: a novel embodiment of the Axel-Brink hypothesis. . . . .	51
2.G	Nuclear van der Waals Cooper pair . . . . .	58
2.H	Hindsight . . . . .	58
<b>3</b>	<b>Simultaneous versus successive transfer</b>	<b>71</b>
3.1	Simultaneous versus successive Cooper pair transfer in nuclei . . . . .	71
3.2	Transfer probabilities, enhancement factor . . . . .	72
3.3	Correlations in Cooper pair tunneling . . . . .	80
3.A	Pair transfer . . . . .	85
3.A.1	Cooper pair dimensions . . . . .	85
3.B	Comments on the optical potential . . . . .	89
3.C	Weak link between superconductors . . . . .	95
3.D	Phase coherence . . . . .	98
3.E	Medium polarization effects and pairing . . . . .	102
3.E.1	Nuclei . . . . .	102
3.E.2	Metals . . . . .	102

3.F	Hindsight . . . . .	102
<b>4</b>	<b>One-particle transfer</b>	<b>109</b>
4.1	General derivation . . . . .	110
4.1.1	Coordinates . . . . .	116
4.1.2	Zero-range approximation . . . . .	117
4.2	Examples and Applications . . . . .	117
4.2.1	$^{120}\text{Sn}(p, d)^{119}\text{Sn}$ and $^{120}\text{Sn}(d, p)^{121}\text{Sn}$ reactions. . . . .	118
4.2.2	Dressing of single-particle states: parity inversion in $^{11}\text{Li}$ . . . . .	122
4.A	Minimal mean field theory . . . . .	128
4.B	Single-particle strength function . . . . .	130
4.C	Vacuum and medium polarization . . . . .	132
4.D	The Lamb Shift . . . . .	134
4.E	Self-energy and vertex corrections . . . . .	135
4.F	Single-nucleon transfer for pedestrians . . . . .	136
4.F.1	Plane-wave limit . . . . .	140
4.G	One-particle knockout within DWBA . . . . .	142
4.G.1	Spinless particles . . . . .	142
4.G.2	Particles with spin . . . . .	149
4.G.3	One-particle transfer . . . . .	155
4.H	Modified formfactors . . . . .	158
4.H.1	Two-particle transfer . . . . .	158
4.H.2	One-particle transfer . . . . .	158
4.H.3	Inelastic scattering . . . . .	158
4.H.4	Elastic scattering . . . . .	158
4.I	Dynamical shell model in a nutshell . . . . .	158
<b>5</b>	<b>Two-particle transfer</b>	<b>169</b>
5.1	Summary of second order DWBA . . . . .	170
5.2	Detailed derivation of second order DWBA . . . . .	175
5.2.1	Simultaneous transfer: distorted waves . . . . .	175
5.2.2	matrix element for the transition amplitude . . . . .	176
5.2.3	Coordinates for the calculation of simultaneous transfer . . . . .	184
5.2.4	Matrix element for the transition amplitude (alternative derivation) . . . . .	187
5.2.5	Coordinates used to derive Eq. (5.2.89) . . . . .	190
5.2.6	Successive transfer . . . . .	192
5.2.7	Coordinates for the successive transfer . . . . .	197
5.2.8	Simplifying the vector coupling . . . . .	198
5.2.9	non-orthogonality term . . . . .	199
5.2.10	Arbitrary orbital momentum transfer . . . . .	200
5.2.11	Successive transfer contribution . . . . .	202
5.A	ZPF and Pauli principle . . . . .	206
5.B	Coherence and effective formfactors . . . . .	209

5.C	Succesive, simultaneous, non-orthogonality . . . . .	214
5.C.1	Independent particle limit . . . . .	220
5.C.2	Strong correlation (cluster) limit . . . . .	221
5.D	Spherical harmonics and angular momenta . . . . .	222
5.D.1	addition theorem . . . . .	222
5.D.2	expansion of the delta function . . . . .	222
5.D.3	coupling and complex conjugation . . . . .	223
5.D.4	angular momenta coupling . . . . .	223
5.D.5	integrals . . . . .	224
5.D.6	symmetry properties . . . . .	225
5.E	distorted waves . . . . .	225
5.F	hole states and time reversal . . . . .	226
5.G	Spectroscopic amplitudes in the BCS approximation . . . . .	228
5.H	Bayman's two-nucleon transfer amplitudes . . . . .	230
<b>6</b>	<b>Structure with two neutrons</b>	<b>233</b>
6.1	Evidence for phonon mediated pairing . . . . .	233
6.1.1	Structure . . . . .	237
6.1.2	Reaction . . . . .	238
6.2	Pairing rotational bands . . . . .	240
6.2.1	Fluctuations . . . . .	241
6.2.2	Pairing rotations . . . . .	242
6.2.3	Pairing vibrations in superfluid nuclei . . . . .	244
6.3	BCS correlation (Cooper pair) . . . . .	245
6.A	Bootstrap mechanism to break gauge invariance . . . . .	247
6.A.1	Gedanken eksperiment . . . . .	247
6.B	Table 1 PRL . . . . .	249
6.C	Formfactors for the reaction ${}^1\text{H}({}^{11}\text{Li}, {}^9\text{Li}){}^3\text{H}$ . . . . .	251
6.D	Software . . . . .	251
6.E	Articulo Belyaev Pairing vibrational band based on $N = 6$ . . . . .	255
6.F	Simple estimates revisited. . . . .	255
6.G	Statistics. . . . .	255
6.H	Correlation length and quantality parameter. . . . .	256
6.I	$k$ -mass in ${}^{11}\text{Li}$ and Pauli principle. . . . .	257



# Preface

The elementary modes of nuclear excitation are vibrations and rotations, single-particle (quasiparticle) motion, and pairing vibrations and rotations. The specific reactions probing these modes are inelastic, single- and two- particle transfer processes respectively. Within this context one can posit that nuclear structure (bound) and reactions (continuum) are but two aspects of the same physics. This is the reason why they can be treated on equal footing in terms of elementary modes of excitation, within the framework of nuclear field theory (NFT). This theory provides the rules to diagonalize in a compact and economic way the nuclear Hamiltonian for both bound and continuum states correcting for overcompleteness of the basis (particle-vibration coupling (structure), non-orthogonality (reaction)), and for Pauli principle violation.

Pairing vibrations and rotations, closely connected with nuclear superfluidity are, arguably, paradigms of quantal nuclear phenomena. They thus play an important role within the field of nuclear structure. It is only natural that two-nucleon transfer plays a similar role concerning direct nuclear reactions. In fact, this is the central subject of the present monograph.

At the basis of fermionic pairing phenomena one finds Cooper pairs, weakly bound, extended, strongly overlapping (quasi-) bosonic entities, made out of pairs of nucleons dressed by collective vibrations and interacting through the exchange of these vibrations as well as through the bare  $NN$ -interaction, eventually corrected by  $3N$  contributions. Cooper pairs not only change the statistics of the nuclear stuff around the Fermi surface and, condensing, the properties of nuclei close to their ground state. They also display a rather remarkable mechanism of tunnelling between target and projectile in direct two-nucleon transfer reaction. In fact, being weakly bound ( $\ll \epsilon_F$ , Fermi energy) they display correlations over distances (correlation length) much larger than nuclear dimensions ( $\gg R$ , nuclear radius). On the other hand, Cooper pairs are forced to be confined within such dimensions by the action of the average potential, which can be viewed as an external field as far as these pairs are concerned.

The correlation length paradigm comes into evidence, for example, when two nuclei are set into weak contact in a direct reaction. In this case, each of the partner nucleons of a Cooper pair has a finite probability to be confined within the mean field of each of the two nuclei. It is then natural that a Cooper pair can tunnel, equally well correlated, between target and projectile, through simultaneous

than through successive transfer processes. Consequently, although one does not expects supercurrents in nuclei, one can study long-range pairing correlations in terms of individual quantal state. The above mentioned weak coupling Cooper pair tunnelling reminds the tunnelling mechanism of electronic Cooper pairs across a barrier (e.g. a dioxide layer) separating two superconductors, known as Josephson junction. The main difference is that, as a rule, in the nuclear time dependent junction efimerely established in direct two-nucleon transfer process, only one or even none of the two weakly interacting nuclei are superfluid (or superconducting). Now, in nuclei, paradigmatic example of fermionic finite many-body system, zero point fluctuations (ZPF) in general, and those associated with pair addition and pair subtraction modes known as pairing vibrations in particular, are much stronger than in condensed matter. Consequently, and in keeping with the fact that pairing vibrations are the nuclear embodiment of Cooper pairs in nuclei, pairing correlations based on even a single Cooper pair can lead to clearly observable effects in two-nucleon transfer processes.

Nucleonic Cooper pair tunnelling has played and is playing a central role in the probing of these subtle quantal phenomena, both in the case of exotic nuclei as well as of nuclei lying along the stability valley, and have been instrumental in shedding light on the subject of pairing in nuclei at large, and on nuclear superfluidity in particular. Consequently, the subject of two-nucleon transfer occupies a central place in the present monograph both concerning the conceptual and the computational aspects of the description of nuclear pairing, as well as regarding the quantitative confrontation of the results and predictions with the experimental findings.

Because of the central role the interweaving of the variety of elementary modes of nuclear excitation, namely single particle motion and collective vibrations play in nuclear superfluidity, the study of Cooper pair tunnelling in nuclei aside from requiring a consistent description of nuclear structure in terms of dressed quasiparticles and vibrations resulting from both bare and induced interactions, also involves the description of one-nucleon transfer as well as knock out processes. consequently, in the present monograph the general physical arguments and technical computational details concerning the calculation of absolute one-and two nucleon transfer cross sections, making use of state of the art nuclear structure information, are discussed in detail. As a consequence, theoretical and experimental nuclear practitioners, as well as fourth year and PhD students can use the present monograph at profit. To make simpler this use, the basic nuclear structure formalism, in particular that associated with pairing and with collectives modes in nuclei, is economically introduced through general physical arguments. This is also in keeping with the availability in the current literature, of detailed discussions of such material.

Within this context, the monographs *Nuclear Superfluidity* by Brink and Broglia and *Oscillations in Finite Quantum Systems* by Bertsch and Broglia, published also by Cambridge University Press can be considered companion volumes to the present one.

Concerning the notation, we have divided each chapter into sections. Each subsection may in turn be broken down into subsections. Equations and Figures are identified by the number of the chapter and that of the section. Thus (6.1.33) labels the thirtythird equation of section 1 of chapter 6. Similarly, Fig. 6.1.2 labels the second figure of section 1 of chapter 6. Concerning the Appendices, they are labelled by the chapter number and by a Latin letter in alphabetical order, e.g. App. 6.A, App. 6.B, etc. Concerning equations and Figures, a sequential number is added. Thus (6.E.15) labels the fifteenth equation of Appendix E of chapter 6, while Fig. 6.F.1 labels the first figure of Appendix F of chapter 6.

Throughout, a number of footnotes are found. This is in keeping with the fact that footnotes can play a special role within the framework of an ellaborated presentation. In particular they allow one to emphasize relevant issues in an economic way. Being outside the main text, they allow to state eventual important results, without the need of elaborating on the proof. Within this context, cf. (Born, 1926), paper introducing the interpretation of the wavefunction squared as a probability, in a footnote. Most of the material contained in this monograph have been the subject of lectures of the four year course “Nuclear Structure Theory” which RAB delivered through the years at the Department of Physics of the University of Milan, as well as at the Niels Bohr Institute and at Stony Brook (State University of New York). It was also presented by the authors in the course Nuclear Reactions held in the academic year 2009 at the PhD School of Physics of the University of Milan.

RAB wants to acknowledge the central role the collaboration with Francisco Barranco and Enrico Vigezzi has played concerning the nuclear structure aspects of the present monograph. Its dept to the late Aage Winther regarding the reaction contents is difficult to express in words. The overall contributions of Daniel Bès, Ben Bayman and Pier Francesco Bortignon are only too explicitly evident throughout the text and constitute a daily source of inspiration.

Gregory Potel Aguilar  
Livermore

Ricardo A. Broglia  
Milano

## Bibliography

M. Born. Zur Quantenmechanik der Stoßvorgänge. *Zeitschr. f. Phys.*, 37:863, 1926.



# **Chapter 1**

## **Introduction**



# Chapter 2

## Pairing with transfer

### 2.1 Nuclear Structure in a nutshell

The low-energy properties of quantal, many-body, Fermi systems displaying sizable values of zero-point-motion (kinetic energy) of localization compared to the strength of the  $NN$ -interaction and quantified by the quantity parameter  $q \gtrsim 0.15$  (see App. 2.A, and 2.D Fig. 2.A.1, Fig. 2.D.2 and Fig. 2.D.3 Table 2.A.1), are determined by the laws which control independent-particle fermion motion close to the Fermi energy  $\epsilon_F$ , and by the relations/correlations operating among these fermions. First of all, the Pauli principle, implying orbitals solidly anchored to the single-particle mean field, as testified by the Hartree–Fock ground state  $|HF\rangle = \prod_i a_i^\dagger |0\rangle$  (Figs. 2.A.2 and 2.A.3), describing a step function separation in the probability of occupied ( $\epsilon_i \leq \epsilon_F$ ) and empty ( $\epsilon_i \geq \epsilon_F$ ) states.

Pairing acting on fermions moving in time reversal states lying close to  $\epsilon_F$  alters this picture in a conspicuous way (cf. e.g. Broglia, R. A. and Zelevinsky, V. (2013)). In particular, in the case of  $S = 0$  configurations, in which case the radial component of the pair wavefunction does not display nodes. Within an energy range of the order of the pair correlation energy  $E_{corr} (\approx 2\Delta$  within BCS) centered around  $\epsilon_F (E_{corr}/\epsilon_F \ll 1)$  the system is now made out of pairs of fermions which flicker in and out of the correlated ( $L = 0, S = 0$ ) configuration (Cooper pairs, App. 2.D; cf. also Brink, D. and Broglia (2005), in particular Apps. A,G,H,I and J of this reference). For temperatures (intrinsic excitation energies) or stress regimes (magnetic field in metals, Coriolis force in nuclei, etc.) smaller than  $\approx E_{corr}/2$  ( $\approx$  critical value), Cooper pairs respect Bose–Einstein statistics (BCS condensation cf. Fig. 2.A.4 and 2.A.5), the single-particle orbits on which they are correlated become dynamically detached from the mean field, leading to a bosonic condensate and, at the same time, reducing in a conspicuous way the inertia of the system. For example the moment of inertia  $\mathcal{I}$  of quadrupole rotational bands of superfluid nuclei with open shells of both protons and neutrons is found to be considerably smaller than the rigid moment of inertia  $\mathcal{I}_r$  ( $\mathcal{I} \approx \mathcal{I}_r/3$ ) expected from independent particle motion (Inglis limit; see Figs. 2.A.3 and 2.D.2; cf. Belyaev (1959),

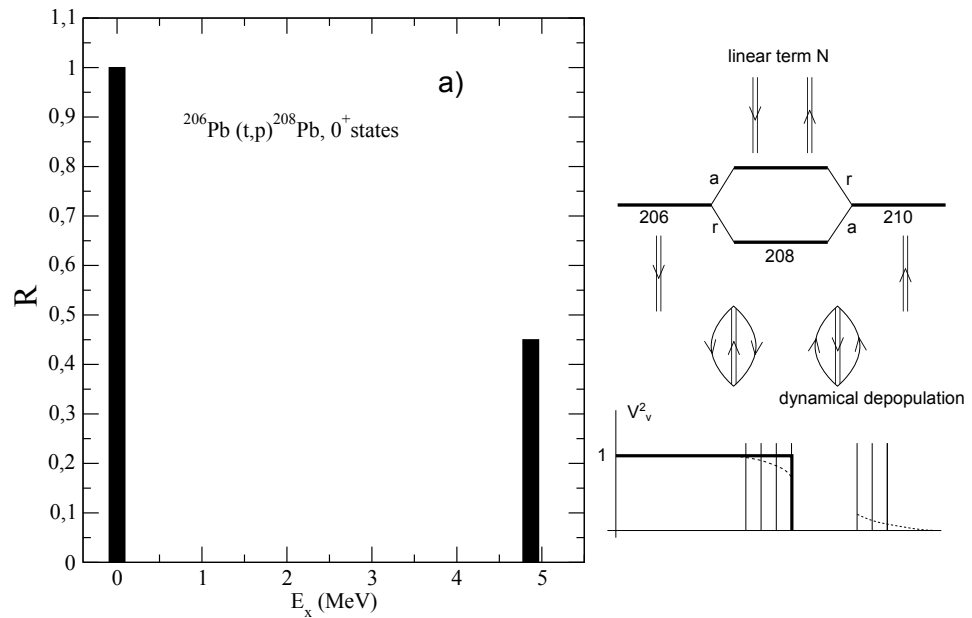


Figure 2.1.1: (a) Ratio of the absolute  $L = 0$  differential cross sections  $d\sigma(E_x, \theta = 59^\circ)/d\sigma(gs, \theta = 59^\circ)$  ( $= (0.05 \text{ mb/sr})/(0.12 \text{ mb/sr})$ ) for the reaction  $^{206}\text{Pb}(t, p)^{208}\text{Pb}$  at the second minimum ( $\theta = 59^\circ$ ; Bjerregaard, J. H. et al. (1966)). It is of notice the large experimental errors associated with the poor statistics of the cross section at the first maximum  $\theta = 5^\circ$ . (b) Schematic representation of the pairing vibrational spectrum around  $^{208}\text{Pb}$ . Concerning the anharmonicities of the modes cf. last paragraph App. 2.E.

Belyaev, S. T. (2013) Bohr, A. and Mottelson (1975) and references therein; within this context see last paragraph of App. 2.D).

Cooper pairs exist also in situations in which the environmental conditions are above critical, e.g. in metals at room temperature, in closed shell nuclei as well as in deformed open shell ones at high values of the angular momentum, although they break as soon as they are generated (pairing vibrations). While these pair addition and subtraction fluctuations have little effect in condensed matter systems with the exception than at  $T \approx T_c$  (Schmid, A. (1966), Schmidt, H. (1968), Schmid, A. (1969) Abrahams, E. and Woo (1968); concerning superfluid  $^3\text{He}$  cf. Wölfe, P. (1978)), they play an important role in mesoscopic systems. In particular in nuclei around closed shells (Fig. 2.1.1 and App. 2.E, Fig. 2.E.6) specially in the case of light, highly polarizable, exotic halo nuclei (see App. 2.F; Bohr, A. and Mottelson (1975) , Bès,D. R. and Broglia (1966), Högaasen-Feldman (1961), Schmidt, H. (1972), Schmidt, H. (1968), Barranco, F. et al. (2001), Potel, G. et al. (2013a), Potel et al. (2014)). From this vantage point of view one can posit that it is not so much, or, at least not only, the superfluid state which is abnormal in the nuclear case, but the normal state associated with closed shell systems. It is of notice nonetheless, the role pairing vibrations play in the transition between superfluid and normal nuclear phases (cf. Fig. 2.1.2) as a function of the rotational frequency (angular momentum) as emerged from the experimental studies of high spin states carried out by, among others, Garrett and collaborators (cf. Shimizu, Y. R. et al. (1989); cf. also Brink, D. and Broglia (2005), Ch. 6 and references therein).

From Fig. 2.1.2 it is seen that while the dynamic pairing gap associated with pairing vibrations leads to a  $\approx 20\%$  increase of the static pairing gap for low rotational frequencies, it becomes the overwhelming contribution above the critical frequency (Shimizu, Y. R. et al. (1989), Shimizu, Y. R. and Broglia (1990), Shimizu, Y. R. (2013), Dönau, F. et al. (1999) Shimizu, Y. R. et al. (2000)). In any case, the central role played by pairing vibrations within the present circumstances is that to restore particle-number conservation, an example of the fact that potential functionals are, as a rule, best profited by special arrangements of fermions (spontaneous symmetry breaking), while fluctuations restore symmetry (cf. Chapter 6 Section 6.2.3). Within this context, there are a number of methods which allows one to go beyond mean-field approximation (HFB). Generally referred to as number projection methods (NP), they make use of a variety of techniques (Generator Coordinate Method, Pfaffians, etc.) as well as protocols (variation after projection, gradient method, etc.; cf. Ring, P. and Schuck (1980), Egido, J. L. (2013), Robledo, R. M. and Bertsch (2013); cf. also Frauendorf, S. (2013), Ring, P. (2013), Heenen, P. H. et al. (2013), and references therein). The advantages of NP methods over the RPA is to lead to smooth functions for both the correlation energy and the pairing gap at the pairing phase transition between normal and superfluid phases. That is, between the pairing vibrational and pairing rotational schemes (Figs. 2.1.1, 2.1.3, 2.1.4, see also Fig. 2.D.1; cf. Bès,D. R. and Broglia (1966), Bohr, A. and Mottelson (1975) and references therein).

The above results underscore the fact that, at the basis of an operative coarse

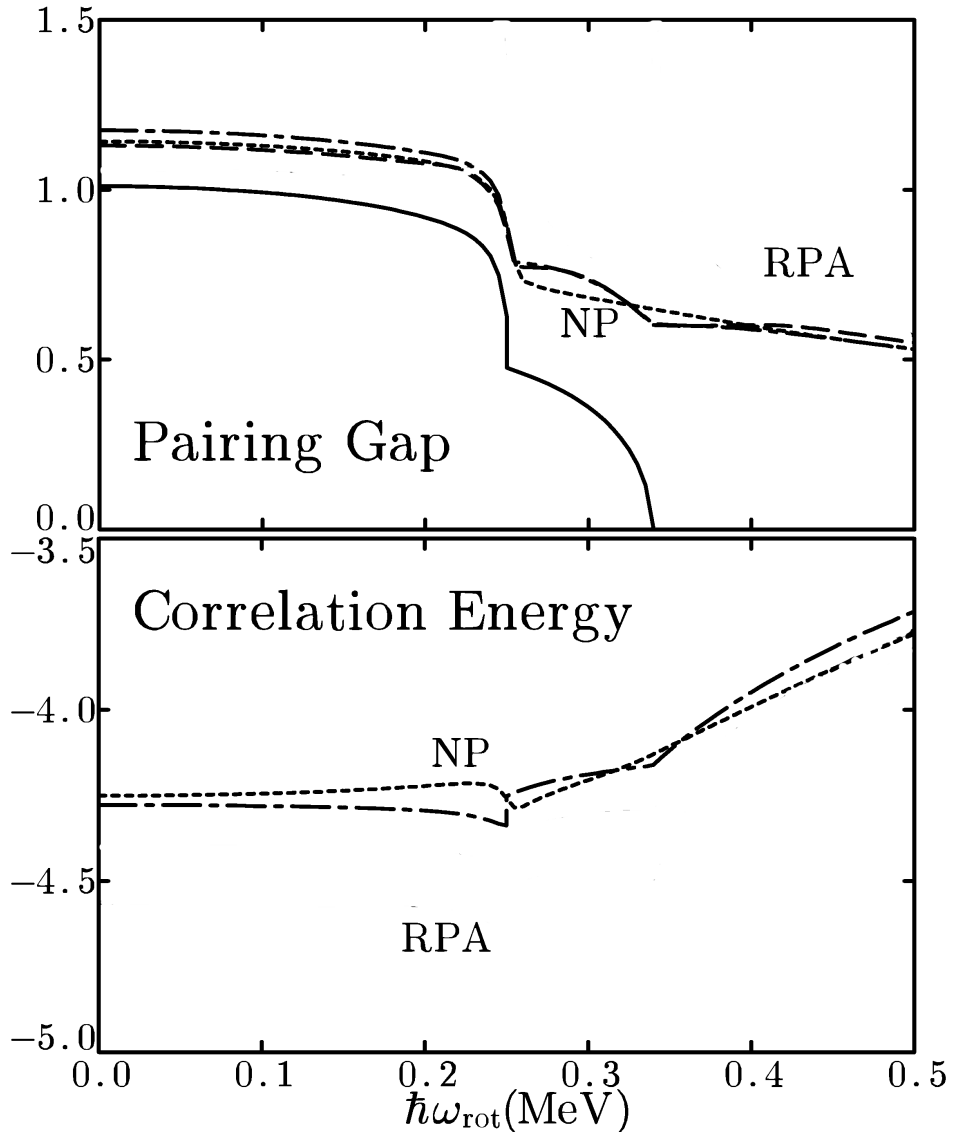


Figure 2.1.2: Pairing gap calculated taking into account the correlation associated with pair vibrations in the RPA approximation ( $\Delta = (\Delta_{BCS}^2 + \frac{1}{2}G^2 S_0(RPA)))^{1/2}$  (upper panel) and RPA correlation energy (lower panel) for neutrons in  $^{164}\text{Er}$  as a function of the rotational frequency. Both quantities are in MeV (dashed-dotted curves). The value of the static (mean-field) pairing gap  $\Delta$ , which vanishes at  $\hbar\omega_{rot} = 0.34$  MeV, is also displayed in the upper panel (continuous curve). The results of the number-projection (NP) calculations are shown as dotted curves.  $S_0(RPA) = \sum_{n \neq AGN} [ \langle n|P|0 \rangle + \langle n|P^\dagger|0 \rangle ]_{RPA}^2$ , where  $\Delta_{BCS} = G \langle BCS|P^\dagger|BCS \rangle$  is the standard, static BCS pairing gap, while  $G$  is the pairing force strength. The non-energy weighted sum rule  $S_0(RPA)$  describes the contribution of pairing fluctuations to the effective (RPA) gap, and is intimately associated with projection in particle number. It is of notice that  $\sum_{n \neq AGN}$  means that the divergent contribution from the zero energy mode (Anderson, Goldstone, Nambu mode, see e.g. Broglia et al. (2000) and references therein), associated with the lowest ( $\hbar\omega_0$ ) solution of the  $H = H'_p + H''_p$  (cf. Sect 6.2.3 and Brink, D. and Broglia (2005) App. J) is to be excluded (after Shimizu, Y. R. and Broglia (1990)).

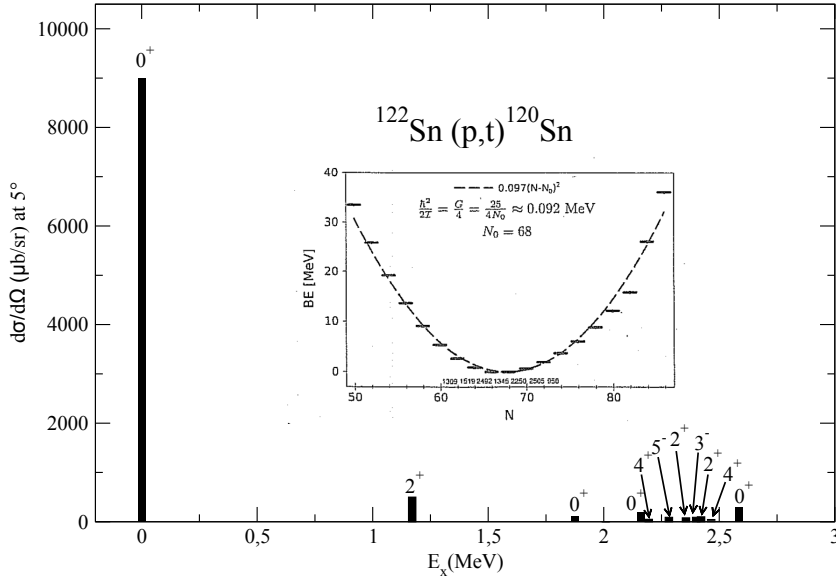


Figure 2.1.3: Excitation function associated with the reaction  $^{122}\text{Sn}(p,t)^{120}\text{Sn}(J^\pi)$ . The absolute experimental values of  $d\sigma(J^\pi)/d\Omega|_{5^\circ}$  are given as a function of the excitation energy  $E_x$  (after Guazzoni, P. et al. (2011)). In the inset the full neutron pairing rotational band between magic numbers  $N = 50$  and  $N = 82$  is also displayed, the absolute  $^{A+2}\text{Sn}(p,t)^A\text{Sn}$  experimental cross sections are reported in the abscissa (Guazzoni, P. et al. (1999), Guazzoni, P. et al. (2004), Guazzoni, P. et al. (2006), Guazzoni, P. et al. (2008), Guazzoni, P. et al. (2011), Guazzoni, P. et al. (2012); see also Potel, G. et al. (2011), Potel, G. et al. (2013b)).

grained approximation to the nuclear many–body problem, one finds a judicious choice of the collective coordinate/s<sup>1</sup>. In other words, pairing vibrations are elementary modes of excitation containing the right physics to restore gauge invariance through their interweaving with quasiparticle states. Within the framework of the above picture, one can introduce at profit a collective coordinate  $\alpha_0$  (order parameter) which measures the number of Cooper pairs participating in the pairing condensate, and define a wavefunction for each pair  $(U_\nu + V_\nu a_\nu^\dagger a_{\bar{\nu}}^\dagger)|0\rangle$  (independent pair motion, BCS approximation, cf. Figs. 2.D.1, 2.D.2 and 2.D.3), adjusting the occupation parameters  $V_\nu$  and  $U_\nu$  (probability amplitudes that the two–fold, Kramer’s–degenerate pair state ( $\nu, \bar{\nu}$ ), is either occupied or empty), so as to mini-

<sup>1</sup>Within this context we quote allegedly from E. Wigner: “In solving a problem you may choose to use the degrees of freedom you like. But if you choose the wrong ones you will be sorry”.

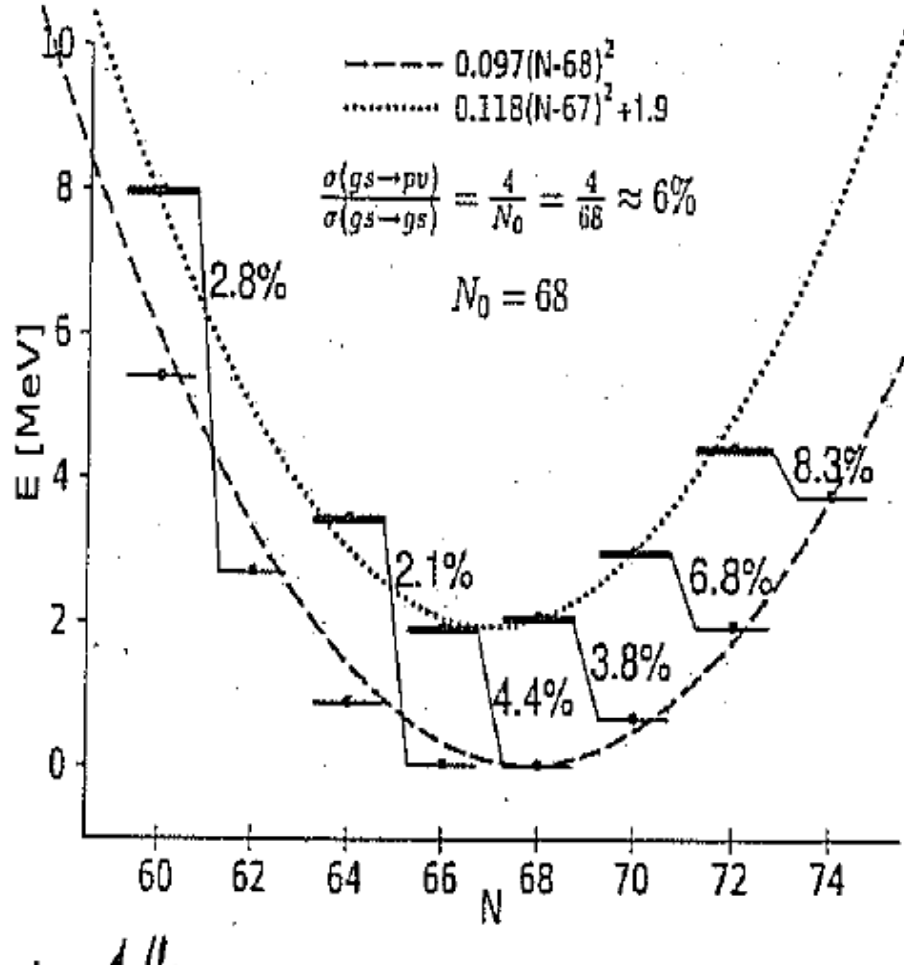


Figure 2.1.4: The weighted average energies ( $E_{exc} = \sum_i E_i \sigma_i / \sum_i \sigma_i$ ) of the excited  $0^+$  states below 3 MeV in the Sn isotopic chain are shown on top of the pairing rotational band, already displayed in Fig. 2.1.3. Also indicated is the percentage of cross section for two-neutron transfer to excited states, normalized to the cross sections populating the ground states (after Potel, G. et al. (2013b)). The estimate of the ratio of cross sections displayed on top of the figure was obtained making use of the single  $j$ -shell model (see, e.g., Brink, D. and Broglia (2005) and references therein).

mize the energy of the system under the condition that the average number of nucleons is equal to  $N_0$  (Coriolis–like force felt, in the intrinsic system in gauge space by the Cooper pairs, being equal to  $-\lambda N_0$ ). Thus,  $|BCS\rangle = \Pi_{\nu>0} (U_\nu + V_\nu a_\nu^\dagger a_\nu^\dagger) |0\rangle$  provides a valid description of the independent pair mean field ground state, and of the associated order parameter  $\alpha_0 = \langle BCS | P^\dagger | BCS \rangle = \sum_{\nu>0} U_\nu V_\nu$ ,  $P^\dagger = \sum_{\nu>0} a_\nu^\dagger a_\nu^\dagger$  being the pair creation operator (cf. Bardeen et al. (1957a), Bardeen et al. (1957b), Schrieffer (1964), Schrieffer, J. R. (1973) and references therein). It is then natural to posit that two-particle transfer reactions are specific to probe pairing correlations in many-body fermionic systems. Examples are provided by the Josephson effect (Josephson (1962)) between e.g. metallic superconductors, and  $(t, p)$  and  $(p, t)$  reactions in atomic nuclei (cf. e.g. Yoshida (1962), Broglia, R.A. et al. (1973), Bayman (1971), Glendenning, N. K. (1965), Bohr (1964), Hansen (2013) and Potel, G. et al. (2013a) and references therein; cf. also Figs. 2.1.3 and 2.1.4.)

Due to the fact that, away from the Fermi energy pair motion becomes independent particle motion (see App. 2.D), one-particle transfer reactions like e.g.  $(d, p)$  and  $(p, d)$  can be used together with  $(t, p)$  and  $(p, t)$  processes as valid tools to cross check pair correlation predictions (see Chapter 4). In particular, to shed light on the origin of pairing in nuclei: in a nutshell, the relative importance of the bare  $NN$ -interaction and the induced pairing interaction (within this context see App. 2.F).

While the calculation of two-nucleon transfer spectroscopic amplitudes and differential cross sections are, a priori, more involved to be worked out than those associated with one-nucleon transfer reactions, the former are, as a rule, more “intrinsically” accurate than the latter ones. This is because, in the case of two nucleon transfer reactions, the quantity (order parameter  $\alpha_0$ ) which expresses the collectivity of the members of a pairing rotational band reflect the properties of a coherent state ( $|BCS\rangle$ ). In other words, it results from the sum over many contributions ( $\sqrt{j_\nu + 1/2} U_\nu V_\nu$ , cf. App. 2.D), all of them having the same phase. Consequently, errors are averaged out in the summed value  $|\alpha_0|$ , conferring the two nucleon transfer cross section  $d\sigma(2n \text{ transfer})/d\Omega \sim |\alpha_0|^2$ , a quantitative accuracy which goes beyond that of the individual contributions. On the other hand,  $d\sigma(1n\text{-transfer})/d\Omega \sim |U_\nu|^4$  ( $\sim |V_\nu|^4$ ) depends on the accuracy with which one is able to calculate the occupancy of a single pure configuration (similar to the relative accuracy with which one can calculate the nuclear density as a whole and the density associated with a single orbital, quantities which can be probed in  $(e, e')$  experiments).

The soundness of the above parlance reflects itself in the calculation of the elements resulting from the encounter of structure and reaction, namely one- and two-nucleon modified transfer formfactors. While it is usually considered that these quantities carry all the structure information associated with the calculation of the corresponding cross sections, a consistent NFT treatment of structure and reaction will posit that equally much is contained in the distorted waves describing the relative motion of the colliding systems. This is because the optical po-

tential ( $U + iW$ ) which determines the scattering waves, emerges from the same modified formfactors, eventually including also inelastic processes (cf. App. 3.B; cf also Broglia, R. A. et al. (1981), Pollarolo et al. (1983), Broglia and Winther (2004), Fernández-García, J.P. et al. (2010), Fernández-García, J.P., M. Rodríguez-Gallardo et al. (2010), Dickhoff, W. and Van Neck (2005), Jenning, B. (2011), Montanari et al. (2014)). In other words, to describe a two-nucleon transfer reaction like  $A + t \rightarrow B (= A + 2) + p$ , one needs to know what the single-particle states and collective modes of the system  $F (= A + 1)$  are, equally well than those of nuclei  $A$  and  $B$ . In principle, also the deuteron wavefunction as one knows the triton wavefunction (see Chapter 3, cf. also Chapter 5, Section 5.1). Furthermore one needs to take into account the interweaving of different modes and degrees of freedom resulting in dressed particle states (quasiparticles; fermions) and renormalized normal vibrational modes of excitation (bosons). But these are essentially all the elements needed to calculate the processes leading to the depopulation of e.g. the flux in the incoming channel ( $A + t$  in the case under discussion). In particular, and assuming to work with spherical nuclei, one-particle transfer is, as a rule, the main depopulation process, in keeping with the long range tail of the associated formfactors as compared to that of other processes, e.g. inelastic processes (cf. e.g. Fig. 3.B.5).

In keeping with this fact, and because  $U$  and  $W$  are connected by the Kramers-Krönig generalized dispersion relation (fluctuation-dissipation theorem, see e.g. Mahaux, C. et al. (1985) and references therein), it is possible to calculate the nuclear dielectric function (optical potential) associated with the elastic channels under discussion (i.e.  $(A, t)$ ,  $(F, d)$  and  $(B, p)$  in the present case) making use of the above described elements.

Concerning the modified formfactor associated with e.g. a  $(t, p)$  process, we shall see in the (Chapter 5, App. 5.B) that it can be written as

$$\begin{aligned} u_{LSJ}^{J_i J_f}(R) = & \sum_{\substack{n_1 l_1 j_1 \\ n_2 l_2 j_2, n}} B(n_1 l_1 j_1, n_2 l_2 j_2; J J_i J_f) \\ & \times \langle S L J | j_1 j_2 J \rangle \times \langle n 0, N L, L | n_1 l_1, n_2 l_2; L \rangle \\ & \times \Omega_n R_{NL}(R), \end{aligned} \quad (2.1.1)$$

where the overlaps

$$\begin{aligned} & B(n_1 l_1 j_1, n_2 l_2 j_2; J J_i J_f) \\ & = \langle \Psi^{J_f}(\xi_{A+2}) | [\phi^J(n_1 l_1 j_1, n_2 l_2 j_2), \Psi^{J_i}(\xi_A)]^{J_f} \rangle, \end{aligned} \quad (2.1.2)$$

and

$$\Omega_n = \langle \phi_{nlm_l}(\mathbf{r}) | \phi_{000}(\mathbf{r}) \rangle, \quad (2.1.3)$$

encode for the physics of particle-particle (but also, to a large extent, particle-hole) correlations in nuclei,  $\langle S L J | j_1 j_2 J \rangle$  and  $\langle n 0, N L, L | n_1 l_1, n_2 l_2; L \rangle$  being  $LS - jj$  and Moshinsky transformation brackets, keeping track of symmetry and number of

degrees of freedom conservation (Glendenning, N. K. (1965), Broglia, R.A. et al. (1973)). In fact, the two–nucleon spectroscopic amplitude (B–coefficient) and the overlap  $\Omega_n$  reflect the parentage with which the nucleus  $B$  can be written in terms of the system  $A$  and a Cooper pair,

$$\Psi_{exit} = \Psi_{M_f}^{J_f}(\xi_{A+2}) \times \chi_{M_{S_f}}^{S_f}(\sigma_p), \quad (2.1.4)$$

where

$$\begin{aligned} \Psi_{M_f}^{J_f}(\xi_{A+2}) &= \sum_{\substack{n_1 l_1 j_1 \\ n_2 l_2 j_2 \\ J, J'_i}} B(n_1 l_1 j_1, n_2 l_2 j_2; J J'_i J_f) \\ &\times [\phi^J(n_1 l_1 j_1, n_2 l_2 j_2) \Psi_{M_f}^{J_i}(\xi_A)]_{M_f}^{J_f}, \end{aligned} \quad (2.1.5)$$

and

$$\Psi_{entrance} = \Psi_{M_i}^{J_i}(\xi_A) \times \phi_t(\mathbf{r}_{n1}, \mathbf{r}_{n2}, r_p; \sigma_{n1}, \sigma_{n2}, \sigma_p), \quad (2.1.6)$$

with

$$\phi_t = [\chi^S(\sigma_{n1}, \sigma_{n2}) \chi^{S'_f}(\sigma_p)]_{M_{S_i}}^{S_i} \times \phi_t^{L=0} \left( \sum_{i>j} |\mathbf{r}_i - \mathbf{r}_j| \right). \quad (2.1.7)$$

Assuming for simplicity a symmetric di–neutron radial wavefunction of the triton (i.e. neglecting the  $d$ –component of the corresponding wavefunction) for the relative and center of mass wavefunctions  $\phi_{nlm}(\mathbf{r})$  and  $\phi_{N\Lambda M}(R)$  ( $n = l = m = 0, N = \Lambda = M = 0$ ), leads to  $\Omega_n$ , a quantity which reflects both the non–orthogonality existing between the di–neutron wavefunctions in the final nucleus (Cooper pair) and in the triton. Another way to say the same thing is that dineutron correlations in these two systems are different, a fact which underscores the limitations of light ion reactions to probe specifically pairing correlations in nuclei (within this context see von Oertzen and Vitturi (2001), von Oertzen, W. (2013)).

One can then conclude that, provided one makes use of a (sensible) complete single–particle basis (eventually including also the continuum), one can capture through  $u_{LSJ}^{J,J_f}(R)$  most of the coherence of Cooper pair transfer, as a major fraction of the associated di–neutron non–locality is taken care of by the n–summation appearing in eq. (2.1.1), the different contributions being weighted by the non–orthogonality overlaps  $\Omega_n$ . This is in keeping with the fact that, making use of a more refined triton wavefunction than that employed above, the  $n – p$  (deuteron–like) correlations of this particle can be described with reasonable accuracy and thus, the emergence of successive transfer (see Chapter 3). On the other hand, being the deuteron a bound system, this effective treatment of the associated resonances is not particularly economic. Furthermore, it is of notice that the zero–range approximation ( $V(\rho)\phi_{000}(\rho) = D_0\delta(\vec{\rho})$ ) eliminates the above mentioned possibilities cf. eq. (5.B.19).

Anyhow, the fact that one can still work out a detailed and reasonably consistent picture of two–nucleon transfer reactions in nuclei in terms of absolute cross

sections with the help of a single parameter ( $D_0^2 \approx (31.6 \pm 9.3)10^4 \text{MeV}^2\text{fm}^2$ ) testifies to the fact that the above picture of Cooper pair transfer (Glendenning, N. K. (1965), Bayman and Kallio (1967)) is a powerful one, as it contains a large fraction of the physics which is at the basis of Cooper pair transfer in nuclei (Broglia, R.A. et al. (1973)). This is in keeping with the fact that the Cooper pair correlation length is much larger than nuclear dimensions and, consequently, simultaneous and successive transfer feel the same pairing correlations (see Chapter 3). In other words, treating explicitly the intermediate deuteron channel in terms of successive transfer, correcting both this and the simultaneous transfer channels for non-orthogonality contributions, makes the above picture the quantitative probe of Cooper pair correlations in nuclei (Fig. 2.2.1; cf. Bayman and Chen (1982) and Potel, G. et al. (2013a)).

Within the above context, we provide below two examples of  $B$ -coefficients associated with coherent states. Namely, one for the case in which  $A$  and  $B (= A+2)$  are members of a pairing rotational band. A second one, in the case in which they are members of a pairing vibrational band. That is,

$$\begin{aligned} \mathbf{1)}, B(nlj, nlj; 000) &= \langle BCS(N+2) | [a_{nlj}^\dagger a_{nlj}^\dagger]_0^0 | BCS(N) \rangle \\ &= \sqrt{j+1/2} U_{nlj}(N) V_{nlj}(N+2), \end{aligned} \quad (2.1.8)$$

and

$$\begin{aligned} \mathbf{2)}, B(nlj, nlj; 000) &= \langle (N_0 + 2)(gs) | [a_{nlj}^\dagger a_{nlj}^\dagger]_0^0 | N_0(gs) \rangle \\ &= \begin{cases} \sqrt{j_k + 1/2} X^a(n_k l_k j_k) & (\epsilon_{j_k} > \epsilon_F) \\ \sqrt{j_k + 1/2} Y^a(n_l l_i j_i) & (\epsilon_{j_k} \leq \epsilon_F). \end{cases} \end{aligned} \quad (2.1.9)$$

Where the  $X$  and  $Y$  coefficients are the forwardgoing and backwardsgoing RPA amplitudes of the pair addition mode. For actual numerical values see App. 2.D, Table 2.D.1 and App. 2.E Tables 2.E.2–2.E.5.

We conclude this section by remarking that, in spite of the fact that one is dealing with the connection between structure and direct transfer reactions, no mention has been made of spectroscopic factors in relation with one-particle transfer processes, let alone when discussing two-particle transfer. In fact, one will be using throughout the present monograph, exception made when explicitly mentioned, absolute cross sections as the sole link between spectroscopic amplitudes and experimental observations.

## 2.2 Connection between theory and experiment

Let us elaborate on the above question in connection with one-particle transfer reactions (Mahaux, C. et al. (1985), Brink, D. and Broglia (2005) and references therein; cf. also App. 4.I). Elementary modes of nuclear excitation, namely single-particle motion, vibrations and rotations, being tailored to economically describe

the nuclear response to external probes, contain a large fraction of the many-body correlations. Consequently, their wavefunctions are non-orthogonal to each other, in keeping with the fact that all the degrees of freedom of the nucleus are exhausted by those of the nucleons (see Chapter 1). The resulting overlaps give a measure of the strength with which the different modes couple to each other. The resulting particle-vibration coupling Hamiltonian can be diagonalized, making use of Nuclear Field Theory (NFT, cf. Bortignon, P. F. et al. (1977), Bortignon, P. F. et al. (1978)), and of the BRST techniques in the case of particle-rotor coupling (cf. Bès, D. R. and Kurchan (1990)) or, approximately in terms of large amplitude plastic-like vibrations (cf. end of Sect. 2.D.1 and App. 2.B).

As a result of the interweaving of single-particle and collective motion, the nucleons acquire a state dependent self energy  $\Delta E_j(\omega)$  which, for levels far away from the Fermi energy can become complex. Consequently, the single-particle potential which was already non-local in space (exchange potential, related to the Pauli principle) becomes also non-local in time (retardation effects; cf. e.g. Fig 2.F.3 (I), also Fig. 4.B.1). There are a number of techniques to make it local. In particular the Local Density Approximation (LDA) and the effective mass approximation. In this last case one can describe the single-particle motion in terms of a local (complex) potential with a real part given by  $U'(r) = (m/m^*)U(r)$ , where  $m^* = m_k m_\omega / m$  is the effective nucleon mass,  $m_k$  being the so-called  $k$ -mass (non-locality in space in keeping with the fact that  $\Delta x \Delta k_x \geq 1$ ), and  $m_\omega = m(1 + \lambda)$  being the  $\omega$ -mass (non-locality in time, as implied by the relation  $\Delta \omega \Delta t \geq 1$ ),  $\lambda = -\partial \Delta E(\omega) / \partial \hbar \omega$  being the so-called mass enhancement factor. It reflects the ability with which vibrations clothe single-particles. In other words, it measures the probability with which a nucleon moving at  $t = -\infty$  in a “pure” orbital  $j$  can be found at a later time in a  $2p - 1h$  like (doorway state)  $|j'L; j\rangle$ ,  $L$  being the multipolarity of a vibrational state. Within this context, the discontinuity taking place at the Fermi energy in the dressed particle picture ( $Z_\omega = (m/m_\omega)$ ; cf. Appendix D introduction) is connected with the single-particle occupancy probability.

It is of notice that dressed particles (cf. e.g Fig. 2.F.3 (I) also Fig. 4.B.1) automatically imply an induced pairing interaction (cf. e.g. Fig. 2.F.3 (II) and Fig. 4.2.6 (b)) resulting from the exchange of the dressing vibrations between pairs of nucleons moving in time reversal states close to the fermi energy. In other words, fluctuations in the normal density ( $\delta \rho$ , cf. Fig. 4.A.1 (i)) and the associated particle-vibration coupling vertices lead to abnormal (superfluid) density (deformation in gauge space). Whether this is a dynamic or static effect, depends on whether the parameter (cf. Fig. 2.E.7)

$$x' = G' N'(0), \quad (2.2.1)$$

product of the effective pairing strength,

$$G' = Z_\omega^2 (v_p^{bare} + v_p^{ind}), \quad (2.2.2)$$

and of the renormalized density of levels  $N'(0)$  is considerable larger (smaller) than  $\approx 1/2$ . The quantity  $G'$  is the sum of the bare and induced pairing interaction,

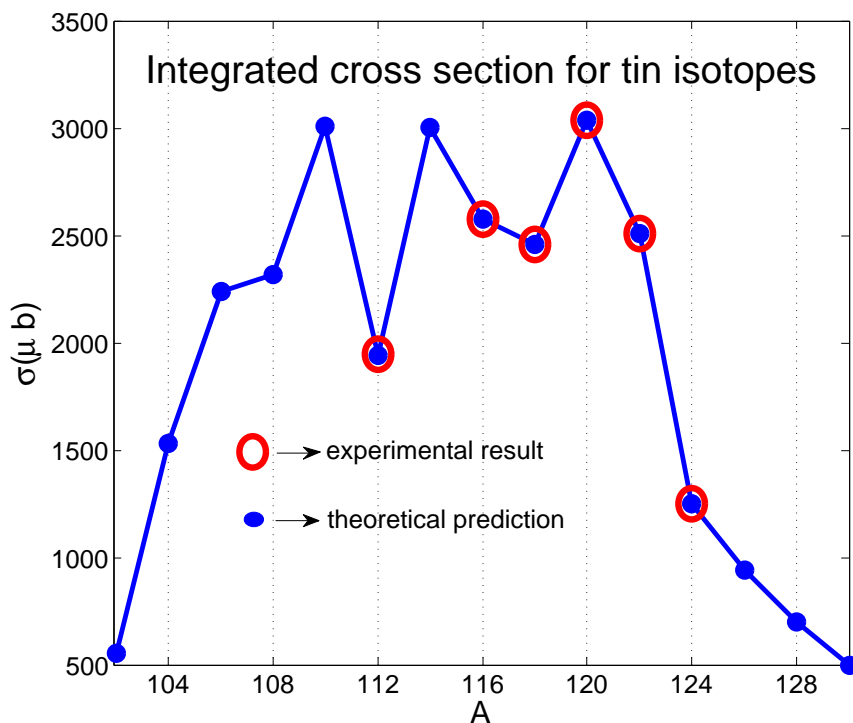


Figure 2.2.1: Absolute value of the calculate two–nucleon transfer cross section  $^{A+2}\text{Sn}(p, t)^A\text{Sn}(\text{gs})$  ( $A = 112, 116, 118, 120, 122, 124$  cf. Potel, G. et al. (2013a) Potel, G. et al. (2013b)) calculated taking into account successive and simultaneous transfer in second order DWBA, properly corrected for non–orthogonality contributions in comparison with the experimental data (Guazzoni, P. et al. (1999), Guazzoni, P. et al. (2004), Guazzoni, P. et al. (2006), Guazzoni, P. et al. (2008), Guazzoni, P. et al. (2011), Guazzoni, P. et al. (2012)).

renormalized by the degree of single-particle content of the levels where nucleons correlate. The quantity

$$N'(0) = Z_\omega^{-1} N(0) = (1 + \lambda) N(0) \quad (2.2.3)$$

is the similarly renormalized density of levels at the Fermi energy. From the above relations one obtains

$$x' = Z_\omega(v_p^{bare} + v_p^{ind})N(0). \quad (2.2.4)$$

All of the above many-body,  $\omega$ -dependent effects which imply in many cases a coherent sum of amplitudes, are not simple to capture in connection with one-particle, let alone two-nucleon transfer processes.

In keeping with the fact that  $m_k \approx 0.6 - 0.7m$  and that  $m^* \approx m$ , as testified by the good fitting standard Saxon-Woods potentials provides for the valence orbitals of nucleons of mass  $m$  around closed shells, one obtains  $m_\omega \approx 1.4 - 1.7m$ . Thus  $Z_\omega \approx 0.6 - 0.7$ . It is still an open question how much of the observed single-particle depopulation can be due to hard core effects, which shifts the associated strength to high momentum levels (cf. Dickhoff, W. and Van Neck (2005), Jenning, B. (2011), Kramer, G. J. et al. (2001), Barbieri, C. (2009), Schiffer, J. P. et al. (2012), Duguet, T. and Hagen (2012), Furnstahl, R. J. and Schwenk (2010)). An estimate of such an effect of about 20% will not quantitative change the long wavelength estimate of  $Z_\omega$  given above. Arguably, a much larger depopulation through hard core effects remains an open problem within the overall picture of elementary modes of nuclear excitation and of medium polarization effects.

## Appendix 2.A Quantality Parameter

The quantality parameter (Nosanow (1976), de Boer (1957), de Boer (1948), de Boer and Lundbeck (1948)) is defined as the ratio of the quantal kinetic energy of localization and potential energy, (cf. Fig. 2.A.1 and Table 2.A.1). Fluctuations, quantal or classical, favor symmetry: gases and liquids are homogeneous. Potential energy on the other hand prefers special arrangements: atoms like to be at specific distances and orientations from each other (spontaneous breaking of translational and of rotational symmetry reflecting the homogeneity and isotropy of empty space, see Anderson (1984); within this context cf. App 2.D, end of Sect. 2.D.1 as well as Sect. 6.2.3)<sup>2</sup>.

---

<sup>2</sup>Within this general context the physics embodied in the quantality parameter is closely related to that which is at the basis of the classical Lindemann criterion (Lindemann (1910)) to measure whether a system is ordered (e.g. a crystal) or disordered (e.g. a melted system) (Bilgram (1987), Löwen, H. (1994), Stillinger (1995)). The above statement is also true for the generalized Lindemann parameter (Stillinger and Stillinger (1990), Zhou et al. (1999)), used to provide similar insight into inhomogeneous finite systems like e.g. proteins (aperiodic crystals Schrödinger, E. (1944), see also Ehrenfest's theorem (Basdevant pag. 138)).

constituents	$M/M_n$	$a(\text{cm})$	$v_0(\text{eV})$	$q$	phase( $T = 0$ )
$^3\text{He}$	3	2.9(-8)	8.6(-4)	0.19	liquid <sup>a)</sup>
$^4\text{He}$	4	2.9(-8)	8.6(-4)	0.14	liquid <sup>a)</sup>
$\text{H}_2$	2	3.3(-8)	32(-4)	0.06	solid <sup>b)</sup>
$^{20}\text{Ne}$	20	3.1(-8)	31(-4)	0.007	solid <sup>b)</sup>
nucleons	1	9(-14)	100(+6)	0.5	liquid <sup>a),c),d)</sup>

Table 2.A.1: Zero temperature phase for a number of systems. a) delocalized (condensed), b) localized, c) non–Newtonian solid (cf. e.g. De Gennes (1994), page 25), that is, systems which react elastically to sudden solicitations and plastically under prolonged strain, d) paradigm of quantal, strongly fluctuating, finite many–body systems. While delocalization or less does not seem to depend much on whether one is dealing with fermions or bosons (Mottelson (1998) and refs. therein; cf also Ebran et al. (2014a), Ebran et al. (2014b), Ebran et al. (2013), Ebran et al. (2012)), the detailed properties of the corresponding single–particle motion are strongly dependent on the statistics obeyed by the associated particle (cf. App. 2.C).

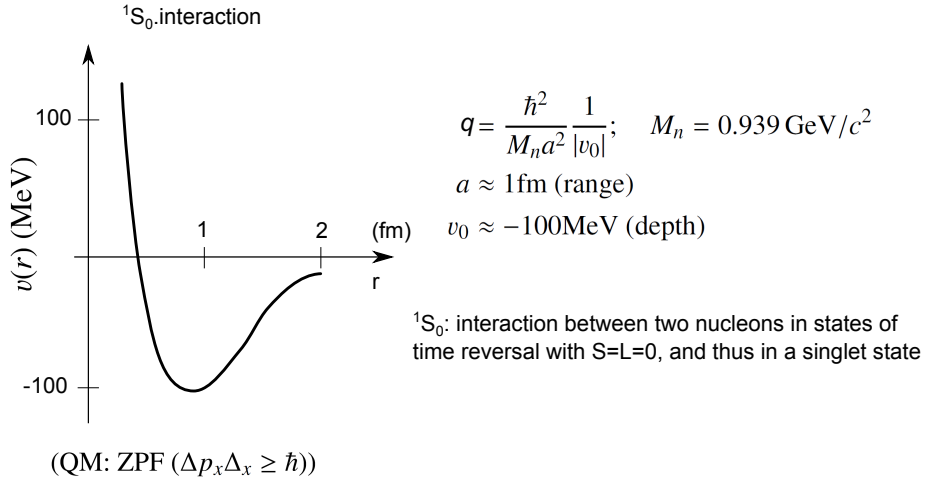


Figure 2.A.1: Schematic representation of the bare  $NN$ –interaction acting among nucleons displayed as a function of the relative coordinate  $r = |\mathbf{r}_1 - \mathbf{r}_2|$ , used to estimate the quantality parameter  $q$ , ratio of the zero point fluctuations (ZPF) of confinement and the potential energy.

When  $q$  is small, quantal effects are small and the lower state for  $T < T_c$  will have a crystalline structure,  $T_c$  denoting the critical temperature. For sufficiently large values of  $q$  ( $> 0.15$ ) the system will display particle delocalization and, likely, be amenable, within some approximation, to a mean field description (Fig. 2.A.2 and Fig. 2.A.3; cf. also 2.D.3 and also Figs. 2.A.4 and 2.A.5). In fact, the step delocalization  $\rightarrow$  mean field is certainly not automatic, neither guaranteed. In any case, not for all properties neither for all levels of the system. Let us elaborate on these points. It is, arguably, true that independent particle motion can be viewed as the most collective of all nuclear properties, reflecting the effect of all nucleons on a given one resulting in a macroscopic effect (confinement). Consequently, mean field should easily be accurately calculated as the sum of many contributions whose relative errors cancel out, in average, against each other, an *ansatz* found at the basis of most collective approximations, like e.g. RPA. On the other hand, this fact does not guarantees that each single contribution is correctly calculated but, alas, the opposite. Thus, it will not be surprising that if one could force each, or at least a number of the virtual individual contributions to become real by acting with an appropriate external field (specific experiment), one would find varied degrees of agreement with experiment. Within this context one may find through mean field approximation a good description for the energy of the valence orbitals of a nucleus but for a specific level (e.g. the  $d_{5/2}$  level of  $^{119-120}\text{Sn}$ , cf. e.g. Fig 4.2.3). It is not said that including higher order particle-vibration coupling corrections the resulting quasiparticle will agree better with the data (cf. e.g. Tarpanov, D. et al. (2014)). Cases like this one constitute a sobering experience concerning the intricacies of the many-body problem in general, and the nuclear one (finite many-body system, FMBS) in particular. In other words, one is dealing with a self-confined, strongly interacting, finite many-body system generated from collisions originally associated with a variety of astrophysical events and thus with the coupling and interweaving of different scattering channels and resonances, a little bit as e.g. the Hoyle monopole one ( $\alpha + \alpha + \alpha \rightarrow ^{12}\text{C}$ ). Within the anthropomorphic (grand design) scenario such phenomena are found in the evolution of the Universe to eventually allow for the presence of organic matter and, arguably, life on earth (cf. e.g. Rees, M. (2000), Meissner, U. G. (2014) and references therein) more likely than to make mean field approximation an “exact” description of nuclear structure and reactions.

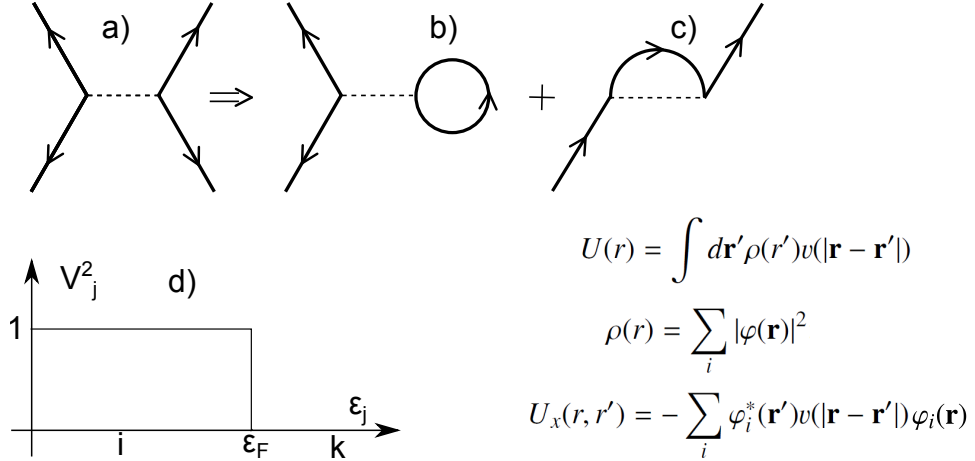


Figure 2.A.2: Schematic representation of (a) nucleon–nucleon scattering through the bare  $NN$ –interaction, (b) the associated contribution to the Hartree potential  $U(r)$  and, (c) to the Fock (exchange) potential  $U_x(r, r')$ ,  $\rho(r)$  being the nucleon density. (d) the Hartree–Fock solution leads to a sharp discontinuity at the Fermi energy  $\epsilon_F$ . That is, single–particle levels with energy  $\epsilon_i \leq \epsilon_F$  are fully occupied. Those with  $\epsilon_k \geq \epsilon_F$  empty.

## Appendix 2.B Relation between collectivity and correlations

## Appendix 2.C Quantality, Pauli principle, closed shells and single particle motion

## Appendix 2.D Cooper pairs

Let us assume that the motion of nucleons is described by the Hamiltonian,

$$H = \sum_{j_1 j_2} \langle j_1 | T | j_2 \rangle a_{j_1}^\dagger a_{j_2} + \frac{1}{4} \sum_{\substack{j_1 j_2 \\ j_3 j_4}} \langle j_1 j_2 | v | j_3 j_4 \rangle a_{j_2}^\dagger a_{j_1}^\dagger a_{j_3} a_{j_4},$$

written in second quantization (cf. e.g. Brink, D. and Broglia (2005), App. A). In what follows it will be schematically shown how mean field is extracted from such a Hamiltonian, both in the case of single–particle motion (HF) and of independent pair motion (BCS).

### 2.D.1 independent-particle motion

In App. 2.A it was shown that the value of the quantality parameter associated with nuclei ( $q \approx 0.5$ ) leads to particle delocalization and likely makes the system

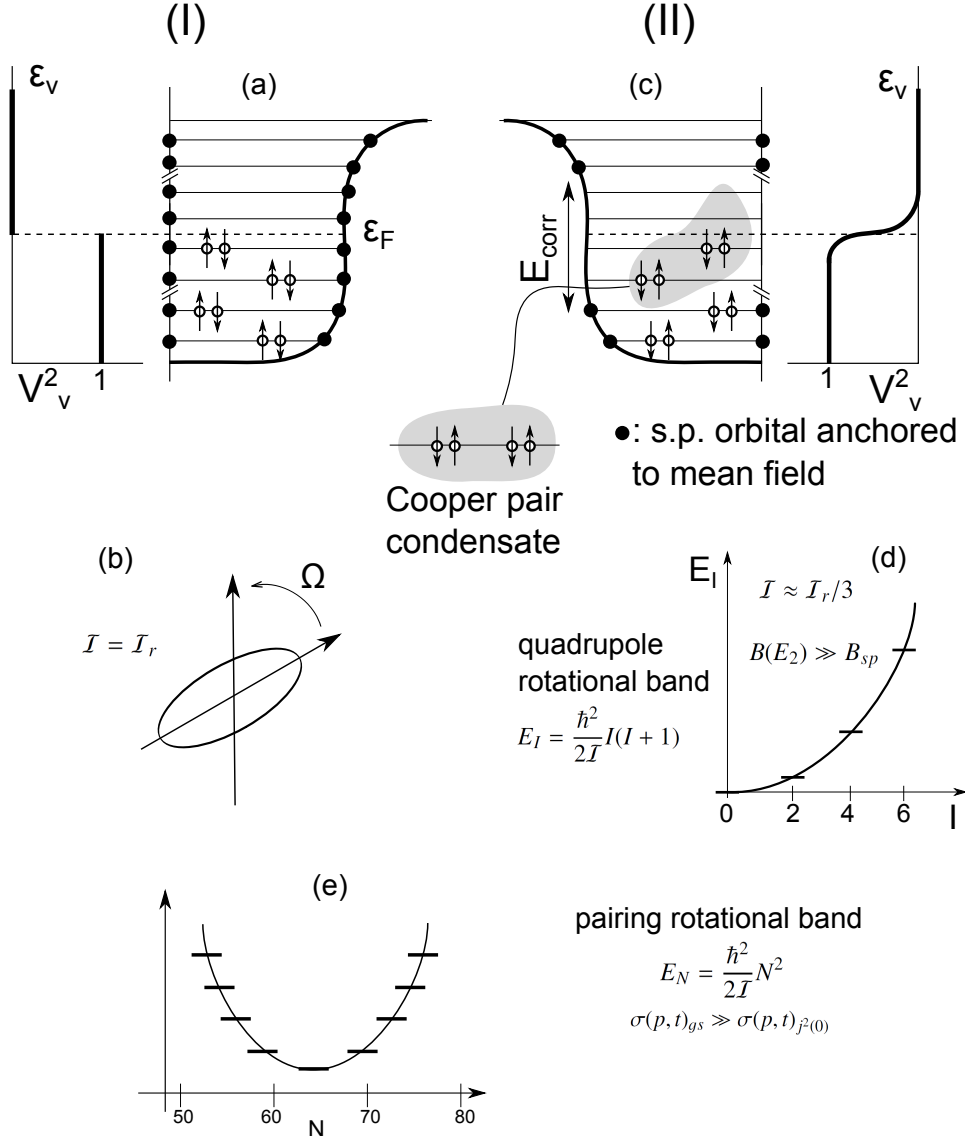


Figure 2.A.3: (I) (a) Schematic representation of “normal” (independent-particle) motion of nucleons in two-fold degenerate (Kramers, time-reversal degeneracy) orbits solidly anchored to the mean field and displaying a sharp, step-function-like, discontinuity in the occupancy at the Fermi energy lead to a deformed (Nilsson (1955)) rotating nucleus with a rigid moment of inertia  $I_r$  (b). (II) Schematic representation of independent nucleon Cooper pair motion in which few (of the order of 5-8) pairs lead to (c) a sigmoidal occupation transition at the Fermi energy and, having uncoupled themselves from the fermionic mean field being now (quasi) bosons they essentially do not contribute to (d) the moment of inertia of quadrupole rotational bands leading to  $I \approx I_r/3$  (cf. Belyaev, S. T. (2013), Belyaev (1959), Bohr, A. and Mottelson (1975) and references therein), (e) pairing rotational bands in gauge space, an example of which is provided by the ground states of the superfluid Sn-isotopes (see also Figs. 2.1.3 and 2.1.4).

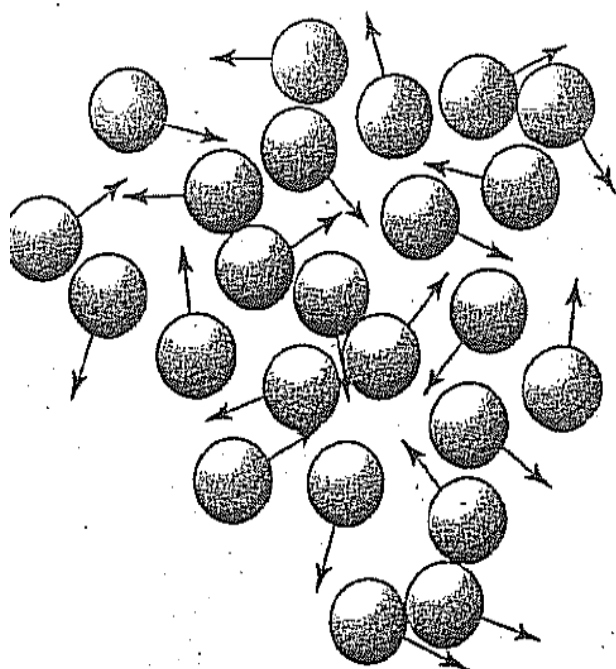


Figure 2.A.4: A system of independent Cooper pairs (Schafroth pairs). This situation corresponds to the incoherent solution of the many Cooper pair problem, the so called Fock state. In cold gases it describes the system after the Feschbach resonance leading to BEC (after Rogovin and Scully (1976)).

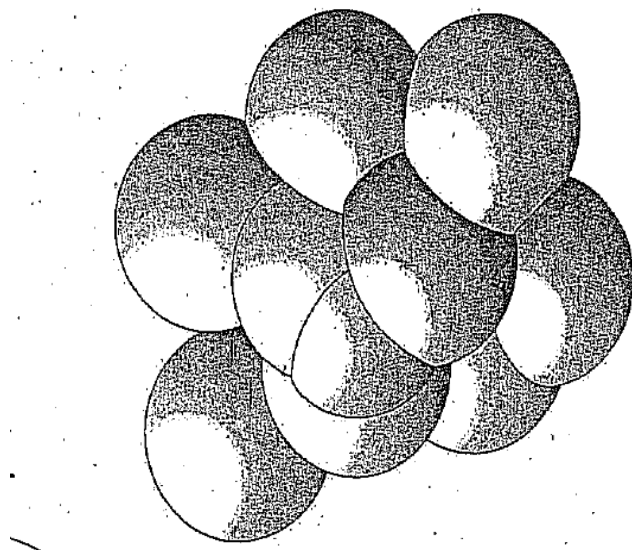


Figure 2.A.5: There are about  $10^{18}$  Cooper pairs per  $\text{cm}^3$  in a superconducting metal. A Cooper pair has a spatial extension of about  $10^{-4}$  cm. Thus a given Cooper pair will overlap with  $10^6$  other Cooper pairs, leading to strong pair–pair correlation, as schematically shown. This solution corresponds to the coherent solution of the many Cooper pair problem (coherent state), also valid in atomic nuclei (cf. Schrieffer (1964), Brink, D. and Broglia (2005), and references therein). (After Rogovin and Scully (1976)).

amenable to a mean field description (Fig. 2.A.2; see however the provisos expressed at the end of App. 2.A). In such a case, Hartree–Fock approximation is tantamount to a selfconsistent relation between density and potential, weighted by the nucleon–nucleon interaction  $v$ , and leading to a complete separation between occupied ( $|i\rangle$ ) and empty ( $|k\rangle$ ) states,

$$(U_\nu^2 + V_\nu^2) = 1; \quad |\varphi_\nu\rangle = \bar{a}_\nu^\dagger |0\rangle = (U_\nu + V_\nu a_\nu^\dagger) |0\rangle; \quad V_\nu^2 = \begin{cases} 1 & \epsilon_i \leq \epsilon_F, \\ 0 & \epsilon_k > \epsilon_F. \end{cases}$$

The Hartree–Fock ground state can then be written as,

$$|HF\rangle = |\det(\varphi_\nu)\rangle = \Pi_\nu \bar{a}_\nu^\dagger |0\rangle = \Pi_i a_i^\dagger |0\rangle = \Pi_{i>0} a_i^\dagger a_i^\dagger |0\rangle.$$

where  $|\tilde{i}\rangle$  is the time reversed state to  $|i\rangle$ .

To be solved, the above self–consistent equations have to be given boundary conditions. In particular, make it explicit whether the system has a spherical or, for example, a quadrupole shape. That is, whether  $\langle HF|Q_2|HF\rangle$  is zero or has a finite value,  $Q_{2M} = \sum_{j_1 j_2} \langle j_2 | r^2 Y_M^2 | j_1 \rangle [a_{j_1}^\dagger a_{j_2}]_M^2$  being the quadrupole operator which carries particle transfer quantum number  $\beta = 0$ , in keeping with its particle–hole character. In the case in which  $\langle Q_{2M} \rangle = 0$ , the system can display a spectrum of low–lying, large amplitude, collective quadrupole vibrations of frequency  $(C/D)^{1/2}$ , the associated ZPF =  $(\hbar^2/(2D\hbar\omega))^{1/2}$ , leading to dynamical violations of rotational invariance (cf. App. 2.B). In the case in which  $\langle Q_{2M} \rangle \neq 0$ , the  $|HF\rangle$  state is known as the Nilsson state,  $|\text{Nilsson}\rangle$ , defining a privileged orientation in 3D–space and thus an intrinsic, body–fixed system of reference  $\mathcal{K}'$  which makes an angle  $\Omega$  (Euler angles) with the laboratory frame  $\mathcal{K}$  (Nilsson (1955)). Because there is no restoring force associated with the different orientations, fluctuations in  $\Omega$  diverge in just the right way to lead to a rotational band displaying a rigid moment of inertia (cf. Fig. 2.A.3), and whose members are the states (Bohr, A. and Mottelson (1975)),

$$|IKM\rangle \sim \int d\Omega \mathcal{D}_{MK}^I(\Omega) |\text{Nilsson}(\Omega)\rangle; \quad E_I = (\hbar^2/2\mathcal{I}) I(I+1); \quad \mathcal{I} = \mathcal{I}_{rig}.$$

One can also view such bands as the limit ( $C \rightarrow 0, D (= \mathcal{I})$  finite) of low energy ( $\omega \rightarrow 0$ ), large–amplitude collective vibration (see App. 2.B). Similar dynamic and static spontaneous symmetry breaking phenomena take place in connection with particle–particle ( $\beta = +2$  transfer quantum number) and hole–hole ( $\beta = -2$ ) correlations, namely in gauge space (see Fig. 2.D.1; subject discussed also in App. 2.E (dynamic: pairing vibration) and also below (static: pairing rotation); see also Figs. 2.1.1, 2.1.3 and 2.1.4). For a consistent discussion of these subjects, see Bès, D. R. and Kurchan (1990).

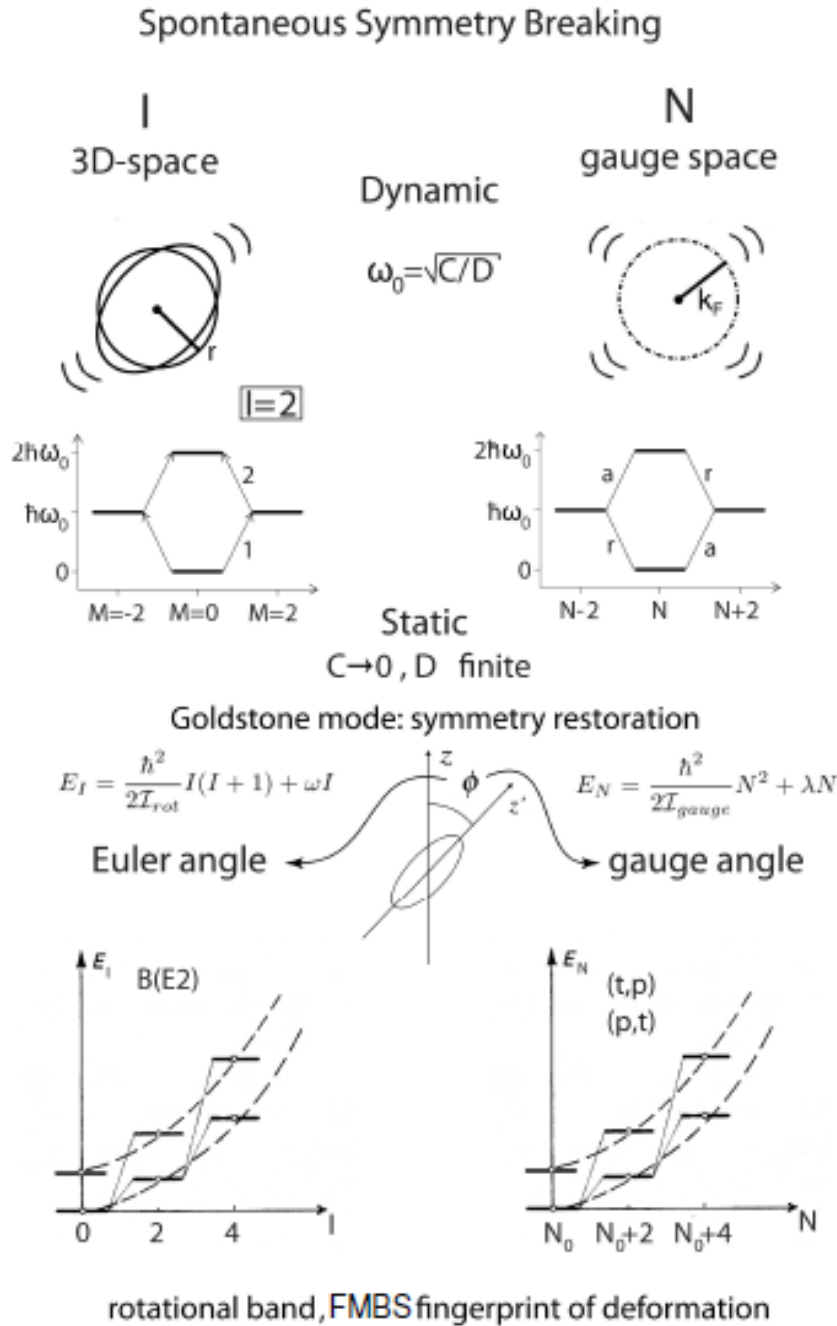


Figure 2.D.1: Parallel between dynamic and static deformations in 3D– and in gauge–space for the nuclear finite many body system (FMBS). In the first case, the angular momentum  $\mathbf{I}$  and the Euler angles are conjugate variables. In the second, particle number  $N$  and gauge angle. While the fingerprint of static (quadrupole and gauge) deformations are quadrupole and pairing rotational bands (see Fig. 2.1.4), vibrational bands are the expression of such phenomena in non deformed systems (after Broglia, R.A. et al. (1973)).

### 2.D.2 independent-pair motion

Let us make use of the constant pairing matrix element approximation  $\langle j_1 j_2 | v | j_3 j_4 \rangle = G$ , that is,

$$H_P = -G \sum_{\nu, \nu' > 0} a_\nu^\dagger a_{\bar{\nu}}^\dagger a_{\nu'} a_{\bar{\nu}'},$$

The abnormal density mean field (cf. e.g. Figs. 2.D.2 and 2.D.3) is related to the finite value of the pair operator that is,

$$\sum \langle a_{j_2}^\dagger a_{j_1}^\dagger \rangle a_{j_3} a_{j_4} + \sum a_{j_2}^\dagger a_{j_1}^\dagger \langle a_{j_3} a_{j_4} \rangle; |\varphi^{COOPER}\rangle = \left( U_j + V_j a_{jm}^\dagger a_{\tilde{j}m}^\dagger \right) |0\rangle,$$

the ground (mean field) state being,

$$|BCS\rangle = \prod_{jm>0} \left( U_j + V_j a_{jm}^\dagger a_{\tilde{j}m}^\dagger \right) |0\rangle; \alpha_0 = \langle BCS | \sum_{jm>0} a_{jm}^\dagger a_{\tilde{j}m}^\dagger |BCS\rangle.$$

Let us introduce the phasing (cf. e.g. Schrieffer, J. R. (1973)),

$$U_\nu = |U_\nu| = U'_\nu; \quad V_\nu = e^{-2i\phi} V'_\nu; \quad (V'_\nu \equiv |V_\nu|) (\nu \equiv j, m),$$

where  $\phi$  is the gauge angle. One can then write the (BCS) wavefunction as,

$$\begin{aligned} |BCS(\phi)\rangle_{\mathcal{K}} &= \prod_{\nu>0} \left( U'_\nu + V'_\nu e^{-2i\phi} a_\nu^\dagger a_{\bar{\nu}}^\dagger \right) |0\rangle = \prod_{\nu>0} \left( U'_\nu + V'_\nu a_\nu^{\dagger'} a_{\bar{\nu}}^{\dagger'} \right) |0\rangle \\ &= |BCS(\phi=0)\rangle_{\mathcal{K}'} : \text{lab. system, } \mathcal{K} : \text{intr. system } \mathcal{K}', \end{aligned}$$

where  $a_\nu^{\dagger'} = e^{-i\phi} a_\nu^\dagger$  is the single-particle creation operator referred to the intrinsic system. The BCS number and gap equations, order parameter, and two-nucleon spectroscopic amplitudes are,

$$\alpha_0 = \alpha'_0 e^{-2i\phi}; \quad \alpha'_0 = \sum_{\nu>0} U'_\nu V'_\nu; \quad ; \Delta = G \alpha_0,$$

$$B_\nu = \langle BCS | [a_\nu'^\dagger a_\nu'^\dagger]_0 | BCS \rangle = (j_\nu + 1/2)^{1/2} U'_\nu V'_\nu,$$

and

$$N_0 = 2 \sum_{\nu>0} V_\nu^2; \quad \frac{1}{G} = \sum_{\nu} \frac{1}{2E_\nu}; \quad \left. \frac{V'_\nu}{U'_\nu} \right\} = \frac{1}{\sqrt{2}} \left( 1 \mp \frac{1}{E_\nu} \right)^{1/2}.$$

Examples of  $B_\nu$ -coefficients for the reaction  $^{124}\text{Sn}(p, t)^{122}\text{Sn}$  (gs) are given in Table 2.D.1.

The wavefunction and energies of the members of the pairing rotational band, can be written as

$$\begin{aligned} |N_0\rangle &\sim \int_0^{2\pi} d\phi e^{-iN_0\phi} |BCS(\phi)\rangle_{\mathcal{K}} \sim \left( \sum_{\nu>0} c_\nu a_\nu^\dagger a_{\bar{\nu}}^\dagger \right)^{N_0/2} |0\rangle; \\ E_N &= (\hbar^2/2I) N^2; \quad I \approx 2\hbar^2/G, \end{aligned}$$

respectively (cf. e.g. Brink, D. and Broglia (2005) App. H).

In the case of a quadrupole deformed nucleus, the system acquires not only a privileged orientation in gauge space, but also in 3D-space. Now, as summarized above, in a superfluid system, Cooper pairs and not single-particles are the building blocks of the system (see Figs. 2.D.2 and 2.D.3)<sup>3</sup>. But while the mean square radius of a nucleon at the Fermi energy ( $\langle r^2 \rangle^{1/2} \approx (3/5)^{1/2} R_0$  ( $R_0 = 1.2 A^{1/3}$  fm)) is about 4.6 fm ( $A \approx 120$ ), that of a Cooper pair is determined by the correlation length ( $\xi \approx \hbar v_F/m \approx 36$  fm) between the two nucleons forming the pair (see Figs. 2.A.3 and 2.A.4). Consequently, orienting the quadrupole deformed potential in different directions (angles  $\Omega$ ), will have less effect on Cooper pairs than on independent particles. Thus the reduction of the moment of inertia from  $I_r$  to  $\approx I_r/3$ . Within this context one can mention the fact that low-lying nuclear collective vibrations (and rotations) are essentially not observed at intrinsic excitation energies corresponding to temperatures of  $\approx 1\text{-}2$  MeV. In this case, this is because the surface is strongly fluctuating and thus not well defined, making it non operative its anisotropic orientation in space.

Because in FMBS quantal fluctuations are very important (see Bertsch and Broglia (2005) and references therein), deformation in such systems explicit themselves through rotational bands. In particular, superfluid nuclei display well defined pairing rotational bands, an example of such bands being provided by the ground states of the superfluid Sn-isotopes. In this case, the moment of inertia is directly related to the pairing interaction. Pairing rotational bands are specifically excited in two nucleon transfer reactions (cf, Figs. 2.1.3 and 2.1.4). A summary of the physics which is at the basis of independent single-particle and single-pair motion is given in Figs. 2.D.2 and 2.D.3.

## Appendix 2.E Two-nucleon spectroscopic amplitudes associated with pairing vibrational modes in closed shell systems: the $^{208}\text{Pb}$ case.

The solution of the pairing Hamiltonian

$$H = H_{sp} + H_p,$$

where

$$H_{sp} = \sum_\nu \epsilon_\nu a_\nu^\dagger a_\nu,$$

and

$$H_p = -GP^\dagger P,$$

---

<sup>3</sup>In connection with Fig. 2.D.2, the estimate  $2R = 20/k_F$  was carried out with the help of the Fermi gas model (cf. e.g. Bohr and Mottelson (1969)), making use of the relation  $k_F \approx (3\pi A/2V)^{1/3}$  connecting the Fermi momentum to the nuclear density  $\rho(0) = A/V$ ,  $A$  being the mass number. Employing  $\rho(0) = 0.17 \text{ fm}^{-3}$  and  $R = r_0 A^{1/3}$  ( $r_0 = 1.2 \text{ fm}$ ) one obtains  $k_F R_0 = 1.63$ . Thus, in the case of a heavy system ( $A = 200$ ,  $A^{1/3} = 5.85$ ),  $2R = 2R_0 A^{1/3} = 2 \times 1.63 \times 5.85/k_F \approx 20/k_F$ .

### Classical localization and quantal ZPF

$$\delta x \delta k \geq 1 \quad \varepsilon = \frac{\hbar^2 k^2}{2M} \quad \delta k = \frac{\delta \varepsilon}{\hbar v_F} \quad (v_F/c \approx 0.3)$$

structure

Independent motion of

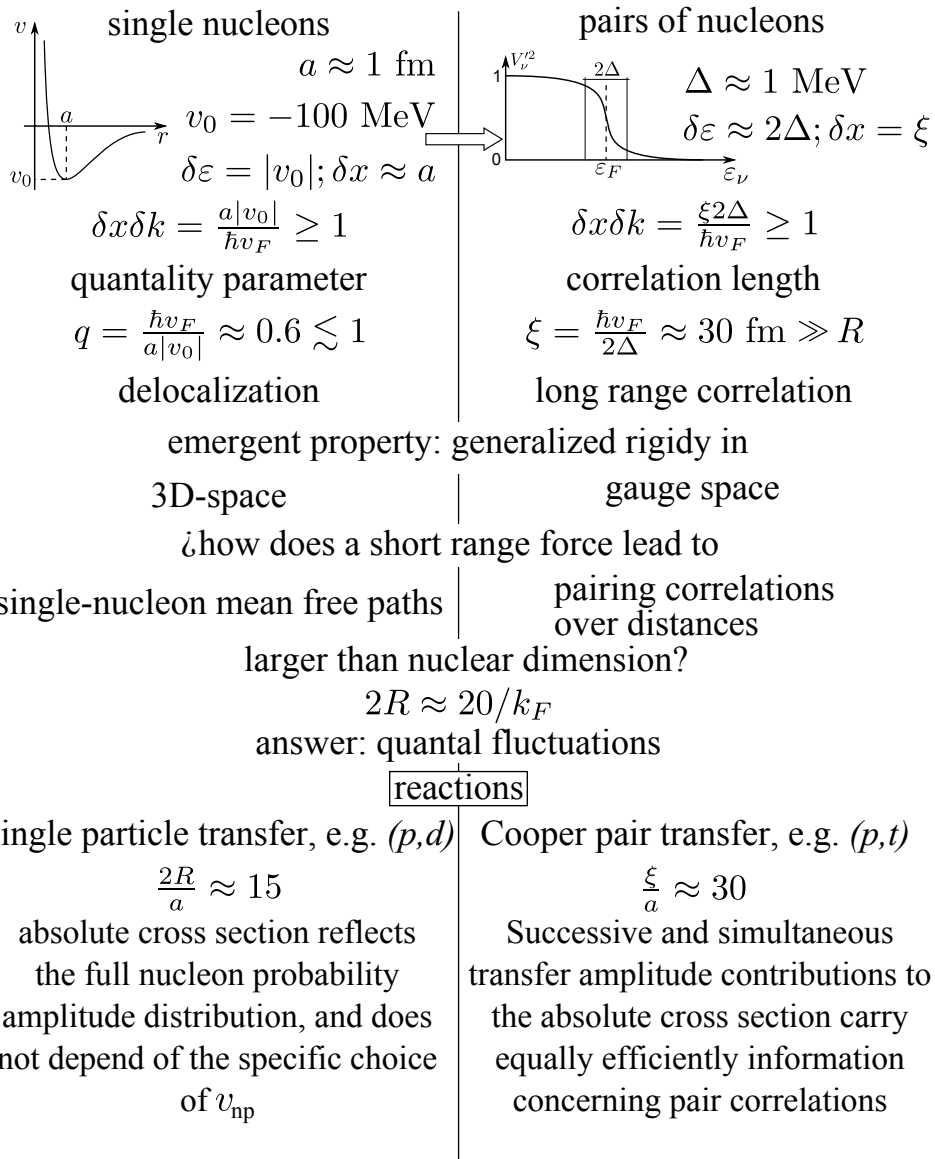
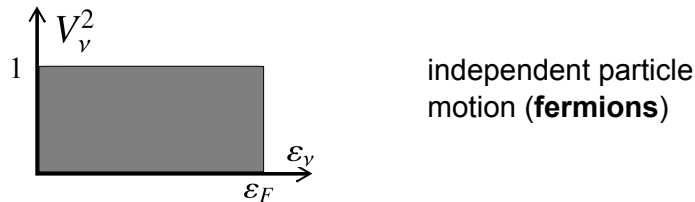


Figure 2.D.2: Classical localization and zero point fluctuations, associated with independent-particle (normal density) and independent-pair motion (abnormal density). In the second part of the figure, fluctuations associated with collective motion are also allowed (e.g. collective surface vibrations and pairing vibrations). Their interweaving lead to dressed particles and to an induced pairing interaction.

$$\begin{aligned}
 H = T + v &= \underbrace{T + U + V_p}_{\text{mean field}} + (v - U - V_p) \\
 \text{diagonalization} &\quad \text{Kramers degeneracy } v\bar{v} \\
 a_v^\dagger &= U_v a_v^\dagger - V_v a_{\bar{v}}^\dagger; \\
 \text{ground state} & \\
 a_v |\tilde{0}\rangle &= 0 \\
 |\tilde{0}\rangle &= \prod_{v>0} a_v a_{\bar{v}}^\dagger |0\rangle \sim \prod_{v>0} (U_v + V_v a_v^\dagger a_{\bar{v}}^\dagger) |0\rangle \\
 a_v |0\rangle &= 0
 \end{aligned}$$

Ansatz 1:  $|\tilde{0}\rangle$  sharp step-funct. occ.

$$|HF\rangle = \prod_{i>0} a_i^\dagger a_i^\dagger |0\rangle = \prod_i a_i^\dagger |0\rangle$$



Ansatz 2:  $|\tilde{0}\rangle$  sigmoidal distr. occ.

$$|BCS\rangle = \prod_{v>0} (U_v + V_v a_v^\dagger a_{\bar{v}}^\dagger) |0\rangle$$

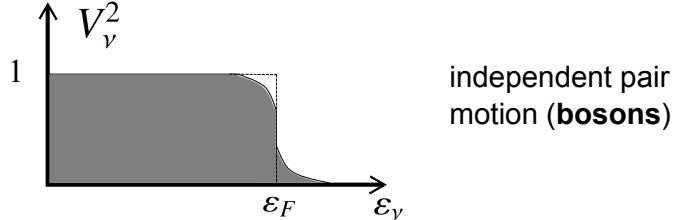


Figure 2.D.3: Schematic representation of the steps to be taken to extract from a two-body interaction independent particle motion ( $U$ , mean field) and independent pair motion ( $V_p = -G\alpha_0(P^\dagger + P)$ , pair potential,  $P^\dagger$  being the pair creation operator), in terms of a generalized quasiparticle transformation, and leading to a sharp step-function occupation distribution and a smooth (sigmoidal) occupation distribution around the Fermi surface respectively.

$nlj^a)$	$^{112}\text{Sn}(p, t)^{110}\text{Sn}(\text{gs})$	$^{124}\text{Sn}(p, t)^{122}\text{Sn}(\text{gs})$	$\text{BCS}^b)$	$V_{low-k}^c)$	$\text{BCS}^d)$	$\text{NuShell}^e)$
$1g_{7/2}$	0.96	-1.1073	0.44	0.63		
$2d_{5/2}$	0.66	-0.7556	0.35	0.60		
$2d_{3/2}$	0.54	-0.4825	0.58	0.72		
$3s_{1/2}$	0.45	-0.3663	0.36	0.52		
$1h_{11/2}$	0.69	-0.6647	1.22	-1.24		

Table 2.D.1: Two–nucleon transfer spectroscopic amplitudes associated with the reactions  $^{112}\text{Sn}(p, t)^{110}\text{Sn}(\text{gs})$  and  $^{124}\text{Sn}(p, t)^{122}\text{Sn}(\text{gs})$ . **a)** quantum numbers of the two–particle configurations  $(nlj)_{J=0}^2$  coupled to angular momentum  $J = 0$ . **b,d)**  $\langle \text{BCS} | P_\nu | \text{BCS} \rangle = \sqrt{2j_\nu + 1} U_\nu(A) V_\nu(A+2)$  ( $A+2 = 112$  and  $124$  respectively), where  $P_\nu = a_\nu a_\nu$  ( $\nu \equiv nlj$ ) (cf. Potel, G. et al. (2011, 2013a,b)) **c)** two–nucleon transfer spectroscopic amplitudes calculated making use of initial and final state wavefunctions obtained by diagonalizing a  $v_{low-k}$ , that is a renormalized, low–momentum interaction derived from the CD–Bonn nucleon–nucleon potential (see Guazzoni, P. et al. (2006) and references therein). **e)** Two–neutron overlap functions obtained making use of the shell–model wavefunctions for the ground state of  $^{122}\text{Sn}$  and  $^{124}\text{Sn}$  calculated with the code NuShell (Brown, B. A. and Rae, 2007). The wavefunctions were obtained starting with a  $G$ –matrix derived from the CD–Bonn nucleon–nucleon interaction Machleidt, R. et al. (1996). These amplitudes were used in the calculation of  $^{124}\text{Sn}(p, t)^{122}\text{Sn}$  absolute cross sections carried out by I.J. Thompson (Thompson, I.J., 2013).

with

$$P^\dagger = \sum_{\nu>0} a_\nu^\dagger a_{\bar{\nu}}^\dagger,$$

lead, in the case of closed shell systems and within the harmonic approximation (RPA), to pair addition ( $a$ ) pair removal ( $r$ ) two–particle, two–hole correlated modes, the associated creation and annihilation operator being

$$\Gamma_a^\dagger(n) = \sum_k X_n^a(k) \Gamma_k^\dagger + \sum_i Y_n^a(i) \Gamma_i,$$

and

$$\Gamma_r^\dagger(n) = \sum_i X_n^r(i) \Gamma_i^\dagger + \sum_k Y_n^r(k) \Gamma_k,$$

with

$$\sum X^2 - Y^2 = 1,$$

and

$$\Gamma_k^\dagger = a_k^\dagger a_{\bar{k}}^\dagger, \quad (\epsilon_k > \epsilon_F).$$

Similarly,

$$\Gamma_i^\dagger = a_i^\dagger a_i, \quad (\epsilon_i \leq \epsilon_F).$$

The relations

$$[H, \Gamma_a^\dagger(n)] = \hbar W_n(\beta = +2),$$

and

$$[H, \Gamma_r^\dagger(n)] = \hbar W_n(\beta = -2),$$

where  $\beta$  is the transfer quantum number, while  $n$  labels the roots of the corresponding dispersion relations (cf. Bès, D. R. and Broglia (1966)),

$$\frac{1}{G(\pm 2)} = \sum_k \frac{(\Omega_k/2)}{2\epsilon_k \mp W_n(\pm 2)} + \sum_i \frac{(\Omega_i/2)}{2\epsilon_i \pm W_n(\pm 2)},$$

$n$  labeling the corresponding solutions in increasing order of energy. In the above equation,  $\Omega_j = j + 1/2$  is the pair degeneracy of the orbital with total angular momentum  $j$ .

For the case of the (neutron) pair addition and pair subtraction modes of  $^{208}\text{Pb}$  the above equations are graphically solved in Fig 2.E.1 (see also Table 2.E.1). The minimum of the dispersion relation defines the Fermi energy of the system under study. This is in keeping with the fact that in the case in which  $W_1(\beta = +2) = W_1(\beta = -2) = 0$ , situation corresponding to the transition between normal and superfluid phases, the energy value at which the dispersion relation touches for the first time the energy axis, coincides with the BCS  $\lambda$  variational parameter. It is of notice that, as a rule, the Fermi energy of closed shell nuclei is empirically defined as half the energy difference between the last occupied and the first empty single particle state (cf. e.g. Mahaux, C. et al. (1985)). Making use of the values (see Fig. 2.E.1)

$$\begin{cases} E_{corr}(+2) = B(208) + B(210) - 2B(209) = 1.248 \text{ MeV}, \\ E_{corr}(-2) = B(208) + B(206) - 2B(207) = 0.630 \text{ MeV}, \end{cases}$$

one obtains  $W_1(+2) + W_1(-2) = (B(208) - B(206)) - (B(210) - B(208)) = 14.11 - 9.115 = 4.995 \text{ MeV}$ . Notice that in the above calculations all energies differences are positive. In particular (see Table 2.E.1)

$$\epsilon_i < \epsilon_F \Rightarrow \epsilon_F - \epsilon_i = -|\epsilon_F| + |\epsilon_i| = |\epsilon_i| - |\epsilon_F| > 0,$$

and

$$\epsilon_k > \epsilon_F \Rightarrow \epsilon_k - \epsilon_F = -|\epsilon_k| + |\epsilon_F| = |\epsilon_F| - |\epsilon_k| > 0.$$

Thus,

$$\begin{cases} 2(\epsilon_F - \epsilon_{p_{1/2}}) = W_1(-2) + E_{corr}(-2) > 0, \\ 2(\epsilon_{g_{9/2}} - \epsilon_F) = W_1(+2) + E_{corr}(+2) > 0. \end{cases}$$

From Fig. 2.E.1 and Table 2.E.1 one can then write,

$$2 \times (-5.825 - (-7.5)) \text{ MeV} = 2.650 \text{ MeV} = W_1(-2) + 0.640 \text{ MeV}$$

and

$$2 \times (-3.74 \text{ MeV} - (-5.825) \text{ MeV}) = 4.17 \text{ MeV} = W_1(+2) + 1.248 \text{ MeV}.$$

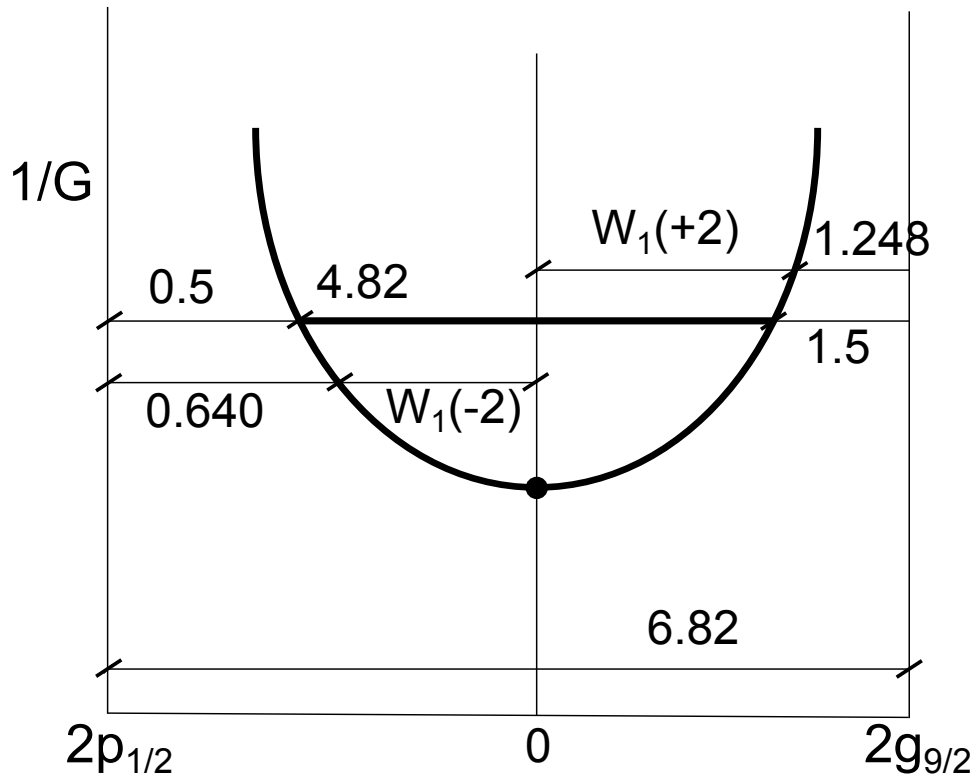


Figure 2.E.1: The right hand side of the RPA pairing vibrational dispersion relation for neutrons in the case of the closed shell system  $^{208}\text{Pb}$  (cf. Bès,D. R. and Broglia (1966)) in the region between the two neighboring shells ( $p_{1/2}$  and  $g_{9/2}$ ). All quantities are in MeV. For each  $G$  there is a straight horizontal line, which is divided by the the curve in three sections. The first one from the left corresponds to the pairing correlation energy of the nucleus  $^{206}\text{Pb}$  (two correlated neutron hole states) while the last segment to the right measures the pairing correlation energy of  $^{210}\text{Pb}$  (two correlated neutrons above closed shell) the intermediate segment measures the energy of the two phonon (correlated  $(2p - 2h)$ ) pairing vibrational state of  $^{208}\text{Pb}$ .

orbit	$\epsilon_j$	$\epsilon_{p_{1/2}} - \epsilon_k \equiv  \epsilon_k  -  \epsilon_{p_{1/2}} $
$0h_{9/2}$	-10.62	3.47
$1f_{7/2}$	-9.50	2.35
$0i_{13/2}$	-8.79	1.64
$2p_{3/2}$	-8.05	0.90
$1f_{5/2}$	-7.72	0.57
$2p_{1/2}$	-7.15	0
$\epsilon_F = -5.825$ keV		$\epsilon_k - \epsilon_{g_{9/2}} \equiv  \epsilon_{g_{9/2}}  -  \epsilon_k $
$1g_{9/2}$	-3.74	0.
$0i_{11/2}$	-2.97	0.77
$0j_{15/2}$	-2.33	1.41
$2d_{5/2}$	-2.18	1.56
$3s_{1/2}$	-1.71	2.03
$1g_{7/2}$	-1.27	2.47
$2d_{3/2}$	-1.23	2.51

Table 2.E.1: Valence single-particle levels of  $^{208}\text{Pb}$ . In the upper part the occupied levels ( $\epsilon_i \leq \epsilon_F$ ) are shown while in the lower part the empty levels ( $\epsilon_k \geq \epsilon_F$ ). Of notice that  $\epsilon_{p_{1/2}} - \epsilon_{g_{9/2}} = 3.41$  MeV, is the single-particle gap associated with  $N = 126$  shell closure (from Nuclear Data Center).

Consequently,

$$W_1(-2) = 2.01 \text{ MeV} \quad \text{and} \quad W_1(+2) = 2.92 \text{ MeV},$$

leading to,

$$W_1(+2) + W_1(-2) = 4.93 \text{ MeV}.$$

### 2.E.1 Pair removal mode

In Fig. 2.E.2 the graphical representation of the forwards going RPA amplitude of the pair removal mode is shown. Its expression is

$$X_1^r(i) = \frac{\frac{1}{2}\Omega_i^{1/2}\Lambda(-2)}{2(\epsilon_F - \epsilon_i) - W_1(-2)},$$

where

$$\begin{aligned} 2 \times (\epsilon_F - \epsilon_i) - W_1(-2) &= 2 \times (\epsilon_F - \epsilon_i) - 2 \times (\epsilon_F - \epsilon_{p_{1/2}}) + E_{corr}(-2) \\ &= 2 \times (\epsilon_{p_{1/2}} - \epsilon_i) + E_{corr}(-2) = 2 \times (|\epsilon_i| - |\epsilon_{p_{1/2}}|) + E_{corr}(-2). \end{aligned}$$

Thus,

$$X_1^r(i) = \frac{\frac{1}{2}\Omega_i^{1/2}\Lambda(-2)}{2(|\epsilon_i| - |\epsilon_{p_{1/2}}|) + E_{corr}(-2)}.$$

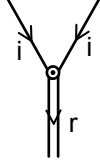


Figure 2.E.2: NFT representation of the forwards going RPA amplitude of the pair removal mode (double downward going arrowed line) describing a two correlated hole state (single downward going arrowed line for each hole with quantum numbers collectively labeled  $i$ ).

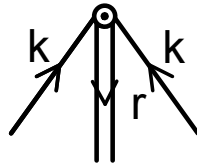


Figure 2.E.3: Same as Fig. 2.E.2 but for the backwards going amplitudes.

Making use of the empirical value of  $E_{corr}(-2)$  worked out above one obtains,

$$X_1^r(i) = \frac{\frac{1}{2}\Omega_i^{1/2}\Lambda(-2)}{2(|\epsilon_i| - |\epsilon_{p_{1/2}}|) + 0.640 \text{ MeV}}.$$

In Fig. 2.E.3 we display the graphical process associated with the backwards going RPA amplitude,

$$Y_1^r(k) = \frac{\frac{1}{2}\Omega_k^{1/2}\Lambda(-2)}{2(\epsilon_k - \epsilon_F) + W_1(-2)}.$$

Making use of

$$2 \times (\epsilon_F - \epsilon_{p_{1/2}}) - E_{corr}(-2) = W_1(-2),$$

one can write

$$2 \times (\epsilon_F - \epsilon_{p_{1/2}}) + 2 \times (\epsilon_k - \epsilon_F) - E_{corr}(-2) = 2 \times (\epsilon_k - \epsilon_F) + W_1(-2),$$

leading to

$$2 \times (|\epsilon_{p_{1/2}}| - |\epsilon_k|) - E_{corr}(-2) = 2 \times (|\epsilon_{p_{1/2}}| - |\epsilon_{g_{9/2}}|) + 2 \times (|\epsilon_{g_{9/2}}| - |\epsilon_k|) - E_{corr}(-2).$$

Thus,

$$Y_1^r(k) = \frac{\frac{1}{2}\Omega_k^{1/2}\Lambda(-2)}{2(|\epsilon_{g_{9/2}}| - |\epsilon_k|) + 2(|\epsilon_{p_{1/2}}| - |\epsilon_{g_{9/2}}|) - E_{corr}(-2)}.$$

With the help of  $2 \times (|\epsilon_{p_{1/2}}| - |\epsilon_{g_{9/2}}|) - E_{corr}(-2) = 6.82 \text{ MeV} - 0.640 \text{ MeV} = 6.18 \text{ MeV}$ , one obtains,

$$Y_1^r(k) = \frac{\frac{1}{2}\Omega_k^{1/2}\Lambda(-2)}{2(|\epsilon_{g_{9/2}}| - |\epsilon_k|) + 6.18 \text{ MeV}}.$$

The above expressions of  $X_1^r(i)$  and  $Y_1^r(k)$  contain the experimental values of the 2-hole correlation energies (0.640 MeV). Because (see Fig. 2.E.1) the associated values of  $G$  does not lead to the observed correlation energy of the pair addition mode (1.248 MeV), we prefer to choose a single intermediate value of  $G$  and use the resulting  $E_{corr}(-2)$  (=0.5 MeV) and  $E_{corr}(+2)$  (=1.5 MeV), correlation energies, to calculate the corresponding  $X, Y$  amplitudes for both the lowest removal and lowest addition pairing modes. Making use of,

$$\begin{aligned} 2 \times (|\epsilon_{p_{1/2}}| - |\epsilon_{g_{9/2}}|) &= 6.82 \text{ MeV} \quad \text{and} \quad 2 \times (|\epsilon_{p_{1/2}}| - |\epsilon_{g_{9/2}}|) - E_{corr}(-2) \\ &= (6.82 - 0.5) \text{ MeV} = 6.32 \text{ MeV}, \end{aligned}$$

one can write

$$\begin{aligned} X_1^r(i) &= \frac{\frac{1}{2}\Omega_i^{1/2}\Lambda(-2)}{2(|\epsilon_i| - |\epsilon_{p_{1/2}}|) + 0.5 \text{ MeV}}, \\ Y_1^r(k) &= \frac{\frac{1}{2}\Omega_k^{1/2}\Lambda(-2)}{2(|\epsilon_{g_{9/2}}| - |\epsilon_k|) + 6.32 \text{ MeV}}. \end{aligned}$$

Tables 2.E.2 and 2.E.3 contain the amplitudes of the pair removal mode of  $^{208}\text{Pb}$  ( $\Gamma_r^\dagger(1) = \sum X_1^r(i)\Gamma_i^\dagger + \sum Y_1^r(k)\Gamma_k$ ), that is of the two neutron correlated hole state describing  $|^{206}\text{Pb}(\text{gs})\rangle = \Gamma_r^\dagger(1)|0\rangle$ .

It is of notice that the coupling strength  $\Lambda(-2)$  with which the pair removal mode couples to the single-particle (-hole) states is calculated by normalizing the amplitudes: 1) (Tamm Dancoff, TD)  $\sum_i A^2(i) = 1.5549 \text{ MeV}^{-2}$  and thus  $\Lambda(-2) = 0.802 \text{ MeV}$ , ( $\sum X(i)_{TD}^2 = 1$ ); 2) RPA,  $\Lambda_1^2(-2) \times (\sum_i A^2(i) - \sum_k B^2(k)) = \Lambda_1^2(-2) \times 1.45073 = 1$ . Thus  $\Lambda_1(-2) = 0.830 \text{ MeV}$ . The above results shows that there is a few percentage difference between the two values of  $\Lambda$  (TD and RPA), as well as for the corresponding  $X$  amplitudes. Nonetheless, ground state correlations as expressed by the  $Y$  amplitudes, gives rise to a 52% increase in the  $^{206}\text{Pb}(t, p)^{208}\text{Pb}(\text{gs})$  absolute cross section, from 0.34 mb to 0.52 mb to be compared with experimental data  $\sigma = 0.68 \pm 0.24 \text{ mb}$  (see Fig. 3.A.4).

## 2.E.2 Pair addition mode

In Fig. 2.E.4 the  $X$ -amplitude of the pair addition mode is shown (NFT diagram). The associated expression

$$X_1^a(k) = \frac{\frac{1}{2}\Omega_k^{1/2}\Lambda_1(+2)}{2(\epsilon_k - \epsilon_F) - W_1(+2)},$$

units		MeV	MeV <sup>-1</sup>	RPA	TD
$nlj$	$\Omega_i$	$ \epsilon_i  -  \epsilon_{p_{1/2}} $	$A(i) = \frac{\frac{1}{2}\Omega_i^{1/2}}{2( \epsilon_i  -  \epsilon_{p_{1/2}} ) + 0.5 \text{ MeV}}$	$X_1^r(i)$	$X_1^r(i)$
$2p_{1/2}$	1	0	1	0.83	0.80
$1f_{5/2}$	3	0.57	0.528	0.44	0.42
$2p_{3/2}$	2	0.90	0.307	0.25	0.25
$0i_{13/2}$	7	1.64	0.350	0.29	0.28
$1f_{7/2}$	4	2.35	0.192	0.16	0.15
$0h_{9/2}$	5	3.47	0.150	0.12	0.12

Table 2.E.2: Forwards going RPA amplitudes of the pair removal mode of  $^{208}\text{Pb}$  (i.e.  $|^{206}\text{Pb}\rangle$  state), cf. Table XVI Broglia, R.A. et al. (1973).

units		MeV	MeV <sup>-1</sup>	RPA
$nlj$	$\Omega_k$	$ \epsilon_{g_{9/2}}  -  \epsilon_k $	$B(k) = \frac{\frac{1}{2}\Omega_k^{1/2}}{2( \epsilon_{g_{9/2}}  -  \epsilon_k ) + 6.23 \text{ MeV}}$	$Y_1^r(i)$
$1g_{9/2}$	5	0	0.179	-0.15
$0i_{11/2}$	6	0.77	0.158	-0.13
$0j_{15/2}$	8	1.41	0.156	-0.13
$2d_{5/2}$	3	1.56	0.093	-0.08
$3s_{1/2}$	1	2.03	0.046	-0.04
$1g_{7/2}$	4	2.47	0.090	-0.07
$2d_{3/2}$	2	2.51	0.063	-0.05

Table 2.E.3: Same as Table 2.E.2 but for the backwards amplitude.

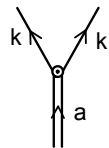


Figure 2.E.4: Same as Fig. 2.E.2 but for the pair addition mode

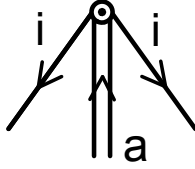


Figure 2.E.5: Same as Fig. 2.E.3 but for the pair addition mode

can be written, making use of

$$\begin{aligned} 2 \times (\epsilon_k - \epsilon_F) - W_1(+2) &= 2 \times (\epsilon_k - \epsilon_F) - 2 \times (\epsilon_{g_{9/2}} - \epsilon_F) + E_{corr}(+2) \\ &= 2 \times (\epsilon_k - \epsilon_{g_{9/2}}) + E_{corr}(+2) = 2 \times (|\epsilon_{g_{9/2}}| - |\epsilon_k|) + E_{corr}(+2), \end{aligned}$$

as

$$X_1^a(k) = \frac{\frac{1}{2}\Omega_k^{1/2}\Lambda_1(+2)}{2(|\epsilon_{g_{9/2}}| - |\epsilon_k|) + E_{corr}(+2)}.$$

Similarly (cf. Fig. 2.E.5),

$$Y_1^a(i) = \frac{\frac{1}{2}\Omega_i^{1/2}\Lambda_1(+2)}{2(\epsilon_F - \epsilon_i) + W_1(+2)},$$

can be written, with the help of the relation

$$\begin{aligned} 2 \times (\epsilon_F - \epsilon_i) + W_1(+2) &= 2 \times (\epsilon_F - \epsilon_i) - 2 \times (\epsilon_{g_{9/2}} - \epsilon_F) - E_{corr}(+2) \\ &= 2 \times (\epsilon_{p_{1/2}} - \epsilon_i) + 2 \times (\epsilon_{g_{9/2}} - \epsilon_{p_{1/2}}) - E_{corr}(+2) \\ &= 2 \times (|\epsilon_i| - |\epsilon_{p_{1/2}}|) + 2 \times (|\epsilon_{p_{1/2}}| - |\epsilon_{g_{9/2}}|) - E_{corr}(+2), \end{aligned}$$

as

$$Y_1^a(i) = \frac{\frac{1}{2}\Omega_i^{1/2}\Lambda_1(+2)}{2(|\epsilon_i| - |\epsilon_{p_{1/2}}|) + 2\Delta\epsilon_{sp} - E_{corr}(+2)}.$$

Making use of  $E_{corr}(+2) = 1.5$  MeV (cf. Fig. 2.E.1) and

$$\Delta\epsilon_{sp} = 2 \times (|\epsilon_{p_{1/2}}| - |\epsilon_{g_{9/2}}|) = 6.28 \text{ MeV},$$

one can write  $2\Delta\epsilon_{sp} - E_{corr}(+2) = (6.82 - 1.5)$  MeV = 5.32 MeV, leading to

$$\begin{cases} X_1^a(k) = \frac{\frac{1}{2}\Omega_k^{1/2}\Lambda(-2)}{2(|\epsilon_{g_{9/2}}| - |\epsilon_k|) + 1.5 \text{ MeV}}, \\ Y_1^a(i) = -\frac{\frac{1}{2}\Omega_i^{1/2}\Lambda(+2)}{2(|\epsilon_i| - |\epsilon_{p_{1/2}}|) + 5.32 \text{ MeV}}. \end{cases}$$

The corresponding numerical values are displayed in Tables 2.E.4 and 2.E.5, while in Fig. 2.E.6 we display a schematic summary of the graphical solution of the dispersion relations.

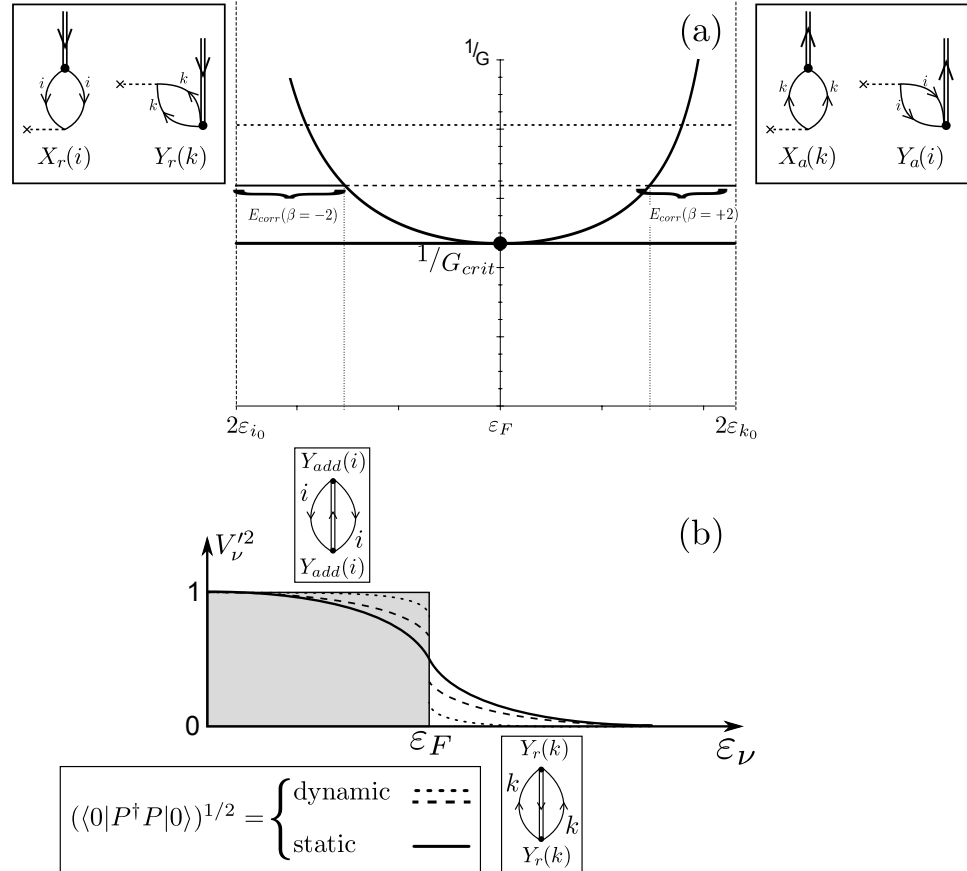


Figure 2.E.6: Schematic representation of the quantal phase transition taking place as a function of the pairing coupling constant in a (model) closed shell nucleus. (a) dispersion relation associated with the RPA diagonalization of the Hamiltonian  $H = H_{sp} + H_p$  for the pair addition and pair removal modes. In the insets are shown the two-particle transfer processes exciting these modes, which testify to the fact that the associated zero point fluctuations (ZPF) which diverge at  $G = G_{crit}$ , blur the distinction between occupied and empty states typical of closed shell nuclei. (b) occupation number associated with the single-particle levels. For  $G < G_{crit}$  there is a dynamical depopulation (population) of levels  $i(k)$  below (above) the Fermi energy. For  $G > G_{crit}$ , the deformation of the Fermi surface becomes static, although with a non-vanishing dynamic component (cf. Fig. 2.1.2).

units		MeV	MeV <sup>-1</sup>	
$nlj$	$\Omega_k$	$ \epsilon_{g_{9/2}}  -  \epsilon_k $	$C(k) = \frac{\frac{1}{2}\Omega_k^{1/2}}{2( \epsilon_{g_{9/2}}  -  \epsilon_k ) + 1.5 \text{ MeV}}^a$	$X_1^a(k)$
$1g_{9/2}$	5	0	0.745	0.82
$0i_{11/2}$	6	0.77	0.403	0.44
$0j_{15/2}$	8	1.41	0.327	0.36
$2d_{5/2}$	3	1.56	0.187	0.21
$3s_{1/2}$	1	2.03	0.090	0.10
$1g_{7/2}$	4	2.47	0.155	0.17
$2d_{3/2}$	2	2.51	0.108	0.12

Table 2.E.4: Forwards going RPA amplitudes associated with the pair addition mode of  $^{208}\text{Pb}$  (cf. Table XVI Broglia, R.A. et al. (1973)). a)  $\sum_k C^2(k) = 0.903$

units		MeV	MeV <sup>-1</sup>	
$nlj$	$\Omega_i$	$ \epsilon_i  -  \epsilon_{p_{1/2}} $	$D(i) = \frac{\frac{1}{2}\Omega_i^{1/2}}{2( \epsilon_i  -  \epsilon_{p_{1/2}} ) + 5.32 \text{ MeV}}^a$	$Y_1^a(i)$
$2p_{1/2}$	1	0	-0.094	-0.1
$1f_{5/2}$	3	0.57	-0.134	-0.15
$2p_{3/2}$	2	0.90	-0.099	-0.11
$0i_{13/2}$	7	1.64	-0.154	-0.17
$1f_{7/2}$	4	2.35	-0.100	-0.11
$0h_{9/2}$	5	3.47	-0.091	-0.10

Table 2.E.5: Same as Table 2.E.4 but for the backwards going amplitude. a)  $\sum_i D^2(i) = 0.079$  and  $\Lambda^2(+2)(\sum_k C^2(k) - D^2(i)) = \Lambda^2(+2)(0.903 - 0.079) \text{ MeV}^{-2} = 0.824 \text{ MeV}^{-2}$ ;  $\Lambda(+2) = (0.824)^{-1/2} \text{ MeV}$ , thus  $\Lambda(+2) = 1.102 \text{ MeV}$ .

Let us conclude this Appendix by noting that while the harmonic (RPA) description of the pair vibrational mode of  $^{208}\text{Pb}$  provides a fair description of the two neutron transfer spectroscopic amplitudes, in keeping with the collective character of these (coherent) states, conspicuous anharmonicities in the multi-phonon spectrum have been observed and calculated (cf. for example Flynn, E. R. et al. (1972), Bortignon, P. F. et al. (1978), Clark, R. M. et al. (2006)). Within the framework of Fig. 2.D.1, we schematically emphasize in Fig. 2.E.7 the relative importance of dynamic and static pairing distortions, in comparison with the corresponding quantities in the case of quadrupole surface distortions in 3D space (for details cf. Bès and Broglia (1977), Broglia, R.A. et al. (1968), Bès, D. R. et al. (1988), Shimizu, Y. R. et al. (1989), Shimizu, Y. R. (2013), Vaquero et al. (2013) and references therein). These results underscore the major role pairing vibrations play in nuclei around closed shells, while those collected in Fig. 2.1.2 their importance in gauge invariance restoration in systems far away from closed shells.

## Appendix 2.F Halo pair addition mode and pigmy: a new symbiotic elementary mode of nuclear excitation

Pairing is intimately connected with particle number violation and thus spontaneous breaking of gauge invariance, as testified by the order parameter  $\langle BCS | P^\dagger | BCS \rangle = \alpha_0$ . In the nuclear case and, at variance with condensed matter, dynamical breaking of gauge symmetry is similarly important to that associated with static distortions (e.g. pairing vibrations around closed shell nuclei, cf. Fig. 2.1.1; see also Fig. 2.D.2 and Fig. 2.E.7). The fact that the average single-particle field acts as an external potential (like e.g. a magnetic field in metallic superconductors) is one of the reasons of the existence of a critical value  $G_c$  of the pairing strength  $G$  to bind Cooper pairs in nuclei. Spatial quantization in finite systems at large and in nuclei in particular, is intimately connected with the paramount role the surface plays in these systems, (cf. Broglia, R. A. (2002) and references therein). Another consequence of this role is the fact that in nuclei an important fraction (30-50%) of Cooper pair binding is due to the exchange of collective vibrations between the partners of the pair (cf. e.g. Barranco et al. (1999), Brink, D. and Broglia (2005), Saperstein and Baldo (2013), Avdeenkov and Kamerdzhiev (2013), Lombardo et al. (2013), and references therein; cf. also Bohr, A. and Motelson (1975), p. 432), the rest being associated with the bare  $NN$ -interaction in the  $^1S_0$  channel (cf. Fig. 2.F.1) plus possible  $3N$  corrections (cf. e.g. Lesinski et al. (2012), Pankratov et al. (2011), Hergert and Roth (2009)).

The study of light exotic nuclei lying along the neutron drip line have revealed a novel aspect of the interplay between shell effects and induced pairing interaction. It has been found that there are situations in which spatial quantization screens, essentially completely, the bare nucleon-nucleon interaction. This happens in the case in which the nuclear valence orbitals are  $s, p$ -states at threshold

$$P^\dagger = \sum_{\nu>0} a_\nu^\dagger a_\nu^\dagger$$

$$x = \frac{2G\Omega}{D} = GN(0)$$

$x > 1$ $\alpha_0 = \langle P^\dagger \rangle = \frac{\Delta}{G} \approx 7$	$x < 1$ $\alpha_{dyn} = \frac{\langle PP^\dagger \rangle^{1/2} + \langle P^\dagger P \rangle^{1/2}}{2}$ $\approx \frac{1}{2} \left( \frac{E_{corr}(A+2)}{G} + \frac{E_{corr}(A-2)}{G} \right) \approx 10$ $\frac{\alpha_0}{\alpha_{dyn}} \approx 0.7$
--	---

$$\frac{\beta_2}{(\beta_2)_{dyn}} \approx 3 - 6$$

Figure 2.E.7: Relative importance of dynamic and static pairing distortion ( $\alpha_{dyn}$  and  $\alpha_0$  respectively) associated with closed shell and open shell nuclei, calculated in terms of a two level model, as compared with similar quantities for the case of quadrupole surface degrees of freedom ( $\beta_2$ -values). The parameter  $x'$  (product of the effective pairing strength  $G' = Z_\omega^2(v_p^{bare} + v_p^{ind})$  and of the effective density of levels at the Fermi energy  $N'(0) = 2\omega/D' = 2\omega/Z_\omega D = Z_\omega^{-1}N(0)$ ), measures the relative importance of the single-particle gap  $D' = Z_\omega D$  and of the pair correlation  $G'\Omega$  (cf. Brink, D. and Broglia (2005) App. H, Sect. H.4).

(pairing anti–halo effect; Bennaceur, K. et al. (2000) , Hamamoto and Mottelson (2003), Hamamoto, I. and Mottelson (2004)). An example of situations of this type is provided by  $N = 6$  (parity inversion; cf. Chapter 4 Section 4.2.2) isotones. In particular, by  $^{11}\text{Li}$ , in which case the strongly renormalized  $s_{1/2}$  and  $p_{1/2}$  valence orbitals are a virtual and a resonant state lying at  $\approx 0.2$  and  $0.5$  MeV in the continuum, respectively. Let us elaborate on this point. The binding provided by a contact pairing interaction  $V_\delta(|\mathbf{r} - \mathbf{r}'|)$  ( $\delta$ –force) to a pair of fermions moving in time–reversal states is (cf. e.g. Eq. (2.12) Brink, D. and Broglia (2005)), is given by the matrix element,

$$M_j = \langle j^2(0)|V_\delta|j^2(0)\rangle = -\frac{(2j+1)}{2}V_0I(j) \approx \frac{(2j+1)}{2}V_0\frac{3}{R^3}.$$

Of notice that  $G = V_0I(j)$  (cf. the expression of  $H_P$  Section 1.D.2). The ratio of the above matrix element for the halo nucleus  $^{11}\text{Li}$  and for an hypothetical normal nucleus of mass  $A = 11$  is

$$r = \frac{(M_j)_{\text{halo}}}{(M_j)_{\text{core}}} = \frac{2}{(2j+1)}\left(\frac{R_0}{R}\right)^3,$$

The quantities  $R_0 = 1.2A^{1/3}\text{fm} = 2.7\text{fm}$  ( $A = 11$ ), and  $R = \sqrt{\frac{5}{3}}\langle r^2 \rangle_{^{11}\text{Li}}^{1/2} = \sqrt{\frac{5}{3}}(3.55 \pm 0.1)\text{ fm} = (4.6 \pm 0.13)\text{ fm}$  are the radius of a stable nucleus of mass  $A = 11$  (systematics), and the measured radius of  $^{11}\text{Li}$ , respectively. The quantity  $j$  is the angular momentum representative for a nucleus of mass  $A = 11$  ( $j \sim k_F R_0 \approx 3 - 4$ ). One thus obtains  $r = 0.048$ . Consequently, the bare  $NN$ –nucleon pairing interaction is expected to become strongly screened, the resulting effective  $G$ –value

$$G' = G \times r = 0.048 \times 25\text{MeV}/A \approx 1\text{MeV}/A \approx 0.1 \quad (2.\text{F}.1)$$

MeV becoming subcritical and thus unable to bind the halo Cooper pair ( $2\epsilon_{s_{1/2}} = 0.4$  MeV) to the  $^9\text{Li}$  core.

Further insight into this question can be shed making use of the multipole expansion of a general interaction

$$v(|\mathbf{r}_1 - \mathbf{r}_2|) = \sum_{\lambda} V_{\lambda}(r_1, r_2)P_{\lambda}(\cos \theta_{12}).$$

Because the function  $P_{\lambda}$  drops from its maximum at  $\theta_{12} = 0$  in an angular distance  $1/\lambda$ , particles 1 and 2 interact through the component  $\lambda$  of the force, only if  $r_{12} = |\mathbf{r}_1 - \mathbf{r}_2| < R/\lambda$ , where  $R$  is the mean value of the radii  $\mathbf{r}_1$  and  $\mathbf{r}_2$ . Thus, as  $\lambda$  increases, the effective force range decreases. For a force of range much greater than the nuclear size, only the  $\lambda \approx 0$  (long wavelength) term is important. At the other extreme, a  $\delta$ –function force has coefficients  $V_{\lambda}(r_1, r_2) \left(= \frac{(2\lambda+1)}{4\pi r_1^2} \delta(r_1 - r_2)\right)$  that increase with  $\lambda$ . In the case of  $^{11}\text{Li}(\text{gs})$  we are thus forced to accept the need for a long range, low  $\lambda$  pairing interaction, as responsible for the binding of the dineutron, halo Cooper pair to the  $^9\text{Li}$  core. This is equivalent to saying, an induced pairing interaction arising from the exchange of vibrations with low  $\lambda$ –value.

### 2.F.1 Cooper pair binding: a novel embodiment of the Axel–Brink hypothesis.

In what follows we discuss a novel test of the Axel–Brink hypothesis<sup>4</sup>. Within the  $s, p$  subspace, the most natural low wavelength vibration is the dipole mode. From systematics, the centroid of these vibrations is  $\hbar\omega_{GDR} \approx 100$  MeV/ $R$ ,  $R$  being the nuclear radius (cf. e.g. Bortignon, P.F. et al. (1998) and Bertsch and Broglia (2005)). Thus, in the case of  $^{11}\text{Li}$ , one expects the centroid of the Giant Dipole Resonance carrying  $\approx 100\%$  of the energy weighted sum rule (EWSR) at  $\hbar\omega_{GDR} \approx 100$  MeV/2.7  $\approx 37$  MeV. Now, such a high frequency mode can hardly be expected to give rise to anything, but polarization effects (see within this context Eqs. ??–?? 3E12–3E14). On the other hand, there exists experimental evidence which testifies to the presence of a rather sharp dipole state with centroid at  $\approx 1$  MeV and carrying  $\approx 8\%$  of the EWSR (Zinser, M. et al. (1997), T. Nakamura et al. (2006), Shimoura et al. (1995), Ieki et al. (1993), Sackett et al. (1993)). The existence of this “pigmy resonance” which can be viewed as a simple consequence of the existence of a low-lying particle–hole state associated with the transition  $s_{1/2} \rightarrow p_{1/2}$  testifies, arguably, to the coexistence of two states with rather different radii in the ground state. One, closely connected with the  $^9\text{Li}$  core, ( $\approx 2.5$  fm), the second with the diffuse halo ( $\approx 4.6$  fm), namely displaying a large radial deformation, and thus able to induce a conspicuous inhomogeneous damping to the dipole mode.

Before proceeding, let us estimate the overlap  $O$  between them. Making use of a schematic expression for the single-particle radial wavefunctions

$$\mathcal{R} = \sqrt{3/R_0^3} \Theta(r - R_0), \quad (2.F.2)$$

where

$$\Theta = 1 \quad (r \leq R_0); \quad 0 \quad (r > R_0),$$

leading to,

$$\int_0^\infty dr r^2 \mathcal{R}^2(r) = \frac{3}{R_0^3} \int_0^{R_0} dr^3 / 3 = 1, \quad (2.F.3)$$

one can work out the overlap  $O$  between the two halo neutrons and the core nucleons.

---

<sup>4</sup>The color of an object can be determined in two ways: by illuminating it with white light and see which wavelength it absorbs, or by heating it up and see the same wavelength it emits. In both cases one is talking about dipole vibrations. To describe the de-excitation process of hot nuclei requires the knowledge of the photon interactions with excited states. The common assumption, known as the Axel–Brink hypothesis has been that each excited state of a nucleus carries a giant dipole resonance (GDR) on top of it, and that the properties of such resonances are unaffected by any excitation of the nucleus (Brink (1955), Lynn (1968) pag. 321, Axel (1962); cf. also Bertsch, G. F. and Broglia (1986) and Bortignon, P.F. et al. (1998))

That is,

$$\begin{aligned} O &= |\langle \mathcal{R}_{\text{halo}} | \mathcal{R}_{\text{core}} \rangle|^2 = \left( \sqrt{\frac{3}{R_0^3}} \sqrt{\frac{3}{R^3}} \int_0^\infty dr r^2 \Theta(r - R) \Theta(r - R_0) \right)^2 \\ &= \left( \sqrt{\frac{3}{R_0^3}} \sqrt{\frac{3}{R^3}} \int_0^{R_0} dr^3 / 3 \right)^2 = (R_0/R)^3 = 0.16, \end{aligned} \quad (2.F.4)$$

where use has been made of  $\Theta(r - R)\Theta(r - R_0) = \Theta(r - R_0)$ ,  $R_0 = 1.2A^{1/3}\text{fm} = 2.5\text{fm}(A = 9)$  and  $R = (4.6 \pm 0.13) \text{ fm}$ . Because of the small value of this overlap, one can posit that a *bona fide* dipole pigmy resonance is a GDR based on an exotic, unusually extended state as compared to systematics ( $A \approx (4.6/1.2)^3 \approx 60$ ), i.e. to a system with an effective  $A$  mass number about 5 times that predicted by systematics.

Of notice that, the small values of  $r$  and of  $O$  have essentially the same origin. On the other hand, they have apparently, rather different physical consequences. In fact, the first makes the bare interaction strength  $G$  subcritical, while the second one screens the repulsive symmetry potential  $V_1(\approx +25 \text{ MeV}$ , cf. e.g. Bortignon, P.F. et al. (1998)), that is, the price one has to pay to separate protons from neutrons. This effect allows for a consistent fraction of the dipole Thomas–Reiche–Kuhn sum rule, that is of the  $J^\pi = 1^-$  energy weighted sum rule (EWSR), to come low in energy from the value  $E_{GDR} \approx (80/A^{1/3}) \text{ MeV}$  and, acting as an intermediate boson between the two halo neutrons, glue them to the  ${}^9\text{Li}$  core. Summing up, the halo anti-pairing effect  $G_{\text{screened}} = r \times G \ll G < G_{\text{crit}}$  triggers ( $OV_1 \ll V_1$ ) the virtual presence of a “gas” of dipole (pigmy) bosons which, exchanged between the two halo neutrons (cf. Fig. 2.F.2), overcompensates the reduction of the bare interaction, leading to the binding of the halo Cooper pair to the core (anti-(halo anti-pairing effect)). It can thus be stated that the halo of  ${}^{11}\text{Li}$  and the pigmy resonance built on top of it constitute a pair of symbiotic states (see also Chapter 6, in particular Fig. 6.1.4).

Let us further elaborate on these issues. Making use of the relation  $\langle r^2 \rangle^{1/2} \approx (3/5)^{1/2} R$  between mean square radius and radius, one may write

$$\langle r^2 \rangle_{{}^{11}\text{Li}} \approx \frac{3}{5} R_{\text{eff}}^2({}^{11}\text{Li}).$$

with

$$R_{\text{eff}}^2({}^{11}\text{Li}) = \left( \frac{9}{11} R_0^2({}^9\text{Li}) + \frac{2}{11} \left( \frac{\xi}{2} \right)^2 \right),$$

where

$$R_0({}^9\text{Li}) = 2.5\text{fm},$$

is the  ${}^9\text{Li}$  radius ( $R_0 = r_0 A^{1/3}$ ,  $r_0 = 1.2\text{fm}$ ), while  $\xi$  is the correlation length of the Cooper pair neutron halo. An estimate of this quantity is provided by the relation

$$\xi = \frac{\hbar v_F}{2E_{\text{corr}}} \approx 20 \text{ fm},$$

## 2.F. HALO PAIR ADDITION MODE AND PIGMY: A NEW SYMBIOTIC ELEMENTARY MODE OF NUCLEAR

in keeping with the fact that in  $^{11}\text{Li}$ ,  $(v_F/c) \approx 0.1$  and  $E_{corr} \approx 0.5$  MeV. Consequently,

$$R_{eff}(^{11}\text{Li}) \approx 4.83 \text{ fm} \quad (2.F.5)$$

and  $\langle r^2 \rangle_{^{11}\text{Li}}^{1/2} \approx 3.74 \text{ fm}$ , in overall agreement with the experimental value  $\langle r^2 \rangle_{^{11}\text{Li}}^{1/2} = 3.55 \pm 0.1 \text{ fm}$  (Kobayashi, T. et al. (1989); thus  $R(^{11}\text{Li})_{exp} = \sqrt{5/3 \langle r^2 \rangle_{^{11}\text{Li}}} = 4.58 \pm 0.13 \text{ fm}$ ).

We now proceed to the calculation of the centroid of the dipole pigmy resonance of  $^{11}\text{Li}$  in the RPA making use of the separable interaction

$$H_D = -\kappa_1 \vec{D} \cdot \vec{D} \quad (2.F.6)$$

where  $\vec{D} = \vec{r}$  and

$$\kappa_1 = \frac{-5V_1}{AR^2}. \quad (2.F.7)$$

The resulting dispersion relation is (cf. (3.30) p.55 of Bortignon, P.F. et al. (1998))

$$W(E) = \sum_{k,i} \frac{2(\epsilon_k - \epsilon_i)|\langle \tilde{i}|F|k \rangle|^2}{(\epsilon_k - \epsilon_i)^2 - E^2}. \quad (2.F.8)$$

Making use of this relation and of the fact that  $\epsilon_{\nu_k} - \epsilon_{\nu_i} = \epsilon_{p_{1/2}} - \epsilon_{s_{1/2}} \approx 0.3 \text{ MeV}$  (see Fig. 2.F.3; see also p.264 Brink, D. and Broglia (2005)), and that the EWSR associated with the  $^{11}\text{Li}$  pigmy resonance is  $\approx 8\%$  of the total Thomas–Reiche–Kuhn sum rule

$$\sum_n |\langle 0|F|n \rangle|^2 (E_n - E_0) = \frac{\hbar^2}{2M} \int d\mathbf{r} |\vec{\nabla} F|^2 \rho(r), \quad (2.F.9)$$

which, for  $F = r$  has the value  $\hbar^2 A / 2M$  (cf. Bertsch and Broglia (2005) pag. 53) one can write,

$$2 \times 0.08 \times \frac{\hbar^2 A}{2M} = \frac{1}{\kappa_1} [(0.3 \text{ MeV})^2 - (\hbar\omega_{pigmy})^2],$$

and thus

$$(\hbar\omega_{pigmy})^2 = (0.3 \text{ MeV})^2 - 2 \times 0.08 \times \frac{\hbar^2 A}{2M} \kappa_1,$$

where (see Bortignon, P.F. et al. (1998))

$$\kappa_1 = -\frac{5V_1}{A(\xi/2)^2} \left( \frac{2}{11} \right) = -\frac{125 \text{ MeV}}{A 100 \text{ fm}^2} \left( \frac{2}{11} \right) \approx \kappa_1^0 \times 0.045 = -\frac{2.5}{A^2} \text{ fm}^{-2} \text{ MeV},$$

the ratio in parenthesis reflecting the fact that only 2 out of 11 nucleons, slosh back and forth in an extended configuration with little overlap with the other nucleons, while

$$\kappa_1^0 = -\frac{5V_1}{AR_{eff}^2(^{11}\text{Li})} \approx 0.49 \text{ MeV fm}^{-2} \quad (2.F.10)$$

is the standard self consistent dipole strength (cf. Bohr, A. and Mottelson (1975)). One then obtains,

$$-2 \times 0.08 \frac{\hbar^2 A}{2M} \kappa_1 = 2 \times 0.08 \times 20 \text{ MeV fm}^2 \times A \times \frac{2.5}{A^2} \text{ fm}^{-2} \text{ MeV} \approx 0.73 \text{ MeV}^2 \approx (0.85 \text{ MeV})^2.$$

Consequently

$$\hbar\omega_{pigmy} = \sqrt{(0.3)^2 + (0.85)^2} \text{ MeV} \approx 1.0 \text{ MeV},$$

in overall agreement with the experimental findings (Zinsler, M. et al., 1997). It is of notice that the centroid of the pigmy resonance calculated in the RPA with the help of a separable dipole interaction is  $\approx (0.6 \text{ MeV} + 1.6 \text{ MeV})/2 \approx 1.0 \text{ MeV}$  (Barranco, F. et al. (2001); see also Fig. 11.3(a) p.269, Brink, D. and Broglia (2005)).

Let us now estimate the binding energy which the exchange of the pigmy resonance between two neutron of the Cooper pair halo of  $^{11}\text{Li}$  can provide. The associated particle-vibration coupling is  $\Lambda = (\partial W(E)/\partial E|_{\hbar\omega_{pigmy}})^{-1/2}$ , (cf. e.g. Brink, D. and Broglia (2005) Eq. (8.42) p.189; note the use in what follows of a dimensionless dipole single-particle field  $F' = F/R_{eff}(^{11}\text{Li})$ ). This is in keeping with the fact that one wants to obtain a quantity with energy dimensions ( $[\Lambda] = \text{MeV}$ ), and that  $\kappa_1$  has been introduced through the Hamiltonian  $H_D$  with the self consistent value normalized in terms of  $R_{eff}^2(^{11}\text{Li})$ . One then obtains

$$\begin{aligned} \Lambda^2 &= \left\{ 2\hbar\omega_{pigmy} \frac{2 \times 0.08(\frac{\hbar^2 A}{2M})/R_{eff}^2(^{11}\text{Li})}{[(\epsilon_{p_{1/2}} - \epsilon_{s_{1/2}})^2 - (\hbar\omega_{pigmy})^2]^2} \right\}^{-1} \\ &= \left\{ 2 \text{ MeV} \frac{0.16(\hbar^2 A/2M)(1/4.83^2 \text{ fm}^2)}{[(0.3)^2 - (1 \text{ MeV})^2]^2 \text{ MeV}^4} \right\}^{-1} \\ &= \left( \frac{3 \text{ MeV}^2}{(0.91)^2 \text{ MeV}^4} \right)^{-1} \\ &= \left( \frac{1}{1.7} \right)^2 \text{ MeV}^2 \approx 0.35 \text{ MeV}^2, \end{aligned}$$

leading to  $\Lambda \approx 0.6 \text{ MeV}$ . The value of the induced interaction matrix elements is then given by,

$$M_{ind} = \frac{2\Lambda^2}{DEN} = -\frac{2\Lambda^2}{\hbar\omega_{pigmy}} \approx -0.7 \text{ MeV}, \quad (2.F.11)$$

the factor of two resulting from the two time ordering contributions (see Fig. 2.F.2). The resulting correlation energy is thus  $E_{corr} = |2\epsilon_{s_{1/2}} - G' + M_{ind}| = |0.4 - 0.1 - 0.7| \approx 0.4 \text{ MeV}$ , in overall agreement with the experimental (C. Bachelet et al. (2008), M. Smith et al. (2008)) findings (0.380 MeV). Of notice that in this estimate the (subcritical) effect of the screened bare pairing interaction has also been used (see Eq. (2.F.1)).

## 2.F. HALO PAIR ADDITION MODE AND PIGMY: A NEW SYMBIOTIC ELEMENTARY MODE OF NUCLEAR

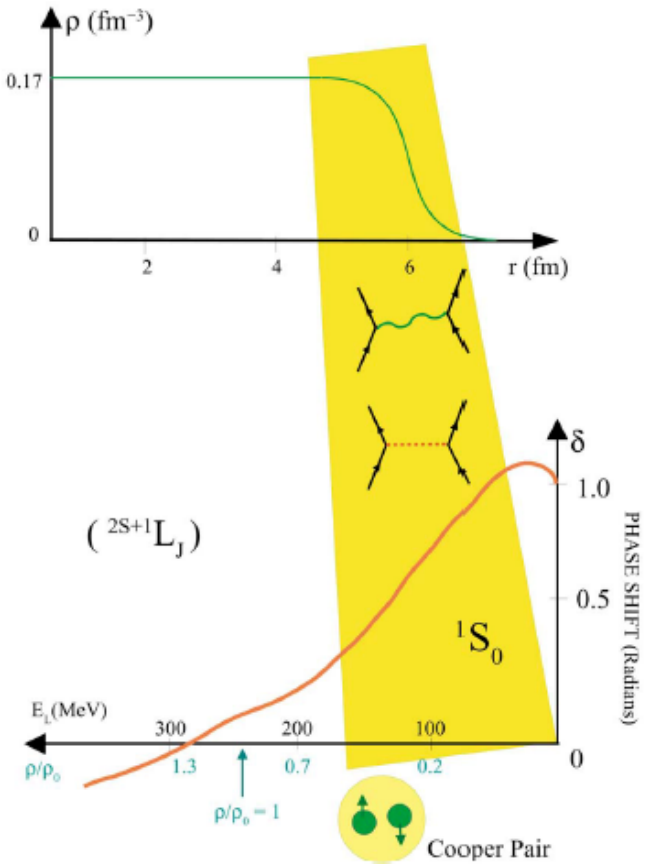


Figure 2.F.1: (top) Nuclear density  $\rho$  in units of  $\text{fm}^{-3}$ , plotted as a function of the distance  $r$  (in units of fm) from the centre of the nucleus (after Bohr and Mottelson (1969)). Saturation density correspond to  $\approx 0.17 \text{ fm}^{-3}$ , equivalent to  $2.8 \times 10^{14} \text{ g/cm}^3$ . Because of the short range of the nuclear force, the strong force, the nuclear density changes from 90% of saturation density to 10% within 0.65 fm, i.e. within the nuclear diffusivity. (bottom) Phase shift parameter associated with the elastic scattering of two nucleons moving in states of time reversal, so called  $^1S_0$  phase shift, in keeping with the fact that the system is in a singlet state of spin zero. The solution of the Schrödinger equation describing the elastic scattering of a nucleon from a scattering centre (in this case another nucleon) is, at large distances from the scattering centre a superposition of the incoming wave and of the outgoing, scattering wave. The interaction of the incoming particle with the target particle changes only the amplitude of the outgoing wave. This amplitude can be written in terms of a real phase shift or scattering phase  $\delta$ . Positive values of  $\delta$  implies an attractive interaction, negative a repulsive one. For low relative velocities (kinetic energies  $E_L$ ), i.e. around the nuclear surface where the density is low, the  $^1S_0$  phase shift arizing from the exchange of mesons (i.g. pions, represented by an horizontal dotted line) between nucleons (represented by upward pointing arrowed lines) is attractive. This mechanism provides about half of the glue to nucleons moving in time reversal states to form Cooper pairs. These pairs behaves like boson and eventually condense in a single quantal state leading to nuclear superfluidity. Cooper pair formation is further assisted by the exchange of collective surface vibrations (wavy curve in the scattering process) between the members of the pair (after Broglia, R. A. (2002)).

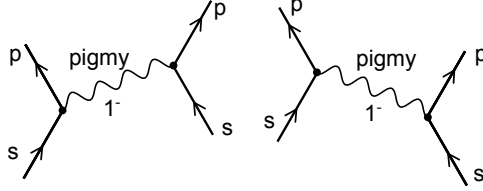


Figure 2.F.2: Diagrammatic representation of the exchange of a collective  $1^-$  pigmy resonance between pairs of nucleons moving in the time-reversal configurations  $s_{1/2}^2(0)$  and  $p_{1/2}^2(0)$ . It is of notice that both these configurations can act as initial states the figure showing only one of the two possibilities. Consequently, the energy denominator to be used in the simple estimate (2.F.11) is the average value  $DEN = (DEN_1 + DEN_2)/2 = -\hbar\omega_{pigmy}$  where  $DEN_1 = \Delta\epsilon - \hbar\omega_{pigmy}$  and  $DEN_2 = -\Delta\epsilon - \hbar\omega_{pigmy}$ , while  $\Delta\epsilon = \epsilon_{s_{1/2}} - \epsilon_{p_{1/2}}$ .

This schematic model has been implemented with microscopic detail (cf. Barancho, F. et al. (2001)) within the framework of a field theoretical description of the interweaving of collective vibrations and single-particle motion (Nuclear Field Theory (NFT); cf. Bortignon, P. F. et al. (1977) and references therein), and is discussed in more detail within the context of single-particle (Chapter 4) and two-particle (Chapter 5) transfer processes. Here we provide a summary of the theoretical findings. In Fig. 2.F.3 (I), the single-particle neutron resonances in  $^{10}\text{Li}$  are given. The position of the levels  $s_{1/2}$  and  $p_{1/2}$  determined making use of mean-field theory is shown (hatched area and thin horizontal line, respectively). The coupling of a single-neutron (upward pointing arrowed line) to a vibration (wavy line) calculated making use of NFT Feynman diagrams (schematically depicted also in terms of either solid dots (neutron) or open circles (neutron hole) moving in a single-particle level around or in the  $^9\text{Li}$  core (hatched area)), leads to conspicuous shifts in the energy centroid of the  $s_{1/2}$  and  $p_{1/2}$  resonances (shown by thick horizontal lines) and eventually to an inversion in their sequence. In Fig. 2.F.3 (II) the processes binding the halo neutron system  $^{11}\text{Li}$  are displayed. Starting with the clothed mean field picture in which two neutrons (solid dots) move in time-reversal states around the core  $^9\text{Li}$  (hatched area) in the  $s_{1/2}$  virtual state leading to an unbound  $s_{1/2}^2(0)$  state where the two neutrons are coupled to angular momentum zero. The associated spatial structure of the uncorrelated pair is shown in **a**). The exchange of vibrations between the two neutrons displayed in the upper part of the figure leads to a density-dependent interaction which, added to the nucleon-nucleon bare interaction (see boxed inset) which, as can be seen from the figure, is subcritical, correlates the two-neutron system leading to a bound state  $|\tilde{0}\rangle$  whose wavefunction is displayed in **b**), together with the spatial structure of the Cooper pair. It is of notice that a large fraction of the induced interaction arises from the exchange of the pigmy resonance (see Fig. 2.F.2) between the two halo neutrons. Within this scenario one can posit that the  $^{11}\text{Li}$  dipole pigmy resonance can hardly be viewed but in symbiosis with the  $^9\text{Li}$  halo neutron pair addition mode and vice

## 2.F. HALO PAIR ADDITION MODE AND PIGMY: A NEW SYMBIOTIC ELEMENTARY MODE OF NUCLEAR

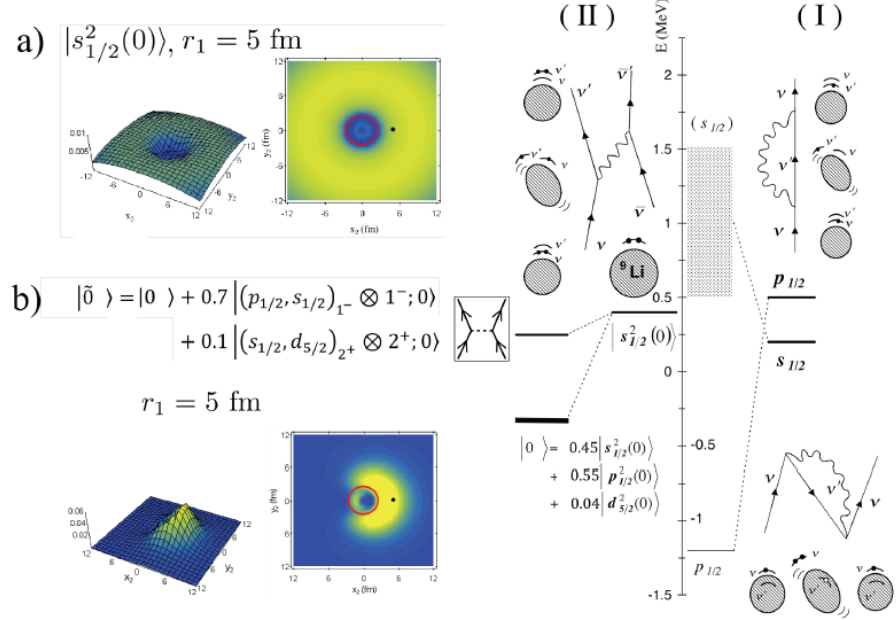


Figure 2.F.3: In (I) and (II) the NFT processes renormalizing the single-particle motion ( ${}^{10}\text{Li}$ ) and leading to the effective interaction, sum of the bare (horizontal dotted lines) and induced (wavy curves) interactions which bind the two-neutron halo to the core of  ${}^9\text{Li}$  thus leading to the  $|{}^{11}\text{Li}\rangle$  state are displayed. In b) the corresponding wavefunction is shown. In a) and b) are also displayed the spatial structure of the pure  $|s_{1/2}^2(0)\rangle$  configuration and that of the two-neutron halo  $|\tilde{0}\rangle$ . The modulus squared wave function  $|\Psi_0(\mathbf{r}_1, \mathbf{r}_2)|^2 = |\langle \mathbf{r}_1, \mathbf{r}_1 | 0^+ \rangle|^2$  describing the motion of the two halo neutrons around the  ${}^9\text{Li}$  core is shown as a function of the cartesian coordinates of particle 2, for fixed values of the position of particle 1 ( $r_1 = 5$  fm) represented by a solid dot, while the core  ${}^9\text{Li}$  is shown as a red circle. The numbers appearing on the  $z$ -axis of the three-dimensional plots displayed on the left side of the figure are in units of  $\text{fm}^{-2}$ . After Barranco, F. et al. (2001).

versa. For details see Chapter 6 as well as Barranco, F. et al. (2001).

Let us conclude this Appendix by stating that the detailed consequences of the diagonalization of self-energy processes and of the bare and induced interactions tantamount to the diagonalization of the many-body Hamiltonian, provides in the case of  $^{10}\text{Li}$  an example of minimal mean field description (cf. apendice D de la introducción and App. 4.A) and in the case of  $^{11}\text{Li}$  an example of the fact that pairs of dressed single-particle states lead to abnormal density (induced pairing interaction), also in the case of closed shell systems, due to the strong ZPF associated with pairing vibrations (Fig. 2.F.3; cf. also discussion around eq. (2.2.1)). In keeping with the fact that  $^9\text{Li}$  is a normal, bound nucleus, while  $^{10}\text{Li}$  is not bound testifies to the fact that the binding of two neutrons to the  $^9\text{Li}$  core leading to  $^{11}\text{Li}$  ground state ( $S_{2n} \approx 380$  keV), is a pairing phenomenon.

## Appendix 2.G Nuclear van der Waals Cooper pair

The atomic van der Waals (dispersive; retarded) interaction acts, like gravitation, between all atoms and molecules, also non-polar, can be written for two systems placed at a distance  $R$  as,

$$\Delta E = -\frac{6 \times e^2 \times a_0^5}{R^6} = -\frac{6 \times e^2}{(R/a_0)^6} \frac{1}{a_0}, \quad (2.G.1)$$

where  $a_0$  is the Bohr radius. A possible nuclear parallel can be established making the following correspondences

$$e^2 \rightarrow \Lambda R_0(^{11}\text{Li}) = 0.6 \text{ MeV} \times 2.7 \text{ fm}; \quad a_0 \rightarrow d = 4 \text{ fm}; \quad R \rightarrow R_{eff}(^{11}\text{Li}) = 4.83 \text{ fm}.$$

That is,

$$\begin{aligned} \Delta E &= -\frac{6 \times \Lambda \times R_0}{R^6} = -\frac{6 \times e^2}{(R_{eff}(^{11}\text{Li})/d)^6} \frac{1}{d} = \frac{6 \times 0.6 \text{ MeV} \times 2.7 \text{ fm}}{(4.83/4)^6} \frac{1}{4 \text{ fm}} \\ &= -\frac{9.72 \text{ MeV}}{12.4} \approx -0.8 \text{ MeV} \rightarrow M_{ind}. \end{aligned}$$

Thus,

$$E_{corr} = |2E_{s_{1/2}} - G' + \Delta E| = |0.4 \text{ MeV} - 0.1 \text{ MeV} - 0.8 \text{ MeV}| \approx 0.5, \text{ MeV} \quad ((S_{2n})_{exp} \approx 0.38 \text{ MeV}).$$

## Appendix 2.H Hindsight

Let us make use of the experimental (empirical),

$$\begin{aligned} \epsilon_{s_{1/2}} &= 0.2 \text{ MeV}, \\ \epsilon_{p_{1/2}} &= 0.5 \text{ MeV}, \\ V_1 &= 25 \text{ MeV}, \end{aligned}$$

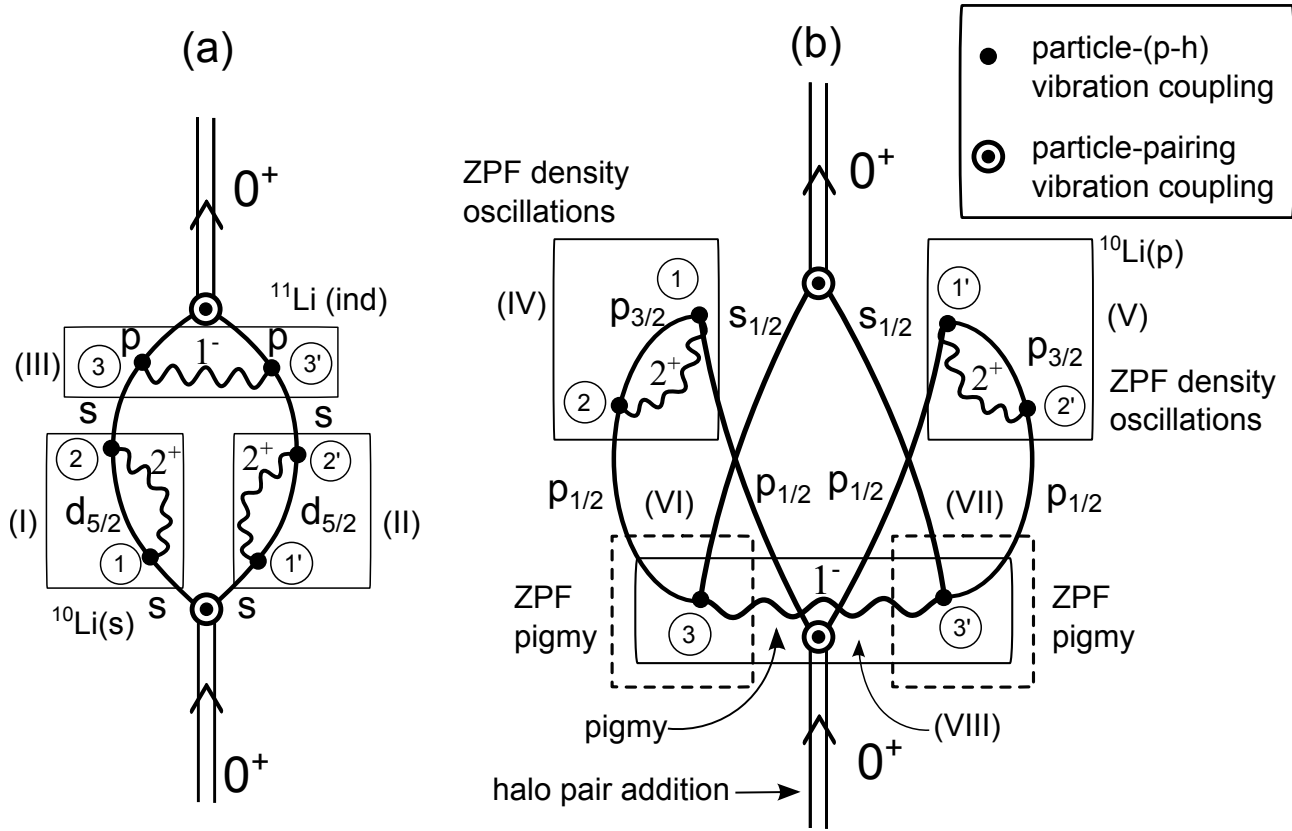


Figure 2.G.1: NFT Feynman diagrams describing the binding of the halo Cooper pair through pigmy. That is, producing the symbiotic mode involving the pair addition mode and the GDPR. The single-particle states  $s_{1/2}$  and  $p_{1/2}$  are labeled in (a)  $s$  and  $p$  for simplicity. The different particle-vibration coupling vertices (either with the quadrupole ( $2^+$ ) or with the pigmy ( $1^-$ ) modes drawn as solid wavy lines) are denoted by a solid dot, and numbered in increasing sequence so as to show that diagram (b) emerges from (a) through time ordering. The motion of the neutrons are drawn in terms of continuous solid curves. In keeping with the fact that the occupation of the single-particle states is neither 1 nor 0 (cf. Eqs. 6.1.1–6.1.3), these states are treated as quasiparticle states. Thus no arrow is drawn on them. Diagram (a) emphasizes the self-energy renormalization of the state  $s_{1/2}$  lying in the continuum and which is brought down by its clothing with the quadrupole mode to a virtual ( $\epsilon_{s_{1/2}} = 0.2$  MeV) state (see (I) and (II)), while (III) contributes to the induced pairing interaction through pigmy (see also Fig. 2.F.2). Diagram (b) provides in (IV) and (V) with Pauli corrections which push the bound state  $p_{1/2}$  into a resonant state in the continuum ( $\epsilon_{p_{1/2}} = 0.5$  MeV). In other words, processes (I), (II), (III), (IV) and (V) are at the basis of parity inversion, and of the appearal of the new magic number  $N = 6$ . Processes (VI) and (VII) are associated with the pigmy ZPF, while (VIII) contributes to the induced pairing interaction through pigmy (van der Waals).

and theoretical

$$\begin{aligned}
 R_0(^{11}\text{Li}) &= 1.2(11)^{1/3} \text{ fm} = 2.7 \text{ fm} \\
 \xi &= 20 \text{ fm} \\
 R_{eff}(^{11}\text{Li}) &= 4.83 \text{ MeV} \\
 G &= \frac{25}{A} \text{ MeV} = 2.3 \text{ fm} \\
 \kappa_1^0 &= -\frac{5V_1}{AR_{eff}(^{11}\text{Li})} \approx -0.49 \text{ MeV fm}^{-2} \\
 \kappa_1 &= -\frac{5V_1}{A(\xi/2)^2} = -0.022 \text{ MeV fm}^{-2}
 \end{aligned}$$

inputs.

One can then calculate the ratio

$$r = \frac{2}{(2j+1)} \frac{R_0}{R_{eff}}^3 \approx 0.042,$$

where use was made of  $(2j+1) \approx (2k_F R_0 + 1) \approx 8.34$ . Thus, the screened bare pairing interaction is,

$$(G)_{scr} = rG = 0.042 \times \frac{25}{A} \text{ MeV} = \frac{1 \text{ MeV}}{A} \approx 0.1 \text{ MeV}.$$

Similarly

$$\kappa_1 = s\kappa_1^0$$

where the screening factor is

$$s = \frac{R_{eff}^2}{(\xi/2)^2} \frac{2}{11} \approx 0.042.$$

Thus, the screened symmetry potential is,

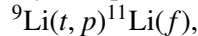
$$(V_1)_{scr} = sV_1 = 0.042 \times 25 \text{ MeV} = 1 \text{ MeV}.$$

The fact that  $r$  and  $s$  coincide within numerical approximations is in keeping with the fact that both quantities are closely related to the overlap

$$O = \left( \frac{R_0}{R_{eff}} \right)^3 = \left( \frac{2.7 \text{ fm}}{4.83 \text{ fm}} \right)^3 = 0.17,$$

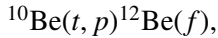
quantity which has a double hit effect concerning the mechanism which is at the basis of much of the nuclear structure of exotic nuclei at threshold: 1) it makes subcritical the screened bare  $NN$ -pairing interaction  $(G)_{scr} = rG < G_c$  ( $(G)_{scr} = 1 \text{ MeV}/A$ ); 2) it screens the symmetry potential drastically, reducing the price one

has to pay to separate protons from delocalized neutrons, thus allowing a consistent chunk ( $\approx 8\%$ ) of the TRK sum rule to essentially becoming degenerate with the ground state ( $(V_1)_{scr} = 1$  MeV), thus allowing for the first nuclear example of a Van der Waals Cooper pair and a novel mechanism to break dynamically gauge invariance. Dipole–dipole fluctuating fields associated with the exchange of the pigmy resonance between the halo neutrons of  $^{11}\text{Li}$ . As a result, a new, composite mode of nuclear excitation join the ranks of the previously known: halo pair addition mode carrying on top of it, a low-lying collective pigmy resonance. This symbiotic mode can be studies through two-particle transfer reactions, eventually in coincidence with  $\gamma$ -decay. In particular, making use of the reactions,



$|f\rangle$ ; ground state ( $L = 0$ ), pigmy ( $L = 1$ ),

and



$|f\rangle$ ; first excited  $0^+$  state ( $E_x = 2.24$  MeV) ( $L = 0$ );  
pigmy on top of it ( $L = 1$ , arguably within  $\approx 1$  MeV).

## Bibliography

- Abrahams, E. and J. W. F. Woo. *Phys. Lett. A*, 27:117, 1968.
- P. W. Anderson. *Basic notions of condensed matter physics*. Benjamin, Menlo Park, California, 1984.
- A. Avdeenkov and S. Kamerdzhiev. Phonon Coupling and the Single-Particle Characteristics of Sn Isotopes. In R. A. Broglia and V. Zelevinsky, editors, *50 Years of Nuclear BCS*, page 274. World Scientific, Singapore, 2013.
- P. Axel. Electric Dipole Ground-State Transition Width Strength Function and 7-Mev Photon Interactions. *Phys. Rev.*, 126:671, 1962.
- Barbieri, C. Role of Long-Range Correlations in the quenching of spectroscopic factors. *Phys. Rev. Lett.*, 103:202502, 2009.
- J. Bardeen, L. N. Cooper, and J. R. Schrieffer. Microscopic theory of superconductivity. *Physical Review*, 106:162, 1957a.
- J. Bardeen, L. N. Cooper, and J. R. Schrieffer. Theory of superconductivity. *Physical Review*, 108:1175, 1957b.
- F. Barranco, R. A. Broglia, G. Gori, E. Vigezzi, P. F. Bortignon, and J. Terasaki. Surface vibrations and the pairing interaction in nuclei. *Phys. Rev. Lett.*, 83: 2147, 1999.
- Barranco, F., P. F. Bortignon, R. A. Broglia, G. Colò, and E. Vigezzi. The halo of the exotic nucleus  $^{11}\text{Li}$ : a single Cooper pair. *Europ. Phys. J. A*, 11:385, 2001.
- B. F. Bayman. Finite-range calculation of the two-neutron transfer reaction. *Nuclear Physics A*, 168:1, 1971.
- B. F. Bayman and J. Chen. One-step and two-step contributions to two-nucleon transfer reactions. *Phys. Rev. C*, 26:1509, 1982.
- B. F. Bayman and A. Kallio. Relative-angular-momentum-zero part of two-nucleon wave functions. *Phys. Rev.*, 156:1121, 1967.
- S. T. Belyaev. *Kgl. Danske Videnskab. Selskab, Mat.-fys. Medd.*, 31:No11, 1959.
- Belyaev, S. T. Pair correlations in nuclei: Copenhagen 1958. In R. A. Broglia and V. Zelevinski, editors, *50 Years of Nuclear BCS*, page 3. World Scientific, Singapore, 2013.
- Bennaceur, K., J. Dobaczewski, and M. Ploszajczak. Pairing anti-halo effect. *Physics Letters B*, 496:154, 2000.
- G. Bertsch and R. Broglia. *Oscillations in Finite Quantum Systems*. Cambridge University Press, Cambridge, 2005.

- Bertsch, G. F. and R. A. Broglia. Giant resonances in hot nuclei. *Physics Today*, 39 (8):44, 1986.
- D. R. Bès and R. A. Broglia. In A. Bohr and R. Broglia, editors, *International School of Physics “Enrico Fermi” Course LXIX, Elementary Modes of Excitation in Nuclei*, page 55, Amsterdam, 1977. North Holland.
- Bès, D. R. and J. Kurchan. *The treatment of Collective Coordinates in Many-Body Systems*. World Scientific, Singapore, 1990.
- Bès, D. R., R. A. Broglia, J. Dudek, W. Nazarewicz, and Z. Szymański. Fluctuation effects in the pairing field of rapidly rotating nuclei. *Annals of Physics*, 182:237, 1988.
- Bès, D. R. and R. A. Broglia. Pairing vibrations. *Nucl. Phys.*, 80:289, 1966.
- J. H. Bilgram. Dynamics at the solid-liquid transition: Experiments at the freezing point. *Physics Reports*, 153:1, 1987.
- Bjerregaard, J. H., O. Hansen, Nathan, and S. Hinds. States of  $^{208}\text{Pb}$  from double triton stripping. *Nucl. Phys.*, 89:337, 1966.
- A. Bohr. In *Comptes Rendus du Congrès International de Physique Nucléaire*, volume 1, page 487. Centre National de la Recherche Scientifique, 1964.
- A. Bohr and B. R. Mottelson. *Nuclear Structure, Vol.I*. Benjamin, New York, 1969.
- Bohr, A. and B. R. Mottelson. *Nuclear Structure, Vol.II*. Benjamin, New York, 1975.
- Bortignon, P. F., R. A. Broglia, D. R. Bès, and R. Liotta. Nuclear field theory. *Physics Reports*, 30:305, 1977.
- Bortignon, P. F., R. A. Broglia, and Bès. On the convergence of nuclear field theory perturbation expansion for strongly anharmonic systems. *Phys. Lett. B*, 76:153, 1978.
- Bortignon, P. F., A. Bracco, and R. Broglia. *Giant Resonances*. Harwood Academic Publishers, Amsterdam, 1998.
- D. M. Brink. *PhD Thesis*. Oxford University, 1955.
- Brink, D. and R. A. Broglia. *Nuclear Superfluidity*. Cambridge University Press, Cambridge, 2005.
- R. Broglia and A. Winther. *Heavy Ion Reactions*. Westview Press, Boulder, CO., 2004.
- R. Broglia, J. Terasaki, and N. Giovanardi. The Anderson–Goldstone–Nambu mode in finite and in infinite systems. *Physics Reports*, 335:1, 2000.

- Broglia, R. A. The surfaces of compact systems: from nuclei to stars. *Surface Science*, 500:759, 2002.
- Broglia, R. A., G. Pollaro, and A. Winther. On the absorptive potential in heavy ion scattering. *Nuclear Physics A*, 361:307, 1981.
- Broglia, R. A. and Zelevinsky, V. . In R. A. Broglia and V. Zelevinsky, editors, *50 Years of Nuclear BCS*. World Scientific, Singapore, 2013.
- Broglia, R.A., C. Riedel, and B. Sørensen. Two-nucleon transfer and pairing phase transition. *Nuclear Physics A*, 107:1, 1968.
- Broglia, R.A., O. Hansen, and C. Riedel. Two-neutron transfer reactions and the pairing model. *Advances in Nuclear Physics*, 6:287, 1973. URL [www.mi.infn.it/~vigezzi/BHR/BrogliaHansenRiedel.pdf](http://www.mi.infn.it/~vigezzi/BHR/BrogliaHansenRiedel.pdf).
- Brown, B. A. and W. D. M. Rae. In *NuShell @ MSU*. MSU–NSCL report, 2007.
- C. Bachelet et al. New Binding Energy for the Two-Neutron Halo of  $^{11}\text{Li}$ . *Phys. Rev. Lett.*, 100:182501, 2008.
- Clark, R. M., A. O. Macchiavelli, L. Fortunato, and R. Krücken. Critical-point description of the transition from vibrational to rotational regimes in the pairing phase. *Phys. Rev. Lett.*, 96:032501, 2006.
- J. de Boer. Quantum theory of condensed permanent gases i the law of corresponding states. *Physica*, 14:139, 1948.
- J. de Boer. Chapter i quantum effects and exchange effects on the thermodynamic properties of liquid helium. volume 2 of *Progress in Low Temperature Physics*, page 1. 1957.
- J. de Boer and R. J. Lundbeck. *Physica*, 14:520, 1948.
- P. G. De Gennes. *Les objets fragiles*. Plon, 1994.
- Dickhoff, W. and D. Van Neck. *Many–Body Theory Exposed: Propagator description of quantum mechanics in many–body systems*. World Scientific, Singapore, 2005.
- Dönau, F., D. Almehed, and R. G. Nazmitdinov. Integral representation of the random–phase approximation correlation energy. *Phys. Rev. Lett.*, 83:280, 1999.
- Duguet, T. and G. Hagen. *Ab initio* approach to effective single-particle energies in doubly closed shell nuclei. *Phys. Rev. C*, 85:034330, 2012.
- J. Ebran, E. Khan, T. Niksic, and D. Vretenar. Density Functional Theory studies of cluster states in nuclei. 2014a.

- J.-P. Ebran, E. Khan, T. Nikšić, and D. Vretenar. How atomic nuclei cluster. *Nature*, 487:341, 2012.
- J.-P. Ebran, E. Khan, T. Nikšić, and D. Vretenar. Localization and clustering in the nuclear fermi liquid. *Phys. Rev. C*, 87:044307, 2013.
- J.-P. Ebran, E. Khan, T. Nikšić, and D. Vretenar. Cluster-liquid transition in finite, saturated fermionic systems. *Phys. Rev. C*, 89:031303, 2014b.
- Egido, J. L. Projection methods, variational diagonalization of the pairing hamiltonian and restoration of rotational and gauge invariance. In R. A. Broglia and V. Zelevinski, editors, *50 Years of Nuclear BCS*, page 553. World Scientific, Singapore, 2013.
- Fernández-García, J.P., M. Alvarez, A. Moro, and M. Rodriguez-Gallardo. Simultaneous analysis of elastic scattering and transfer/breakup channels for the  $^6\text{He} + ^{208}\text{Pb}$  reaction at energies near the Coulomb barrier. *Phys.Lett.*, B693:310, 2010.
- Fernández-García, J.P., M. Rodríguez-Gallardo, M. Alvarez, and A. Moro. Long range effects on the optical model of  $^6\text{He}$  around the Coulomb barrier. *Nuclear Physics A*, 840:19, 2010.
- Flynn, E. R., G. J. Igo, and R. A. Broglia. Three-phonon monopole and quadrupole pairing vibrational states in  $^{206}\text{Pb}$ . *Phys. Lett. B*, 41:397, 1972.
- Frauendorf, S. Pairing at high spin. In R. A. Broglia and V. Zelevinski, editors, *50 Years of Nuclear BCS*, page 536. World Scientific, Singapore, 2013.
- Furnstahl, R. J. and A. Schwenk. How should one formulate, extract and interpret 'non-observables' for nuclei? *Journal of Physics G*, 37:064005, 2010.
- Glendenning, N. K. Nuclear Spectroscopy with Two-Nucleon Transfer Reactions. *Phys. Rev.*, 137:B102, 1965.
- Guazzoni, P., M. Jaskola, L. Zetta, A. Covello, A. Gargano, Y. Eisermann, G. Graw, R. Hertenberger, A. Metz, F. Nuoffer, and G. Staudt. Level structure of  $^{120}\text{Sn}$ : High resolution ( $p, t$ ) reaction and shell model description. *Phys. Rev. C*, 60: 054603, 1999.
- Guazzoni, P., L. Zetta, A. Covello, A. Gargano, G. Graw, R. Hertenberger, H.-F. Wirth, and M. Jaskola. High-resolution study of the  $^{116}\text{Sn}$  ( $p, t$ ) reaction and shell model structure of  $^{114}\text{Sn}$ . *Phys. Rev. C*, 69:024619, 2004.
- Guazzoni, P., L. Zetta, A. Covello, A. Gargano, B. F. Bayman, G. Graw, R. Hertenberger, H.-F. Wirth, and M. Jaskola. Spectroscopy of  $^{110}\text{Sn}$  via the high-resolution  $^{112}\text{Sn}(p, t)$   $^{110}\text{Sn}$  reaction. *Phys. Rev. C*, 74:054605, 2006.

- Guazzoni, P., L. Zetta, A. Covello, A. Gargano, B. F. Bayman, T. Faestermann, G. Graw, R. Hertenberger, H.-F. Wirth, and M. Jaskola.  $^{118}\text{Sn}$  levels studied by the  $^{120}\text{Sn}(p, t)$  reaction: High-resolution measurements, shell model, and distorted-wave Born approximation calculations. *Phys. Rev. C*, 78:064608, 2008.
- Guazzoni, P., L. Zetta, A. Covello, A. Gargano, B. F. Bayman, T. Faestermann, G. Graw, R. Hertenberger, H.-F. Wirth, and M. Jaskola. High-resolution measurement of the  $^{118,124}\text{Sn}(p,t)^{116,122}$  reactions: Shell-model and microscopic distorted-wave Born approximation calculations. *Phys. Rev. C*, 83:044614, 2011.
- Guazzoni, P., L. Zetta, A. Covello, A. Gargano, B. F. Bayman, G. Graw, R. Hertenberger, H. F. Wirth, T. Faestermann, and M. Jaskola. High resolution spectroscopy of  $^{112}\text{Sn}$  through the  $^{114}\text{Sn}(p,t)^{112}\text{Sn}$  reaction. *Phys. Rev. C*, 85:054609, 2012.
- I. Hamamoto and B. R. Mottelson. Pair correlation in neutron drip line nuclei. *Phys. Rev. C*, 68:034312, 2003.
- Hamamoto, I. and B. R. Mottelson. Weakly bound  $s_{1/2}$  neutrons in the many-body pair correlation of neutron drip line nuclei. *Phys. Rev. C*, 69:064302, 2004.
- O. Hansen. Experimental establishment of the nuclear pairing phases. In R. A. Broglia and V. Zelevinsky, editors, *50 Years of Nuclear BCS*, page 449. World Scientific, Singapore, 2013.
- Heenen, P. H., V. Hellemans, and R. V. F. Janssens. Pairing correlations at superdeformation. In R. A. Broglia and V. Zelevinski, editors, *50 Years of Nuclear BCS*, page 579. World Scientific, Singapore, 2013.
- H. Hergert and R. Roth. Pairing in the framework of the unitary correlation operator method (UCOM): Hartree-Fock-Bogoliubov calculations. *Phys. Rev. C*, 80: 024312, 2009.
- J. Högaasen-Feldman. A study of some approximations of the pairing force. *Nuclear Physics*, 28:258, 1961.
- K. Ieki, D. Sackett, A. Galonsky, C. A. Bertulani, J. J. Kruse, W. G. Lynch, D. J. Morrissey, N. A. Orr, H. Schulz, B. M. Sherrill, A. Sustich, J. A. Winger, F. Deák, A. Horváth, A. Kiss, Z. Seres, J. J. Kolata, R. E. Warner, and D. L. Humphrey. Coulomb dissociation of  $^{11}\text{Li}$ . *Phys. Rev. Lett.*, 70:730, 1993.
- Jenning, B. Non observability of spectroscopic factors. *arXiv: 1102.3721ve [nucl-th]*, 2011.
- B. D. Josephson. Possible new effects in superconductive tunnelling. *Phys. Lett.*, 1:251, 1962.

- Kobayashi, T., S. Shimoura, I. Tanihata, K. Katori, K. Matsuta, T. Minamisono, K. Sugimoto, W. Mller, D. L. Olson, T. J. M. Symons, and H. Wieman. Electromagnetic dissociation and soft giant dipole resonance of the neutron-dripline nucleus  $^{11}\text{Li}$ . *Physics Letters B*, 232:51, 1989.
- Kramer, G. J., H. P. Blok, and L. Lapikás. A consistence analisys of  $(e, e' p)$  and  $(d, ^3\text{He})$  experiments. *Nucl. Phys. A*, 679:267, 2001.
- T. Lesinski, K. Hebeler, T. Duguet, and A. Schwenk. Chiral three-nucleon forces and pairing in nuclei. *Journal of Physics G: Nuclear and Particle Physics*, 39: 015108, 2012.
- F. A. Lindemann. The calculation of molecular vibration frequancies. *Physik. Z.*, 11:609, 1910.
- U. Lombardo, H. J. Schulze, and W. Zuo. Induced Pairing Interaction in Neutron Star Matter. In R. A. Broglia and V. Zelevinsky, editors, *50 Years of Nuclear BCS*, page 338. World Scientific, Singapore, 2013.
- Löwen, H. Melting, freezing and colloidal suspensions. *Phys. Rep.*, 237:249, 1994.
- J. E. Lynn. *Theory of neutron resonance reactions*. Oxford University Press, Oxford, 1968.
- M. Smith et al. First penning-trap mass measurement of the exotic halo nucleus  $^{11}\text{Li}$ . *Phys. Rev. Lett.*, 101:202501, 2008.
- Machleidt, R., F. Sammarruca, and Y. Song. Nonlocal nature of the nuclear force and its impact on nuclear structure. *Phys. Rev. C*, 53:R1483, 1996.
- Mahaux, C., P. F. Bortignon, R. A. Broglia, and C. H. Dasso. Dynamics of the shell model. *Physics Reports*, 120:1–274, 1985.
- Meissner, U. G. Anthropic considerations in nuclear physics. *arXiv:1409.2959v1[hep-th]*, 2014.
- D. Montanari, L. Corradi, S. Szilner, G. Pollarolo, E. Fioretto, G. Montagnoli, F. Scarlassara, A. M. Stefanini, S. Courtin, A. Goasduff, F. Haas, D. Jelavić Malenica, C. Michelagnoli, T. Mijatović, N. Soić, C. A. Ur, and M. Varga Pajtler. Neutron Pair Transfer in  $^{60}\text{Ni} + ^{116}\text{Sn}$  Far below the Coulomb Barrier. *Phys. Rev. Lett.*, 113:052501, 2014.
- B. Mottelson. Elementary features of nuclear structure. In Niefnecker, Blaizot, Bertsch, Weise, and David, editors, *Trends in Nuclear Physics, 100 years later, Les Houches, Session LXVI*, page 25, Amsterdam, 1998. Elsevier.
- S. G. Nilsson. Binding states of individual nucleons in strongly deformed nuclei. *Mat. Fys. Medd. Dan. Vid. Selk.*, 29, 1955.

- L. Nosanow. On the possible superfluidity of  $^6\text{He}$ ?Its phase diagram and those of  $^6\text{He}$ - $^4\text{He}$  and  $^6\text{He}$ - $^3\text{He}$  mixtures. *Journal of Low Temperature Physics*, 23:605, 1976.
- S. S. Pankratov, M. V. Zverev, M. Baldo, U. Lombardo, and E. E. Saperstein. Semi-microscopic model of pairing in nuclei. *Phys. Rev. C*, 84:014321, 2011.
- G. Pollarolo, R. Broglia, and A. Winther. Calculation of the imaginary part of the heavy ion potential. *Nuclear Physics A*, 406:369, 1983.
- G. Potel, A. Idini, F. Barranco, E. Vigezzi, and R. A. Broglia. Nuclear Field Theory predictions for  $^{11}\text{Li}$  and  $^{12}\text{Be}$ : shedding light on the origin of pairing in nuclei. *Yad. Fiz.*, *in press*: arXiv:1210.5085 [nucl-th], 2014.
- Potel, G., F. Barranco, F. Marini, A. Idini, E. Vigezzi, and R. A. Broglia. Calculation of the Transition from Pairing Vibrational to Pairing Rotational Regimes between Magic Nuclei  $^{100}\text{Sn}$  and  $^{132}\text{Sn}$  via Two-Nucleon Transfer Reactions. *Physical Review Letters*, 107:092501, 2011.
- Potel, G., A. Idini, F. Barranco, E. Vigezzi, and R. A. Broglia. Cooper pair transfer in nuclei. *Rep. Prog. Phys.*, 76:106301, 2013a.
- Potel, G., A. Idini, F. Barranco, E. Vigezzi, and R. A. Broglia. Quantitative study of coherent pairing modes with two-neutron transfer: Sn isotopes. *Phys. Rev. C*, 87:054321, 2013b.
- Rees, M. *Just six numbers*. Basic Books, New York, 2000.
- Ring, P. Berry phase and backbending. In R. A. Broglia and V. Zelevinski, editors, *50 Years of Nuclear BCS*, page 522. World Scientific, Singapore, 2013.
- Ring, P. and P. Schuck. *The Nuclear Many-Body Problem*. Springer, Berlin, 1980.
- Robledo, R. M. and G. F. Bertsch. Pairing in Finite Systems: Beyond the HFB Theory. In R. A. Broglia and V. Zelevinski, editors, *50 Years of Nuclear BCS*, page 89. World Scientific, Singapore, 2013.
- D. Rogovin and M. Scully. Superconductivity and macroscopic quantum phenomena. *Physics Reports*, 25:175, 1976.
- D. Sackett, K. Ieki, A. Galonsky, C. A. Bertulani, H. Esbensen, J. J. Kruse, W. G. Lynch, D. J. Morrissey, N. A. Orr, B. M. Sherrill, H. Schulz, A. Sustich, J. A. Winger, F. Deák, A. Horváth, A. Kiss, Z. Seres, J. J. Kolata, R. E. Warner, and D. L. Humphrey. Electromagnetic excitation of  $^{11}\text{Li}$ . *Phys. Rev. C*, 48:118, 1993.
- E. E. Saperstein and M. Baldo. Microscopic Origin of Pairing. In R. A. Broglia and V. Zelevinsky, editors, *50 Years of Nuclear BCS*, page 263. World Scientific, Singapore, 2013.

- Schiffer, J. P., C. R. Hoffman, B. P. Kay, J. A. Clark, C. M. Deibel, S. J. Freeman, A. M. Howard, A. J. Mitchell, P. D. Parker, D. K. Sharp, and J. S. Thomas. Test of sum rules in nucleon transfer reactions. *Phys. Rev. Lett.*, 108:022501, 2012.
- Schmid, A. A time dependent Ginzburg–Landau equation and its application to the problem of resistivity in the mixed state. *Phys. d. Kond. Materie*, 5:302, 1966.
- Schmid, A. Diamagnetic susceptibility at the transition to the superconducting state. *Phys. Rev.*, 180:527, 1969.
- Schmidt, H. The onset of superconductivity in the time dependent ginzburg-landau theory. *Zeits. Phys.*, 216:336, 1968.
- Schmidt, H. Pairing vibrations in nuclei and solids. In Morinaga H., editor, *Proceedings of the International School of Physics “Enrico Fermi” Course LIII*, page 144, NY, 1972. Academic Press.
- J. Schrieffer. *Superconductivity*. Benjamin, New York, 1964.
- Schrieffer, J. R. Macroscopic quantum phenomena from pairing in superconductors. *Physics Today*, 26 (7):23, 1973.
- Schrödinger, E. *What is life? The physical aspect of the living cell*. Cambridge University Press, 1944.
- Shimizu, Y. R. Pairing fluctuations and gauge symmetry restoration in rotating superfluid nuclei. In R. A. Broglia and V. Zelevinsky, editors, *50 Years of Nuclear BCS*, page 567. World Scientific, Singapore, 2013.
- Shimizu, Y. R. and R. A. Broglia. A comparison of the RPA and number projection approach for calculations of pairing fluctuations in fast rotating nuclei. *Nucl. Phys. A*, 515:38, 1990.
- Shimizu, Y. R., J. D. Garrett, R. A. Broglia, M. Gallardo, and E. Vigezzi. Pairing fluctuations in rapidly rotating nuclei. *Reviews of Modern Physics*, 61:131, 1989.
- Shimizu, Y. R., P. Donati, and R. A. Broglia. Response function technique for calculating the random-phase approximation correlation energy. *Phys. Rev. Lett.*, 85:2260, 2000.
- S. Shimoura, T. Nakamura, M. Ishihara, N. Inabe, T. Kobayashi, T. Kubo, R. Siemssen, I. Tanihata, and Y. Watanabe. Coulomb dissociation reaction and correlations of two halo neutrons in  $^{11}\text{Li}$ . *Physics Letters B*, 348:29, 1995.
- F. H. Stillinger. A topographic view of supercooled liquids and glass formation. *Science*, 237:1935, 1995.
- F. H. Stillinger and D. K. Stillinger. Computational study of transition dynamics in 55-atom clusters. *J. Chem. Phys.*, 93:6013, 1990.

- T. Nakamura et al. Observation of Strong Low-Lying E1 Strength in the Two-Neutron Halo Nucleus  $^{11}\text{Li}$ . *Phys. Rev. Lett.*, 96:252502, 2006.
- Tarpanov, D., J. Dobaczewski, J. Toivanen, and B. G. Carlsson. Spectroscopic properties of nuclear Skyrme energy density functionals. *arXiv:1405.4823v1 [nucl-th]*, 2014.
- Thompson, I.J. Reaction mechanism of pair transfer. In R. A. Broglia and V. Zelevinsky, editors, *50 Years of Nuclear BCS*, page 455. World Scientific, Singapore, 2013.
- N. L. Vaquero, J. L. Egido, and T. R. Rodríguez. Large amplitude pairing fluctuations in atomic nuclei. *arXiv:1311.7573[nucl-th]*, 2013.
- W. von Oertzen and A. Vitturi. Pairing correlations of nucleons and multi-nucleon transfer between heavy nuclei. *Reports on Progress in Physics*, 64:1247, 2001.
- von Oertzen, W. Enhanced two-nucleon transfer due to pairing correlations. In R. A. Broglia and V. Zelevinsky, editors, *50 Years of Nuclear BCS*, page 405. World Scientific, Singapore, 2013.
- Wölfe, P. Sound propagation an kinetic coefficients in superfluid  $^3\text{He}$ . *Progr. Low Temp. Phys.*, 7:191, 1978.
- S. Yoshida. Note on the two-nucleon stripping reaction. *Nuclear Physics*, 33:685, 1962.
- Y. Zhou, D. Vitkup, and M. Karplus. Native proteins are surface–molten solids: applications of the Lindemann Criterion for the solid versus liquid state. *J. Mol. Biol.*, 285:1371, 1999.
- Zinser, M., F. Humbert, T. Nilsson, W. Schwab, H. Simon, T. Aumann, M. J. G. Borge, L. V. Chulkov, J. Cub, T. W. Elze, H. Emling, H. Geissel, D. Guillemaud-Mueller, P. G. Hansen, R. Holzmann, H. Irnich, B. Jonson, J. V. Kratz, R. Kulessa, Y. Leifels, H. Lenske, A. Magel, A. C. Mueller, G. Mnzenberg, F. Nickel, G. Nyman, A. Richter, K. Riisager, C. Scheidenberger, G. Schrieder, K. Stelzer, J. Stroth, A. Surowiec, O. Tengblad, E. Wajda, and E. Zude. Invariant-mass spectroscopy of  $^{10}\text{Li}$  and  $^{11}\text{Li}$ . *Nuclear Physics A*, 619:151, 1997.

# Chapter 3

## Pair transfer in a nutshell

### 3.1 Simultaneous versus successive Cooper pair transfer in nuclei

Cooper pair transfer is commonly thought to be tantamount to simultaneous transfer. In this process a nucleon goes over through the  $NN$ -interaction  $v$ , the second one does it making use of the correlations with its partner (cf. Figs. 3.1.1 and 5.C.1 (I)). Consequently, in the independent particle limit, simultaneous transfer should not be possible (see Sect. 5.C.1). Nonetheless, it remains operative. This is because, in this limit, the particle transferred through  $v$  does it together with a second one which profits from the non-orthogonality of the wavefunctions describing the single-particle motion in target and projectile (Figs. 3.1.2 and 5.C.1 (II)). This is the reason why this (non-orthogonality) transfer amplitude has to be treated on equal footing with the previous one representing, within the overcomplete basis employed, a natural contribution to simultaneous transfer (cf. also discussion carried out in Ch.2 in connection with the overlap  $\Omega_n$  Eq. (2.1.3)). In other words,  $T^{(1)}$  gives the wrong cross section, even at the level of simultaneous transfer, as it violates two-nucleon transfer sum rules (Broglia, R. A. et al. (1972), Bayman, B. F. and Clement (1972); cf. also Chapter 1). In fact  $(T^{(1)} - T_{NO}^{(1)})$  is the correct, sum rule conserving two-nucleon transfer amplitude to lowest order (first) in  $v$  (Fig. 3.1.2). The resulting cancellation is quite conspicuous in actual nuclei, in keeping with the fact that Cooper pairs are weakly correlated systems (see e.g. Figs. 3.A.2 (b) and 3.A.3). This is the reason why the successive transfer process in which  $v$  acts twice, is the dominant mechanism in pair transfer reactions (within this context see Sect. 3.3). While this mechanism seems antithetical to the transfer of correlated fermions pairs (bosons), it probes, in the nuclear case, the same pairing correlations as simultaneous transfer does (App. 3.A). This is because nuclear Cooper pairs (quasi-bosons) are quite extended objects, the two nucleons being (virtually) correlated over distances much larger than typical nuclear dimensions (cf. Fig. 3.1.3; cf. also Sect. 2.F.1). In a two-nucleon transfer process this virtual property becomes real, the difference between the character of simultaneity and of

succession becoming strongly blurred.

Within this context, let us refer to the Josephson effect, associated with the Cooper pair tunneling across a thin barrier separating two metallic superconductors. Because the probability of one-electron-tunneling is of the order of  $10^{-10}$ , (conventional) simultaneous tunneling associated with a probability of  $(10^{-10})^2$  would hardly be observed (cf. Sect 3.3). Nonetheless, Josephson currents are standard measures in low temperature laboratories (cf. e.g. Rogalla and Kes (2012) and references therein).

The same arguments related to the large value of the correlation length is operative in explaining the fact that Coulomb repulsion is rather weak between partners of Cooper pairs which are, in average, at a distance  $\xi (\approx 10^4 \text{ \AA})$  much larger than the Wigner–Seitz radius  $r_s$  typical of metallic elements ( $\approx 1 - 2 \text{ \AA}$ ). Consequently, it can be overwhelmed by the long range electron phonon pairing. Similarly, in widely extended light halo nuclei, the short range bare pairing interaction plays little role, becoming subcritical (cf. App 2.F). The fact that such systems are nonetheless bound, although weakly, testifies to the dominant role the exchange of collective vibrations between halo nucleons have in binding the associated halo Cooper pair (e.g.  $^{11}\text{Li(gs)}$ , and, arguably, also of  $^{12}\text{Be}$  ( $0^{++}$ ; 2.251 MeV; cf. e.g. Johansen et al. (2013))) to the core ( $^9\text{Li(gs)}$  and  $^{10}\text{Be}$  respectively) (cf. Section 6.1.2 and Fig. 6.1.4).

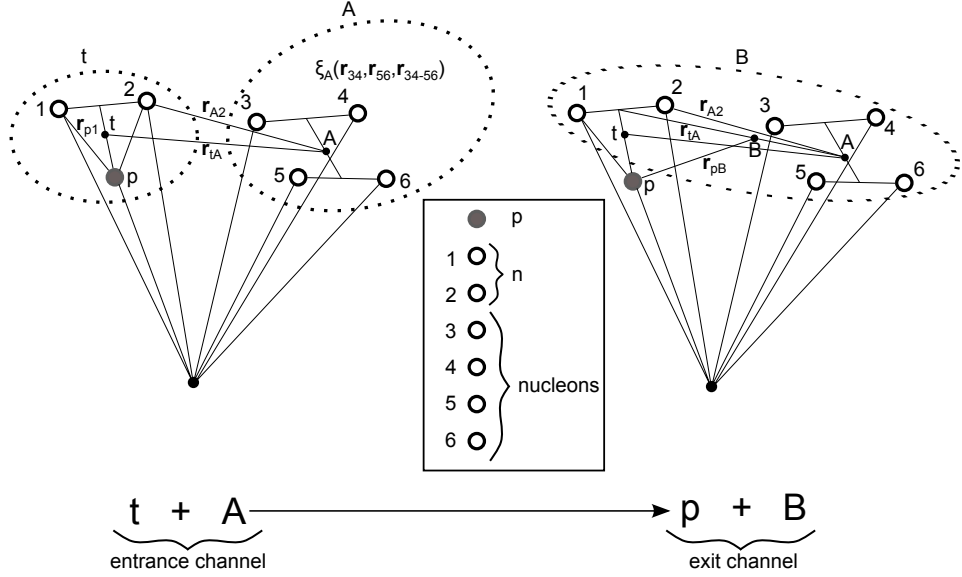
The above arguments are at the basis of the fact that second order DWBA theory which add both successive and non-orthogonality contributions to the simultaneous transfer amplitudes, provides a quantitative account of the experimental findings (cf. e.g. Fig. 2.2.1 and Chapter 6).

### 3.2 Two-nucleon transfer probabilities, enhancement factor

As discussed in Chapter ?? the enhancement factor in a two-nucleon transfer reaction can be defined in terms of two-particle units (cf. e.g. Broglia, R. A. et al. (1972); Broglia, R.A. et al. (1973) and references therein), similar to what is done in the case of electromagnetic decay (Weisskopf units, see e.g. Bohr and Mottelson (1969)). Let us, for simplicity, write such a relation as

$$\left( \frac{d\sigma}{d\Omega} \right)_{2n} = |\langle f | P^\dagger | i \rangle|^2 \left( \frac{d\sigma}{d\Omega} \right)_{2n}^{(0)}, \quad (3.2.1)$$

where  $\left( \frac{d\sigma}{d\Omega} \right)_{2n}^{(0)}$  is the absolute differential cross section associated with a typical pure single-pair configuration  $|j^2(0)\rangle$  (or the average value over pairs based on the valence orbitals). In the case of a superfluid nucleus like e.g.  $^{120}\text{Sn}$  and for  $i = \text{gs(A)}$



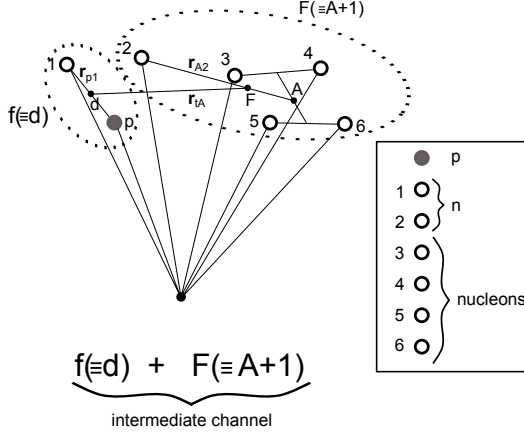
$$\phi_t(\mathbf{r}_{p1}, \sigma_1, \mathbf{r}_{p2}, \sigma_2) \chi_{m_s}^{1/2}(\sigma_p) \psi_A(\xi_A) \chi_{tA}^{(+)}(\mathbf{r}_{tA}) \quad \chi_{m_s}^{1/2}(\sigma_p) \psi_B(\xi_B) \chi_{pB}^{(-)}(\mathbf{r}_{pB})$$

$$(\phi_d(\mathbf{r}_{p1}, \sigma_1) \phi_d(\mathbf{r}_{p2}, \sigma_2) \chi_{tA}^{(+)}(\mathbf{r}_{tA}))$$

$$\begin{aligned} \Psi_{A+2}(\xi_A, \mathbf{r}_{A1}, \sigma_1, \mathbf{r}_{A2}, \sigma_2) &= \psi_A(\xi_A) \sum_{l_i, j_i} [\phi_{l_i, j_i}^{A+2}(\mathbf{r}_{A1}, \sigma_1, \mathbf{r}_{A2}, \sigma_2)]_0^0 \\ &= \psi_A(\xi_A) \sum_{nm} a_{nm} [\varphi_{n, l_i, j_i}^{A+2}(\mathbf{r}_{A1}, \sigma_1) \varphi_{m, l_i, j_i}^{A+2}(\mathbf{r}_{A2}, \sigma_2)]_0^0 \end{aligned}$$

$$\begin{aligned} T^{(1)} &= 2 \sum_{\sigma_1, \sigma_2, \sigma_p} \int d\xi_A d\mathbf{r}_{tA} d\mathbf{r}_{p1} d\mathbf{r}_{A2} \psi_A(\xi_A) \sum_{l_i, j_i} [\phi_{l_i, j_i}^{A+2}(\mathbf{r}_{A1}, \sigma_1, \mathbf{r}_{A2}, \sigma_2)]_0^{0*} \\ &\times \chi_{pB}^{(-)*}(\mathbf{r}_{pB}) \chi_{m_s}^{1/2*}(\sigma_p) v(r_{p1}) \phi_t(\mathbf{r}_{p1}, \sigma_1, \mathbf{r}_{p2}, \sigma_2) \chi_{m_s}^{1/2}(\sigma_p) \psi_A(\xi_A) \chi_{tA}^{(+)}(\mathbf{r}_{tA}) \\ &= 2 \sum_{\sigma_1, \sigma_2, \sigma_p} \int d\mathbf{r}_{tA} d\mathbf{r}_{p1} d\mathbf{r}_{A2} \sum_{l_i, j_i} [\phi_{l_i, j_i}^{A+2}(\mathbf{r}_{A1}, \sigma_1, \mathbf{r}_{A2}, \sigma_2)]_0^{0*} \\ &\times \chi_{pB}^{(-)*}(\mathbf{r}_{pB}) \chi_{m_s}^{1/2*}(\sigma_p) v(r_{p1}) \phi_t(\mathbf{r}_{p1}, \sigma_1, \mathbf{r}_{p2}, \sigma_2) \chi_{m_s}^{1/2}(\sigma_p) \chi_{tA}^{(+)}(\mathbf{r}_{tA}) \end{aligned}$$

Figure 3.1.1: Contribution of simultaneous transfer, in first order DWBA, to the reaction  $A(t, p)B (\equiv A + 2)$ . The nucleus  $A$  is schematically assumed to contain four nucleons, the triton being composed of two neutrons and one proton. The set of coordinates used to describe the entrance and exit channels are shown in the upper part, while in the lower part the simultaneous two-nucleon transfer amplitude is written in detail (cf. Potel, G. et al. (2013b)). Of notice that the expression of  $T^{(1)}$  violates, in the independent particle basis used, the two-nucleon transfer sum rule by exactly  $T_{NO}^{(1)}$ , amplitude operative also in lowest order of  $v$  (Fig. 3.1.2; see also text). It is of notice that of all the relative motion coordinates, only those describing the relative motion of  $(t, A)$  and of  $(p, B)$  have asymptotic values.



$$\chi_{m_s}^{1/2}(\sigma_p)\phi_d(\mathbf{r}_{p1}, \sigma_1)\psi_A(\xi_A)\varphi_{l_f, j_f, m_f}^{A+1}(\mathbf{r}_{A2}, \sigma_2)$$

$$\begin{aligned} T_{succ}^{(2)} &= 2 \sum_{l_i, j_i} \sum_{l_f, j_f, m_f} \sum_{\sigma_1 \sigma_2} \int d\xi_A d\mathbf{r}_{dF} d\mathbf{r}_{p1} d\mathbf{r}_{A2} \chi_{pB}^{(-)*}(\mathbf{r}_{pB}) \chi_B^*(\xi_B) v(\mathbf{r}_{p1}) \phi_d(\mathbf{r}_{p1}) \varphi_{l_f, j_f, m_f}^{A+1}(\mathbf{r}_{A2}, \sigma_2) \\ &\quad \times \chi_{m_s}^{1/2}(\sigma_p) \Psi_A(\xi_A) \frac{2\mu_{dF}}{\hbar^2} \int d\xi'_A d\mathbf{r}'_{dF} d\mathbf{r}'_{p1} d\mathbf{r}'_{A2} G(\mathbf{r}_{dF}, \mathbf{r}'_{dF}) \\ &\quad \times \chi_{IA}^{(+)}(\mathbf{r}_{IA}) \psi_A^*(\xi'_A) v(\mathbf{r}'_{p2}) \phi_d(\mathbf{r}'_{p1}) \varphi_{l_f, j_f, m_f}^{A+1}(\mathbf{r}'_{A2}, \sigma'_2) \\ &= 2 \sum_{l_i, j_i} \sum_{l_f, j_f, m_f} \sum_{\sigma_1 \sigma_2} \int d\mathbf{r}_{dF} d\mathbf{r}_{p1} d\mathbf{r}_{A2} \chi_{pB}^{(-)*}(\mathbf{r}_{pB}) v(\mathbf{r}_{p1}) \phi_d(\mathbf{r}_{p1}) \left[ \varphi_{l_f, j_f, m_f}^{A+2}(\mathbf{r}_{A1}, \sigma_1, \mathbf{r}_{A2}, \sigma_2) \right]_0^0 \\ &\quad \times \frac{2\mu_{dF}}{\hbar^2} \int d\mathbf{r}'_{dF} d\mathbf{r}'_{p1} d\mathbf{r}'_{A2} G(\mathbf{r}_{dF}, \mathbf{r}'_{dF}) \chi_{IA}^{(+)}(\mathbf{r}'_{IA}) v(\mathbf{r}'_{p2}) \phi_d(\mathbf{r}'_{p1}, \sigma'_1) \phi_d(\mathbf{r}'_{p2}, \sigma'_2) \varphi_{l_f, j_f, m_f}^{A+1}(\mathbf{r}'_{A2}, \sigma'_2) \end{aligned}$$

$$\begin{aligned} T_{NO}^{(1)} &= 2 \sum_{l_i, j_i} \sum_{l_f, j_f, m_f} \sum_{\sigma_1 \sigma_2} \int d\xi_A d\mathbf{r}_{dF} d\mathbf{r}_{p1} d\mathbf{r}_{A2} \chi_{pB}^{(-)*}(\mathbf{r}_{pB}) \chi_B^*(\xi_B) v(\mathbf{r}_{p1}) \phi_d(\mathbf{r}_{p1}) \varphi_{l_f, j_f, m_f}^{A+1}(\mathbf{r}_{A2}, \sigma_2) \\ &\quad \times \chi_{m_s}^{1/2}(\sigma_p) \Psi_A(\xi_A) \frac{2\mu_{dF}}{\hbar^2} \int d\xi'_A d\mathbf{r}'_{dF} d\mathbf{r}'_{p1} d\mathbf{r}'_{A2} \\ &\quad \times \chi_{IA}^{(+)}(\mathbf{r}_{IA}) \psi_A^*(\xi'_A) \phi_d(\mathbf{r}'_{p1}) \mathbb{I} \varphi_{l_f, j_f, m_f}^{A+1}(\mathbf{r}'_{A2}, \sigma'_2) \\ &= 2 \sum_{l_i, j_i} \sum_{l_f, j_f, m_f} \sum_{\sigma_1 \sigma_2} \int d\mathbf{r}_{dF} d\mathbf{r}_{p1} d\mathbf{r}_{A2} \chi_{pB}^{(-)*}(\mathbf{r}_{pB}) v(\mathbf{r}_{p1}) \phi_d(\mathbf{r}_{p1}) \left[ \varphi_{l_f, j_f, m_f}^{A+2}(\mathbf{r}_{A1}, \sigma_1, \mathbf{r}_{A2}, \sigma_2) \right]_0^0 \\ &\quad \times \frac{2\mu_{dF}}{\hbar^2} \int d\mathbf{r}'_{dF} d\mathbf{r}'_{p1} d\mathbf{r}'_{A2} \chi_{IA}^{(+)}(\mathbf{r}'_{IA}) \phi_d(\mathbf{r}'_{p1}, \sigma'_1) \phi_d(\mathbf{r}'_{p2}, \sigma'_2) \varphi_{l_f, j_f, m_f}^{A+1}(\mathbf{r}'_{A2}, \sigma'_2) \end{aligned}$$

Figure 3.1.2: Successive and non-orthogonality contributions to the amplitude describing two-nucleon transfer in second order DWBA, entering in the expression of the absolute differential cross section  $d\sigma/d\Omega = \frac{\mu_i \mu_f}{(4\pi\hbar^2)^2} \frac{k_f}{k_i} |T^{(1)} + T_{succ}^{(2)} - T_{NO}^{(2)}|^2$ . Concerning  $T^{(1)}$  we refer to Fig. 3.1.1. In the upper part of the figure the coordinates used to describe the intermediate channel  $d + F(\equiv A + 1)$  are given, while in the lower part the corresponding expressions are displayed (Potel, G. et al., 2013b) in the case of a  $(t, p)$  process. Schematically, the three contributions  $T^{(1)}$ ,  $T_{succ}^{(2)}$  and  $T_{NO}^{(2)}$  to the transfer amplitude can be written as  $\langle pB|v|tA \rangle$ ,  $\sum \langle pB|v|dF \rangle \langle dF|v|tA \rangle$  and  $\sum \langle pB|v|dF \rangle \langle dF|\mathbf{1}|tA \rangle$  respectively, where  $v$  is the proton-neutron interaction and  $\mathbf{1}$  the unit operator. Within this context, while  $T_{NO}^{(2)}$  receives contributions from the intermediate (virtual) closed  $(d + F)$  channel as  $T_{succ}^{(2)}$  does, it is first order in  $v$  as  $T^{(1)}$ .

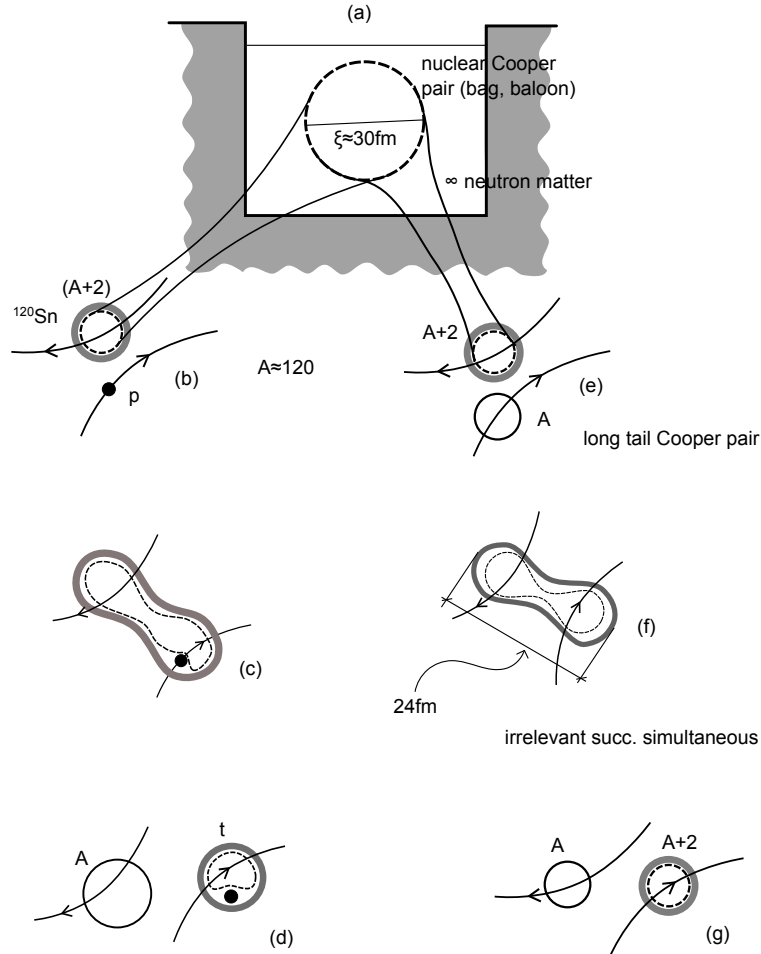


Figure 3.1.3: The correlation length associated with a nuclear Cooper pair is of the order of  $\xi \approx \hbar v_F / \Delta \approx 30 \text{ fm}$  (see App. 3.A). (a) in neutron matter at typical densities of the order of 0.5–0.8 saturation density, the  $NN - ^1S_0$  short range force, eventually renormalized by medium polarization effects, makes pairs of nucleons moving in time reversal states to correlate over distances of the order of 5–6 times typical nuclear radii. How can one get evidence for such an extended object? Certainly not when the Cooper bag (balloon) is introduced in (b) the mean field of a superfluid nucleus which, acting as an external field, constrains the Cooper pair to be within the nuclear radius with some spill out (long tail of Cooper pair, grey, shaded area extending outside the nuclear surface defined by  $R_0 = 1.2A^{1/3} \text{ fm}$ ). But yes in (c), (d) that is in the case of two-nucleon transfer process (e.g.  $(p, t)$  reaction) in which the absolute cross section can change by orders of magnitude in going from pure two-particle (uncorrelated configurations) to long tail Cooper pair spill outs. This effect is expected to become stronger by allowing , pair transfer between similar superfluid nuclei, in which case one profits of the same type of correlations (superfluidity) as resulting from very similar pair mean fields (e), (f), (g) (cf. e.g. von Oertzen, W. (2013) and references therein; see also Eqs. (2.1.2) and (2.1.3). For the case under discussion  $\Omega = 1$ ). Within this context, it is apparent that pairs of nucleons will feel equally well pairing correlations whether they are transferred simultaneously or one after the other. (cf. (c) and (f)).

and  $f = gs(A+2)$  as well as  $f = 2qp(A+2)$  one can write

$$\left| \langle f | P^\dagger | i \rangle \right|^2 = \begin{cases} \alpha_0'^2 = (\sum_{\nu>0} U_\nu' V_\nu')^2 = \left( \frac{A}{G} \right)^2 = \left( \frac{12A}{\sqrt{A}25} \right)^2 \approx \frac{A}{4} \approx 30 \ (f = gs), \\ U_\nu^4 \approx 1 \ (f = 2qp). \end{cases} \quad (3.2.2)$$

Thus, the expected enhancement factor (see e.g. Brink, D. and Broglia (2005) p. 324) is given by the ratio,

$$R = \frac{\left( \frac{d\sigma}{d\Omega}(gs \rightarrow gs) \right)_{2n}}{\left( \frac{d\sigma}{d\Omega}(gs \rightarrow 2qp) \right)_{2n}} \approx 30. \quad (3.2.3)$$

In other words, in superfluid nuclei one expects the  $0^+$  pairing vibrational states to carry a (summed) cross section of the order of 3% that of the  $gs \rightarrow gs$  transition (cf. Fig. 2.1.4). Now, in defining the quantity  $R$  used was made of (3.2.1). Because both numerator and denominator are linear in  $\left( \frac{d\sigma}{d\Omega} \right)_{2n}^{(0)}$ , one could as well posit that one has used (3.2.2) in defining  $R$ .

The situation is quite different when one intends to define the probability associated with a transfer process. One could be tempted again to use (3.2.1) for the case of  $2n$ -transfer and eventually

$$\left( \frac{d\sigma}{d\Omega} \right)_{1n} = S \left( \frac{d\sigma}{d\Omega} \right)_{1n}^{(0)}, \quad (3.2.4)$$

in the case of  $1n$ -transfer,  $S$  being known in the literature as the spectroscopic factor, and used here for illustration purposes only. However, in trying to define an enhancement factor in terms of  $P_{2n}/P_{1n}^2$ , the approximate relations (3.2.1) and (3.2.4) will now condition the physics one is trying to extract from the experimental (empirical) information. In fact, in this case the actual values of  $\left( \frac{d\sigma}{d\Omega} \right)_{1n}^{(0)}$  and of  $\left( \frac{d\sigma}{d\Omega} \right)_{2n}^{(0)}$  will play an important role, and this could be hardly correct. In fact, the proper definition of the transfer probabilities is to be made in terms of the total reaction cross section.

For this purpose let us remind some useful relations. In particular that of the differential reaction cross section

$$\frac{d\sigma}{d\Omega} = |f(\theta)|^2 \quad (3.2.5)$$

where

$$f(\theta) = \frac{1}{k} \sum_l (2l+1) e^{i\delta_l} \sin \delta_l P_l(\cos \theta), \quad (3.2.6)$$

$\delta_l$  being the partial wave  $l$  phase shift. Let us now use for simplicity the result associated with hard sphere scattering (cf. e.g. Sakurai (1994)) in the low and high

energy limit. Making use of the fact that in the case under discussion the phase shift  $\delta_l$  are related to the regular and irregular spherical Bessel functions,

$$\tan \delta_l = \frac{j_l(kR)}{n_l(kR)}, \quad (3.2.7)$$

and that  $\sin^2 \delta_l = \tan^2 \delta_l / (1 + \tan^2 \delta_l)$ , one can write in the case in which  $kR \ll 1$ , i.e. in the low-energy, long wavelength, regime

$$\tan \delta_l \approx \frac{-(kR)^{2l+1}}{(2l+1)[(2l-1)!!]^2}, \quad (3.2.8)$$

implying that one can ignore all  $\delta_l$  with  $l \neq 0$ . Because  $\delta_0 = -kR$  (cf. (3.2.7)) regardless the value of  $k$ , one obtains,

$$\frac{d\sigma}{d\Omega} = \frac{\sin^2 \delta_0}{k^2} = R^2, \quad (3.2.9)$$

and thus

$$\sigma_{tot} = \int \frac{d\sigma}{d\Omega} d\Omega = 4\pi R^2 \quad (kR \ll 1), \quad (3.2.10)$$

a cross section which is four times the geometric cross section  $\pi R^2$ , namely the area of the disc of radius  $R$  that blocks the propagation of the incoming (plane) wave, and has the same value as that of a hard sphere. Because  $kR \ll 1$  implies long wavelength scattering, it is not surprising that quantal effects are important, so as to overwhelm the classical picture. Let us now consider the high energy limit  $kR \gg 1$ . The total cross section is in this case, given by

$$\begin{aligned} \sigma_{tot} &= \int |f_l(\theta)|^2 d\Omega = \frac{1}{k^2} \int_0^{2\pi} d\phi \int_{-1}^1 d(\cos \theta) \sum_{l=1}^{kR} \sum_{l'=1}^{kR} (2l+1)(2l'+1) \\ &\times e^{i\delta_l} \sin \delta_l e^{-i\delta_{l'}} \sin \delta_{l'} P_l P_{l'} = \frac{4\pi}{k^2} \sum_{l=1}^{kR} (2l+1) \sin^2 \delta_l. \end{aligned} \quad (3.2.11)$$

Making use of the relation

$$\sin^2 \delta_l = \frac{\tan^2 \delta_l}{1 + \tan^2 \delta_l} = \frac{[j_l(kR)]^2}{[j_l(kR)]^2 + [n_l(kR)]^2} \approx \sin^2 \left( kR - \frac{\pi l}{2} \right), \quad (3.2.12)$$

and the fact that so many  $l$ -values contribute to (3.2.11), one can replace  $\sin^2 \delta_l$  by its average value  $1/2$ . Because the number of terms of the sum is roughly  $kR$ , the same being true for the average value of  $(2l+1)$ . Thus one can write

$$\sigma_{tot} = \frac{4\pi}{k^2} (kR)^2 \frac{1}{2} = 2\pi R^2, \quad (kR \gg 1) \quad (3.2.13)$$

which, in this short wavelength limit, is not the geometric cross section either. In fact, (3.2.13) can be split into two contributions each of value  $\pi R^2$ . One due to reflection in which it can be shown that there is no interference amongst contributions from different  $l$ -values. A second one (coherent contribution in the forward direction) called shadow because for hard-sphere scattering at high energies, waves with impact parameter less than  $R$  must be deflected. Consequently, behind the scatterer there must be zero probability for finding the scattered particle and a shadow must be generated.

In term of wave mechanics, this shadow is due to the destructive interference between the original wave (which would be there even if the scatterer was absent), and the newly scattered wave. Thus one needs scattering in order to create a shadow. This contribution is intimately related to the optical theorem (Sakurai (1994) pp. 420–421)

$$\sigma_{tot} = \frac{4\pi}{k} \Im[f(\theta = 0, k)] = \frac{4\pi}{k} [f_{shad}(\theta = 0, k)] = \frac{4\pi}{k^2} \sum_l (2l + 1) \sin^2 \delta_l, \quad (3.2.14)$$

to which it provides its physical interpretation. In fact, in a similar way in which there are two independent ways to determine the “colour” of an object, namely to shine light on it and observe which wavelengths it absorbs, or to heat it up and measure which wavelengths it emits, there are two independent ways of measuring  $\sigma_{tot}$ , namely: i) by integrating the differential cross section  $d\sigma/d\Omega = |f(\theta)|^2$  moving around the detector, ii) measuring the attenuation of the incoming beam. Both procedures should give the same result. One then identifies  $(4\pi/k)f(\theta = 0, k)$  with the attenuation arising from the interference of the elastic wave with the incoming wave. Of notice that in (3.2.11) the factor  $(\pi/k^2)(2l + 1) = \pi\lambda(2l + 1)$  is the area of a ring with radius  $b = (l + 1/2)\lambda$  and width  $\lambda$  due to quantal uncertainties. Thus

$$\sigma_{tot} = 2\pi(R + \lambda/2)^2 \quad (kR \gg 1). \quad (3.2.15)$$

The quantity

$$\lambda = \frac{\lambda}{2\pi} = \frac{h}{2\pi p} = \frac{\hbar}{p} = \frac{1}{k} = \frac{\hbar}{\sqrt{2mE}}, \quad (3.2.16)$$

is the reduced de Broglie wavelength for a massive particle ( $E = p^2/2m$ ). For a proton of energy  $E_p \approx 20$  MeV, typical of beams used in  $^{120}\text{Sn}(p, t)^{118}\text{Sn}(\text{gs})$  and  $^{120}\text{Sn}(p, d)^{119}\text{Sn}(\text{j})$  reactions (cf. Figs. 4.2.1, 4.2.3 and 6.2.1)<sup>1</sup>  $\lambda \approx 1$  fm, to be compared with the value  $R \approx 6$  fm of the radius of  $^{120}\text{Sn}$ . Consequently, we are in a situation of type (3.2.15), that is,

$$\sigma_{tot} = 2\pi(6 + 0.5)^2 \text{ fm}^2 \approx 2.7 \text{ b}. \quad (3.2.17)$$

---

<sup>1</sup>Of notice that the reduced wavelength of a photon ( $p = E/c$ ) of the same energy  $E = 20$  MeV is  $\lambda (= \lambda/2\pi = \hbar/p = \hbar c/E) \approx 10$  fm (cf. Table 2.1 p. 22 Satchler (1980)).

Because typical values of the absolute one-particle cross section associated with the  $(p, d)$  reaction mentioned above are few mb (cf. Fig. 4.2.3 right panel) one can use, for order of estimate purposes,

$$P_1 \approx \frac{5.35 \text{ mb}}{2.7 \text{ b}} \approx 10^{-3}, \quad (3.2.18)$$

as the typical probability for such processes. Consequently, one may argue that the probability for a (Cooper) pair of nucleons to simultaneously tunnel in e.g. the  $(p, t)$  process mentioned above is  $(P_1)^2 \approx 10^{-6}$ , as near impossible as no matter. Within this context we note that the integrated  $\text{gs} \rightarrow \text{gs}$  absolute cross section  $\sigma(^{120}\text{Sn}(p, t)^{118}\text{Sn(gs)}) \approx 2.5 \pm 0.2 \text{ mb}$  (cf. Figs. 2.2.1 and 6.2.1). This fact implies that the empirical two-nucleon transfer probability is of the order of  $P_2 \approx 10^{-3}$ . Consequently,  $P_2/(P_1)^2 \approx 10^3$ , a ratio which can hardly be explained in terms of a physical enhancement factor.

The above contradictions<sup>2</sup> are, to a large extent, connected with the fact that one is addressing the subject of pairing correlations in nuclei as probed by two-nucleon transfer reactions, treating separately the associated questions of structure and reactions, while they are but complementary aspects of the same physics. Let us elaborate on this point.

When one turns on, in an open shell atomic nucleus like e.g.  $^{120}_{50}\text{Sn}_{70}$ , a pairing interaction of strength larger than critical, the system moves into an independent pair regime (cf. e.g. Sects. 2.D.1 and 2.D.2 as well as Fig. 2.D.3; see Fig. 3.2.1). This fact has essentially no consequence concerning the one-particle transfer mechanism, exception made regarding the size of the mismatch between the relative motion–incoming ( $p+^{120}\text{Sn(gs)}$ ) and –outgoing ( $d+^{119}\text{Sn(gs)}$ ) trajectories ( $Q$ -value and recoil effect), in keeping with the fact that one has to break a Cooper pair to populate a single quasiparticle state. From a structure point of view the depletion of the occupation probability measured in a  $(p, d)$  process is correlated with the corresponding increase in occupation observed in  $(d, p)$  ( $U^2, V^2$  factors). Aside from the quantitative values, this is also observed in dressed single-particle states, the single-particle sum rule implying both the (A-1) and (A+1) system (see App. 4.I). Concerning the phase coherence of the pair correlated wavefunction it has no consequence for one-particle transfer process, in keeping with the fact that  $|e^{i\phi} \sqrt{P_1}|^2 = P_1$ .

The situation is very different concerning (Cooper) pair transfer. From a reaction point of view, and in keeping with the non-orthogonality existing between the wavefunctions in target and projectile, the associated contributions to the transfer

---

<sup>2</sup>Within this context it is of notice that similar questions were raised by Bardeen (1962, 1961); Pippard (2012); Cohen et al. (1962); McDonald (2001) in connection with the prediction of Josephson (Josephson (1962)) that there should be a contribution to the current through an insulating barrier between two superconductors which would behave like direct tunneling of condensed pairs. This is in keeping with the fact that a single electron has a probability of  $\approx 10^{-10}$  of getting through, the “classical” estimate of simultaneous pair tunneling being  $\approx 10^{-20}$ , an impossible observation as stated above.

process have to be eliminated. This is in keeping with the fact that simultaneous two-nucleon transfer can take place also in first order in the proton–neutron interaction  $v_{np}$ . When this is a consequence of the correlation between the partners of the Cooper pair (cf. Fig. 5.C.1 (I)) it constitutes a *bona fide* contribution. Not when it is a consequence of non-orthogonality (see Fig. 5.C.1 (II)). Continuing within the realm of reaction theory, second order processes in  $v_{np}$  are to be included (Fig. 5.C.2) and as a rule neglect higher orders in keeping with the small value of  $P_2$  ( $\approx 10^{-3}$ , cf. also Table 6.B.1). Let us now bring structure into the discussion. The fact that the wave function of the electrons in the pair are phase-coherent ( $(U_\nu + V_\nu e^{2i\phi} a_\nu^\dagger a_{\bar{\nu}}^\dagger) |0\rangle$ ) implies that one has to add the amplitudes before one takes modulus squared (cf. also App. 3.C and App. 3.D), that is,

$$\begin{aligned} P_2 &= \lim_{\epsilon \rightarrow 0} \left| \frac{1}{\sqrt{2}} (e^{i\phi'} \sqrt{P_1} + e^{i\phi} \sqrt{P_1}) \right|^2 \\ &= P_1 \lim_{\epsilon \rightarrow 0} (1 + \cos \epsilon) = 2P_1 \quad (\epsilon = \phi - \phi'), \end{aligned} \quad (3.2.19)$$

again, an unexpected quantum mechanical result as e.g. (3.2.13). Because the range of  $v_{np}$  ( $a \approx 1$  fm) is much smaller than the correlation length ( $\xi \approx 20$ – $30$  fm), in the successive process (3.2.19), the Cooper pair tunnels between target and projectile equally formed and “unharmed” as in the simultaneous process. Think again that in the nuclear pairing correlated system only Cooper pair exist (in which the partners nucleons are at 20–30 fm from each other) and not single nucleons (normal system) at  $\approx 4$  fm (2 fm being the radius of the Wigner–Seitz nucleus cell) from each other (cf. Fig. 3.2.1). In fact, as one switches on the pairing interaction, the average relative distance of pairs of correlated fermions move away from each other, so as to lower the relative momentum. This explains the importance of long-range induced pairing interaction (exchange of phonons) in general, let alone in very extended light halo nuclei like  $^{11}\text{Li}$ .

The fact that pairs of nucleons in nuclei are closer when pair correlated as compared to angular momentum coupled ( $j^2(0)$ ), is in keeping with the fact that the extended Cooper correlated pair is forced, by the single-particle “external field” to elastically reflect on its surface (cf. e.g.  $|\Psi(\mathbf{r}_1, \mathbf{r}_2)|^2$  displayed in a) and b) of Fig 2.F.3). Within this context, it is of notice that lattice phonon exchange (few meV) can bind Cooper pairs in metals (e.g. Pb) because the Coulomb repulsion between Cooper partners ( $e^2/\xi$  ( $\xi \approx 10^2$ – $10^3$  Å) instead of  $e^2/r_s$  ( $r_s \approx 1$ – $2$  Å)), let alone the exchange of plasmons, particularly important in small metallic clusters (cf. e.g. Broglia et al. (2004) and references therein).

### 3.3 Correlations between nucleons in Cooper pair tunneling

Let us call  $x_1$  and  $x_2$  the coordinates of the Cooper pair partners. Let us furthermore assume they can only take two values: 0 when they are bound to the target

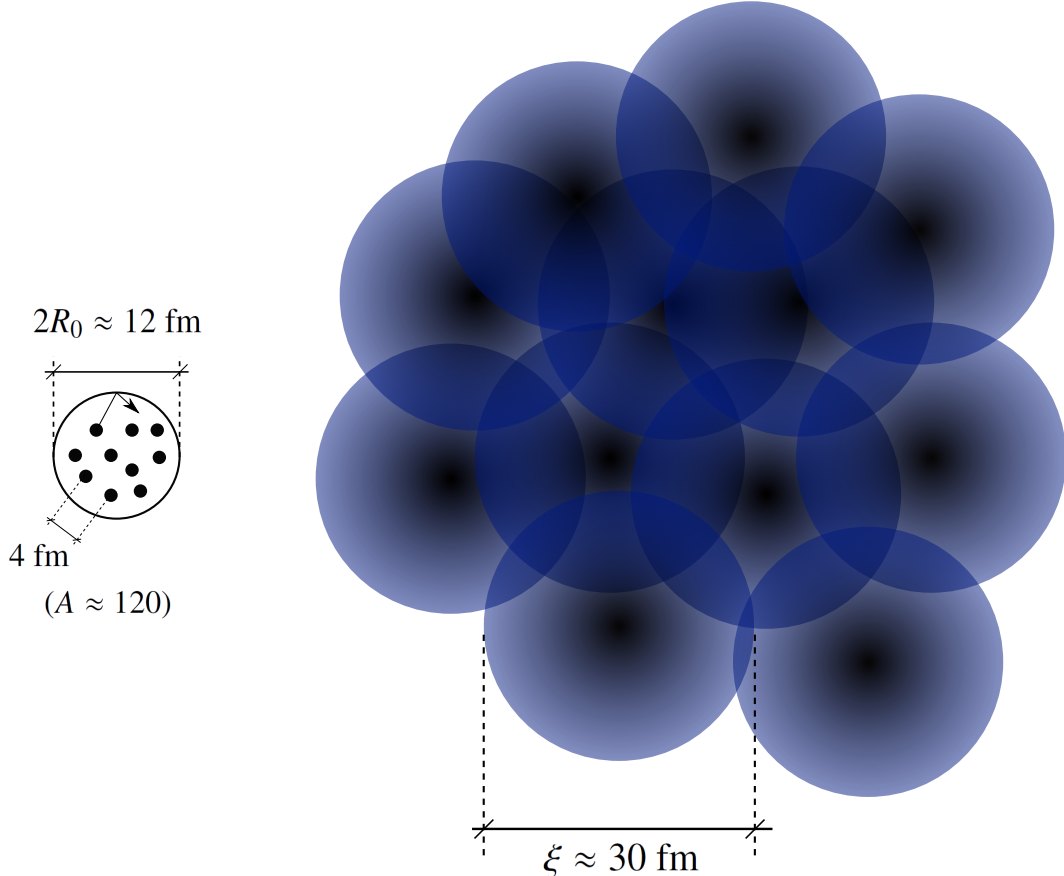


Figure 3.2.1: Schematic representation of independent-particle motion (left) and independent-pair motion (right). In the first case nucleons (fermions) move independently of each other reflecting elastically from the wall of the mean field created by all the other nucleons, each of which is associated with a Wigner–Seitz cell of radius  $d = ((4\pi/3)R_0^3/A)^{1/3}$  implying a relative distance of  $2d$  (the actual numbers correspond to e.g.  $^{120}\text{Sn}$ ). Switching on the pairing interaction (bare plus induced) leads to Cooper pair formation in which the correlation length is  $\xi$ . Thus, pair of nucleons moving in time reversal states close to the Fermi energy recede from each other lowering their relative momentum ( $2d \rightarrow \xi$ ) thus boosting the stability of the system. From this point on, and at least for the levels lying close to the Fermi surface, one cannot talk about particles but about Cooper pairs (unless one does not intervene the system with an external field, e.g.  $(p, d)$  and provides the energy, angular and linear momentum needed to break a pair). Of course that the system to the right under the influence of an external field (like e.g. the HF of  $^{120}\text{Sn}$ ) Cooper pairs will be constrained within its boundaries. But this will be true with two nuclei of  $^{120}\text{Sn}$  at a relative (CM) distance much larger than  $2R_0$  ( $\approx 12$  fm). The pair field associated with a Cooper pair, will extend in the empty region between the two nuclei allowing two nucleons to correlate over  $\xi$  and, eventually, in a reaction like e.g.  $\text{Sn}+\text{Sn} \rightarrow \text{Sn(gs)}+\text{Sn(gs)}$  allow for the transfer of two nucleons correlated over tens of fm. This is in keeping with the fact that  $\langle BCS | P^\dagger | BCS \rangle = \sum_{v>0} U_v V_v$  can be different from zero, also in regions in which the pairing interaction vanishes  $G_{eff} = 0$  (cf. App. 3.F). An example of the fact that a Cooper pair will “expand” if the external HF field is weakened, is provided by  $^{11}\text{Li}$  in which case, and profiting of the weak binding ( $\approx 380$  keV), the extension of the Cooper pair ( $\approx 4.55$  fm  $\pm 0.3$  fm) is similar to that of a nucleus of mass number  $A \approx 60$  assuming a standard behavior, i.e.  $R_0 = 1.2A^{1/3}$  fm.

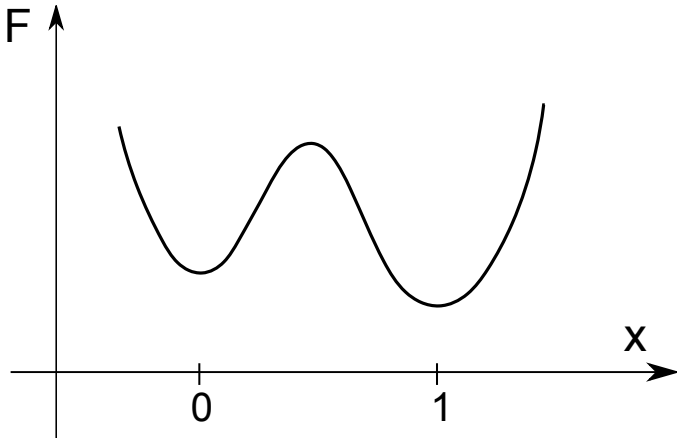


Figure 3.3.1: A schematic representation of nucleon tunneling between target and projectile. The free energy  $F = U - TS$  which for the zero temperature situation under consideration (e.g.  $^{120}\text{Sn}(p, d)^{119}\text{Sn}$ ,  $^{120}\text{Sn}(p, d)^{118}\text{Sn}$ ) coincides with the potential energy as a function of the nucleon coordinate  $x$ . For  $x = 0$  the nucleon is assumed to be bound to the target system. For  $x = 1$  the nucleon has undergone tunneling becoming bound to the outgoing particle. In other words  $x_1$  jumps from the value 0 to the value 1 in the tunneling process ( $x_1, 0 \rightarrow 1$ ), the same for the coordinate of the second nucleon.

nucleus, 1 when they have tunneled and become part of the outgoing particle (see Fig. 3.3.1).

The correlation between the two nucleons is measured by the value

$$\langle x_1 x_2 \rangle - \langle x_1 \rangle \langle x_2 \rangle = \int d\gamma P_2 \times 1 \times 1 - \int d\gamma P_1 \times 1 \int d\gamma' P'_1 \times 1 = P_2 - P_1 P'_1, \quad (3.3.1)$$

$d\gamma$  being the differential volume in phase space, normalized with respect to the corresponding standard deviations, that is, with respect to

$$\sigma_{x_1} \sigma_{x_2} = [(\langle x_1^2 \rangle - \langle x_1 \rangle^2)(\langle x_2^2 \rangle - \langle x_2 \rangle^2)]^{1/2}. \quad (3.3.2)$$

Making use of the fact that

$$\langle x_1^2 \rangle = \int d\gamma P_1 \times 1^2 = P_1, \quad (3.3.3)$$

and

$$\langle x_1 \rangle = \int d\gamma P_1 \times 1 = P_1, \quad (3.3.4)$$

One obtains the function which measures the correlations between nucleons 1 and 2, namely,

$$C = \frac{\langle x_1 x_2 \rangle - \langle x_1 \rangle \langle x_2 \rangle}{\sqrt{(\langle x_1^2 \rangle - \langle x_1 \rangle^2)(\langle x_2^2 \rangle - \langle x_2 \rangle^2)}} = \frac{P_2 - P_1 P'_1}{\sqrt{(P_1 - P_1^2)(P'_1 - P'^2_1)}}. \quad (3.3.5)$$

Because both nucleons are identical and thus interchangeable,  $P_1 = P'_1$ . Thus

$$C = \frac{P_2 - P_1^2}{P_1 - P_1^2}. \quad (3.3.6)$$

Making use of the empirical values

$$P_1 \approx P_2 \approx 10^{-3} \quad (3.3.7)$$

leads to,

$$C = \frac{10^{-3} - 10^{-6}}{10^{-3} - 10^{-6}} \approx 1. \quad (3.3.8)$$

In other words, within the independent pair motion regime, nucleon partners are solidly anchored to each other: if one nucleon goes over, the other does it also. This is so in spite of the very liable and fragile structure of the nuclear Cooper pairs ( $\Delta/\epsilon_F \ll 1$ ), a clear example of which is being provided by  $^{11}\text{Li}$ . In fact, if one picks-up a neutron from  $^{11}\text{Li}$  ( $^{11}\text{Li}(p, d)^{10}\text{Li}$ ), the other one breaks up essentially instantaneously,  $^{10}\text{Li}$  being unbound. In spite of this fact, the probability associated with the reaction  $^{11}\text{Li}(^{11}\text{Li}, ^9\text{Li(gs)})^1\text{H}$  is (see Table II Potel et al. (2010) and eq. (2.F.5) as well as Sect. 2.H) is given by,

$$P_2 = \frac{5.7 \pm 0.9 \text{ mb}}{2\pi(4.83 \text{ fm})^2} \approx 4 \times 10^{-3}, \quad (3.3.9)$$

a value which is much larger than the value of  $4.81 \times 10^{-6}$  associated with the breakup process mentioned above (see  $l = 0$  columns 1 and 3 of Table 6.B.1), let alone  $P_1^2 (1.02 \times 10^{-3})^2 \approx 10^{-6}$  as given in Table 3.3.1. One may be surprised of this result, in keeping with the fact that most of the two-nucleon transfer reaction cross section ( $\approx 80\%$ ) is associated with successive transfer (see Fig. 6.B.3). The answer is in any case contained in the relation (3.2.19), applicable both for static and dynamic pair modes, in keeping with the fact that in nuclei, dynamic spontaneous breaking of gauge invariance is of similar importance as the static one (cf. Fig. 2.E.7, cf. also App. 3.F and Fig. 4 Potel, G. et al. (2013b); cf. Fig. 3.3.2). Of notice that in successive transfer processes the one-particle channels are virtual, that is with no outgoing running waves and thus with a very different coupling to the continuum states than in the case of real asymptotic waves. This coupling influences in an important way the structure aspects of the problem, less the reaction one.

$$\text{Order parameter} \quad \left( \langle \tilde{0} | PP^\dagger | \tilde{0} \rangle \right)^{1/2} = \begin{cases} \alpha_0 = \sum_{\nu>0} U'_\nu V'_\nu \\ \alpha_{dyn} = \sum_{\nu>0} U_\nu^{eff} V_\nu^{eff} \end{cases}$$

pairing vibrations

$$(U_\nu^{eff})^2 = 2Y_a^2(j_\nu)/\Omega_{j_\nu} (V_\nu^{eff})^2 = 1 - (U_\nu^{eff})^2$$

$$\begin{aligned} X_n(j_\nu) \\ Y_n(j_\nu) \end{aligned} \Big\} = \frac{\left(\sqrt{\Omega_j}/2\right)\Lambda_n}{2|E_j| \mp W_n}$$

pairing rotations

$$U'_\nu, V'_\nu \text{ BCS}$$

Figure 3.3.2: Order parameter associated with static and dynamic pair correlations.

1	
0	$1.02 \times 10^{-3}$
1	$2.40 \times 10^{-3}$
2	$1.26 \times 10^{-2}$
3	$1.84 \times 10^{-2}$
4	$6.13 \times 10^{-3}$
5	$1.39 \times 10^{-3}$
6	$2.89 \times 10^{-4}$
7	$5.04 \times 10^{-5}$
8	$6.51 \times 10^{-6}$
9	$5.87 \times 10^{-7}$

Table 3.3.1: Probabilities  $p_l$  (cf. Eq. (3.2.14) and App. 6.B) associated with the reaction  ${}^1\text{H}({}^{11}\text{Li}, {}^{10}\text{Li(gs)}){}^2\text{H}$  calculated with the same bombarding conditions as those associated with  ${}^1\text{H}({}^{11}\text{Li}, {}^9\text{Li(gs)}){}^3\text{H}$  cf. Table 6.B.1. It was assumed that the amplitude with which the single particle orbital  $s_{1/2}$  enters in the  $|{}^{10}\text{Li}(1/2^+)\rangle$  (gs) is  $\sqrt{0.5}$  (cf. Eqs. (6.1.1)–(6.1.3)).

But again, the simple answer is that the halo Cooper pair in its tunneling between  $^{11}\text{Li}$  and  $^1\text{H}$  does not see neither  $^{10}\text{Li}$  nor  $^2\text{H}$ , behaving as an entity. Surprisingly, the regime of independent pair motion extends also to the single pair situation. Two-particle tunneling can specifically probe such a regime.

A direct consequence of the above parlance is the fact that the Cooper pair rigidity emerges from phase coherence (in gauge space), and leads to the generalized rigidity of pairing rotational (static) and vibrational (dynamic) bands which can be instantaneously set into rotation (vibration) with just the push imparted in gauge space by the transferred pair, without this fact violating any limiting velocity, neither of medium propagating signals nor of light.

## Appendix 3.A Pair transfer

The semiclassical two-nucleon transfer amplitudes fulfill, in the **independent particle limit** (ademas figura capitulo 7 correspondiente a la figura 7 review), the relations (see App. 5.C, also Potel, G. et al. (2013a)),

$$a_{sim}^{(1)} = a_{NO}^{(1)}, \quad (3.A.1)$$

and

$$a_{succ}^{(2)} = a_{one-part}^{(1)} \times a_{one-part}^{(1)}, \quad (3.A.2)$$

with

$$a + A \rightarrow f + F \rightarrow b + B, \quad (3.A.3)$$

corresponding to the product of two single nucleon transfer processes. On the other hand, in the **strong correlation limit** one can write, making use of the post-prior representation

$$\tilde{a}_{succ}^{(2)} = a_{succ}^{(2)} - a_{NO}^{(1)}. \quad (3.A.4)$$

Thus

$$\lim_{E_{corr} \rightarrow \infty} \tilde{a}_{succ}^{(2)} = 0, \quad (3.A.5)$$

and all transfer is, in this case, due to simultaneous transfer. Actual nuclei are close to the independent particle limit ( $E_{corr}$  (1–2 MeV)  $\ll \epsilon_F \approx 37$  MeV). Then successive transfer is the major contribution to pair transfer processes. But successive transfer seems to break the pair *right? Wrong. Why?* let us see below.

### 3.A.1 Cooper pair dimensions

Typical correlation energies of Cooper pairs are 1–2 MeV. Now, such a system (dineutron or diproton) is not bound and needs of an external field to be confined. This is the role played by the single-particle field (cf. Fig. 3.1.3). Let us now calculate the dimensions of a Cooper pair (correlation length). We start with the relation

$$\delta x \delta p \geq \hbar \quad \delta \epsilon \approx 2E_{corr}, \quad (3.A.6)$$

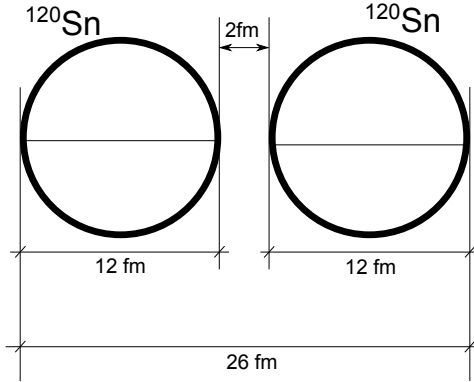


Figure 3.A.1: Schematic representation of two Sn-isotopes (radius  $R_0 \approx 6$  fm) at the distance of closest approach in a heavy ion collision.

where

$$\epsilon = \frac{p^2}{2m}; \quad \delta\epsilon = \frac{2p\delta p}{m} \approx v_F\delta p, \quad (3.A.7)$$

and thus

$$\delta\epsilon \approx 2E_{corr} \approx v_F\delta p, \quad (3.A.8)$$

leading to

$$\xi = \delta x = \frac{\hbar}{\delta p} \approx \frac{\hbar v_F}{2E_{corr}} \quad (\text{correlation length}). \quad (3.A.9)$$

Making use of the fact that in nuclei,

$$\frac{v_F}{c} \approx 0.3, \quad (3.A.10)$$

one obtains

$$\xi \approx \frac{200 \text{ MeV fm} \times 0.3}{2 \text{ MeV}} \approx 30 \text{ fm}. \quad (3.A.11)$$

Consequently, successive and simultaneous transfer feel equally well the pairing correlations giving rise to long range order. This virtual property can become (see von Oertzen, W. (2013)) real in e.g. a pair transfer between two superfluid tin isotopes (Fig. 3.A.1).

### Objection

What about  $v_{pairing}(= G)$  becoming zero, e.g. between the two nuclei?

### Answer

$$\frac{d\sigma(a(= b + 2) + A \rightarrow b + B(= A + 2))}{d\Omega} \sim |\alpha_0|^2, \quad (3.A.12)$$

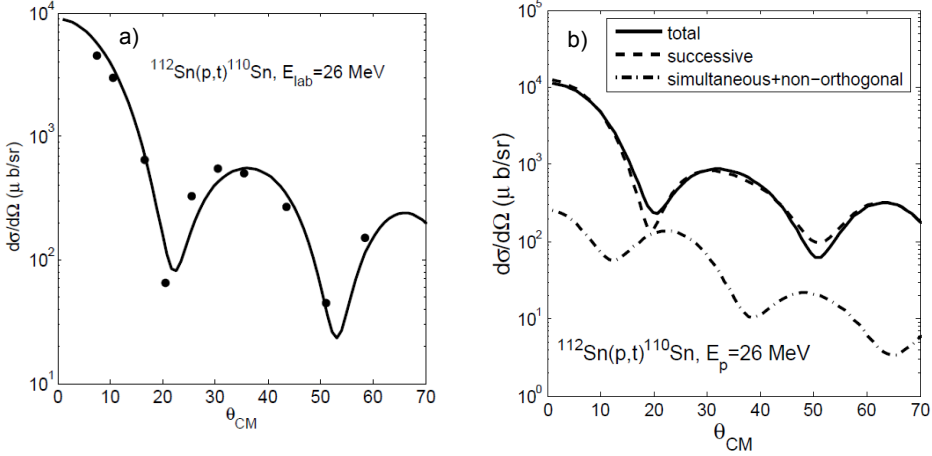


Figure 3.A.2: a) Absolute differential cross section associated with the reaction  $^{112}\text{Sn}(p,t)^{110}\text{Sn}(\text{gs})$  calculated with the software COOPER (mencionar apéndice software) in comparison with the experimental data (Guazzoni, P. et al. (2006)). b) Details of the different contributions to the total absolute ( $p, t$ ) differential cross section (for details see Potel, G. et al. (2013a), Potel, G. et al. (2013b)).

$$\alpha_0 = \langle BCS(A+2)|P^\dagger|BCS(A) \rangle = \sum_{\nu>0} U_\nu(A) V_\nu(A+2). \quad (3.A.13)$$

(cf. also App. 3.F).

### Objection

Relation (3.A.13) is only valid for simultaneous transfer, *right? Wrong.*

### Answer

The order parameter can also be written as,

$$\begin{aligned} \alpha_0 &= \sum_{\nu, \nu' > 0} \langle BCS | a_\nu^\dagger | int(\nu') \rangle \langle int(\nu') | a_{\bar{\nu}}^\dagger | BCS \rangle \\ &\approx \sum_{\nu, \nu' > 0} \langle BCS(A+2) | a_\nu^\dagger a_{\nu'}^\dagger | BCS(A+1) \rangle \langle BCS(A+1) | a_{\nu'} a_{\bar{\nu}}^\dagger | BCS(A) \rangle \\ &= \sum_{\nu, \nu' > 0} \langle BCS(A+2) | V_\nu(A+2) \alpha_{\bar{\nu}} \alpha_{\nu'}^\dagger | BCS(A+1) \rangle \\ &\times \langle BCS(A+1) | \alpha_{\nu'} U_\nu(A) a_{\bar{\nu}}^\dagger | BCS(A) \rangle = \sum_{\nu > 0} V_\nu(A+2) U_\nu(A), \quad (3.A.14) \end{aligned}$$

where the (inverse) quasiparticle transformation relation  $a_\nu^\dagger = U_\nu a_\nu^\dagger + V_\nu \alpha_{\bar{\nu}}$  was used. Examples of two-nucleon spectroscopic amplitudes involving superfluid targets, namely those associated with the reactions  $^{112}\text{Sn}(p,t)^{110}\text{Sn}(\text{gs})$  and

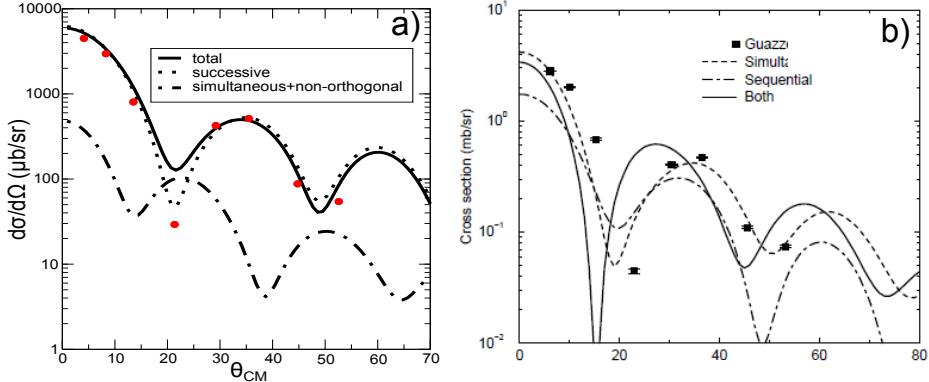


Figure 3.A.3: Absolute differential cross section associated with the reaction  $^{124}\text{Sn}(p,t)^{122}\text{Sn}(\text{gs})$  calculated making use of: a) second order DWBA taking into account non-orthogonality corrections and the two-nucleon spectroscopic amplitudes resulting from BCS (see Table 2.D.1, third column; for details see Potel, G. et al. (2013a), Potel, G. et al. (2013b)) in comparison with experimental data (Guazzoni, P. et al. (2011)). b) As above, but making use of FRESCO (reaction) and of shell model two-nucleon overlaps (structure); cf. Table 2.D.1 fourth column (for details cf. Thompson, I.J. (2013)).

$^{124}\text{Sn}(p,t)^{122}\text{Sn}(\text{gs})$  are given in Table 2.D.1. Making use of these amplitudes (first column) and of global optical parameters, the two-nucleon transfer absolute differential cross section of the reaction  $^{112}\text{Sn}(p,t)^{110}\text{Sn}(\text{gs})$  at center of mass bombarding energy of  $E_p = 26$  MeV, was calculated making use of the software COOPER based on second order DWBA and taking into account successive and simultaneous transfer properly corrected for non-orthogonality (cf. Chapter 5 and App. 6.D). It is compared with experimental data in Fig. 3.A.2 (a). The corresponding absolute integrated cross sections are  $1310 \mu\text{b}$  and  $1309 \pm 200 \mu\text{b}$  respectively. The largest contribution to the cross section arises from successive transfer, the cancellation between simultaneous and non-orthogonality amplitudes being important (Fig. 3.A.2 (b)). The above is a typical example of results of a systematic study of two-nucleon transfer reactions in terms of absolute cross sections (Potel, G. et al. (2013a), Potel, G. et al. (2013b) see also Ch. 6, in particular Fig. 6.2.1).

Making use of two-nucleon spectroscopic amplitudes worked out within the framework of an extended shell model calculation (Table 2.D.1, second column) one obtains very similar results to those displayed in Fig. 3.A.2 (a). In Fig. 3.A.3 (a) we report results similar to those displayed in Fig. 3.A.2, but for the case of the reaction  $^{124}\text{Sn}(p,t)^{122}\text{Sn}(\text{gs})$  calculated within second order DWBA making use of the BCS spectroscopic amplitudes (Table 2.D.1 third column). We display in Fig. 3.A.3 (b) the absolute differential cross section calculated with NuShell spectroscopic amplitudes and the coupled channel software FRESCO (Thompson, I.J.

(2013)).

Let us now provide an example of two–nucleon transfer around a closed shell nucleus displaying well defined collective pairing vibrational modes. We refer, in particular, to the pair removal mode of  $^{206}\text{Pb}$ , that is, to the reaction,  $^{206}\text{Pb}(t, p)^{208}\text{Pb}(\text{gs})$ . Making use of the spectroscopic amplitudes displayed in Tables 2.E.2 and 2.E.3 and of global optical parameters, the associated absolute differential cross sections was calculated again with the software COOPER. It is displayed in Fig. 3.A.4 in comparison with experimental findings. In the same figure, the total differential cross section is compared with that associated with the TD (Tamm–Dankoff) description of  $^{206}\text{Pb}(\text{gs})$ , that is, setting the pairing ground state correlations to zero ( $\sum_i X_r^2(i) = 1, Y_r(k) \equiv 0$ , see Table 2.E.2). In this case, theory underpredicts observation by about a factor of 2, let alone the fact that the TD solution does not conserve the two–nucleon transfer sum rule. Also given in Fig. 3.A.4 is the predicted cross section associated with the pure configuration  $|p_{1/2}^{-2}(0)\rangle$ . These results underscore the role pairing correlations play in the properties of  $^{208}\text{Pb}$  pair removal mode  $|r\rangle \equiv |^{206}\text{Pb}(\text{gs})\rangle$ . Not only they make the two holes come closer to each other as required by the calculated correlation length  $\xi$  (Bertsch, G. F. et al. (1967), Ferreira, L. et al. (1984) see also Figs. 2.F.3 a) and b) i.e. left part) but they also lower the relative momentum. This in keeping with the fact that  $\Omega_0(\approx 0.97)$ , that is  $l = n = 0$  give a much larger contribution to the two–nucleon transfer process than  $\Omega_1$  and  $\Omega_2$  which are 0.25 and 0.06 respectively, cf. Eq. (2.1.3). All these features boost the absolute two–nucleon pure configuration transfer cross section to the observed experimental value. While the results displayed in Fig. 3.A.4 were calculated making use of the full formalism of second order DWBA (cf. Figs. 3.1.1 and 3.1.2) the simplified expressions given in Eqs. (2.1.1–2.1.7) are useful to gain physical insight into the two–nucleon transfer process.

## Appendix 3.B Comments on the optical potential

As a rule, the depopulation of the entrance, elastic channel  $\alpha(a, A)$  (see Fig. 3.B.1) is mainly due to one–particle transfer channels  $\phi(f(= a - 1), F(= A + 1))$ . Other channels, like e.g. inelastic ones  $\beta(a^*, A)$ ,  $\gamma(a, A^*)$  being operative in particular situations, for example, when deformed nuclei are involved in the reaction process. Let us assume that this is not the case. Thus, quite likely, the one–particle transfer channel  $\phi$  is expected to be the main depopulating channel of the entrance channel  $\alpha$  (cf. Fig. 3.B.2). This is also in keeping with the fact that the tail of the corresponding form factors, reaches further away than that of any other channel (cf. Fig. 3.B.5). In this case, the calculation of the optical potential<sup>3</sup>, is quite reminiscent to

---

<sup>3</sup>It is of notice that the optical potential can be viewed as the complex “dielectric” function of direct nuclear reactions. In other words, the function describing the properties of the medium in which incoming and outgoing distorted waves propagate, properties which are, as a rule determined through the analysis of elastic scattering processes, under the assumption that the coupling between the relative motion(reaction) and intrinsic (structure) coordinates, occur only through a Galilean transforma-

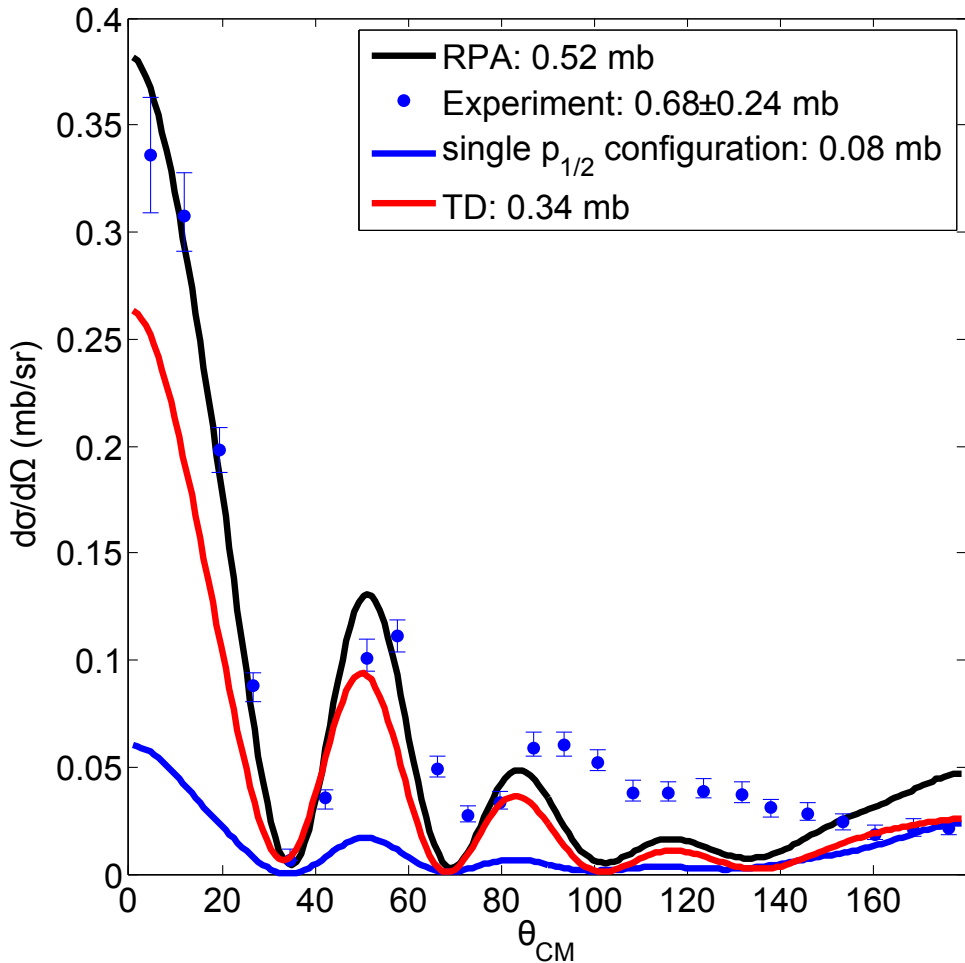


Figure 3.A.4: Absolute two–nucleon transfer differential cross section associated with the  $^{206}\text{Pb}(t, p)^{208}\text{Pb}(\text{gs})$  transfer reaction, that is, the annihilation of the pair removal mode of  $^{208}\text{Pb}$  in comparison with the data (Bjerregaard, J. H. et al. (1966)). The theoretical cross sections were calculated making use of the spectroscopic amplitudes given in Tables 2.E.2 and 2.E.3 and of global optical parameters as reported in the reference above. Both RPA and TD amplitudes were used as well as a pure configuration  $p_{1/2}^2(0)$ .

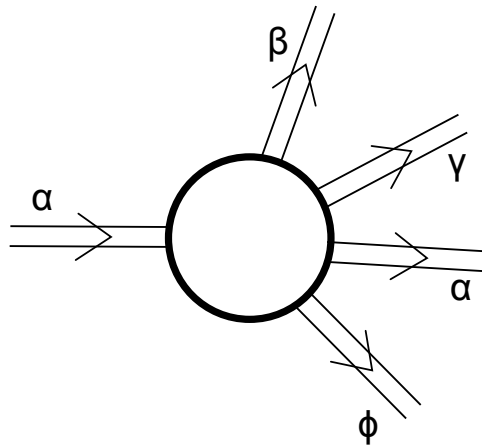


Figure 3.B.1: Schematic representation of entrance ( $\alpha$ ) and exit channels ( $\beta, \gamma, \alpha, \phi$ ) of a nuclear reaction and of the interaction region.

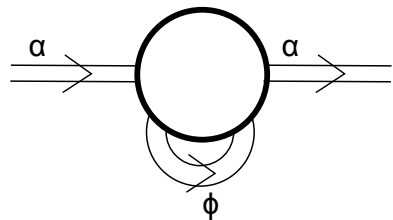


Figure 3.B.2: Schematic representation of the change in role of the one-nucleon transfer channel  $\phi$  from being an open channel, (Fig. 3.B.1) to one which acts as a virtual channel contributing to the optical potential.

the calculation of two-particle transfer (2nd order process), and can be carried out with essentially the same tools. In fact,

$$\begin{aligned} T_{succ}^{(2)} &\sim \langle fin|v|int\rangle\langle int|v|in\rangle \\ T_{NO}^{(2)} &\sim \langle fin|v|int\rangle\langle int|\mathbf{1}|in\rangle, \end{aligned} \quad (3.B.1)$$

where  $|in\rangle = |a, A\rangle$ ,  $|int\rangle = |f, F\rangle$  and  $|fin\rangle = |b, B\rangle$  are the initial, intermediate, and final channels in a two-nucleon transfer reactions, which become

$$\begin{aligned} \langle in|v|int\rangle\langle int|v|in\rangle \\ \langle in|v|int\rangle\langle int|\mathbf{1}|in\rangle, \end{aligned} \quad (3.B.2)$$

as contributions to the optical potential (Fig. 3.B.2).

Let us elaborate on the above arguments within the context, for concreteness, of  $^{11}\text{Li}$  and of the reaction  $^{11}\text{Li}(p, t)^9\text{Li}$ . In keeping with the fact that structure and reactions are just but two aspects of the same physics and that in the study of light halo nuclei, continuum states are to be treated on, essentially, equal footing in the calculation of the wavefunctions describing bound states (structure) as well as of the asymptotic distorted waves entering in the calculation of the absolute two-particle transfer differential cross sections (reaction; see Figs. 3.B.3 (a) and (b), the calculation of the optical potentials is essentially within reach (reaction, see Figs. 3.B.3 (c) and 3.B.4). Because the real and imaginary parts of complex functions are related by simple dispersion relations (see, e.g., Mahaux, C. et al. (1985) and references therein) it is sufficient to calculate only one of the two (real or imaginary) components of the self-energy function to obtain the full scattering, complex, nuclear dielectric function (optical potentials). Now, absorption is controlled by on-the-energy-shell contributions. Within this scenario it is likely that the simplest way to proceed is that of calculating the absorptive potential and then obtain the real part by dispersion. Of notice that in heavy-ion reactions, one is dealing with leptodermous systems. Thus, the real part of the optical potential can, in principle, be obtained by convolution of the nuclear densities and of the surface tension (cf. Broglia and Winther (2005) and references therein). Within the present context, one can mention the ambiguities encountered in trying to properly define a parentage coefficient relating the system of  $(A + 1)$  nucleons to the system of  $A$

---

tion (recoil effect) which smoothly matches the incoming with the outgoing waves (trajectories). Now, within the present context, namely that of the microscopic calculation of  $U + iW$ , non-locality and  $\omega$ -dependence can be microscopically treated on equal footing through the calculation of structure properties. In particular, within the framework of NFT, taking into account the variety of correlations and couplings between single-particle and collective motion, elementary modes of nuclear excitation. Such an approach to structure and reaction provides the elements and rules for an *ab initio* calculations of the texture of the corresponding vacuum states, and thus of the bound and continuum properties of the nuclear quantal system by itself and in interaction. It is of notice that such a scenario includes also limiting situations like sub-barrier fusion processes (cf. e.g. Sargsyan, V. V. et al. (2013) and refs. therein) and also exotic decay (cf. e.g. Barranco, F. et al. (1988, 1990); Montanari et al. (2014), cf. also Brink, D. and Broglia (2005)), and eventually compound nucleus formation.

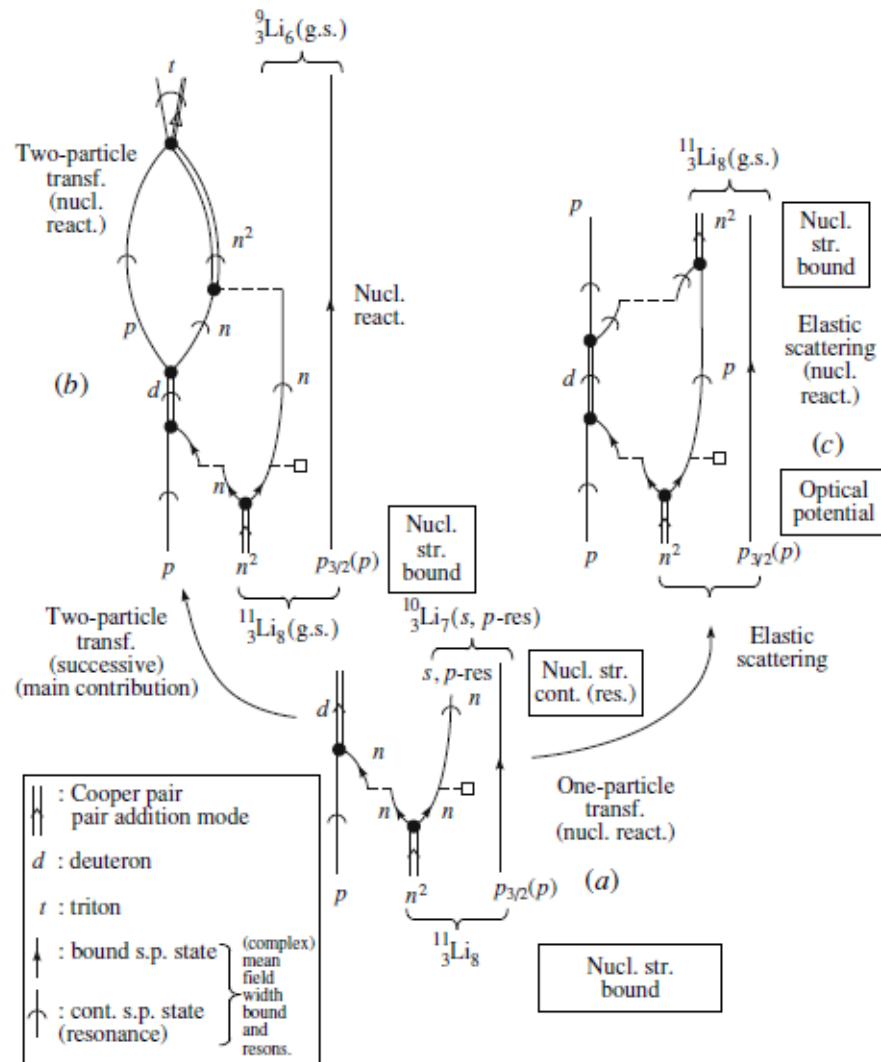


Figure 3.B.3: NFT diagrams summarizing the physics which is at the basis of the structure of  $^{11}\text{Li}$  (Barranco, F. et al. (2001)) and of the analysis of the  $^{11}\text{Li}(p, t)^9\text{Li}(\text{g.s.})$  reaction (Potel et al. (2010)). In the figure emphasis is set on intermediate (like, e.g.,  $^{10}\text{Li} + d$ , see (a) and (b)) and elastic (see (c), see also Fig. 3.B.4) channels.

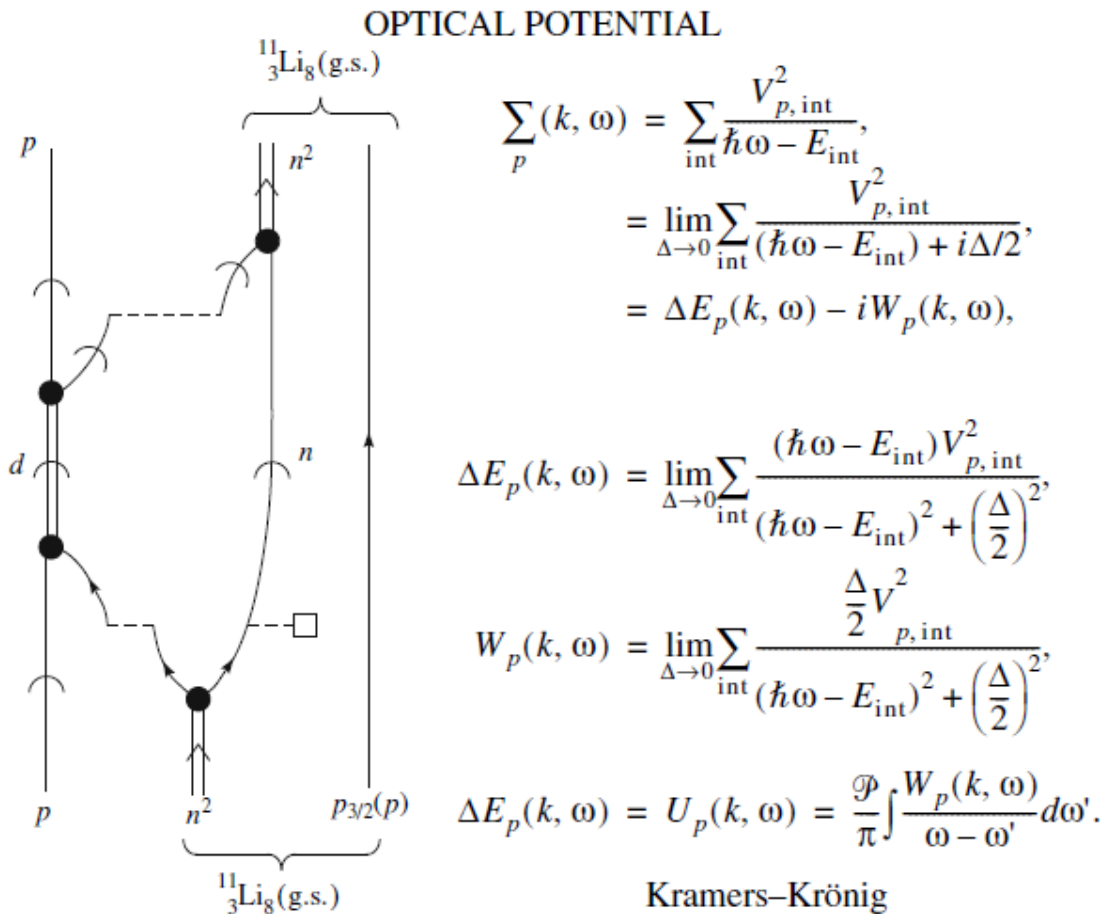


Figure 3.B.4: NFT diagrams and summary of the expression (see, e.g., Mahaux, C. et al. (1985) and references therein) entering the calculation of one of the contributions (that associated with one-particle transfer and, arguably, the dominant one) to the  $^{11}_3\text{Li} + p$  elastic channel optical potential. The self-energy function is denoted  $\Sigma_p$ , while the real and imaginary parts are denoted  $\Delta E_p (= U_p)$  and  $W_p$ , respectively, the subindex  $p$  indicating the incoming proton. These quantities are, in principle, functions of frequency and momentum.

nucleons, and thus a spectroscopic amplitude. In other words, a prefactor which allows to express the absolute one-particle transfer differential cross section in terms of the elastic cross section. Making use of NFT diagrams like the one shown in Fig. 3.B.4 , it is possible to calculate, one at a time, the variety of contributions leading to one- and two-particle transfer processes as well as of the associated optical potential. Summing up the different contributions, taking also proper care of those arising from four-point vertex, tadpole processes, etc., a consistent description of the different channels can be worked out, in which the predicted quantities to be directly compared with observables are absolute differential cross sections, or, more generally, absolute values of strength functions for different scattering angles.

## Appendix 3.C Weak link between superconductors

In this appendix we essentially reproduce the description of the tunneling of Cooper pairs between two weakly coupled superconductors to be found in Anderson (1964), arguably, the best physical presentation of the Josephson effect (Josephson (1962)).

One starts with the many-body Hamiltonian of Cohen et al. (1962)

$$H = H_1 + H_2 + \sum_{kq} T_{kq} (a_{k\uparrow}^\dagger a_{k\uparrow} + a_{-q\downarrow}^\dagger a_{-q\downarrow}) + HC \quad (3.C.1)$$

where  $H_1$  and  $H_2$  are the separate Hamiltonian of the two superconductors on each side of the barrier,  $T_{kq}$  being the (exponentially) small tunneling matrix element from state  $k$  on one side to  $q$  on the other.

One can arrive to (3.C.1) by first finding sets of single-particle wavefunctions for each side separately, in the absence of the potential of the other system. Then one eliminates the non-orthogonality effects by perturbation theory. It is of notice that a nuclear embodiment of such strategy but for the case superfluid-normal<sup>4</sup> tunneling is discussed in App. 3.A as well as App. 5.A and implemented in COOPER (cf. App. 6.D; cf. also Broglia and Winther (2005)).

Let us now calculate the second order expression of (3.C.1) in the case in which the gaps of the two weakly linked superconductors are different. Making use of relations presented in Sect. 2.D.2 one can write for  $T = 0$ ,

$$\Delta E_2 = -2 \sum_{kq} |T_{kq}|^2 \frac{|V_k U_q + V_q U_k|^2}{E_k + E_q}. \quad (3.C.2)$$

---

<sup>4</sup>Within this context it is of notice that at the level of single Cooper pair transfer, the nuclear and the condensed matter expressions are very similar. Of course no supercurrent is expected between nuclei. However, the systems <sup>120</sup>Sn(gs), <sup>119</sup>Sn(j), <sup>118</sup>Sn(gs) form an ensemble of weakly coupled Fermi superfluids, with different (average) number of particles ( $N, N-1, N-2$ ), to which essentially all the BCS techniques, including those of the present Appendix can be applied (cf. Fig. 3.D.1). Of notice the parallel of this scenario with that associated with nuclei excited rather high energies for which one defines a temperature. This is possible, because the excited (thermalized) nucleus is in equilibrium with the particles, namely neutrons and *gamma*-rays it emits, particles which act as a thermal bath, let alone the very high density of levels, of the compound nucleus (cf. Bertsch and Broglia (2005) p 171).

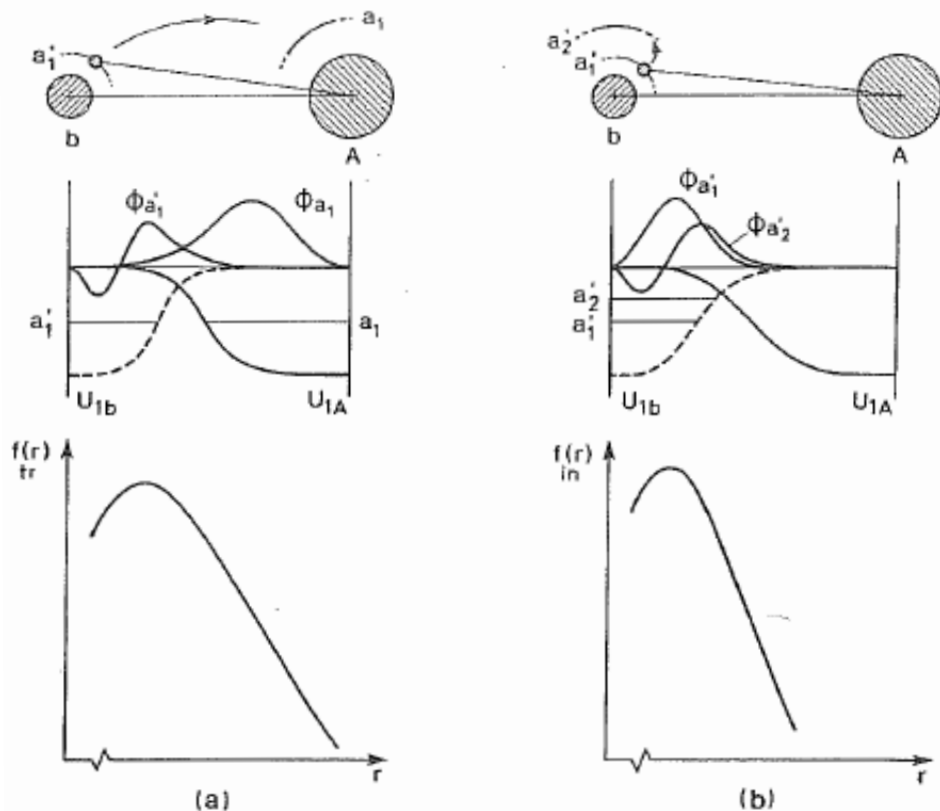


Figure 3.B.5: Schematic representation of the radial dependence of the one-particle transfer and inelastic form factors. In (a) a nucleon moving in the orbital with quantum numbers  $a'_1$  in the projectile  $a$  is transferred under the action  $f$  the shell model potential  $U_{1A}$  to the target nucleus  $A$  into an orbital  $a_1$ . The dependence of the form factor on the distance between the two nuclei is determined by the overlap of the product of the single-particle wavefunctions  $\phi_{a'_1}$  and  $\phi_{a_1}$  with the potential  $U_{1A}$ . A schematic representation of this dependence is given at the bottom of target field (a). In (b) a nucleon in the projectile  $a$  is excited under the influence of the target field  $U_{1A}$  from the single-particle orbital with quantum numbers  $a'_1$  to the orbital with quantum numbers  $a'_2$ . The dependence of the form factor on the distance between the cores is here determined by the overlap of the product of the functions  $\phi_{a'_1}$  and  $\phi_{a'_2}$  with the potential  $U_{1A}$ . A representation of this dependence is shown at the bottom of (b) (after Broglia and Winther (2005)).

With the help of

$$2U_k V_k^* = \frac{\Delta_k}{E_k}, \quad 2U_q V_q^* = \frac{\Delta_q}{E_q}, \quad (3.C.3)$$

and

$$|U_k|^2 - |V_k|^2 = \frac{\epsilon_k}{E_k}, \quad |U_q|^2 - |V_q|^2 = \frac{\epsilon_q}{E_q}, \quad (3.C.4)$$

where

$$E = \sqrt{\epsilon^2 + \Delta^2} \quad (3.C.5)$$

and

$$\Delta_k = \Delta_1 e^{i\phi_1}, \quad \Delta_q = \Delta_2 e^{i\phi_2} \quad (3.C.6)$$

one can write for the numerator of Eq. (3.C.2),

$$\begin{aligned} NUM &= (V_k U_q + V_q U_k)(V_k^* U_q^* + V_q^* U_k^*) \\ &= \{V_k^2 U_q^2 + V_q^2 U_k^2\} + [(U_k^* V_k)(U_q V_q^*) + (U_q^* V_q)(U_k V_k^*)]. \end{aligned} \quad (3.C.7)$$

It is of notice that, for simplicity, throughout this Appendix

$$V^2 \equiv |V|^2. \quad (3.C.8)$$

With the help of (3.C.3) the expression in the squared bracket in (3.C.7) can be written as

$$[ ] = \frac{1}{4E_k E_q} (\Delta_k^* \Delta_q + (\Delta_k^* \Delta_q)^*) = \frac{1}{4E_k E_q} 2\Re(\Delta_k^* \Delta_q). \quad (3.C.9)$$

Making use of the relations

$$\begin{aligned} (U_k^2 - V_k^2)(U_q^2 - V_q^2) &= U_k^2 U_q^2 - U_k^2 V_q^2 - V_k^2 U_q^2 + V_k^2 V_q^2 \\ &= -(U_k^2 V_q^2 + V_k^2 U_q^2) + (U_k^2 U_q^2 + V_k^2 V_q^2), \end{aligned} \quad (3.C.10)$$

and

$$\begin{aligned} 1 &= (U_k^2 + V_k^2)(U_q^2 + V_q^2) = U_k^2 U_q^2 + U_k^2 V_q^2 + V_k^2 U_q^2 + V_k^2 V_q^2 \\ &= (U_k^2 V_q^2 + V_k^2 U_q^2) + (U_k^2 U_q^2 + V_k^2 V_q^2), \end{aligned} \quad (3.C.11)$$

one obtains,

$$1 - (U_k^2 - V_k^2)(U_q^2 - V_q^2) = 2(U_k^2 V_q^2 + V_k^2 U_q^2), \quad (3.C.12)$$

that is, twice the expression written in curly brackets in (3.C.7). Consequently

$$\{ \} = \frac{1}{2} (1 - (U_k^2 - V_k^2)(U_q^2 - V_q^2)) = \frac{1}{2} \left( 1 - \frac{\epsilon_k \epsilon_q}{E_k E_q} \right). \quad (3.C.13)$$

Thus, the sum of (3.C.9) and (3.C.13) leads to,

$$NUM = \frac{1}{2} \left( 1 - \frac{\epsilon_k \epsilon_q}{E_k E_q} + \frac{\Re(\Delta_q^* \Delta_k)}{E_k E_q} \right) \quad (3.C.14)$$

and

$$\Delta E_2 = - \sum_{kq} \frac{|T_{kq}|^2}{E_k + E_q} \left( 1 - \frac{\epsilon_k \epsilon_q}{E_k E_q} + \frac{\Re(\Delta_q^* \Delta_k)}{E_k E_q} \right). \quad (3.C.15)$$

With the help of (3.C.6) one can write

$$\Delta_k \Delta_q^* = \Delta_1 \Delta_2 e^{i(\phi_1 - \phi_2)} = \Delta_1 \Delta_2 (\cos(\phi_1 - \phi_2) + i \sin(\phi_1 - \phi_2)). \quad (3.C.16)$$

Thus

$$\Re \Delta_k \Delta_q^* = \Delta_1 \Delta_2 \cos(\phi_1 - \phi_2), \quad (3.C.17)$$

where  $\Re$  stands for real part. Making use of

$$\sum_k \rightarrow N_1 \int d\epsilon_1, \quad \sum_q \rightarrow N_2 \int d\epsilon_2 \quad (3.C.18)$$

where  $N_1$  and  $N_2$  are the density of levels of one spin at the Fermi energy one finally obtains

$$\begin{aligned} \Delta E_2 &\approx -N_1 N_2 \Delta_1 \Delta_2 \langle |T_{kq}|^2 \rangle \cos(\phi_1 - \phi_2) \int_{-\infty}^{\infty} \int_{-\infty}^{\infty} \frac{d\epsilon_1 d\epsilon_2}{E_1 E_2 (E_1 + E_2)} \\ &\approx -N_1 N_2 \langle |T_{kq}|^2 \rangle \cos(\phi_1 - \phi_2) 2\pi^2 \frac{\Delta_1 \Delta_2}{\Delta_1 + \Delta_2} \end{aligned} \quad (3.C.19)$$

Consequently, the maximum possible supercurrent is the same as the normal current at a voltage  $V_{equiv}$  equal to  $\pi \Delta_1 \Delta_2 / (\Delta_1 + \Delta_2)$ .

## Appendix 3.D Phase coherence

The phase of a wavefunction and the number of nucleons (electrons in condensed matter) are conjugate variables: gauge invariance, i.e. invariance under phase changes, implies number conservation in the same way that rotational invariance implies angular momentum conservation.

Example:

$$\Psi = a_1^\dagger a_2^\dagger \cdots a_N^\dagger \Psi_{vac}.$$

Multiply the creation operators by a phase factor,

$$a'^\dagger = e^{-i\phi} a^\dagger,$$

one can rewrite

$$\begin{aligned}\Psi &= (e^{i\phi} a_1'^\dagger)(e^{i\phi} a_2'^\dagger) \cdots (e^{i\phi} a_N'^\dagger) \Psi_{vac} \\ &= e^{iN\phi} \Psi'.\end{aligned}$$

Thus

$$-i \frac{\partial}{\partial \phi} \Phi = N e^{iN\phi} \Psi' = \Psi,$$

where

$$N = -i \frac{\partial}{\partial \phi}; \quad \phi = i \frac{\partial}{\partial N}$$

and

$$[\phi, N] = 1 \quad \Delta\phi \Delta N = 1$$

In this case  $\Psi$  (wavefunction referred to laboratory system) and  $\Psi'$  (wavefunction referred to intrinsic system) represent the same state. A phase change for a gauge invariant function is just a trivial operation. Like to rotate a rotational invariant function. Quantum mechanically nothing happens rotating a spherical system (in 3D-, gauge, etc.) space.

The situation is very different in the case of the wavefunction

$$\begin{aligned}|BCS(\phi)\rangle_{\mathcal{K}} &= \prod_{\nu>0} (U_\nu + V_\nu a_\nu^\dagger a_{\bar{\nu}}^\dagger) |0\rangle, \\ &= \prod_{\nu>0} (U_\nu + e^{2i\phi} V_\nu a_\nu'^\dagger a_{\bar{\nu}}'^\dagger) |0\rangle, \\ &= \prod_{\nu>0} (U'_\nu + V'_\nu a_\nu'^\dagger a_{\bar{\nu}}'^\dagger) |0\rangle, \\ &= |BCS(\phi=0)\rangle_{\mathcal{K}'},\end{aligned}$$

where

$$U_\nu = |U_\nu| = U'_\nu; \quad V_\nu = e^{2i\phi} V'_\nu (V'_\nu = |V_\nu|),$$

and

$$|BCS(\phi)\rangle_{\mathcal{K}} = \left( \prod_{\nu>0} U_\nu \right) \sum_{n=0,1,2}^{N_0/2} e^{i2n\phi} \left( \sum_{\nu>0}^{N/2} \frac{c_\nu}{\sqrt{n}} P_\nu'^\dagger \right)^n |0\rangle,$$

with

$$c_\nu = \frac{V_\nu}{U_\nu}; \quad n : \# \text{ of pairs}; \quad P'_\nu^\dagger = a'_\nu a'_{\bar{\nu}},$$

is a wavepacket in particle number,

$$\begin{aligned} |BCS(\phi)\rangle_{\mathcal{K}} &= \left( \prod_{\nu>0} U_\nu \right) \sum_n e^{i2n\phi} |2n\rangle, \\ &= \left( \prod_{\nu>0} U_\nu \right) \sum_n e^{i2n\phi} |N\rangle. \end{aligned} \quad (3.D.1)$$

Let us now apply the gauge angle operator

$$\begin{aligned} \hat{\phi}|BCS(\phi)\rangle_{\mathcal{K}} &= i \frac{\partial}{\partial N} |BCS(\phi)\rangle_{\mathcal{K}} \\ &= -\phi \left( \prod_{\nu>0} U_\nu \right) \sum_n e^{i2n\phi} |N\rangle = -\phi|BCS(\phi)\rangle_{\mathcal{K}}. \end{aligned}$$

Thus the state  $|BCS(\phi)\rangle_{\mathcal{K}} = |BCS(\phi = 0)\rangle_{\mathcal{K}'}$  is rigidly aligned in gauge space in which it defines a privileged orientation ( $z'$ ).

An isolated nucleus will not remain long in this product type state. Due to the term  $(G/4) \left( \sum_{\nu>0} (U_\nu^2 + V_\nu^2) (\Gamma_\nu^\dagger - \Gamma_\nu) \right)^2$  in the residual quasiparticle Hamiltonian it will fluctuate, (QM ZPF Goldstone mode) it will decay in a state

$$|N\rangle \sim \int d\phi e^{iN\phi} |BCS(\phi)\rangle_{\mathcal{K}}, \quad (3.D.2)$$

member of a pairing rotational band around neutron mass number  $N$ : for example the ground states of the Sn-isotopes around  $N_0 = 68$  (see Fig. 2.1.3). Because  $E_R = (\hbar^2/2I)(N - N_0)^2 = (G/4)(N - N_0)^2 = G/4(\frac{1}{\delta\phi})^2$  is the kinetic energy of rotation in (nuclear) gauge space, and  $G/4 \approx 25/(4N_0) \approx 0.0092$  MeV, the wavepacket (3.D.1) will decay<sup>5</sup> in the state (3.D.2) in a time of the order of  $\hbar/E_R \approx \hbar/(4 \times 0.0092 \text{ MeV}) (N = N_0 \pm 2) \approx 10^{-19} \text{ sec}$ . In other words, superfluid nuclei cannot be prepared, in isolation, in states with coherent superposition of different  $N$ -values. The common assumption that  $N$  is fixed,  $\phi$  meaningless is

---

<sup>5</sup>Within this context note that setting in phase at  $t = 0$  all the states in which a GDR breaks down through the hierarchy of doorway-states-coupling, they would dissipate like a wavepacket of free particles after  $10^{-22}$  sec (assuming  $\Gamma_{GDR} \approx 3 - 4$  MeV). It is of notice that the GDR will eventually branch into the ground state, although  $\Gamma_\gamma \ll \Gamma_{GDR}$ , in keeping with the fact that the  $t = 0$  phase coherent states are individually stationary. What is not stationary is its phase coherence. Pushing the analogy a step further, one can say that in quantum mechanics, while the outcome of an experiment is probabilistic the associated probability evolve in a deterministic way (?). This is the reason why a large gamma ray detector will reveal a well defined peak of the resonant state long after its (damping width) lifetime deadline ( $\hbar/\Gamma$ ) also, that one can obtain a completely (classical) picture of a face making use of single photons if one waits long enough.

correct. This is also the case for real superconductors. In fact, the corresponding state (3.D.1) even if prepared in isolation would dissipate because there is actually a term in the energy of the superconductor depending on  $N$ , namely the electrostatic energy  $e(N - N_0)^2/2C = e^2/2C(\partial/\partial\phi)^2$ , where  $C$  is the electrostatic capacity. The system will dissipate, no matter how small  $\delta\phi$  is. In fact, let us assume  $\delta\phi = 1$  degree ( $= \pi/180 = 0.017$ ). The kinetic energy of rotation in gauge space is  $\sim (e^2/2C)(1/\delta)^2(\delta N\delta\phi/2\pi \sim 1)$ , and

$$\Delta E = \frac{1.44 \text{ fm MeV}}{1 \text{ cm } (1^\circ)^2} \sim 1.44 \times 10^{-13} \text{ MeV}, \quad (3.D.3)$$

which corresponds to an interval of time

$$\Delta t \approx \frac{\hbar}{1 \text{ MeV}} \frac{10^{13}}{1.44} \approx \frac{0.667 \times 10^{-21} \text{ sec}}{1.44} \times 10^{13} \approx 10^{-9} \text{ sec.} \quad (3.D.4)$$

The opposite situation is the case when one consider different parts of the same superconductor. In this case one can define relative variables  $n = N_1 - N_2$  and  $\phi = \phi_1 - \phi_2$  and again  $n = -i\partial/\partial\phi$  and  $\phi = i\partial/\partial n$ . Thus, locally there is a superposition of different  $n$  states:  $\phi$  is fixed so  $n$  is uncertain. It is clear that there must be a dividing line between these two behaviors, perfect phase coherence and negligible coherence, namely the Josephson effect.

In the nuclear case, one can view the systems  $|BCS(A+2)\rangle$  and  $|BCS(A)\rangle$  as parts of a fermion superfluid (superconductor) which, in presence of a proton ( $p + (A+2)$ ) are in weak contact to each other, the  $d + |BCS(A+1)\rangle$  system (without scattering, running waves, but as a closed, virtual, channel) acting as the dioxide layer of a Josephson junction.

Clearly, again, the total phase of the assembly is not physical. However the relative phases can be given a meaning when one observes, as one does in e.g. metallic superconductors, that electrons can pass back and forth through the barrier, leading to the possibility of coherence between states in which the total number of electrons is not fixed *locally*. Under such conditions, there is for instance, a coherence between the state with  $N/2$  electrons in one half of the block and  $N/2$  in the other, and that with  $(N/2) + 2$  on one side side and  $(N/2) - 2$  on the other.

Under favorable conditions, in particular of  $Q$ -values for the different channels involved, and similarly to the so called backwards rise effect, one may, arguably, observe signals of the coherence between systems  $(A+2)$  and  $A$  in the elastic scattering process  ${}^{A+2}X + p \rightarrow {}^{A+2}X + p$ ,  ${}^{A+2}X$  denoting a member of a pairing rotational band (cf. Fig. 3.D.1, see also Fig 2.1.3). It is of notice that the process  ${}^{A+2}X + p \rightarrow {}^{A+1}X + d \rightarrow {}^{A+2}X + p$  is likely to be the dominant one concerning the optical potential describing the  ${}^{A+2}X + p$  scattering process. Because  $P_2 \approx P_1$ , a likely better estimate of  $U + iW$  can be obtained taking into account also the transfer back and forth of two nucleons. In keeping with the fact that the sum of the simultaneous and on-orthogonality contributions are much smaller than the successive transfer, only this last process is shown in the NFT reaction-structure diagram displayed in Fig. 3.D.1 Whether an effect which may parallel that shown

in (c) (backwards rise) can be seen or not depends on a number of factors, but very likely is expected to be a weak effect. This was also true in the case of the Josephson effect in its varied versions (AC, DC, etc.). In fact, its observation required to take into account the effect of the earth magnetic field, let alone quantal and thermal fluctuations.

## Appendix 3.E Medium polarization effects and pairing

### 3.E.1 Nuclei

### 3.E.2 Metals

## Appendix 3.F Hindsight

The formulation of superconductivity (BCS theory) described in Gor'kov, L.P. (1959) allows, among other things for a simple visualization of spatial dependences. In this formulation  $F(\mathbf{x}, \mathbf{x}')$  is the amplitude for two Fermions (electrons) at  $\mathbf{x}, \mathbf{x}'$ , to belong to the Cooper pair (within the framework of nuclear physics cf. e.g. Fig. 2.F.3  $\Psi_0(\mathbf{r}_1, \mathbf{r}_2)$ ). The phase of  $F$  is closely related to the angular orientation of the spin variable in Anderson's quasiparticle formulation of BCS theory (Anderson (1958); within the framework of nuclear physics cf. e.g. Bohr and Ulfbeck (1988), Potel, G. et al. (2013b) and references therein). The gap function  $\Delta(x)$  is given by  $V(\mathbf{x})F(\mathbf{x}, \mathbf{x})$  where  $V(\mathbf{x})$  is the local two-body interaction at the point  $\mathbf{x}$ . In the insulating barrier between the two superconductors of a Josephson junction,  $V(\mathbf{x})$  is zero and thus  $\Delta(x)$  is also zero.

The crucial point is that vanishing  $\Delta(x)$  does not imply vanishing  $F$ . On the contrary,  $F(\mathbf{x}, \mathbf{x}')$  can have large amplitude for electron separated by distances  $|\mathbf{x} - \mathbf{x}'|$  up to the coherence length. Hence, for barriers thin compared with that length, two electrons on opposite sides of the barrier can still be correlated and the pair current can be consistent. An evaluation of its value shows that, at zero temperature, the pair current is equal to the single particle current at an equivalent voltage  $\pi\Delta/2e$  (Ambegaokar and Baratoff (1963)).

The translation of the above parlance to the language of nuclear physics has to come to terms with the basic fact that these objects are strongly interacting, finite many-body systems (self bound drops of pairing correlated nuclear matter<sup>6</sup>). Under the influence of the associated mean field acting as a very strong external field ( $|V_0| \approx 50$  MeV), Cooper pairs ( $E_{corr} \approx 1 - 2$  MeV) will become constrained

---

<sup>6</sup>Within this context a very successful nuclear model, able to accurately describe not only large amplitude motion (fission, exotic decay, low-lying collective density and surface vibrations, cf. e.g. Bohr and Wheeler (1939), Barranco, F. et al. (1990), Bertsch (1988), see also Brink, D. and Broglia (2005) and references therein), but also the masses of nuclides (cf. e.g. Moller and Nix), provided the superfluid inertia and shell corrections respectively, are properly considered. Within this context it is an open question whether in the quest of developing more predictive theoretical tools of the global nuclear properties one should develop ever more "accurate" zero range (Skyrme-like) forces, or deal with the long wavelength, renormalization effects and induced interaction.

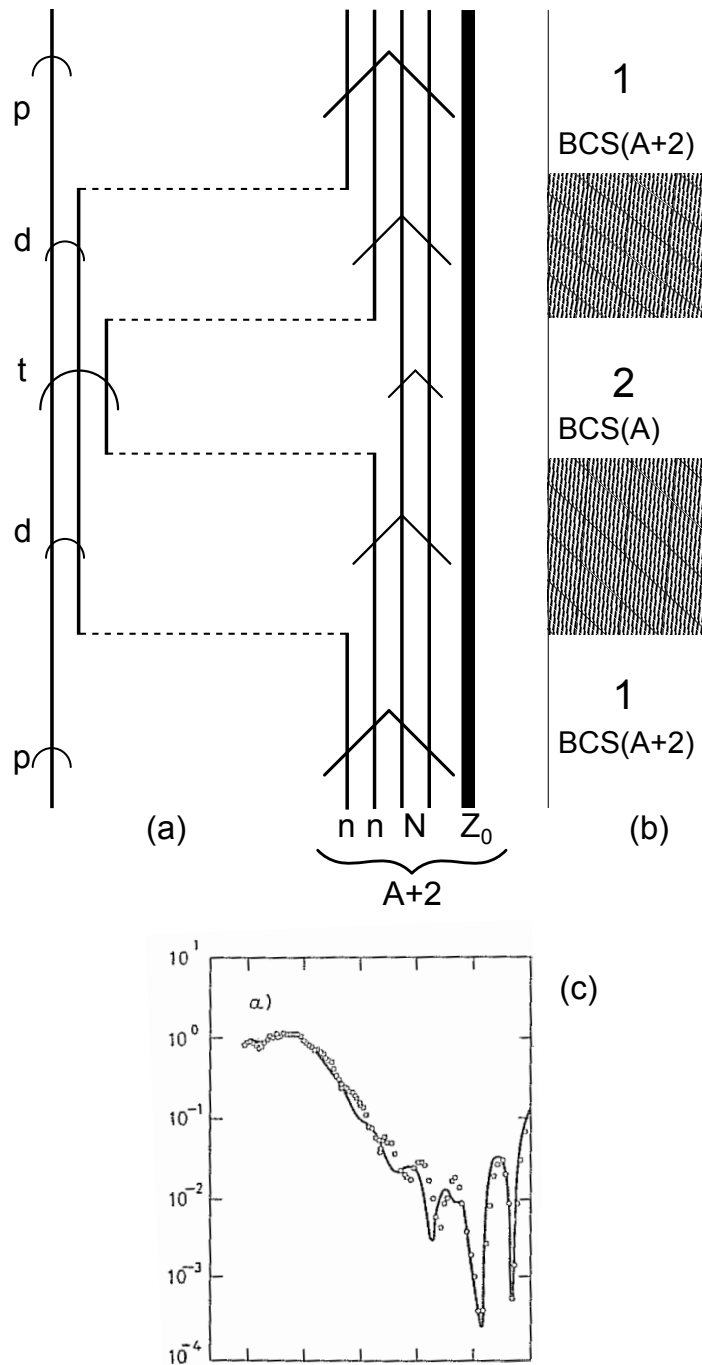


Figure 3.D.1: Gedanken experiment concerning the possibility of observing weak coupling coherence phenomena between states  $|\text{BCS}(A + 2)\rangle$  and  $|\text{BCS}(A)\rangle$  in an elastic reaction involving superfluid nuclei (a), e.g.  $p + ^{120}\text{Sn} \rightarrow p + ^{120}\text{Sn}$ , the system  $^{119}\text{Sn} + d$  acting as a dynamical barrier between the two even  $N$  superfluid systems arising from the successive transfer of two nucleons (b) and eventually allowing for a time dependent gauge phase difference between the  $(A + 2)$  and  $A$  superfluid systems, thus leading, in the case in which  $Q$ -value effects are appropriate, to an oscillating enhancement of the elastic cross section at large angles as observed for quite different reasons in the case of the elastic angular distribution of the reaction  $^{16}\text{O} + ^{28}\text{Si}$  (c) (cf. Pollarolo and Broglia (1984)).

within its boundaries which e.g. in the case of  $^{120}\text{Sn}$  is  $R_0 \approx 6 \text{ fm}$  ( $\ll \xi \approx 30 \text{ fm}$ ). This will be also the case in a Sn+Sn reaction, corresponding e.g. to a distance of closest approach of  $\approx 14 \text{ fm}$  in which the two nuclear surfaces are separated by  $\approx 2 \text{ fm}$  (cf. Fig 3.A.1).

The pair field associated with a Cooper pair, will extend into the empty region between the two nuclei allowing nucleons, eventually at distances as large as 26 fm from each other to correlate and, eventually in a reaction like  $\text{Sn}+\text{Sn} \rightarrow \text{Sn(gs)}+\text{Sn(gs)}$  allow for transfer of two nucleons distant from each other by tens of fm. This is in keeping with the fact that  $a'_0(\alpha_{dyn})$  (see Fig. 3.3.2) can be different from zero, also in regions in which the nuclear pairing interaction vanishes. An example of the fact that Cooper pairs will “expand” if the external mean field is weakened, is provided by  $^{11}\text{Li}$  in which case, profiting of the weak binding ( $\approx 380 \text{ keV}$ ), the extension of the constrained Cooper pair ( $\approx 4.55 \text{ fm} \pm 0.3 \text{ fm}$ ) is similar to a nucleus of mass number  $A \approx 60$ , assuming a standard radial behavior, i.e.  $r_0 A^{1/3} \text{ fm}$  (cf. Fig. 3.F.1). In fact moving from one neutron pair addition  $0^+$  mode of the  $N = 6$  isotones to another one ( $|^{11}\text{Li(gs)}\rangle$ ,  $|^{12}\text{Be(gs)}\rangle$  and  $|^{12}\text{Be}(0^{+*}; 2.24 \text{ MeV})\rangle$ ) one would see it expanding, contracting and expanding again, respectively, in keeping with the fact that the external (mean) field is weak, strong, weak respectively, as testified by  $S_{2n}$  ( $0.380 \text{ MeV}, \dots \text{ MeV}, \dots \text{ MeV}$ ). Furthermore, and physically more relevant, is the fact that the dipole state built on top of them is expected to vary in energy from low ( $0.6 \text{ MeV}$ ) to high ( $\dots \text{ MeV}$ ) to low ( $\dots \text{ MeV}$ ).

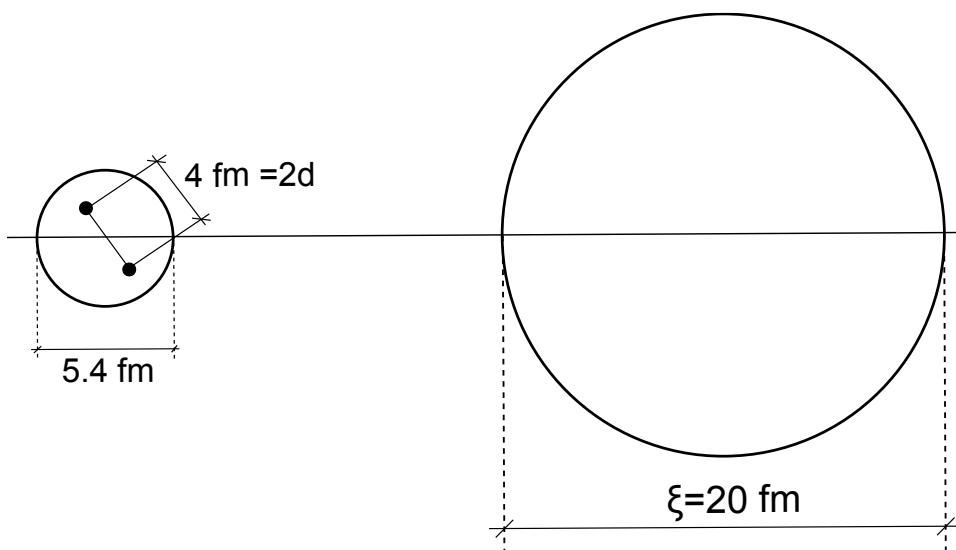


Figure 3.F.1: Schematic representation of the  $^{11}\text{Li}$  nuclear radius and of the associated halo Cooper pair field. Twice the radius of  $^{11}\text{Li}$  should be, according to systematics, given by  $2R_0(^{11}\text{Li})=2\times(1.2\times 11^{1/3})=5.4\text{ fm}$ . The average distance between nucleons is  $2\times d$ , where  $d$  is the Wigner-Seitz radius  $d=\left((4\pi/3)R_0^3/A\right)^{1/3}=(4\pi/3)^{1/3}R_0\approx 2\text{ fm}$ .

## Bibliography

- V. Ambegaokar and A. Baratoff. Tunneling between superconductors. *Phys. Rev. Lett.*, 10:486, 1963.
- P. W. Anderson. New method in the theory of superconductivity. *Phys. Rev.*, 110: 985, 1958.
- P. W. Anderson. *The Many-Body Problem, Vol.2.* Academic Press, New York, 1964.
- J. Bardeen. Tunnelling from a many-particle point of view. *Phys. Rev. Lett.*, 6:57, 1961.
- J. Bardeen. Tunneling into superconductors. *Physical Review Letters*, 9:147, 1962.
- Barranco, F., R. A. Broglia, and G. F. Bertsch. Exotic radioactivity as a superfluid tunneling phenomenon. *Phys. Rev. Lett.*, 60:507, 1988.
- Barranco, F., G. Bertsch, R. Broglia, and E. Vigezzi. Large-amplitude motion in superfluid fermi droplets. *Nuclear Physics A*, 512:253, 1990.
- Barranco, F., P. F. Bortignon, R. A. Broglia, G. Colò, and E. Vigezzi. The halo of the exotic nucleus  $^{11}\text{Li}$ : a single Cooper pair. *Europ. Phys. J. A*, 11:385, 2001.
- Bayman, B. F. and C. F. Clement. Sum rules for two-nucleon transfer reactions. *Phys. Rev. Lett.*, 29:1020, 1972.
- G. Bertsch. In R. Broglia and J. R. Schrieffer, editors, *International School of Physics “Enrico Fermi” Collective motion in Fermi droplets*, page 41, Amsterdam, 1988. North Holland.
- G. Bertsch and R. Broglia. *Oscillations in Finite Quantum Systems*. Cambridge University Press, Cambridge, 2005.
- Bertsch, G. F., R. A. Broglia, and C. Riedel. Qualitative description of nuclear collectivity. *Nucl. Phys. A*, 91:123, 1967.
- Bjerregaard, J. H., O. Hansen, Nathan, and S. Hinds. States of  $^{208}\text{Pb}$  from double triton stripping. *Nucl. Phys.*, 89:337, 1966.
- A. Bohr and B. R. Mottelson. *Nuclear Structure, Vol.I*. Benjamin, New York, 1969.
- A. Bohr and O. Ulfbeck. Quantal structure of superconductivity gauge angle. In *First Topsøe summer School on Superconductivity and Workshop on Superconductors*, Roskilde, Denmark Riso/M/2756, 1988.
- N. Bohr and J. A. Wheeler. The mechanism of nuclear fission. *Phys. Rev.*, 56:426, 1939.

- Brink, D. and R. A. Broglia. *Nuclear Superfluidity*. Cambridge University Press, Cambridge, 2005.
- R. Broglia and A. Winther. *Heavy Ion Reactions*, 2nd ed. Westview Press, Perseus Books, Boulder, 2005.
- R. Broglia, G. Coló, G. Onida, and H. Roman. *Solid State Physics of Finite Systems: metal clusters, fullerenes, atomic wires*. Springer Verlag, Berlin, Heidelberg, 2004.
- Broglia, R. A., C. Riedel, and T. Udagawa. Sum rules and two-particle units in the analysis of two-neutron transfer reactions. *Nuclear Physics A*, 184:23, 1972.
- Broglia, R.A., O. Hansen, and C. Riedel. Two-neutron transfer reactions and the pairing model. *Advances in Nuclear Physics*, 6:287, 1973. URL [www.mi.infn.it/~vigezzi/BHR/BrogliaHansenRiedel.pdf](http://www.mi.infn.it/~vigezzi/BHR/BrogliaHansenRiedel.pdf).
- M. H. Cohen, L. M. Falicov, and J. C. Phillips. Superconductive tunneling. *Phys. Rev. Lett.*, 8:316, 1962.
- Ferreira, L., R. Liotta, C. Dasso, R. A. Broglia, and A. Winther. Spatial correlations of pairing collective states. *Nuclear Physics A*, 426:276, 1984.
- Gor'kov, L.P. Microscopic derivation of the Ginzburg–Landau equations in the theory of superconductivity. *Soviet Phys. JETP*, 9:1364, 1959.
- Guazzoni, P., L. Zetta, A. Covello, A. Gargano, B. F. Bayman, G. Graw, R. Hertenberger, H.-F. Wirth, and M. Jaskola. Spectroscopy of  $^{110}\text{Sn}$  via the high-resolution  $^{112}\text{Sn}(p, t) ^{110}\text{Sn}$  reaction. *Phys. Rev. C*, 74:054605, 2006.
- Guazzoni, P., L. Zetta, A. Covello, A. Gargano, B. F. Bayman, T. Faestermann, G. Graw, R. Hertenberger, H.-F. Wirth, and M. Jaskola. High-resolution measurement of the  $^{118,124}\text{Sn}(p, t) ^{116,122}$  reactions: Shell-model and microscopic distorted-wave Born approximation calculations. *Phys. Rev. C*, 83:044614, 2011.
- J. G. Johansen, V. Bildstein, M. J. G. Borge, M. Cubero, J. Diriken, J. Elseviers, L. M. Fraile, H. O. U. Fynbo, L. P. Gaffney, R. Gernhäuser, B. Jonson, G. T. Koldste, J. Konki, T. Kröll, R. Krücken, D. Mücher, T. Nilsson, K. Nowak, J. Pakarinen, V. Pesudo, R. Raabe, K. Riisager, M. Seidlitz, O. Tengblad, H. Törnqvist, D. Voulot, N. Warr, F. Wenander, K. Wimmer, and H. De Witte. Experimental study of bound states in  $^{12}\text{Be}$  through low-energy  $^{11}\text{Be}(d, p)$ -transfer reactions. *Phys. Rev. C*, 88:044619, 2013.
- B. D. Josephson. Possible new effects in superconductive tunnelling. *Phys. Lett.*, 1:251, 1962.
- Mahaux, C., P. F. Bortignon, R. A. Broglia, and C. H. Dasso. Dynamics of the shell model. *Physics Reports*, 120:1–274, 1985.

- D. G. McDonald. The nobel laureate versus the graduate student. *Physics Today*, page 46, July 2001.
- D. Montanari, L. Corradi, S. Szilner, G. Pollarolo, E. Fioretto, G. Montagnoli, F. Scarlassara, A. M. Stefanini, S. Courtin, A. Goasduff, F. Haas, D. Jelavić Malenica, C. Michelagnoli, T. Mijatović, N. Soić, C. A. Ur, and M. Varga Pajtler. Neutron Pair Transfer in  $^{60}\text{Ni} + ^{116}\text{Sn}$  Far below the Coulomb Barrier. *Phys. Rev. Lett.*, 113:052501, 2014.
- A. B. Pippard. The historical context of Josephson discovery. In H. Rogalla and P. H. Kes, editors, *100 years of superconductivity*, page 30. CRC Press, Taylor and Francis, FL, 2012.
- G. Pollarolo and R. A. Broglia. Microscopic Description of the Backward Rise of the Elastic Angular Distribution  $^{16}\text{O} + ^{28}\text{Si}$ . *Nuovo Cimento*, 81:278, 1984.
- G. Potel, F. Barranco, E. Vigezzi, and R. A. Broglia. Evidence for phonon mediated pairing interaction in the halo of the nucleus  $^{11}\text{Li}$ . *Phys. Rev. Lett.*, 105:172502, 2010.
- Potel, G., A. Idini, F. Barranco, E. Vigezzi, and R. A. Broglia. Cooper pair transfer in nuclei. *Rep. Prog. Phys.*, 76:106301, 2013a.
- Potel, G., A. Idini, F. Barranco, E. Vigezzi, and R. A. Broglia. Quantitative study of coherent pairing modes with two-neutron transfer: Sn isotopes. *Phys. Rev. C*, 87:054321, 2013b.
- H. Rogalla and P. H. Kes. . In H. Rogalla and P. H. Kes, editors, *100 years of superconductivity*. CRC Press, Taylor and Francis, FL, 2012.
- J. J. Sakurai. *Modern Quantum Mechanics*. Addison-Wesley, Cambridge, MA, 1994.
- Sargsyan, V. V., G. Scamps, G. G. Adamian, N. V. Antonenko, and D. Lacroix. Neutron pair transfer in sub-barrier capture processes. *arXiv:1311.4353v1*, 2013.
- G. Satchler. *Introduction to Nuclear Reactions*. Mc Millan, New York, 1980.
- Thompson, I.J. Reaction mechanism of pair transfer. In R. A. Broglia and V. Zelevinsky, editors, *50 Years of Nuclear BCS*, page 455. World Scientific, Singapore, 2013.
- von Oertzen, W. Enhanced two-nucleon transfer due to pairing correlations. In R. A. Broglia and V. Zelevinsky, editors, *50 Years of Nuclear BCS*, page 405. World Scientific, Singapore, 2013.

## Chapter 4

# One-particle transfer

In what follows we present a derivation of the one-particle transfer differential cross section within the framework of the distorted wave Born approximation (DWBA) (cf. Tobocman (1961), Austern (1963), Satchler (1980); Broglia and Winther (2004), Satchler (1983), Austern (1970), Glendenning, N. K. (2004) and refs. therein). The structure input for the calculations are mean field potentials and single-particle states dressed, within the formalism of Nuclear Field Theory, through the coupling with the variety of collective, (quasi-) bosonic vibrations, leading to modified formfactors<sup>1</sup> resulting from the interweaving of these vibrations and a number of orbitals with the original, unperturbed single-particle states (Bohr, A. and Mottelson, 1975; Bès et al., 1974; Bès and Broglia, 1975; Bès et al., 1976a,b,c; Mottelson, 1976; Broglia et al., 1976; Bès and Broglia, 1977; Bortignon, P. F. et al., 1977; Bès, D. R. and Kurchan, 1990). With the help of these modified formfactors (cf. also Vaagen et al. (1979); Bang et al. (1980); Hamamoto (1970) and refs. therein), and of global optical potentials, one can calculate the absolute differential cross sections, quantities which can be directly compared with the experimental findings.

In this way one avoids to introduce, let alone use spectroscopic factors, quantities which are rather elusive to calculate consistently (cf. Duguet, T. and Hagen (2012); Jenning, B. (2011); Dickhoff and Barbieri (2004); Dickhoff, W. and Van Neck (2005), and refs. therein). This is in keeping with the fact that as a nucleon moves through the nucleus it feels the presence of the other nucleons whose configurations change as time proceeds. It takes time for this information to be fed back on the nucleon. This renders the average potential nonlocal in time (cf. Mahaux, C. et al. (1985) and references therein, cf. also App. 4.I). A time-dependent operator can always be transformed into an energy-dependent operator, implying an  $\omega$ -dependence of the properties which are usually ascribed to parti-

---

<sup>1</sup>It is of notice that single-particle modified formfactors have their counterpart in the renormalised transition densities (Apéndice introducción (inelastic scattering)) and in the modified two-nucleon transfer formfactors (Chapter 5, Eqs. (5.2.48; simultaneous), (5.2.135–5.2.136; successive) and (5.2.155–5.2.156; non-orthogonality) associated with inelastic and with pair transfer reactions (cf. Broglia, R.A. et al. (1973); Potel, G. et al. (2013) and refs. therein), respectively (cf. App. 4.H).

cles like (effective) mass, charge, etc (see App. 4.B). Furthermore, due to Pauli principle, the average potential is also non local in space (cf. App. 4.A). Consequently, one is forced to deal with nucleons which carry around a cloud of (quasi) bosons, aside from exchanging its position with that of the other nucleons, properties which eventually result in a dynamical shell model. It is of notice that the above mentioned phenomena are not only found in nuclear physics, but are universal within the framework of many-body systems as well as of field theories like quantum electrodynamics (QED). In fact, a basic result of such theories is that nothing is really free (Feynman, 1975). A textbook example of this fact is provided by the Lamb shift, resulting from the dressing of the hydrogen's atom electron, as a result of the exchange of this electron with those participating in the spontaneous, virtual excitation (zero point fluctuations (ZPF)) of the QED vacuum (cf. Apps 4.C, 4.D and 4.E). Within this context, in Section 4.2.1 we provide examples of one-particle transfer processes between nuclei lying along the stability valley, populating strongly renormalized quasiparticle states. In Section 4.2.2 (Poner aqui el apendice W) we again take up the subject, but in this case for the exotic, halo nucleus  $^{11}\text{Li}$ , in particular in connection with the phenomenon of parity inversion in connection with  $N=6$  magic number.

## 4.1 General derivation

We now proceed to derive the transition amplitude for the reaction (cf. Fig. 4.1.1).

$$A + a (= b + 1) \longrightarrow B (= A + 1) + b. \quad (4.1.1)$$

For a simplified version we refer to App 4.F, while for an alternative derivation within the framework of one-particle knock-out reactions we refer to App 4.G. Let us assume that the nucleon bound initially to the core  $b$  is in a single-particle state with orbital and total angular momentum  $l_i$  and  $j_i$  respectively, and that the nucleon in the final state (bound to core  $A$ ) is in the  $l_f, j_f$  state. The total spin and magnetic quantum numbers of nuclei  $A, a, B, b$  are  $\{J_A, M_A\}, \{J_a, M_a\}, \{J_B, M_B\}, \{J_b, M_b\}$  respectively. Denoting  $\xi_A$  and  $\xi_b$  the intrinsic coordinates of the wavefunctions describing the structure of nuclei  $A$  and  $b$  respectively, and  $\mathbf{r}_{An}$  and  $\mathbf{r}_{bn}$  the relative coordinates of the transferred nucleon with respect to the CM of nuclei  $A$  and  $b$  respectively, one can write the “intrinsic” wavefunctions of the colliding nuclei  $A, a$  as

$$\begin{aligned} & \phi_{M_A}^{J_A}(\xi_A), \\ & \Psi(\xi_b, \mathbf{r}_{b1}) = \sum_{m_i} \langle J_b \ j_i \ M_b \ m_i | J_a \ M_a \rangle \phi_{M_b}^{J_b}(\xi_b) \psi_{m_i}^{j_i}(\mathbf{r}_{bn}, \sigma), \end{aligned} \quad (4.1.2)$$

while the “intrinsic” wavefunctions describing the structure of nuclei  $B$  and  $b$  are

$$\begin{aligned} & \phi_{M_b}^{J_b}(\xi_b), \\ & \Psi(\xi_A, \mathbf{r}_{A1}) = \sum_{m_f} \langle J_A \ j_f \ M_A \ m_f | J_B \ M_B \rangle \phi_{M_A}^{J_A}(\xi_A) \psi_{m_f}^{j_f}(\mathbf{r}_{An}, \sigma). \end{aligned} \quad (4.1.3)$$

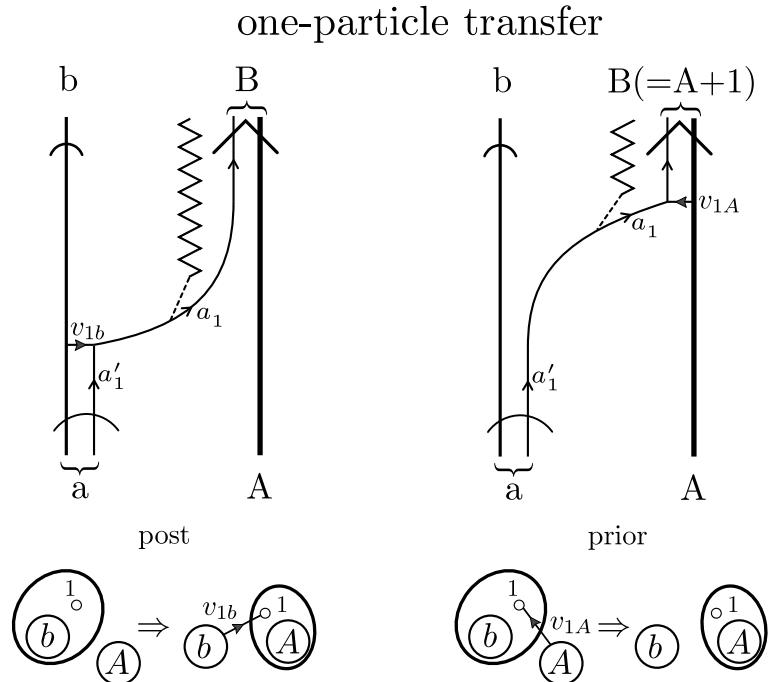


Figure 4.1.1: NFT graphical representation of the one-particle transfer reaction  $a (= b + 1) + A \rightarrow b + B (= A + 1)$  (for details in the notation we refer to Figs. 5.C.1 and 5.C.2 and to the last paragraph before Sect. 5.C.1 of App. 5.C). The time arrow is assumed to point upwards. The quantum numbers characterizing the states in which the transferred nucleon moves in projectile and target are denoted  $a'_1$  and  $a_1$  respectively. The interaction inducing the nucleon to be transferred can act either in the entrance channel  $((a, A); v_{1A}$ , prior representation) or in the exit channel  $((b, B); v_{1b}$ , post representation), in keeping with energy conservation. In the transfer process, the nucleon changes orbital at the same time that a change in the mass partition takes place. The corresponding relative motion mismatch is known as the recoil process, and is represented by a jagged curve (this is the recoil elementary mode, mode which couples to the particle degrees of freedom through a Galilean transformation operator). The recoil mode provides information on the evolution of  $r_{1A}$  ( $r_{1b}$ ). In other words, on the coupling between structure and reaction (relative motion) degrees of freedom.

For an unpolarized incident beam (sum over  $M_A, M_a$  and divide by  $(2J_A + 1), (2J_a + 1)$ ), and assuming that one does not detect the final polarization (sum over  $M_B, M_b$ ), the differential cross section in the DWBA can be written as

$$\frac{d\sigma}{d\Omega} = \frac{k_f}{k_i} \frac{\mu_i \mu_f}{4\pi^2 \hbar^4} \frac{1}{(2J_A + 1)(2J_a + 1)} \times \sum_{\substack{M_A, M_a \\ M_B, M_b}} \left| \sum_{m_i, m_f} \langle J_b j_i M_b m_i | J_a M_a \rangle \langle J_A j_f M_A m_f | J_B M_B \rangle T_{m_i, m_f} \right|^2, \quad (4.1.4)$$

where  $k_i$  and  $k_f$  are the relative motion linear momentum in both initial and final channels (flux), while  $\mu_i$  and  $\mu_f$  are the corresponding relative masses. The two quantities within  $\langle \rangle$  brackets are Clebsch–Gordan coefficients taking care of angular momentum conservation (cf. Brink and Satchler (1968) and Edmonds (1960), also Bohr and Mottelson (1969)).

The transition amplitude  $T_{m_i, m_f}$  is

$$T_{m_i, m_f} = \sum_{\sigma} \int d\mathbf{r}_f d\mathbf{r}_{bn} \chi^{(-)*}(\mathbf{r}_f) \psi_{m_f}^{j_f*}(\mathbf{r}_{An}, \sigma) V(r_{bn}) \psi_{m_i}^{j_i}(\mathbf{r}_{bn}, \sigma) \chi^{(+)}(\mathbf{r}_i), \quad (4.1.5)$$

where

$$\psi_{m_i}^{j_i}(\mathbf{r}_{An}, \sigma) = u_{j_i}(r_{bn}) \left[ Y^{l_i}(\hat{r}_i) \chi(\sigma) \right]_{j_i m_i}, \quad (4.1.6)$$

is the single-particle wavefunction describing the motion of the nucleon to be transferred, when in the initial state,  $u$ ,  $Y$  and  $\chi$  being the radial, angular (spherical harmonics) and spin components. Similarly for  $\psi_{m_f}^{j_f}$ . The distorted waves describing the relative motion of the incoming projectile and of the target nucleus and of the outgoing system and the residual nucleus are,

$$\chi^{(+)}(\mathbf{k}_i, \mathbf{r}_i) = \frac{4\pi}{k_i r_i} \sum_{l'} i^{l'} e^{i\sigma_i^{l'}} g_{l'}(\hat{r}_i) \left[ Y^{l'}(\hat{r}_i) Y^{l'}(\hat{k}_i) \right]_0^0, \quad (4.1.7)$$

and

$$\chi^{(-)*}(\mathbf{k}_f, \mathbf{r}_f) = \frac{4\pi}{k_f r_f} \sum_l i^{-l} e^{i\sigma_f^{l'}} f_l(\hat{r}_f) \left[ Y^l(\hat{r}_f) Y^l(\hat{k}_f) \right]_0^0, \quad (4.1.8)$$

respectively. In the above relations  $f$  and  $g$  are, respectively, **the regular and irregular radial solutions** describing the relative motion associated with the corresponding optical potential (“elastic” scattering). Let us now discuss the angular components involved in the reaction process, starting with the relation

$$\begin{aligned} \left[ Y^l(\hat{r}_f) Y^l(\hat{k}_f) \right]_0^0 \left[ Y^{l'}(\hat{r}_i) Y^{l'}(\hat{k}_i) \right]_0^0 &= \sum_K ((ll)_0 (l'l')_0 | (ll')_K (ll')_K)_0 \\ &\times \left\{ \left[ Y^l(\hat{r}_f) Y^{l'}(\hat{r}_i) \right]^K \left[ Y^l(\hat{k}_f) Y^{l'}(\hat{k}_i) \right]^K \right\}_0^0. \end{aligned} \quad (4.1.9)$$

The 9j-symbol can be explicitly evaluated to give,

$$((ll)_0(l'l')_0|(ll')_K(l'l')_K)_0 = \sqrt{\frac{2K+1}{(2l+1)(2l'+1)}}, \quad (4.1.10)$$

while the coupled expression can be written as

$$\begin{aligned} & \left\{ \left[ Y^l(\hat{r}_f)Y^{l'}(\hat{r}_i) \right]^K \left[ Y^l(\hat{k}_f)Y^{l'}(\hat{k}_i) \right]^K \right\}_0^0 = \sum_M \langle K \ K \ M \ -M | 0 \ 0 \rangle \left[ Y^l(\hat{r}_f)Y^{l'}(\hat{r}_i) \right]_M^K \\ & \times \left[ Y^l(\hat{k}_f)Y^{l'}(\hat{k}_i) \right]_{-M}^K = \sum_M \frac{(-1)^{K+M}}{\sqrt{2K+1}} \left[ Y^l(\hat{r}_f)Y^{l'}(\hat{r}_i) \right]_M^K \left[ Y^l(\hat{k}_f)Y^{l'}(\hat{k}_i) \right]_{-M}^K. \end{aligned} \quad (4.1.11)$$

Thus,

$$\begin{aligned} & \left[ Y^l(\hat{r}_f)Y^l(\hat{k}_f) \right]_0^0 \left[ Y^{l'}(\hat{r}_i)Y^{l'}(\hat{k}_i) \right]_0^0 \\ & = \sum_{K,M} \frac{(-1)^{K+M}}{\sqrt{(2l+1)(2l'+1)}} \left[ Y^l(\hat{r}_f)Y^{l'}(\hat{r}_i) \right]_M^K \left[ Y^l(\hat{k}_f)Y^{l'}(\hat{k}_i) \right]_{-M}^K. \end{aligned} \quad (4.1.12)$$

For the angular integral to be different from zero, the integrand must be coupled to zero angular momentum (scalar). Noting that the only variables over which one integrates in the above expression are  $\hat{r}_i, \hat{r}_f$ , we have to couple the remaining functions of the angular variables, namely the wavefunctions  $\psi_{m_f}^{j_f*}(\mathbf{r}_{An}, \sigma) = (-1)^{j_f-m_f} \psi_{-m_f}^{j_f}(\mathbf{r}_{An}, -\sigma)$  and  $\psi_{m_i}^{j_i}(\mathbf{r}_{bn}, \sigma)$  to angular momentum  $K$ , as well as to fulfill  $M = m_f - m_i$ . Let us then consider

$$\begin{aligned} & (-1)^{j_f-m_f} \psi_{-m_f}^{j_f}(\mathbf{r}_{An}, -\sigma) \psi_{m_i}^{j_i}(\mathbf{r}_{bn}, \sigma) = (-1)^{j_f-m_f} u_{j_f}(r_{An}) u_{j_i}(r_{bn}) \\ & \times \sum_P \langle j_f \ j_i \ -m_f \ m_i | P \ m_i - m_f \rangle \left\{ \left[ Y^{l_f}(\hat{r}_{An}) \chi^{1/2}(-\sigma) \right]^{j_f} \left[ Y^{l_i}(\hat{r}_{bn}) \chi^{1/2}(\sigma) \right]^{j_i} \right\}_{m_i-m_f}^P. \end{aligned} \quad (4.1.13)$$

Recoupling the spherical harmonics to angular momentum  $K$  and the spinors to  $S = 0$ , only one term survives the angular integral in (4.1.5), namely

$$\begin{aligned} & (-1)^{j_f-m_f} u_{j_f}(r_{An}) u_{j_i}(r_{bn}) ((l_f \frac{1}{2})_{j_f} (l_i \frac{1}{2})_{j_i} | (l_f l_i)_K (\frac{1}{2} \frac{1}{2})_0)_K \\ & \times \langle j_f \ j_i \ -m_f \ m_i | K \ m_i - m_f \rangle \left[ Y^{l_f}(\hat{r}_{An}) Y^{l_i}(\hat{r}_{bn}) \right]_{m_i-m_f}^K [\chi(-\sigma) \chi(\sigma)]_0^0. \end{aligned} \quad (4.1.14)$$

Making use of the fact that the sum over spins yields a factor  $-\sqrt{2}$ , and in

keeping with the fact that  $M = m_f - m_i$ , one obtains,

$$\begin{aligned} T_{m_i, m_f} &= (-1)^{j_f - m_f} \frac{-16\sqrt{2}\pi^2}{k_f k_i} \sum_{ll'} i^{l'-l} e^{\sigma'_f + \sigma'_i} \sum_K ((l_f \frac{1}{2})_{j_f} (l_i \frac{1}{2})_{j_i} | (l_f l_i)_K (\frac{1}{2} \frac{1}{2})_0)_K \\ &\times \langle j_f \ j_i \ -m_f \ m_i | K \ m_i - m_f \rangle \left[ Y^l(\hat{k}_f) Y^{l'}(\hat{k}_i) \right]_{m_i - m_f}^K \int d\mathbf{r}_f d\mathbf{r}_{bn} \frac{f_l(r_f) g_{l'}(r_i)}{r_f r_i} \\ &\times u_{j_f}(r_{An}) u_{j_i}(r_{bn}) V(r_{bn}) (-1)^{K+m_f-m_i} \left[ Y^l(\hat{r}_f) Y^{l'}(\hat{r}_i) \right]_{m_f - m_i}^K \left[ Y^{l_f}(\hat{r}_{An}) Y^{l_i}(\hat{r}_{bn}) \right]_{m_i - m_f}^K. \end{aligned} \quad (4.1.15)$$

Again, the only term of the expression

$$\begin{aligned} &(-1)^{K+m_f-m_i} \left[ Y^l(\hat{r}_f) Y^{l'}(\hat{r}_i) \right]_{m_f - m_i}^K \left[ Y^{l_f}(\hat{r}_{An}) Y^{l_i}(\hat{r}_{bn}) \right]_{m_i - m_f}^K = \\ &(-1)^{K+m_f-m_i} \sum_P \langle K \ K \ m_f - m_i \ m_i - m_f | P \ 0 \rangle \left\{ \left[ Y^l(\hat{r}_f) Y^{l'}(\hat{r}_i) \right]^K \left[ Y^{l_f}(\hat{r}_{An}) Y^{l_i}(\hat{r}_{bn}) \right]^K \right\}_0^P \end{aligned}$$

which survives after angular integration is the one with  $P = 0$ , that is,

$$\begin{aligned} &\frac{1}{\sqrt{(2K+1)}} \left\{ \left[ Y^l(\hat{r}_f) Y^{l'}(\hat{r}_i) \right]^K \left[ Y^{l_f}(\hat{r}_{An}) Y^{l_i}(\hat{r}_{bn}) \right]^K \right\}_0^0 \\ &= \frac{1}{\sqrt{(2K+1)}} \sum_{M_K} \langle K \ K \ M_K \ -M_K | 0 \ 0 \rangle \left[ Y^l(\hat{r}_f) Y^{l'}(\hat{r}_i) \right]_{M_K}^K \\ &\times \left[ Y^{l_f}(\hat{r}_{An}) Y^{l_i}(\hat{r}_{bn}) \right]_{-M_K}^K = \frac{1}{\sqrt{(2K+1)}} \sum_{M_K} \frac{(-1)^{K+M_K}}{\sqrt{(2K+1)}} \left[ Y^l(\hat{r}_f) Y^{l'}(\hat{r}_i) \right]_{M_K}^K \\ &\times \left[ Y^{l_f}(\hat{r}_{An}) Y^{l_i}(\hat{r}_{bn}) \right]_{-M_K}^K \\ &= \frac{1}{2K+1} \sum_{M_K} (-1)^{K+M_K} \left[ Y^l(\hat{r}_f) Y^{l'}(\hat{r}_i) \right]_{M_K}^K \left[ Y^{l_f}(\hat{r}_{An}) Y^{l_i}(\hat{r}_{bn}) \right]_{-M_K}^K, \end{aligned}$$

an expression which is spherically symmetric. One can evaluate it for a particular configuration, for example setting  $\hat{r}_f = \hat{z}$  and the center of mass  $A, b, n$  in the  $x - z$  plane (see Fig. 4.1.2). Once the orientation in space of this “standard” configuration is specified (through, for example, a rotation  $0 \leq \alpha \leq 2\pi$  around  $\hat{z}$ , a rotation  $0 \leq \beta \leq \pi$  around the new  $x$  axis and a rotation  $0 \leq \gamma \leq 2\pi$  around  $\hat{r}_{bB}$ ), the only remaining angular coordinate is  $\theta$ , while the integral over the other three angles yields  $8\pi^2$ . Setting  $\hat{r}_f = \hat{z}$  one obtains

$$\left[ Y^l(\hat{r}_f) Y^{l'}(\hat{r}_i) \right]_{M_K}^K = \langle l \ l' \ 0 \ M_K | K \ M_K \rangle \sqrt{\frac{2l+1}{4\pi}} Y_{M_K}^{l'}(\hat{r}_i). \quad (4.1.16)$$

Because of  $M = m_i - m_f$ , and  $m = m_f$ ,  $T_{m_i, m_f} \equiv T_{m, M}$  where

$$\begin{aligned} T_{m, M} &= (-1)^{j_f - m} \frac{-64\sqrt{2}\pi^{7/2}}{k_f k_i} \sum_{ll'} i'^l - l e^{\sigma_f^l + \sigma_i'^l} \sqrt{2l+1} \sum_K \frac{(-1)^K}{2K+1} ((l_f \frac{1}{2})_{j_f} (l_i \frac{1}{2})_{j_i} | (l_f l_i)_K (\frac{1}{2} \frac{1}{2})_0)_K \\ &\times \langle j_f j_i - m | M + m | K M \rangle [Y^l(\hat{k}_f) Y^{l'}(\hat{k}_i)]_M^K \int d\mathbf{r}_f d\mathbf{r}_{bn} \frac{f_l(r_f) g_{l'}(r_i)}{r_f r_i} \\ &\times u_{j_f}(r_{An}) u_{j_i}(r_{bn}) V(r_{bn}) \sum_{M_K} (-1)^{M_K} \langle l l' 0 | M_K | K M_K \rangle [Y^{l_f}(\hat{r}_{An}) Y^{l_i}(\hat{r}_{bn})]_{-M_K}^K Y^{l'}_{M_K}(\hat{r}_i). \end{aligned} \quad (4.1.17)$$

We now turn our attention to the sum

$$\sum_{\substack{M_A, M_a \\ M_B, M_b}} \left| \sum_{m, M} \langle J_b j_i M_b m | J_a M_a \rangle \langle J_A j_f M_A M | J_B M_B \rangle T_{m, M} \right|^2, \quad (4.1.18)$$

appearing in the expression for the differential cross section (4.1.4). For any given value  $m', M'$  of  $m, M$ , the sum will be

$$\begin{aligned} &\sum_{M_a, M_b} |\langle J_b j_i M_b m' | J_a M_a \rangle|^2 \sum_{M_A, M_B} |\langle J_A j_f M_A M' | J_B M_B \rangle|^2 |T_{m', M'}|^2 \\ &= \frac{(2J_a + 1)(2J_B + 1)}{(2j_i + 1)(2j_f + 1)} \sum_{M_a, M_b} |\langle J_b J_a M_b - M_a | j_i m' \rangle|^2 \\ &\times \sum_{M_A, M_B} |\langle J_A J_B M_A - M_B | j_f M' \rangle|^2 |T_{m', M'}|^2, \end{aligned} \quad (4.1.19)$$

by virtue of the symmetry property of Clebsch–Gordan coefficients

$$\langle J_b j_i M_b m | J_a M_a \rangle = (-1)^{J_b - M_b} \sqrt{\frac{(2J_a + 1)}{(2j_i + 1)}} \langle J_b J_a M_b - M_a | j_i m \rangle. \quad (4.1.20)$$

The sum over the Clebsch–Gordan coefficients in (4.1.19) is equal to 1, so (4.1.18) becomes

$$\frac{(2J_a + 1)(2J_B + 1)}{(2j_i + 1)(2j_f + 1)} \sum_{m, M} |T_{m, M}|^2, \quad (4.1.21)$$

and the differential cross section can be written as,

$$\frac{d\sigma}{d\Omega} = \frac{k_f}{k_i} \frac{\mu_i \mu_f}{4\pi^2 \hbar^4} \frac{(2J_B + 1)}{(2j_i + 1)(2j_f + 1)(2J_A + 1)} \sum_{m, M} |T_{m, M}|^2. \quad (4.1.22)$$

where

$$T_{m, M} = \sum_{Kll'} (-1)^{-m} \langle j_f j_i - m | M + m | K M \rangle [Y^l(\hat{k}_f) Y^{l'}(\hat{k}_i)]_M^K t_{ll'}^K. \quad (4.1.23)$$

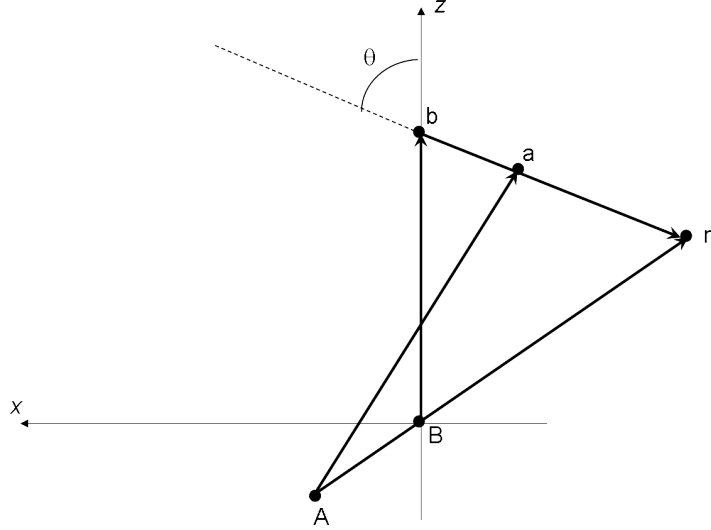


Figure 4.1.2: Coordinate system in the “standard” configuration. Note that  $\mathbf{r}_f \equiv \mathbf{r}_{Bb}$ , and  $\mathbf{r}_i \equiv \mathbf{r}_{Aa}$ .

Orienting  $\hat{k}_i$  along the incident  $z$ -direction leads to,

$$\left[ Y^l(\hat{k}_f) Y^{l'}(\hat{k}_i) \right]_M^K = \langle l l' M 0 | K M \rangle \sqrt{\frac{2l'+1}{4\pi}} Y_M^l(\hat{k}_f), \quad (4.1.24)$$

and

$$T_{m,M} = \sum_{Kll'} (-1)^{-m} \langle l l' M 0 | K M \rangle \langle j_f j_i - m | M + m | K M \rangle Y_M^l(\hat{k}_f) t_{ll'}^K, \quad (4.1.25)$$

with

$$\begin{aligned} t_{ll'}^K &= (-1)^{K+j_f} \frac{-32\sqrt{2}\pi^3}{k_f k_i} i^{l'-l} e^{\sigma_f^l + \sigma_i^{l'}} \frac{\sqrt{(2l+1)(2l'+1)}}{2K+1} ((l_f \frac{1}{2})_{j_f} (l_i \frac{1}{2})_{j_i} | (l_f l_i)_K (\frac{1}{2} \frac{1}{2})_0)_K \\ &\times \int dr_f dr_{bn} d\theta r_{bn}^2 \sin \theta r_f \frac{f_l(r_f) g_{l'}(r_i)}{r_i} u_{j_f}(r_{An}) u_{j_i}(r_{bn}) V(r_{bn}) \\ &\times \sum_{M_K} (-1)^{M_K} \langle l l' 0 | M_K | K M_K \rangle \left[ Y^{l_f}(\hat{r}_{An}) Y^{l_i}(\hat{r}_{bn}) \right]_{-M_K}^K Y_{M_K}^{l'}(\hat{r}_i). \end{aligned} \quad (4.1.26)$$

### 4.1.1 Coordinates

To perform the integral in (4.1.26), one needs the expression of  $r_i, r_{An}, \hat{r}_{An}, \hat{r}_{bn}, \hat{r}_i$  in term of the integration variables  $r_f, r_{bn}, \theta$ . Because one is interested in evaluating

these quantities in the particular configuration depicted in Fig. 4.1.2, one has

$$\mathbf{r}_f = r_f \hat{z}, \quad (4.1.27)$$

$$\mathbf{r}_{bn} = -r_{bn}(\sin \theta \hat{x} + \cos \theta \hat{z}), \quad (4.1.28)$$

$$\mathbf{r}_{Bn} = \mathbf{r}_f + \mathbf{r}_{bn} = -r_{bn} \sin \theta \hat{x} + (r_f - r_{bn} \cos \theta) \hat{z}. \quad (4.1.29)$$

One can then write

$$\mathbf{r}_{An} = \frac{A+1}{A} \mathbf{r}_{Bn} = -\frac{A+1}{A} r_{bn} \sin \theta \hat{x} + \frac{A+1}{A} (r_f - r_{bn} \cos \theta) \hat{z}, \quad (4.1.30)$$

$$\mathbf{r}_{an} = \frac{b}{b+1} \mathbf{r}_{bn} = -\frac{b}{b+1} r_{bn} (\sin \theta \hat{x} + \cos \theta \hat{z}), \quad (4.1.31)$$

and

$$\mathbf{r}_i = \mathbf{r}_{An} - \mathbf{r}_{an} = -\frac{2A+1}{(A+1)A} r_{bn} \sin \theta \hat{x} + \left( \frac{A+1}{A} r_f - \frac{2A+1}{(A+1)A} r_{bn} \cos \theta \right) \hat{z}, \quad (4.1.32)$$

where  $A, b$  are the number of nucleons of nuclei  $A$  and  $b$  respectively.

### 4.1.2 Zero-range approximation

In the zero range approximation,

$$\int dr_{bn} r_{bn}^2 u_{j_i}(r_{bn}) V(r_{bn}) = D_0; \quad u_{j_i}(r_{bn}) V(r_{bn}) = \delta(r_{bn}) / r_{bn}^2. \quad (4.1.33)$$

It can be shown (see Fig. 4.1.2) that for  $r_{bn} = 0$

$$\mathbf{r}_{An} = \frac{m_A + 1}{m_A} \mathbf{r}_f, \quad \mathbf{r}_i = \frac{m_A + 1}{m_A} \mathbf{r}_f. \quad (4.1.34)$$

One then obtains

$$\begin{aligned} t_{ll'}^K &= \frac{-16 \sqrt{2} \pi^2}{k_f k_i} (-1)^K \frac{D_0}{\alpha} l'^{-l} e^{\sigma_f^l + \sigma_i^{l'}} \frac{\sqrt{(2l+1)(2l'+1)(2l_i+1)(2l_f+1)}}{2K+1} ((l_f \frac{1}{2})_{j_f} (l_i \frac{1}{2})_{j_i} | (l_f l_i)_K (\frac{1}{2} \frac{1}{2})_0)_K \\ &\times \langle l' l' 0 0 | K 0 \rangle \langle l_f l_i 0 0 | K 0 \rangle \int dr_f f_l(r_f) g_{l'}(ar_f) u_{j_f}(ar_f), \end{aligned} \quad (4.1.35)$$

with

$$\alpha = \frac{A+1}{A}. \quad (4.1.36)$$

## 4.2 Examples and Applications

In this section we discuss some examples which illustrate the workings of single-particle transfer processes.

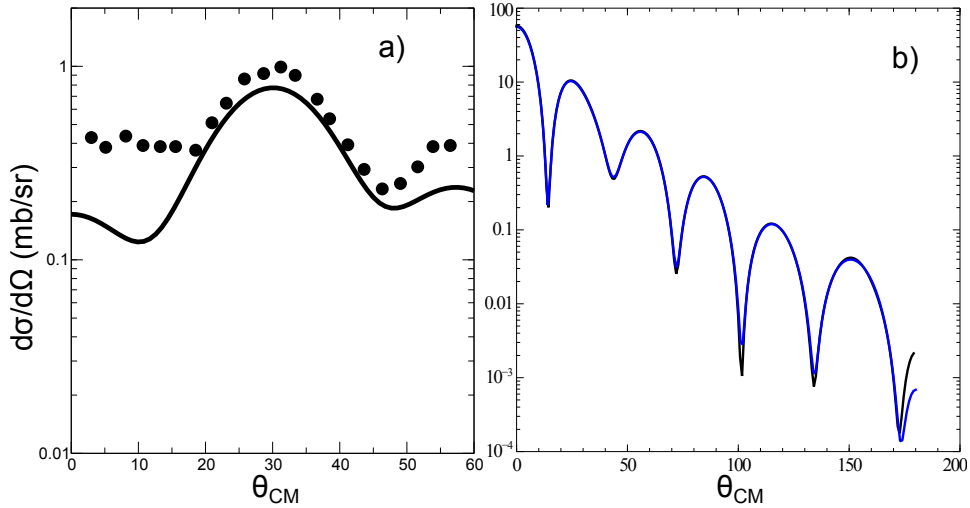


Figure 4.2.1: The absolute differential cross section  $^{120}\text{Sn}(p, d)^{119}\text{Sn}(j^\pi)$  associated with the state  $j^\pi = 7/2^+$ . a) the theoretical prediction discussed in the text are displayed in comparison with the experimental data (Dickey, S. A. et al. (1982)). The corresponding integrated cross sections are 5.0 and  $5.2 \pm 0.6$  mb respectively. b) Comparison of the results of ONE and of the software FRESCO for the same reaction as in (a) but populating the  $s_{1/2}$  state.

#### 4.2.1 $^{120}\text{Sn}(p, d)^{119}\text{Sn}$ and $^{120}\text{Sn}(d, p)^{121}\text{Sn}$ reactions.

In the calculation of absolute reaction cross section two elements melt together: reaction and structure. In the case of weakly coupled probes like, as a rule, direct one-particle transfer processes are, the first element can be further divided into two essentially separated components: elastic scattering (optical potentials), and transfer amplitudes connecting entrance and exit channels. In other words, the habitat of DWBA.

In Fig. 4.2.1 (a) a concrete embodiment of the formalism presented in the first part of this Chapter, worked out with the help of the software ONE (Potel, G. (2012)), of global optical parameters (Dickey, S. A. et al. (1982)) and of NFT spectroscopic amplitudes (cf. Table 4.2.1), is given. In it, the absolute differential cross section associated with the population of the low-lying state  $|^{119}\text{Sn}(11/2^-; 88\text{keV})\rangle$  in the one-particle pick-up process  $^{120}\text{Sn}(p, d)^{119}\text{Sn}$  is compared with the experimental data. In Fig. 4.2.1 (b) the theoretical predictions were obtained with the help of ONE.

Similar calculations (ONE, NFT spectroscopic amplitudes and global optical parameters), have been carried for the reaction  $^{120}\text{Sn}(d, p)^{121}\text{Sn}(j^\pi; E_x)$  in connection with the population of the  $|3/2^+; \text{gs}\rangle$  and  $|11/2^-; E_x \approx 0 \text{ MeV}\rangle$  states. In the stripping experiment (Bechara, M. J. and Dietzsche (1975)) the ground state and the  $11/2^-$  state were not resolved in energy. This is the reason why theory and experiment are only compared to the data for the summed  $l = 2 + 5$  differential cross

section (cf. Fig. 4.2.2 (a)), the separate theoretical predictions been displayed in Figs. 4.2.2 (b) and (c).

Let us now turn to the most fragmented low-lying quasiparticle state around  $^{120}\text{Sn}$ , namely that associated with the  $d_{5/2}$  orbital (cf. Idini, A. (2013), Idini, A. et al. (2012)) As shown in Fig. 4.2.3 five low-lying  $5/2^+$  states have been populated in the reaction  $^{120}\text{Sn}(p, d)^{119}\text{Sn}$  with a summed cross section  $\sum_{i=1}^5 \sigma(2^\circ - 25^\circ) \approx 8 \text{ mb} \pm 2 \text{ mb}$  (Dickey, S. A. et al. (1982)) while four are theoretically predicted with  $\sum_{i=1}^4 \sigma(2^\circ - 25^\circ) = 6.2 \text{ mb}$  (cf. also Idini, A. et al. (2014)). Within the present context, namely that of probing the single-particle content of an elementary excitation, the study of the  $5/2^+$  quasiparticle strength is a rather trying situation. Arguably, it provides a measure of the limitations encountered in such studies.

Analysis of the type presented above allows one to posit that structure and reactions are but just two aspects of the same physics. If one adds to this picture the fact that the optical potential –that is, the energy and momentum dependent nuclear dielectric function describing the medium where direct nuclear chemistry takes place– can be calculated microscopically (cf. Mahaux, C. et al. (1985), Fernández-García, J.P. et al. (2010), Fernández-García, J.P., M. Rodríguez-Gallardo et al. (2010), Broglia, R. A. et al. (1981), Pollarolo et al. (1983), Broglia and Winther (2004), Dickhoff, W. and Van Neck (2005), Jenning, B. (2011), Montanari et al. (2014)) in terms of the same elements entering structure calculations (i.e. spectroscopic amplitudes, single-particle wavefunctions, transition densities and eventually effective formfactors), the structure reaction loop closes itself.

Allowing halo nuclei to be part of the daily nuclear structure paradigm, the equivalence between structure and reactions becomes even stronger, explaining in simple terms why one-particle transfer is likely to be, as a rule, the main channel contributing to the entrance channel depopulation (absorptive optical potential), in keeping with the large overlap displayed by the corresponding single-particle wavefunctions, as compared to particle-hole configuration controlling inelastic processes (cf. Fig. 3.B.5).

Searching for further contact points between structure and reactions, one can posit that the above parlance, although being essentially correct, does not emphasize enough the central role virtual, correlated particle-hole excitations play in the single-particle transfer process. In fact, as a result of the interweaving of single-particle (quasiparticle) motion and e.g. collective surface vibrations, particles become dressed, being able to contribute less (differently) to the direct transfer process but, eventually, opening new doorway channels (states) (cf. Feshbach (1958), Rawitscher, G. H. (1987), Bortignon and Broglia (1981), Bertsch et al. (1983)) to depopulate the entrance channel (cf. figura 1D4 de la introducción), similar to those responsible for the breaking of the single-particle strength ( $Z_\omega (= m/m_\omega)$ ) and of the damping of giant resonances and of the renormalization of low-lying collective states (cf. Figs. 4.C.2, 4.C.3, 4.E.1, 4.E.2, cf. also App. 4.I).

It seems then fair to state that the importance of the coupled channels approach to reactions (cf. e.g. Thompson (1988), Thompson, I.J. (2013), Tamura, T. et al. (1970), Ascuitto and Glendenning (1969), Ascuitto, R. J. and Glendenning (1970),

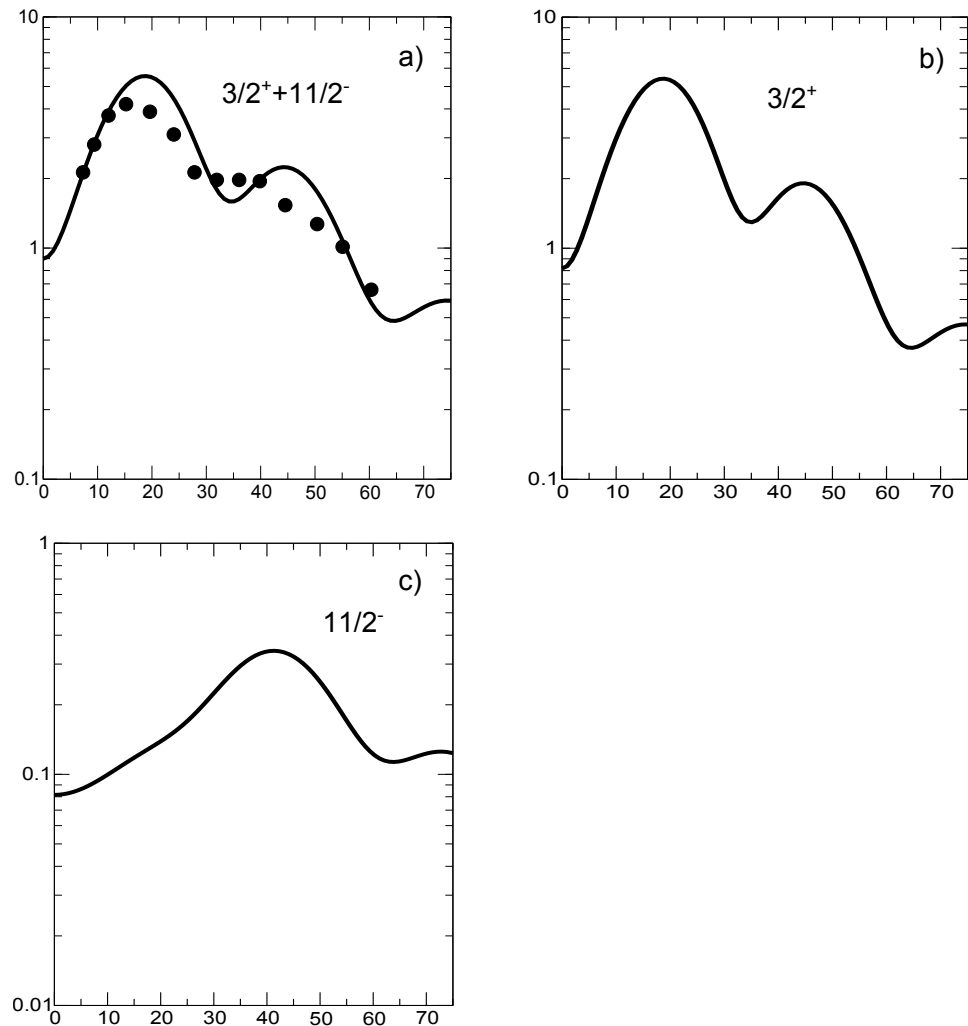


Figure 4.2.2: The theoretical absolute differential cross section (continuous curve) associated with the reaction  $^{120}\text{Sn}(d, p)^{121}\text{Sn}$  and populating the low-lying states  $3/2^+$  and  $11/2^-$  are shown in b) and c), while the summed differential cross section is displayed in a) in comparison with the data (Bechara, M. J. and Dietzsch (1975)).

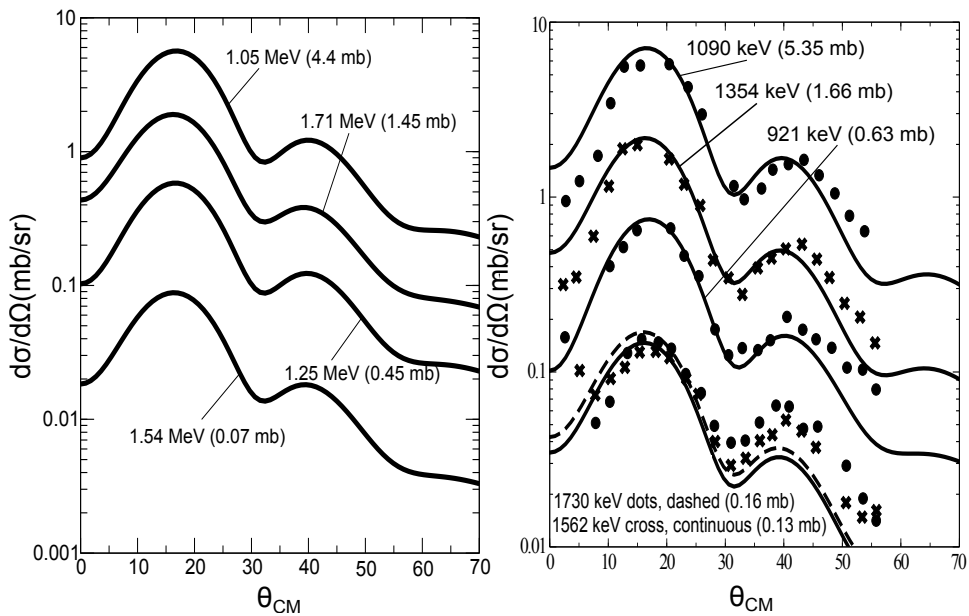


Figure 4.2.3:  $^{120}\text{Sn}(p, d)^{119}\text{Sn}(5/2^+)$  absolute experimental cross sections (dots, Dickey, S. A. et al. (1982)), together with the DWBA fit carried out in the analysis of the data (right panel) in comparison with the finite range, full recoil DWBA calculations carried out with global optical potentials making use of NFT structure inputs as explained in the text (after Idini, A. et al. (2014)) and of the software ONE (Potel, G. (2012)); see also App. 6.D.

		$^{120}\text{Sn}(p, d)^{119}\text{Sn}(j)$	$^{120}\text{Sn}(d, p)^{121}\text{Sn}(j)$
$j$	$E_j$ (MeV)	$\bar{V}_j^2$	$\bar{U}_j^2$
$h_{11/2}$	1.54	(1.34) 0.25 (0.28)	(1.25) 0.55 (0.49)
$d_{3/2}$	1.27	(1.27) 0.35 (0.41)	(1.25) 0.41 (0.44)

Table 4.2.1: The properties of the main peaks of the  $h_{11/2}$  and  $d_{3/2}$  strength functions of  $^{120}\text{Sn}$  calculated taking into account the interweaving of fermionic and bosonic elementary modes of excitation within NFT and of their consequences in both the normal and abnormal densities (cf. Idini, A. et al. (2012); Idini, A. (2013) see also Idini, A. et al. (2014) where the spin degrees of freedom, solely repulsive pairing channel ( ${}^1S_0$ ) in finite nuclei, has also been included). In parenthesis, experimental (energies) and empirical (single-particle strength) data are given (Bechara, M. J. and Dietzsch (1975), Dickey, S. A. et al. (1982)).

Asciutto R. J. et al. (1971), Asciutto R.J. and Sørensen (1972); cf. also Fernández-García, J.P. et al. (2010), Fernández-García, J.P., M. Rodríguez-Gallardo et al. (2010)) is not so much, or at least not only, that it is able to handle situations like for example one-particle transfer to members of a rotational band, alas at the expenses of eventually adjusting the optical potential, but that it reminds us how intimately connected probed and probe are in nuclei.

On the other hand for most of the situations dealt in the present monography, it is transparent the power, also to reflect the physics, of perturbative DWBA (e.g. 1st order for one-nucleon transfer and 2nd for Cooper pair tunneling), coupled together with NFT elementary modes of nuclear excitation approach.

To which extent a FRESCO like software built on a NFT basis will ever be attempted is an open question. Note in any case the serious attempts made at incorporating so called core excitations within the FRESCO framework (Fernández-García, J.P. et al. (2010), Fernández-García, J.P., M. Rodríguez-Gallardo et al. (2010)).

We conclude this section by recalling the fact that the dressing of single particles with pairing vibrations plays also a central role in the structure properties of nuclei (cf. e.g. Barranco et al. (1987), Bès, D. R. et al. (1988), Baroni, S. et al. (2004) and refs. therein; see Sect. 2.1 and Fig. 2.E.1 of App. 2.E).

#### 4.2.2 Dressing of single-particle states: parity inversion in $^{11}\text{Li}$ .

The  $N = 6$  isotope of  ${}^9\text{Li}$  displays quite ordinary structural properties and can, at first glance, be thought of a two-neutron hole system in the  $N = 8$  closed shell. That this is not the case emerges clearly from the fact that  ${}^{10}\text{Li}$  is not bound. In addition, the observation that the two lowest unoccupied states are the virtual ( $1/2^+$ ) and the resonant ( $1/2^-$ ) states, testify to the fact that, in the present case,  $N = 6$  is a far better magic neutron number than  $N = 8$ . In addition the observation that the unbound  $s_{1/2}$  state lies lower than the unbound  $p_{1/2}$  state, a phenomenon known in the literature as parity inversion (see Fig. 4.2.4), is in plain contradiction with static mean field theory. Dressing the (standard) mean field (e.g. Saxon-Woods

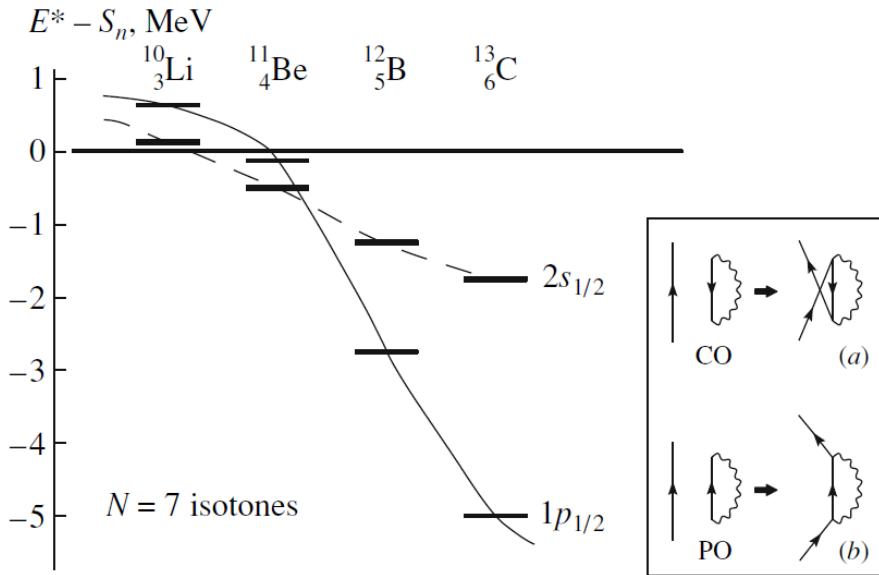


Figure 4.2.4: Single-particle states for  $N = 7$  isotones around  $^{11}\text{Be}$  associated with parity inversion. The thin horizontal lines represent the  $1p_{1/2}$  single-particle state, while the thick ones the  $2s_{1/2}$  orbital. In the case of  $^{10}\text{Li}$  one reports the centroid of the virtual and of the resonant states.  $E^*$  stands for excitation energy and  $S_n$  is the neutron separation energy. In the case of  $^{10}\text{Li}$  e.g.  $S_n = 0$ , while  $E^*_{s_{1/2}} = 0.2$  MeV and  $E^*_{p_{1/2}} = 0.5$  MeV. In the inset the correlation (CO) and polarization (PO) (virtual) contribution to the single-particle self-energy are shown. An arrowed line pointing upwards represents a particle moving in a level with energy  $\epsilon_k > \epsilon_F$ , a downwards pointing line represents a hole state  $\epsilon_i < \epsilon_F$ , while a wavy line stands for a ph-like vibrational state. Their contribution to the real (single-particle “legs” propagating to  $\pm\infty$ times) processes dressing the  $1p_{1/2}$  and  $2s_{1/2}$  neutron states of  $^{10}\text{Li}$  and  $^{11}\text{Be}$  are (a) and (b), respectively. In the first case the phonon corresponds essentially only to the  $2^+$  vibration of the corresponding core ( $^9\text{Li}$  and  $^{10}\text{Be}$ , respectively) and pushes the orbital upwards (Pauli principle, Lamb-shift-like process) making the dressed  $p_{1/2}$  orbital more strongly unbound than what it was originally in the SaxonWoods potential. In the case of the  $2s_{1/2}$  orbital, it is mainly the process (b) which dresses the state making it almost bound (virtual state) as compared with the SaxonWoods state. Within this context, it is of notice that in the binding of the two halo neutrons of  $^{11}\text{Li}$  to the  $^9\text{Li}$  core, it is essentially the pigmy resonance of  $^{11}\text{Li}$  which provides the largest contribution, the coupling to the  $2^+$  vibration of the core  $^9\text{Li}$  giving a small shift in energy (nonetheless, it is this weak component of the self energy which is responsible for the excitation, in the  $^{11}\text{Li}(p,t)^9\text{Li}$  reaction, of the  $1/2, 2.69$  MeV state). In the case of  $^{11}\text{Be}$  the ( $ph$ ) vibrations are the  $2^+, 1$ , and  $3$  of the core  $^{10}\text{Be}$ , in keeping also with the fact that  $^{12}\text{Be}$  does not display a pigmy  $1$  resonance, not at least based on the ground state. It is of notice that graphs (a) and (b) give rise to an effective mass known as the  $\omega$ -mass. Associated with it are the  $Z(\omega) = (m_\omega/m) - 1$  occupation factors (discontinuity at the Fermi energy).

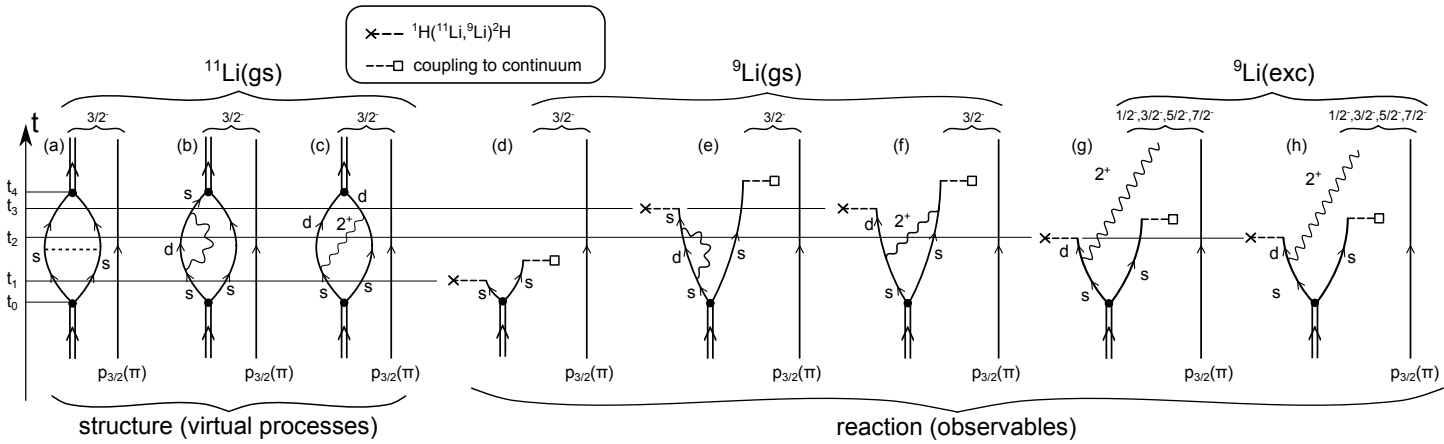


Figure 4.2.5: Nuclear Field Theory diagrams describing the basic, lowest order processes, by which the di-neutron halo binds to the  $^9\text{Li}_6$  core to give rise to  $^{11}\text{Li}$  ground state (**structure**), and those associated with a one-neutron pick-up process, e.g.  $^1\text{H}(^{11}\text{Li}, ^{10}\text{Li})^2\text{H}$  (**reaction**).

potential, cf. Bohr and Mottelson (1969) Eqs. (2–181)–(2–182) single-particle states with vibrations of the  $^9\text{Li}$  core in terms of polarization (effective mass-like) and correlation (vacuum zero point fluctuations (ZPF)) diagrams, similar to those associated with the (lowest order) Lamb shift Feynman diagrams, (cf. App 4.D), shifts the  $s_{1/2}$  and  $p_{1/2}$  mean field levels around. In particular the  $p_{1/2}$  from a bound state ( $\approx -1.2\text{ MeV}$ ) to a resonant state lying at  $\approx 0.5\text{ MeV}$  (Pauli principle, vacuum ZPF process), the  $s_{1/2}$  being lowered and becoming a virtual state ( $\approx 0.2\text{ MeV}$ ) (cf. Fig. 2.F.3 1F3; cf. also Barranco, F. et al. (2001)).

While  $^{10}\text{Li}$  is not bound, adding a second dressed neutron and allowing them to exchange density vibrations of the core, as well as the pigmy giant resonance resulting from the sloshing back and forth of the outer neutrons as well as those of  $^9\text{Li}$  against the protons (cf. Appendix 1F y App. 6.A) binds the Cooper pair to  $^9\text{Li}$ . In fact  $^{11}\text{Li}_8$  displays a two-neutron separation energy  $S_{2n} \approx 400\text{ keV}$  (for further details we refer to Ch. 6, Sect. 6.1).

The two dimensional landscapes (surfaces) displayed in Figs. 2.F.3 figura 1F3 (II) a) and b) attempt at describing the becoming of the neutron halo Cooper pair of  $^{11}\text{Li}$ , from an uncorrelated  $s_{1/2}^2(0)$  configuration to a correlated, (weakly) bound two-neutron state. It is of notice that the bare interaction (boxed inset in (II)), lowers the  $s_{1/2}^2(0)$  (as well as the  $p_{1/2}^2(0)$ ) pure configurations by only 100 keV, and thus it is not able, by itself, to bind the pair, nor to give rise to any significant mixing between these two configurations. The surfaces display the modulus square of the two-neutron wavefunction as a function of the coordinates of the two nucleons (left) and the probability distribution of one neutron with respect to the second one held fixed on the x-axis (at a radius of 5fm, solid dot). The red circle schematically represents the core.

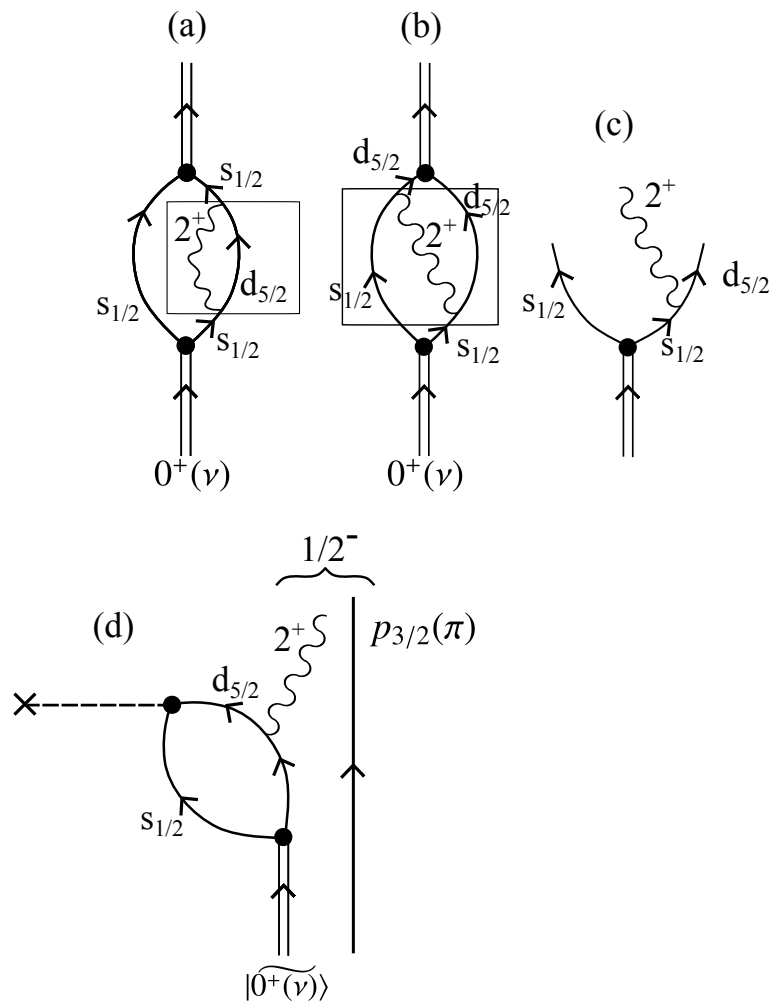


Figure 4.2.6: (a) Self-energy (see boxed process) and (b) vertex (pairing induced interaction) renormalization process, both diagrams associated with (c) a (two-particle)-(quadrupole vibration) intermediate (virtual state) which can be forced to became real in a  $(p, t)$  reaction like e.g.  ${}^1\text{H}({}^{11}\text{Li}, {}^9\text{Li}){}^3\text{H}$  exciting the first excited state  $|2.69\text{MeV}; 1/2^-\rangle$  of  ${}^9\text{Li}$  (see Ch.6).

How can one check that CO and PO like processes as the ones shown in Fig. 2.F.3 1F3 (I) (cf. also Fig. 4.B.1) are the basic processes dressing the odd neutron of  $^{10}\text{Li}$ , and thus the mechanism at the basis of parity inversion? The answer is, forcing these virtual processes to become real. In other words, act on the system with an external field so that certain off-the-energy shell states become on-the-energy shell. In fact, a reaction like  $^1\text{H}(^{11}\text{Li}, ^{10}\text{Li})^2\text{H}$  can populate single-particle states in  $^{10}\text{Li}$  (see Fig. 4.2.5), in particular the two lowest states of  $^{10}\text{Li}$ , namely the virtual and the resonant  $|s_{1/2}\rangle$  and  $|p_{1/2}\rangle$  states respectively (see Orrigo, S. E. A. and Lenske (2009) and Jeppesen, H. B. et al. (2004)). Being these states embedded in the continuum the system will eventually decay into both the ground and excited states of  $^9\text{Li}$  (cf. Fig. 4.2.5) (referir al apendice W).

Now, indirect information on this questions can be obtained with the help of two-particle transfer processes, namely that associated with inverse kinematics ( $p, t$ ) reaction  $^1\text{H}(^{11}\text{Li}, ^9\text{Li}(2.69\text{MeV}; 1/2^-))^3\text{H}$  populating the first excited state of  $^9\text{Li}$ , thought to be the lowest member of the multiplet  $2^+ \otimes p_{3/2}(\pi)$  (cf. Fig. 6.1.1–6.1.3 and 4.2.6). Such a reaction is feasible and has been studied (Tanihata, I. et al., 2008). A price to pay for not using the specific probe for single-particle modes (one-particle transfer), is that of adding to the self-energy contributions in question those corresponding to vertex corrections (for details cf. App 4.E, Figs 4.E.1 and 4.E.2 and Ch. 6).

Within the present context, it is difficult if not impossible to talk about single-particle motion without also referring to collective vibrational states (cf. e.g. Fig. 2.F.3 1F3 (II)), or to talk about pair addition and pair subtraction modes, without at the same time talking about correlated particle-hole (e.g. density) vibrations and dressed quasiparticle motion (see e.g. Fig. 4.2.6 (a) and (b) ), again concerning both structure and reactions. Within the framework of the present monograph, the above facts imply that Chapters ver introduccion, en particular apendice E (inelastic), 4 (one-particle transfer) 5 and 6 (two-particle transfer and applications) form a higher unity. This unity extends also to the content of App 4.G (knock-out reactions), as well as to the question of inelastic channels and of final state interactions, and thus of the possibility that the population of the excited state  $1/2^-$  receives contributions other, and more involved, than those associated with the direct two-nucleon pick-up process depicted in Figs. 4.2.5 (g) and (h) and 4.2.6 (d) (for details cf. Ch. 6, in particular App. 6.B, Table 6.B.1; cf. also (Potel et al., 2010)).

Let us now return to the discussion of the one-particle transfer process  $^1\text{H}(^{11}\text{Li}, ^{10}\text{Li})^2\text{H}$ , that is the pickup of a neutron from the pair addition halo state  $|^{11}\text{Li(gs)}\rangle$  (cf. Fig. 4.2.5). In keeping with the fact that  $^{10}\text{Li}$  is not bound, such a reaction populates only transiently the virtual and resonant states of  $^{10}\text{Li}$  and eventually, after the second neutron of the pair spoliated of its dynamical glue leaves the system by decaying into the continuum, a state in  $^9\text{Li}$  is populated (cf. Figs. 4.2.5 (d)–(f) and 4.2.5 (g) and (h)). In drawing the different NFT diagrams time  $t$  is assumed to run upwards. External fields and the bare  $NN$ -interaction are assumed to act instantaneously, while the couplings to the phonon modes (wavy lines) lead to retarded

( $\omega$ -dependent) effects. For simplicity, only the quadrupole vibrational mode of the  ${}^8\text{He}$  core is considered, as well as only the virtual  $s$ - and continuum  $d$ - single-particle states are taken into account. The halo Cooper pair (pair addition mode of the  $N = 6$  closed shell system) carries angular momentum  $0^+$  and is represented by a double arrowed line, the odd proton ( $\pi$ ) which occupies a  $p_{3/2}$  state, is represented by a single arrowed line and is here treated as a spectator. The di-neutron system binds to the core through (a) the bare interaction (horizontal dashed line) acting between the two-neutron, each represented by a single arrowed line, and through the renormalizing processes associated with the coupling of the neutrons with vibrations; (b) effective mass processes associated with the quadrupole vibration of  ${}^8\text{He}$  (wavy line) renormalizing the energy of the  $s_{1/2}$  continuum state and leading to an almost bound (virtual) state ( $\approx 0.2$  MeV). (c) Vertex correction (induced pairing interaction) associated with the quadrupole vibration of  ${}^8\text{He}$ . (d) Intervening the process (a) at any time after  $t_0$  and before  $t_4$  with an external single-neutron pick-up field (cross followed by an horizontal dashed line), and processes (b) and (c) at  $t_0 < t < t_1$ , leads to the ground state of  ${}^9\text{Li}$ , in keeping with the fact that the second neutron will leave the system almost immediately,  ${}^{10}\text{Li}$  not being stable. (e) Same as above but in connection with process (b) and now after the nucleon has reabsorbed the quadrupole phonon and before  $t_4$ , i.e. acting at  $t_3 < t < t_4$  leads again to the population of the  ${}^9\text{Li}$  ground state. (f) same as (e) but in this case the external field acts on the process (c). Let us now consider the one-nucleon pickup processes populating the  $(2 \otimes p_{3/2}(\pi))_{J^\pi}$ , ( $J^\pi = 1/2^-, 3/2^-, 5/2^-$  and  $7/2^-$ ) multiplet of  ${}^9\text{Li}$ , in particular the lowest  $|1/2^-; 2.69 \text{ MeV}\rangle$  state. In this case the external field has to act at a time  $t_2$  on (b) and on (c) leading to identical final states displayed in (g) and on (h). While the single contribution associated with mass renormalization process ((b) $\rightarrow$ (g)) and vertex corrections ((c) $\rightarrow$ (h)) cannot be distinguished experimentally, one can estimate the relative contribution to the corresponding absolute cross section making use of, microscopic wavefunctions (cf. e.g. Barranco, F. et al. (2001)).

Before concluding the present section, and in connection with Figs. 4.2.5 (g,h) and 4.2.6 (d), it may be useful to remind us what, within the framework of quantum mechanics, one can learn from a reaction experiment. It is not “what is the state after the collision” but “how probable is a given effect of the collision”. Within this context: “The motion of particles follows probability laws, but the probability itself propagates according to the laws of causality” (Born, 1926)<sup>2</sup>.

<sup>2</sup>If there is a lesson to be learned from the above discussion is the fact that, in dealing with a specific feature of a quantal many-body system, e.g. single-particle motion in nuclei (structure) and one-particle transfer process (reaction), one can hardly avoid to talk about other elementary modes of excitation and reaction channels, respectively. Within the scenario of the chosen example, this is because a nucleon which, in first approximation is in a mean field stationary state, can actually be viewed as a fermion moving through a gas of ephemeral  $2p - 2h$  composite virtual excitations, that is  $(p - h) +$  density and/or  $2h(2p)$  + pair addition (subtraction) modes, arising from vacuum (ground state) ZPF and giving rise to the nuclear vacuum  $\omega$ -dependent dielectric function. Because of Pauli principle (Pauli, 1947) the nucleon in question is forced to exchange role with the virtual, off-the-energy-shell nucleons, thus leading to CO processes (cf. Fig. 4.B.1 (b)) and eventually,

## Appendix 4.A Minimal requirements for a consistent mean field theory

In what follows the question of why, rigorously speaking, one cannot talk about single-particle motion, let alone spectroscopic factors, not even within the framework of Hartree–Fock theory, is briefly touched upon (see also App. 4.I).

As can be seen from Fig. 4.A.1 the minimum requirements of selfconsistency to be imposed upon single-particle motion requires both non-locality in space (HF) and in time (TDHF)

$$i\hbar \frac{\partial \varphi_\nu}{\partial t} = -\frac{\hbar^2}{2m} \nabla^2 \varphi_\nu(x, t) + \int dx' dt' U(x - x', t - t') \varphi_\nu(x', t'), \quad (4.A.1)$$

and consequently also of collective vibrations and, consequently, from their interweaving to dressed single-particles (quasiparticles), let alone renormalized collective modes (cf. Fig. 4.C.3). Assuming for simplicity infinite nuclear matter (confined by a constant potential of depth  $V_0$ ), and thus plane wave solutions, the above time-dependent Schrödinger equation leads to the quasiparticle dispersion relation

$$\hbar\omega = \frac{\hbar^2 k^2}{2m^*} + \frac{m}{m^*} V_0, \quad (4.A.2)$$

where the effective mass

$$m^* = \frac{m_k m_\omega}{m}, \quad (4.A.3)$$

in the product of the  $k$ -mass

$$m_k = m \left( 1 + \frac{m}{\hbar^2 k} \frac{\partial U}{\partial k} \right)^{-1}, \quad (4.A.4)$$

closely connected with the Pauli principle ( $\frac{\partial U}{\partial k} \approx \frac{\partial U_x}{\partial k}$ ), while the  $\omega$ -mass

$$m_\omega = m \left( 1 - \frac{\partial U}{\partial \hbar\omega} \right), \quad (4.A.5)$$

results from the dressing of the nucleon through the coupling with the (quasi) bosons. Because typically  $m_k \approx 0.7m$  and  $m_\omega \approx 1.4m$ ,  $m^* \approx m$ , one could be tempted to conclude that the results embodied in the dispersion relation (4.A.2) reflects the fact that the distribution of levels around the Fermi energy can be described in terms of the solutions of a Schrödinger equation in which nucleons of mass equal to the bare nucleon mass  $m$  move in a Saxon–Woods potential of depth  $V_0$ .

---

through time ordering, to PO ones (cf. Fig. 4.B.1 (a)). Such processes, eventually carried on to higher orders of perturbation in the nucleon–vibration coupling, eventually diagonalize the nuclear Hamiltonian, taking care of the overcompleteness (non-orthogonality) and of Pauli violations of the basis made out of elementary modes of nuclear excitation, thus leading to dressed (observable) modes, single-particle states in the present case, whose properties, e.g. absolute single-particle transfer cross sections, can be compared with the data without further ado.

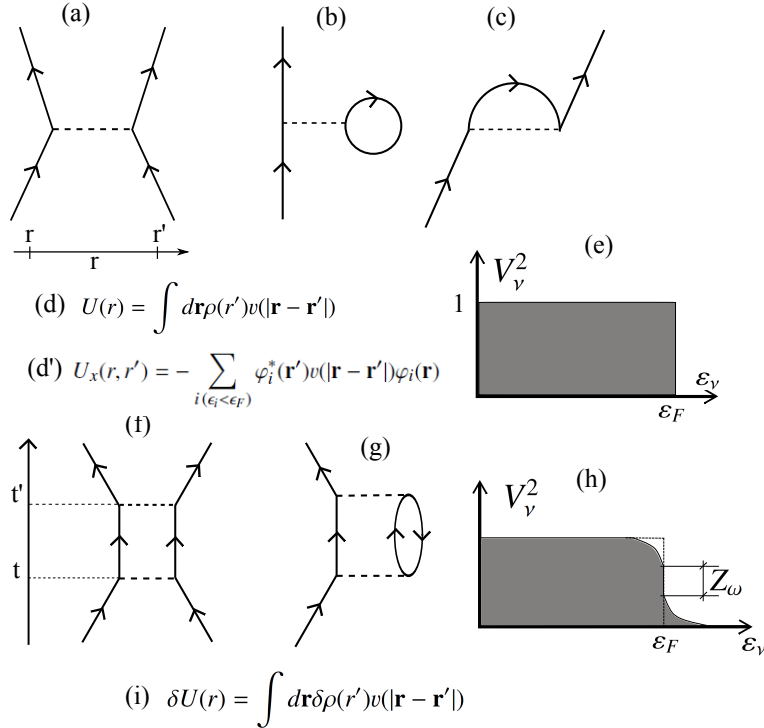


Figure 4.A.1: (a) Scattering of two nucleons through the bare  $NN$  interaction  $v|\mathbf{r} - \mathbf{r}'|$ , (b) contribution to the direct ( $U$ , Hartree) and (c) to the exchange ( $U_x$ , Fock) potential, resulting in (d) the (static) self-consistent relation between potential and density (non-local (d')), which (e) uncouples occupied ( $\varepsilon_\nu \leq \varepsilon_F$ ) from empty states ( $\varepsilon_\nu > \varepsilon_F$ ), (f) multiple scattering of two nucleons lead, through processes like the one depicted in (g), eventually propagated to all orders, to: (h) softening of the discontinuity of the occupancy of levels at  $\varepsilon_F$ , as well as to: (i) generalization of the static selfconsistency into a dynamic relation encompassing also collective vibrations (Time-Dependent HF solutions of the nuclear Hamiltonian, conserving energy weighted sum rules (EWSR)).

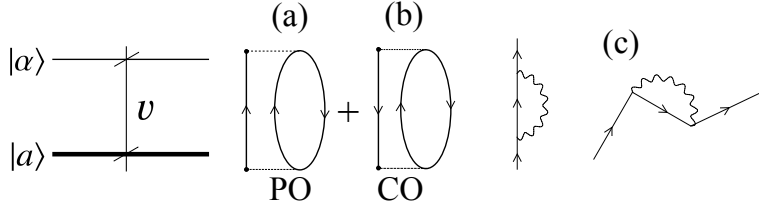


Figure 4.B.1: Two state schematic model describing the breaking of the strength of the pure single-particle state  $|a\rangle$ , through the coupling to collective vibrations (wavy line) associated with polarization (PO) and correlation (CO) processes.

Now, it can be shown that the occupancy of levels around  $\varepsilon_F$  is related to  $Z_\omega$ , a quantity which measures the discontinuity at the Fermi energy (cf. Fig. 4.A.1 (h)) and which is equal to  $m/m_\omega = 1/(1+\lambda_{p-v}) \approx 0.7$ ,  $\lambda_{p-v}$  being the mass enhancement factor ( $\lambda_{p-v} = N(0)g_{p-v}$ ), product of the density of levels at the Fermi energy and the particle–vibration coupling parameter (cf. e.g. Bohr, A. and Mottelson (1975); Brink, D. and Broglia (2005) and refs. therein). This is in keeping with the fact that the time the nucleon is coupled to the vibrations it cannot behave as a single-particle and can thus not contribute to e.g. the single-particle pickup cross section.

It is of notice that the selfconsistence requirements for the iterative solution of Eq. (4.A.1) (see Fig. 4.A.1 (d) and (d')) remind very much those associated with the solution of the Kohn–Sham equations in finite systems,

$$H^{KS} \varphi_\gamma(\mathbf{r}) = \lambda_\gamma \varphi_\gamma(\mathbf{r}), \quad (4.A.6)$$

where

$$H^{KS} = -\frac{\hbar^2}{2m_e} \nabla^2 + U_H(\mathbf{r}) + V_{ext}(\mathbf{r}) + U_{xc}(\mathbf{r}), \quad (4.A.7)$$

$H^{KS}$  being known as the Kohn–Sham Hamiltonian,  $V_{ext}(\mathbf{r})$  being the field created by the ions and acting on the electrons. Both the Hartree and the exchange–correlation potentials  $U_H(\mathbf{r})$  and  $U_{xc}(\mathbf{r})$  depend on the (local) density, hence on the whole set of wavefunctions  $\varphi_\gamma(\mathbf{r})$ . Thus, the set of  $KS$ –equations must be solved selfconsistently (cf. e.g. (Broglia et al., 2004) and refs. therein).

## Appendix 4.B Model for single-particle strength function: Dyson equation

In the previous Appendix we schematically introduced the argument concerning the “impossibility” of defining a “bona fide” single-particle spectroscopic factor. It was done with the help of Feynman (NFT) diagrams. In what follows we essentially repeat the arguments, but this time in terms of Dyson’s (Schwinger) language. For simplicity, we consider a two-level model where the pure single-particle state  $|a\rangle$  couples to a more complicated (doorway) state  $|\alpha\rangle$ , made out of a fermion (particle or hole), coupled to a particle–hole excitation which, if iterated to all orders

can give rise to a collective state (cf. Fig. 4.B.1). The Hamiltonian describing the system is (Bohr and Mottelson, 1969)

$$H = H_0 + v, \quad (4.B.1)$$

where

$$H_0|a\rangle = E_a|a\rangle, \quad (4.B.2)$$

and

$$H_0|\alpha\rangle = E_\alpha|\alpha\rangle. \quad (4.B.3)$$

Let us call  $\langle a|v|\alpha\rangle = v_{a\alpha}$  and assume  $\langle a|v|a\rangle = \langle \alpha|v|\alpha\rangle = 0$ .

From the secular equation

$$\begin{pmatrix} E_\alpha & v_{a\alpha} \\ v_{a\alpha} & E_a - E_i \end{pmatrix} \begin{pmatrix} C_\alpha(i) \\ C_a(i) \end{pmatrix} = 0, \quad (4.B.4)$$

and associated normalization condition

$$C_a^2(i) + C_\alpha^2(i) = 0, \quad (4.B.5)$$

one obtains

$$C_a^2(i) = \left( 1 + \frac{v_{a\alpha}^2}{(E_\alpha - E_i)^2} \right)^{-1}, \quad (4.B.6)$$

and

$$\Delta E_a(E) = E_a - E = \frac{v_{a\alpha}^2}{E_a - E}. \quad (4.B.7)$$

The energy of the correlated state

$$|\tilde{a}\rangle = C_a(i)|a\rangle + C_\alpha(i)|\alpha\rangle, \quad (4.B.8)$$

is obtained by the (iterative) solution of the Dyson equation (4.B.7), which propagate the bubble diagrams shown in Figs 4.B.1 (a) and (b) to infinite order leading to collective vibrations (see Fig. 4.B.1 (c))

With the help of the definition given in eq (4.A.5), and making use of the fact that in the present case, the quantity  $U$  appearing in this equation coincides, within the present context with  $\Delta E_a(E)$ , one obtains that the discontinuity of the single-particle levels at the Fermi energy is given by

$$Z_\omega = C_a^2(i) = \left( \frac{m_\omega}{m} \right)^{-1}. \quad (4.B.9)$$

Making use of the solution of the Dyson equation (4.B.7), and of the relations (4.B.5) and (4.B.6), one can calculate the renormalized state  $|\tilde{a}\rangle$  (Eq. 4.B.8) to be employed in working out the associated, modified, single-particle transfer form factor needed in the calculation of the absolute value of one-particle transfer cross sections (cf. e.g. Sect. 4.2.1, where the above concepts and techniques are applied to the study of one-neutron transfer reactions in open shell, superfluid ( $^{120}\text{Sn}$ )).

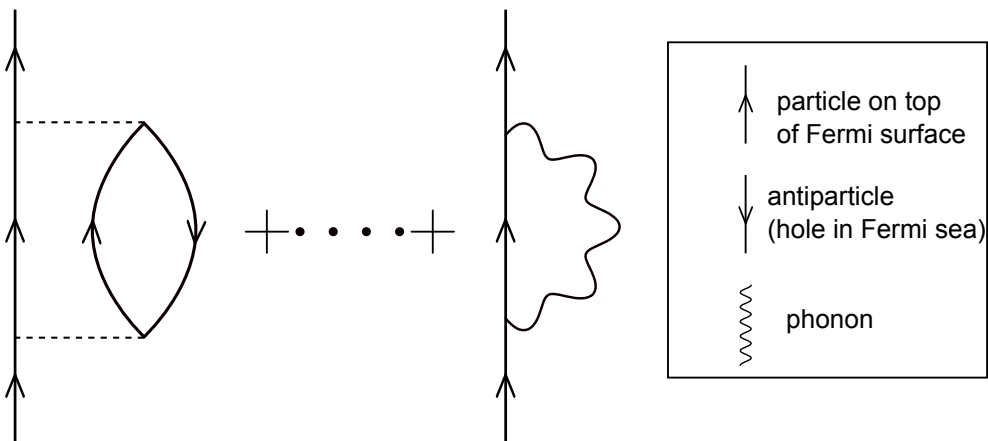


Figure 4.C.1: Feynman diagrams renormalizing the properties of a fermion.

## Appendix 4.C Antiparticles: proof of concept of the quantal vacuum and of medium polarization effects

Let us consider a massive quantal particle, e.g., an electron, which moves at a velocity close of that of light. Because of Heisenberg relations, there exists a finite possibility to observe the particle moving at a velocity larger than its average velocity, and thus faster than light, a possibility ruled out by special relativity. The only way to avoid this, is by introducing antiparticles, that is a hole in the “vacuum” filled to the rim (Fermi energy) with particles, thus providing the physics to the negative energy solutions of Dirac equation.

In other words, when an electron approaches the maximum speed with which information propagate in a medium, like e.g. in the case of an electron in the QED vacuum, processes like the one depicted in Fig. 4.C.1 become operative. In other words, one can take care of the position indeterminacy of a quantal particle (electron) accepting the possibility to observe it through specific measurements which unavoidably create different particles, each of them identical to the original one, but with different positions, to keep track of conserved quantum numbers, these particles are to be accompanied by an equal number of antiparticles (positrons).

Similar results can be obtained by considering vacuum fluctuations (ZPF), and forcing them to become real through e.g. the Pauli principle (Pauli, 1947), as observed in the Lamb shift (Fig. 4.C.2, cf. also Fig. 4.D.1).

In the nuclear case the medium can, due to spatial quantization typical of Finite Many-Body Systems (FMBS), propagate information with varied frequency. Typically, few MeV (low-lying collective vibrations) and tens of MeV (giant resonances), leading to a rich number of CO and PO processes. This is in keeping with the fact that the intermediate boson (photon QED, vibrations of nuclear medium) propagates in a medium which is not isotropic, thus undergoing fragmentation of

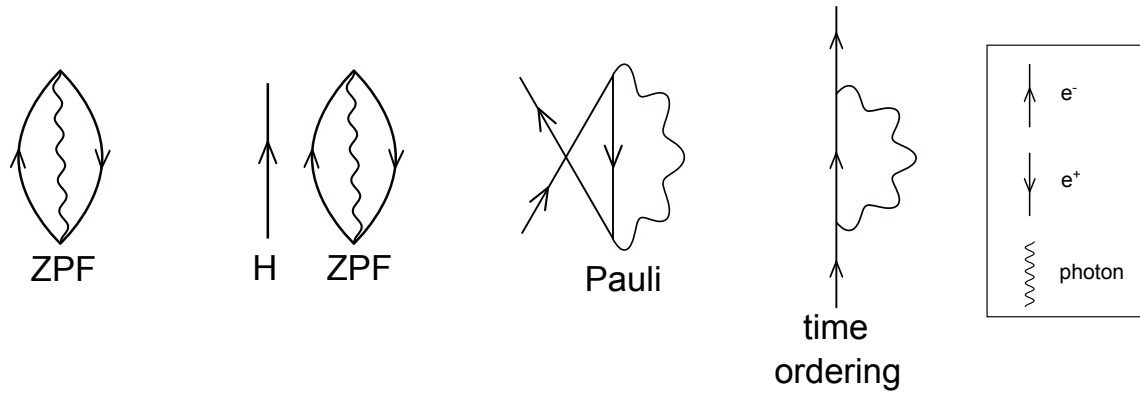


Figure 4.C.2: QED vacuum fluctuation (ZPF). In presence of e.g. an hydrogen atom (H), its electron is forced by Pauli principle to exchange with that of the ZPF, leading to a CO (correlation) like process. Time ordering leads to PO (polarization) processes.

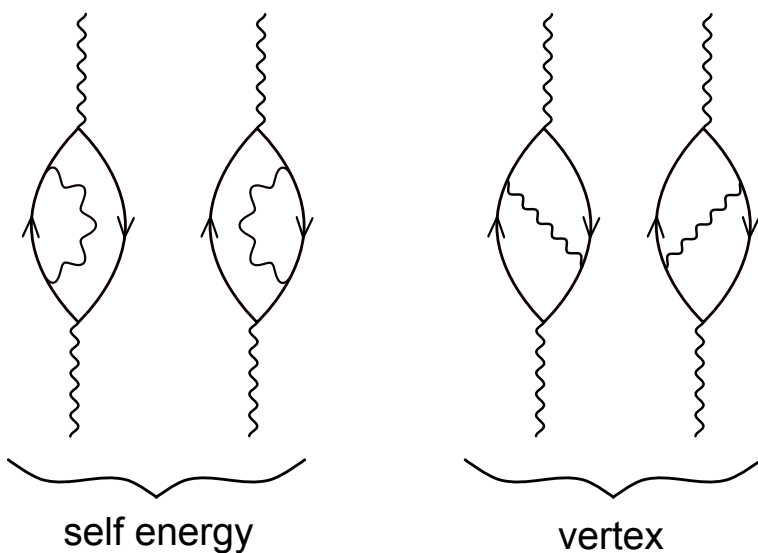


Figure 4.C.3: Lowest order diagrams which dress collective nuclear vibrations and GR.

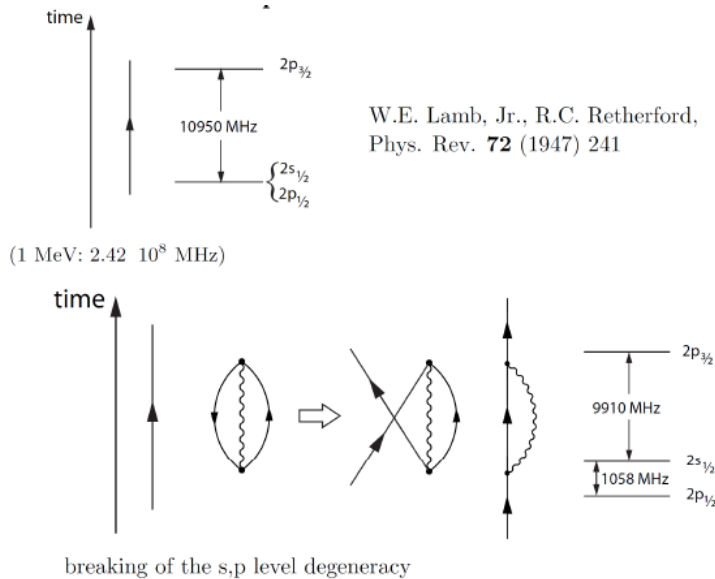


Figure 4.D.1: Schematic representation of the processes associated with the Lamb shift.

the associated strength (inhomogeneous damping). To make even richer the nuclear scenario, collisional damping plays also a role in the strength function of GR. Nonetheless, the associated widths (lifetimes) are controlled by the coupling to doorway states (cf. figura1d6 apendice D introducción), even at nuclear temperatures of 1–2 MeV, let alone when the GR is based on the ground state (Fig. 4.C.3; cf. Bortignon, P.F. et al. (1998) and refs. therein, cf. also Broglia, R. A. et al. (1987)). The strong cancellation found between self-energy and vertex correction diagrams, testify to the collectivity of nuclear vibrations (generalized Ward identities), and reminds of Furry's theorem (no coupling between one- and two-photon states). Summing up, nothing is really free in the quantal world (cf. also App. 4.E). Selected measurements carried out with specific probes, can make virtual processes become real, and shed light on the variety of these processes leading to renormalized elementary modes of nuclear excitation (dressed fermions and bosons).

## Appendix 4.D The Lamb Shift

In Fig. 4.D.1 we display a schematic summary of the electron–photon processes, associated with Pauli principle corrections, leading to the splitting of the lowest  $s, p$  states of the hydrogen atom known as the Lamb shift.

In the upper part of the figure the predicted position of the electronic single-particle levels of the hydrogen atom as resulting from the solution of the Schrödinger equation (Coulomb field). In the lowest part of the figure one displays the electron

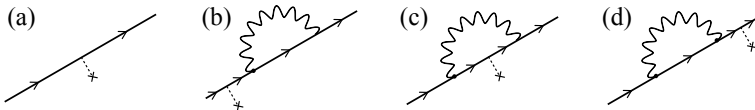


Figure 4.E.1: Self energy (effective–mass–like) processes. The result of the probing with an external field (dotted line started with a cross, observer) of the properties (mass, single–particle energy, etc) of a fermion (e.g. an electron or a nucleon, arrowed line) dressed through the coupling of (quasi) bosons (photons or collective vibrations, wavy line), corresponds to the modulus squared of the sum of the amplitudes associated with each of the four diagrams (a)–(d) (cf. (Feynman, 1975)). A concrete embodiment of the above parlance is provided by the process  $^1\text{H}(^{11}\text{Li}, ^9\text{Li})^3\text{H}$  (cf. Figs. 4.2.5 and 4.2.6).

of an hydrogen atom (upwards going arrowed line) in presence of vacuum ZPF (electron–positron pair plus photon, oyster–like diagram) (within this scenario we refer to App. 4.C concerning to the central role ZPF of the vacuum and the concept of antiparticle (hole) has in the description of physical, dressed observable states of quantal many–body systems). Because the associate electron virtually occupies states already occupied by the hydrogen’s electron, thus violating Pauli principle, one has to antisymmetrize the corresponding two–electron state. Such process gives rise to the exchange of the corresponding fermionic lines and thus to CO–like diagrams as well as, through time ordering, to PO–like diagrams. The results provide a quantitative account of the experimental findings.

## Appendix 4.E Self–energy and vertex corrections

In Fig. 4.E.1 an example of the fact that in field theories (e.g. QED or NFT), nothing is really free and that e.g., the bare mass of a fermion (electron or nucleon), is the parameter one adjusts ( $m_k$ ) so that the result of a measurement gives the observed mass (single particle energy). In Fig. 4.E.2, lowest order diagrams associated with the renormalization of the fermion–boson interaction (vertex corrections) are given. The sum of contributions (a) and (b) can, in principle, be represented by a renormalized vertex (cf. diagram (c)). It is of notice, however, that there is, as a rule, conspicuous interference (e.g. cancellation) in the nuclear case between vertex and self–energy contributions (cf. diagrams (a) and (d)+(e) of Fig. 4.E.2, a phenomenon closely related with conservation laws (generalized Ward identities); cf. also Fig. 4.C.3 and refs. Bortignon and Broglia (1981); Bertsch et al. (1983) and Bortignon, P.F. et al. (1998) pp. 82–86). In particular, cancellation in the case in which the bosonic modes are isoscalar (Bortignon et al., 1983). Consequently, one has to sum explicitly the different amplitudes with the corresponding phases and eventually take the modulus squared of the result to eventually obtain

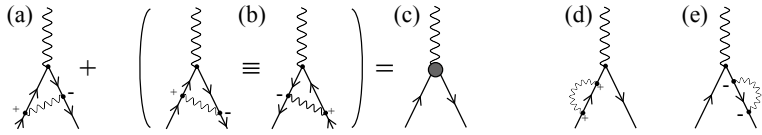


Figure 4.E.2: Vertex corrections. These are triple–interaction diagrams (phonon, particle and hole lines) in which none of the incoming lines can be detached from either of the other two by cutting one line. In connection with condensed matter Migdal’s theorem (Migdal (1958)) states that for phonons, (Bardeen and Pines (1955), Fröhlich, H. (1952)) vertex corrections can be neglected (cf. also Anderson (1984)). Vertex corrections are, as a rule, important in the nuclear case where they lead to conspicuous cancellations of the self–energy contributions (cf. e.g. Bortignon et al. (1983), cf. also Anderson (1984)). The solid grey circle in (c) represents the effective, renormalized vertex.

the quantities to be compared with the data, a fact that precludes the use of an effective,  $\omega$ –independent (renormalized) vertex.

Within the framework of QED the above mentioned cancellations are exact implying that the interaction between one– and two–photon states vanishes (Furry theorem). The physics at the basis of the cancellation found in the nuclear case can be exemplified by looking at a spherical nucleus displaying a low–lying collective quadrupole vibration. The associated zero point fluctuations (ZPF) lead to time dependent shapes with varied instantaneous values of the quadrupole moment, and of its orientation (dynamical spontaneous breaking of rotational invariance, ver apendice 1B correlations and fluctuations). In other words, a component of the ground state wavefunction ( $| (j_p \otimes j_h^{-1})_{2+} \otimes 2^+; 0^+ \rangle$ ), which can be viewed as a gas of quadrupole (quasi) bosons promoting a nucleon across the Fermi energy (particle–hole excitation) will lead to fermionic states which behave as having a positive (particle) and a negative (hole) effective quadrupole moment, in keeping with the fact that the closed shell system is spherical, thus carrying zero quadrupole moment.

## Appendix 4.F Single–nucleon transfer for pedestrians

In this Appendix we discuss some aspects of the relations existing between nuclear structure and one–particle transfer cross sections. To do so, we repeat some of the steps carried out in the text but this time in a simpler and straightforward way, ignoring the complications associated with the spin carried out by the particles, the spin–orbit dependence of the optical model potential, the recoil effect, etc.

We consider the case of  $A(d, p)A + 1$  reaction, namely that of neutron stripping.

The intrinsic wave functions  $\psi_\alpha$  and  $\psi_\beta$ , where  $\alpha = (A, d)$  and  $\beta = ((A + 1), p)$ ,

$$\psi_\alpha = \psi_{M_A}^{I_A}(\xi_A) \phi_d(\vec{r}_{np}), \quad (4.F.1a)$$

$$\begin{aligned} \psi_\beta &= \psi_{M_{A+1}}^{I_{A+1}}(\xi_{A+1}) \\ &= \sum_{l, I'_A} (I'_A; l | I_{A+1}) [\psi_{M_A}^{I_A}(\xi_A) \phi^l(\vec{r}_n)]_{M_{A+1}-M_A}^{I_{A+1}}, \end{aligned} \quad (4.F.1b)$$

where  $(I'_A; l | I_{A+1})$  is a generalized fractional parentage coefficient. It is of notice that this fractional parentage expansion is not well defined. In fact, as a rule,  $(I'_A; l | I_{A+1}) \phi^l(\vec{r}_n)_{M_{A+1}-M_A}$  is an involved, dressed quasiparticle state containing only a fraction of the “pure” single particle strength (cf. Apps 4.A and 4.B). For simplicity we assume the expansion to be operative. To further simplify the derivation we assume we are dealing with spinless particles. This is the reason why no “intrinsic” proton wavefunction appears in (4.F.1b). The variable  $\vec{r}_{np}$  is the relative coordinate of the proton and the neutron (see Fig. 4.F.1).

The transition matrix element can now be written as

$$\begin{aligned} T_{d,p} &= \langle \psi_{M_{A+1}}^{I_{A+1}}(\xi_{A+1}) \chi_p^{(-)}(k_p, \vec{r}_p), V'_\beta \psi_{M_A}^{I_A}(\xi_A) \chi_d^{(+)}(k_d, \vec{r}_d) \rangle \\ &= \sum_{l, I'_A} (I'_A; l | I_{A+1}) (I'_A M'_A l M_{A+1} - M' A | I_{A+1} M_{A+1}) \\ &\quad \times \int d\vec{r}_n d\vec{r}_p \chi_p^{*(-)}(k_p, \vec{r}_p) \phi_{M_{A+1}-M_A}^{*l}(\vec{r}_n) (\psi_{M_A}^{I_A}(\xi_A), V'_\beta \psi_{M'_A}^{I'_A}(\xi_A)) \\ &\quad \times \phi_d(\vec{r}_{np}) \chi_d^{(+)}(k_d, \vec{r}_d) \delta_{I'_A, I_A} \delta_{M'_A, M_A}. \end{aligned} \quad (4.F.2)$$

In the stripping approximation

$$\begin{aligned} V'_\beta &= V_\beta(\xi, \vec{r}_\beta) - \bar{U}_\beta(r_\beta) \\ &= V_\beta(\xi_A, \vec{r}_{pA}) + V_\beta(\vec{r}_{pn}) - \bar{U}_\beta(r_{pA}). \end{aligned} \quad (4.F.3)$$

Then

$$\begin{aligned} (\psi_{M_A}^{I_A}(\xi_A), V'_\beta \psi_{M_A}^{I_A}(\xi_A)) &= (\psi_{M_A}^{I_A}(\xi_A), V_\beta(\xi_A, \vec{r}_{pA}) \psi_{M_A}^{I_A}(\xi_A)) \\ &\quad + (\psi_{M_A}^{I_A}(\xi_A), V_\beta(\vec{r}_{pn}) \psi_{M_A}^{I_A}(\xi_A)) - \bar{U}_\beta(r_{pA}). \end{aligned} \quad (4.F.4)$$

We assume

$$U_\beta(r_{pA}) = (\psi_{M_A}^{I_A}(\xi_A), V_\beta(\xi_A, \vec{r}_{pA}) \psi_{M_A}^{I_A}(\xi_A)). \quad (4.F.5)$$

Then

$$(\psi_{M_A}^{I_A}(\xi_A), V'_\beta \psi_{M_A}^{I_A}(\xi_A)) = V_{np}(\vec{r}_{pn}). \quad (4.F.6)$$

Inserting eq. (4.F.6) into eq. (4.F.2) we obtain

$$\begin{aligned} T_{d,p} &= \sum_l (I_A; l | I_{A+1}) (I_A M_A l M_{A+1} - M_A | I_{A+1} M_{A+1}) \\ &\quad \times \int d\vec{r}_n d\vec{r}_p \chi_p^{*(-)}(k_p, \vec{r}_p) \phi_{M_{A+1}-M_A}^{*l}(\vec{r}_n) V(\vec{r}_{pn}) \phi_d(\vec{r}_{np}) \chi_d^{(+)}(k_d, \vec{r}_d) \end{aligned} \quad (4.F.7)$$

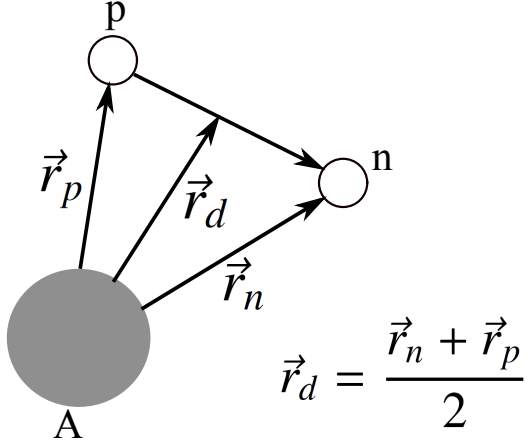


Figure 4.F.1: Coordinates used in the description of the  $A(d, p)(A + 1)$  stripping process.

The differential cross section is then equal to

$$\frac{d\sigma}{d\Omega} = \frac{2}{3} \frac{\mu_p \mu_d}{(2\pi\hbar^2)^2} \frac{(2I_{A+1} + 1)}{(2I_A + 1)} \frac{k_p}{k_d} \sum_{l,m_l} \frac{(I_A; l||I_{A+1})^2}{2l + 1} |B_{m_l}^l|^2, \quad (4.F.8)$$

where

$$B_{m_l}^l(\theta) = \int d\vec{r}_n d\vec{r}_p \chi_p^{*(-)}(k_p, \vec{r}_p) Y_m^{*l}(\hat{r}_n) u_{nl}(r_n) V(\vec{r}_{pn}) \phi_d(\vec{r}_{np}) \chi_d^{(+)}(k_d, \vec{r}_d) \quad (4.F.9)$$

and

$$\phi_m^l(\vec{r}_n) = u_{nl}(r_n) Y_m^l(\hat{r}_n), \quad (4.F.10)$$

is the single-particle wave function of a neutron bound to the core A. For simplicity, the radial wave function  $u_{nl}(r_n)$  can be assumed to be a solution of a Saxon-Woods potential of parameters  $V_0 \approx 50$  MeV,  $a = 0.65$  fm and  $r_0 = 1.25$  fm.

The relation (4.F.8) gives the cross section for the stripping from the projectile of a neutron that would correspond to the  $n^{\text{th}}$  valence neutron in the nucleus  $(A + 1)$ . If we now want the cross section for stripping any of the valence neutrons of the final nucleus from the projectile, we must multiply eq. (4.F.8) by  $n$ . A more careful treatment of the antisymmetry with respect to the neutrons shows this to be the correct answer.

Finally we get

$$\frac{d\sigma}{d\Omega} = \frac{(2I_{A+1} + 1)}{(2I_A + 1)} \sum_l S_l \sigma_l(\theta), \quad (4.F.11)$$

where

$$S_l = n(I_A; l||I_{A+1})^2, \quad (4.F.12)$$

and

$$\sigma_l(\theta) = \frac{2}{3} \frac{\mu_p \mu_d}{(2\pi\hbar^2)^2} \frac{k_p}{k_d} \frac{1}{2l + 1} \sum_m |B_m^l|^2 \quad (4.F.13)$$

The distorted wave softwares evaluate numerically the quantity  $B_{m_l}^l(\theta)$ , using for the wave functions  $\chi^{(-)}$  and  $\chi^{(+)}$  the solution of the optical potentials that fit the elastic scattering, i.e.

$$(-\nabla^2 + \bar{U} - k^2)\chi = 0, \quad (4.F.14)$$

Note that if the target nucleus is even–even,  $I_A = 0$ ,  $l = I_{A+1}$ . That is, only one  $l$  value contributes in Eq. (4.F.8), and the angular distribution is uniquely given by  $\sum_m |B_m^l|^2$ . The  $l$ -dependence of the angular distributions helps to identify  $l = I_{A+1}$ . The factor  $S_l$  needed to normalize the calculated function to the data yields (assuming a good fit to the angular distribution), is known in the literature as the spectroscopic factor. It was assumed in the early stages of studies of nuclear structure with one-particle transfer reactions not only that it could be defined, but also that it contained all the nuclear structure information (aside from that associated with the angular distribution) which could be extracted from single-particle transfer. In other words, that it was the bridge directly connecting theory with experiment. Because nucleons are never bare, but are dressed by the coupling to collective modes as previously discussed in this chapter, the spectroscopic factor approximation is at best a helpful tool to get order of magnitude information from one-particle transfer data.

There is a fundamental problem which makes the handling of integrals like that of (4.F.9) difficult to handle, if not numerically at least conceptually. This difficulty is connected with the so called recoil effect <sup>3</sup>, namely the fact that the center of mass of the two interacting particles in entrance ( $\mathbf{r}_\alpha : \alpha = a + A$ ) and exit ( $\mathbf{r}_\beta : \beta = b + B$ ) channels is different. This is at variance with what one is accustomed to deal with in nuclear structure calculations, in which the Hartree potential depends on a single coordinate, as well as in the case of elastic and inelastic reactions, situations in which  $\mathbf{r}_\alpha = \mathbf{r}_\beta$ . When  $\mathbf{r}_\alpha \neq \mathbf{r}_\beta$  we enter a rather more complex many-body problem, in particular if continuum states are to be considered, than nuclear structure practitioners were accustomed to.

Of notice that similar difficulties have been faced in connection with the non-local Fock (exchange) potential. As a rule, the corresponding (HF) mean field equations are rendered local making use of the  $k$ -mass approximation or within the framework of Local Density Functional Theory (DFT), in particular with the help of the Kohn–Sham equations (see e.g. Mahaux, C. et al. (1985), Broglia et al. (2004) and refs. therein; cf. also App. 4.A). Although much of the work in this field is connected with the correlation potential (interweaving of single-particle and collective motion), an important fraction is connected with the exchange potential.

In any case, and returning to the subject of the present appendix, it is always useful to be able to introduce approximations which can help the physics which is at the basis of the phenomenon under discussion (single-particle motion) emerge

---

<sup>3</sup>While this effect could be treated in a cavalier fashion in the case of light ion reactions ( $m_a/m_A \ll 1$ ), this was not possible in the case of heavy ion reactions, as the change in momenta involved was always sizeable (cf. Broglia and Winther (2004) and refs. therein).

in a natural way, if not to compare in detail with the experimental data. Within this context, to reduce the integral (4.F.9) one can assume that the proton-neutron interaction  $V_{np}$  has zero-range, i.e.

$$V_{np}(\vec{r}_{np})\phi_d(\vec{r}_{np}) = D_0\delta(\vec{r}_{np}) \quad (4.F.15)$$

so that  $B_m^l$  becomes equal to

$$B_{m_l}^l(\theta) = D_0 \int d\vec{r} \chi_p^{*(-)}(k_p, \vec{r}) Y_{m_l}^{*l}(\hat{r}) u_l(r) \chi_d^{(+)}(k_d, \vec{r}), \quad (4.F.16)$$

which is a three dimensional integral, but in fact essentially a one-dimensional integral, as the integration over the angles can be worked out analytically.

#### 4.F.1 Plane-wave limit

If in Eq. (4.F.14) one sets  $\bar{U} = 0$ , the distorted waves become plane waves i.e.

$$\chi_d^{(+)}(k_d, \vec{r}) = e^{i\vec{k}_d \cdot \vec{r}}, \quad (4.F.17a)$$

$$\chi_d^{*(-)}(k_p, \vec{r}) = e^{-i\vec{k}_p \cdot \vec{r}}. \quad (4.F.17b)$$

Equation (4.F.16) can now be written as

$$B_m^l = D_0 \int d\vec{r} e^{i(\vec{k}_d - \vec{k}_p) \cdot \vec{r}} Y_m^{*l}(\hat{r}) u_l(r). \quad (4.F.18)$$

The linear momentum transferred to the nucleus is  $\vec{k}_d - \vec{k}_p = \vec{q}$ . Let us expand  $e^{i\vec{q} \cdot \vec{r}}$  in spherical harmonics, i.e.

$$\begin{aligned} e^{i\vec{q} \cdot \vec{r}} &= \sum_l i^l j_l(qr) (2l+1) P_l(\hat{q} \cdot \hat{r}) \\ &= 4\pi \sum_l i^l j_l(qr) \sum_m Y_m^{*l}(\hat{q}) Y_m^l(\hat{r}), \end{aligned} \quad (4.F.19)$$

so

$$\int d\hat{r} e^{i\vec{q} \cdot \vec{r}} Y_m^l(\hat{r}) = 4\pi i^l j_l(qr) Y_m^{*l}(\hat{q}). \quad (4.F.20)$$

Then

$$\begin{aligned} \sum_m |B_m^l|^2 &= \sum_m |Y_m^l(\hat{q})|^2 D_0^2 16\pi^2 \times \\ &\quad \left| \int r^2 dr j_l(qr) u_l(r) \right|^2 = \\ &\quad \frac{2l+1}{4\pi} D_0^2 16\pi^2 \left| \int r^2 dr j_l(qr) u_l(r) \right|^2. \end{aligned} \quad (4.F.21)$$

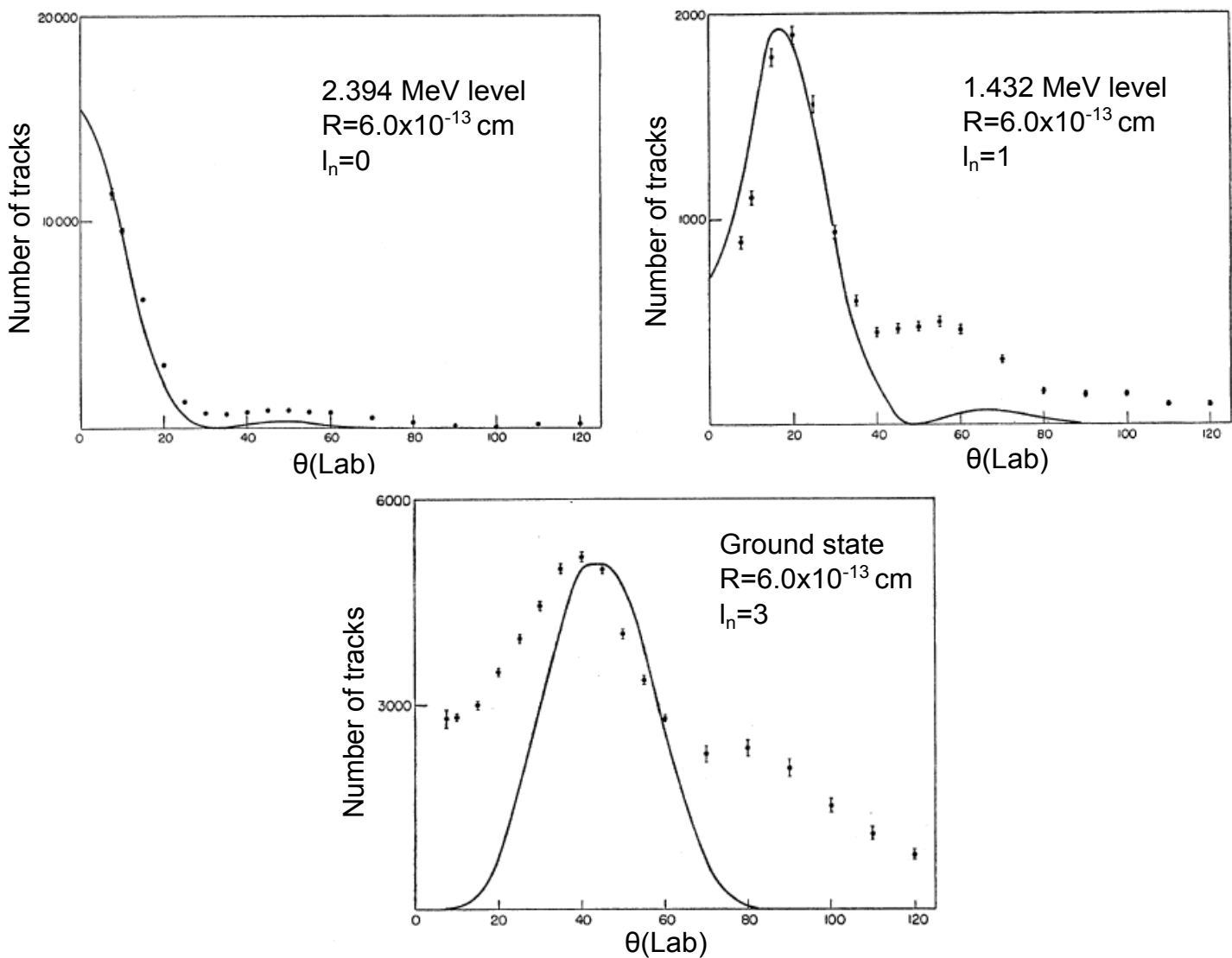


Figure 4.F.2: Plane wave approximation analysis of three  $^{44}\text{Ca}(\text{d},\text{p})^{45}\text{Ca}$  differential cross sections leading to the ground state ( $l_n = 3$ ) and to the 1.9 MeV state ( $l_n = 1$ ) and 2.4 MeV ( $l_n = 0$ ) excited states, i.e.  $f_{9/2}$ ,  $p_{1/2}$  and  $s_{1/2}$  states (Cobb and Guthe, 1957).

Thus, the angular distribution is given by the integral  $\left| \int r^2 dr j_l(qr) u_l(r) \right|^2$ . If one assumes that the process takes place mostly on the surface, the angular distribution will be given by  $|j_l(qR_0)|^2$ , where  $R_0$  is the nuclear radius.

We then have

$$\begin{aligned} q^2 &= k_d^2 + k_p^2 - 2k_d k_p \cos(\theta) \\ &= (k_d^2 + k_p^2 - 2k_d k_p) + 2k_d k_p (1 - \cos(\theta)) \\ &= (k_d - k_p)^2 + 4k_d k_p (\sin(\theta/2))^2 \\ &\approx 4k_d k_p (\sin(\theta/2))^2, \end{aligned} \quad (4.F.22)$$

since  $k_d \approx k_p$  for stripping reactions at typical energies. Thus the angular distribution has a diffraction-like structure given by

$$|j_l(qR_0)|^2 = j_l^2(2R_0 \sqrt{k_d k_p} \sin(\theta/2)). \quad (4.F.23)$$

The function  $j_l(x)$  has its first maximum at  $x = l$ , i.e. where

$$\sin(\theta/2) = \frac{l}{2R_0 k}, \quad (k_p \approx k_d = k), \quad (4.F.24)$$

Examples of the above relation are provided in Fig. 4.F.2.

## Appendix 4.G One-particle knockout within DWBA

### 4.G.1 Spinless particles

We are going to consider the reaction  $A + a \rightarrow a + b + c$ , in which the cluster  $b$  is knocked out from the nucleus  $A (= c + b)$ . Cluster  $b$  is thus initially bound, while the final states of  $a, b$  and the initial state of  $a$  are all in the continuum, and can be described with distorted waves defined as scattering solutions of an optical potential. A schematic depiction of the situation is shown in Fig. 4.G.1. While the derivation presented below is quite general, special emphasis is set to one-particle knock-out processes.

#### Transition amplitude

A first derivation will be given in which, for simplicity, all the “particles” (nuclei) involved in the reaction process are spinless and inert. Use is made of central, complex optical potentials ( $U(r_{aA}), U(r_{cb}), U(r_{ac})$ ) potentials without a spin-orbit term. In addition, the interaction  $v(r_{ab})$  between  $a$  and  $b$  is taken to be a function of the distance  $r_{ab}$ . Within this scenario, the transition amplitude which is at the basis of the evaluation of the multi-differential cross section is the 6-dimensional integral

$$T_{mb} = \int d\mathbf{r}_{aA} d\mathbf{r}_{bc} \chi^{(-)*}(\mathbf{r}_{ac}) \chi^{(-)*}(\mathbf{r}_{bc}) v(r_{ab}) \chi^{(+)}(\mathbf{r}_{aA}) u_{lb}(r_{bc}) Y_{mb}^{lb}(\hat{\mathbf{r}}_{bc}). \quad (4.G.1)$$

### Coordinates

The vectors  $\mathbf{r}_{ab}, \mathbf{r}_{ac}$  can easily be written in function of the integration variables  $\mathbf{r}_{aA}, \mathbf{r}_{bc}$  (see Fig. 4.G.1), namely

$$\begin{aligned}\mathbf{r}_{ac} &= \mathbf{r}_{aA} + \frac{b}{A} \mathbf{r}_{bc}, \\ \mathbf{r}_{ab} &= \mathbf{r}_{aA} - \frac{c}{A} \mathbf{r}_{bc},\end{aligned}\quad (4.G.2)$$

where  $b, c, A$  stand for the number of nucleons of the species  $b, c$  and  $A$  respectively.

### Distorted waves in the continuum

A standard way to reduce the dimensionality of the integral (4.G.1) consists in expanding the continuum wave functions  $\chi^{(+)}(\mathbf{r}_{aA}), \chi^{(-)*}(\mathbf{r}_{ac}), \chi^{(-)*}(\mathbf{r}_{bc})$  in a basis of eigenstates of the angular momentum operator (partial waves). Then one can exploit the transformation properties of these eigenstates under rotations to conveniently carry out the angular integrations. Making use of time-reversed phasing, that is

$$Y_m^l(\theta, \phi) = i^l \sqrt{\frac{2l+1}{4\pi} \frac{(l-m)!}{(l+m)!}} P_l^m(\cos \theta) e^{im\phi}, \quad (4.G.3)$$

the general form of these expansions is

$$\chi^{(+)}(\mathbf{k}, \mathbf{r}) = \sum_l \frac{4\pi}{kr} i^l \sqrt{2l+1} e^{i\sigma^l} F_l(r) [Y^l(\hat{\mathbf{r}}) Y^l(\hat{\mathbf{k}})]_0^0, \quad (4.G.4)$$

and

$$\chi^{(-)*}(\mathbf{k}, \mathbf{r}) = \sum_l \frac{4\pi}{kr} i^{-l} \sqrt{2l+1} e^{i\sigma^l} F_l(r) [Y^l(\hat{\mathbf{r}}) Y^l(\hat{\mathbf{k}})]_0^0, \quad (4.G.5)$$

$\sigma_l$  being the Coulomb phase shift. The radial functions  $F_l(r)$  are regular (finite at  $r = 0$ ) solutions of the one-dimensional Schrödinger equation with an effective potential  $U(r) + \frac{\hbar^2 l(l+1)}{2\mu r^2}$  and suitable asymptotic behaviour at  $r \rightarrow \infty$  as boundary conditions. Thus, the distorted waves appearing in (4.G.1) are,

$$\chi^{(+)}(\mathbf{k}_a, \mathbf{r}_{aA}) = \sum_{l_a} \frac{4\pi}{k_a r_{aA}} i^{l_a} \sqrt{2l_a+1} e^{i\sigma^{l_a}} F_{l_a}(r_{aA}) [Y^{l_a}(\hat{\mathbf{r}}_{aA}) Y^{l_a}(\hat{\mathbf{k}}_a)]_0^0, \quad (4.G.6)$$

describing the relative motion of  $A$  and  $a$  in the entrance channel as determined by the complex optical potential  $U(r_{Aa})$ ,

$$\chi^{(-)*}(\mathbf{k}'_a, \mathbf{r}_{ac}) = \sum_{l'_a} \frac{4\pi}{k'_a r_{ac}} i^{-l'_a} \sqrt{2l'_a+1} e^{i\sigma^{l'_a}} F_{l'_a}(r_{ac}) [Y^{l'_a}(\hat{\mathbf{r}}_{ac}) Y^{l'_a}(\hat{\mathbf{k}}'_a)]_0^0, \quad (4.G.7)$$

which describes the relative motion of  $c$  and  $a$ , in the final channel controlled by the complex optical potential  $U(r_{ac})$ , and finally

$$\chi^{(-)*}(\mathbf{k}'_b, \mathbf{r}_{bc}) = \sum_{l'_b} \frac{4\pi}{k'_b r_{bc}} i^{-l'_b} \sqrt{2l'_b+1} e^{i\sigma^{l'_b}} F_{l'_b}(r_{bc}) [Y^{l'_b}(\hat{\mathbf{r}}_{bc}) Y^{l'_b}(\hat{\mathbf{k}}'_b)]_0^0, \quad (4.G.8)$$

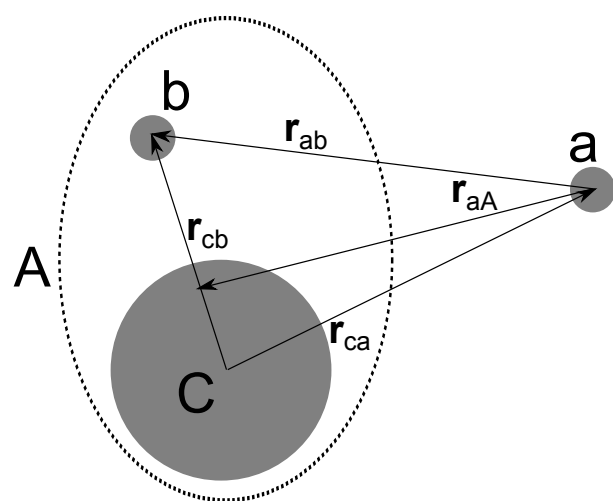


Figure 4.G.1: System of coordinates used to describe the reaction  $A + a \rightarrow a + b + c$ . The nucleus  $A$  is viewed as an inert cluster  $b$  bounded to an inert core  $c$ .

final channel wavefunction describing the relative motion of  $b$  and  $c$ , as defined by the complex optical potential  $U(r_{bc})$ .

### Recoupling of angular momenta

One now proceeds to the evaluation of the 6-dimensional integral

$$\begin{aligned} & \frac{64\pi^3}{k_a k'_a k'_b} \int d\mathbf{r}_{aA} d\mathbf{r}_{bc} u_{l_b}(r_{cb}) v(r_{ab}) \sum_{l_a, l'_a, l'_b} \sqrt{(2l_a + 1)(2l'_a + 1)(2l'_b + 1)} \\ & \times e^{i(\sigma^{l_a} + \sigma'^{l'_a} + \sigma'^{l'_b})} \frac{F_{l_a}(r_{aA}) F_{l'_a}(r_{ac}) F_{l'_b}(r_{bc})}{r_{ac} r_{aA} r_{bc}} \\ & \times [Y^{l_a}(\hat{\mathbf{r}}_{aA}) Y^{l_a}(\hat{\mathbf{k}}_a)]_0^0 [Y^{l'_a}(\hat{\mathbf{r}}_{ac}) Y^{l'_a}(\hat{\mathbf{k}}'_a)]_0^0 [Y^{l'_b}(\hat{\mathbf{r}}_{bc}) Y^{l'_b}(\hat{\mathbf{k}}'_b)]_0^0 Y_{m_b}^{l_b}(\hat{\mathbf{r}}_{bc}), \end{aligned} \quad (4.G.9)$$

an expression which explicitly depends on the asymptotic kinetic energies and scattering angles  $(\hat{\mathbf{k}}_a, \hat{\mathbf{k}}'_a, \hat{\mathbf{k}}'_b)$  of  $a, b$  as determined by  $k_a, k'_a, k'_b$  and  $\hat{\mathbf{k}}_a, \hat{\mathbf{k}}'_a, \hat{\mathbf{k}}'_b$  respectively. In what follows we will take advantage of the partial wave expansion to reduce the dimensionality of the integral from 6 to 3. A possible strategy to follow is that of recoupling together all the terms that depend on the integration variables to a global angular momentum and retain only the term coupled to 0 as the only one surviving the integration. Let us start to separately couple the terms corresponding to particles  $a$  and  $b$ . For particle  $a$  we write

$$\begin{aligned} & [Y^{l_a}(\hat{\mathbf{r}}_{aA}) Y^{l_a}(\hat{\mathbf{k}}_a)]_0^0 [Y^{l'_a}(\hat{\mathbf{r}}_{ac}) Y^{l'_a}(\hat{\mathbf{k}}'_a)]_0^0 = \sum_K ((l_a l_a)_0 (l'_a l'_a)_0 | (l_a l'_a)_K (l_a l'_a)_K)_0 \\ & \times \left\{ [Y^{l_a}(\hat{\mathbf{r}}_{aA}) Y^{l'_a}(\hat{\mathbf{r}}_{ac})]_M^K [Y^{l_a}(\hat{\mathbf{k}}_a) Y^{l'_a}(\hat{\mathbf{k}}'_a)]_0^K \right\}_0^0. \end{aligned} \quad (4.G.10)$$

We can now evaluate the  $9j$ -symbol,

$$((l_a l_a)_0 (l'_a l'_a)_0 | (l_a l'_a)_K (l_a l'_a)_K)_0 = \sqrt{\frac{2K+1}{(2l'_a+1)(2l_a+1)}}, \quad (4.G.11)$$

and expand the coupling,

$$\begin{aligned} & \left\{ [Y^{l_a}(\hat{\mathbf{r}}_{aA}) Y^{l'_a}(\hat{\mathbf{r}}_{ac})]_M^K [Y^{l_a}(\hat{\mathbf{k}}_a) Y^{l'_a}(\hat{\mathbf{k}}'_a)]_0^K \right\}_0^0 = \sum_M \langle K \ K \ M \ - M | 0 \ 0 \rangle \\ & \times [Y^{l_a}(\hat{\mathbf{r}}_{aA}) Y^{l'_a}(\hat{\mathbf{r}}_{ac})]_M^K [Y^{l_a}(\hat{\mathbf{k}}_a) Y^{l'_a}(\hat{\mathbf{k}}'_a)]_{-M}^K = \sum_M \frac{(-1)^{K+M}}{\sqrt{2K+1}} \\ & \times [Y^{l_a}(\hat{\mathbf{r}}_{aA}) Y^{l'_a}(\hat{\mathbf{r}}_{ac})]_M^K [Y^{l_a}(\hat{\mathbf{k}}_a) Y^{l'_a}(\hat{\mathbf{k}}'_a)]_{-M}^K. \end{aligned} \quad (4.G.12)$$

Thus,

$$\begin{aligned} \left[ Y^{l_a}(\hat{\mathbf{r}}_{aA}) Y^{l_a}(\hat{\mathbf{k}}_a) \right]_0^0 \left[ Y^{l'_a}(\hat{\mathbf{r}}_{ac}) Y^{l'_a}(\hat{\mathbf{k}}'_a) \right]_0^0 &= \sqrt{\frac{1}{(2l'_a + 1)(2l_a + 1)}} \\ &\times \sum_{KM} (-1)^{K+M} \left[ Y^{l_a}(\hat{\mathbf{r}}_{aA}) Y^{l'_a}(\hat{\mathbf{r}}_{ac}) \right]_M^K \left[ Y^{l_a}(\hat{\mathbf{k}}_a) Y^{l'_a}(\hat{\mathbf{k}}'_a) \right]_{-M}^K. \end{aligned} \quad (4.G.13)$$

One can further simplify the above expression by choosing the direction of the initial momentum to be parallel to the  $z$  axis, so that  $Y_m^{l_a}(\hat{\mathbf{k}}_a) = Y_m^{l_a}(\hat{\mathbf{z}}) = \sqrt{\frac{2l_a + 1}{4\pi}} \delta_{m,0}$ . Then,

$$\begin{aligned} \left[ Y^{l_a}(\hat{\mathbf{r}}_{aA}) Y^{l_a}(\hat{\mathbf{k}}_a) \right]_0^0 \left[ Y^{l'_a}(\hat{\mathbf{r}}_{ac}) Y^{l'_a}(\hat{\mathbf{k}}'_a) \right]_0^0 &= \sqrt{\frac{1}{4\pi(2l'_a + 1)}} \sum_{KM} (-1)^{K+M} \\ &\times \langle l_a \ 0 \ l'_a \ -M | K \ -M \rangle \left[ Y^{l_a}(\hat{\mathbf{r}}_{aA}) Y^{l'_a}(\hat{\mathbf{r}}_{ac}) \right]_M^K Y_{-M}^{l'_a}(\hat{\mathbf{k}}'_a). \end{aligned} \quad (4.G.14)$$

For particle  $b$  we have

$$Y_{m_b}^{l_b}(\hat{\mathbf{r}}_{bc}) \left[ Y^{l'_b}(\hat{\mathbf{r}}_{bc}) Y^{l'_b}(\hat{\mathbf{k}}'_b) \right]_0^0 = Y_{m_b}^{l_b}(\hat{\mathbf{r}}_{cb}) \sum_m \frac{(-1)^{l'_b+m}}{\sqrt{2l'_b + 1}} Y_m^{l'_b}(\hat{\mathbf{r}}_{bc}) Y_{-m}^{l'_b}(\hat{\mathbf{k}}'_b), \quad (4.G.15)$$

and can write

$$Y_{m_b}^{l_b}(\hat{\mathbf{r}}_{bc}) Y_m^{l'_b}(\hat{\mathbf{r}}_{bc}) = \sum_{K'} \langle l_b \ m_b \ l'_b \ m | K' \ m_b + m \rangle \left[ Y^{l_b}(\hat{\mathbf{r}}_{bc}) Y^{l'_b}(\hat{\mathbf{r}}_{bc}) \right]_{m_b+m}^{K'}. \quad (4.G.16)$$

In order to couple to 0 angular momentum with (4.G.14) we must only keep the term with  $K' = K$ ,  $m = -M - m_b$  so

$$\begin{aligned} Y_{m_b}^{l_b}(\hat{\mathbf{r}}_{bc}) \left[ Y^{l'_b}(\hat{\mathbf{r}}_{bc}) Y^{l'_b}(\hat{\mathbf{k}}'_b) \right]_0^0 &= \frac{(-1)^{l'_b-M-m_b}}{\sqrt{2l'_b + 1}} \langle l_b \ m_b \ l'_b \ -M - m_b | K \ -M \rangle \\ &\times \left[ Y^{l_b}(\hat{\mathbf{r}}_{bc}) Y^{l'_b}(\hat{\mathbf{r}}_{bc}) \right]_{-M}^{K'} Y_{-M-m_b}^{l'_b}(\hat{\mathbf{k}}'_b), \end{aligned} \quad (4.G.17)$$

and (4.G.9) becomes

$$\begin{aligned} \frac{32\pi^2}{k_a k'_a k'_b} \sum_{KM} (-1)^{K+l'_b-m_b} \langle l_a \ 0 \ l'_a \ -M | K \ -M \rangle \langle l_b \ m_b \ l'_b \ -M - m_b | K \ -M \rangle \\ \times \sum_{l_a, l'_a, l'_b} \sqrt{(2l_a + 1)} e^{i(\sigma^{l_a} + \sigma^{l'_a} + \sigma^{l'_b})} Y_{-M-m_b}^{l'_b}(\hat{\mathbf{k}}'_b) Y_{-M}^{l'_a}(\hat{\mathbf{k}}'_a) \int d\mathbf{r}_{aA} d\mathbf{r}_{bc} u_{l_b}(r_{bc}) v(r_{ab}) \\ \times \frac{F_{l_a}(r_{aA}) F_{l'_a}(r_{ac}) F_{l'_b}(r_{bc})}{r_{ac} r_{aA} r_{bc}} \left[ Y^{l_a}(\hat{\mathbf{r}}_{aA}) Y^{l'_a}(\hat{\mathbf{r}}_{ac}) \right]_M^K \left[ Y^{l_b}(\hat{\mathbf{r}}_{bc}) Y^{l'_b}(\hat{\mathbf{r}}_{bc}) \right]_{-M}^K. \end{aligned} \quad (4.G.18)$$

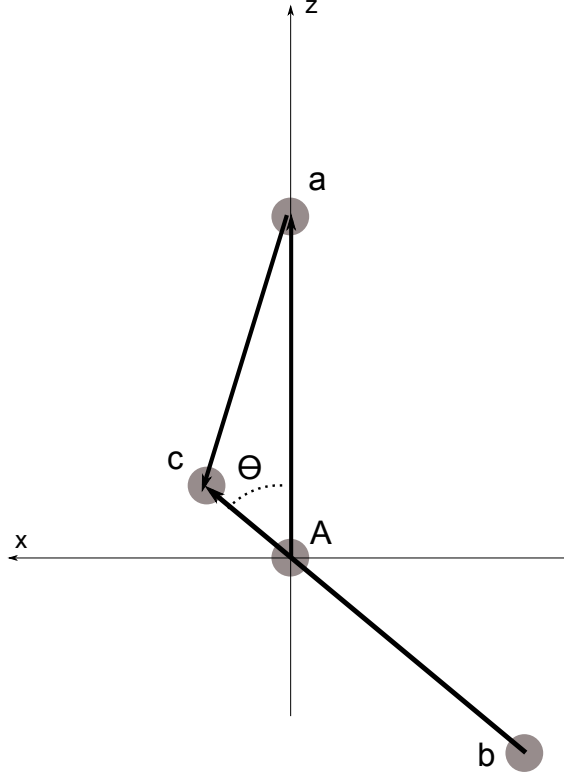


Figure 4.G.2: Coordinates in the “standard” configuration.

Note that

$$\begin{aligned} \left[ Y^{l_a}(\hat{\mathbf{r}}_{aA}) Y^{l'_a}(\hat{\mathbf{r}}_{ac}) \right]_M^K \left[ Y^{l_b}(\hat{\mathbf{r}}_{bc}) Y^{l'_b}(\hat{\mathbf{r}}_{bc}) \right]_{-M}^K &= \sum_P \langle K M K - M | P 0 \rangle \\ &\times \left\{ \left[ Y^{l_a}(\hat{\mathbf{r}}_{aA}) Y^{l'_a}(\hat{\mathbf{r}}_{ac}) \right]_0^K \left[ Y^{l_b}(\hat{\mathbf{r}}_{bc}) Y^{l'_b}(\hat{\mathbf{r}}_{bc}) \right]_0^K \right\}_0^P, \end{aligned} \quad (4.G.19)$$

and that to survive the integration the rotational tensors must be coupled to  $P = 0$ . Keeping only this term in the sum over  $P$ , we get

$$\begin{aligned} \left[ Y^{l_a}(\hat{\mathbf{r}}_{aA}) Y^{l'_a}(\hat{\mathbf{r}}_{ac}) \right]_M^K \left[ Y^{l_b}(\hat{\mathbf{r}}_{bc}) Y^{l'_b}(\hat{\mathbf{r}}_{bc}) \right]_{-M}^K &= \\ \frac{(-1)^{K+M}}{\sqrt{2K+1}} \left\{ \left[ Y^{l_a}(\hat{\mathbf{r}}_{aA}) Y^{l'_a}(\hat{\mathbf{r}}_{ac}) \right]_0^K \left[ Y^{l_b}(\hat{\mathbf{r}}_{bc}) Y^{l'_b}(\hat{\mathbf{r}}_{bc}) \right]_0^K \right\}_0^0. \end{aligned} \quad (4.G.20)$$

The coordinate-dependent part of the latter expression is a rotationally invariant scalar, so it can be evaluated in any conventional “standard” configuration such as the one depicted in Fig. 4.G.2. It must then be multiplied by a factor resulting

of the integration of the remaining angular variables, which accounts for the rigid rotations needed to connect any arbitrary configuration to one of this type. This factor turns out to be  $8\pi^2$  (a  $4\pi$  factor for all possible orientations of, say,  $\mathbf{r}_{aA}$  and a  $2\pi$  factor for a complete rotation around its direction). According to Fig. 4.G.2,

$$\begin{aligned}\mathbf{r}_{bc} &= r_{bc} (\sin \theta \hat{x} + \cos \theta \hat{z}), \\ \mathbf{r}_{aA} &= -r_{aA} \hat{z}, \\ \mathbf{r}_{ac} &= \frac{b}{A} r_{bc} \sin \theta \hat{x} + \left( \frac{b}{A} r_{bc} \cos \theta - r_{aA} \right) \hat{z}.\end{aligned}\quad (4.G.21)$$

As  $\mathbf{r}_{aA}$  lies parallel to the  $z$  axis,  $Y_{M_K}^{l_a}(\hat{\mathbf{r}}_{aA}) = \sqrt{\frac{2l_a+1}{4\pi}} \delta_{M_K,0}$  and

$$\begin{aligned}\left[ Y^{l_a}(\hat{\mathbf{r}}_{aA}) Y^{l'_a}(\hat{\mathbf{r}}_{ac}) \right]_{M_K}^K &= \sum_m \langle l_a \ m \ l'_a \ M_K - m | K \ M_K \rangle Y_m^{l_a}(\hat{\mathbf{r}}_{aA}) Y_{M_K-m}^{l'_a}(\hat{\mathbf{r}}_{ac}) = \\ &\sqrt{\frac{2l_a+1}{4\pi}} \langle l_a \ 0 \ l'_a \ M_K | K \ M_K \rangle Y_{M_K}^{l'_a}(\hat{\mathbf{r}}_{ac}).\end{aligned}\quad (4.G.22)$$

Then

$$\begin{aligned}\left\{ \left[ Y^{l_a}(\hat{\mathbf{r}}_{aA}) Y^{l'_a}(\hat{\mathbf{r}}_{ac}) \right]^K \left[ Y^{l_b}(\hat{\mathbf{r}}_{bc}) Y^{l'_b}(\hat{\mathbf{r}}_{bc}) \right]^K \right\}_0^0 &= \\ \sum_{M_K} \langle K \ M_K \ K - M_K | 0 \ 0 \rangle \left[ Y^{l_a}(\hat{\mathbf{r}}_{aA}) Y^{l'_a}(\hat{\mathbf{r}}_{ac}) \right]_{M_K}^K \left[ Y^{l_b}(\hat{\mathbf{r}}_{bc}) Y^{l'_b}(\hat{\mathbf{r}}_{bc}) \right]_{-M_K}^K &= \\ \sqrt{\frac{2l_a+1}{4\pi}} \sum_{M_K} \frac{(-1)^{K+M_K}}{\sqrt{2K+1}} \langle l_a \ 0 \ l'_a \ M_K | K \ M_K \rangle \\ \times \left[ Y^{l_b}(\hat{\mathbf{r}}_{bc}) Y^{l'_b}(\hat{\mathbf{r}}_{bc}) \right]_{-M_K}^K Y_{M_K}^{l'_a}(\hat{\mathbf{r}}_{ac}).\end{aligned}\quad (4.G.23)$$

Remembering the  $8\pi^2$  factor, the term arising from (4.G.20) to be considered in the integral is

$$\begin{aligned}4\pi^{3/2} \frac{\sqrt{2l_a+1}}{2K+1} (-1)^K \sum_{M_K} (-1)^{M_K} \langle l_a \ 0 \ l'_a \ M_K | K \ M_K \rangle \\ \times \left[ Y^{l_b}(\cos \theta, 0) Y^{l'_b}(\cos \theta, 0) \right]_{-M_K}^K Y_{M_K}^{l'_a}(\cos \theta_{ac}, 0),\end{aligned}\quad (4.G.24)$$

with

$$\cos \theta_{ac} = \frac{\frac{b}{A} r_{bc} \cos \theta - r_{aA}}{\sqrt{\left( \frac{b}{A} r_{bc} \sin \theta \right)^2 + \left( \frac{b}{A} r_{bc} \cos \theta - r_{aA} \right)^2}},\quad (4.G.25)$$

(see (4.G.21)). The final expression of the transition amplitude is

$$\begin{aligned} T_{m_b}(\mathbf{k}'_a, \mathbf{k}'_b) = & \frac{128\pi^{7/2}}{k_a k'_a k'_b} \sum_{KM} \frac{(-1)^{l'_b+m_b}}{2K+1} \langle l_a 0 l'_a - M | K - M \rangle \langle l_b m_b l'_b - M - m_b | K - M \rangle \\ & \times \sum_{l_a, l'_a, l'_b} (2l_a + 1) e^{i(\sigma^{l_a} + \sigma^{l'_a} + \sigma^{l'_b})} Y_{-M-m_b}^{l'_b}(\hat{\mathbf{k}}'_b) Y_{-M}^{l'_a}(\hat{\mathbf{k}}'_a) \mathcal{I}(l_a, l'_a, l'_b, K), \end{aligned} \quad (4.G.26)$$

where

$$\begin{aligned} \mathcal{I}(l_a, l'_a, l'_b, K) = & \int dr_{aA} dr_{bc} d\theta_{r_{aA}} r_{bc} \frac{\sin \theta}{r_{ac}} u_{l_b}(r_{bc}) v(r_{ab}) F_{l_a}(r_{aA}) F_{l'_a}(r_{ac}) F_{l'_b}(r_{bc}) \\ & \times \sum_{M_K} (-1)^{M_K} \langle l_a 0 l'_a M_K | K M_K \rangle \left[ Y^{l_b}(\cos \theta, 0) Y^{l'_b}(\cos \theta, 0) \right]_{-M_K}^K Y_{M_K}^{l'_a}(\cos \theta_{ac}, 0) \end{aligned} \quad (4.G.27)$$

is a 3-dimensional integral that can be numerically evaluated with the help of, e.g., Gaussian integration.

## 4.G.2 Particles with spin

We now treat the case in which the clusters have a definite spin (see Fig. 4.G.3), and the complex optical potentials  $U(r_{aA}), U(r_{cb}), U(r_{ac})$  contain now a spin-orbit term proportional to the product  $\mathbf{l} \cdot \mathbf{s} = 1/2(j(j+1) - l(l+1) - 3/4)$  for particles with spin 1/2. In addition, the interaction  $V(r_{ab}, \sigma_a, \sigma_b)$  between  $a$  and  $b$  is taken to be a separable function of the distance  $r_{ab}$  and of the spin orientations,  $V(r_{ab}, \sigma_a, \sigma_b) = v(r_{ab})v_\sigma(\sigma_a, \sigma_b)$ . Note that this ansatz rules out spin-orbit as well as tensor terms in the  $NN$ -interaction. For the time being we will assume that the spin-dependent interaction is rotationally invariant (scalar with respect to rotations), such as, e.g.,  $v_\sigma(\sigma_a, \sigma_b) \propto \sigma_a \cdot \sigma_b$ . Again, this assumption excludes tensor terms in the interaction. The transition amplitude is then,

$$\begin{aligned} T_{m_a, m_b}^{m'_a, m'_b} = & \sum_{\sigma_a, \sigma_b} \int d\mathbf{r}_{aA} d\mathbf{r}_{bc} \chi_{m'_a}^{(-)*}(\mathbf{r}_{ac}, \sigma_a) \chi_{m'_b}^{(-)*}(\mathbf{r}_{bc}, \sigma_b) \\ & \times v(r_{ab}) v_\sigma(\sigma_a, \sigma_b) \chi_{m_a}^{(+)}(\mathbf{r}_{aA}, \sigma_a) \psi_{m_b}^{l_b, j_b}(\mathbf{r}_{bc}, \sigma_b). \end{aligned} \quad (4.G.28)$$

### Distorted waves

The distorted waves in (4.G.28)  $\chi_m(\mathbf{r}, \sigma) = \chi(\mathbf{r})\phi_m^{1/2}(\sigma)$  have a spin dependence contained in the spinor  $\phi_m^{1/2}(\sigma)$ , where  $\sigma$  is the spin degree of freedom and  $m$  the projection of the spin along the quantization axis. The superscript 1/2 reminds us that we are considering spin 1/2 particles, which have important consequences when dealing with the spin-orbit term of the optical potentials. As for the spin-dependent term  $v_\sigma(\sigma_a, \sigma_b)$ , the actual value of the spin of particles involved in the

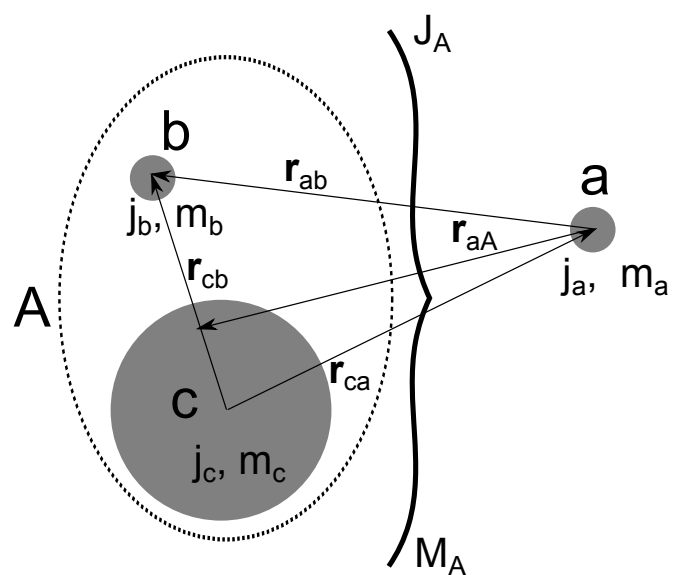


Figure 4.G.3: In the present case all three clusters  $a, b, c$  have definite spins and projections. The nucleus  $A$  is coupled to total spin  $J_A, M_A$ .

reaction process do not make much difference, *as long as this term is rotationally invariant*. Following (4.G.4),

$$\chi^{(+)}(\mathbf{k}, \mathbf{r})\phi_m(\sigma) = \sum_{l,j} \frac{4\pi}{kr} i^l \sqrt{2l+1} e^{i\sigma l} F_{l,j}(r) [Y^l(\hat{\mathbf{r}}) Y^l(\hat{\mathbf{k}})]_0^0 \phi_m^{1/2}(\sigma). \quad (4.G.29)$$

Note that now one also sums over the total angular momentum  $j$ , as the radial functions  $F_{l,j}(r)$  depend both on  $j$  as well as on  $l$ , in keeping with the fact that they are solutions of an optical potential containing a spin-orbit term proportional to  $1/2(j(j+1) - l(l+1) - 3/4)$ . One must then couple the radial and spin functions to total angular momentum  $j$ , noting that

$$\begin{aligned} [Y^l(\hat{\mathbf{r}}) Y^l(\hat{\mathbf{k}})]_0^0 \phi_m^{1/2}(\sigma) &= \sum_{m_l} \langle l m_l | 0 0 \rangle Y_{m_l}^l(\hat{\mathbf{r}}) Y_{-m_l}^l(\hat{\mathbf{k}}) \phi_m^{1/2}(\sigma) = \\ &\sum_{m_l} \frac{(-1)^{l-m_l}}{\sqrt{2l+1}} Y_{m_l}^l(\hat{\mathbf{r}}) Y_{-m_l}^l(\hat{\mathbf{k}}) \phi_m^{1/2}(\sigma), \end{aligned} \quad (4.G.30)$$

and

$$Y_{m_l}^l(\hat{\mathbf{r}}) \phi_m^{1/2}(\sigma) = \sum_j \langle l m_l | 1/2 m | j m_l + m \rangle [Y^l(\hat{\mathbf{r}}) \phi^{1/2}(\sigma)]_{m_l+m}^j, \quad (4.G.31)$$

we can write

$$\begin{aligned} [Y^l(\hat{\mathbf{r}}) Y^l(\hat{\mathbf{k}})]_0^0 \phi_m^{1/2}(\sigma) &= \sum_{m_l, j} \frac{(-1)^{l+m_l}}{\sqrt{2l+1}} \langle l m_l | 1/2 m | j m_l + m \rangle \\ &\times [Y^l(\hat{\mathbf{r}}) \phi^{1/2}(\sigma)]_{m_l+m}^j Y_{-m_l}^l(\hat{\mathbf{k}}), \end{aligned} \quad (4.G.32)$$

and the distorted waves in (4.G.28) are

$$\begin{aligned} \chi_{m_a}^{(+)}(\mathbf{r}_{aA}, \mathbf{k}_a, \sigma_a) &= \sum_{l_a, m_{l_a}, j_a} \frac{4\pi}{k_a r_{aA}} i^{l_a} (-1)^{l_a+m_{l_a}} e^{i\sigma l_a} F_{l_a, j_a}(r_{aA}) \\ &\times \langle l_a m_{l_a} | 1/2 m_a | j_a m_{l_a} + m_a \rangle [Y^{l_a}(\hat{\mathbf{r}}_{aA}) \phi^{1/2}(\sigma_a)]_{m_{l_a}+m_a}^{j_a} Y_{-m_{l_a}}^{l_a}(\hat{\mathbf{k}}_a), \end{aligned} \quad (4.G.33)$$

$$\begin{aligned} \chi_{m'_b}^{(-)*}(\mathbf{r}_{bc}, \mathbf{k}'_b, \sigma_b) &= \sum_{l'_b, m'_{l'_b}, j'_b} \frac{4\pi}{k'_b r_{bc}} i^{-l'_b} (-1)^{l'_b+m'_{l'_b}} e^{i\sigma l'_b} F_{l'_b, j'_b}(r_{bc}) \\ &\times \langle l'_b m'_{l'_b} | 1/2 m'_b | j'_b m'_{l'_b} + m'_b \rangle [Y^{l'_b}(\hat{\mathbf{r}}_{bc}) \phi^{1/2}(\sigma_b)]_{m'_{l'_b}+m'_b}^{j'_b} Y_{-m'_{l'_b}}^{l'_b}(\hat{\mathbf{k}}'_b), \end{aligned} \quad (4.G.34)$$

$$\begin{aligned} \chi_{m'_a}^{(-)*}(\mathbf{r}_{ac}, \mathbf{k}'_a, \sigma_a) &= \sum_{l'_a, m'_{l'_a}, j'_a} \frac{4\pi}{k'_a r_{ac}} i^{-l'_a} (-1)^{l'_a+m'_{l'_a}} e^{i\sigma l'_a} F_{l'_a, j'_a}(r_{ac}) \\ &\times \langle l'_a m'_{l'_a} | 1/2 m'_a | j'_a m'_{l'_a} + m'_a \rangle [Y^{l'_a}(\hat{\mathbf{r}}_{ac}) \phi^{1/2}(\sigma_a)]_{m'_{l'_a}+m'_a}^{j'_a} Y_{-m'_{l'_a}}^{l'_a}(\hat{\mathbf{k}}'_a). \end{aligned} \quad (4.G.35)$$

The initial bound particle  $b$  wavefunction is

$$\psi_{m_b}^{l_b, j_b}(\mathbf{r}_{bc}, \sigma_b) = u_{l_b, j_b}(r_{bc}) [Y^{l_b}(\hat{\mathbf{r}}_{bc}) \phi^{1/2}(\sigma_b)]_{m_b}^{j_b}, \quad (4.G.36)$$

Substituting in (4.G.28), one obtains,

$$\begin{aligned} T_{m_a, m_b}^{m'_a, m'_b}(\mathbf{k}'_a, \mathbf{k}'_b) &= \frac{64\pi^3}{k_a k'_a k'_b} \sum_{\sigma_a, \sigma_b} \sum_{l_a, m_{l_a}} \sum_{j_a, l'_a, m'_{l'_a}, j'_a} \sum_{l'_b, m'_{l'_b}, j'_b} e^{i(\sigma'^{l_a} + \sigma'^{l'_a} + \sigma'^{l'_b})} i^{l_a - l'_a - l'_b} (-1)^{l_a - m_{l_a} + l'_a - j'_a + l'_b - j'_b} \\ &\times \langle l'_a m'_{l'_a} | 1/2 m'_a | j'_a m'_{l'_a} + m'_a \rangle \langle l_a m_{l_a} | 1/2 m_a | j_a m_{l_a} + m_a \rangle \langle l'_b m'_{l'_b} | 1/2 m'_b | j'_b m'_{l'_b} + m'_b \rangle \\ &\times Y_{-m_{l_a}}^{l_a}(\hat{\mathbf{k}}_a) Y_{-m'_{l'_a}}^{l'_a}(\hat{\mathbf{k}}'_a) Y_{-m'_{l'_b}}^{l'_b}(\hat{\mathbf{k}}'_b) \int d\mathbf{r}_{aA} d\mathbf{r}_{bc} [Y^{l'_a}(\hat{\mathbf{r}}_{ac}) \phi^{1/2}(\sigma_a)]_{-m'_{l'_a} - m'_a}^{j'_a} [Y^{l'_b}(\hat{\mathbf{r}}_{bc}) \phi^{1/2}(\sigma_b)]_{-m'_{l'_b} - m'_b}^{j'_b} \\ &\times \frac{F_{l_a, j_a}(r_{aA}) F_{l'_a, j'_a}(r_{ac}) F_{l'_b, j'_b}(r_{bc})}{r_{ac} r_{aA} r_{bc}} u_{l_b, j_b}(r_{bc}) v(r_{ab}) v_\sigma(\sigma_a, \sigma_b) \\ &\times [Y^{l_a}(\hat{\mathbf{r}}_{aA}) \phi^{1/2}(\sigma_a)]_{m_{l_a} + m_a}^{j_a} [Y^{l_b}(\hat{\mathbf{r}}_{bc}) \phi^{1/2}(\sigma_b)]_{m_b}^{j_b}, \quad (4.G.37) \end{aligned}$$

where use was made of the relation

$$[Y^l(\hat{\mathbf{r}}) \phi^{1/2}(\sigma)]_m^{j*} = (-1)^{j-m} [Y^l(\hat{\mathbf{r}}) \phi^{1/2}(\sigma)]_{-m}^j. \quad (4.G.38)$$

### Recoupling of angular momenta

Let us now separate spatial and spin coordinates, noting that the spin functions must be coupled to  $S = 0$ , a consequence of the fact that the interaction  $v_\sigma(\sigma_a, \sigma_b)$  is rotationally invariant. Starting with particle  $a$ ,

$$\begin{aligned} [Y^{l'_a}(\hat{\mathbf{r}}_{ac}) \phi^{1/2*}(\sigma_a)]_{-m'_{l'_a} - m'_a}^{j'_a} [Y^{l_a}(\hat{\mathbf{r}}_{aA}) \phi^{1/2}(\sigma_a)]_{m_{l_a} + m_a}^{j_a} &= \\ \sum_K ((l'_a \frac{1}{2})_{j'_a} (l_a \frac{1}{2})_{j_a} | (l_a l'_a)_K (\frac{1}{2} \frac{1}{2})_0)_K &\\ \times [Y^{l'_a}(\hat{\mathbf{r}}_{ac}) Y^{l_a}(\hat{\mathbf{r}}_{aA})]_{-m'_{l'_a} - m'_a + m_{l_a} + m_a}^K [\phi^{1/2*}(\sigma_a) \phi^{1/2}(\sigma_a)]_0^0. \quad (4.G.39) & \end{aligned}$$

For particle  $b$ ,

$$\begin{aligned} [Y^{l'_b}(\hat{\mathbf{r}}_{bc}) \phi^{1/2*}(\sigma_b)]_{-m'_{l'_b} - m'_b}^{j'_b} [Y^{l_b}(\hat{\mathbf{r}}_{bc}) \phi^{1/2}(\sigma_b)]_{m_b}^{j_b} &= \\ \sum_{K'} ((l'_b \frac{1}{2})_{j'_b} (l_b \frac{1}{2})_{j_b} | (l_b l'_b)_{K'} (\frac{1}{2} \frac{1}{2})_0)_{K'} &\\ \times [Y^{l'_b}(\hat{\mathbf{r}}_{bc}) Y^{l_b}(\hat{\mathbf{r}}_{bc})]_{-m'_{l'_b} - m'_b + m_b}^{K'} [\phi^{1/2*}(\sigma_b) \phi^{1/2}(\sigma_b)]_0^0. \quad (4.G.40) & \end{aligned}$$

The spin summation yields a constant factor,

$$\sum_{\sigma_a, \sigma_b} [\phi^{1/2*}(\sigma_a) \phi^{1/2}(\sigma_a)]_0^0 [\phi^{1/2*}(\sigma_b) \phi^{1/2}(\sigma_b)]_0^0 v_\sigma(\sigma_a, \sigma_b) \equiv T_\sigma, \quad (4.G.41)$$

and what we have yet to do is very similar to what we have done in the case of spinless particles. First of all note that the constrain of coupling all angular momenta to 0, imposes  $K' = K$  and  $m_{l_a} + m_a - m_{l'_a} - m'_a = m_{l'_b} + m'_b - m_b$  (see (4.G.39) and (4.G.40)). If we set  $M = m_{l_a} + m_a - m_{l'_a} - m'_a$  and take, as before,  $\hat{\mathbf{k}}_a \equiv \hat{z}$

$$\begin{aligned} T_{m_a, m_b}^{m'_a, m'_b}(\mathbf{k}'_a, \mathbf{k}'_b) &= \frac{32\pi^{5/2}}{k_a k'_a k'_b} T_\sigma \sum_{l_a, j_a} \sum_{l'_a, j'_a} \sum_{l'_b, j'_b} \sum_{K, M} e^{i(\sigma^{l_a} + \sigma^{l'_a} + \sigma^{l'_b})} i^{l_a - l'_a - l'_b} (-1)^{l_a + l'_a + l'_b - j'_a - j'_b} \\ &\times \sqrt{2l_a + 1} ((l'_a \frac{1}{2})_{j'_a} (l_a \frac{1}{2})_{j_a} | (l_a l'_a)_K (\frac{1}{2} \frac{1}{2})_0)_K ((l'_b \frac{1}{2})_{j'_b} (l_b \frac{1}{2})_{j_b} | (l_b l'_b)_K (\frac{1}{2} \frac{1}{2})_0)_K \\ &\times \langle l'_a m_a - m'_a - M \ 1/2 \ m'_a | j'_a m_a - M \rangle \langle l_a 0 \ 1/2 \ m_a | j_a m_a \rangle \langle l'_b m_b - m'_b + M \ 1/2 \ m'_b | j'_b M + m_b \rangle \\ &\times Y_{m'_b - m_b - M}^{l'_b}(\hat{\mathbf{k}}'_b) Y_{m'_a - m_a + M}^{l'_a}(\hat{\mathbf{k}}'_a) \int d\mathbf{r}_{aA} d\mathbf{r}_{bc} \frac{F_{l_a, j_a}(r_{aA}) F_{l'_a, j'_a}(r_{ac}) F_{l'_b, j'_b}(r_{bc})}{r_{ac} r_{aA} r_{bc}} \\ &\times u_{l_b, j_b}(r_{bc}) v(r_{ab}) \left[ Y^{l_a}(\hat{\mathbf{r}}_{aA}) Y^{l'_a}(\hat{\mathbf{r}}_{ac}) \right]_M^K \left[ Y^{l_b}(\hat{\mathbf{r}}_{bc}) Y^{l'_b}(\hat{\mathbf{r}}_{bc}) \right]_{-M}^K. \quad (4.G.42) \end{aligned}$$

The integral of the above expression is similar to the one in (4.G.18), so we obtain

$$\begin{aligned} T_{m_a, m_b}^{m'_a, m'_b}(\mathbf{k}'_a, \mathbf{k}'_b) &= \frac{128\pi^4}{k_a k'_a k'_b} T_\sigma \sum_{l_a, j_a} \sum_{l'_a, j'_a} \sum_{l'_b, j'_b} \sum_{K, M} e^{i(\sigma^{l_a} + \sigma^{l'_a} + \sigma^{l'_b})} i^{l_a - l'_a - l'_b} (-1)^{l_a + l'_a + l'_b - j'_a - j'_b} \\ &\times \frac{2l_a + 1}{2K + 1} ((l'_a \frac{1}{2})_{j'_a} (l_a \frac{1}{2})_{j_a} | (l_a l'_a)_K (\frac{1}{2} \frac{1}{2})_0)_K ((l'_b \frac{1}{2})_{j'_b} (l_b \frac{1}{2})_{j_b} | (l_b l'_b)_K (\frac{1}{2} \frac{1}{2})_0)_K \\ &\times \langle l'_a m_a - m'_a - M \ 1/2 \ m'_a | j'_a m_a - M \rangle \langle l'_b m_b - m'_b + M \ 1/2 \ m'_b | j'_b M + m_b \rangle \\ &\times \langle l_a 0 \ 1/2 \ m_a | j_a m_a \rangle Y_{m'_b - m_b - M}^{l'_b}(\hat{\mathbf{k}}'_b) Y_{m'_a - m_a + M}^{l'_a}(\hat{\mathbf{k}}'_a) \mathcal{I}(l_a, l'_a, l'_b, j_a, j'_a, j'_b, K), \quad (4.G.43) \end{aligned}$$

with

$$\begin{aligned} \mathcal{I}(l_a, l'_a, l'_b, j_a, j'_a, j'_b, K) &= \int dr_{aA} dr_{bc} d\theta r_{aA} r_{bc} \frac{\sin \theta}{r_{ac}} u_{l_b}(r_{bc}) v(r_{ab}) \\ &\times F_{l_a, j_a}(r_{aA}) F_{l'_a, j'_a}(r_{ac}) F_{l'_b, j'_b}(r_{bc}) \\ &\times \sum_{M_K} \langle l_a 0 \ l'_a M_K | K M_K \rangle \left[ Y^{l_b}(\cos \theta, 0) Y^{l'_b}(\cos \theta, 0) \right]_{-M_K}^K Y_{M_K}^{l'_a}(\cos \theta_{ac}, 0). \quad (4.G.44) \end{aligned}$$

Again, this is a 3-dimensional integral that can be evaluated with the method of Gaussian quadratures. The transition amplitude  $T_{m_a, m_b}^{m'_a, m'_b}(\mathbf{k}'_a, \mathbf{k}'_b)$  depends explicitly on the initial  $(m_a, m'_a)$  and final  $(m'_a, m'_b)$  polarizations of  $a, b$ . If the particle  $b$  is initially coupled to core  $c$  to total angular momentum  $J_A, M_A$ , the amplitude to be considered is rather

$$T_{m_a}^{m'_a, m'_b}(\mathbf{k}'_a, \mathbf{k}'_b) = \sum_{m_b} \langle j_b m_b j_c M_A - m_b | J_A M_A \rangle T_{m_a, m_b}^{m'_a, m'_b}(\mathbf{k}'_a, \mathbf{k}'_b), \quad (4.G.45)$$

and the multi-differential cross section for detecting particle  $c$  (or  $a$ ) is

$$\frac{d\sigma}{d\mathbf{k}'_a d\mathbf{k}'_b} \Big|_{m_a}^{m'_a, m'_b} = \frac{k'_a}{k_a} \frac{\mu_{aA} \mu_{ac}}{4\pi^2 \hbar^4} \left| \sum_{m_b} \langle j_b \ m_b \ j_c \ M_A - m_b | J_A \ M_A \rangle T_{m_a, m_b}^{m'_a, m'_b}(\mathbf{k}'_a, \mathbf{k}'_b) \right|^2. \quad (4.G.46)$$

All spin-polarization observables (analysing powers, etc.,) can be derived from this expression. But let us now work out the expression of the cross section for an unpolarized beam (sum over initial spin orientations divided by the number of such orientations) and when we do not detect the final polarizations (sum over final spin orientations),

$$\begin{aligned} \frac{d\sigma}{d\mathbf{k}'_a d\mathbf{k}'_b} &= \frac{k'_a}{k_a} \frac{\mu_{aA} \mu_{ac}}{4\pi^2 \hbar^4} \frac{1}{(2J_A + 1)(2j_a + 1)} \\ &\times \sum_{\substack{m_a, m'_a \\ M_A, m'_b}} \left| \sum_{m_b} \langle j_b \ m_b \ j_c \ M_A - m_b | J_A \ M_A \rangle T_{m_a, m_b}^{m'_a, m'_b}(\mathbf{k}'_a, \mathbf{k}'_b) \right|^2. \end{aligned} \quad (4.G.47)$$

The sum above can be simplified a bit. Let us consider a single particular value of  $m_b$  in the sum over  $m_b$ ,

$$\begin{aligned} \sum_{m_a, m'_a, m'_b} \left| T_{m_a, m_b}^{m'_a, m'_b}(\mathbf{k}'_a, \mathbf{k}'_b) \right|^2 \sum_{M_A} \left| \langle j_b \ m_b \ j_c \ M_A - m_b | J_A \ M_A \rangle \right|^2 = \\ \frac{2J_A + 1}{2j_b + 1} \sum_{m_a, m'_a, m'_b} \left| T_{m_a, m_b}^{m'_a, m'_b}(\mathbf{k}'_a, \mathbf{k}'_b) \right|^2 \\ \times \sum_{M_A} \left| \langle J_A - M_A \ j_c \ M_A - m_b | j_b \ m_b \rangle \right|^2, \end{aligned} \quad (4.G.48)$$

where we have used

$$\langle j_b \ m_b \ j_c \ M_A - m_b | J_A \ M_A \rangle = (-1)^{j_c - M_A + m_b} \sqrt{\frac{2J_A + 1}{2j_b + 1}} \langle J_A - M_A \ j_c \ M_A - m_b | j_b \ m_b \rangle. \quad (4.G.49)$$

As

$$\sum_{M_A} \left| \langle J_A - M_A \ j_c \ M_A - m_b | j_b \ m_b \rangle \right|^2 = 1, \quad (4.G.50)$$

we finally have

$$\frac{d\sigma}{d\mathbf{k}'_a d\mathbf{k}'_b} = \frac{k'_a}{k_a} \frac{\mu_{aA} \mu_{ac}}{4\pi^2 \hbar^4} \frac{1}{(2j_b + 1)(2j_a + 1)} \sum_{m_a, m'_a, m'_b} \left| \sum_{m_b} T_{m_a, m_b}^{m'_a, m'_b}(\mathbf{k}'_a, \mathbf{k}'_b) \right|^2. \quad (4.G.51)$$

### Zero range approximation.

The zero range approximation consists in taking  $v(r_{ab}) = D_0\delta(r_{ab})$ . Then, (see (4.G.21))

$$\begin{aligned}\mathbf{r}_{aA} &= \frac{c}{A}\mathbf{r}_{bc}, \\ \mathbf{r}_{ac} &= \mathbf{r}_{bc}.\end{aligned}\quad (4.G.52)$$

The angular dependence of the integral can be readily evaluated. From (5.D.20), noting that  $\hat{\mathbf{r}}_{aA} = \hat{\mathbf{r}}_{ac} = \hat{\mathbf{r}}_{bc} \equiv \hat{\mathbf{r}}$ ,

$$\begin{aligned}&\left[ Y^{l_a}(\hat{\mathbf{r}}) Y'^{l'_a}(\hat{\mathbf{r}}) \right]_M^K \left[ Y^{l_b}(\hat{\mathbf{r}}) Y'^{l'_b}(\hat{\mathbf{r}}) \right]_{-M}^K = \\ &\frac{(-1)^{K-M}}{\sqrt{2K+1}} \left\{ \left[ Y^{l_a}(\hat{\mathbf{r}}) Y'^{l'_a}(\hat{\mathbf{r}}) \right]_0^K \left[ Y^{l_b}(\hat{\mathbf{r}}) Y'^{l'_b}(\hat{\mathbf{r}}) \right]_0^K \right\}_0^0.\end{aligned}\quad (4.G.53)$$

We can as before evaluate this expression in the configuration shown in Fig. 4.G.2 ( $\hat{\mathbf{r}} = \hat{z}$ ), but now the multiplicative factor is  $4\pi$ . The corresponding contribution to the integral is

$$\frac{(-1)^K}{4\pi(2K+1)} \langle l_a 0 l'_a 0 | K 0 \rangle \sqrt{(2l_a + 1)(2l'_a + 1)(2l_b + 1)(2l'_b + 1)}, \quad (4.G.54)$$

and

$$\begin{aligned}T_{m_a, m_b}^{m'_a, m'_b}(\mathbf{k}'_a, \mathbf{k}'_b) &= \frac{16\pi^2}{k_a k'_a k'_b A} D_0 T_\sigma \sum_{l_a, j_a} \sum_{l'_a, j'_a} \sum_{l'_b, j'_b} \sum_{K, M} e^{i(\sigma^{l_a} + \sigma^{l'_a} + \sigma^{l'_b})} i^{l_a - l'_a - l'_b} (-1)^{l_a + l'_a + l'_b - j'_a - j'_b} \\ &\times \sqrt{(2l_a + 1)(2l'_a + 1)(2l_b + 1)(2l'_b + 1)} \langle l_a 0 l'_a 0 | K 0 \rangle \\ &\times \frac{2l_a + 1}{2K + 1} ((l'_a \frac{1}{2})_{j'_a} (l_a \frac{1}{2})_{j_a} | (l_a l'_a)_K (\frac{1}{2} \frac{1}{2})_0)_K ((l'_b \frac{1}{2})_{j'_b} (l_b \frac{1}{2})_{j_b} | (l_b l'_b)_K (\frac{1}{2} \frac{1}{2})_0)_K \\ &\times \langle l'_a m_a - m'_a - M 1/2 m'_a | j'_a m_a - M \rangle \langle l'_b m_b - m'_b + M 1/2 m'_b | j'_b M + m_b \rangle \\ &\times \langle l 0 1/2 m_a | j m_a \rangle Y_{M+m_b+m'_b}^{l'_b}(\hat{\mathbf{k}}'_b) Y_{m_a+m'_a-M}^{l'_a}(\hat{\mathbf{k}}'_a) \mathcal{I}_{ZR}(l_a, l'_a, l'_b, j_a, j'_a, j'_b),\end{aligned}\quad (4.G.55)$$

where now the 1-dimensional integral to solve is

$$\mathcal{I}_{ZR}(l_a, l'_a, l'_b, j_a, j'_a, j'_b) = \int dr u_{l_b}(r) F_{l_a, j_a}(\frac{c}{A}r) F_{l'_a, j'_a}(r) F_{l'_b, j'_b}(r)/r. \quad (4.G.56)$$

### 4.G.3 One-particle transfer

It may be interesting to state the expression for the one particle transfer reaction within the same context and using the same elements, in order to better compare these two type of experiments. In particle transfer, the final state of  $b$  is a bound

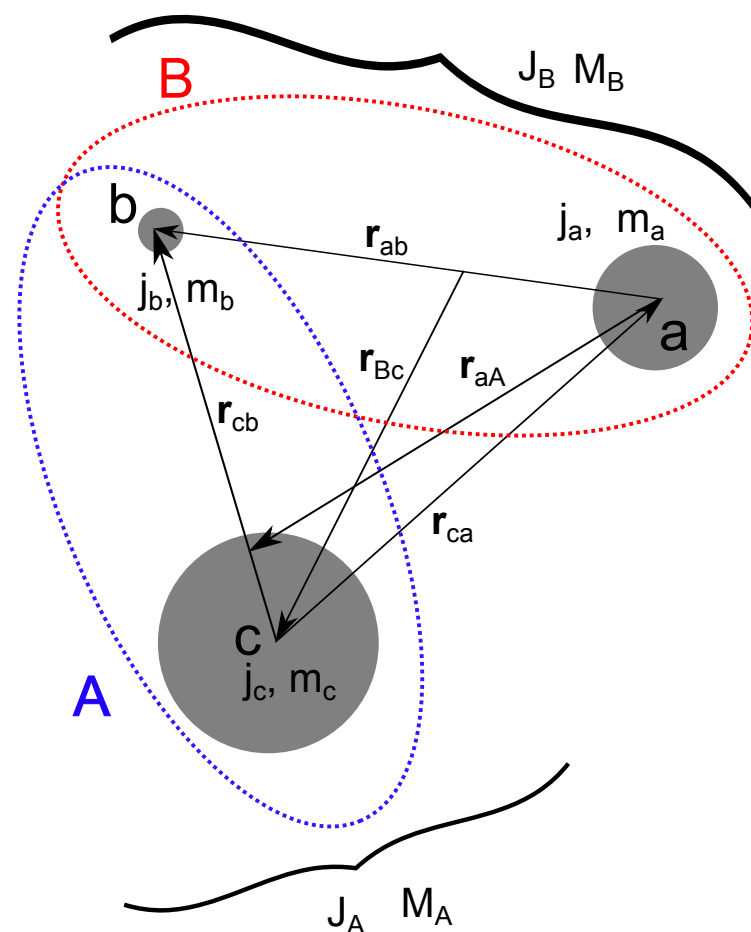


Figure 4.G.4: One particle transfer reaction  $A(= c + b) + a \rightarrow B(= a + b) + c$ .

state of the  $B (= a + b)$  nucleus (cf. Fig. 4.G.4), and we can carry on in a similar way as done previously just by substituting the distorted wave (continuum) wave function (4.G.34) with

$$\psi_{m'_b}^{l'_b, j'_b *}(r_{ab}, \sigma_b) = u_{l'_b, j'_b}^*(r_{ab}) [Y^{l'_b}(\hat{\mathbf{r}}_{ab}) \phi^{1/2}(\sigma_b)]_{m'_b}^{j'_b *}, \quad (4.G.57)$$

so the transition amplitude is now

$$\begin{aligned} T_{m_a, m_b}^{m'_a, m'_b}(\mathbf{k}'_a) &= \frac{8\pi^{3/2}}{k_a k'_a} \sum_{\sigma_a, \sigma_b} \sum_{l_a, j_a} \sum_{l'_a, m_{l'_a}, j'_a} e^{i(\sigma^{l_a} + \sigma^{l'_a})} i^{l_a - l'_a} (-1)^{l_a + l'_a - j'_a - j'_b} \\ &\times \sqrt{2l_a + 1} \langle l'_a | m_{l'_a} 1/2 | m'_a | j'_a | m_{l'_a} + m'_a \rangle \langle l_a 0 1/2 | m_a | j_a | m_a \rangle \\ &\times Y_{-m_{l'_a}}^{l'_a}(\hat{\mathbf{k}}'_a) \int d\mathbf{r}_{aA} d\mathbf{r}_{bc} [Y^{l'_a}(\hat{\mathbf{r}}_{bc}) \phi^{1/2}(\sigma_a)]_{-m_{l'_a} - m'_a}^{j'_a} [Y^{l'_b}(\hat{\mathbf{r}}_{ab}) \phi^{1/2}(\sigma_b)]_{-m'_b}^{j'_b} \\ &\times \frac{F_{l_a, j_a}(r_{aA}) F_{l'_a, j'_a}(r_{bc})}{r_{bc} r_{aA}} u_{l'_b, j'_b}^*(r_{ab}) u_{l_b, j_b}(r_{bc}) v(r_{ab}) v_\sigma(\sigma_a, \sigma_b) \\ &\times [Y^{l_a}(\hat{\mathbf{r}}_{aA}) \phi^{1/2}(\sigma_a)]_{m_a}^{j_a} [Y^{l_b}(\hat{\mathbf{r}}_{bc}) \phi^{1/2}(\sigma_b)]_{m_b}^{j_b}. \quad (4.G.58) \end{aligned}$$

Using (4.G.39), (4.G.40), (5.F.4), and setting  $M = m_a - m'_a - m_{l'_a}$

$$\begin{aligned} T_{m_a, m_b}^{m'_a, m'_b}(\mathbf{k}'_a) &= \frac{8\pi^{3/2}}{k_a k'_a} T_\sigma \sum_{l_a, j_a} \sum_{l'_a, j'_a} \sum_{K, M} e^{i(\sigma^{l_a} + \sigma^{l'_a})} i^{l_a - l'_a} (-1)^{l_a + l'_a - j'_a - j'_b} \\ &\times ((l'_a \frac{1}{2})_{j'_a} (l_a \frac{1}{2})_{j_a} | (l_a l'_a)_K (\frac{1}{2} \frac{1}{2})_0)_K ((l'_b \frac{1}{2})_{j'_b} (l_b \frac{1}{2})_{j_b} | (l_b l'_b)_K (\frac{1}{2} \frac{1}{2})_0)_K \\ &\times \sqrt{2l_a + 1} \langle l'_a | m_a - m'_a - M 1/2 | m'_a | j'_a | m_a - M \rangle \langle l_a 0 1/2 | m_a | j_a | m_a \rangle \\ &\times Y_{m_a - m'_a - M}^{l'_a}(\hat{\mathbf{k}}'_a) \int d\mathbf{r}_{aA} d\mathbf{r}_{bc} \frac{F_{l_a, j_a}(r_{aA}) F_{l'_a, j'_a}(r_{bc})}{r_{bc} r_{aA}} u_{l'_b, j'_b}^*(r_{ab}) u_{l_b, j_b}(r_{bc}) v(r_{ab}) \\ &\times [Y^{l_a}(\hat{\mathbf{r}}_{aA}) Y^{l'_a}(\hat{\mathbf{r}}_{bc})]_M^K [Y^{l_b}(\hat{\mathbf{r}}_{bc}) Y^{l'_b}(\hat{\mathbf{r}}_{ab})]_{-M}^K. \quad (4.G.59) \end{aligned}$$

Aside from (4.G.21), we also need

$$\mathbf{r}_{bc} = \frac{a + B}{B} \mathbf{r}_{aA} + \frac{b}{A} \mathbf{r}_{bc}. \quad (4.G.60)$$

From (4.G.20–4.G.25), one gets

$$\begin{aligned} T_{m_a, m_b}^{m'_a, m'_b}(\mathbf{k}'_a) &= \frac{32\pi^3}{k_a k'_a} T_\sigma \sum_{l_a, j_a} \sum_{l'_a, j'_a} \sum_{K, M} e^{i(\sigma^{l_a} + \sigma^{l'_a})} i^{l_a - l'_a} (-1)^{l_a + l'_a - j'_a - j'_b} \\ &\times ((l'_a \frac{1}{2})_{j'_a} (l_a \frac{1}{2})_{j_a} | (l_a l'_a)_K (\frac{1}{2} \frac{1}{2})_0)_K ((l'_b \frac{1}{2})_{j'_b} (l_b \frac{1}{2})_{j_b} | (l_b l'_b)_K (\frac{1}{2} \frac{1}{2})_0)_K \\ &\times \frac{2l_a + 1}{2K + 1} \langle l'_a | m_a - m'_a - M 1/2 | m'_a | j'_a | m_a - M \rangle \\ &\times \langle l_a 0 1/2 | m_a | j_a | m_a \rangle Y_{m_a - m'_a - M}^{l'_a}(\hat{\mathbf{k}}'_a) \mathcal{I}(l_a, l'_a, j_a, j'_a, j'_b, K), \quad (4.G.61) \end{aligned}$$

with

$$\begin{aligned}
 I(l_a, l'_a, j_a, j'_a, K) = & \int dr_{aA} dr_{bc} d\theta r_{aA} r_{bc}^2 \frac{\sin \theta}{r_{bc}} \\
 & \times F_{l_a, j_a}(r_{aA}) F_{l'_a, j'_a}(r_{ac}) u_{l'_b, j'_b}^*(r_{ab}) u_{l_b, j_b}(r_{bc}) v(r_{ab}) \\
 & \times \sum_{M_K} \langle l_a 0 | l'_a M_K | K M_K \rangle [Y^{l_b}(\cos \theta, 0) Y^{l'_b}(\cos \theta_{ab}, 0)]_{-M_K}^K Y_{M_K}^{l'_a}(\cos \theta_{Bc}, 0),
 \end{aligned} \tag{4.G.62}$$

where (see (4.G.21), (4.G.60) and Fig. 4.G.2)

$$\cos \theta_{ab} = \frac{-r_{aA} - \frac{c}{A} r_{bc} \cos \theta}{\sqrt{\left(\frac{c}{A} r_{bc} \sin \theta\right)^2 + \left(r_{aA} + \frac{c}{A} r_{bc} \cos \theta\right)^2}}, \tag{4.G.63}$$

$$\cos \theta_{Bc} = \frac{\frac{a+B}{B} r_{aA} + \frac{b}{A} r_{bc} \cos \theta}{\sqrt{\left(\frac{b}{A} r_{bc} \sin \theta\right)^2 + \left(\frac{a+B}{B} r_{aA} + \frac{b}{A} r_{bc} \cos \theta\right)^2}}, \tag{4.G.64}$$

and

$$r_{Bc} = \sqrt{\left(\frac{b}{A} r_{bc} \sin \theta\right)^2 + \left(\frac{a+B}{B} r_{aA} + \frac{b}{A} r_{bc} \cos \theta\right)^2}. \tag{4.G.65}$$

By the way, (4.G.61) can also be used when particle  $b$  populates a resonant state in the continuum of nucleus  $B$ .

## Appendix 4.H Modified formfactors

### 4.H.1 Two-particle transfer

### 4.H.2 One-particle transfer

### 4.H.3 Inelastic scattering

### 4.H.4 Elastic scattering

## Appendix 4.I Dynamical shell model in a nutshell

In the extreme shell model the nucleons move independently, feeling the presences of the other nucleons when bouncing elastically off the nuclear surface of the average potential. The properly normalized probability for removing nucleon from such orbitals is one for  $\omega$  equal to the (unperturbed) energy of the orbital  $k$  and zero otherwise. (cf. Fig 4.I.1)

In the dynamical shell model (cf. Mahaux, C. et al. (1985) and references therein) the nucleons can bounce inelastically off the nuclear surface setting the nucleus in a vibrational state and changing the state of motion (Fig. 4.I.1). In this case the strength of the levels becomes in general distributed over a range of

energies both below and above the Fermi energy. That is, the state  $k$  is found both in the system ( $A - 1$ ) produced in a pick-up process and in the system ( $A + 1$ ) populated through a stripping reaction as indicated in Fig 4.I.1.

It is still an open question whether this distribution is concentrated in discrete states or displays a continuous behavior. Both situations can in principle be found depending of whether the original single-particle state is close or far away from the Fermi energy. The sum of the spectroscopic factors associated with all the states excited in the pick-up process of a nucleon with quantum numbers  $k$  gives the occupation number associated with the orbital, i.e.  $\int_{-\infty}^{\epsilon_F} S_h(k; \omega) d\omega = n_k$ , where  $S_h$  is the (hole) strength function. The full single-particle strength is found adding to this quantity the spectroscopic factors associated with the excitation of states in the ( $A + 1$ ) system where a particle with quantum numbers  $k$  is deposited in the target.

It is noted that the fact that in the dynamical shell model the single-particle strength is distributed not only over an energy range in the ( $A - 1$ ) system but also on the ( $A + 1$ ) system is intimately connected with the ground state correlations associated with the vibrational modes which produce particle-hole excitations in the ground state (also pair addition and subtraction modes). In this way single-particle states which originally were filled become partially empty, and vice versa.

The transfer process shown in (b) for both stripping and pick-up reactions are closely associated with the polarization and correlation contributions to the mass operator  $\mathcal{M}(k; \omega) = \mathcal{V}(k; \omega) + i\mathcal{W}(k; \omega)$ . The associated total strength distribution

$$\begin{aligned} S(k; \omega) &= S_h(k; \omega) + S_p(k; \omega) \\ &= \frac{1}{2\pi} \frac{\mathcal{W}(k; \omega) + \Delta}{(E_k + \mathcal{V}(k; \omega) - E)^2 + \frac{1}{4}\mathcal{W}(k; \omega)^2} \end{aligned}$$

can display a variety of shapes, as  $\mathcal{V}(k; \omega)$  and  $\mathcal{W}(k; \omega)$  are energy dependent.

The intermediate states of the polarization and correlation diagrams which in the present discussion are the doorway states to the renormalization of the single-particle motion must be mixed with more complicated configurations. The mechanism for these couplings and their consequences are quite involved and, to some extent, open problems. Thus, the extension in the complex plane of the associated expressions in terms of an imaginary parameter  $\Delta$  is made to take these effects into account in some average way. In any case, most of the results are not dependent on the detailed value this quantity has.

The picture shown in Fig. 4.I.1 (b) although accurate and controlled by only few parameters is much ..... rich as compared to the originally extreme shell model picture.

A major simplification can be achieved recognizing that the essential difference between the situation depicted in Figs 4.I.1 (a) and (b) is the value of the mean free path. In the first case it is infinite while in the second it is finite, i.e. due to the coupling to the surface modes (and eventually pair modes) single-particle motion acquires a lifetime. In this sense the detailed shape of the strength distribution which reflects the specificity of the different couplings and which is of central

important for a detailed analysis of the data becomes of secondary importance within the present context.

Making the ansatz that the single-particle motion decays exponentially a Breit-Wigner shape can be fitted to the different strength concentration resulting from the detailed calculation (cf. Fig. 4.I.1 (a)) The centroid of the corresponding peaks defines an energy which can be viewed as the energy of the dressed single-particle state. On the other hand, caution should be exercised in interpreting the area under the fitted curve as a spectroscopic factor, if only because this quantity can become larger than one. It is only for the levels not too far away from the Fermi energy that such interpretation can be reasonably accurate.

another quantity which can be used to characterize the dressed single-particle states is the rate of change of the energy shift as a function of the energy, i.e. the effective mass. Again, for the orbitals close to the Fermi energy this quantity is inversely proportional to the area under the Breit-Wigner shapes. The energy range over which the effective mass deviates from one determine the region where the dynamical couplings change the density of single-particle levels.

The trend of the effective masses shown in Fig. 4.I.1 (d) can be quantitatively understood as follows. For single-particle states close to the Fermi energy the intermediate states have all energies larger than the unperturbed single-particle energy, and the resulting shape is  $\delta$ -like with a tail extending away from the Fermi energy. For single-particle orbital 5–7 MeV away from  $E_F$  there are a number of intermediate states which have the same energy of the initial state leading to zero energy denominators and thus to a marked structure in the strength function. Finally, for single-particle states far away from  $E_F$ , the density of intermediate states is so large that the matrix elements of these couplings average out to a constant with a value much larger than typical distances between successive intermediate states. These are the conditions which lead to a Breit-Wigner shape.

It is then to be expected that the single-particle levels in the intermediate region will be associated with strength functions which deviate much from a smooth function and for which comparatively large errors can be made through a Breit-Wigner fitting. This is also seen from Fig. 4.I.1 (d) where the effective mass becomes smaller than one, indicating that the area of the fitted shapes are larger than that of the original strength function  $S(k; \omega)$ . This result emphasizes the difficulties found in trying to translate effective masses into spectroscopic factors in a general situation.

Starting from the extreme picture shown in Fig. 4.I.1 (a) where the relation  $\omega = \hbar^2 k^2 / 2m$  holds one arrives at the picture (c) where the relation  $d\omega = \hbar^2 k \delta k / m*$  again accounts for the main properties of the single-particle motion and where the effect of the couplings are contained in  $m*$ . .... implementation of the single-particle self energies have been carried out for different regions of the mass table. In particular, for the valence levels of  $^{208}\text{Pb}$ . In this case the mass operator associated with each orbital was calculated as a function of the energy. The numerical derivative of the real part of the mass operator was then calculated and the  $\omega$ -dependent effective mass obtained as a function of the energy.

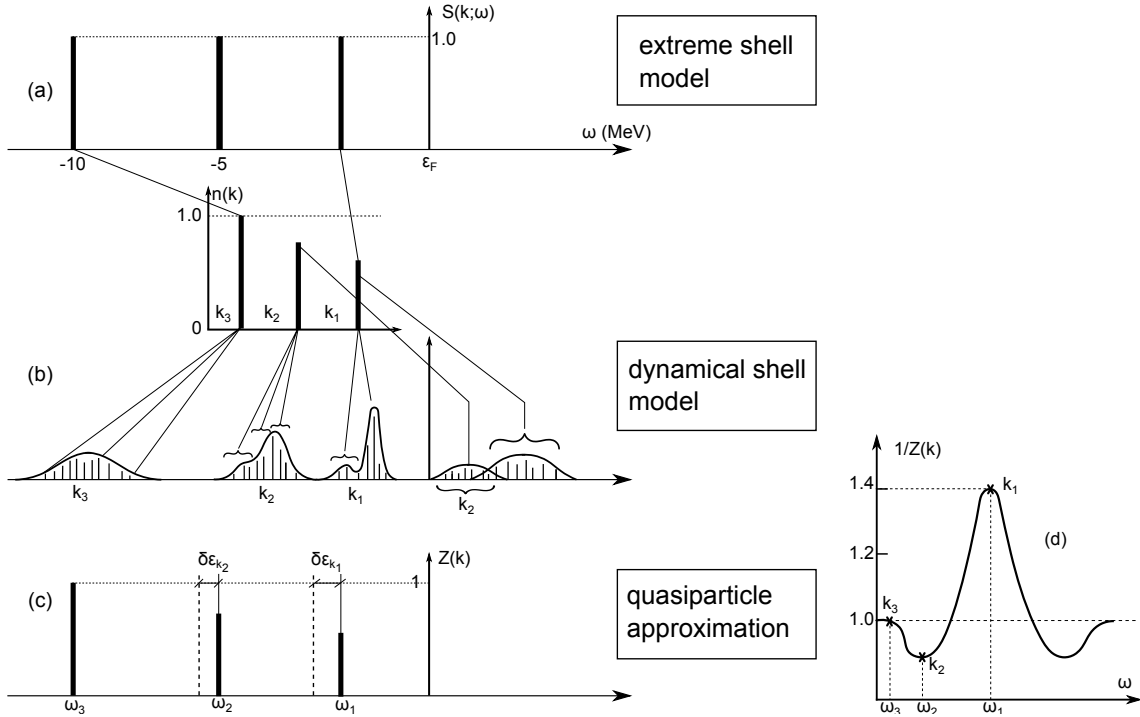


Figure 4.I.1: Schematic representation of the main quantities characterizing the single-particle motion in the nuclear shell model taking into account the residual interaction among the particles at different levels of approximation. In (a) the interaction is treated in the Hartree–Fock approximation and the particles feel the presence of the other particles through their own confinement in the average field. The strength function shows sharp peaks, each of them carrying the full strength of the states. In fact the occupation number associated with each state  $k$  contains only one contribution. In (b) the particles couple still only with the average field. However in this case they can set the surface into vibrations by changing its state of notion. The strength associated with each orbital is distributed over a finite energy range. The corresponding occupation numbers arise from the sum of many contributions. Fitting a Lorentzian shape to each peak one can regain the simplicity of the extreme shell model by defining new levels with energy equal to that of the centroid and strength equal to that of the area covered by the Lorentzian shape (cf. (c)). In (d) the energy variation of the shift of the centroids is contained into an effective  $\omega$ –mass according to the standard relation  $\frac{m_\omega}{m} = \left(1 - \frac{\partial \Delta E}{\partial \hbar \omega}\right)$  (see Eq. (4.A.5)). The resulting curve resembles the shape obtained by calculating the inverse of the area below the different Lorentzians (quasiparticle approximation).

The question then arises of how to define an average quantity which depends only on the energy of the orbital and is state independent. Rather different prescriptions have been used to deal with the question. In any case the main result obtained was that the  $\omega$ -dependent effective mass shows a well defined peak at the Fermi surface, its maximum value being considerably larger than one ( $\approx 1.4$ ). The associated full width at half maximum is of the order of 10 MeV. This quantity is much smaller than the Fermi energy ( $\sim 36$  MeV) and is essentially determined by the energy of the low-lying collective modes and of the single-particle gap around  $^{208}\text{Pb}$ .

## Bibliography

- H. An and C. Cai. Global deuteron optical model potential for the energy range up to 183 MeV. *Phys. Rev. C*, 73:054605, 2006.
- P. W. Anderson. *Basic notions of condensed matter physics*. Benjamin, Menlo Park, California, 1984.
- R. J. Ascuitto and N. K. Glendenning. Inelastic processes in particle transfer reactions. *Physical Review*, 181:1396, 1969.
- Ascuitto, R. J. and N. K. Glendenning. Assessment of two-step processes in  $(p, t)$  reactions. *Phys. Rev. C*, 2:1260, 1970.
- Ascuitto R. J., N. K. Glendenning, and B. Sørensen. Confirmation of strong second order processes in  $(p, t)$  reactions on deformed nuclei. *Physics Letters B*, 34:17, 1971.
- Ascuitto R.J. and B. Sørensen. Coupling effects in  $^{208}\text{Pb}$ . *Nuclear Physics A*, 186: 641, 1972.
- N. Austern. Direct reactions. In F. Janouch, editor, *Select Topics in Nuclear Theory*, Vienna, 1963. IAEA.
- N. Austern. *Direct nuclear reaction theories*. Interscience monographs and texts in physics and astronomy. Wiley-Interscience, 1970.
- J. Bang, S. Ershov, F. Gareev, and G. Kazacha. Discrete expansions of continuum wave functions. *Nuclear Physics A*, 339:89, 1980.
- J. Bardeen and D. Pines. Electron-phonon interaction in metals. *Phys. Rev.*, 99: 1140, 1955.
- Baroni, S., M. Armati, F. Barranco, R. A. Broglia, G. Colò, G. Gori, and E. Vigezzi. Correlation energy contribution to nuclear masses. *Journal of Physics G: Nuclear and Particle Physics*, 30:1353, 2004.

- F. Barranco, M. Gallardo, and R. A. Broglia. Nuclear field theory of spin dealignment in strongly rotating nuclei and the vacuum polarization induced by pairing vibrations. *Phys. Lett. B*, 198:19, 1987.
- Barranco, F., P. F. Bortignon, R. A. Broglia, G. Colò, and E. Vigezzi. The halo of the exotic nucleus  $^{11}\text{Li}$ : a single Cooper pair. *Europ. Phys. J. A*, 11:385, 2001.
- Bechara, M. J. and O. Dietzsch. States in  $^{121}\text{Sn}$  from the  $^{120}\text{Sn}(d, p)^{121}\text{Sn}$  reaction at 17 mev. *Phys. Rev. C*, 12:90, 1975.
- G. F. Bertsch, P. F. Bortignon, and R. A. Broglia. Damping of nuclear excitations. *Rev. Mod. Phys.*, 55:287, 1983.
- Bertsch, G. F., R. A. Broglia, and C. Riedel. Qualitative description of nuclear collectivity. *Nucl. Phys. A*, 91:123, 1967.
- D. R. Bès and R. A. Broglia. Equivalence between Feynman–Goldstone and particle–phonon diagrams for finite many body systems. In G. Alaga, V. Paar, and L. Sips, editors, *Problems of Vibrational Nuclei, in Procs. of the topical Conference on Problems of Vibrational Nuclei*, page 1, Amsterdam, 1975. North Holland.
- D. R. Bès and R. A. Broglia. In A. Bohr and R. Broglia, editors, *International School of Physics “Enrico Fermi” Course LXIX, Elementary Modes of Excitation in Nuclei*, page 55, Amsterdam, 1977. North Holland.
- D. R. Bès, G. G. Dussel, R. Broglia, R. Liotta, and B. R. Mottelson. Nuclear field theory as a method of treating the problem of overcompleteness in descriptions involving elementary modes of both quasi-particles and collective type. *Phys. Lett. B*, 52:253, 1974.
- D. R. Bès, R. A. Broglia, G. G. Dussel, R. J. Liotta, and R. P. J. Perazzo. On the many-body foundation of the Nuclear Field Theory. *Nucl. Phys. A*, 260:77, 1976a.
- D. R. Bès, R. A. Broglia, G. G. Dussel, R. J. Liotta, and H. M. Sofía. The nuclear field treatment of some exactly soluble models. *Nucl. Phys. A*, 260:1, 1976b.
- D. R. Bès, R. A. Broglia, G. G. Dussel, R. J. Liotta, and H. M. Sofía. Application of the nuclear field theory to monopole interactions which include all the vertices of a general force. *Nucl. Phys. A*, 260:27, 1976c.
- Bès, D. R. and J. Kurchan. *The treatment of Collective Coordinates in Many–Body Systems*. World Scientific, Singapore, 1990.
- Bès, D. R., R. A. Broglia, J. Dudek, W. Nazarewicz, and Z. Szymański. Fluctuation effects in the pairing field of rapidly rotating nuclei. *Annals of Physics*, 182:237, 1988.

- Bès,D. R. and R. A. Broglia. Pairing vibrations. *Nucl. Phys.*, 80:289, 1966.
- Bjerregaard, J. H., O. Hansen, Nathan, and S. Hinds. States of  $^{208}\text{Pb}$  from double triton stripping. *Nucl. Phys.*, 89:337, 1966.
- A. Bohr and B. R. Mottelson. *Nuclear Structure, Vol.I.* Benjamin, New York, 1969.
- Bohr, A. and B. R. Mottelson. *Nuclear Structure, Vol.II.* Benjamin, New York, 1975.
- M. Born. Zur Quantenmechanik der Stoßvorgänge. *Zeitschr.f. Phys.*, 37:863, 1926.
- P. F. Bortignon and R. A. Broglia. Role of the nuclear surface in a unified description of the damping of single-particle states and giant resonances. *Nucl. Phys. A*, 371:405, 1981.
- P. F. Bortignon, R. A. Broglia, and C. H. Dasso. Quenching of the mass operator associated with collective states in many-body systems. *Nuclear Physics A*, 398: 221, 1983.
- Bortignon, P. F., R. A. Broglia, D. R. Bès, and R. Liotta. Nuclear field theory. *Physics Reports*, 30:305, 1977.
- Bortignon, P.F., A. Bracco, and R. Broglia. *Giant Resonances*. Harwood Academic Publishers, Amsterdam, 1998.
- D. Brink and G. R. Satchler. *Angular Momentum*. Clarendon Press, 1968.
- Brink, D. and R. A. Broglia. *Nuclear Superfluidity*. Cambridge University Press, Cambridge, 2005.
- R. Broglia and A. Winther. *Heavy Ion Reactions*. Westview Press, Boulder, CO., 2004.
- R. Broglia, G. Coló, G. Onida, and H. Roman. *Solid State Physics of Finite Systems: metal clusters, fullerenes, atomic wires*. Springer Verlag, Berlin, Heidelberg, 2004.
- R. A. Broglia and C. Riedel. Pairing vibration and particle-hole states excited in the reaction  $^{206}\text{Pb}(\text{t}, \text{p})^{208}\text{Pb}$ . *Nucl. Phys.*, 92:145, 1967.
- R. A. Broglia, B. R. Mottelson, D. R. Bès, R. Liotta, and H. M. Sofía. Treatment of the spurious state in Nuclear Field Theory. *Physics Letters B*, 64:29, 1976.
- Broglia, R. A., G. Pollarolo, and A. Winther. On the absorptive potential in heavy ion scattering. *Nuclear Physics A*, 361:307, 1981.
- Broglia, R. A., T. Døssing, B. Lauritzen, and B. R. Mottelson. Nuclear rotational damping: Finite-system analogue to motional narrowing in nuclear magnetic resonances. *Phys. Rev. Lett.*, 58:326, 1987.

- Broglia, R.A., O. Hansen, and C. Riedel. Two-neutron transfer reactions and the pairing model. *Advances in Nuclear Physics*, 6:287, 1973. URL [www.mi.infn.it/?vigezzi/BHR/BrogliaHansenRiedel.pdf](http://www.mi.infn.it/?vigezzi/BHR/BrogliaHansenRiedel.pdf).
- W. R. Cobb and D. B. Guthe. Angular distribution of protons from the  $^{44}\text{Ca}(d, p)^{45}\text{Ca}$  reaction. *Phys. Rev.*, 107:181, 1957.
- Dickey, S. A., J. Kraushaar, R. Ristinen, and M. Rumore. The  $^{120}\text{Sn}(p, d)^{119}\text{Sn}$  reaction at 26.3 MeV. *Nuclear Physics A*, 377:137, 1982.
- W. H. Dickhoff and C. Barbieri. Self-consistent Green's function method for nuclei and nuclear matter. *Progress in Particle and Nuclear Physics*, 52:377, 2004.
- Dickhoff, W. and D. Van Neck. *Many-Body Theory Exposed: Propagator description of quantum mechanics in many-body systems*. World Scientific, Singapore, 2005.
- Duguet, T. and G. Hagen. *Ab initio* approach to effective single-particle energies in doubly closed shell nuclei. *Phys. Rev. C*, 85:034330, 2012.
- A. R. Edmonds. *Angular momentum in quantum mechanics*. Princeton University Press, 1960.
- Fernández-García, J.P., M. Alvarez, A. Moro, and M. Rodriguez-Gallardo. Simultaneous analysis of elastic scattering and transfer/breakup channels for the  $^6\text{He}+^{208}\text{Pb}$  reaction at energies near the Coulomb barrier. *Phys.Lett.*, B693:310, 2010.
- Fernández-García, J.P., M. Rodríguez-Gallardo, M. Alvarez, and A. Moro. Long range effects on the optical model of  $^6\text{He}$  around the Coulomb barrier. *Nuclear Physics A*, 840:19, 2010.
- H. Feshbach. Unified Theory of Nuclear Reactions. *Annals of Physics*, 5:357, 1958.
- R. Feynman. *Theory of fundamental processes*. Benjamin, Reading, Mass., 1975.
- Fröhlich, H. Interaction of electrons with lattice vibrations. *Procs. Royal Soc.*, 215:291, 1952.
- Glendenning, N. K. *Direct nuclear reactions*. World Scientific, Singapore, 2004.
- I. Hamamoto. Single-particle components of particle-vibrational states in the nuclei  $^{209}\text{Pb}$ ,  $^{209}\text{Bi}$ ,  $^{207}\text{Pb}$  and  $^{207}\text{Tl}$ . *Nuclear Physics A*, 141:1, 1970.
- Idini, A. Renormalization effects in nuclei. *Ph.D. thesis, University of Milan*, 2013.
- Idini, A., F. Barranco, and E. Vigezzi. Quasiparticle renormalization and pairing correlations in spherical superfluid nuclei. *Phys. Rev. C*, 85:014331, 2012.

- Idini, A., G. Potel, Barranco, E. Vigezzi, and R. A. Broglia. Dual origin of pairing in nuclei. *arXiv:1404.7365v1 [nucl-th]*, 2014.
- Jenning, B. Non observability of spectroscopic factors. *arXiv: 1102.3721v1 [nucl-th]*, 2011.
- Jeppesen, H. B. et al. Experimental investigation of the  ${}^9\text{Li}+\text{d}$  reaction at REX-ISOLDE. *Nucl. Phys. A*, 738:511, 2004.
- Mahaux, C., P. F. Bortignon, R. A. Broglia, and C. H. Dasso. Dynamics of the shell model. *Physics Reports*, 120:1–274, 1985.
- A. Migdal. Interaction between electrons and lattice vibrations in a normal metal. *Soviet Physics JETP*, 7:996, 1958.
- D. Montanari, L. Corradi, S. Szilner, G. Pollarolo, E. Fioretto, G. Montagnoli, F. Scarlassara, A. M. Stefanini, S. Courtin, A. Goasduff, F. Haas, D. Jelavić Malenica, C. Michelagnoli, T. Mijatović, N. Soić, C. A. Ur, and M. Varga Pajtler. Neutron Pair Transfer in  ${}^{60}\text{Ni}+{}^{116}\text{Sn}$  Far below the Coulomb Barrier. *Phys. Rev. Lett.*, 113:052501, 2014.
- B. R. Mottelson. *Elementary Modes of Excitation in Nuclei, Le Prix Nobel en 1975*. Imprimerie Royale Norstedts Tryckeri, Stockholm, 1976. p. 80.
- Orrigo, S. E. A. and H. Lenske. Pairing resonances and the continuum spectroscopy of  ${}^{10}\text{Li}$ . *Phys. Lett. B*, 677:214, 2009.
- W. Pauli. *Exclusion principle and quantum mechanics, Nobel Lecture 1945*. Editions du Griffon, Neuchâtel, Switzerland, 1947.
- G. Pollarolo, R. Broglia, and A. Winther. Calculation of the imaginary part of the heavy ion potential. *Nuclear Physics A*, 406:369, 1983.
- G. Potel, F. Barranco, E. Vigezzi, and R. A. Broglia. Evidence for phonon mediated pairing interaction in the halo of the nucleus  ${}^{11}\text{Li}$ . *Phys. Rev. Lett.*, 105:172502, 2010.
- Potel, G. ONE: single-particle transfer DWBA software for both light and heavy ions. *Private communication*, 2012.
- Potel, G., A. Idini, F. Barranco, E. Vigezzi, and R. A. Broglia. Cooper pair transfer in nuclei. *Rep. Prog. Phys.*, 76:106301, 2013.
- Rawitscher, G. H. The microscopic Feshbach optical potential for a schematic coupled channel example. *Nuclear Physics A*, 475:519, 1987.
- G. Satchler. *Introduction to Nuclear Reactions*. Mc Millan, New York, 1980.
- G. Satchler. *Direct Nuclear Reactions*. Clarendon Press, Oxford, 1983.

- Tamura, T., D. R. Bès, R. A. Broglia, and S. Landowne. Coupled-channel born-approximation calculation of two-nucleon transfer reactions in deformed nuclei. *Physical Review Letters*, 25:1507, 1970.
- Tanikawa, I., M. Alcorta, D. Bandyopadhyay, R. Bieri, L. Buchmann, B. Davids, N. Galinski, D. Howell, W. Mills, S. Mythili, R. Openshaw, E. Padilla-Rodal, G. Ruprecht, G. Sheffer, A. C. Shotter, M. Trinczek, P. Walden, H. Savajols, T. Roger, M. Caamano, W. Mittig, P. Roussel-Chomaz, R. Kanungo, A. Gallant, M. Notani, G. Savard, and I. J. Thompson. Measurement of the two-halo neutron transfer reaction  $^1\text{H}(^{11}\text{Li}, ^9\text{Li})^3\text{H}$  at 3A MeV. *Phys. Rev. Lett.*, 100:192502, 2008.
- I. J. Thompson. Coupled reaction channels calculations in nuclear physics. *Computer Physics Reports*, 7(4):167, 1988.
- Thompson, I.J. Reaction mechanism of pair transfer. In R. A. Broglia and V. Zelevinsky, editors, *50 Years of Nuclear BCS*, page 455. World Scientific, Singapore, 2013.
- W. Tobocman. *Theory of direct reactions*. Oxford University Press, Oxford, 1961.
- J. Vaagen, B. Nilsson, J. Bang, and R. Ibarra. One- and two-nucleon overlaps generated by a Sturmian method. *Nuclear Physics A*, 319:143, 1979.



# Chapter 5

## Two-particle transfer

Cooper pairs are the building blocks of pairing correlations in many-body fermionic systems. In particular in atomic nuclei. As a consequence, nuclear superfluidity can be specifically probed through Cooper pair tunneling. In the simultaneous transfer of two nucleons, one nucleon goes over from target to projectile, or viceversa, under the influence of the nuclear interaction responsible of the existence of a mean field potential, while the other follows suit by profiting of: 1) pairing correlations (simultaneous transfer); 2) the fact that the single-particle wavefunctions describing the motion of Cooper pair partners in both target and projectile are solutions of different single-particle potentials (non-orthogonality term). In the limit of independent particle motion, in which all of the nucleon-nucleon interaction is used up in generating a mean field, both contributions to the transfer process (simultaneous and non-orthogonality) cancel out exactly (cf. App. 5.C)

In keeping with the fact that nuclear Cooper pairs are weakly bound ( $E_{corr} \ll \epsilon_F$ ), this cancellation is, in actual nuclei, quite strong. Consequently, successive transfer, a process in which the nuclear interaction acts twice is, as a rule, the main mechanism at the basis of Cooper pair transfer. Because of the same reason (weak binding), the correlation length of Cooper pairs is larger than nuclear dimensions ( $\xi = \hbar v_F / (2E_{corr}) \gg R$ ), a fact which allows the two members of a Cooper pair to move between target and projectile, essentially as a whole, also in the case of successive transfer. In other words, because of its (intrinsic, virtual extension) Cooper pair transfer display equivalent pairing correlations both in simultaneous as in successive transfer.<sup>1</sup>

---

<sup>1</sup>In order for a nucleon to display independent particle motion, all other nucleons must act coherently so as to leave the way free making feel their pullings and pushings only when the nucleon in question tries to leave the self-bound system, thus acting as a reflecting surface which inverts the momentum of the particle. It is then natural to consider the nuclear mean field the most striking and fundamental collective feature in all nuclear phenomena (Mottelson (1962)). A close second is provided by the BCS mean field, resulting from the condensation of a number of strongly overlapping Cooper pairs ( $\approx \langle BCS | \sum_{\nu>0} a_\nu^\dagger a_\nu^\dagger | BCS \rangle = \alpha_0 \neq 0$ ) and leading to independent pair motion. It is a rather unfortunate perversity of popular terminology that regards these collective fields (HF and HFB) as well as successive transfer, as in some sense an antithesis to the nuclear collective modes and to simultaneous transfer respectively. Within this context it is of notice that the differential cross

The present Chapter is structured in the following way. In section 5.1 we present a summary of two-nucleon transfer reaction theory. It provides, together with Section 3.1 the elements needed to calculate the absolute two-nucleon transfer differential cross sections in second order DWBA, and thus to compare theory with experiment. Within this context one can, after reading this section, move directly to Chapter 6 containing examples of applications of this formalism. For the practitioner in search of details and clarification we present in section 5.2 a derivation of the equations presented in section 5.1. These equations are implemented and made operative in the software COOPER used in the applications (cf. App. 6.D).

A number of Appendices are provided. Appendix 5.A briefly reminds the quantum basis for the dressing of elementary modes of excitation and of pairing interaction. In App. 5.B the derivation of first order DWBA simultaneous transfer is worked out within a formalism tailored to focus the attention on the nuclear structure correlations aspects of the process leading to effective two-nucleon transfer form factors. In App. 5.C the variety of contributions to two-nucleon transfer amplitudes (successive, simultaneous and non-orthogonality) are discussed in detail within the framework of the semi-classical approximation which provides a rather intuitive vision of the different processes. Appendices 5.D–5.G contain relations used in Sect. 5.2 as well as in the derivation of two-nucleon transfer spectroscopic amplitudes. Finally Appendix 5.H provides a glimpse of original material due to Ben Bayman (Bayman and Kallio (1967), Bayman (1970), Bayman (1971), Bayman and Chen (1982)) which was instrumental to render quantitative, studies of two-nucleon transfer, studies which can now be carried out in terms of absolute cross sections and not relative ones as done previously.

## 5.1 Summary of second order DWBA

Let us illustrate the theory of second order DWBA two-nucleon transfer reactions with the  $A + t \rightarrow B(\equiv A + 2) + p$  reaction, in which  $A + 2$  and  $A$  are even nuclei in their  $0^+$  ground state. The extension of the expressions to the transfer of pairs coupled to arbitrary angular momentum is discussed in subsection 5.2.10.

The wavefunction of the nucleus  $A + 2$  can be written as

$$\Psi_{A+2}(\xi_A, \mathbf{r}_{A1}, \sigma_1, \mathbf{r}_{A2}, \sigma_2) = \psi_A(\xi_A) \sum_{l_i, j_i} [\phi_{l_i, j_i}^{A+2}(\mathbf{r}_{A1}, \sigma_1, \mathbf{r}_{A2}, \sigma_2)]_0^0, \quad (5.1.1)$$

where

$$[\phi_{l_i, j_i}^{A+2}(\mathbf{r}_{A1}, \sigma_1, \mathbf{r}_{A2}, \sigma_2)]_0^0 = \sum_{nm} a_{nm} [\varphi_{n, l_i, j_i}^{A+2}(\mathbf{r}_{A1}, \sigma_1) \varphi_{m, l_i, j_i}^{A+2}(\mathbf{r}_{A2}, \sigma_2)]_0^0, \quad (5.1.2)$$

---

section associated with the two-nucleon transfer transitions between the ground state of superfluid nuclei is proportional to  $\alpha_0^2$  and not to  $\Delta^2$ . In fact, Cooper pairs partners remain correlated even over regions in which  $G = 0$ .

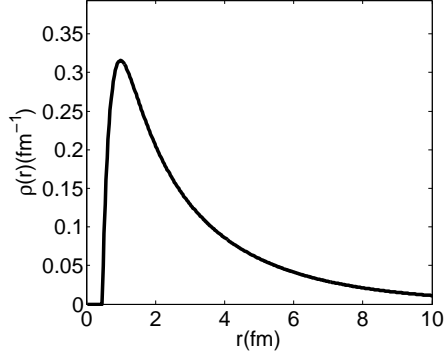


Figure 5.1.1: Radial function  $\rho(r)$  (hard core 0.45 fm) entering the tritium wavefunction (cf. Tang and Herndon (1965)).

while the wavefunctions  $\varphi_{n,l_i,j_i}^{A+2}(\mathbf{r})$  are eigenfunctions of a Saxon–Woods potential

$$U(r) = -\frac{V_0}{1 + \exp\left[\frac{r-R_0}{a}\right]}, \quad R_0 = r_0 A^{1/3}, \quad (5.1.3)$$

of depth  $V_0$  adjusted to reproduce the experimental single-particles energies, together with a standard spin-orbit potential. The radial dependence of the wavefunction of the two neutrons in the triton is written as  $\phi_t(\mathbf{r}_{p1}, \mathbf{r}_{p2}) = \rho(r_{p1})\rho(r_{p2})\rho(r_{12})$ , where  $r_{p1}, r_{p2}, r_{12}$  are the distances between neutron 1 and the proton, neutron 2 and the proton and between neutrons 1 and 2 respectively, while  $\rho(r)$  is the hard core ( $r_{core} = 0.45$  fm) potential wavefunction depicted in Fig 5.1.1.

The two-nucleon transfer differential cross section is written as

$$\frac{d\sigma}{d\Omega} = \frac{\mu_i \mu_f}{(4\pi\hbar^2)^2} \frac{k_f}{k_i} \left| T^{(1)}(\theta) + T_{succ}^{(2)}(\theta) - T_{NO}^{(2)}(\theta) \right|^2, \quad (5.1.4)$$

where (see e.g. Bayman and Chen (1982) and App. 5.H),

$$\begin{aligned} T^{(1)}(\theta) = 2 \sum_{l_i,j_i} \sum_{\sigma_1\sigma_2} \int d\mathbf{r}_{tA} d\mathbf{r}_{p1} d\mathbf{r}_{A2} & [\phi_{l_i,j_i}^{A+2}(\mathbf{r}_{A1}, \sigma_1, \mathbf{r}_{A2}, \sigma_2)]_0^{0*} \chi_{pB}^{(-)*}(\mathbf{r}_{pB}) \\ & \times v(\mathbf{r}_{p1}) \phi_t(\mathbf{r}_{p1}, \mathbf{r}_{p2}) \chi_{tA}^{(+)}(\mathbf{r}_{tA}), \end{aligned} \quad (5.1.5a)$$

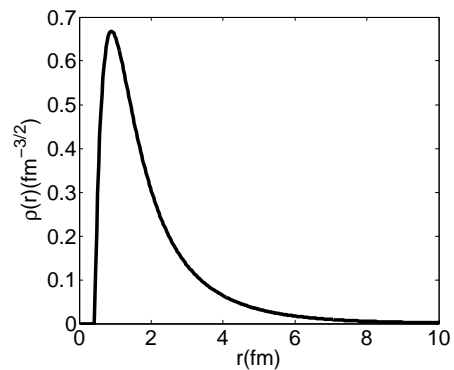


Figure 5.1.2: Radial wavefunction  $\rho_d(r)$  (hard core 0.45 fm) entering the deuteron wavefunction (cf. Tang and Herndon (1965)).

$$\begin{aligned}
T_{succ}^{(2)}(\theta) = & 2 \sum_{l_i, j_i} \sum_{l_f, j_f, m_f} \sum_{\substack{\sigma_1 \sigma_2 \\ \sigma'_1 \sigma'_2}} \int d\mathbf{r}_{dF} d\mathbf{r}_{p1} d\mathbf{r}_{A2} [\phi_{l_i, j_i}^{A+2}(\mathbf{r}_{A1}, \sigma_1, \mathbf{r}_{A2}, \sigma_2)]_0^{0*} \chi_{pB}^{(-)*}(\mathbf{r}_{pB}) v(\mathbf{r}_{p1}) \\
& \times \phi_d(\mathbf{r}_{p1}) \varphi_{l_f, j_f, m_f}^{A+1}(\mathbf{r}_{A2}) \int d\mathbf{r}'_{dF} d\mathbf{r}'_{p1} d\mathbf{r}'_{A2} G(\mathbf{r}_{dF}, \mathbf{r}'_{dF}) \\
& \times \phi_d(\mathbf{r}'_{p1})^* \varphi_{l_f, j_f, m_f}^{A+1*}(\mathbf{r}'_{A2}) \frac{2\mu_{dF}}{\hbar^2} v(\mathbf{r}'_{p2}) \phi_d(\mathbf{r}'_{p1}) \phi_d(\mathbf{r}'_{p2}) \chi_{tA}^{(+)}(\mathbf{r}'_{tA}), \quad (5.1.5b)
\end{aligned}$$

$$\begin{aligned}
T_{NO}^{(2)}(\theta) = & 2 \sum_{l_i, j_i} \sum_{l_f, j_f, m_f} \sum_{\substack{\sigma_1 \sigma_2 \\ \sigma'_1 \sigma'_2}} \int d\mathbf{r}_{dF} d\mathbf{r}_{p1} d\mathbf{r}_{A2} [\phi_{l_i, j_i}^{A+2}(\mathbf{r}_{A1}, \sigma_1, \mathbf{r}_{A2}, \sigma_2)]_0^{0*} \chi_{pB}^{(-)*}(\mathbf{r}_{pB}) v(\mathbf{r}_{p1}) \\
& \times \phi_d(\mathbf{r}_{p1}) \varphi_{l_f, j_f, m_f}^{A+1}(\mathbf{r}_{A2}) \int d\mathbf{r}'_{p1} d\mathbf{r}'_{A2} d\mathbf{r}'_{dF} \\
& \times \phi_d(\mathbf{r}'_{p1})^* \varphi_{l_f, j_f, m_f}^{A+1*}(\mathbf{r}'_{A2}) \phi_d(\mathbf{r}'_{p1}) \phi_d(\mathbf{r}'_{p2}) \chi_{tA}^{(+)}(\mathbf{r}'_{tA}). \quad (5.1.5c)
\end{aligned}$$

The quantities  $\mu_i, \mu_f (k_i, k_f)$  are the reduced masses (relative linear momenta) in both entrance (initial,  $i$ ) and exit (final,  $f$ ) channels, respectively. In the above expressions,  $\varphi_{l_f, j_f, m_f}^{A+1}(\mathbf{r}_{A1})$  are the wavefunctions describing the intermediate states of the nucleus  $F (\equiv (A + 1))$ , generated as solutions of a Woods–Saxon potential,  $\phi_d(\mathbf{r}_{p2})$  being the deuteron bound wavefunction (see Fig. 5.1.2). Note that some or all of the single-particle states described by the wavefunctions  $\varphi_{l_f, j_f, m_f}^{A+1}(\mathbf{r}_{A1})$  may lie in the continuum (case in which the nucleus  $F$  is loosely bound or unbound). Although there are a number of ways to exactly treat such states, discretization processes may be sufficiently accurate. They can be implemented by, for example, embedding the Woods–Saxon potential in a spherical box of sufficiently large radius. In actual calculations involving the halo nucleus  $^{11}\text{Li}$ , and where  $|F\rangle = |^{10}\text{Li}\rangle$ , one achieved convergence making use of approximately 20 continuum states and a box of 30 fm of radius. Concerning the components of the triton wavefunction describing the relative motion of the dineutron, it was generated with the  $p - n$  interaction (Tang and Herndon, 1965)

$$v(r) = -v_0 \exp(-k(r - r_c)) \quad r > r_c \quad (5.1.6)$$

$$v(r) = \infty \quad r < r_c, \quad (5.1.7)$$

where  $k = 2.5 \text{ fm}^{-1}$  and  $r_c = 0.45 \text{ fm}$ , the depth  $v_0$  being adjusted to reproduce the experimental separation energies. The positive-energy wavefunctions  $\chi_{tA}^{(+)}(\mathbf{r}_{tA})$  and  $\chi_{pB}^{(-)}(\mathbf{r}_{pB})$  are the ingoing distorted wave in the initial channel and the outgoing distorted wave in the final channel respectively. They are continuum solutions of the Schrödinger equation associated with the corresponding optical potentials.

The transition potential responsible for the transfer of the pair is, in the *post* representation (cf. Fig. 5.C.1),

$$V_\beta = v_{pB} - U_\beta, \quad (5.1.8)$$

where  $v_{pB}$  is the interaction between the proton and nucleus  $B$ , and  $U_\beta$  is the optical potential in the final channel. We make the assumption that  $v_{pB}$  can be decomposed into a term containing the interaction between  $A$  and  $p$  and the potential describing the interaction between the proton and each of the transferred nucleons, namely

$$v_{pB} = v_{pA} + v_{p1} + v_{p2}, \quad (5.1.9)$$

where  $v_{p1}$  and  $v_{p2}$  is the hard–core potential (5.1.6). The transition potential is

$$V_\beta = v_{pA} + v_{p1} + v_{p2} - U_\beta. \quad (5.1.10)$$

Assuming that  $\langle \beta | v_{pA} | \alpha \rangle \approx \langle \beta | U_\beta | \alpha \rangle$  (i.e, assuming that the matrix element of the core–core interaction between the initial and final states is very similar to the matrix element of the real part of the optical potential), one obtains the final expression of the transfer potential in the *post* representation, namely,

$$V_\beta \simeq v_{p1} + v_{p2} = v(\mathbf{r}_{p1}) + v(\mathbf{r}_{p2}). \quad (5.1.11)$$

We make the further approximation of using the same interaction potential in all the (i.e. initial, intermediate and final) channels.

The extension to a heavy-ion reaction  $A + a (\equiv b+2) \longrightarrow B (\equiv A+2) + b$  imply no essential modifications in the formalism. The deuteron and triton wavefunctions appearing in Eqs. (5.1.5a), (5.1.5b) and (5.1.5c) are to be substituted with the corresponding wavefunctions  $\Psi_{b+2}(\xi_b, \mathbf{r}_{b1}, \sigma_1, \mathbf{r}_{b2}, \sigma_2)$ , constructed in a similar way as those appearing in (5.1.1 and 5.1.2). The interaction potential used in Eqs. (5.1.5a), (5.1.5b) and (5.1.5c) will now be the Saxon–Woods used to define the initial (final) state in the post (prior) representation, instead of the proton–neutron interaction (5.1.6).

The Green’s function  $G(\mathbf{r}_{dF}, \mathbf{r}'_{dF})$  appearing in (5.1.5b) propagates the intermediate channel  $d, F$ . It can be expanded in partial waves as,

$$G(\mathbf{r}_{dF}, \mathbf{r}'_{dF}) = i \sum_l \sqrt{2l+1} \frac{f_l(k_{dF}, r_<) g_l(k_{dF}, r_>)}{k_{dF} r_{dF} r'_{dF}} \left[ Y^l(\hat{r}_{dF}) Y^l(\hat{r}'_{dF}) \right]_0^0. \quad (5.1.12)$$

The  $f_l(k_{dF}, r)$  and  $g_l(k_{dF}, r)$  are the regular and the irregular solutions of a Schrödinger equation for a suitable optical potential and an energy equal to the kinetic energy of the intermediate state. In most cases of interest, the result is hardly altered if we use the same energy of relative motion for all the intermediate states. This representative energy is calculated when both intermediate nuclei are in their corresponding ground states. It is of notice that the validity of this approximation can break down in some particular cases. If, for example, some relevant intermediate state become off shell, its contribution is significantly quenched. An interesting situation can arise when this happens to all possible intermediate states, so they can only be virtually populated.

## 5.2 Detailed derivation of second order DWBA

### 5.2.1 Simultaneous transfer: distorted waves

For a  $(t, p)$  reaction, the triton is represented by an incoming distorted wave. We make the assumption that the two neutrons are in an  $S = L = 0$  state, and that the relative motion of the proton with respect to the dineutron is also  $l = 0$ . Consequently, the total spin of the triton is entirely due to the spin of the proton. We will explicitly treat it, as we will consider a spin-orbit term in the optical potential acting between the triton and the target. In what follows we will use the notation of Bayman (1971) (cf. also App. 5.H).

Following (5.E.1), we can write the triton distorted wave as

$$\psi_{m_t}^{(+)}(\mathbf{R}, \mathbf{k}_i, \sigma_p) = \sum_{l_t} \exp(i\sigma_{l_t}^t) g_{l_t j_t} Y_0^{l_t}(\hat{\mathbf{R}}) \frac{\sqrt{4\pi(2l_t + 1)}}{k_i R} \chi_{m_t}(\sigma_p), \quad (5.2.1)$$

where use was made of  $Y_0^{l_t}(\hat{\mathbf{k}}_i) = i^{l_t} \sqrt{\frac{2l_t + 1}{4\pi}} \delta_{m_t, 0}$ , in keeping with the fact that  $\mathbf{k}_i$  is oriented along the  $z$ -axis. Note the phase difference with eq. (7) of Bayman (1971), due to the use of time-reversal rather than Condon–Shortley phase convention. Making use of the relation

$$Y_0^{l_t}(\hat{\mathbf{R}}) \chi_{m_t}(\sigma_p) = \sum_{j_t} \langle l_t 0 1/2 m_t | j_t m_t \rangle [Y^{l_t}(\hat{\mathbf{R}}) \chi(\sigma_p)]_{m_t}^{j_t}, \quad (5.2.2)$$

we have

$$\begin{aligned} \psi_{m_t}^{(+)}(\mathbf{R}, \mathbf{k}_i, \sigma_p) &= \sum_{l_t, j_t} \exp(i\sigma_{l_t}^t) \frac{\sqrt{4\pi(2l_t + 1)}}{k_i R} g_{l_t j_t}(R) \\ &\times \langle l_t 0 1/2 m_t | j_t m_t \rangle [Y^{l_t}(\hat{\mathbf{R}}) \chi(\sigma_p)]_{m_t}^{j_t}. \end{aligned} \quad (5.2.3)$$

We now turn our attention to the outgoing proton distorted wave, which, following (5.E.3) can be written as

$$\psi_{m_p}^{(-)}(\zeta, \mathbf{k}_f, \sigma_p) = \sum_{l_p j_p} \frac{4\pi}{k_f \zeta} i^{l_p} \exp(-i\sigma_{l_p}^p) f_{l_p j_p}^*(\zeta) \sum_m Y_m^{l_p}(\hat{\zeta}) Y_m^{l_p*}(\hat{\mathbf{k}}_f) \chi_{m_p}(\sigma_p). \quad (5.2.4)$$

Making use of the relation

$$\begin{aligned} \sum_m Y_m^{l_p}(\hat{\zeta}) Y_m^{l_p*}(\hat{\mathbf{k}}_f) \chi_{m_p}(\sigma_p) &= \sum_{m, j_p} Y_m^{l_p*}(\hat{\mathbf{k}}_f) \langle l_p m 1/2 m_p | j_p m + m_p \rangle \\ &\times [Y^{l_p}(\hat{\zeta}) \chi_{m_p}(\sigma_p)]_{m+m_p}^{j_p} \\ &= \sum_{m, j_p} Y_{m-m_p}^{l_p*}(\hat{\mathbf{k}}_f) \langle l_p m - m_p 1/2 m_p | j_p m \rangle [Y^{l_p}(\hat{\zeta}) \chi_{m_p}(\sigma_p)]_m^{j_p}, \end{aligned} \quad (5.2.5)$$

one obtains

$$\begin{aligned} \psi_{m_p}^{(-)}(\zeta, \mathbf{k}_f, \sigma_p) &= \frac{4\pi}{k_f \zeta} \sum_{l_p j_p, m} i^{l_p} \exp\left(-i\sigma_{l_p}^p\right) f_{l_p j_p}^*(\zeta) Y_{m-m_p}^{l_p*}(\hat{\mathbf{k}}_f) \\ &\quad \times \langle l_p \ m - m_p \ 1/2 \ m_p | j_p \ m \rangle [Y^{l_p}(\hat{\zeta}) \chi(\sigma_p)]_m^{j_p}. \end{aligned} \quad (5.2.6)$$

### 5.2.2 matrix element for the transition amplitude

We now turn our attention to the evaluation of

$$\begin{aligned} \langle \Psi_f^{(-)}(\mathbf{k}_f) | V(r_{1p}) | \Psi_i^{(+)}(k_i, \hat{\mathbf{z}}) \rangle &= \frac{(4\pi)^{3/2}}{k_i k_f} \sum_{l_p l_t j_p j_t, m} ((\lambda \frac{1}{2})_k (\lambda \frac{1}{2})_k | (\lambda \lambda)_0 (\frac{1}{2} \frac{1}{2})_0)_0 \sqrt{2l_t + 1} \\ &\quad \times \langle l_p \ m - m_p \ 1/2 \ m_p | j_p \ m \rangle \langle l_t \ 0 \ 1/2 \ m_t | j_t \ m_t \rangle i^{-l_p} \exp[i(\sigma_{l_p}^p + \sigma_{l_t}^t)] \\ &\quad \times 2Y_{m-m_p}^{l_p}(\hat{\mathbf{k}}_f) \sum_{\sigma_1 \sigma_2 \sigma_p} \int \frac{d\zeta d\mathbf{r} d\boldsymbol{\eta}}{\zeta R} u_{\lambda k}(r_1) u_{\lambda k}(r_2) [Y^\lambda(\hat{\mathbf{r}}_1) Y^\lambda(\hat{\mathbf{r}}_2)]_0^{0*} \\ &\quad \times f_{l_p j_p}(\zeta) g_{l_t j_t}(R) [\chi(\sigma_1) \chi(\sigma_2)]_0^{0*} [Y^{l_p}(\hat{\zeta}) \chi(\sigma_p)]_m^{j_p*} V(r_{1p}) \\ &\quad \times \theta_0^0(\mathbf{r}, \mathbf{s}) [\chi(\sigma_1) \chi(\sigma_2)]_0^0 [Y^{l_t}(\hat{\mathbf{R}}) \chi(\sigma_p)]_{m_t}^{j_t}, \end{aligned} \quad (5.2.7)$$

where

$$\begin{aligned} \mathbf{r} &= \mathbf{r}_2 - \mathbf{r}_1, \\ \mathbf{s} &= \frac{1}{2} (\mathbf{r}_1 + \mathbf{r}_2) - \mathbf{r}_p, \\ \boldsymbol{\eta} &= \frac{1}{2} (\mathbf{r}_1 + \mathbf{r}_2), \\ \zeta &= \mathbf{r}_p - \frac{\mathbf{r}_1 + \mathbf{r}_2}{A+2}. \end{aligned} \quad (5.2.8)$$

The sum over  $\sigma_1, \sigma_2$  in (5.2.7) is found to be equal to 1. We will now simplify the term  $[Y^{l_p}(\hat{\zeta}) \chi(\sigma_p)]_m^{j_p*} [Y^{l_t}(\hat{\mathbf{R}}) \chi(\sigma_p)]_{m_t}^{j_t}$ , noting that, (5.D.13)

$$[Y^{l_p}(\hat{\zeta}) \chi(\sigma_p)]_m^{j_p*} = (-1)^{1/2 - \sigma_p + j_p - m} [Y^{l_p}(\hat{\zeta}) \chi(-\sigma_p)]_{-m}^{j_p}. \quad (5.2.9)$$

and that

$$\begin{aligned} [Y^{l_p}(\hat{\zeta}) \chi(-\sigma_p)]_{-m}^{j_p} [Y^{l_t}(\hat{\mathbf{R}}) \chi(\sigma_p)]_{m_t}^{j_t} &= \sum_{JM} \langle j_p \ -m \ j_t \ m_t | J \ M \rangle \\ &\quad \times \left\{ [Y^{l_p}(\hat{\zeta}) \chi(-\sigma_p)]_{-m}^{j_p} [Y^{l_t}(\hat{\mathbf{R}}) \chi(\sigma_p)]_{m_t}^{j_t} \right\}_M^J \end{aligned} \quad (5.2.10)$$

The only term which does not vanish after the integration is performed is the one in which the angular and spin functions are coupled to  $L = 0, S = 0, J = 0$ .

Thus,

$$\begin{aligned} \langle j_p - m | j_t | 0 \rangle & \left\{ \left[ Y^{l_p}(\hat{\zeta}) \chi(-\sigma_p) \right]^{j_p} \left[ Y^{l_t}(\hat{\mathbf{R}}) \chi(\sigma_p) \right]^{j_t} \right\}_0^0 \delta_{l_p l_t} \delta_{j_p j_t} \delta_{m m_t} \\ & = \frac{(-1)^{j_p + m_t}}{\sqrt{2j_p + 1}} \left\{ \left[ Y^{l_p}(\hat{\zeta}) \chi(-\sigma_p) \right]^{j_p} \left[ Y^{l_t}(\hat{\mathbf{R}}) \chi(\sigma_p) \right]^{j_t} \right\}_0^0 \delta_{l_p l_t} \delta_{j_p j_t} \delta_{m m_t}. \end{aligned} \quad (5.2.11)$$

Coupling separately the spin and angular functions, one obtains

$$\begin{aligned} & \left\{ \left[ Y^l(\hat{\zeta}) \chi(-\sigma_p) \right]^j \left[ Y^l(\hat{\mathbf{R}}) \chi(\sigma_p) \right]^j \right\}_0^0 \\ & = ((l \frac{1}{2})_j (l \frac{1}{2})_j | (ll)_0 (\frac{1}{2} \frac{1}{2})_0)_0 \left[ \chi(-\sigma_p) \chi(\sigma_p) \right]_0^0 \left[ Y^l(\hat{\zeta}) Y^l(\hat{\mathbf{R}}) \right]_0^0. \end{aligned} \quad (5.2.12)$$

We substitute (5.2.9), (5.2.30), (5.2.31) in (5.2.7) to obtain

$$\begin{aligned} \langle \Psi_f^{(-)}(\mathbf{k}_f) | V(r_{1p}) | \Psi_i^{(+)}(k_i, \hat{\mathbf{z}}) \rangle & = -\frac{(4\pi)^{3/2}}{k_i k_f} \sum_{lj} ((\lambda \frac{1}{2})_k (\lambda \frac{1}{2})_k | (\lambda \lambda)_0 (\frac{1}{2} \frac{1}{2})_0)_0 \sqrt{\frac{2l+1}{2j+1}} \\ & \times \langle l | m_t - m_p | 1/2 | m_p | j | m_t \rangle \langle l | 0 | 1/2 | m_t | j | m_t \rangle i^{-l} \exp[i(\sigma_l^p + \sigma_l^t)] \\ & \times 2Y_{m_t - m_p}^l(\hat{\mathbf{k}}_f) \int \frac{d\zeta d\mathbf{r} d\boldsymbol{\eta}}{\zeta R} u_{\lambda k}(r_1) u_{\lambda k}(r_2) \left[ Y^\lambda(\hat{\mathbf{r}}_1) Y^\lambda(\hat{\mathbf{r}}_2) \right]_0^{0*} \\ & \times f_{lj}(\zeta) g_{lj}(R) \left[ Y^l(\hat{\zeta}) Y^l(\hat{\mathbf{R}}) \right]_0^0 V(r_{1p}) \theta_0^0(\mathbf{r}, \mathbf{s}) \\ & \times ((l \frac{1}{2})_j (l \frac{1}{2})_j | (ll)_0 (\frac{1}{2} \frac{1}{2})_0)_0 \sum_{\sigma_p} (-1)^{1/2 - \sigma_p} \left[ \chi(-\sigma_p) \chi(\sigma_p) \right]_0^0. \end{aligned} \quad (5.2.13)$$

The last sum over  $\sigma_p$  leads to

$$\begin{aligned} \sum_{\sigma_p} (-1)^{1/2 - \sigma_p} \left[ \chi(-\sigma_p) \chi(\sigma_p) \right]_0^0 & = \sum_{\sigma_p m} (-1)^{1/2 - \sigma_p} \langle 1/2 | m | 1/2 | -m | 0 \rangle \\ & \times \chi_m(-\sigma_p) \chi_{-m}(\sigma_p) \\ & = \frac{1}{\sqrt{2}} \sum_{\sigma_p m} (-1)^{1/2 - \sigma_p} (-1)^{1/2 - m} \delta_{m, -\sigma_p} \delta_{-m, \sigma_p} = -\sqrt{2}. \end{aligned} \quad (5.2.14)$$

The 9j-symbols can be evaluated to find

$$\begin{aligned} ((\lambda \frac{1}{2})_k (\lambda \frac{1}{2})_k | (\lambda \lambda)_0 (\frac{1}{2} \frac{1}{2})_0)_0 & = \sqrt{\frac{2k+1}{2(2\lambda+1)}} \\ ((l \frac{1}{2})_j (l \frac{1}{2})_j | (ll)_0 (\frac{1}{2} \frac{1}{2})_0)_0 & = \sqrt{\frac{2j+1}{2(2l+1)}}, \end{aligned} \quad (5.2.15)$$

and consequently,

$$\begin{aligned} \langle \Psi_f^{(-)}(\mathbf{k}_f) | V(r_{1p}) | \Psi_i^{(+)}(k_i, \hat{\mathbf{z}}) \rangle &= \frac{(4\pi)^{3/2}}{k_i k_f} \sum_{lj} \sqrt{\frac{2k+1}{2\lambda+1}} \\ &\times \langle l m_t - m_p 1/2 m_p | j m_t \rangle \langle l 0 1/2 m_t | j m_t \rangle i^{-l} \exp[i(\sigma_l^p + \sigma_l^t)] \quad (5.2.16) \\ &\times \sqrt{2} Y_{m_t - m_p}^l(\hat{\mathbf{k}}_f) \int \frac{d\zeta d\mathbf{r} d\boldsymbol{\eta}}{\zeta R} u_{\lambda k}(r_1) u_{\lambda k}(r_2) [Y^\lambda(\hat{\mathbf{r}}_1) Y^\lambda(\hat{\mathbf{r}}_2)]_0^{0*} \\ &\times f_{lj}(\zeta) g_{lj}(R) [Y^l(\hat{\zeta}) Y^l(\hat{\mathbf{R}})]_0^0 V(r_{1p}) \theta_0^0(\mathbf{r}, \mathbf{s}). \end{aligned}$$

The values of the Clebsh–Gordan coefficients are, for  $j = l - 1/2$ ,

$$\begin{aligned} \langle l m_t - m_p 1/2 m_p | l - 1/2 m_t \rangle \langle l 0 1/2 m_t | l - 1/2 m_t \rangle \\ = \begin{cases} \frac{l}{2l+1} & \text{if } m_t = m_p \\ -\frac{\sqrt{l(l+1)}}{2l+1} & \text{if } m_t = -m_p \end{cases} \quad (5.2.17) \end{aligned}$$

and, for  $j = l + 1/2$ :

$$\begin{aligned} \langle l m_t - m_p 1/2 m_p | l + 1/2 m_t \rangle \langle l 0 1/2 m_t | l + 1/2 m_t \rangle \\ = \begin{cases} \frac{l+1}{2l+1} & \text{if } m_t = m_p \\ \frac{\sqrt{l(l+1)}}{2l+1} & \text{if } m_t = -m_p \end{cases} \quad (5.2.18) \end{aligned}$$

One thus can write,

$$\begin{aligned} \langle \Psi_f^{(-)}(\mathbf{k}_f) | V(r_{1p}) | \Psi_i^{(+)}(k_i, \hat{\mathbf{z}}) \rangle &= \frac{(4\pi)^{3/2}}{k_i k_f} \sum_l \frac{1}{(2l+1)} \sqrt{\frac{(2k+1)}{(2\lambda+1)}} \exp[i(\sigma_l^p + \sigma_l^t)] i^{-l} \\ &\times \sqrt{2} Y_{m_t - m_p}^l(\hat{\mathbf{k}}_f) \int \frac{d\zeta d\mathbf{r} d\boldsymbol{\eta}}{\zeta R} u_{\lambda k}(r_1) u_{\lambda k}(r_2) [Y^\lambda(\hat{\mathbf{r}}_1) Y^\lambda(\hat{\mathbf{r}}_2)]_0^{0*} \\ &\times V(r_{1p}) \theta_0^0(\mathbf{r}, \mathbf{s}) [Y^l(\hat{\zeta}) Y^l(\hat{\mathbf{R}})]_0^0 \\ &\times \left[ (f_{ll+1/2}(\zeta) g_{ll+1/2}(R)(l+1) + f_{ll-1/2}(\zeta) g_{ll-1/2}(R)l) \delta_{m_p, m_t} \right. \\ &\left. + (f_{ll+1/2}(\zeta) g_{ll+1/2}(R) \sqrt{l(l+1)} - f_{ll-1/2}(\zeta) g_{ll-1/2}(R) \sqrt{l(l+1)}) \delta_{m_p, -m_t} \right]. \quad (5.2.19) \end{aligned}$$

We can further simplify this expression using

$$\begin{aligned}
 [Y^\lambda(\hat{\mathbf{r}}_1)Y^\lambda(\hat{\mathbf{r}}_2)]_0^{0*} &= [Y^\lambda(\hat{\mathbf{r}}_1)Y^\lambda(\hat{\mathbf{r}}_2)]_0^0 = \sum_m \langle \lambda m \lambda - m | 0 0 \rangle Y_m^\lambda(\hat{\mathbf{r}}_1)Y_{-m}^\lambda(\hat{\mathbf{r}}_2) \\
 &= \sum_m (-1)^{\lambda-m} \langle \lambda m \lambda - m | 0 0 \rangle Y_m^\lambda(\hat{\mathbf{r}}_1)Y_m^{\lambda*}(\hat{\mathbf{r}}_2) \\
 &= \frac{1}{\sqrt{2\lambda+1}} \sum_m Y_m^\lambda(\hat{\mathbf{r}}_1)Y_m^{\lambda*}(\hat{\mathbf{r}}_2) \\
 &= \frac{\sqrt{(2\lambda+1)}}{4\pi} P_\lambda(\cos \theta_{12}).
 \end{aligned} \tag{5.2.20}$$

Note that when using Condon–Shortley phases this last expression is to be multiplied by  $(-1)^\lambda$ , and that

$$\begin{aligned}
 [Y^l(\hat{\boldsymbol{\zeta}})Y^l(\hat{\mathbf{R}})]_0^0 &= \sum_m \langle l m l - m | 0 0 \rangle Y_m^l(\hat{\boldsymbol{\zeta}})Y_{-m}^l(\hat{\mathbf{R}}) \\
 &= \frac{1}{\sqrt{(2l+1)}} \sum_m (-1)^{l+m} Y_m^l(\hat{\boldsymbol{\zeta}})Y_{-m}^l(\hat{\mathbf{R}}).
 \end{aligned} \tag{5.2.21}$$

Because the integral of the above expression is independent of  $m$ , one can eliminate the  $m$ -sum and multiply by  $2l+1$  the  $m=0$  term, leading to

$$\begin{aligned}
 [Y^l(\hat{\boldsymbol{\zeta}})Y^l(\hat{\mathbf{R}})]_0^0 &\Rightarrow (-1)^l \sqrt{(2l+1)} Y_0^l(\hat{\boldsymbol{\zeta}})_0 Y^l(\hat{\mathbf{R}}) \\
 &= \sqrt{(2l+1)} Y_0^l(\hat{\boldsymbol{\zeta}}) Y_0^{l*}(\hat{\mathbf{R}}).
 \end{aligned} \tag{5.2.22}$$

We now change the integration variables from  $(\boldsymbol{\zeta}, \mathbf{r}, \boldsymbol{\eta})$  to  $(\mathbf{R}, \alpha, \beta, \gamma, r_{12}, r_{1p}, r_{2p})$ , the quantity

$$\left| \frac{\partial(\mathbf{r}, \boldsymbol{\eta}, \boldsymbol{\zeta})}{\partial(\mathbf{R}, \alpha, \beta, \gamma, r_{12}, r_{1p}, r_{2p})} \right| = r_{12} r_{1p} r_{2p} \sin \beta, \tag{5.2.23}$$

being the Jacobian of the transformation. Finally,

$$\begin{aligned}
 \langle \Psi_f^{(-)}(\mathbf{k}_f) | V(r_{1p}) | \Psi_i^{(+)}(k_i, \hat{\mathbf{z}}) \rangle &= \frac{\sqrt{8\pi}}{k_i k_f} \sum_l \sqrt{\frac{2k+1}{2l+1}} \exp[i(\sigma_l^p + \sigma_l^t)] i^{-l} \\
 &\times Y_{m_t-m_p}^l(\hat{\mathbf{k}}_f) \int d\mathbf{R} Y_0^{l*}(\hat{\mathbf{R}}) \int \frac{d\alpha d\beta d\gamma dr_{12} dr_{1p} dr_{2p} \sin \beta}{\zeta R} Y_0^l(\hat{\boldsymbol{\zeta}}) \\
 &\times u_{\lambda k}(r_1) u_{\lambda k}(r_2) V(r_{1p}) \theta_0^0(\mathbf{r}, \mathbf{s}) P_\lambda(\cos \theta_{12}) r_{12} r_{1p} r_{2p} \\
 &\times \left[ \left( f_{ll+1/2}(\zeta) g_{ll+1/2}(R)(l+1) + f_{ll-1/2}(\zeta) g_{ll-1/2}(R) l \right) \delta_{m_p, m_t} \right. \\
 &\quad \left. + \left( f_{ll+1/2}(\zeta) g_{ll+1/2}(R) \sqrt{l(l+1)} - f_{ll-1/2}(\zeta) g_{ll-1/2}(R) \sqrt{l(l+1)} \right) \delta_{m_p, -m_t} \right].
 \end{aligned} \tag{5.2.24}$$

It is noted that the second integral is a function of solely  $\mathbf{R}$  transforming under rotations as  $Y_0^l(\hat{\mathbf{R}})$ , in keeping with the fact that the full dependence on the orientation

of  $\mathbf{R}$  is contained in the spherical harmonic  $Y_0^l(\hat{\zeta})$ . The second integral can thus be cast into the form

$$\begin{aligned} A(R)Y_0^l(\hat{\mathbf{R}}) &= \int d\alpha d\beta d\gamma dr_{12} dr_{1p} dr_{2p} \sin\beta \\ &\quad \times F(\alpha, \beta, \gamma, r_{12}, r_{1p}, r_{2p}, R_x, R_y, R_z). \end{aligned} \quad (5.2.25)$$

To evaluate  $A(R)$ , we set  $\mathbf{R}$  along the  $z$ -axis

$$\begin{aligned} A(R) &= 2\pi i^{-l} \sqrt{\frac{4\pi}{2l+1}} \int d\beta d\gamma dr_{12} dr_{1p} dr_{2p} \sin\beta \\ &\quad \times F(\alpha, \beta, \gamma, r_{12}, r_{1p}, r_{2p}, 0, 0, R), \end{aligned} \quad (5.2.26)$$

where a factor  $2\pi$  results from the integration over  $\alpha$ , the integrand not depending on  $\alpha$ . Substituting (5.2.25) and (5.2.26) in (5.2.24) and, after integration over the angular variables of  $\mathbf{R}$ , we obtain

$$\begin{aligned} \langle \Psi_f^{(-)}(\mathbf{k}_f) | V(r_{1p}) | \Psi_i^{(+)}(k_i, \hat{\mathbf{z}}) \rangle &= 2 \frac{(2\pi)^{3/2}}{k_i k_f} \sum_l \sqrt{\frac{2k+1}{2l+1}} \exp[i(\sigma_l^p + \sigma_l^t)] i^{-l} \\ &\quad \times Y_{m_t - m_p}^l(\hat{\mathbf{k}}_f) \int dR d\beta d\gamma dr_{12} dr_{1p} dr_{2p} R \sin\beta r_{12} r_{1p} r_{2p} \\ &\quad \times u_{\lambda k}(r_1) u_{\lambda k}(r_2) V(r_{1p}) \theta_0^0(\mathbf{r}, \mathbf{s}) P_\lambda(\cos\theta_{12}) P_l(\cos\theta_\zeta) \\ &\quad \times \left[ (f_{ll+1/2}(\zeta) g_{ll+1/2}(R)(l+1) + f_{ll-1/2}(\zeta) g_{ll-1/2}(R)l) \delta_{m_p, m_t} \right. \\ &\quad \left. + (f_{ll+1/2}(\zeta) g_{ll+1/2}(R) \sqrt{l(l+1)} - f_{ll-1/2}(\zeta) g_{ll-1/2}(R) \sqrt{l(l+1)}) \delta_{m_p, -m_t} \right] / \zeta, \end{aligned} \quad (5.2.27)$$

where use was made of the relation

$$Y_0^l(\hat{\zeta}) = i^l \sqrt{\frac{2l+1}{4\pi}} P_l(\cos\theta_\zeta). \quad (5.2.28)$$

The final expression of the differential cross section involves a sum over the spin orientations:

$$\frac{d\sigma}{d\Omega}(\hat{\mathbf{k}}_f) = \frac{k_f}{k_i} \frac{\mu_i \mu_f}{(2\pi\hbar^2)^2} \frac{1}{2} \sum_{m_p m_t} |\langle \Psi_f^{(-)}(\mathbf{k}_f) | V(r_{1p}) | \Psi_i^{(+)}(k_i, \hat{\mathbf{z}}) \rangle|^2. \quad (5.2.29)$$

When  $m_p = 1/2, m_t = 1/2$  or  $m_p = -1/2, m_t = -1/2$ , the terms proportional to  $\delta_{m_p, m_t}$  including the factor

$$|Y_{m_t - m_p}^l(\hat{\mathbf{k}}_f) \delta_{m_p, m_t}| = |Y_0^l(\hat{\mathbf{k}}_f)| = \left| i^l \sqrt{\frac{2l+1}{4\pi}} P_l^0(\cos\theta) \right|, \quad (5.2.30)$$

in the case in which  $m_p = -1/2, m_t = 1/2$

$$|Y_{m_t - m_p}^l(\hat{\mathbf{k}}_f) \delta_{m_p, -m_t}| = |Y_1^l(\hat{\mathbf{k}}_f)| = \left| i^l \sqrt{\frac{2l+1}{4\pi}} \frac{1}{l(l+1)} P_l^1(\cos\theta) \right|, \quad (5.2.31)$$

and

$$|Y_{m_t-m_p}^l(\hat{\mathbf{k}}_f)\delta_{m_p,-m_t}| = |Y_{-1}^l(\hat{\mathbf{k}}_f)| = |Y_1^l(\hat{\mathbf{k}}_f)| = \left| i^l \sqrt{\frac{2l+1}{4\pi}} \frac{1}{l(l+1)} P_l^1(\cos \theta) \right|, \quad (5.2.32)$$

when  $m_p = 1/2, m_t = -1/2$ . Taking the squared modulus of (5.2.27), the sum over  $m_t$  and  $m_p$  yields a factor 2 multiplying each one of the 2 different terms of the sum ( $m_t = m_p$  and  $m_t = -m_p$ ). This is equivalent to multiply each amplitude by  $\sqrt{2}$ , so the final constant that multiply the amplitudes is

$$\frac{8\pi^{3/2}}{k_i k_f}. \quad (5.2.33)$$

Now, for the triton wavefunction we use

$$\theta_0^0(\mathbf{r}, \mathbf{s}) = \rho(r_{1p})\rho(r_{2p})\rho(r_{12}), \quad (5.2.34)$$

$\rho(r)$  being a Tang–Herndon (1965) wave function also used by Bayman (1971). We obtain

$$\frac{d\sigma}{d\Omega}(\hat{\mathbf{k}}_f) = \frac{1}{2E_i^{3/2} E_f^{1/2}} \sqrt{\frac{\mu_f}{\mu_i}} (|I_{\lambda k}^{(0)}(\theta)|^2 + |I_{\lambda k}^{(1)}(\theta)|^2), \quad (5.2.35)$$

where

$$\begin{aligned} I_{\lambda k}^{(0)}(\theta) &= \sum_l P_l^0(\cos \theta) \sqrt{2k+1} \exp[i(\sigma_l^p + \sigma_l^t)] \\ &\times \int dR d\beta d\gamma dr_{12} dr_{1p} dr_{2p} R \sin \beta \rho(r_{1p})\rho(r_{2p})\rho(r_{12}) \\ &\times u_{\lambda k}(r_1)u_{\lambda k}(r_2)V(r_{1p})P_\lambda(\cos \theta_{12})P_l(\cos \theta_\zeta)r_{12}r_{1p}r_{2p} \\ &\times (f_{ll+1/2}(\zeta)g_{ll+1/2}(R)(l+1) + f_{ll-1/2}(\zeta)g_{ll-1/2}(R)l)/\zeta, \end{aligned} \quad (5.2.36)$$

and

$$\begin{aligned} I_{\lambda k}^{(1)}(\theta) &= \sum_l P_l^1(\cos \theta) \sqrt{2k+1} \exp[i(\sigma_l^p + \sigma_l^t)] \\ &\times \int dR d\beta d\gamma dr_{12} dr_{1p} dr_{2p} R \sin \beta \rho(r_{1p})\rho(r_{2p})\rho(r_{12}) \\ &\times u_{\lambda k}(r_1)u_{\lambda k}(r_2)V(r_{1p})P_\lambda(\cos \theta_{12})P_l(\cos \theta_\zeta)r_{12}r_{1p}r_{2p} \\ &\times (f_{ll+1/2}(\zeta)g_{ll+1/2}(R) - f_{ll-1/2}(\zeta)g_{ll-1/2}(R))/\zeta. \end{aligned} \quad (5.2.37)$$

Note that the absence of the  $(-1)^l$  factor with respect to what is found in Bayman (1971), is due to the use of time-reversed phases instead of Condon–Shortley phasing. This is compensated in the total result by a similar difference in the expression of the spectroscopic amplitudes. This ensures that, in either case, the contribution of all the single particle transitions tend to have the same phase for superfluid nuclei, adding coherently to enhance the transfer cross section.

### Heavy-ion Reactions

In dealing with a heavy ion reaction,  $\theta_0^0(\mathbf{r}, \mathbf{s})$  are be the spatial part of the wavefunction

$$\begin{aligned}\Psi(\mathbf{r}_{b1}, \mathbf{r}_{b2}, \sigma_1, \sigma_2) &= [\psi^{j_i}(\mathbf{r}_{b1}, \sigma_1)\psi^{j_i}(\mathbf{r}_{b2}, \sigma_2)]_0^0 \\ &= \theta_0^0(\mathbf{r}, \mathbf{s})[\chi(\sigma_1)\chi(\sigma_2)]_0^0,\end{aligned}\quad (5.2.38)$$

where  $\mathbf{r}_{b1}, \mathbf{r}_{b2}$  are the positions of the two neutrons with respect to the  $b$  core. It can be shown to be

$$\theta_0^0(\mathbf{r}, \mathbf{s}) = \frac{u_{l_i j_i}(r_{b1})u_{l_i j_i}(r_{b2})}{4\pi} \sqrt{\frac{2j_i + 1}{2}} P_{l_i}(\cos \theta_i), \quad (5.2.39)$$

where  $\theta_i$  is the angle between  $\mathbf{r}_{b1}$  and  $\mathbf{r}_{b2}$ . Neglecting the spin-orbit term in the optical potential, as is usually done for heavy ion reactions, one obtains

$$\frac{d\sigma}{d\Omega}(\hat{\mathbf{k}}_f) = \frac{\mu_f \mu_i}{16\pi^2 \hbar^4 k_i^3 k_f} |T^{(1)}(\theta)|^2, \quad (5.2.40)$$

where

$$\begin{aligned}T^{(1)}(\theta) &= \sum_l (2l + 1) P_l(\cos \theta) \sqrt{(2j_i + 1)(2j_f + 1)} \exp[i(\sigma_l^p + \sigma_l^t)] \\ &\times \int dR d\beta d\gamma dr_{12} dr_{b1} dr_{b2} R \sin \beta u_{l_i j_i}(r_{b1})u_{l_i j_i}(r_{b2}) \\ &\times u_{l_f j_f}(r_{A1})u_{l_f j_f}(r_{A2}) V(r_{b1}) P_\lambda(\cos \theta_{12}) P_l(\cos \theta_\zeta) \\ &\times r_{12} r_{b1} r_{b2} P_{l_i}(\cos \theta_i) \frac{f_l(\zeta) g_l(R)}{\zeta},\end{aligned}\quad (5.2.41)$$

obtained by using Eq. (5.2.39) in Eq. (5.2.7) instead of (5.2.34),  $\mathbf{r}_{A1}, \mathbf{r}_{A2}$  being the coordinates of the two transferred neutrons with respect to the  $A$  core.

For control, in what follows we work out the same transition amplitude but starting from the distorted waves for a reaction taking place between spinless nuclei, namely

$$\psi^{(+)}(\mathbf{r}_{Aa}, \mathbf{k}_{Aa}) = \sum_l \exp(i\sigma_l^i) g_l Y_0^l(\hat{\mathbf{r}}_{aA}) \frac{\sqrt{4\pi(2l+1)}}{k_{aA} r_{aA}}, \quad (5.2.42)$$

and

$$\psi^{(-)}(\mathbf{r}_{bB}, \mathbf{k}_{bB}) = \frac{4\pi}{k_{bB} r_{bB}} \sum_{\tilde{l}} i^{\tilde{l}} \exp(-i\sigma_{\tilde{l}}^f) f_{\tilde{l}}^*(r_{bB}) \sum_m Y_m^{\tilde{l}*}(\hat{\mathbf{k}}_{bB}) Y_m^{\tilde{l}}(\hat{\mathbf{r}}_{bB}). \quad (5.2.43)$$

One can then write,

$$\begin{aligned}
T_{2N}^{1step} = \langle \Psi_f^{(-)}(\mathbf{k}_{bB}) | V(r_{1p}) | \Psi_i^{(+)}(k_{aA}, \hat{\mathbf{z}}) \rangle &= \frac{(4\pi)^{3/2}}{k_{aA} k_{bB}} \sum_{\tilde{l}\tilde{m}} ((l_f \frac{1}{2})_{j_f} (l_f \frac{1}{2})_{j_f} | (l_f l_f)_0 (\frac{1}{2} \frac{1}{2})_0)_0 \\
&\times ((l_i \frac{1}{2})_{j_i} (l_i \frac{1}{2})_{j_i} | (l_i l_i)_0 (\frac{1}{2} \frac{1}{2})_0)_0 \sqrt{2l+1} i^{-l_p} \exp[i(\sigma_{\tilde{l}}^f + \sigma_l^i)] \\
&\times 2Y_m^{\tilde{l}}(\hat{\mathbf{k}}_{bB}) \sum_{\sigma_1 \sigma_2} \int \frac{d\mathbf{r}_{bB} d\mathbf{r} d\boldsymbol{\eta}}{r_{bB} r_{aA}} u_{l_f j_f}(r_{A1}) u_{l_f j_f}(r_{A2}) u_{l_i j_i}(r_{b1}) u_{l_i j_i}(r_{b2}) \\
&\times [Y^{l_f}(\hat{\mathbf{r}}_{A1}) Y^{l_f}(\hat{\mathbf{r}}_{A2})]_0^{0*} [Y^{l_i}(\hat{\mathbf{r}}_{b1}) Y^{l_i}(\hat{\mathbf{r}}_{b2})]_0^0 \\
&\times f_{\tilde{l}}(r_{bB}) g_l(r_{aA}) [\chi(\sigma_1) \chi(\sigma_2)]_0^{0*} Y_m^{\tilde{l}*}(\hat{\mathbf{r}}_{bB}) V(r_{1p}) \\
&\times [\chi(\sigma_1) \chi(\sigma_2)]_0^0 Y_0^l(\hat{\mathbf{r}}_{aA}),
\end{aligned} \tag{5.2.44}$$

which, after a number of simplifications becomes

$$\begin{aligned}
\langle \Psi_f^{(-)}(\mathbf{k}_{bB}) | V(r_{1p}) | \Psi_i^{(+)}(k_{aA}, \hat{\mathbf{z}}) \rangle &= \frac{(4\pi)^{3/2}}{k_{aA} k_{bB}} \sum_{\tilde{l}\tilde{m}} \sqrt{\frac{(2j_f+1)(2j_i+1)}{(2l_f+1)(2l_i+1)}} \\
&\times \sqrt{2l+1} i^{-\tilde{l}} \exp[i(\sigma_{\tilde{l}}^f + \sigma_l^i)] \\
&\times Y_m^{\tilde{l}}(\hat{\mathbf{k}}_{bB}) \int \frac{d\mathbf{r}_{bB} d\mathbf{r} d\boldsymbol{\eta}}{r_{bB} r_{aA}} u_{l_f j_f}(r_{A1}) u_{l_f j_f}(r_{A2}) u_{l_i j_i}(r_{b1}) u_{l_i j_i}(r_{b2}) \\
&\times [Y^{l_f}(\hat{\mathbf{r}}_{A1}) Y^{l_f}(\hat{\mathbf{r}}_{A2})]_0^{0*} [Y^{l_i}(\hat{\mathbf{r}}_{b1}) Y^{l_i}(\hat{\mathbf{r}}_{b2})]_0^0 \\
&\times f_{\tilde{l}}(r_{bB}) g_l(r_{aA}) Y_m^{\tilde{l}*}(\hat{\mathbf{r}}_{bB}) V(r_{1p}) Y_0^l(\hat{\mathbf{r}}_{aA}),
\end{aligned} \tag{5.2.45}$$

where  $l = \tilde{l}$  and  $m = 0$ . Making use of Legendre polynomials leads to,

$$\begin{aligned}
\langle \Psi_f^{(-)}(\mathbf{k}_{bB}) | V(r_{1p}) | \Psi_i^{(+)}(k_{aA}, \hat{\mathbf{z}}) \rangle &= \frac{(4\pi)^{-1/2}}{k_{aA} k_{bB}} \sum_l \sqrt{(2j_f+1)(2j_i+1)} \\
&\times \sqrt{2l+1} i^{-l} \exp[i(\sigma_l^f + \sigma_l^i)] Y_0^l(\hat{\mathbf{k}}_{bB}) \\
&\times \int \frac{d\mathbf{r}_{bB} d\mathbf{r} d\boldsymbol{\eta}}{r_{bB} r_{aA}} u_{l_f j_f}(r_{A1}) u_{l_f j_f}(r_{A2}) u_{l_i j_i}(r_{b1}) u_{l_i j_i}(r_{b2}) \\
&\times P_{l_f}(\cos \theta_A) P_{l_i}(\cos \theta_b) \\
&\times f_l(r_{bB}) g_l(r_{aA}) Y_0^{l*}(\hat{\mathbf{r}}_{bB}) V(r_{1p}) Y_0^l(\hat{\mathbf{r}}_{aA}).
\end{aligned} \tag{5.2.46}$$

Changing the integration variables and proceeding as in last section, (implying the

multiplicative factor  $2\pi \sqrt{\frac{4\pi}{2l+1}}$ , the above expression becomes

$$\begin{aligned} \langle \Psi_f^{(-)}(\mathbf{k}_{bB}) | V(r_{1p}) | \Psi_i^{(+)}(k_{aA}, \hat{\mathbf{z}}) \rangle &= \frac{2\pi}{k_{aA} k_{bB}} \sum_l \sqrt{(2j_f + 1)(2j_i + 1)} \\ &\times i^{-l} \exp[i(\sigma_l^f + \sigma_l^i)] Y_0^l(\hat{\mathbf{k}}_{bB}) \\ &\times \int dr_{aA} d\beta d\gamma dr_{12} dr_{b1} dr_{b2} r_{aA} \sin\beta r_{12} r_{b1} r_{b2} \\ &\times P_{l_f}(\cos\theta_A) P_{l_i}(\cos\theta_b) u_{l_f j_f}(r_{A1}) u_{l_f j_f}(r_{A2}) u_{l_i j_i}(r_{b1}) u_{l_i j_i}(r_{b2}) \\ &\times f_l(r_{bB}) g_l(r_{aA}) Y_0^{l*}(\hat{\mathbf{r}}_{bB}) V(r_{1p}) / r_{bB}, \end{aligned} \quad (5.2.47)$$

which eventually can be recasted, through the use of Legendre polynomials, in the expression,

$$\begin{aligned} T_{2N}^{1step} = \langle \Psi_f^{(-)}(\mathbf{k}_{bB}) | V(r_{1p}) | \Psi_i^{(+)}(k_{aA}, \hat{\mathbf{z}}) \rangle &= \frac{1}{2k_{aA} k_{bB}} \sum_l \sqrt{(2j_f + 1)(2j_i + 1)} \\ &\times i^{-l} \exp[i(\sigma_l^f + \sigma_l^i)] P_l(\cos\theta) (2l + 1) \\ &\times \int dr_{aA} d\beta d\gamma dr_{12} dr_{b1} dr_{b2} r_{aA} \sin\beta r_{12} r_{b1} r_{b2} \\ &\times P_{l_f}(\cos\theta_A) P_{l_i}(\cos\theta_b) u_{l_f j_f}(r_{A1}) u_{l_f j_f}(r_{A2}) V(r_{1p}) \\ &\times u_{l_i j_i}(r_{b1}) u_{l_i j_i}(r_{b2}) f_l(r_{bB}) g_l(r_{aA}) P_l(\cos\theta_{if}) / r_{bB}, \end{aligned} \quad (5.2.48)$$

expression which gives the same results as (5.2.41)

### 5.2.3 Coordinates for the calculation of simultaneous transfer

In what follows we explicit the coordinates used in the calculation of the above equations. Making use of the notation of Bayman (1971), we find the expression of the variables appearing in the integral as functions of the integration variables  $r_{1p}, r_{2p}, r_{12}, R, \beta, \gamma$  (remember that  $\mathbf{R} = R \hat{\mathbf{z}}$ , see last section).  $\mathbf{R}$  being the center of mass coordinate. Thus, one can write

$$\mathbf{R} = \frac{1}{3} (\mathbf{r}_1 + \mathbf{r}_2 + \mathbf{r}_p) = \frac{1}{3} (\mathbf{R} + \mathbf{d}_1 + \mathbf{R} + \mathbf{d}_2 + \mathbf{R} + \mathbf{d}_p), \quad (5.2.49)$$

so

$$\mathbf{d}_1 + \mathbf{d}_2 + \mathbf{d}_p = 0. \quad (5.2.50)$$

Together with

$$\mathbf{d}_1 + \mathbf{r}_{12} = \mathbf{d}_2 \quad \mathbf{d}_2 + \mathbf{r}_{2p} = \mathbf{d}_p, \quad (5.2.51)$$

we find

$$\mathbf{d}_1 = \frac{1}{3} (2\mathbf{r}_{12} + \mathbf{r}_{2p}), \quad (5.2.52)$$

and

$$d_1^2 = \frac{1}{9} (4r_{12}^2 + r_{2p}^2 + 4\mathbf{r}_{12}\mathbf{r}_{2p}). \quad (5.2.53)$$

Making use of

$$\begin{aligned} \mathbf{r}_{12} + \mathbf{r}_{2p} &= \mathbf{r}_{1p} \\ r_{1p}^2 &= r_{12}^2 + r_{2p}^2 + 2\mathbf{r}_{12}\mathbf{r}_{2p} \\ 2\mathbf{r}_{12}\mathbf{r}_{2p} &= r_{1p}^2 - r_{12}^2 - r_{2p}^2. \end{aligned} \quad (5.2.54)$$

one obtains

$$d_1 = \frac{1}{3} \sqrt{2r_{12}^2 + 2r_{1p}^2 - r_{2p}^2}. \quad (5.2.55)$$

Similarly,

$$d_2 = \frac{1}{3} \sqrt{2r_{12}^2 + 2r_{2p}^2 - r_{1p}^2} \quad d_p = \frac{1}{3} \sqrt{2r_{2p}^2 + 2r_{1p}^2 - r_{12}^2}. \quad (5.2.56)$$

We now express the angle  $\alpha$  between  $\mathbf{d}_1$  and  $\mathbf{r}_{12}$ . We have

$$-\mathbf{d}_1 \mathbf{r}_{12} = r_{12} d_1 \cos(\alpha), \quad (5.2.57)$$

and

$$\begin{aligned} \mathbf{d}_1 + \mathbf{r}_{12} &= \mathbf{d}_2 \\ d_1^2 + r_{12}^2 + 2\mathbf{d}_1\mathbf{r}_{12} &= d_2^2. \end{aligned} \quad (5.2.58)$$

Consequently,

$$\cos(\alpha) = \frac{d_1^2 + r_{12}^2 - d_2^2}{2r_{12}d_1}. \quad (5.2.59)$$

The complete determination of  $\mathbf{r}_1$ ,  $\mathbf{r}_2$ ,  $\mathbf{r}_{12}$  can be made by writing their expression in a simple configuration, in which the triangle lies in the  $xz$ -plane with  $\mathbf{d}_1$  pointing along the positive  $z$ -direction, and  $\mathbf{R} = 0$ . Then, a first rotation  $\mathcal{R}_z(\gamma)$  of an angle  $\gamma$  around the  $z$ -axis, a second rotation  $\mathcal{R}_y(\beta)$  of an angle  $\beta$  around the  $y$ -axis, and a translation along  $\mathbf{R}$  will bring the vectors to the most general configuration. In other words,

$$\begin{aligned} \mathbf{r}_1 &= \mathbf{R} + \mathcal{R}_y(\beta)\mathcal{R}_z(\gamma)\mathbf{r}'_1, \\ \mathbf{r}_{12} &= \mathcal{R}_y(\beta)\mathcal{R}_z(\gamma)\mathbf{r}'_{12}, \\ \mathbf{r}_2 &= \mathbf{r}_1 + \mathbf{r}_{12}, \end{aligned} \quad (5.2.60)$$

with

$$\mathbf{r}'_1 = \begin{bmatrix} 0 \\ 0 \\ d_1 \end{bmatrix}, \quad (5.2.61)$$

$$\mathbf{r}'_{12} = r_{12} \begin{bmatrix} \sin(\alpha) \\ 0 \\ -\cos(\alpha) \end{bmatrix}, \quad (5.2.62)$$

and the rotation matrixes are

$$\mathcal{R}_y(\beta) = \begin{bmatrix} \cos(\beta) & 0 & \sin(\beta) \\ 0 & 1 & 0 \\ -\sin(\beta) & 0 & \cos(\beta) \end{bmatrix}, \quad (5.2.63)$$

and

$$\mathcal{R}_z(\gamma) = \begin{bmatrix} \cos(\gamma) & -\sin(\gamma) & 0 \\ \sin(\gamma) & \cos(\gamma) & 0 \\ 0 & 0 & 1 \end{bmatrix}. \quad (5.2.64)$$

then

$$\mathbf{r}_1 = \begin{bmatrix} d_1 \sin(\beta) \\ 0 \\ R + d_1 \cos(\beta) \end{bmatrix}, \quad (5.2.65)$$

$$\mathbf{r}_{12} = \begin{bmatrix} r_{12} \cos(\beta) \cos(\gamma) \sin(\alpha) - r_{12} \sin(\beta) \cos(\alpha) \\ r_{12} \sin(\gamma) \sin(\alpha) \\ -r_{12} \sin(\beta) \cos(\gamma) \sin(\alpha) - r_{12} \cos(\alpha) \cos(\beta) \end{bmatrix}, \quad (5.2.66)$$

$$\mathbf{r}_2 = \begin{bmatrix} d_1 \sin(\beta) + r_{12} \cos(\beta) \cos(\gamma) \sin(\alpha) - r_{12} \sin(\beta) \cos(\alpha) \\ r_{12} \sin(\gamma) \sin(\alpha) \\ R + d_1 \cos(\beta) - r_{12} \sin(\beta) \cos(\gamma) \sin(\alpha) - r_{12} \cos(\alpha) \cos(\beta) \end{bmatrix}. \quad (5.2.67)$$

We also need  $\cos(\theta_{12})$ ,  $\zeta$  and  $\cos(\theta_\zeta)$ ,  $\theta_{12}$  being the angle between  $\mathbf{r}_1$  and  $\mathbf{r}_2$ ,  $\zeta = \mathbf{r}_p - \frac{\mathbf{r}_1 + \mathbf{r}_2}{A+2}$  the position of the proton with respect to the final nucleus, and  $\theta_\zeta$  the angle between  $\zeta$  and the  $z$ -axis:

$$\cos(\theta_{12}) = \frac{\mathbf{r}_1 \cdot \mathbf{r}_2}{r_1 r_2}, \quad (5.2.68)$$

and

$$\zeta = 3\mathbf{R} - \frac{A+3}{A+2}(\mathbf{r}_1 + \mathbf{r}_2), \quad (5.2.69)$$

where we have used (5.2.49).

For heavy ions, we find instead

$$\mathbf{R} = \frac{1}{m_a} (\mathbf{r}_{A1} + \mathbf{r}_{A2} + m_b \mathbf{r}_{Ab}), \quad (5.2.70)$$

$$\mathbf{d}_1 = \frac{1}{m_a} (m_b \mathbf{r}_{b2} - (m_b + 1) \mathbf{r}_{12}), \quad (5.2.71)$$

$$d_1 = \frac{1}{m_a} \sqrt{(m_b + 1)r_{12}^2 + m_b(m_b + 1)r_{b1}^2 - m_b r_{b2}^2}, \quad (5.2.72)$$

$$d_2 = \frac{1}{m_a} \sqrt{(m_b + 1)r_{12}^2 + m_b(m_b + 1)r_{b2}^2 - m_b r_{b1}^2}, \quad (5.2.73)$$

and

$$\zeta = \frac{m_a}{m_b} \mathbf{R} - \frac{m_B + m_b}{m_b m_B} (\mathbf{r}_{A1} + \mathbf{r}_{A2}). \quad (5.2.74)$$

The rest of the formulae are identical to the  $(t, p)$  ones. We list them for convenience,

$$\mathbf{r}_{A1} = \begin{bmatrix} d_1 \sin(\beta) \\ 0 \\ R + d_1 \cos(\beta) \end{bmatrix}, \quad (5.2.75)$$

$$\mathbf{r}_{A2} = \begin{bmatrix} d_1 \sin(\beta) + r_{12} \cos(\beta) \cos(\gamma) \sin(\alpha) - r_{12} \sin(\beta) \cos(\alpha) \\ r_{12} \sin(\gamma) \sin(\alpha) \\ R + d_1 \cos(\beta) - r_{12} \sin(\beta) \cos(\gamma) \sin(\alpha) - r_{12} \cos(\alpha) \cos(\beta) \end{bmatrix}. \quad (5.2.76)$$

We we also find

$$\mathbf{r}_{b1} = \frac{1}{m_b} (\mathbf{r}_{A2} + (m_b + 1)\mathbf{r}_{A1} - m_a \mathbf{R}), \quad (5.2.77)$$

and

$$\mathbf{r}_{b2} = \frac{1}{m_b} (\mathbf{r}_{A1} + (m_b + 1)\mathbf{r}_{A2} - m_a \mathbf{R}). \quad (5.2.78)$$

One can readily obtain

$$\cos \theta_{12} = \frac{r_{A1}^2 + r_{A2}^2 - r_{12}^2}{2r_{A1}r_{A2}}, \quad (5.2.79)$$

and

$$\cos \theta_i = \frac{r_{b1}^2 + r_{b2}^2 - r_{12}^2}{2r_{b1}r_{b2}}. \quad (5.2.80)$$

#### 5.2.4 Matrix element for the transition amplitude (alternative derivation)

In what follows we work out an alternative derivation of  $T_{2N}^{1\text{step}}$ , more closely related to heavy ion reactions. Following Bayman and Chen (1982) it can be written as

$$\begin{aligned} T^{(1)}(\theta) = & 2 \frac{(4\pi)^{3/2}}{k_{Aa} k_{Bb}} \sum_{l_p j_p m_l j_p} i^{-l_p} \exp[i(\sigma_{l_p}^p + \sigma_{l_t}^t)] \sqrt{2l_t + 1} \\ & \times \langle l_p m - m_p 1/2 m_p | j_p m \rangle \langle l_t 0 1/2 m_t | j_t m_t \rangle Y_{m-m_p}^{l_p}(\hat{\mathbf{k}}_{Bb}) \\ & \times \sum_{\sigma_1 \sigma_2 \sigma_p} \int d\mathbf{r}_{Cc} d\mathbf{r}_{b1} d\mathbf{r}_{A2} [\psi^{j_f}(\mathbf{r}_{A1}, \sigma_1) \psi^{j_f}(\mathbf{r}_{A2}, \sigma_2)]_0^{0*} \\ & \times v(r_{b1}) [\psi^{j_i}(\mathbf{r}_{b1}, \sigma_1) \psi^{j_i}(\mathbf{r}_{b2}, \sigma_2)]_0^0 \frac{g_{l_t j_t}(r_{Aa}) f_{l_p j_p}(r_{Bb})}{r_{Aa} r_{Bb}} \\ & \times [Y^{l_t}(\hat{\mathbf{r}}_{Aa}) \chi(\sigma_p)]_{m_t}^{j_t} [Y^{l_p}(\hat{\mathbf{r}}_{Bb}) \chi(\sigma_p)]_m^{j_p*}. \end{aligned} \quad (5.2.81)$$

As shown above one can write,

$$\begin{aligned} \sum_{\sigma_p} \langle l_p m - m_p 1/2 m_p | j_p m \rangle \langle l_t 0 1/2 m_t | j_t m_t \rangle & \left[ Y^{l_t}(\hat{\mathbf{r}}_{Aa}) \chi(\sigma_p) \right]_{m_t}^{j_t} \left[ Y^{l_p}(\hat{\mathbf{r}}_{Bb}) \chi(\sigma_p) \right]_m^{j_p*} \\ &= -\frac{\delta_{l_p, l_t} \delta_{j_p, j_t} \delta_{m, m_t}}{\sqrt{2l+1}} \left[ Y^l(\hat{\mathbf{r}}_{Aa}) Y^l(\hat{\mathbf{r}}_{Bb}) \right]_0^0 \begin{cases} \frac{l}{2l+1} & \text{if } m_t = m_p \\ -\frac{\sqrt{l(l+1)}}{2l+1} & \text{if } m_t = -m_p \end{cases} \end{aligned} \quad (5.2.82)$$

when  $j = l - 1/2$  and

$$\begin{aligned} \sum_{\sigma_p} \langle l_p m - m_p 1/2 m_p | j_p m \rangle \langle l_t 0 1/2 m_t | j_t m_t \rangle & \left[ Y^{l_t}(\hat{\mathbf{r}}_{Aa}) \chi(\sigma_p) \right]_{m_t}^{j_t} \left[ Y^{l_p}(\hat{\mathbf{r}}_{Bb}) \chi(\sigma_p) \right]_m^{j_p*} \\ &= -\frac{\delta_{l_p, l_t} \delta_{j_p, j_t} \delta_{m, m_t}}{\sqrt{2l+1}} \left[ Y^l(\hat{\mathbf{r}}_{Aa}) Y^l(\hat{\mathbf{r}}_{Bb}) \right]_0^0 \begin{cases} \frac{l+1}{2l+1} & \text{if } m_t = m_p \\ \frac{\sqrt{l(l+1)}}{2l+1} & \text{if } m_t = -m_p \end{cases} \end{aligned} \quad (5.2.83)$$

if  $j = l + 1/2$ . One then gets

$$\begin{aligned} T^{(1)}(\mu = 0; \theta) &= 2 \frac{(4\pi)^{3/2}}{k_{Aa} k_{Bb}} \sum_l i^{-l} \frac{\exp[i(\sigma_l^p + \sigma_l^t)]}{2l+1} Y_{m_t - m_p}^l(\hat{\mathbf{k}}_{Bb}) \\ &\times \sum_{\sigma_1 \sigma_2} \int \frac{d\mathbf{r}_{Ccd} d\mathbf{r}_{b1} d\mathbf{r}_{A2}}{r_{Aa} r_{Bb}} \left[ \psi^{j_f}(\mathbf{r}_{A1}, \sigma_1) \psi^{j_f}(\mathbf{r}_{A2}, \sigma_2) \right]_0^{0*} \\ &\times v(r_{b1}) \left[ \psi^{j_i}(\mathbf{r}_{b1}, \sigma_1) \psi^{j_i}(\mathbf{r}_{b2}, \sigma_2) \right]_0^0 \left[ Y^l(\hat{\mathbf{r}}_{Aa}) Y^l(\hat{\mathbf{r}}_{Bb}) \right]_0^0 \\ &\times \left[ (f_{ll+1/2}(r_{Bb}) g_{ll+1/2}(r_{Aa})(l+1) + f_{ll-1/2}(r_{Bb}) g_{ll-1/2}(r_{Aa})l) \delta_{m_p, m_t} \right. \\ &\left. + (f_{ll+1/2}(r_{Bb}) g_{ll+1/2}(r_{Aa}) \sqrt{l(l+1)} - f_{ll-1/2}(r_{Bb}) g_{ll-1/2}(r_{Aa}) \sqrt{l(l+1)}) \delta_{m_p, -m_t} \right]. \end{aligned} \quad (5.2.84)$$

Making use of the relations,

$$\begin{aligned} & \left[ \psi^{j_f}(\mathbf{r}_{A1}, \sigma_1) \psi^{j_f}(\mathbf{r}_{A2}, \sigma_2) \right]_0^{0*} \\ &= ((l_f \frac{1}{2})_{j_f} (l_f \frac{1}{2})_{j_f} | (l_f l_f)_0 (\frac{1}{2} \frac{1}{2})_0)_0 u_{l_f}(r_{A1}) u_{l_f}(r_{A2}) \\ &\times \left[ Y^{l_f}(\hat{\mathbf{r}}_{A1}) Y^{l_f}(\hat{\mathbf{r}}_{A2}) \right]_0^{0*} [\chi(\sigma_1) \chi(\sigma_2)]_0^{0*} \\ &= \sqrt{\frac{2j_f + 1}{2(2l_f + 1)}} u_{l_f}(r_{A1}) u_{l_f}(r_{A2}) \\ &\times \left[ Y^{l_f}(\hat{\mathbf{r}}_{A1}) Y^{l_f}(\hat{\mathbf{r}}_{A2}) \right]_0^{0*} [\chi(\sigma_1) \chi(\sigma_2)]_0^{0*} \\ &= \sqrt{\frac{2j_f + 1}{2}} \frac{u_{l_f}(r_{A1}) u_{l_f}(r_{A2})}{4\pi} P_{l_f}(\cos \omega_A) [\chi(\sigma_1) \chi(\sigma_2)]_0^{0*}, \end{aligned} \quad (5.2.85)$$

and

$$\begin{aligned}
& \left[ \psi^{j_i}(\mathbf{r}_{b1}, \sigma_1) \psi^{j_i}(\mathbf{r}_{b2}, \sigma_2) \right]_0^0 \\
&= ((l_i \frac{1}{2})_{j_i} (l_i \frac{1}{2})_{j_i} | (l_i l_i)_0 (\frac{1}{2} \frac{1}{2})_0)_0 u_{l_i}(r_{b1}) u_{l_i}(r_{b2}) \\
&\quad \times \left[ Y^{l_i}(\hat{\mathbf{r}}_{b1}) Y^{l_i}(\hat{\mathbf{r}}_{b2}) \right]_0^0 [\chi(\sigma_1) \chi(\sigma_2)]_0^0 \\
&= \sqrt{\frac{2j_i + 1}{2(2l_i + 1)}} u_{l_i}(r_{b1}) u_{l_i}(r_{b2}) \\
&\quad \times \left[ Y^{l_i}(\hat{\mathbf{r}}_{b1}) Y^{l_i}(\hat{\mathbf{r}}_{b2}) \right]_0^0 [\chi(\sigma_1) \chi(\sigma_2)]_0^0 \\
&= \sqrt{\frac{2j_i + 1}{2}} \frac{u_{l_i}(r_{b1}) u_{l_i}(r_{b2})}{4\pi} P_{l_i}(\cos \omega_b) [\chi(\sigma_1) \chi(\sigma_2)]_0^0,
\end{aligned} \tag{5.2.86}$$

where  $\omega_A$  is the angle between  $\mathbf{r}_{A1}$  and  $\mathbf{r}_{A2}$ , and  $\omega_b$  is the angle between  $\mathbf{r}_{b1}$  and  $\mathbf{r}_{b2}$ . Consequently

$$\begin{aligned}
T^{(1)}(\theta) &= (4\pi)^{-3/2} \frac{\sqrt{(2j_i + 1)(2j_f + 1)}}{k_{Aa} k_{Bb}} \sum_l i^{-l} \frac{\exp[i(\sigma_l^p + \sigma_l^t)]}{\sqrt{2l + 1}} Y_{m_t - m_p}^l(\hat{\mathbf{k}}_{Bb}) \\
&\quad \times \int \frac{d\mathbf{r}_{Cc} d\mathbf{r}_{b1} d\mathbf{r}_{A2}}{r_{Aa} r_{Bb}} P_{l_f}(\cos \omega_A) P_{l_i}(\cos \omega_b) P_l(\cos \omega_{if}) \\
&\quad \times v(r_{b1}) u_{l_i}(r_{b1}) u_{l_i}(r_{b2}) u_{l_f}(r_{A1}) u_{l_f}(r_{A2}) \\
&\quad \times \left[ (f_{ll+1/2}(r_{Bb}) g_{ll+1/2}(r_{Aa})(l+1) + f_{ll-1/2}(r_{Bb}) g_{ll-1/2}(r_{Aa})l) \delta_{m_p, m_t} \right. \\
&\quad \left. + (f_{ll+1/2}(r_{Bb}) g_{ll+1/2}(r_{Aa}) \sqrt{l(l+1)} - f_{ll-1/2}(r_{Bb}) g_{ll-1/2}(r_{Aa}) \sqrt{l(l+1)}) \delta_{m_p, -m_t} \right],
\end{aligned} \tag{5.2.87}$$

where  $\omega_{if}$  is the angle between  $\mathbf{r}_{Aa}$  and  $\mathbf{r}_{Bb}$ . For heavy ions, we can consider that the optical potential does not have a spin-orbit term, and the distorted waves are independent of  $j$ . We thus have

$$\begin{aligned}
T^{(1)}(\theta) &= (4\pi)^{-3/2} \frac{\sqrt{(2j_i + 1)(2j_f + 1)}}{k_{Aa} k_{Bb}} \sum_l i^{-l} \exp[i(\sigma_l^p + \sigma_l^t)] Y_0^l(\hat{\mathbf{k}}_{Bb}) \sqrt{2l + 1} \\
&\quad \times \int \frac{d\mathbf{r}_{Cc} d\mathbf{r}_{b1} d\mathbf{r}_{A2}}{r_{Aa} r_{Bb}} P_{l_f}(\cos \omega_A) P_{l_i}(\cos \omega_b) P_l(\cos \omega_{if}) \\
&\quad \times v(r_{b1}) u_{l_i}(r_{b1}) u_{l_i}(r_{b2}) u_{l_f}(r_{A1}) u_{l_f}(r_{A2}) f_l(r_{Bb}) g_l(r_{Aa}).
\end{aligned} \tag{5.2.88}$$

Changing variables one obtains,

$$\begin{aligned}
 T^{(1)}(\theta) = & (4\pi)^{-1} \frac{\sqrt{(2j_i+1)(2j_f+1)}}{k_{Aa}k_{Bb}} \sum_l \exp[i(\sigma_l^p + \sigma_l')] P_l(\cos \theta) (2l+1) \\
 & \times \int dr_{1A} dr_{2A} dr_{Aa} d(\cos \beta) d(\cos \omega_A) d\gamma r_{1A}^2 r_{2A}^2 r_{Aa}^2 \\
 & \times P_{l_f}(\cos \omega_A) P_{l_i}(\cos \omega_b) P_l(\cos \omega_{if}) v(r_{b1}) \\
 & \times u_{l_i}(r_{b1}) u_{l_i}(r_{b2}) u_{l_f}(r_{A1}) u_{l_f}(r_{A2}) f_l(r_{Bb}) g_l(r_{Aa}).
 \end{aligned} \tag{5.2.89}$$

### 5.2.5 Coordinates used to derive Eq. (5.2.89)

We determine the relation between the integration variables in (5.2.87) and the coordinates needed to evaluate the quantities in the integrand. Noting that

$$\mathbf{r}_{Aa} = \frac{\mathbf{r}_{A1} + \mathbf{r}_{A2} + m_b \mathbf{r}_{Ab}}{m_b + 2}, \tag{5.2.90}$$

one has

$$\mathbf{r}_{b1} = \mathbf{r}_{bA} + \mathbf{r}_{A1} = \frac{(m_b + 1)\mathbf{r}_{A1} + \mathbf{r}_{A2} - (m_b + 2)\mathbf{r}_{Aa}}{m_b}, \tag{5.2.91}$$

$$\mathbf{r}_{b2} = \mathbf{r}_{bA} + \mathbf{r}_{A2} = \frac{(m_b + 1)\mathbf{r}_{A2} + \mathbf{r}_{A1} - (m_b + 2)\mathbf{r}_{Aa}}{m_b}, \tag{5.2.92}$$

and

$$\begin{aligned}
 \mathbf{r}_{Cc} = \mathbf{r}_{CA} + \mathbf{r}_{A1} + \mathbf{r}_{1c} &= -\frac{1}{m_A + 1} \mathbf{r}_{A2} + \mathbf{r}_{A1} - \frac{m_b}{m_b + 1} \mathbf{r}_{b1} \\
 &= \frac{m_b + 2}{m_b + 1} \mathbf{r}_{Aa} - \frac{m_b + 2 + m_A}{(m_b + 1)(m_A + 1)} \mathbf{r}_{A2}
 \end{aligned} \tag{5.2.93}$$

Since,

$$\mathbf{r}_{AB} = \frac{\mathbf{r}_{A1} + \mathbf{r}_{A2}}{m_A + 2}, \tag{5.2.94}$$

one obtains

$$\mathbf{r}_{Bb} = \mathbf{r}_{BA} + \mathbf{r}_{Ab} = \frac{m_b + 2}{m_b} \mathbf{r}_{Aa} - \frac{m_A + m_b + 2}{(m_A + 2)m_b} (\mathbf{r}_{A1} + \mathbf{r}_{A2}). \tag{5.2.95}$$

Using the same rotations as those used in Section 5.2.3 one gets,

$$\mathbf{r}_{A1} = r_{A1} \begin{bmatrix} \sin \alpha \\ 0 \\ \cos \alpha \end{bmatrix}, \tag{5.2.96}$$

and

$$\mathbf{r}_{A2} = r_{A2} \begin{bmatrix} -\cos \alpha \cos \gamma \sin \omega_A + \sin \alpha \cos \omega_A \\ -\sin \gamma \sin \omega_A \\ \sin \alpha \cos \gamma \sin \omega_A + \cos \alpha \cos \omega_A \end{bmatrix}, \tag{5.2.97}$$

with

$$\cos \alpha = \frac{r_{A1}^2 - d_1^2 + r_{Aa}^2}{2r_{A1}r_{Aa}}, \quad (5.2.98)$$

and

$$d_1 = \sqrt{r_{A1}^2 - r_{Aa}^2 \sin^2 \beta} - r_{Aa} \cos \beta. \quad (5.2.99)$$

Note that though  $\beta, r_{1A}, r_{Aa}$  are independent integration variables, they have to fulfill the condition

$$r_{Aa} \sin \beta \leq r_{A1}, \quad \text{for } 0 \leq \beta \leq \pi. \quad (5.2.100)$$

The expression of the remaining quantities appearing in the integral are now straightforward,

$$\begin{aligned} r_{b1} &= m_b^{-1} |(m_b + 1)\mathbf{r}_{A1} + \mathbf{r}_{A2} - (m_b + 2)\mathbf{r}_{Aa}| \\ &= m_b^{-1} \left( (m_b + 2)^2 r_{Aa}^2 + (m_b + 1)^2 r_{A1}^2 + r_{A2}^2 \right. \\ &\quad \left. - 2(m_b + 2)(m_b + 1)\mathbf{r}_{Aa} \mathbf{r}_{A1} - 2(m_b + 2)\mathbf{r}_{Aa} \mathbf{r}_{A2} + 2(m_b + 1)\mathbf{r}_{A1} \mathbf{r}_{A2} \right)^{1/2}, \end{aligned} \quad (5.2.101)$$

$$\begin{aligned} r_{b2} &= m_b^{-1} |(m_b + 1)\mathbf{r}_{A2} + \mathbf{r}_{A1} - (m_b + 2)\mathbf{r}_{Aa}| \\ &= m_b^{-1} \left( (m_b + 2)^2 r_{Aa}^2 + (m_b + 1)^2 r_{A2}^2 + r_{A1}^2 \right. \\ &\quad \left. - 2(m_b + 2)(m_b + 1)\mathbf{r}_{Aa} \mathbf{r}_{A2} - 2(m_b + 2)\mathbf{r}_{Aa} \mathbf{r}_{A1} + 2(m_b + 1)\mathbf{r}_{A2} \mathbf{r}_{A1} \right)^{1/2}, \end{aligned} \quad (5.2.102)$$

$$\begin{aligned} r_{Bb} &= \left| \frac{m_b + 2}{m_b} \mathbf{r}_{Aa} - \frac{m_A + m_b + 2}{(m_A + 2)m_b} (\mathbf{r}_{A1} + \mathbf{r}_{A2}) \right| \\ &= \left[ \left( \frac{m_b + 2}{m_b} \right)^2 r_{Aa}^2 + \left( \frac{m_A + m_b + 2}{(m_A + 2)m_b} \right)^2 (r_{A1}^2 + r_{A2}^2 + 2\mathbf{r}_{A1} \mathbf{r}_{A2}) \right. \\ &\quad \left. - 2 \frac{(m_b + 2)(m_A + m_b + 2)}{(m_A + 2)m_b^2} \mathbf{r}_{Aa}(\mathbf{r}_{A1} + \mathbf{r}_{A2}) \right]^{1/2}, \end{aligned} \quad (5.2.103)$$

$$\begin{aligned} r_{Cc} &= \left| \frac{m_b + 2}{m_b + 1} \mathbf{r}_{Aa} - \frac{m_b + 2 + m_A}{(m_b + 1)(m_A + 1)} \mathbf{r}_{A2} \right| \\ &= \left[ \left( \frac{m_a}{(m_a - 1)} \right)^2 r_{Aa}^2 + \left( \frac{m_A + m_a}{(m_A + 1)(m_a - 1)} \right)^2 r_{A2}^2 \right. \\ &\quad \left. - 2 \frac{m_A m_a + m_a^2}{(m_A + 1)(m_a - 1)^2} \mathbf{r}_{Aa} \mathbf{r}_{A2} \right]^{1/2}, \end{aligned} \quad (5.2.104)$$

$$\cos \omega_b = \frac{\mathbf{r}_{b1} \mathbf{r}_{b2}}{r_{b1} r_{b2}}, \quad (5.2.105)$$

$$\cos \omega_{if} = \frac{\mathbf{r}_{Aa} \mathbf{r}_{Bb}}{r_{Aa} r_{Bb}}, \quad (5.2.106)$$

with

$$\mathbf{r}_{Aa}\mathbf{r}_{A1} = r_{Aa}r_{A1} \cos \alpha, \quad (5.2.107)$$

$$\mathbf{r}_{Aa}\mathbf{r}_{A2} = r_{Aa}r_{A2}(\sin \alpha \cos \gamma \sin \omega_A + \cos \alpha \cos \omega_A), \quad (5.2.108)$$

$$\mathbf{r}_{A1}\mathbf{r}_{A2} = r_{A1}r_{A2} \cos \omega_A. \quad (5.2.109)$$

### 5.2.6 Successive transfer

The successive two-neutron transfer amplitudes can be written as (Bayman and Chen (1982)):

$$\begin{aligned} T_{succ}^{(2)}(\theta) = & \frac{4\mu_{Cc}}{\hbar^2} \sum_{\substack{\sigma_1 \sigma_2 \\ \sigma'_1 \sigma'_2 \\ KM}} \int d^3 r_{Cc} d^3 r_{b1} d^3 r_{A2} d^3 r'_{Cc} d^3 r'_{b1} d^3 r'_{A2} \chi^{(-)*}(\mathbf{k}_{Bb}, \mathbf{r}_{Bb}) \\ & \times \left[ \psi^{j_f}(\mathbf{r}_{A1}, \sigma_1) \psi^{j_f}(\mathbf{r}_{A2}, \sigma_2) \right]_0^{0*} v(r_{b1}) \left[ \psi^{j_f}(\mathbf{r}_{A2}, \sigma_2) \psi^{j_i}(\mathbf{r}_{b1}, \sigma_1) \right]_M^K \\ & \times G(\mathbf{r}_{Cc}, \mathbf{r}'_{Cc}) \left[ \psi^{j_f}(\mathbf{r}'_{A2}, \sigma'_2) \psi^{j_i}(\mathbf{r}'_{b1}, \sigma'_1) \right]_M^{K*} v(r'_{c2}) \\ & \times \left[ \psi^{j_i}(\mathbf{r}'_{b1}, \sigma'_1) \psi^{j_i}(\mathbf{r}'_{b2}, \sigma'_2) \right]_0^0 \chi^{(+)}(\mathbf{r}'_{Aa}). \end{aligned} \quad (5.2.110)$$

It is of notice that the time-reversal phase convention is used throughout. Expanding the Green function and the distorted waves in a basis of angular momentum eigenstate one can write,

$$\chi^{(-)*}(\mathbf{k}_{Bb}, \mathbf{r}_{Bb}) = \sum_{\tilde{l}} \frac{4\pi}{k_{Bb}r_{Bb}} i^{-\tilde{l}} e^{i\sigma_f^{\tilde{l}}} F_{\tilde{l}} \sum_m Y_{\tilde{l}}^{\tilde{l}}(\hat{r}_{Bb}) Y_{\tilde{l}}^{\tilde{l}*}(\hat{k}_{Bb}), \quad (5.2.111)$$

the sum over  $m$  being

$$\sum_m (-1)^{\tilde{l}-m} Y_{\tilde{l}}^{\tilde{l}}(\hat{r}_{Bb}) Y_{-m}^{\tilde{l}}(\hat{k}_{Bb}) = \sqrt{2\tilde{l}+1} \left[ Y_{\tilde{l}}^{\tilde{l}}(\hat{r}_{Bb}) Y_{\tilde{l}}^{\tilde{l}}(\hat{k}_{Bb}) \right]_0^0, \quad (5.2.112)$$

where we have used (5.D.2) and (5.D.18), so

$$\chi^{(-)*}(\mathbf{k}_{Bb}, \mathbf{r}_{Bb}) = \sum_{\tilde{l}} \sqrt{2\tilde{l}+1} \frac{4\pi}{k_{Bb}r_{Bb}} i^{-\tilde{l}} e^{i\sigma_f^{\tilde{l}}} F_{\tilde{l}}(r_{Bb}) \left[ Y_{\tilde{l}}^{\tilde{l}}(\hat{r}_{Bb}) Y_{\tilde{l}}^{\tilde{l}}(\hat{k}_{Bb}) \right]_0^0. \quad (5.2.113)$$

Similarly,

$$\chi^{(+)}(\mathbf{r}'_{Aa}) = \sum_l i^l \sqrt{2l+1} \frac{4\pi}{k_{Aa}r'_{Aa}} e^{i\sigma_i^l} F_l(r'_{Aa}) \left[ Y^l(\hat{r}'_{Aa}) Y^l(\hat{k}_{Aa}) \right]_0^0 \quad (5.2.114)$$

where we have taken into account the choice  $\hat{k}_{Aa} \equiv \hat{z}$ . The Green function can be written as

$$G(\mathbf{r}_{Cc}, \mathbf{r}'_{Cc}) = i \sum_{l_c} \sqrt{2l_c + 1} \frac{f_{l_c}(k_{Cc}, r_<) P_{l_c}(k_{Cc}, r_>)}{k_{Cc} r_{Cc} r'_{Cc}} \left[ Y^{l_c}(\hat{r}_{Cc}) Y^{l_c}(\hat{r}'_{Cc}) \right]_0^0. \quad (5.2.115)$$

Finally

$$\begin{aligned} T_{succ}^{(2)}(\theta) &= \frac{4\mu_{Cc}(4\pi)^2 i}{\hbar^2 k_{Aa} k_{Bb} k_{Cc}} \sum_{l, l_c, \tilde{l}} e^{i(\sigma_i^l + \sigma_f^{\tilde{l}})} i^{l-\tilde{l}} \sqrt{(2l+1)(2l_c+1)(2\tilde{l}+1)} \\ &\times \sum_{\substack{\sigma_1 \sigma_2 \\ \sigma'_1 \sigma'_2}} \int d^3 r_{Cc} d^3 r_{b1} d^3 r_{A2} d^3 r'_{Cc} d^3 r'_{b1} d^3 r'_{A2} v(r_{b1}) v(r'_{c2}) \left[ Y^{\tilde{l}}(\hat{r}_{Bb}) Y^{\tilde{l}}(\hat{k}_{Bb}) \right]_0^0 \\ &\times \left[ Y^l(\hat{r}'_{Aa}) Y^l(\hat{k}'_{Aa}) \right]_0^0 \left[ Y^{l_c}(\hat{r}_{Cc}) Y^{l_c}(\hat{r}'_{Cc}) \right]_0^0 \frac{F_l(r_{Bb})}{r_{Bb}} \frac{F_l(r'_{Aa})}{r'_{Aa}} \\ &\times \frac{f_{l_c}(k_{Cc}, r_<) P_{l_c}(k_{Cc}, r_>)}{r_{Cc} r'_{Cc}} \left[ \psi^{j_f}(\mathbf{r}_{A1}, \sigma_1) \psi^{j_f}(\mathbf{r}_{A2}, \sigma_2) \right]_0^{0*} \\ &\times \left[ \psi^{j_i}(\mathbf{r}'_{b1}, \sigma'_1) \psi^{j_i}(\mathbf{r}'_{b2}, \sigma'_2) \right]_0^0 \sum_{KM} \left[ \psi^{j_f}(\mathbf{r}_{A2}, \sigma_2) \psi^{j_i}(\mathbf{r}_{b1}, \sigma_1) \right]_M^K \\ &\times \left[ \psi^{j_f}(\mathbf{r}'_{A2}, \sigma'_2) \psi^{j_i}(\mathbf{r}'_{b1}, \sigma'_1) \right]_M^{K*}. \end{aligned} \quad (5.2.116)$$

Let us now perform the integration over  $\mathbf{r}_{A2}$ ,

$$\begin{aligned} &\sum_{\sigma_1, \sigma_2} \int d\mathbf{r}_{A2} \left[ \psi^{j_f}(\mathbf{r}_{A1}, \sigma_1) \psi^{j_f}(\mathbf{r}_{A2}, \sigma_2) \right]_0^{0*} \left[ \psi^{j_f}(\mathbf{r}_{A2}, \sigma_2) \psi^{j_i}(\mathbf{r}_{b1}, \sigma_1) \right]_M^K \\ &= \sum_{\sigma_1, \sigma_2} (-1)^{1/2-\sigma_1+1/2-\sigma_2} \int d\mathbf{r}_{A2} \left[ \psi^{j_f}(\mathbf{r}_{A1}, -\sigma_1) \psi^{j_f}(\mathbf{r}_{A2}, -\sigma_2) \right]_0^0 \left[ \psi^{j_f}(\mathbf{r}_{A2}, \sigma_2) \psi^{j_i}(\mathbf{r}_{b1}, \sigma_1) \right]_M^K \\ &= - \sum_{\sigma_1, \sigma_2} (-1)^{1/2-\sigma_1+1/2-\sigma_2} \int d\mathbf{r}_{A2} \left[ \psi^{j_f}(\mathbf{r}_{A2}, -\sigma_2) \psi^{j_f}(\mathbf{r}_{A1}, -\sigma_1) \right]_0^0 \left[ \psi^{j_f}(\mathbf{r}_{A2}, \sigma_2) \psi^{j_i}(\mathbf{r}_{b1}, \sigma_1) \right]_M^K \\ &= -((j_f j_f)_0 (j_f j_i)_K |(j_f j_f)_0 (j_f j_i)_K)_K \sum_{\sigma_1, \sigma_2} (-1)^{1/2-\sigma_1+1/2-\sigma_2} \\ &\times \int d\mathbf{r}_{A2} \left[ \psi^{j_f}(\mathbf{r}_{A2}, -\sigma_2) \psi^{j_f}(\mathbf{r}_{A2}, \sigma_2) \right]_0^0 \left[ \psi^{j_f}(\mathbf{r}_{A1}, -\sigma_1) \psi^{j_i}(\mathbf{r}_{b1}, \sigma_1) \right]_M^K \\ &= \frac{1}{2j_f + 1} \sqrt{2j_f + 1} ((l_f \frac{1}{2})_{j_f} (l_i \frac{1}{2})_{j_i} |(l_f l_i)_K (\frac{1}{2} \frac{1}{2})_0)_K \\ &\times u_{l_f}(r_{A1}) u_{l_i}(r_{b1}) \left[ Y^{l_f}(\hat{r}_{A1}) Y^{l_i}(\hat{r}_{b1}) \right]_M^K \sum_{\sigma_1} (-1)^{1/2-\sigma_1} \left[ \chi^{1/2}(-\sigma_1) \chi^{1/2}(\sigma_1) \right]_0^0 \\ &= -\sqrt{\frac{2}{2j_f + 1}} ((l_f \frac{1}{2})_{j_f} (l_i \frac{1}{2})_{j_i} |(l_f l_i)_K (\frac{1}{2} \frac{1}{2})_0)_K \left[ Y^{l_f}(\hat{r}_{A1}) Y^{l_i}(\hat{r}_{b1}) \right]_M^K u_{l_f}(r_{A1}) u_{l_i}(r_{b1}), \end{aligned} \quad (5.2.117)$$

where we have evaluated the 9*j*-symbol

$$((j_f j_f)_0 (j_f j_i)_K | (j_f j_f)_0 (j_f j_i)_K)_K = \frac{1}{2j_f + 1}, \quad (5.2.118)$$

as well as (5.D.19). We proceed in a similar way to evaluate the integral over  $\mathbf{r}'_{b1}$ ,

$$\begin{aligned} & \sum_{\sigma'_1, \sigma'_2} \int d\mathbf{r}'_{b1} [\psi^{j_i}(\mathbf{r}'_{b1}, \sigma'_1) \psi^{j_i}(\mathbf{r}'_{b2}, \sigma'_2)]_0^0 [\psi^{j_f}(\mathbf{r}'_{A2}, \sigma'_2) \psi^{j_i}(\mathbf{r}'_{b1}, \sigma'_1)]_M^{K*} \\ &= -(-1)^{K-M} \sum_{\sigma'_1, \sigma'_2} \int d\mathbf{r}'_{b1} [\psi^{j_f}(\mathbf{r}'_{A2}, -\sigma'_2) \psi^{j_i}(\mathbf{r}'_{b1}, -\sigma'_1)]_{-M}^K \\ & \times [\psi^{j_i}(\mathbf{r}'_{b2}, \sigma'_2) \psi^{j_i}(\mathbf{r}'_{b1}, \sigma'_1)]_0^0 (-1)^{1/2-\sigma'_1+1/2-\sigma'_2} \\ &= -(-1)^{K-M} ((j_f j_i)_K (j_i j_i)_0 | (j_f j_i)_K (j_i j_i)_0)_K (-\sqrt{2j_i + 1}) \\ & \times ((l_f \frac{1}{2})_{j_f} (l_i \frac{1}{2})_{j_i} | (l_f l_i)_K (\frac{1}{2} \frac{1}{2})_0)_K (-\sqrt{2}) u_{l_f}(r'_{A2}) u_{l_i}(r'_{b2}) [Y^{l_f}(\hat{r}'_{A2}) Y^{l_i}(\hat{r}'_{b2})]_{-M}^K \\ &= -\sqrt{\frac{2}{2j_i + 1}} ((l_f \frac{1}{2})_{j_f} (l_i \frac{1}{2})_{j_i} | (l_f l_i)_K (\frac{1}{2} \frac{1}{2})_0)_K [Y^{l_f}(\hat{r}'_{A2}) Y^{l_i}(\hat{r}'_{b2})]_M^{K*} u_{l_f}(r'_{A2}) u_{l_i}(r'_{b2}). \end{aligned} \quad (5.2.119)$$

Setting the different elements together one obtains

$$\begin{aligned} T_{succ}^{(2)}(\theta) &= \frac{4\mu_{Cc}(4\pi)^2 i}{\hbar^2 k_{Aa} k_{Bb} k_{Cc}} \frac{2}{\sqrt{(2j_i + 1)(2j_f + 1)}} \sum_{K,M} ((l_f \frac{1}{2})_{j_f} (l_i \frac{1}{2})_{j_i} | (l_f l_i)_K (\frac{1}{2} \frac{1}{2})_0)_K^2 \\ & \times \sum_{l_c, l_{\tilde{l}}} e^{i(\sigma'_i + \sigma'_{\tilde{l}})} \sqrt{(2l_c + 1)(2l + 1)(2\tilde{l} + 1)} t^{l-\tilde{l}} \\ & \times \int d^3 r_{Cc} d^3 r_{b1} d^3 r'_{Cc} d^3 r'_{A2} v(r_{b1}) v(r'_{c2}) u_{l_f}(r_{A1}) u_{l_i}(r_{b1}) u_{l_f}(r'_{A2}) u_{l_i}(r'_{b2}) \\ & \times [Y^{l_f}(\hat{r}'_{A2}) Y^{l_i}(\hat{r}'_{b2})]_M^{K*} [Y^{l_f}(\hat{r}_{A1}) Y^{l_i}(\hat{r}_{b1})]_M^K \frac{F_l(r'_{Aa}) F_{\tilde{l}}(r'_{Bb}) f_{l_c}(k_{Cc}, r_{<}) P_{l_c}(k_{Cc}, r_{>})}{r'_{Aa} r_{Bb} r_{Cc} r'_{Cc}} \\ & \times [Y^{\tilde{l}}(\hat{r}_{Bb}) Y^{\tilde{l}}(\hat{k}_{Bb})]_0^0 [Y^l(\hat{r}'_{Aa}) Y^l(\hat{k}_{Aa})]_0^0 [Y^{l_c}(\hat{r}_{Cc}) Y^{l_c}(\hat{r}'_{Cc})]_0^0. \end{aligned} \quad (5.2.120)$$

We now proceed to write this expression in a more compact way. For this purpose one writes

$$\begin{aligned} & [Y^{\tilde{l}}(\hat{r}_{Bb}) Y^{\tilde{l}}(\hat{k}_{Bb})]_0^0 [Y^l(\hat{r}'_{Aa}) Y^l(\hat{k}_{Aa})]_0^0 = \\ & ((l l)_0 (\tilde{l} \tilde{l})_0 | (l \tilde{l})_0 (\tilde{l} l)_0)_0 [Y^{\tilde{l}}(\hat{r}_{Bb}) Y^l(\hat{r}'_{Aa})]_0^0 [Y^{\tilde{l}}(\hat{k}_{Bb}) Y^l(\hat{k}_{Aa})]_0^0 \\ & = \frac{\delta_{ll}}{2l + 1} [Y^l(\hat{r}_{Bb}) Y^l(\hat{r}'_{Aa})]_0^0 [Y^l(\hat{k}_{Bb}) Y^l(\hat{k}_{Aa})]_0^0. \end{aligned} \quad (5.2.121)$$

Taking into account the relations

$$\left[ Y^l(\hat{k}_{Bb}) Y^l(\hat{k}_{Aa}) \right]_0^0 = \frac{(-1)^l}{\sqrt{4\pi}} Y_0^l(\hat{k}_{Bb}) i^l, \quad (5.2.122)$$

and

$$\begin{aligned} & \left[ Y^l(\hat{r}_{Bb}) Y^l(\hat{r}'_{Aa}) \right]_0^0 \left[ Y^{l_c}(\hat{r}_{Cc}) Y^{l_c}(\hat{r}'_{Cc}) \right]_0^0 = \\ & ((ll)_0(l_c l_c)_0 | (ll_c)_K (ll_c)_K)_0 \left\{ \left[ Y^l(\hat{r}_{Bb}) Y^{l_c}(\hat{r}_{Cc}) \right]^K \left[ Y^l(\hat{r}'_{Aa}) Y^{l_c}(\hat{r}'_{Cc}) \right]^K \right\}_0^0 \\ & = \sqrt{\frac{2K+1}{(2l+1)(2l_c+1)}} \\ & \times \sum_{M'} \frac{(-1)^{K+M'}}{\sqrt{2K+1}} \left[ Y^l(\hat{r}_{Bb}) Y^{l_c}(\hat{r}_{Cc}) \right]_{-M'}^K \left[ Y^l(\hat{r}'_{Aa}) Y^{l_c}(\hat{r}'_{Cc}) \right]_{M'}^K \\ & = \sqrt{\frac{1}{(2l+1)(2l_c+1)}} \\ & \times \sum_{M'} \left[ Y^l(\hat{r}_{Bb}) Y^{l_c}(\hat{r}_{Cc}) \right]_{M'}^{K*} \left[ Y^l(\hat{r}'_{Aa}) Y^{l_c}(\hat{r}'_{Cc}) \right]_{M'}^K. \end{aligned} \quad (5.2.123)$$

It is of notice that the integrals

$$\int d\hat{r}_{Cc} d\hat{r}_{b1} \left[ Y^l(\hat{r}_{Bb}) Y^{l_c}(\hat{r}_{Cc}) \right]_M^{K*} \left[ Y^{l_f}(\hat{r}_{A1}) Y^{l_i}(\hat{r}_{b1}) \right]_M^K, \quad (5.2.124)$$

and

$$\int d\hat{r}'_{Cc} d\hat{r}'_{A2} \left[ Y^l(\hat{r}'_{Aa}) Y^{l_c}(\hat{r}'_{Cc}) \right]_M^K \left[ Y^{l_f}(\hat{r}'_{A2}) Y^{l_i}(\hat{r}'_{b2}) \right]_M^{K*}, \quad (5.2.125)$$

over the angular variables do not depend on  $M$ . Let us see why this is so with the help of (5.2.124),

$$\begin{aligned} & \left[ Y^l(\hat{r}_{Bb}) Y^{l_c}(\hat{r}_{Cc}) \right]_M^{K*} \left[ Y^{l_f}(\hat{r}_{A1}) Y^{l_i}(\hat{r}_{b1}) \right]_M^K = (-1)^{K-M} \left[ Y^l(\hat{r}_{Bb}) Y^{l_c}(\hat{r}_{Cc}) \right]_{-M}^K \\ & \times \left[ Y^{l_f}(\hat{r}_{A1}) Y^{l_i}(\hat{r}_{b1}) \right]_M^K = (-1)^{K-M} \sum_J \langle K \ K \ M - M | J \ 0 \rangle \\ & \times \left\{ \left[ Y^l(\hat{r}_{Bb}) Y^{l_c}(\hat{r}_{Cc}) \right]^K \left[ Y^{l_f}(\hat{r}_{A1}) Y^{l_i}(\hat{r}_{b1}) \right]^K \right\}_0^J. \end{aligned} \quad (5.2.126)$$

After integration, only the term

$$\begin{aligned} & (-1)^{K-M} \langle K \ K \ M - M | 0 \ 0 \rangle \left\{ \left[ Y^l(\hat{r}_{Bb}) Y^{l_c}(\hat{r}_{Cc}) \right]^K \left[ Y^{l_f}(\hat{r}_{A1}) Y^{l_i}(\hat{r}_{b1}) \right]^K \right\}_0^0 = . \\ & \frac{1}{\sqrt{2K+1}} \left\{ \left[ Y^l(\hat{r}_{Bb}) Y^{l_c}(\hat{r}_{Cc}) \right]^K \left[ Y^{l_f}(\hat{r}_{A1}) Y^{l_i}(\hat{r}_{b1}) \right]^K \right\}_0^0 \end{aligned} \quad (5.2.127)$$

corresponding to  $J = 0$  survives, which is indeed independent of  $M$ . We can thus omit the sum over  $M$  in (5.2.120) and multiply by  $(2K + 1)$ , obtaining

$$\begin{aligned} T_{succ}^{(2)}(\theta) &= \frac{64\mu_{Cc}(\pi)^{3/2}i}{\hbar^2 k_{Aa} k_{Bb} k_{Cc}} \frac{i^{-l}}{\sqrt{(2j_i + 1)(2j_f + 1)}} \\ &\times \sum_K (2K + 1) ((l_f \frac{1}{2})_{jf} (l_i \frac{1}{2})_{ji} | (l_f l_i)_K (\frac{1}{2} \frac{1}{2})_0)_K^2 \\ &\times \sum_{l_c, l} \frac{e^{i(\sigma_i^l + \sigma_f^l)}}{\sqrt{(2l + 1)}} Y_0^l(\hat{k}_{Bb}) S_{K, l, l_c}, \end{aligned} \quad (5.2.128)$$

where

$$\begin{aligned} S_{K, l, l_c} &= \int d^3 r_{Cc} d^3 r_{b1} v(r_{b1}) u_{l_f}(r_{A1}) u_{l_i}(r_{b1}) \frac{s_{K, l, l_c}(r_{Cc})}{r_{Cc}} \frac{F_l(r_{Bb})}{r_{Bb}} \\ &\times [Y^{l_f}(\hat{r}_{A1}) Y^{l_i}(\hat{r}_{b1})]_M^K [Y^{l_c}(\hat{r}_{Cc}) Y^l(\hat{r}_{Bb})]_M^{K*}, \end{aligned} \quad (5.2.129)$$

and

$$\begin{aligned} s_{K, l, l_c}(r_{Cc}) &= \int_{r_{Cc} \text{fixed}} d^3 r'_{Cc} d^3 r'_{A2} v(r'_{c2}) u_{l_f}(r'_{A2}) u_{l_i}(r'_{b2}) \frac{F_l(r'_{Aa})}{r'_{Aa}} \frac{f_l(k_{Cc}, r_{<}) P_{l_c}(k_{Cc}, r_{>})}{r'_{Cc}} \\ &\times [Y^{l_f}(\hat{r}'_{A2}) Y^{l_i}(\hat{r}'_{b2})]_M^{K*} [Y^{l_c}(\hat{r}'_{Cc}) Y^l(\hat{r}'_{Aa})]_M^K. \end{aligned} \quad (5.2.130)$$

It can be shown that the integrand in (5.2.129) is independent of  $M$ . Consequently, one can sum over  $M$  and divide by  $(2K + 1)$ , to get

$$\begin{aligned} \frac{1}{2K + 1} v(r_{b1}) u_{l_f}(r_{A1}) u_{l_i}(r_{b1}) \frac{s_{K, l, l_c}(r_{Cc})}{r_{Cc}} \frac{F_l(r_{Bb})}{r_{Bb}} \\ \times \sum_M [Y^{l_f}(\hat{r}_{A1}) Y^{l_i}(\hat{r}_{b1})]_M^K [Y^{l_c}(\hat{r}_{Cc}) Y^l(\hat{r}_{Bb})]_M^{K*}. \end{aligned} \quad (5.2.131)$$

This integrand is rotationally invariant (it is proportional to a  $T_M^L$  spherical tensor with  $L = 0, M = 0$ ), so one can evaluate it in the “standard” configuration in which  $\mathbf{r}_{Cc}$  is directed along the  $z$ -axis and multiply by  $8\pi^2$  (see Bayman and Chen (1982)), obtaining the final expression for  $S_{K, l, l_c}$ :

$$\begin{aligned} S_{K, l, l_c} &= \frac{4\pi^{3/2} \sqrt{2l_c + 1}}{2K + 1} i^{-l_c} \\ &\times \int r_{Cc}^2 dr_{Cc} r_{b1}^2 dr_{b1} \sin \theta d\theta v(r_{b1}) u_{l_f}(r_{A1}) u_{l_i}(r_{b1}) \\ &\times \frac{s_{K, l, l_c}(r_{Cc})}{r_{Cc}} \frac{F_l(r_{Bb})}{r_{Bb}} \\ &\times \sum_M \langle l_c 0 l M | K M \rangle [Y^{l_f}(\hat{r}_{A1}) Y^{l_i}(\theta + \pi, 0)]_M^K Y_M^{l*}(\hat{r}_{Bb}). \end{aligned} \quad (5.2.132)$$

Similarly, one has

$$\begin{aligned}
 s_{K,l,l_c}(r_{Cc}) &= \frac{4\pi^{3/2} \sqrt{2l_c + 1}}{2K + 1} i^{l_c} \\
 &\times \int r'_{Cc}^2 dr'_{Cc} r'^2_{A2} dr'_{A2} \sin \theta' d\theta' v(r'_{c2}) u_{l_f}(r'_{A2}) u_{l_i}(r'_{b2}) \\
 &\times \frac{F_l(r'_{Aa}) f_{l_c}(k_{Cc}, r_<) P_{l_c}(k_{Cc}, r_>)}{r'_{Aa} r'_{Cc}} \\
 &\times \sum_M \langle l_c 0 l M | K M \rangle [Y^{l_f}(\hat{r}'_{A2}) Y^{l_i}(\hat{r}'_{b2})]_M^{K*} Y_M^l(\hat{r}'_{Aa}). \tag{5.2.133}
 \end{aligned}$$

Introducing the further approximations  $\mathbf{r}_{A1} \approx \mathbf{r}_{C1}$  and  $\mathbf{r}_{b2} \approx \mathbf{r}_{c2}$ , one obtains the final expression

$$\begin{aligned}
 T_{succ}^{(2)}(\theta) &= \frac{1024\mu_{Cc}\pi^{9/2}i}{\hbar^2 k_{Aa} k_{Bb} k_{Cc}} \frac{1}{\sqrt{(2j_i+1)(2j_f+1)}} \\
 &\times \sum_K \frac{1}{2K+1} ((l_f \frac{1}{2})_{j_f} (l_i \frac{1}{2})_{j_i} | (l_f l_i)_K (\frac{1}{2} \frac{1}{2})_0)_K^2 \\
 &\times \sum_{l_c, l} e^{i(\sigma_i^l + \sigma_f^l)} \frac{(2l_c + 1)}{\sqrt{2l + 1}} Y_0^l(\hat{k}_{Bb}) S_{K,l,l_c}, \tag{5.2.134}
 \end{aligned}$$

with

$$\begin{aligned}
 S_{K,l,l_c} &= \int r_{Cc}^2 dr_{Cc} r_{b1}^2 dr_{b1} \sin \theta d\theta v(r_{b1}) u_{l_f}(r_{C1}) u_{l_i}(r_{b1}) \\
 &\times \frac{s_{K,l,l_c}(r_{Cc})}{r_{Cc}} \frac{F_l(r_{Bb})}{r_{Bb}} \\
 &\times \sum_M \langle l_c 0 l M | K M \rangle [Y^{l_f}(\hat{r}_{C1}) Y^{l_i}(\theta + \pi, 0)]_M^K Y_M^{l*}(\hat{r}_{Bb}), \tag{5.2.135}
 \end{aligned}$$

and

$$\begin{aligned}
 s_{K,l,l_c}(r_{Cc}) &= \int r'_{Cc}^2 dr'_{Cc} r'^2_{A2} dr'_{A2} \sin \theta' d\theta' v(r'_{c2}) u_{l_f}(r'_{A2}) u_{l_i}(r'_{c2}) \\
 &\times \frac{F_l(r'_{Aa})}{r'_{Aa}} \frac{f_{l_c}(k_{Cc}, r_<) P_{l_c}(k_{Cc}, r_>)}{r'_{Cc}} \\
 &\times \sum_M \langle l_c 0 l M | K M \rangle [Y^{l_f}(\hat{r}'_{A2}) Y^{l_i}(\hat{r}'_{c2})]_M^{K*} Y_M^l(\hat{r}'_{Aa}). \tag{5.2.136}
 \end{aligned}$$

### 5.2.7 Coordinates for the successive transfer

In the standard configuration in which the integrals (5.2.135) and (5.2.136) are to be evaluated, we have

$$\mathbf{r}_{Cc} = r_{Cc} \hat{\mathbf{z}}, \quad \mathbf{r}_{b1} = r_{b1}(-\cos \theta \hat{\mathbf{z}} - \sin \theta \hat{\mathbf{x}}). \tag{5.2.137}$$

Now,

$$\begin{aligned}\mathbf{r}_{C1} &= \mathbf{r}_{Cc} + \mathbf{r}_{c1} = \mathbf{r}_{Cc} + \frac{m_b}{m_b + 1} \mathbf{r}_{b1} \\ &= \left( r_{Cc} - \frac{m_b}{m_b + 1} r_{b1} \cos \theta \right) \hat{\mathbf{z}} - \frac{m_b}{m_b + 1} r_{b1} \sin \theta \hat{\mathbf{x}},\end{aligned}\quad (5.2.138)$$

and

$$\mathbf{r}_{Bb} = \mathbf{r}_{BC} + \mathbf{r}_{Cb} = -\frac{1}{m_B} \mathbf{r}_{C1} + \mathbf{r}_{Cb}. \quad (5.2.139)$$

Substituting the relation

$$\mathbf{r}_{Cb} = \mathbf{r}_{Cc} + \mathbf{r}_{cb} = \mathbf{r}_{Cc} - \frac{1}{m_b + 1} \mathbf{r}_{b1}, \quad (5.2.140)$$

in (5.2.139) one gets

$$\mathbf{r}_{Bb} = \left( \frac{m_B - 1}{m_B} r_{Cc} + \frac{m_b + m_B}{m_B(m_b + 1)} r_{b1} \cos \theta \right) \hat{\mathbf{z}} + \frac{m_b + m_B}{m_B(m_b + 1)} r_{b1} \sin \theta \hat{\mathbf{x}}. \quad (5.2.141)$$

The primed variables are arranged in a similar fashion,

$$\mathbf{r}'_{Cc} = r'_{Cc} \hat{\mathbf{z}}, \quad \mathbf{r}'_{A2} = r'_{A2} (-\cos \theta' \hat{\mathbf{z}} - \sin \theta' \hat{\mathbf{x}}). \quad (5.2.142)$$

Thus,

$$\mathbf{r}'_{c2} = \left( -r'_{Cc} - \frac{m_A}{m_A + 1} r'_{A2} \cos \theta' \right) \hat{\mathbf{z}} - \frac{m_A}{m_A + 1} r'_{A2} \sin \theta' \hat{\mathbf{x}}, \quad (5.2.143)$$

and

$$\mathbf{r}'_{Aa} = \left( \frac{m_a - 1}{m_a} r'_{Cc} - \frac{m_A + m_a}{m_a(m_A + 1)} r'_{A2} \cos \theta' \right) \hat{\mathbf{z}} - \frac{m_A + m_a}{m_a(m_A + 1)} r'_{A2} \sin \theta' \hat{\mathbf{x}}. \quad (5.2.144)$$

### 5.2.8 Simplifying the vector coupling

We will now turn our attention to the vector-coupled quantities in (5.2.135) and (5.2.136),

$$\sum_M \langle l_c 0 l M | K M \rangle \left[ Y^{l_f}(\hat{r}_{C1}) Y^{l_i}(\theta + \pi, 0) \right]_M^K Y_M^{l_*}(\hat{r}_{Bb}), \quad (5.2.145)$$

and

$$\sum_M \langle l_c 0 l M | K M \rangle \left[ Y^{l_f}(\hat{r}_{A2}) Y^{l_i}(\hat{r}'_{c2}) \right]_M^{K*} Y_M^l(\hat{r}'_{Aa}). \quad (5.2.146)$$

We can express them both as

$$\sum_M f(M), \quad (5.2.147)$$

where e.g. in the case of (5.2.145), one has

$$f(M) = \langle l_c 0 l M | K M \rangle \left[ Y_f^{l_f}(\hat{r}_{C1}) Y_i^{l_i}(\theta + \pi, 0) \right]_M^K Y_M^{l_*}(\hat{r}_{Bb}). \quad (5.2.148)$$

Note that all the vectors that come into play in the above expressions are in the  $(x, z)$ -plane. Consequently, the azimuthal angle  $\phi$  is always equal to zero. Under these circumstances and for time-reversed phases, ( $Y_M^{L*}(\theta, 0) = (-1)^L Y_M^L(\theta, 0)$ ) one has

$$f(-M) = (-1)^{l_c + l_f + l_i + l} f(M). \quad (5.2.149)$$

Consequently,

$$\begin{aligned} \sum_M \langle l_c 0 l M | K M \rangle f(M) &= \langle l_c 0 l 0 | K 0 \rangle f(0) \\ &+ \sum_{M>0} \langle l_c 0 l M | K M \rangle f(M) \left( 1 + (-1)^{l_c + l + l_i + l_f} \right). \end{aligned} \quad (5.2.150)$$

Consequently, in the case in which  $l_c + l + l_i + l_f$  is odd, we have only to evaluate the  $M = 0$  contribution. This consideration is useful to restrict the number of numerical operations needed to calculate the transition amplitude.

### 5.2.9 non-orthogonality term

We write the non-orthogonality contribution to the transition amplitude (see Bayman and Chen (1982)):

$$\begin{aligned} T_{NO}^{(2)}(\theta) = & 2 \sum_{\substack{\sigma_1 \sigma_2 \\ \sigma'_1 \sigma'_2 \\ KM}} \int d^3 r_{Cc} d^3 r_{b1} d^3 r_{A2} d^3 r'_{b1} d^3 r'_{A2} \chi^{(-)*}(\mathbf{k}_{Bb}, \mathbf{r}_{Bb}) \\ & \times \left[ \psi^{j_f}(\mathbf{r}_{A1}, \sigma_1) \psi^{j_f}(\mathbf{r}_{A2}, \sigma_2) \right]_0^{0*} v(r_{b1}) \left[ \psi^{j_f}(\mathbf{r}_{A2}, \sigma_2) \psi^{j_i}(\mathbf{r}_{b1}, \sigma_1) \right]_M^K \\ & \times \left[ \psi^{j_f}(\mathbf{r}'_{A2}, \sigma'_2) \psi^{j_i}(\mathbf{r}'_{b1}, \sigma'_1) \right]_M^{K*} \left[ \psi^{j_i}(\mathbf{r}'_{b1}, \sigma'_1) \psi^{j_i}(\mathbf{r}'_{b2}, \sigma'_2) \right]_0^0 \chi^{(+)}(\mathbf{r}'_{Aa}). \end{aligned} \quad (5.2.151)$$

This expression is equivalent to (5.2.110) if we make the replacement

$$\frac{2\mu_{Cc}}{\hbar^2} G(\mathbf{r}_{Cc}, \mathbf{r}'_{Cc}) v(r'_{A2}) \rightarrow \delta(\mathbf{r}_{Cc} - \mathbf{r}'_{Cc}). \quad (5.2.152)$$

Looking at the partial-wave expansions of  $G(\mathbf{r}_{Cc}, \mathbf{r}'_{Cc})$  and  $\delta(\mathbf{r}_{Cc} - \mathbf{r}'_{Cc})$  (see App. 5.D), we find that we can use the above expressions for the successive transfer with the replacement

$$i \frac{2\mu_{Cc}}{\hbar^2} \frac{f_{l_c}(k_{Cc}, r_<) P_{l_c}(k_{Cc}, r_>)}{k_{Cc}} \rightarrow \delta(r_{Cc} - r'_{Cc}). \quad (5.2.153)$$

We thus have

$$\begin{aligned} T_{2NT}^{NO} = & \frac{512\pi^{9/2}}{k_{Aa}k_{Bb}} \frac{1}{\sqrt{(2j_i+1)(2j_f+1)}} \\ & \times \sum_K ((l_f \frac{1}{2})_{j_f} (l_i \frac{1}{2})_{j_i} | (l_f l_i)_K (\frac{1}{2} \frac{1}{2})_0)_K^2 \\ & \times \sum_{l_c, l} e^{i(\sigma_i^l + \sigma_f^l)} \frac{(2l_c+1)}{\sqrt{2l+1}} Y_0^l(\hat{k}_{Bb}) S_{K,l,l_c}, \end{aligned} \quad (5.2.154)$$

with

$$\begin{aligned} S_{K,l,l_c} = & \int r_{Cc}^2 dr_{Cc} r_{b1}^2 dr_{b1} \sin \theta d\theta v(r_{b1}) u_{l_f}(r_{C1}) u_{l_i}(r_{b1}) \\ & \times \frac{s_{K,l,l_c}(r_{Cc})}{r_{Cc}} \frac{F_l(r_{Bb})}{r_{Bb}} \\ & \times \sum_M \langle l_c 0 l M | K M \rangle [Y^{l_f}(\hat{r}_{C1}) Y^{l_i}(\theta + \pi, 0)]_M^K Y_M^{l*}(\hat{r}_{Bb}), \end{aligned} \quad (5.2.155)$$

and

$$\begin{aligned} s_{K,l,l_c}(r_{Cc}) = & r_{Cc} \int dr'_{A2} r'^2_{A2} \sin \theta' d\theta' u_{l_f}(r'_{A2}) u_{l_i}(r'_{c2}) \frac{F_l(r'_{Aa})}{r'_{Aa}} \\ & \times \sum_M \langle l_c 0 l M | K M \rangle [Y^{l_f}(\hat{r}'_{A2}) Y^{l_i}(\hat{r}'_{c2})]_M^{K*} Y_M^l(\hat{r}'_{Aa}). \end{aligned} \quad (5.2.156)$$

### 5.2.10 Arbitrary orbital momentum transfer

We will now examine the case in which the two transferred nucleons carry an angular momentum  $\Lambda$  different from 0. Let us assume that two nucleons coupled to angular momentum  $\Lambda$  in the initial nucleus  $a$  are transferred into a final state of zero angular momentum in nucleus  $B$ . The transition amplitude is given by the integral

$$\begin{aligned} 2 \sum_{\sigma_1 \sigma_2} \int d\mathbf{r}_{cC} d\mathbf{r}_{A2} d\mathbf{r}_{b1} \chi^{(-)*}(\mathbf{r}_{bB}) [\psi^{j_f}(\mathbf{r}_{A1}, \sigma_1) \psi^{j_f}(\mathbf{r}_{A2}, \sigma_2)]_0^{0*} \\ \times v(r_{b1}) \Psi^{(+)}(\mathbf{r}_{aA}, \mathbf{r}_{b1}, \mathbf{r}_{b2}, \sigma_1, \sigma_2). \end{aligned} \quad (5.2.157)$$

If we neglect core excitations, the above expression is exact as long as  $\Psi^{(+)}(\mathbf{r}_{aA}, \mathbf{r}_{b1}, \mathbf{r}_{b2}, \sigma_1, \sigma_2)$  is the exact wavefunction. We can instead obtain an approximation for the transfer amplitude using

$$\begin{aligned} \Psi^{(+)}(\mathbf{r}_{aA}, \mathbf{r}_{b1}, \mathbf{r}_{b2}, \sigma_1, \sigma_2) \approx & \chi^{(+)}(\mathbf{r}_{aA}) [\psi^{j_{i1}}(\mathbf{r}_{b1}, \sigma_1) \psi^{j_{i2}}(\mathbf{r}_{b2}, \sigma_2)]_\mu^\Lambda \\ & + \sum_{K,M} \mathcal{U}_{K,M}(\mathbf{r}_{cC}) [\psi^{j_f}(\mathbf{r}_{A2}, \sigma_2) \psi^{j_{i1}}(\mathbf{r}_{b1}, \sigma_1)]_M^K \end{aligned} \quad (5.2.158)$$

as an approximation for the incoming state. The first term of (5.2.158) gives rise to the simultaneous amplitude, while from second one leads to both the successive and the non-orthogonality contributions. To extract the amplitude  $\mathcal{U}_{K,M}(\mathbf{r}_{cC})$ , we define  $f_{KM}(\mathbf{r}_{cC})$  as the scalar product

$$f_{KM}(\mathbf{r}_{cC}) = \left\langle \left[ \psi^{j_f}(\mathbf{r}_{A2}, \sigma_2) \psi^{j_{i1}}(\mathbf{r}_{b1}, \sigma_1) \right]_M^K \middle| \Psi^{(+)}(\mathbf{r}_{aA}, \mathbf{r}_{b1}, \mathbf{r}_{b2}, \sigma_1, \sigma_2) \right\rangle \quad (5.2.159)$$

for fixed  $\mathbf{r}_{cC}$ , which can be seen to obey the equation

$$\begin{aligned} & \left( \frac{\hbar^2}{2\mu_{cC}} k_{cC}^2 + \frac{\hbar^2}{2\mu_{cC}} \nabla_{r_{cC}}^2 - U(r_{cC}) \right) f_{KM}(\mathbf{r}_{cC}) \\ &= \left\langle \left[ \psi^{j_f}(\mathbf{r}_{A2}, \sigma_2) \psi^{j_{i1}}(\mathbf{r}_{b1}, \sigma_1) \right]_M^K \middle| v(r_{c2}) \middle| \Psi^{(+)}(\mathbf{r}_{aA}, \mathbf{r}_{b1}, \mathbf{r}_{b2}, \sigma_1, \sigma_2) \right\rangle. \end{aligned} \quad (5.2.160)$$

The solution can be written in terms of the Green function  $G(\mathbf{r}_{cC}, \mathbf{r}'_{cC})$  defined by

$$\left( \frac{\hbar^2}{2\mu_{cC}} k_{cC}^2 + \frac{\hbar^2}{2\mu_{cC}} \nabla_{r_{cC}}^2 - U(r_{cC}) \right) G(\mathbf{r}_{cC}, \mathbf{r}'_{cC}) = \frac{\hbar^2}{2\mu_{cC}} \delta(\mathbf{r}_{cC} - \mathbf{r}'_{cC}). \quad (5.2.161)$$

Thus,

$$\begin{aligned} f_{KM}(\mathbf{r}_{cC}) &= \frac{2\mu_{cC}}{\hbar^2} \int d\mathbf{r}'_{cC} G(\mathbf{r}_{cC}, \mathbf{r}'_{cC}) \left\langle \left[ \psi^{j_f}(\mathbf{r}'_{A2}, \sigma'_2) \psi^{j_{i1}}(\mathbf{r}'_{b1}, \sigma'_1) \right]_M^K \middle| v(r_{c2}) \middle| \Psi^{(+)}(\mathbf{r}'_{aA}, \mathbf{r}'_{b1}, \mathbf{r}'_{b2}, \sigma'_1, \sigma'_2) \right\rangle \\ &\approx \frac{2\mu_{cC}}{\hbar^2} \sum_{\sigma'_1 \sigma'_2} \int d\mathbf{r}'_{cC} d\mathbf{r}'_{A2} d\mathbf{r}'_{b1} G(\mathbf{r}_{cC}, \mathbf{r}'_{cC}) \left[ \psi^{j_f}(\mathbf{r}'_{A2}, \sigma'_2) \psi^{j_{i1}}(\mathbf{r}'_{b1}, \sigma'_1) \right]_M^{K*} \\ &\quad \times v(r'_{c2}) \chi^{(+)}(\mathbf{r}'_{aA}) \left[ \psi^{j_{i1}}(\mathbf{r}'_{b1}, \sigma'_1) \psi^{j_{i2}}(\mathbf{r}'_{b2}, \sigma'_2) \right]_\mu^\Lambda = \mathcal{U}_{K,M}(\mathbf{r}_{cC}) \\ &\quad + \left\langle \left[ \psi^{j_f}(\mathbf{r}'_{A2}, \sigma_2) \psi^{j_{i1}}(\mathbf{r}'_{b1}, \sigma_1) \right]_M^K \middle| \chi^{(+)}(\mathbf{r}'_{aA}) \left[ \psi^{j_{i1}}(\mathbf{r}'_{b1}, \sigma'_1) \psi^{j_{i2}}(\mathbf{r}'_{b2}, \sigma'_2) \right]_\mu^\Lambda \right\rangle. \end{aligned} \quad (5.2.162)$$

Therefore

$$\begin{aligned} \mathcal{U}_{K,M}(\mathbf{r}_{cC}) &= \frac{2\mu_{cC}}{\hbar^2} \sum_{\sigma'_1 \sigma'_2} \int d\mathbf{r}'_{cC} d\mathbf{r}'_{A2} d\mathbf{r}'_{b1} G(\mathbf{r}_{cC}, \mathbf{r}'_{cC}) \left[ \psi^{j_f}(\mathbf{r}'_{A2}, \sigma'_2) \psi^{j_{i1}}(\mathbf{r}'_{b1}, \sigma'_1) \right]_M^{K*} \\ &\quad \times v(r'_{c2}) \chi^{(+)}(\mathbf{r}'_{aA}) \left[ \psi^{j_{i1}}(\mathbf{r}'_{b1}, \sigma'_1) \psi^{j_{i2}}(\mathbf{r}'_{b2}, \sigma'_2) \right]_\mu^\Lambda \\ &\quad - \left\langle \left[ \psi^{j_f}(\mathbf{r}'_{A2}, \sigma_2) \psi^{j_{i1}}(\mathbf{r}'_{b1}, \sigma_1) \right]_M^K \middle| \chi^{(+)}(\mathbf{r}'_{aA}) \left[ \psi^{j_{i1}}(\mathbf{r}'_{b1}, \sigma'_1) \psi^{j_{i2}}(\mathbf{r}'_{b2}, \sigma'_2) \right]_\mu^\Lambda \right\rangle. \end{aligned} \quad (5.2.163)$$

When we substitute  $\mathcal{U}_{K,M}(\mathbf{r}_{cC})$  into (5.2.158) and (5.2.157), the first term gives rise to the successive amplitude for the two-particle transfer, while the second term is responsible for the non-orthogonal contribution.

### 5.2.11 Successive transfer contribution

We need to evaluate the integral

$$\begin{aligned} T_{succ}^{(2)}(\theta; \mu) = & \frac{4\mu_{cC}}{\hbar^2} \sum_{\sigma_1 \sigma_2} \sum_{KM} \int d\mathbf{r}_{cC} d\mathbf{r}_{A2} d\mathbf{r}_{b1} d\mathbf{r}'_{cC} d\mathbf{r}'_{A2} d\mathbf{r}'_{b1} [\psi^{j_f}(\mathbf{r}_{A1}, \sigma_1) \psi^{j_f}(\mathbf{r}_{A2}, \sigma_2)]_0^{0*} \\ & \times \chi^{(-)*}(\mathbf{r}_{bB}) G(\mathbf{r}_{cC}, \mathbf{r}'_{cC}) [\psi^{j_f}(\mathbf{r}'_{A2}, \sigma'_2) \psi^{j_{i1}}(\mathbf{r}'_{b1}, \sigma'_1)]_M^{K*} \chi^{(+)}(\mathbf{r}'_{aA}) v(r'_{c2}) v(r_{b1}) \\ & \times [\psi^{j_{i1}}(\mathbf{r}'_{b1}, \sigma'_1) \psi^{j_{i2}}(\mathbf{r}'_{b2}, \sigma'_2)]_\mu^K [\psi^{j_f}(\mathbf{r}_{A2}, \sigma_2) \psi^{j_{i1}}(\mathbf{r}_{b1}, \sigma_1)]_M^K, \end{aligned} \quad (5.2.164)$$

where we must substitute the Green function and the distorted waves by their partial wave expansions (see App. 5.E). The integral over  $\mathbf{r}'_{b1}$  is:

$$\begin{aligned} & \sum_{\sigma'_1} \int d\mathbf{r}'_{b1} [\psi^{j_f}(\mathbf{r}'_{A2}, \sigma'_2) \psi^{j_{i1}}(\mathbf{r}'_{b1}, \sigma'_1)]_M^{K*} [\psi^{j_{i1}}(\mathbf{r}'_{b1}, \sigma'_1) \psi^{j_{i2}}(\mathbf{r}'_{b2}, \sigma'_2)]_\mu^K \\ = & \sum_{\sigma'_1} \int d\mathbf{r}'_{b1} (-1)^{-M+j_f+j_{i1}-\sigma_1-\sigma_2} [\psi^{j_{i1}}(\mathbf{r}'_{b1}, -\sigma'_1) \psi^{j_f}(\mathbf{r}'_{A2}, -\sigma'_2)]_{-M}^K [\psi^{j_{i1}}(\mathbf{r}'_{b1}, \sigma'_1) \psi^{j_{i2}}(\mathbf{r}'_{b2}, \sigma'_2)]_\mu^K \\ = & \sum_{\sigma'_1} \int d\mathbf{r}'_{b1} (-1)^{-M+j_f+j_{i1}-\sigma_1-\sigma_2} \sum_P \langle K \Lambda - M \mu | P \mu - M \rangle ((j_{i1} j_f)_K (j_{i1} j_{i2})_\Lambda | (j_{i1} j_{i1})_0 (j_f j_{i2})_P)_P \\ & \times [\psi^{j_{i1}}(\mathbf{r}'_{b1}, -\sigma'_1) \psi^{j_{i1}}(\mathbf{r}'_{b1}, \sigma'_1)]_0^0 [\psi^{j_f}(\mathbf{r}'_{A2}, -\sigma'_2) \psi^{j_{i2}}(\mathbf{r}'_{b2}, \sigma'_2)]_{\mu-M}^P \\ = & (-1)^{-M+j_f+j_{i1}} \sqrt{2j_{i1} + 1} u_{l_f}(r_{A2}) u_{l_{i2}}(r'_{b2}) \sum_P \langle K \Lambda - M \mu | P \mu - M \rangle \\ & \times ((j_{i1} j_f)_K (j_{i1} j_{i2})_\Lambda | (j_{i1} j_{i1})_0 (j_f j_{i2})_P)_P ((l_f \frac{1}{2})_{j_f} (l_{i2} \frac{1}{2})_{j_{i2}} | (l_f l_{i2})_P (\frac{1}{2} \frac{1}{2})_0)_P \\ & \times [Y^{l_f}(\hat{\mathbf{r}}'_{A2}) Y^{l_{i2}}(\hat{\mathbf{r}}'_{b2})]_{\mu-M}^P u_{l_f}(r_{A2}) u_{l_{i2}}(r_{b2}). \end{aligned} \quad (5.2.165)$$

Integrating over  $\mathbf{r}_{A2}$  (see (5.2.117)) leads to,

$$\begin{aligned} & \sum_{\sigma_2} \int d\mathbf{r}_{A2} [\psi^{j_f}(\mathbf{r}_{A1}, \sigma_1) \psi^{j_f}(\mathbf{r}_{A2}, \sigma_2)]_0^{0*} [\psi^{j_f}(\mathbf{r}_{A2}, \sigma_2) \psi^{j_{i1}}(\mathbf{r}_{b1}, \sigma_1)]_M^K \\ = & - \sqrt{\frac{2}{2j_f + 1}} ((l_f \frac{1}{2})_{j_f} (l_{i1} \frac{1}{2})_{j_{i1}} | (l_f l_{i1})_K (\frac{1}{2} \frac{1}{2})_0)_K [Y^{l_f}(\hat{\mathbf{r}}_{A1}) Y^{l_{i1}}(\hat{\mathbf{r}}_{b1})]_M^K u_{l_f}(r_{A1}) u_{l_{i1}}(r_{b1}). \end{aligned} \quad (5.2.166)$$

Let us examine the term

$$\sum_M (-1)^M \langle K \Lambda - M \mu | P \mu - M \rangle [Y^{l_f}(\hat{\mathbf{r}}_{A1}) Y^{l_{i1}}(\hat{\mathbf{r}}_{b1})]_M^K [Y^{l_f}(\hat{\mathbf{r}}'_{A2}) Y^{l_{i2}}(\hat{\mathbf{r}}'_{b2})]_{\mu-M}^P. \quad (5.2.167)$$

Making use of the relation

$$\langle l_1 l_2 m_1 m_2 | L M_L \rangle = (-1)^{l_2-m_2} \sqrt{\frac{2L+1}{2l_1+1}} \langle L l_2 - M_L m_2 | l_1 - m_1 \rangle, \quad (5.2.168)$$

the expression (5.2.168) is equivalent to,

$$(-1)^K \sqrt{\frac{2P+1}{2\Lambda+1}} \left\{ \left[ Y^{l_f}(\hat{\mathbf{r}}'_{A2}) Y^{l_{i2}}(\hat{\mathbf{r}}'_{b2}) \right]^P \left[ Y^{l_f}(\hat{\mathbf{r}}_{A1}) Y^{l_{i1}}(\hat{\mathbf{r}}_{b1}) \right]^K \right\}_\mu^\Lambda. \quad (5.2.169)$$

We now recouple the term

$$\left[ Y^{l_a}(\hat{\mathbf{r}}'_{aA}) Y^{l_a}(\hat{\mathbf{k}}_{aA}) \right]_0^0 \left[ Y^{l_b}(\hat{\mathbf{r}}_{bB}) Y^{l_b}(\hat{\mathbf{k}}_{bB}) \right]_0^0, \quad (5.2.170)$$

arising from the partial wave expansion of the incoming and outgoing distorted waves to have,

$$((l_a l_a)_0 (l_b l_b)_0 | (l_a l_b)_\Lambda (l_a l_b)_\Lambda)_0 \left\{ \left[ Y^{l_a}(\hat{\mathbf{r}}'_{aA}) Y^{l_b}(\hat{\mathbf{r}}_{bB}) \right]^\Lambda \left[ Y^{l_a}(\hat{\mathbf{k}}_{aA}) Y^{l_b}(\hat{\mathbf{k}}_{bB}) \right]^\Lambda \right\}_0^0. \quad (5.2.171)$$

The only term which does not vanish upon integration is

$$\frac{(-1)^{\Lambda-\mu}}{\sqrt{(2l_a+1)(2l_b+1)}} \left[ Y^{l_a}(\hat{\mathbf{r}}'_{aA}) Y^{l_b}(\hat{\mathbf{r}}_{bB}) \right]_{-\mu}^\Lambda \left[ Y^{l_a}(\hat{\mathbf{k}}_{aA}) Y^{l_b}(\hat{\mathbf{k}}_{bB}) \right]_\mu^\Lambda. \quad (5.2.172)$$

Again, the only term surviving

$$\left\{ \left[ Y^{l_f}(\hat{\mathbf{r}}'_{A2}) Y^{l_{i2}}(\hat{\mathbf{r}}'_{b2}) \right]^P \left[ Y^{l_f}(\hat{\mathbf{r}}_{A1}) Y^{l_{i1}}(\hat{\mathbf{r}}_{b1}) \right]^K \right\}_\mu^\Lambda \left[ Y^{l_a}(\hat{\mathbf{r}}'_{aA}) Y^{l_b}(\hat{\mathbf{r}}_{bB}) \right]_{-\mu}^\Lambda \quad (5.2.173)$$

is

$$\frac{(-1)^{\Lambda+\mu}}{\sqrt{2\Lambda+1}} \left[ \left\{ \left[ Y^{l_f}(\hat{\mathbf{r}}'_{A2}) Y^{l_{i2}}(\hat{\mathbf{r}}'_{b2}) \right]^P \right. \right. \\ \left. \left. \left[ Y^{l_f}(\hat{\mathbf{r}}_{A1}) Y^{l_{i1}}(\hat{\mathbf{r}}_{b1}) \right]^K \right\}^\Lambda \left[ Y^{l_a}(\hat{\mathbf{r}}'_{aA}) Y^{l_b}(\hat{\mathbf{r}}_{bB}) \right]_\mu^\Lambda \right]_0^0. \quad (5.2.174)$$

We now couple this last term with the term  $\left[ Y^{l_c}(\hat{\mathbf{r}}'_{cC}) Y^{l_c}(\hat{\mathbf{r}}_{cC}) \right]_0^0$ , arising from the partial wave expansion of the Green function. That is,

$$\begin{aligned}
& \left[ \left\{ \left[ Y^{l_f}(\hat{\mathbf{r}}'_{A2}) Y^{l_{i2}}(\hat{\mathbf{r}}'_{b2}) \right]^P \left[ Y^{l_f}(\hat{\mathbf{r}}_{A1}) Y^{l_{i1}}(\hat{\mathbf{r}}_{b1}) \right]^K \right\}^\Lambda \left[ Y^{l_a}(\hat{\mathbf{r}}'_{aA}) Y^{l_b}(\hat{\mathbf{r}}_{bB}) \right]^\Lambda \right]_0^0 \left[ Y^{l_c}(\hat{\mathbf{r}}'_{cC}) Y^{l_c}(\hat{\mathbf{r}}_{cC}) \right]_0^0 \\
&= ((l_a l_b)_\Lambda (l_c l_c)_0 | (l_a l_c)_P (l_b l_c)_K)_\Lambda \left[ \left\{ \left[ Y^{l_f}(\hat{\mathbf{r}}'_{A2}) Y^{l_{i2}}(\hat{\mathbf{r}}'_{b2}) \right]^P \left[ Y^{l_f}(\hat{\mathbf{r}}_{A1}) Y^{l_{i1}}(\hat{\mathbf{r}}_{b1}) \right]^K \right\}^\Lambda \right. \\
&\quad \left. \left\{ \left[ Y^{l_a}(\hat{\mathbf{r}}'_{aA}) Y^{l_c}(\hat{\mathbf{r}}'_{cC}) \right]^P \left[ Y^{l_b}(\hat{\mathbf{r}}_{bB}) Y^{l_c}(\hat{\mathbf{r}}_{cC}) \right]^K \right\}^\Lambda \right]_0^0 = ((l_a l_b)_\Lambda (l_c l_c)_0 | (l_a l_c)_P (l_b l_c)_K)_\Lambda \\
&\quad \times ((PK)_\Lambda (PK)_\Lambda | (PP)_0 (KK)_0)_0 \left\{ \left[ Y^{l_f}(\hat{\mathbf{r}}'_{A2}) Y^{l_{i2}}(\hat{\mathbf{r}}'_{b2}) \right]^P \left[ Y^{l_a}(\hat{\mathbf{r}}'_{aA}) Y^{l_c}(\hat{\mathbf{r}}'_{cC}) \right]^P \right\}_0^0 \\
&\quad \times \left\{ \left[ Y^{l_f}(\hat{\mathbf{r}}_{A1}) Y^{l_{i1}}(\hat{\mathbf{r}}_{b1}) \right]^K \left[ Y^{l_b}(\hat{\mathbf{r}}_{bB}) Y^{l_c}(\hat{\mathbf{r}}_{cC}) \right]^K \right\}_0^0 = ((l_a l_b)_\Lambda (l_c l_c)_0 | (l_a l_c)_P (l_b l_c)_K)_\Lambda \\
&\quad \times \sqrt{\frac{2\Lambda + 1}{(2K+1)(2P+1)}} \left\{ \left[ Y^{l_f}(\hat{\mathbf{r}}'_{A2}) Y^{l_{i2}}(\hat{\mathbf{r}}'_{b2}) \right]^P \left[ Y^{l_a}(\hat{\mathbf{r}}'_{aA}) Y^{l_c}(\hat{\mathbf{r}}'_{cC}) \right]^P \right\}_0^0 \\
&\quad \times \left\{ \left[ Y^{l_f}(\hat{\mathbf{r}}_{A1}) Y^{l_{i1}}(\hat{\mathbf{r}}_{b1}) \right]^K \left[ Y^{l_b}(\hat{\mathbf{r}}_{bB}) Y^{l_c}(\hat{\mathbf{r}}_{cC}) \right]^K \right\}_0^0. \tag{5.2.175}
\end{aligned}$$

Collecting all the contributions (including the constants and phases arising from the partial wave expansion of the distorted waves and the Green function), we get

$$\begin{aligned}
T_{succ}^{(2)}(\theta; \mu) &= (-1)^{j_f + j_{i1}} \frac{2048\pi^5 \mu_{Cc}}{\hbar^2 k_{Aa} k_{Bb} k_{Cc}} \sqrt{\frac{(2j_{i1} + 1)}{(2\Lambda + 1)(2j_f + 1)}} \sum_{K,P} ((l_f \frac{1}{2})_{j_f} (l_{i2} \frac{1}{2})_{j_{i2}} | (l_f l_{i2})_P (\frac{1}{2} \frac{1}{2})_0)_P \\
&\quad \times ((l_f \frac{1}{2})_{j_f} (l_{i1} \frac{1}{2})_{j_{i1}} | (l_f l_{i1})_K (\frac{1}{2} \frac{1}{2})_0)_K ((j_{i1} j_f)_K (j_{i1} j_{i2})_\Lambda | (j_{i1} j_{i1})_0 (j_f j_{i2})_P)_P \\
&\quad \times \frac{(-1)^K}{(2K+1)\sqrt{2P+1}} \sum_{l_c, l_a, l_b} ((l_a l_b)_\Lambda (l_c l_c)_0 | (l_a l_c)_P (l_b l_c)_K)_\Lambda e^{i(\sigma_i^{l_a} + \sigma_f^{l_b})} i^{l_a - l_b} \\
&\quad \times (2l_c + 1)^{3/2} \left[ Y^{l_a}(\hat{\mathbf{k}}_{aA}) Y^{l_b}(\hat{\mathbf{k}}_{bB}) \right]_\mu^K S_{K,P,l_a,l_b,l_c}, \tag{5.2.176}
\end{aligned}$$

with (note that we have reduced the dimensionality of the integrals in the same fashion as for the  $L=0$ -angular momentum transfer calculation, see (5.2.132))

$$\begin{aligned}
S_{K,P,l_a,l_b,l_c} &= \int r_{Cc}^2 dr_{Cc} r_{b1}^2 dr_{b1} \sin \theta d\theta v(r_{b1}) u_{l_f}(r_{C1}) u_{l_i}(r_{b1}) \\
&\quad \times \frac{s_{P,l_a,l_c}(r_{Cc})}{r_{Cc}} \frac{F_{l_b}(r_{Bb})}{r_{Bb}} \\
&\quad \times \sum_M \langle l_c 0 l_b M | K M \rangle \left[ Y^{l_f}(\hat{r}_{C1}) Y^{l_{i1}}(\theta + \pi, 0) \right]_M^K Y_{-M}^{l_b}(\hat{r}_{Bb}), \tag{5.2.177}
\end{aligned}$$

and

$$\begin{aligned} s_{P,l_a,l_c}(r_{Cc}) &= \int r'_{Cc}^2 dr'_{Cc} r'_{A2}^2 dr'_{A2} \sin \theta' d\theta' v(r'_{c2}) u_{l_f}(r'_{A2}) u_{l_i}(r'_{c2}) \\ &\times \frac{F_{l_a}(r'_{Aa})}{r'_{Aa}} \frac{f_{l_c}(k_{Cc}, r_<) P_{l_c}(k_{Cc}, r_>)}{r'_{Cc}} \\ &\times \sum_M \langle l_c 0 l_a M | P M \rangle \left[ Y^{l_f}(\hat{r}'_{A2}) Y^{l_{i2}}(\hat{r}'_{c2}) \right]_M^P Y^{l_a}_{-M}(\hat{r}'_{Aa}). \end{aligned} \quad (5.2.178)$$

We have evaluated the transition matrix element for a particular projection  $\mu$  of the initial angular momentum of the two transferred nucleons. If they are coupled to a core of angular momentum  $J_f$  to total angular momentum  $J_i, M_i$ , the fraction of the initial wavefunction with projection  $\mu$  is  $\langle \Lambda \mu J_f M_i - \mu | J_i M_i \rangle$ , and the cross section will be

$$\frac{d\sigma}{d\Omega}(\hat{\mathbf{k}}_{bB}) = \frac{k_{bB}}{k_{aA}} \frac{\mu_{aA}\mu_{bB}}{(2\pi\hbar^2)^2} \left| \sum_\mu \langle \Lambda \mu J_f M_i - \mu | J_i M_i \rangle T_{succ}^{(2)}(\theta; \mu) \right|^2. \quad (5.2.179)$$

For a non polarized incident beam,

$$\frac{d\sigma}{d\Omega}(\hat{\mathbf{k}}_{bB}) = \frac{k_{bB}}{k_{aA}} \frac{\mu_{aA}\mu_{bB}}{(2\pi\hbar^2)^2} \frac{1}{2J_i + 1} \sum_{M_i} \left| \sum_\mu \langle \Lambda \mu J_f M_i - \mu | J_i M_i \rangle T_{succ}^{(2)}(\theta; \mu) \right|^2. \quad (5.2.180)$$

This would be the differential cross section for a transition to a definite final state  $M_f$ . If we do not measure  $M_f$  we have to sum for all  $M_f$ ,

$$\frac{d\sigma}{d\Omega}(\hat{\mathbf{k}}_{bB}) = \frac{k_{bB}}{k_{aA}} \frac{\mu_{aA}\mu_{bB}}{(2\pi\hbar^2)^2} \frac{1}{2J_i + 1} \sum_\mu |T_{succ}^{(2)}(\theta; \mu)|^2 \sum_{M_i, M_f} |\langle \Lambda \mu J_f M_f | J_i M_i \rangle|^2. \quad (5.2.181)$$

The sum over  $M_i, M_f$  of the Clebsh–Gordan coefficients gives  $(2J_i + 1)/(2\Lambda + 1)$  (see Eq. (5.D.26)). One then gets,

$$\frac{d\sigma}{d\Omega}(\hat{\mathbf{k}}_{bB}) = \frac{k_{bB}}{k_{aA}} \frac{\mu_{aA}\mu_{bB}}{(2\pi\hbar^2)^2} \frac{1}{(2\Lambda + 1)} \sum_\mu |T_{succ}^{(2)}(\theta; \mu)|^2, \quad (5.2.182)$$

where one can write

$$\begin{aligned} T_{succ}^{(2)}(\theta; \mu) &= \sum_{l_a, l_b} C_{l_a, l_b} \left[ Y^{l_a}(\hat{\mathbf{k}}_{aA}) Y^{l_b}(\hat{\mathbf{k}}_{bB}) \right]_\mu^\Lambda \\ &= \sum_{l_a, l_b} C_{l_a, l_b} i^{l_a} \sqrt{\frac{2l_a + 1}{4\pi}} \langle l_a l_b 0 \mu | \Lambda \mu \rangle Y_\mu^{l_b}(\hat{\mathbf{k}}_{bB}). \end{aligned} \quad (5.2.183)$$

Note that (5.2.182) takes into account only the spins of the heavy nucleus. In a  $(t, p)$  or  $(p, t)$  reaction, we have to sum over the spins of the proton and of the triton

and divide by 2. If a spin-orbit term is present in the optical potential, the sum yields the combination of terms shown in Section (5.2.2),

$$\frac{d\sigma}{d\Omega}(\hat{\mathbf{k}}_{bB}) = \frac{k_{bB}}{k_{aA}} \frac{\mu_{aA}\mu_{bB}}{(2\pi\hbar^2)^2} \frac{1}{2(2\Lambda+1)} \sum_{\mu} |A_{\mu}|^2 + |B_{\mu}|^2. \quad (5.2.184)$$

## Appendix 5.A ZPF and Pauli principle at the basis of medium polarization effects: self-energy, vertex corrections and induced interaction

In keeping with a central objective of the formulation of quantum mechanics, namely that the basic concepts on which it is based relate directly to experiment<sup>2</sup> (Heisenberg (1925)), elementary modes of nuclear excitation (single-particle, collective vibrations and rotations), are solidly anchored on observation (inelastic and Coulomb excitation, one- and two-particle transfer reactions). Of all quantal phenomena, zero point fluctuations (ZPF), closely connected with virtual states, are likely to be most representative of the essential difference existing between quantum and classical mechanics. In fact, ZPF are intimately connected with the complementary principle (Bohr (1928)), and thus with indeterminacy (Heisenberg (1927)) and non-commutative (Born and Jordan (1925), Born et al. (1926)) relations, and with the probabilistic interpretation (Born, 1926) of the (modulus squared) of the wavefunctions, solution of Schrödinger's or Dirac's equations (Schrödinger, E. (1926), Dirac (1930)). Pauli principle (Pauli, 1925) brings about essential modifications of the virtual fluctuations of the many-body system, modifications which are instrumental in the dressing and interweaving of the elementary modes of excitation (within the present context, see also Schrieffer (1964)).

In Fig. 5.A.1, NFT diagrams corresponding to the lowest order medium polarization effects renormalizing the properties of a particle-hole collective mode (wavy line), correlated particle-hole excitation which in the shell model basis corresponds to a linear combination of particle-hole excitations ((up-going)-(down-going) arrowed lines) calculated within the random phase approximation (RPA), and leading to the particle-vibration coupling vertex (formfactor and strength, i.e. transition density (solid dot), see inset (I), bottom). The action of an external field on the zero point fluctuations (ZPF) of the vacuum (inset (II)), forces a virtual process to become real, leading to a collective vibration by annihilating a (virtual, spontaneous) particle-hole excitation (backwards RPA amplitude) or, in the time

---

<sup>2</sup>The abstract of this reference reads: "In this paper it will be attempted to secure foundations for a quantum theoretical mechanics which is exclusively based on relations between quantities which in principle are observables". Within the present context, namely that of probing the nuclear structure (e.g. pairing correlations) with direct nuclear reactions, in particular Cooper pair transfer, one can hardly think of a better *incipit* for the introduction of elementary modes of excitation, modes which carry within them most of the correlations thus requiring for their theoretical treatment an effective field theory, like e.g. NFT to properly take into account the essential overcompleteness of the basis (non-orthogonality) as well as of Pauli violating processes.

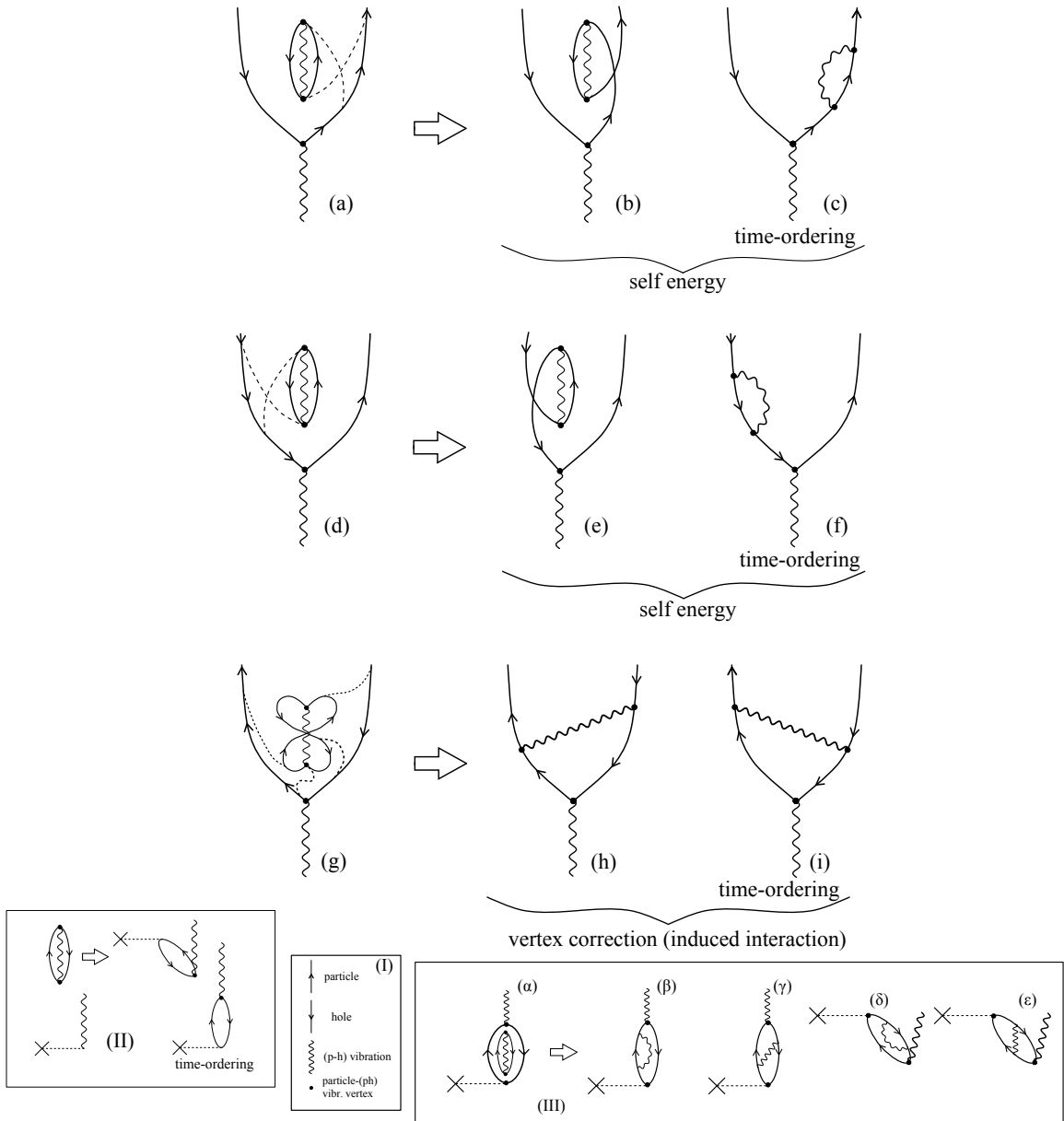


Figure 5.A.1: Nuclear field theory (NFT) diagrams describing renormalization processes associated with ZPF. For details cf. caption to Fig. 5.A.2.

ordered process, by creating a particle–hole excitation which eventually, through the particle–vibration coupling vertex, correlate into the collective (coherent state; forwardgoing amplitudes). Now, oyster-like diagrams associated with the vacuum ZPF can occur at any time (see inset (III)). Because the texture of the vacuum is permeated by symmetry rules (while one can violate energy conservation in a

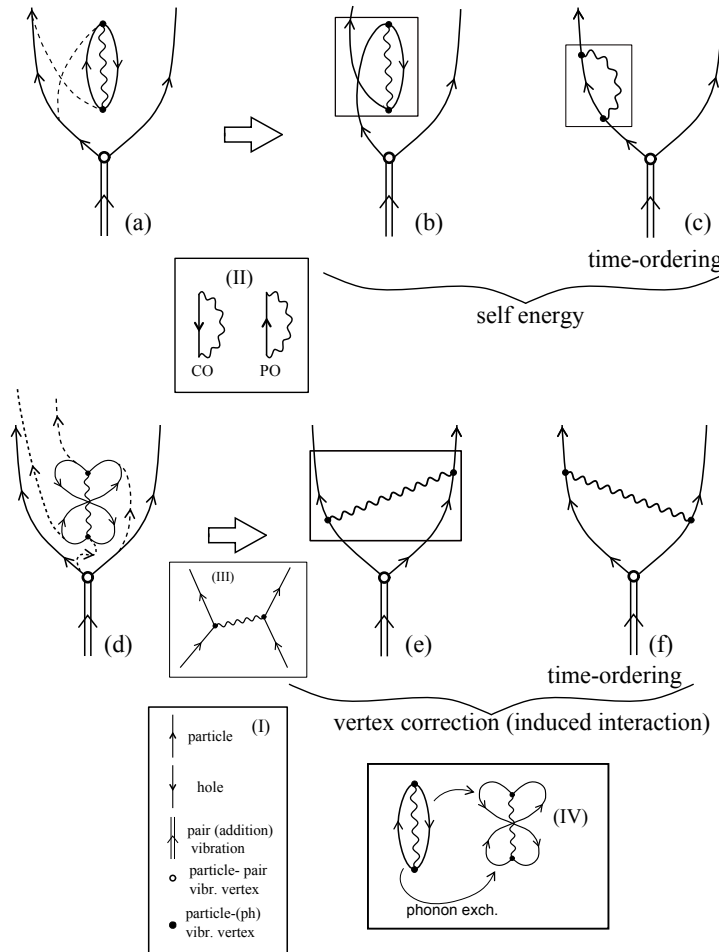


Figure 5.A.2: Pauli effects associated (p-h) ZPF dressing a pairing vibrational (pair addition) mode (see inset I) in terms of self-energy (graphs (a)–(c); correlation (CO) and polarization (PO) diagrams, inset II) and vertex correction (graphs (d)–(f); induced particle–particle (pairing) interaction, ) processes (inset (III)), associated with phonon exchange (inset (IV)).

virtual state one cannot violate e.g. angular momentum conservation or the Pauli principle), the process shown in the inset III ( $\alpha$ ) leads, through Pauli principle correcting processes (exchange of fermionic arrowed lines) to self-energy (inset III ( $\beta$ ), ( $\delta$ )) and vertex corrections (induced p-h interaction; inset III ( $\gamma$ ), ( $\varepsilon$ )) processes (phonon exchange, cf. inset (IV) of Fig. 5.A.2). The first ones are detailed in graphs (a)–(f), while the second ones in graphs (g)–(i). In keeping with the fact that the vibrational states can be viewed as a coherent state exhausting a consistent fraction of the EWSR (e.g. a Giant Resonance) for which the associated uncertainty relations in momentum and coordinate fulfills the absolute minimum con-

sistent with quantum mechanics ( $\Delta\alpha_{\lambda\mu}\Delta\pi_{\lambda\mu} = \hbar/2$ ,  $\alpha_{\lambda\mu} = (\hbar\omega_\mu/2C_\lambda^{1/2})(\Gamma_{\lambda\mu}^\dagger + \Gamma_{\lambda\mu})$  being the (harmonic) collective coordinate,  $\pi_{\lambda\mu}$  being the conjugate momentum; cf. e.g. Glauber (1969)), there is a strong cancellation between the contribution of self-energy and vertex correction diagrams (Bortignon and Broglia, 1981), implying small anharmonicities and long lifetimes ( $\Gamma/E \ll 1$ , where  $\Gamma$  is the width and  $E$  the centroid of the mode  $|\lambda\mu\rangle = \Gamma_{\lambda\mu}^\dagger|0\rangle$ ,  $(\hbar\omega_\lambda/2C_\lambda)^{1/2}$  being the ZPF amplitude (cf. e.g. Brink, D. and Broglia (2005))).

## Appendix 5.B Coherence and effective formfactors

In what follows we shall work out a simplified derivation of the simultaneous two-nucleon transfer amplitude, within the framework of first order DWBA specially suited to discuss correlation aspects of pair transfer in general, and of the associated effective formfactors in particular.

We will concentrate on  $(t, p)$  reaction, namely reactions of the type  $A(\alpha, \beta)B$  where  $\alpha = \beta + 2$  and  $B = A + 2$ .

The intrinsic wave functions are in this case

$$\begin{aligned} \psi_\alpha &= \psi_{M_i}^{J_i}(\xi_A) \sum_{ss'_f} \left[ \chi^s(\sigma_\alpha) \chi^{s'_f}(\sigma_\beta) \right]_{M_{s_i}}^{s_i} \phi_t^{L=0} \left( \sum_{i<j} |\vec{r}_i - \vec{r}_j| \right) \\ &= \psi_{M_i}^{J_i}(\xi_A) \sum_{M_s M'_{s_f}} (s M'_s s'_f M'_{s_f} | s_i M_{s_i}) \chi_{M'_s}^s(\sigma_\alpha) \chi_{M'_{s_f}}^{s'_f}(\sigma_\beta) \\ &\quad \times \phi_t^{L=0} \left( \sum_{i<j} |\vec{r}_i - \vec{r}_j| \right) \end{aligned} \quad (5.B.1)$$

while

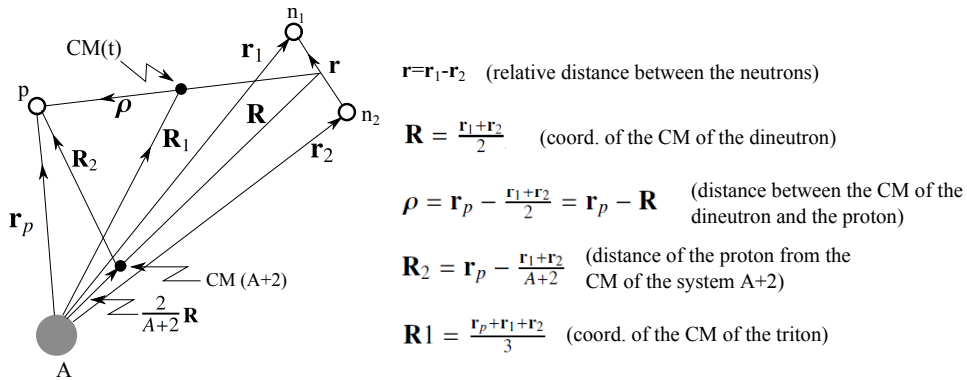


Figure 5.B.1: Coordinate system used in the calculation of the two-nucleon transfer amplitude.

$$\begin{aligned}
\psi_\beta &= \psi_{M_f}^{J_f}(\xi_{A+2}) \chi_{M_{s_f}}^{s_f}(\sigma_\beta) \\
&= \sum_{\substack{n_1 l_1 j_1 \\ n_2 l_2 j_2}} B(n_1 l_1 j_1, n_2 l_2 j_2; J J'_i J_f) [\phi^J(j_1 j_2) \phi^{J'_i}(\xi_A)]_{M_f}^{J_f} \\
&\quad \times \chi_{M_{s_f}}^{s_f}(\sigma_\beta)
\end{aligned} \tag{5.B.2}$$

Making use of the above equation one can define the spectroscopic amplitude  $B$  as

$$\begin{aligned}
&B(n_1 l_1 j_1, n_2 l_2 j_2; J J'_i J_f) \\
&= \left\langle \psi^{J_f}(\xi_{A+2}) \left[ [\phi^J(j_1 j_2) \phi^{J_i}(\xi_A)]_{M_f}^{J_f} \right] \right\rangle,
\end{aligned} \tag{5.B.3}$$

where

$$\phi^J(j_1 j_2) = \frac{[\phi_{j_1}(\vec{r}_1) \phi_{j_2}(\vec{r}_2)]^J - [\phi_{j_1}(\vec{r}_2) \phi_{j_2}(\vec{r}_1)]^J}{\sqrt{1 + \delta(j_1, j_2)}}, \tag{5.B.4}$$

is an antisymmetrized, normalized wave function of the two transferred particles. The function  $\chi_{M_s}^s(\sigma_\beta)$  appearing both in eq. (5.B.1) and (5.B.2) is the spin wave function of the proton while

$$\chi^s(\sigma_\alpha) = [\chi^{s_1}(\sigma_{n_1}) \chi^{s_2}(\sigma_{n_2})]^s, \tag{5.B.5}$$

is the spin function of the two-neutron system.

A convenient description of the intrinsic degrees of freedom of the triton is obtained by using a wavefunction symmetric in the coordinates of all particles, i.e.

$$\begin{aligned}
\phi_t^{L=0} \left( \sum_{i < j} |\vec{r}_i - \vec{r}_j| \right) &= N_t e^{[(r_1 - r_2)^2 + (r_1 - r_p)^2 + (r_2 - r_p)^2]} \\
&= \phi_{000}(\vec{r}) \phi_{000}(\vec{\rho}),
\end{aligned} \tag{5.B.6}$$

where

$$\phi_{000}(\vec{r}) = R_{nl}(v^{1/2} r) Y_{lm}(\hat{r}). \tag{5.B.7}$$

The coordinate  $\vec{\rho}$  is the radius vector which measures the distance between the center of mass of the dineutron and the proton, while the vector  $\vec{r}$  is the dineutron relative coordinate (cf. Fig. 5.B.1).

To obtain the DWBA cross section we have to calculate the integral

$$T(\theta) = \int d\xi_A d\vec{r}_1 d\vec{r}_2 d\vec{r}_p \chi_p^{(-)}(\vec{R}_2) \psi_\beta^*(\xi_{A+2}, \sigma_\beta) V_\beta \psi_\alpha(\xi_A, \sigma_\alpha, \sigma_\beta) \psi_t^{(+)}(\vec{R}_1) \tag{5.B.8}$$

where the final state effective interaction  $V_\beta(\rho)$  is assumed to depend only on the distance  $\rho$  between the center of mass of the di-neutron and of the proton. Instead

of integrating over  $\xi_A, \vec{r}_1, \vec{r}_2$  and  $\vec{r}_p$  we would integrate over  $\xi_A, \vec{r}', \vec{r}'$  and  $\vec{r}_p$ . The Jacobian of the transformation is equal to 1, i.e.  $\partial(\vec{r}_1, \vec{r}_2)/\partial(\vec{r}', \vec{r}') = 1$ .

To carry out the integral (5.B.8) we transform the wave function (5.B.4) into center of mass and relative coordinates. If we assume that both  $\phi_{j_1}(\vec{r}_1)$  and  $\phi_{j_2}(\vec{r}_2)$  are harmonic oscillator wave functions (used as a basis to expand the Saxon–Woods single-particle wavefunctions), this transformation can be carried with the aid of the Moshinsky brackets. If  $|n_1 l_1, n_2 l_2; \lambda \mu\rangle$  is a complete system of wave functions in the harmonic oscillator basis, depending on  $\vec{r}_1$  and  $\vec{r}_2$  and  $|nl, NL; \lambda \mu\rangle$  is the corresponding one depending on  $\vec{r}$  and  $\vec{R}$ , we can write

$$\begin{aligned} |n_1 l_1, n_2 l_2; \lambda \mu\rangle &= \sum_{nlNL} |nl, NL; \lambda \mu\rangle \langle nl, NL; \lambda \mu| |n_1 l_1, n_2 l_2; \lambda \mu\rangle \\ &= \sum_{nlNL} |nl, NL; \lambda \mu\rangle \langle nl, NL; \lambda \mu| n_1 l_1, n_2 l_2; \lambda \rangle \end{aligned} \quad (5.B.9)$$

The labels  $n, l$  are the principal and angular momentum quantum numbers of the relative motion, while  $N, L$  are the corresponding ones corresponding to the center of mass motion of the two-neutron system. Because of energy and parity conservation we have

$$\begin{aligned} 2n_1 + l_1 + 2n_2 + l_2 &= 2n + l + 2N + L \\ (-1)^{l_1+l_2} &= (-1)^{l+L}. \end{aligned} \quad (5.B.10)$$

The coefficients  $\langle nl, NL, L | n_1 l_1, n_2 l_2, L \rangle$  are tabulated and were first discussed by (Moshinsky, 1959)

With the help of eq. (5.B.9) we can write the wave function  $\psi_{M_f}^{J_f}(\xi_{A+2})$  as

$$\begin{aligned} \psi_{M_f}^{J_f}(\xi_{A+2}) &= \sum_{\substack{n_1 l_1 j_1 \\ n_2 l_2 j_2 \\ JJ_i}} B(n_1 l_1 j_1, n_2 l_2 j_2; JJ'_i J_f) [\phi^J(j_1 j_2) \phi^{J'_i}(\xi_A)]_{M_f}^{J_f} \\ &= \sum_{n_1 l_1 j_1} \sum_{JJ_i} B(n_1 l_1 j_1, n_2 l_2 j_2; JJ'_i J_f) \\ &\quad \times \sum_{M_J M'_{J_i}} \langle JM_J J'_i M_{J_i} | J_f M_{J_f} \rangle \psi_{M'_{J_i}}^{J'_i}(\xi_A) \\ &\quad \times \sum_{LS'} \langle S' LJ | j_1 j_2 J \rangle \sum_{M_L M'_S} \langle LM_L S' M'_S | JM_J \rangle \chi_{M'_S}^{S'}(\sigma_\alpha) \\ &\quad \times \sum_{nlN\Lambda} \langle nl, N\Lambda, L | n_1 l_1, n_2 l_2, L \rangle \\ &\quad \times \sum_{m_l M_\Lambda} \langle lm_l \Lambda M_\Lambda | LM_L \rangle \phi_{nlm_l}(\vec{r}) \phi_{N\Lambda M_\Lambda}(\vec{R}) \end{aligned} \quad (5.B.11)$$

Integration over  $\vec{r}$  gives

$$\langle \phi_{nlm_l}(\vec{r}) | \phi_{000}(\vec{r}) \rangle = \delta(l, 0) \delta(m_l, 0) \Omega_n \quad (5.B.12)$$

where

$$\Omega_n = \int R_{nl}(\nu_1^{1/2} r) R_{00}(\nu_2^{1/2} r) r^2 dr \quad (5.B.13)$$

Note that there is no selection rule in the principal quantum number  $n$ , as the potential in which the two neutrons move in the triton has a frequency  $\nu_2$  which is different from the one that the two neutrons are subjected to, when moving in the system  $A$  (non-orthogonality effect).

Integration over  $\xi_A$  and multiplication of the spin functions gives

$$\begin{aligned} (\psi_{M_{J_i}}^{J_i}, V'_\beta(\rho) \psi_{M'_{J'_i}}^{J'_i}) &= \delta(J_i, J'_i) \delta(M_{J_i}, M_{J'_i}) V(\rho), \\ (\chi_{M_S}^S(\sigma_\alpha), \chi_{M_{S'}}^{S'}(\sigma_\alpha)) &= \delta(S, S') \delta(M_S, M_{S'}), \\ (\chi_{M_{S_f}}^{S_f}(\sigma_\beta), \chi_{M_{S'_f}}^{S'_f}(\sigma_\beta)) &= \delta(S_f, S'_f) \delta(M_{S_f}, M_{S'_f}). \end{aligned} \quad (5.B.14)$$

The integral (5.B.8) can then be written as

$$\begin{aligned} T(\theta) &= \sum_{\substack{n_1 l_1 j_1 \\ n_2 l_2 j_2}} \sum_{JM_J} \sum_{nN} \sum_S B(n_1 l_1 j_1, n_2 l_2 j_2; JJ'_i J_f) \\ &\times \langle JM_J J_i M_{J_i} | J_f M_{J_f} \rangle \langle SLJ | j_1 j_2 J \rangle \\ &\times \langle LM_L S M_S | JM_J \rangle \langle n0, NL, L | n_1 l_1, n_2 l_2, L \rangle \\ &\times \langle S M_S S_f M_{S_f} | S_i M_{S_i} \rangle \Omega_n \\ &\times \int d\vec{R} d\vec{r}_p \chi_t^{(+)*}(\vec{R}_1) \phi_{NLM_L}^*(\vec{R}) V(\rho) \phi_{000}(\vec{\rho}) \chi_t^{(+)}(\vec{R}_1), \end{aligned} \quad (5.B.15)$$

where we have approximated  $V'_\beta$  by an effective interaction depending on  $\rho = |\vec{\rho}|$ .

We now define the effective two-nucleon transfer form factor as

$$\begin{aligned} u_{LSJ}^{j_i J_f}(R) &= \sum_{n_1 l_1 j_1} B(n_1 l_1 j_1, n_2 l_2 j_2; JJ_i J_f) \langle SLJ | j_1 j_2 J \rangle \\ &\langle n0, NL, L | n_1 l_1, n_2 l_2, L \rangle \Omega_n R_{nL}(R). \end{aligned} \quad (5.B.16)$$

We can now rewrite eq. (5.B.15) as

$$\begin{aligned} T(\theta) &= \sum_J \sum_L \sum_S (JM_J J_i M_{J_i} | J_f M_{J_f} ) (S M_S S_f M_{S_f} | S_i M_{S_i} ) (LM_L S M_S | JM_J ) \\ &\times \int d\vec{R} d\vec{r}_p \chi_p^{*(-)}(\vec{R}_2) u_{LSJ}^{j_i J_f}(R) Y_{LM_L}^* V(\rho) \phi_{000}(\vec{\rho}) \chi_t^{(+)}(\vec{R}_1). \end{aligned} \quad (5.B.17)$$

Because the di-neutron has  $S = 0$ , we have that

$$(LM_L 00|JM_J) = \delta(J, L)\delta(M_L, M_J), \quad (5.B.18)$$

and the summations over  $S$  and  $L$  disappear from eq. (5.B.17). Let us now make also here, as done in App. 4.F, Eq. (4.F.15) for one-particle transfer reactions, the zero range approximation, that is,

$$V(\rho)\phi_{000}(\vec{\rho}) = D_0\delta(\vec{\rho}). \quad (5.B.19)$$

This means that the proton interacts with the center of mass of the di-neutron, only when they are at the same point in space. Within this approximation (cf. Fig. 5.B.1)

$$\begin{aligned} \vec{R} &= \vec{R}_1 = \vec{r}, \\ \vec{R}_2 &= \frac{A}{A+2}\vec{R}, \end{aligned} \quad (5.B.20)$$

Then eq. (5.B.15) can be written as

$$\begin{aligned} T &= D_0 \sum_L (LM_L J_i M_{J_i} | J_f M_{J_f}) \\ &\times \int d\vec{R} \chi_p^{*(-)}\left(\frac{A}{A+2}\vec{R}\right) u_L^{j_i J_f}(R) Y_{LM_L}^*(\hat{R}) \chi_t^{(+)}(\vec{R}) \end{aligned} \quad (5.B.21)$$

From Eq. (5.B.21) it is seen that the change in parity implied by the reaction is given by  $\Delta\pi = (-1)^L$ . Consequently, the selection rules for  $(t, p)$  and  $(p, t)$  reactions in zero-range approximation are,

$$\begin{aligned} \Delta S &= 0 \\ \Delta J &= \Delta L = L \\ \Delta\pi &= (-1)^L \end{aligned} \quad (5.B.22)$$

i.e. only normal parity states are excited.

The integral appearing in Eq. (5.B.21) has the same structure as the DWBA integral appearing in Eq. (4.F.16) which was derived for the case of one-nucleon transfer reactions.

The difference between the two processes manifests itself through the different structure of the two form factors. While  $u_l(r)$  is a single-particle bound state wave function (cf. Eq. (4.F.1a)),  $u_L^{j_i J_f}$  is a coherent summation over the center of mass states of motion of the two transferred neutrons (see Eq. (5.B.16)). In other words, an effective quantity (function). It is of notice that this difference essentially vanishes, when one considers dressed particles resulting from the coupling to collective motion, and leading, among other things, to  $\omega$ -dependent effective masses. Examples of two-nucleon transfer form factors are given in Figs 5.B.2, 5.B.3 and 5.B.4.

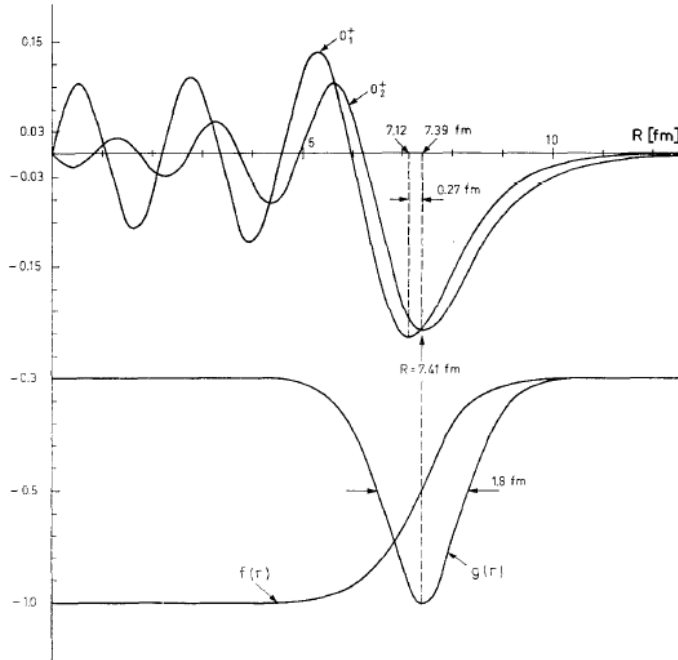


Figure 5.B.2: The upper part of the figure shows the modified formfactor for the  $^{206}\text{Pb}(t,\text{p})^{208}\text{Pb}$  transition to the ground state ( $0_1^+$ ) and the pairing vibrational state ( $0_2^+$ ) at 4.87 MeV. Both curves are matched with appropriate Hankel functions. In the lower part the form factors of the real ( $f(r)$ ) and the imaginary ( $g(r)$ ) part of the optical potential used to calculate the differential cross sections (cf. Fig. 3.A.4), are given in the same scale for the radius. After Broglia and Riedel (1967).

### Appendix 5.C Relative importance of successive and simultaneous transfer and non-orthogonality corrections

In what follows we discuss the relative importance of successive and simultaneous two-neutron transfer and of non-orthogonality corrections associated with the reaction

$$\alpha \equiv a (= b + 2) + A \rightarrow b + B (= A + 2) \equiv \beta \quad (5.C.1)$$

in the limits of independent particles and of strongly correlated Cooper pairs, making use for simplicity of the semiclassical approximation (for details cf. Broglia and Winther (2004), Broglia and refs. therein), in which case the two-particle transfer differential cross section can be written as

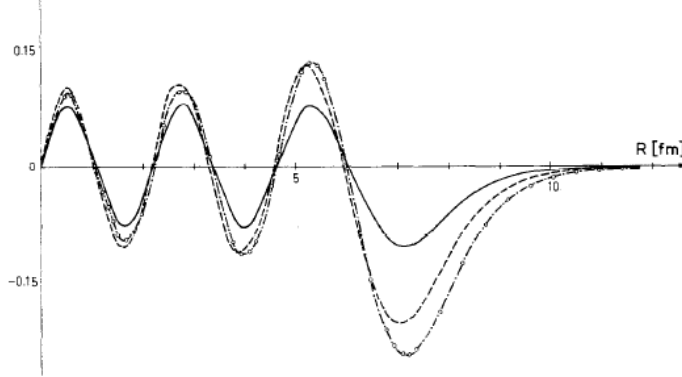


Figure 5.B.3: Modified formfactor for the transition to the ground state ( $^{206}\text{Pb}(\text{t},\text{p})^{208}\text{Pb}(\text{gs})$ ; see Fig. 3.A.4 2A4) calculated in different spectroscopic models (pure shell-model configuration —, shell model plus pairing residual interaction ——, including ground state correlations -o-o-). After Broglia and Riedel (1967).

$$\frac{d\sigma_{\alpha \rightarrow \beta}}{d\Omega} = P_{\alpha \rightarrow \beta}(t = +\infty) \sqrt{\left( \frac{d\sigma_\alpha}{d\Omega} \right)_{el}} \sqrt{\left( \frac{d\sigma_\beta}{d\Omega} \right)_{el}}, \quad (5.C.2)$$

where  $P$  is the absolute value squared of a quantum mechanical transition amplitude. It gives the probability that the system at  $t = +\infty$  is found in the final channel. The quantities  $(d\sigma/d\Omega)_{el}$  are the classical elastic cross sections in the center of mass system, calculated in terms of the deflection function, namely the functional relating the impact parameter and the scattering angle.

The transfer amplitude can be written as

$$a(t = +\infty) = a^{(1)}(\infty) - a^{(NO)}(\infty) + \tilde{a}^{(2)}(\infty), \quad (5.C.3)$$

where  $\tilde{a}^{(2)}(\infty)$  at  $t = +\infty$  labels the successive transfer amplitude expressed in the post-prior representation (see below). The simultaneous transfer amplitude is given by (see Fig. 5.C.1 (I))

$$\begin{aligned} a^{(1)}(\infty) &= \frac{1}{i\hbar} \int_{-\infty}^{\infty} dt (\psi^b \psi^B, (V_{bB} - V_{bB}) \psi^a \psi^A) \times \exp\left[\frac{i}{\hbar}(E^{bB} - E^{aA})t\right] \\ &\approx \frac{2}{i\hbar} \int_{-\infty}^{\infty} dt \left( \phi^{B(A)}(S_{(2n)}^B; \vec{r}_{1A}, \vec{r}_{2A}), U(r_{1b}) e^{i(\sigma_1 + \sigma_2)} \phi^{a(b)}(S_{(2n)}^a; \vec{r}_{1b}, \vec{r}_{2b}) \right) \\ &\quad \times \exp\left[\frac{i}{\hbar}(E^{bB} - E^{aA})t + \gamma(t)\right] \end{aligned} \quad (5.C.4)$$

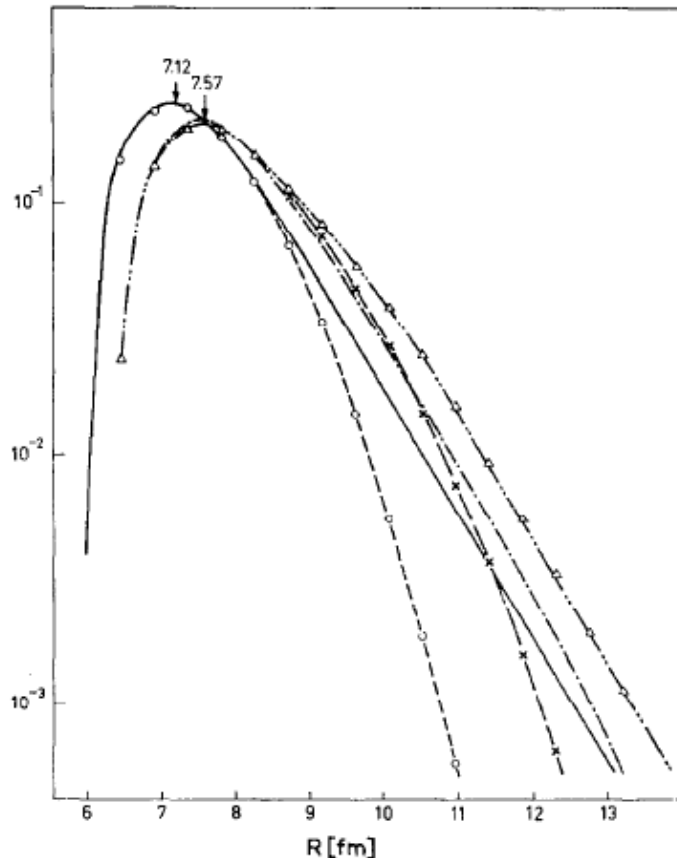


Figure 5.B.4: Asymptotic behavior of the modified formfactor for the  $^{206}(\text{t},\text{p})^{208}\text{Pb(gs)}$  ground state transition for oscillator plus Hankel wave functions (continuous solid curve), oscillator wave functions alone (dash point dashed curve), and Saxon-Woods wave functions with a variety of asymptotic matchings (cf. Broglia and Riedel (1967)).

where

$$\sigma_1 + \sigma_2 = \frac{1}{\hbar} \frac{m_n}{m_A} (m_{aA} \vec{v}_{aA}(t) + m_{bB} \vec{v}_{bB}(t)) \cdot (\vec{r}_{1\alpha} - \vec{r}_{2\alpha}), \quad (5.C.5)$$

in keeping with the fact that  $\exp(i(\sigma_1 + \sigma_2))$  takes care of recoil effects (Galilean transformation associated with the mismatch between entrance and exit channels). The phase  $\gamma(t)$  is related with the effective  $Q$ -value of the reaction. In the above expression,  $\phi$  indicates an antisymmetrized, correlated two-particle (Cooper pair) wavefunction,  $S(2n)$  being the two-neutron separation energy (see Fig. 5.C.3),  $U(r_{1b})$  being the single particle potential generated by nucleus  $b$  ( $U(r) = \int d^3r' \rho^b(r') v(|r - r'|)$ ). The contribution arising from non-orthogonality effects can be written as (see Fig. 5.C.1 (II))

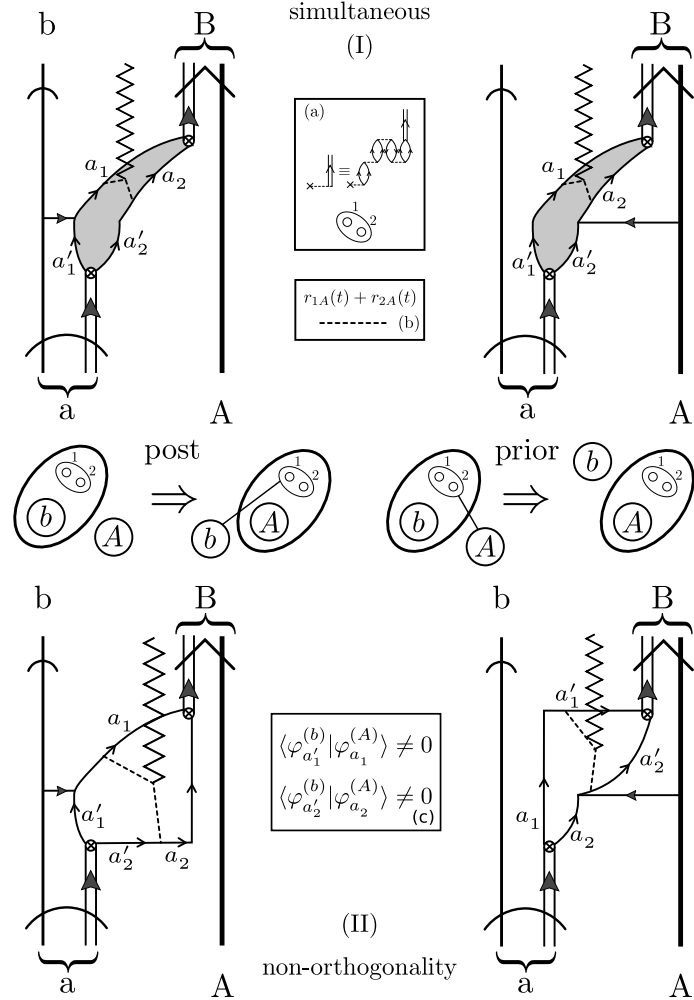


Figure 5.C.1: Graphical representation of simultaneous (I) and non-orthogonality (II) transfer processes. For details see text and cf. caption to Fig. 5.C.2.

$$\begin{aligned}
 a^{(NO)}(\infty) &= \frac{1}{i\hbar} \int_{-\infty}^{\infty} dt (\psi^b \psi^B, (V_{bB} - \langle V_{bB} \rangle) \psi^f \psi^F) (\psi^f \psi^F, \psi^a \psi^A) \exp\left[\frac{i}{\hbar}(E^{bB} - E^{aA})t\right] \\
 &\approx \frac{2}{i\hbar} \int_{-\infty}^{\infty} \phi^{B(F)}(S_{(n)}^B, \vec{r}_{1A}), U(r_{1b}) e^{i\sigma_1} (\phi^{f(b)}(S^f(n), \vec{r}_{1b}) \\
 &\quad \times \phi^{F(A)}(S^F(n), \vec{r}_{2A}) e^{i\sigma_2} \phi^{a(f)}(S^a(n), \vec{r}_{2b})) \exp\left[\frac{i}{\hbar}(E^{bB} - E^{aA})t + \gamma(t)\right],
 \end{aligned} \tag{5.C.6}$$

the reaction channel  $f = (b+1) + F (= A+1)$  having been introduced, the quantity  $S(n)$  being the one-neutron separation energy (see Fig. 5.C.3). The summation

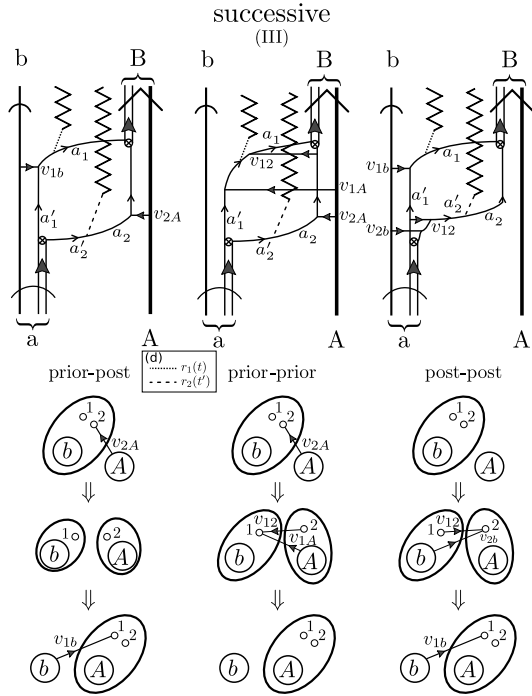


Figure 5.C.2: Graphical representation of the successive transfer of two nucleons. For details see text.

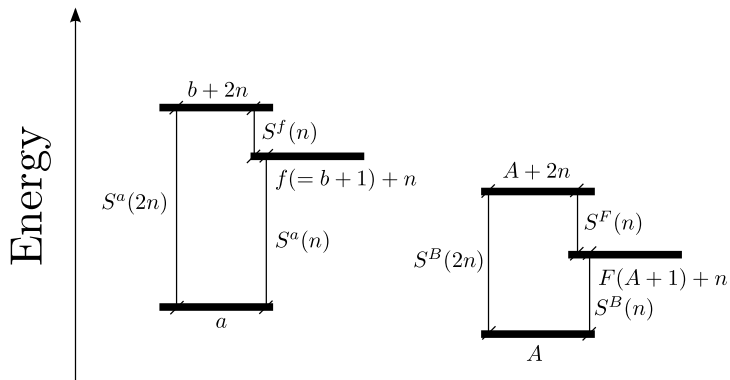


Figure 5.C.3: One- and two-neutron separation energies  $S(n)$  and  $S(2n)$  associated with the channels  $\alpha \equiv a (= b + 2) + A \rightarrow \gamma \equiv f (= b + 1) + F (= A + 1) \rightarrow \beta \equiv b + B (= A + 2)$ .

over  $f (\equiv a'_1, a'_2)$  and  $F (\equiv a_1, a_2)$  involves a restricted number of states, namely the valence shells in nuclei  $B$  and  $a$ .

The successive transfer amplitude  $\tilde{a}_\infty^{(2)}$  written making use of the post-prior

representation is equal to (see Fig. 5.C.2 (III))

$$\begin{aligned} \tilde{a}^{(2)}(\infty) &= \frac{1}{i\hbar} \int_{-\infty}^{\infty} dt (\psi^b \psi^B, (V_{bB} - \langle V_{bB} \rangle) e^{i\sigma_1} \psi^f \psi^F) \\ &\quad \times \exp\left[\frac{i}{\hbar}(E^{bB} - E^{fF})t + \gamma_1(t)\right] \\ &\quad \times \frac{1}{i\hbar} \int_{-\infty}^t dt' (\psi^f \psi^F, (V_{fF} - \langle V_{fF} \rangle) e^{i\sigma_2} \psi^a \psi^A) \\ &\quad \times \exp\left[\frac{i}{\hbar}(E^{fF} - E^{aA})t' + \gamma_2(t)\right]. \end{aligned} \quad (5.C.7)$$

To gain insight into the relative importance of the three terms contributing to Eq. (5.C.3) we discuss two situations, namely, the independent-particle model and the strong-correlation limits.

Before doing so, let us describe in some detail the graphical description of the transfer amplitudes (5.C.4) (5.C.6) and (5.C.7) displayed in Figs. 5.C.1 and 5.C.2. It is of notice that the time arrow is assumed to point upwards: (I) Simultaneous transfer, in which one particle is transferred by the nucleon-nucleon interaction (note that  $U(r) = \int d^3r' \rho(r') v(|\vec{r} - \vec{r}'|)$ ) acting either in the entrance  $\alpha \equiv a + A$  channel (prior) or in the final  $\beta \equiv b + B$  channel (post), while the other particle follows suit making use of the particle-particle correlation (grey area) which binds the Cooper pair (see upper inset labelled (a)), represented by a solid arrow on a double line, to the projectile (curved arrowed lines) or to the target (opened arrowed lines). The above argument provides the explanation why when e.g.  $v_{1b}$  acts on one nucleon, the other nucleon also reacts instantaneously. In fact a Cooper pair displays generalized rigidity (emergent property in gauge space). A crossed open circle represents the particle-pair vibration coupling. The associated strength, together with an energy denominator, determines the amplitude  $X_{a'_1 a'_2}$  with which the pair mode (Cooper pair) is in the (time reversed) two particle configuration  $a'_1 a'_2$ . In the transfer process, the relative motion orbits changes, the readjustement of the corresponding trajectory mismatch being operated by a Galilean transformation induced by the operator ( $\exp\{\vec{k} \cdot (\vec{r}_{1A}(t) + \vec{r}_{2A}(t))\}$ ). This phenomenon, known as recoil process, is represented by a jagged line which provides simultaneous information on the two transferred nucleons (single time appearing as argument of both single-particle coordinates  $r_1$  and  $r_2$ ; see inset labeled (b)). In other words, information on the coupling of structure and reaction modes. (II) Non-orthogonality contribution. While one of the nucleons of the Cooper pairs is transferred under the action of  $v$ , the other goes, uncorrelatedly over, profiting of the non-orthogonality of the associated single-particle wavefunctions (see inset (c)). In other words of the non-vanishing values of the overlaps, as shown in the inset. (III) Successive transfer. In this case, there are two time dependences associated with the acting of the nucleon-nucleon interaction twice (see inset (d)).

### 5.C.1 Independent particle limit

In the independent particle limit, the two transferred particles do not interact among themselves but for antisymmetrization. Thus, the separation energies fulfill the relations (see Fig. 5.C.3)

$$S^B(2n) = 2S^B(n) = 2S^F(n), \quad (5.C.8)$$

and

$$S^a(2n) = 2S^a(n) = 2S^f(n). \quad (5.C.9)$$

In this case

$$\phi^{B(A)}(S^B(2n), \vec{r}_{1A}, \vec{r}_{2A}) = \sum_{a_1 a_2} \phi_{a_1}^{B(F)}(S^B(n), \vec{r}_{1A}) \phi_{a_2}^{F(A)}(S^F(n), \vec{r}_{2a}), \quad (5.C.10)$$

and

$$\phi^{a(b)}(S^a(2n), \vec{r}_{1b}, \vec{r}_{2b}) = \sum_{a'_1 a'_2} \phi_{a'_1}^{a(f)}(S^a(n), \vec{r}_{2b}) \phi_{a'_2}^{f(b)}(S^f(n), \vec{r}_{1b}), \quad (5.C.11)$$

where  $(a_1, a_2) \equiv F$  and  $(a'_1, a'_2) \equiv f$  span, as mentioned above, shells in nuclei  $B$  and  $a$  respectively.

Inserting Eqs. (5.C.8–5.C.11) in Eq. (5.C.4) one can show that

$$a^{(1)}(\infty) = a^{(NO)}(\infty). \quad (5.C.12)$$

It can be further demonstrated that within the present approximation,  $\text{Im } \tilde{a}^{(2)} = 0$ , and that

$$\begin{aligned} \tilde{a}^{(2)}(\infty) &= \frac{1}{i\hbar} \int_{-\infty}^{\infty} dt (\psi^b \psi^B, (V_{bB} - \langle V_{bB} \rangle) e^{i\sigma_1} \psi^f \psi^F) \\ &\quad \times \exp\left[\frac{i}{\hbar}(E^{bB} - E^{fF})t + \gamma_1(t)\right] \\ &\quad \times \frac{1}{i\hbar} \int_{-\infty}^{\infty} dt' (\psi^f \psi^F, (V_{fF} - \langle V_{fF} \rangle) e^{i\sigma_2} \psi^a \psi^A) \\ &\quad \times \exp\left[\frac{i}{\hbar}(E^{fF} - E^{aA})t' + \gamma_2(t)\right]. \end{aligned} \quad (5.C.13)$$

The total absolute differential cross section (5.C.2), where  $P = |a(\infty)|^2 = |\tilde{a}^{(2)}|^2$ , is then equal to the product of two one-particle transfer cross sections (see Fig. 4.1.1), associated with the (virtual) reaction channels

$$\alpha \equiv a + A \rightarrow f + F \equiv \gamma, \quad (5.C.14)$$

and

$$\gamma \equiv f + F \rightarrow b + B \equiv \beta. \quad (5.C.15)$$

In fact, Eq.(5.C.13) involves no time ordering and consequently the two processes above are completely independent of each other. This result was expected because being  $v_{12} = 0$ , the transfer of one nucleon cannot influence, aside from selecting the initial state for the second step, the behaviour of the other nucleon.

### 5.C.2 Strong correlation (cluster) limit

The second limit to be considered is the one in which the correlation between the two nucleons is so strong that (see Fig. 5.C.3)

$$S^a(2n) \approx S^a(n) \gg S^f(n), \quad (5.C.16)$$

and

$$S^B(2n) \approx S^B(n) \gg S^F(n). \quad (5.C.17)$$

That is, the magnitude of the one-nucleon separation energy is strongly modified by the pair breaking.

There is a different, although equivalent way to express (5.C.3) which is more convenient to discuss the strong coupling limit. In fact, making use of the post-prior representation one can write

$$\begin{aligned} a^{(2)}(t) = \tilde{a}^{(2)}(t) - a^{(NO)}(t) &= \frac{1}{i\hbar} \int_{-\infty}^{\infty} dt (\psi^b \psi^B, (V_{bB} - \langle V_{bB} \rangle) e^{i\sigma_1} \psi^f \psi^F) \\ &\times \exp\left[\frac{i}{\hbar}(E^{bB} - E^{fF})t + \gamma_1(t)\right] \\ &\times \frac{1}{i\hbar} \int_{-\infty}^t dt' (\psi^f \psi^F, (V_{aA} - \langle V_{aA} \rangle) \psi^a \psi^A) \\ &\times \exp\left[\frac{i}{\hbar}(E^{fF} - E^{aA})t' + \gamma_2(t')\right]. \end{aligned} \quad (5.C.18)$$

The relations (5.C.16), (5.C.17) imply

$$E^{fF} - E^{aA} = S^a(n) - S^F(n) \gg \frac{\hbar}{\tau}, \quad (5.C.19)$$

where  $\tau$  is the collision time. Consequently the real part of  $a^{(2)}(\infty)$  vanishes exponentially with the  $Q$ -value of the intermediate transition, while the imaginary part vanishes inversely proportional to this energy. One can thus write,

$$\operatorname{Re} a^{(2)}(\infty) \approx 0, \quad (5.C.20)$$

and

$$\begin{aligned} a^{(2)}(\infty) &\approx \frac{1}{i\hbar} \frac{\tau}{\langle E^{fF} \rangle - \langle E^{bB} \rangle} \sum_{fF} (\psi^b \psi^B, (V_{bB} - \langle V_{bB} \rangle) \psi^f \psi^F)_{t=0} \\ &\times (\psi^f \psi^F, (V_{aA} - \langle V_{aA} \rangle) \psi^a \psi^A)_{t=0}, \end{aligned} \quad (5.C.21)$$

where one has utilized the fact that  $E^{bB} \approx E^{aA}$ . For  $v_{12} \rightarrow \infty$ , ( $\langle E^{fF} \rangle - \langle E^{bB} \rangle \rightarrow \infty$ ) and, consequently,

$$\lim_{v_{12} \rightarrow \infty} a^{(2)}(\infty) = 0. \quad (5.C.22)$$

Thus the total two-nucleon transfer amplitude is equal, in the strong coupling limit, to the amplitude  $a^{(1)}(\infty)$ .

Summing up, only when successive transfer and non-orthogonal corrections are included in the description of the two-nucleon transfer process, does one obtain a consistent description of the process, which correctly converges to the weak and strong correlation limiting values.

## Appendix 5.D Spherical harmonics and angular momenta

With Condon–Shortley phases

$$Y_m^l(\hat{z}) = \delta_{m,0} \sqrt{\frac{2l+1}{4\pi}}, \quad Y_m^{l*}(\hat{r}) = (-1)^m Y_{-m}^l(\hat{r}). \quad (5.D.1)$$

Time-reversed phases consist in multiplying Condon–Shortley phases with a factor  $i^l$ , so

$$Y_m^l(\hat{z}) = \delta_{m,0} i^l \sqrt{\frac{2l+1}{4\pi}}, \quad Y_m^{l*}(\hat{r}) = (-1)^{l-m} Y_{-m}^l(\hat{r}). \quad (5.D.2)$$

With this phase convention, the relation with the associated Legendre polynomials includes an extra  $i^l$  factor with respect to the Condon–Shortley phase,

$$Y_m^l(\theta, \phi) = i^l \sqrt{\frac{2l+1}{4\pi} \frac{(l-m)!}{(l+m)!}} P_l^m(\cos \theta) e^{im\phi}. \quad (5.D.3)$$

### 5.D.1 addition theorem

The addition theorem for the spherical harmonics states that

$$P_l(\cos \theta_{12}) = \frac{4\pi}{2l+1} \sum_m Y_m^l(\mathbf{r}_1) Y_m^{l*}(\mathbf{r}_2), \quad (5.D.4)$$

where  $\theta_{12}$  is the angle between the vectors  $\mathbf{r}_1$  and  $\mathbf{r}_2$ . This result is independent of the phase convention. With *time-reversed phases*,

$$P_l(\cos \theta_{12}) = \frac{4\pi}{\sqrt{2l+1}} \left[ Y^l(\hat{\mathbf{r}}_1) Y^l(\hat{\mathbf{r}}_2) \right]_0^0. \quad (5.D.5)$$

With *Condon–Shortley phases*,

$$P_l(\cos \theta_{12}) = (-1)^l \frac{4\pi}{\sqrt{2l+1}} \left[ Y^l(\hat{\mathbf{r}}_1) Y^l(\hat{\mathbf{r}}_2) \right]_0^0. \quad (5.D.6)$$

### 5.D.2 expansion of the delta function

The Dirac delta function can be expanded in multipoles, yielding

$$\begin{aligned} \delta(\mathbf{r}_2 - \mathbf{r}_1) &= \sum_l \delta(r_1 - r_2) \frac{2l+1}{4\pi r_1^2} P_l(\cos \theta_{12}) \\ &= \sum_l \delta(r_1 - r_2) \frac{1}{r_1^2} \sum_m Y_m^l(\mathbf{r}_1) Y_m^{l*}(\mathbf{r}_2). \end{aligned} \quad (5.D.7)$$

This result is independent of the phase convention. With *time-reversed phases*,

$$\delta(\mathbf{r}_2 - \mathbf{r}_1) = \sum_l \delta(r_1 - r_2) \frac{\sqrt{2l+1}}{r_1^2} \left[ Y^l(\hat{\mathbf{r}}_1) Y^l(\hat{\mathbf{r}}_2) \right]_0^0. \quad (5.D.8)$$

### 5.D.3 coupling and complex conjugation

If  $\Psi_{M_1}^{I_1*} = (-1)^{I_1-M_1} \Psi_{-M_1}^{I_1}$  and  $\Phi_{M_2}^{I_2*} = (-1)^{I_2-M_2} \Phi_{-M_2}^{I_2}$ , as it happens to be the case for spherical harmonics with time-reversed phases, then

$$\begin{aligned} [\Psi^{I_1} \Phi^{I_2}]_M^{I*} &= \sum_{\substack{M_1 M_2 \\ (M_1 + M_2 = M)}} \langle I_1 I_2 M_1 M_2 | IM \rangle \Psi_{M_1}^{I_1*} \Phi_{M_2}^{I_2*} \\ &= \sum_{\substack{M_1 M_2 \\ (M_1 + M_2 = M)}} (-1)^{I-M_1-M_2} \langle I_1 I_2 - M_1 - M_2 | I - M \rangle \Psi_{-M_1}^{I_1} \Phi_{-M_2}^{I_2} \\ &= (-1)^{I-M} \sum_{\substack{M_1 M_2 \\ (M_1 + M_2 = M)}} \langle I_1 I_2 - M_1 - M_2 | I - M \rangle \Psi_{-M_1}^{I_1} \Phi_{-M_2}^{I_2} \\ &= (-1)^{I-M} [\Psi^{I_1} \Phi^{I_2}]_{-M}^I, \end{aligned} \quad (5.D.9)$$

where we have used (5.D.23).

Let us care now about the spinor functions  $\chi_m^{1/2}(\sigma)$ , which have the form

$$\chi^{1/2}(\sigma = 1/2) = \begin{bmatrix} 1 \\ 0 \end{bmatrix}, \quad \chi^{1/2}(\sigma = -1/2) = \begin{bmatrix} 0 \\ 1 \end{bmatrix}, \quad (5.D.10)$$

or

$$\chi_m^{1/2}(\sigma) = \delta_{m,\sigma}. \quad (5.D.11)$$

Thus,  $\chi_m^{1/2*}(\sigma) = \chi_m^{1/2}(\sigma) = \delta_{m,\sigma}$ , but we can also write

$$\chi_m^{1/2*}(\sigma) = (-1)^{1/2-m+1/2-\sigma} \chi_{-m}^{1/2}(-\sigma). \quad (5.D.12)$$

This trick enable us to write

$$[Y^l(\hat{r}) \chi^{1/2}(\sigma)]_M^{J*} = (-1)^{1/2-\sigma+J-M} [Y^l(\hat{r}) \chi^{1/2}(-\sigma)]_{-M}^J, \quad (5.D.13)$$

which can be derived in a similar way as (5.D.9).

### 5.D.4 angular momenta coupling

Relation between Clebsh–Gordan and  $3j$  coefficients:

$$\langle j_1 j_2 m_1 m_2 | JM \rangle = (-1)^{j_1-j_2+M} \sqrt{2J+1} \begin{pmatrix} j_1 & j_2 & J \\ m_1 & m_2 & -M \end{pmatrix}. \quad (5.D.14)$$

Relation between Wigner and  $9j$  coefficients:

$$\begin{aligned} ((j_1 j_2)_{j_{12}} (j_3 j_4)_{j_{34}} | (j_1 j_3)_{j_{13}} (j_2 j_4)_{j_{24}})_j = \\ \sqrt{(2j_{12}+1)(2j_{13}+1)(2j_{24}+1)(2j_{34}+1)} \begin{Bmatrix} j_1 & j_2 & j_{12} \\ j_3 & j_4 & j_{34} \\ j_{13} & j_{24} & j \end{Bmatrix}. \end{aligned} \quad (5.D.15)$$

### 5.D.5 integrals

Let us now prove

$$\int d\Omega \left[ Y^l(\hat{r}) Y^l(\hat{r}) \right]_M^I = \delta_{M,0} \delta_{I,0} \sqrt{2l+1}. \quad (5.D.16)$$

$$\begin{aligned} \int d\Omega \left[ Y^l(\hat{r}) Y^l(\hat{r}) \right]_M^I &= \sum_{\substack{m_1, m_2 \\ (m_1 + m_2 = M)}} \langle l \ l \ m_1 \ m_2 | IM \rangle \int d\Omega Y_{m_1}^l(\hat{r}) Y_{m_2}^l(\hat{r}) \\ &= \sum_{\substack{m_1, m_2 \\ (m_1 + m_2 = M)}} (-1)^{l+m_1} \langle l \ l - m_1 \ m_2 | IM \rangle \int d\Omega Y_{m_1}^{l*}(\hat{r}) Y_{m_2}^l(\hat{r}) \\ &= \delta_{M,0} \sum_m (-1)^{l+m} \langle l \ l - m \ m | I0 \rangle \\ &= \delta_{M,0} \sqrt{2l+1} \sum_m \langle l \ l - m \ m | I0 \rangle \langle l \ l - m \ m | 00 \rangle \\ &= \delta_{M,0} \delta_{I,0} \sqrt{2l+1}, \end{aligned} \quad (5.D.17)$$

where we have used

$$\langle l \ l - m \ m | 0 \ 0 \rangle = \frac{(-1)^{l+m}}{\sqrt{2l+1}} \quad (5.D.18)$$

Let us now prove

$$\sum_{\sigma} \int d\Omega (-1)^{1/2-\sigma} \left[ \Psi^j(\hat{r}, -\sigma) \Psi^j(\hat{r}, \sigma) \right]_M^I = -\delta_{M,0} \delta_{I,0} \sqrt{2j+1}. \quad (5.D.19)$$

$$\begin{aligned} \sum_{\sigma} \int d\Omega (-1)^{1/2-\sigma} \left[ \Psi^j(\hat{r}, -\sigma) \Psi^j(\hat{r}, \sigma) \right]_M^I &= \sum_{\substack{m_1, m_2 \\ (m_1 + m_2 = M)}} \langle j \ j \ m_1 \ m_2 | IM \rangle \sum_{\sigma} \int d\Omega \Psi_{m_1}^j(\hat{r}, -\sigma) \Psi_{m_2}^j(\hat{r}, \sigma) \\ &= \sum_{\substack{m_1, m_2 \\ (m_1 + m_2 = M)}} \langle j \ j \ m_1 \ m_2 | IM \rangle \sum_{\sigma} (-1)^{j+m_1} \int d\Omega \Psi_{-m_1}^{j*}(\hat{r}, \sigma) \Psi_{m_2}^j(\hat{r}, \sigma) \\ &= \sum_{\substack{m_1, m_2 \\ (m_1 + m_2 = M)}} \langle j \ j \ m_1 \ m_2 | IM \rangle (-1)^{j+m_1} \delta_{-m_1, m_2} \\ &= \delta_{M,0} \sum_m (-1)^{j+m} \langle j \ j \ m - m | I0 \rangle \\ &= -\delta_{M,0} \sqrt{2j+1} \sum_m (-1)^{j+m} \langle j \ j \ m - m | I0 \rangle \langle j \ j \ m - m | 00 \rangle \\ &= -\delta_{M,0} \delta_{I,0} \sqrt{2j+1}. \end{aligned} \quad (5.D.20)$$

### 5.D.6 symmetry properties

Note also another useful property

$$[\Psi^{I_1} \Psi^{I_2}]^I_M = (-1)^{I_1+I_2-I} [\Psi^{I_2} \Psi^{I_1}]^I_M, \quad (5.D.21)$$

by virtue of the symmetry property of the Clebsh-Gordan coefficients

$$\langle I_1 I_2 m_1 m_2 | IM \rangle = (-1)^{I_1+I_2-I} \langle I_2 I_1 m_2 m_1 | IM \rangle. \quad (5.D.22)$$

Here's another symmetry property of the Clebsh-Gordan coefficients

$$\langle I_1 I_2 m_1 m_2 | IM \rangle = (-1)^{I_1+I_2-I} \langle I_1 I_2 -m_2 -m_1 | I - M \rangle. \quad (5.D.23)$$

Another one, which can be derived from the simpler properties of  $3j$ -symbols

$$\langle I_1 I_2 m_1 m_2 | IM \rangle = (-1)^{I_1-m_1} \sqrt{\frac{2I+1}{2I_2+1}} \langle I_1 I m_1 -M | I_2 m_2 \rangle. \quad (5.D.24)$$

Let us use this last property to calculate sums of the type

$$\sum_{m_1, m_3} |\langle I_1 I_2 m_1 m_2 | I_3 m_3 \rangle|^2. \quad (5.D.25)$$

Using (5.D.24), we have

$$\begin{aligned} \sum_{m_1, m_3} |\langle I_1 I_2 m_1 m_2 | I_3 m_3 \rangle|^2 &= \\ \frac{2I_3 + 1}{2I_2 + 1} \sum_{m_1, m_3} |\langle I_1 I_3 m_1 -m_3 | I_2 m_2 \rangle|^2 &= \frac{2I_3 + 1}{2I_2 + 1}, \end{aligned} \quad (5.D.26)$$

since

$$\sum_{m_1, m_3} |\langle I_1 I_3 m_1 -m_3 | I_2 m_2 \rangle|^2 = \sum_{m_1, m_3} |\langle I_1 I_3 m_1 m_3 | I_2 m_2 \rangle|^2 = 1. \quad (5.D.27)$$

## Appendix 5.E distorted waves

Let us have a closer look at the partial wave expansion of the distorted waves

$$\chi^{(+)}(\mathbf{k}, \mathbf{r}) = \sum_l \frac{4\pi}{kr} i^l e^{i\sigma l} F_l \sum_m Y_m^l(\hat{r}) Y_m^{l*}(\hat{k}). \quad (5.E.1)$$

Of notice the very important fact that *this definition is independent of the phase convention*, since the  $l$ -dependent phase is multiplied by its complex conjugate.

$$\chi^{(-)}(\mathbf{k}, \mathbf{r}) = \chi^{(+)*}(-\mathbf{k}, \mathbf{r}) = \sum_l \frac{4\pi}{kr} i^{-l} e^{-i\sigma l} F_l^* \sum_m Y_m^{l*}(\hat{r}) Y_m^l(-\hat{k}). \quad (5.E.2)$$

As  $Y_m^l(-\hat{k}) = (-1)^l Y_m^l(\hat{k})$ , we have

$$\chi^{(-)}(\mathbf{k}, \mathbf{r}) = \sum_l \frac{4\pi}{kr} i^l e^{-i\sigma^l} F_l^* \sum_m Y_m^{l*}(\hat{r}) Y_m^l(\hat{k}), \quad (5.E.3)$$

which is also independent of the phase convention. With time-reversed phase convention

$$\chi^{(+)}(\mathbf{k}, \mathbf{r}) = \sum_l \frac{4\pi}{kr} i^l \sqrt{2l+1} e^{i\sigma^l} F_l [Y^l(\hat{r}) Y^l(\hat{k})]_0^0, \quad (5.E.4)$$

while with Condon–Shortley phase convention we get an extra  $(-1)^l$  factor:

$$\chi^{(+)}(\mathbf{k}, \mathbf{r}) = \sum_l \frac{4\pi}{kr} i^{-l} \sqrt{2l+1} e^{i\sigma^l} F_l [Y^l(\hat{r}) Y^l(\hat{k})]_0^0. \quad (5.E.5)$$

The partial-wave expansion of the Green function  $G(\mathbf{r}, \mathbf{r}')$  is

$$G(\mathbf{r}, \mathbf{r}') = i \sum_l \frac{f_l(k, r_<) P_l(k, r_>)}{krr'} \sum_m Y_m^l(\hat{r}) Y_m^{l*}(\hat{r}'), \quad (5.E.6)$$

where  $f_l(k, r_<)$  and  $P_l(k, r_>)$  are the regular and the irregular solutions of the homogeneous problem respectively. With *time-reversed* phase convention

$$G(\mathbf{r}, \mathbf{r}') = i \sum_l \sqrt{2l+1} \frac{f_l(k, r_<) P_l(k, r_>)}{krr'} [Y^l(\hat{r}) Y^l(\hat{r}')]_0^0. \quad (5.E.7)$$

## Appendix 5.F hole states and time reversal

Let us consider the state  $|(jm)^{-1}\rangle$  obtained by removing a  $\psi_{jm}$  single-particle state from a  $J = 0$  closed shell  $|0\rangle$ . The antisymmetrized product state

$$\sum_m \mathcal{A}\{\psi_{jm}|(jm)^{-1}\} \propto |0\rangle \quad (5.F.1)$$

is clearly proportional to  $|0\rangle$ . This gives us the transformation rules of  $|(jm)^{-1}\rangle$  under rotations, which must be such that, when multiplied by a  $j, m$  spherical tensor and summed over  $m$ , yields a  $j = 0$  tensor. It can be seen that these properties imply that  $|(jm)^{-1}\rangle$  transforms like  $(-1)^{j-m} T_{j-m}$ ,  $T_{j-m}$  being a spherical tensor. It also follows that the hole state  $|(j\bar{m})^{-1}\rangle$  transforms like a  $j, m$  spherical tensor if  $\psi_{j\bar{m}}$  is defined as the  $\mathcal{R}$ -conjugate to  $\psi_{jm}$  by the relation

$$\psi_{j\bar{m}} \equiv (-1)^{j+m} \psi_{j-m}. \quad (5.F.2)$$

In other words, with the latter definition a *hole state* transforms under rotations with the right phase. We will now show that  $\mathcal{R}$ -conjugation is equivalent to a rotation of spin and spatial coordinates through an angle  $-\pi$  about the  $y$ -axis:

$$e^{i\pi J_y} \psi_{jm} = (-1)^{j+m} \psi_{j-m} \equiv \psi_{j\bar{m}}. \quad (5.F.3)$$

Let us begin by calculating  $e^{i\pi L_y} Y_l^m$ . The rotation matrix about the  $y$ -axis is

$$R_y(\theta) = \begin{pmatrix} \cos(\theta) & 0 & \sin(\theta) \\ 0 & 1 & 0 \\ -\sin(\theta) & 0 & \cos(\theta) \end{pmatrix}, \quad (5.F.4)$$

so for  $R_y(-\pi)$  we get

$$R_y(-\pi) = \begin{pmatrix} -1 & 0 & 0 \\ 0 & 1 & 0 \\ 0 & 0 & -1 \end{pmatrix}. \quad (5.F.5)$$

When applied to the generic direction  $(\sin(\theta)\cos(\phi), \sin(\theta)\sin(\phi), \cos(\theta))$ , we obtain  $(-\sin(\theta)\cos(\phi), \sin(\theta)\sin(\phi), -\cos(\theta))$ , which corresponds to making the substitutions

$$\theta \rightarrow \pi - \theta, \quad \phi \rightarrow \pi - \phi. \quad (5.F.6)$$

When we substitute these angular transformations in the spherical harmonic  $Y_l^m(\theta, \phi)$ , we obtain the rotated  $Y_l^m(\theta, \phi)$ :

$$e^{i\pi L_y} Y_l^m = (-1)^{l+m} Y_l^{-m}. \quad (5.F.7)$$

Let us now turn our attention to the spin coordinates rotation  $e^{i\pi s_y} \chi_m$ . The rotation matrix in spin space is

$$\begin{pmatrix} \cos(\theta/2) & -\sin(\theta/2) \\ \sin(\theta/2) & \cos(\theta/2) \end{pmatrix}, \quad (5.F.8)$$

which, for  $\theta = -\pi$  is

$$\begin{pmatrix} 0 & 1 \\ -1 & 0 \end{pmatrix}. \quad (5.F.9)$$

Applying it to the spinors, we find the rule

$$e^{i\pi s_y} \chi_m = (-1)^{1/2+m} \chi_{-m}, \quad (5.F.10)$$

so

$$\begin{aligned} e^{i\pi J_y} \psi_{jm} &= \sum_{m_l m_s} \langle l m_l 1/2 m_s | j m \rangle e^{i\pi L_y} Y_l^{m_l} e^{i\pi s_y} \chi_{m_s} \\ &= \sum_{m_l m_s} (-1)^{1/2+m_s+l+m_l} \langle l m_l 1/2 m_s | j m \rangle Y_l^{-m_l} \chi_{-m_s} \\ &= \sum_{m_l m_s} (-1)^{1+m-j+2l} \langle l -m_l 1/2 -m_s | j -m \rangle Y_l^{-m_l} \chi_{-m_s} \\ &= (-1)^{m+j} \psi_{j-m} \equiv \psi_{j\bar{m}}, \end{aligned} \quad (5.F.11)$$

where we have used  $(-1)^{1+m-j+2l} = -(-1)^{m-j} = (-1)^{m+j}$ , as  $j, m$  are always half-integers and  $l$  is always an integer.

We now turn our attention to the time reversal operation, which amounts to the transformations

$$\mathbf{r} \rightarrow \mathbf{r}, \quad \mathbf{p} \rightarrow -\mathbf{p}. \quad (5.F.12)$$

This is enough to define the operator of time reversal of a spinless particle (see Messiah). In the position representation, in which  $\mathbf{r}$  is real and  $\mathbf{p}$  pure imaginary, this (unitary antilinear) operator is the complex conjugation operator.

As angular momentum  $\mathbf{l} = \mathbf{r} \times \mathbf{p}$  changes sign under time reversal, so does spin:

$$\mathbf{s} \rightarrow -\mathbf{s}, \quad (5.F.13)$$

which, along with (5.F.12), completes the set of rules that define the time reversal operation on a particle with spin. In the representation of eigenstates of  $\mathbf{s}^2$  and  $s_z$ , complex conjugation alone changes only the sign of  $s_y$ , so an additional rotation of  $-\pi$  around the  $y$ -axis is necessary to change the sign of  $s_x, s_z$  and implement the transformation (5.F.13). If we call  $K$  the time-reversal operator, we have

$$K\psi_{jm} = e^{i\pi s_y} \psi_{jm}^*. \quad (5.F.14)$$

This is completely general and independent of the phase convention. It only depends on the fact that we have used the  $\mathbf{r}$  representation for the spatial wave function and the representation of the eigenstates of  $\mathbf{s}^2$  and  $s_z$  for the spin part. *If we use time-reversal phases for the spherical harmonics* (see (5.D.2)),

$$Y_m^{l*} = (-1)^{l+m} Y_{-m}^l = e^{i\pi L_y} Y_m^l. \quad (5.F.15)$$

So we can write

$$K\psi_{jm} = e^{i\pi J_y} \psi_{jm} = \psi_{j\bar{m}}. \quad (5.F.16)$$

Note again that this last expression is valid only if we use time-reversal phases for the spherical harmonics. Only in this case time-reversal coincides with  $\mathcal{R}$ -conjugation and hole states.

In BCS theory, the quasiparticles are defined in terms of linear combinations of particles and holes. With time-reversal phases, holes are equivalent to time-reversed states, and we get the definitions

$$\begin{aligned} \alpha_\nu^\dagger &= u_\nu a_\nu^\dagger - v_\nu a_{\bar{\nu}}^\dagger & a_\nu^\dagger &= u_\nu \alpha_\nu^\dagger + v_\nu \alpha_{\bar{\nu}} \\ a_{\bar{\nu}}^\dagger &= u_\nu a_{\bar{\nu}}^\dagger + v_\nu a_\nu^\dagger & a_{\bar{\nu}}^\dagger &= u_\nu \alpha_{\bar{\nu}}^\dagger - v_\nu \alpha_\nu \\ \alpha_\nu &= u_\nu a_\nu - v_\nu a_{\bar{\nu}}^\dagger & a_\nu &= u_\nu \alpha_\nu + v_\nu \alpha_{\bar{\nu}}^\dagger \\ a_{\bar{\nu}} &= u_\nu a_{\bar{\nu}} + v_\nu a_\nu^\dagger & a_{\bar{\nu}} &= u_\nu \alpha_{\bar{\nu}} - v_\nu \alpha_\nu^\dagger \end{aligned} \quad (5.F.17)$$

## Appendix 5.G Spectroscopic amplitudes in the BCS approximation

The creation operator of a pair of fermions coupled to  $J, M$  can be expressed in second quantization as

$$P^\dagger(j_1, j_2, JM) = N \sum_m \langle j_1 m | j_2 M - m | J M \rangle a_{j_1 m}^\dagger a_{j_2 M-m}^\dagger, \quad (5.G.1)$$

where  $N$  is a normalization constant. To determine it, we write the wave function resulting from the action of (5.G.1) on the vacuum

$$\begin{aligned}\Psi = P^\dagger(j_1, j_2, JM)|0\rangle &= \frac{N}{\sqrt{2}} \sum_m \langle j_1 m j_2 M - m | J M \rangle \\ &\times (\phi_{j_1 m}(\mathbf{r}_1) \phi_{j_2 M-m}(\mathbf{r}_2) - \phi_{j_2 M-m}(\mathbf{r}_1) \phi_{j_1 m}(\mathbf{r}_2)).\end{aligned}\quad (5.G.2)$$

The norm is

$$\begin{aligned}|\Psi|^2 &= \frac{N^2}{2} \sum_{mm'} \langle j_1 m j_2 M - m | J M \rangle \langle j_1 m' j_2 M - m' | J M \rangle \\ &\times (\phi_{j_1 m}(\mathbf{r}_1) \phi_{j_2 M-m}(\mathbf{r}_2) - \phi_{j_2 M-m}(\mathbf{r}_1) \phi_{j_1 m}(\mathbf{r}_2)) \\ &\times (\phi_{j_1 m'}(\mathbf{r}_1) \phi_{j_2 M-m'}(\mathbf{r}_2) - \phi_{j_2 M-m'}(\mathbf{r}_1) \phi_{j_1 m'}(\mathbf{r}_2)).\end{aligned}\quad (5.G.3)$$

Integrating we get

$$\begin{aligned}1 &= \frac{N^2}{2} \sum_{mm'} \langle j_1 m j_2 M - m | J M \rangle \langle j_1 m' j_2 M - m' | J M \rangle \\ &\times (2\delta_{m,m'} - 2\delta_{j_1,j_2}\delta_{m,M-m'}) \\ &= N^2 \left( \sum_m \langle j_1 m j_2 M - m | J M \rangle^2 \right. \\ &\quad \left. - \delta_{j_1,j_2} \sum_m \langle j_1 m j_2 M - m | J M \rangle \langle j_1 M - m j_2 m | J M \rangle \right) \\ &= N^2 (1 - \delta_{j_1,j_2}(-1)^{2j-J}),\end{aligned}\quad (5.G.4)$$

where we have used the closure condition for Clebsh–Gordan coefficients and (5.D.22), and  $\delta_{j_1,j_2}$  must be interpreted as a  $\delta$  function regarding all the quantum numbers but the magnetic one. We see that two fermions with identical quantum numbers (but the magnetic one) *cannot couple to  $J$  odd*. If  $J$  is even, the normalization constant is

$$N = \frac{1}{\sqrt{1 + \delta_{j_1,j_2}}}.\quad (5.G.5)$$

To sum up,

$$P^\dagger(j_1, j_2, JM) = \frac{1}{\sqrt{1 + \delta_{j_1,j_2}}} \sum_m \langle j_1 m j_2 M - m | J M \rangle a_{j_1 m}^\dagger a_{j_2 M-m}^\dagger.\quad (5.G.6)$$

The spectroscopic amplitude for finding in a  $A + 2, J_f, M_f$  nucleus a couple of nucleons with quantum numbers  $j_1, j_2$  coupled to  $J$  on top of a  $A, J_i$  nucleus is

$$B(J, j_1, j_2) = \sum_{M, M_i} \langle J_i M_i JM | J_f M_f \rangle \langle \Psi_{J_f M_f} | P^\dagger(j_1, j_2, JM) | \Psi_{J_i M_i} \rangle.\quad (5.G.7)$$

This is completely general. It depends on the structure model only through the way the  $A + 2$  and  $A$  nuclei are treated. We now want to turn our attention to the expression of  $B(J, j_1, j_2)$  in the BCS approximation when both the  $A + 2$  and the  $A$  are  $0^+$ , zero-quasiparticle ground states. In order to do this, we write (5.G.6) in terms of quasiparticle operators using (5.F.17)<sup>3</sup>:

$$\begin{aligned} P^\dagger(j_1, j_2, JM) = & \frac{1}{\sqrt{1 + \delta_{j_1, j_2}}} \sum_{m_1, m_2} \langle j_1 \ m_1 \ j_2 \ m_2 | J \ M \rangle \left( U_{j_1} U_{j_2} \alpha_{j_1 m_1}^\dagger \alpha_{j_2 m_2}^\dagger \right. \\ & + (-1)^{j_1 + j_2 - M} V_{j_1} V_{j_2} \alpha_{j_1 - m_1} \alpha_{j_2 - m_2} \\ & + (-1)^{j_2 - m_2} U_{j_1} V_{j_2} \alpha_{j_1 m_1}^\dagger \alpha_{j_2 - m_2} \\ & - (-1)^{j_1 - m_1} V_{j_1} U_{j_2} \alpha_{j_2 m_2}^\dagger \alpha_{j_1 - m_1} \\ & \left. + (-1)^{j_1 - m_1} V_{j_1} U_{j_2} \delta_{j_1 j_2} \delta_{-m_1 m_2} \right). \end{aligned} \quad (5.G.8)$$

If both nuclei are in zero-quasiparticle states, the only term that survives is the last one in the above expression, and (5.G.7) becomes (see also Sect. 2.D.2 and equation 2.1.8).

$$\begin{aligned} B_j = B(j^2(0)) = & \frac{1}{\sqrt{2}} \sum_m \langle j \ m \ j - m | 0 \ 0 \rangle (-1)^{j-m} V_j U_j \\ = & \frac{1}{\sqrt{2}} \sum_m \frac{(-1)^{j-m}}{\sqrt{(2j+1)}} (-1)^{j-m} V_j U_j \\ = & \frac{1}{\sqrt{2}} \sum_m \frac{1}{\sqrt{(2j+1)}} V_j U_j. \end{aligned} \quad (5.G.9)$$

After carrying out the summation one finds,

$$B_j = B(j^2(0)) = \sqrt{j + 1/2} V_j U_j. \quad (5.G.10)$$

Note that in this final expression  $V_j$  refers to the  $A$  nucleus, while  $U_j$  is related to the  $A + 2$  nucleus. In practice, it does not make a big difference to calculate both for the same nucleus.

## Appendix 5.H Derivation of two-nucleon transfer transition amplitudes including recoil, non-orthogonality and successive transfer.

In the present Appendix we reproduce what, arguably, was the first complete derivation (Bayman (1970)(unpublished)) of the different contributions needed to calculate absolute two-nucleon transfer cross sections in a systematic way (cf. Bayman (1971) and Bayman and Chen (1982)). Within this context we refer to Broglia, R.A. et al. (1973) and Potel, G. et al. (2013) in particular Fig. 10 of this reference.

---

<sup>3</sup>In what follows, we use the phase convention  $\alpha_{j\bar{m}}=(-1)^{j-m}\alpha_{j-m}$  instead of  $\alpha_{j\bar{m}}=(-1)^{j+m}\alpha_{j-m}$ , consistent with (5.F.2). Had we stick to the definition (5.F.2), the amplitude  $B(0, j, j)$  calculated below would have a minus sign, which would not have any physical consequence.

## Bibliography

- B. F. Bayman. Finite-range calculation of the two-neutron transfer reaction. *Phys. Rev. Lett.*, 25:1768, 1970.
- B. F. Bayman. Finite-range calculation of the two-neutron transfer reaction. *Nuclear Physics A*, 168:1, 1971.
- B. F. Bayman and J. Chen. One-step and two-step contributions to two-nucleon transfer reactions. *Phys. Rev. C*, 26:1509, 1982.
- B. F. Bayman and A. Kallio. Relative-angular-momentum-zero part of two-nucleon wave functions. *Phys. Rev.*, 156:1121, 1967.
- N. Bohr. The quantum postulate and the recent development of atomic theory. *Nature*, 121:580, 1928.
- M. Born. Zur Quantenmechanik der Stoßvorgänge. *Zeitschr. f. Phys.*, 37:863, 1926.
- M. Born and Jordan. Zur quantenmechanik. *Zeitschr. Phys.*, 34:858, 1925.
- M. Born, Jordan, and W. Heisenberg. Zur Quantenmechanik II. *Zeitschr. Phys.*, 35:557, 1926.
- P. F. Bortignon and R. A. Broglia. Role of the nuclear surface in an unified description of the damping of single-particle states and giant resonances. *Nucl. Phys. A*, 371:405, 1981.
- Brink, D. and R. A. Broglia. *Nuclear Superfluidity*. Cambridge University Press, Cambridge, 2005.
- R. Broglia and A. Winther. *Heavy Ion Reactions*. Westview Press, Boulder, CO., 2004.
- R. A. Broglia. Heavy ion reaction, notes of lectures delivered during the academic years 1974–1976 at SUNY, Stony Brook at Brookhaven National Laboratory, and at Niels Bohr Institute, unpublished.
- R. A. Broglia and C. Riedel. Pairing vibration and particle-hole states excited in the reaction  $^{206}\text{Pb}(\text{t}, \text{p})^{208}\text{Pb}$ . *Nucl. Phys.*, 92:145, 1967.
- Broglia, R.A., O. Hansen, and C. Riedel. Two-neutron transfer reactions and the pairing model. *Advances in Nuclear Physics*, 6:287, 1973. URL [www.mi.infn.it/?vigezzi/BHR/BrogliaHansenRiedel.pdf](http://www.mi.infn.it/?vigezzi/BHR/BrogliaHansenRiedel.pdf).
- P. A. M. Dirac. *The principles of quantum mechanics*. Oxford University Press, London, 1930.

- R. J. Glauber. In R. J. Glauber, editor, *International School of Physics “Enrico Fermi” Course XLII on Quantum Optics*, page 15, Academic Press, 1969. New York.
- W. Heisenberg. Über quantentheoretische umdeutung kinematischer und mechanischer beziehungen. *Z. Phys.*, 33:879, 1925.
- W. Heisenberg. Über der anschaulichen inhalt der quantentheoretischen kinematik und mechanik. *Z. Phys.*, 43:172, 1927.
- M. Moshinsky. Transformation brackets for harmonic oscillator functions. *Nucl. Phys.*, 13:104, 1959.
- B. Mottelson. Selected topics in the theory of collective phenomena in nuclei. In G. Racah, editor, *International School of Physics “Enrico Fermi” Course XV, Nuclear Spectroscopy*, page 44, New York, 1962. Academic Press.
- W. Pauli. Zur quantenmechanik ii. *Zeitschr. Phys.*, 31:625, 1925.
- Potel, G., A. Idini, F. Barranco, E. Vigezzi, and R. A. Broglia. Cooper pair transfer in nuclei. *Rep. Prog. Phys.*, 76:106301, 2013.
- J. Schrieffer. *Superconductivity*. Benjamin, New York, 1964.
- Schrödinger, E. Quantisierung als eigenwertproblem. *Annalen der Phys.*, 384:273, 1926.
- Y. C. Tang and R. C. Herndon. Form factors of  $^3\text{H}$  and  $^4\text{He}$  with repulsive–core potentials. *Phys. Lett.*, 18:42, 1965.

## Chapter 6

# Nuclear Structure with two-nucleon transfer

In what follows, we apply the formalism worked out in the previous chapter with the help of software developed to calculate absolute two-particle transfer differential cross sections, associated with reactions induced by both light and heavy ions (cf. App. 6.D COOPER, ONE, KNOCK-OUT). A number of examples are treated with special detail. Namely, two-particle transfer in light pairing vibrational nuclei, including the halo unstable nucleus  $^{11}\text{Li}$ , in superfluid medium heavy nuclei lying along the stability valley (Sn-isotopes) and in heavy closed shell systems (Pb). In this last case both for light and heavy ion projectiles.

### 6.1 The $^1\text{H}(^{11}\text{Li}, ^9\text{Li})^3\text{H}$ reaction: evidence for phonon mediated pairing

We start by discussing the analysis of the two-neutron pickup reaction  $^1\text{H}(^{11}\text{Li}, ^9\text{Li})^3\text{H}$  (Tanihata, I. et al., 2008). Particular attention is paid to the excitation of the  $1/2^-$  first excited state of  $^9\text{Li}$  lying at 2.69 MeV (cf. Figs. 6.1.1 and 6.1.2). To assess the direct character of the  $1/2^-$  excitation process, the importance of inelastic (cf. Appendix 1E de la introducción inelastic scattering) and knockout (cf. Ch.4) channels were considered and found to be small (see App. 6.B). The results thus provide evidence for a new mechanism of pairing correlations in nuclei: pigmy resonance mediated pairing interaction (Barranco, F. et al. (2001), see also App. 6.A), which strongly renormalizes the bare,  $NN^{-1}S_0$  interaction (Potel et al., 2010). This is but a particular embodiment of phonon mediated pairing interaction found throughout in nuclei (cf. e.g. Barranco et al. (1999); Gori et al. (2004) cf. also Brink, D. and Broglia (2005)). The main difference between light halo exotic nuclei and medium heavy superfluid nuclei lying along the valley of stability is the role fluctuations play in dressing particles (quasiparticles) and in renormalizing their properties (mass, charge, etc.) and their interactions. In fact, in the case of e.g. Sn

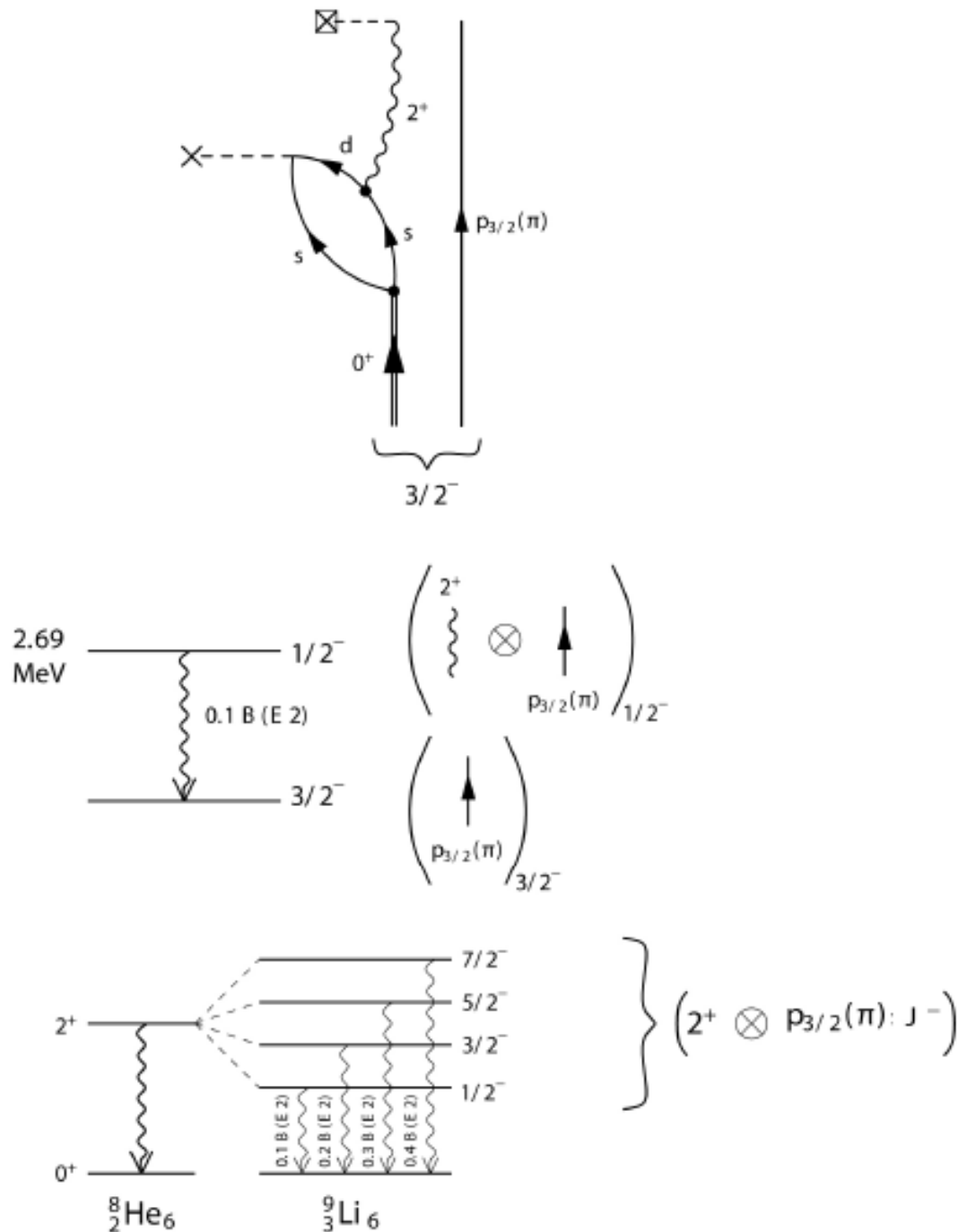


Figure 6.1.1: *Gedanken* (two-particle transfer) coincidence experiments aimed at better individuating the couplings involved in the neutron halo Cooper pair correlations in  $^{11}\text{Li}$  and of the  $1/2^-$  first excited state of  $^9\text{Li}$  populated in the  $^1\text{H}(^{11}\text{Li}, ^9\text{Li})^3\text{H}$  reaction (Barranco, F. et al. (2001); Potel et al. (2010)). From Potel et al. (2014).

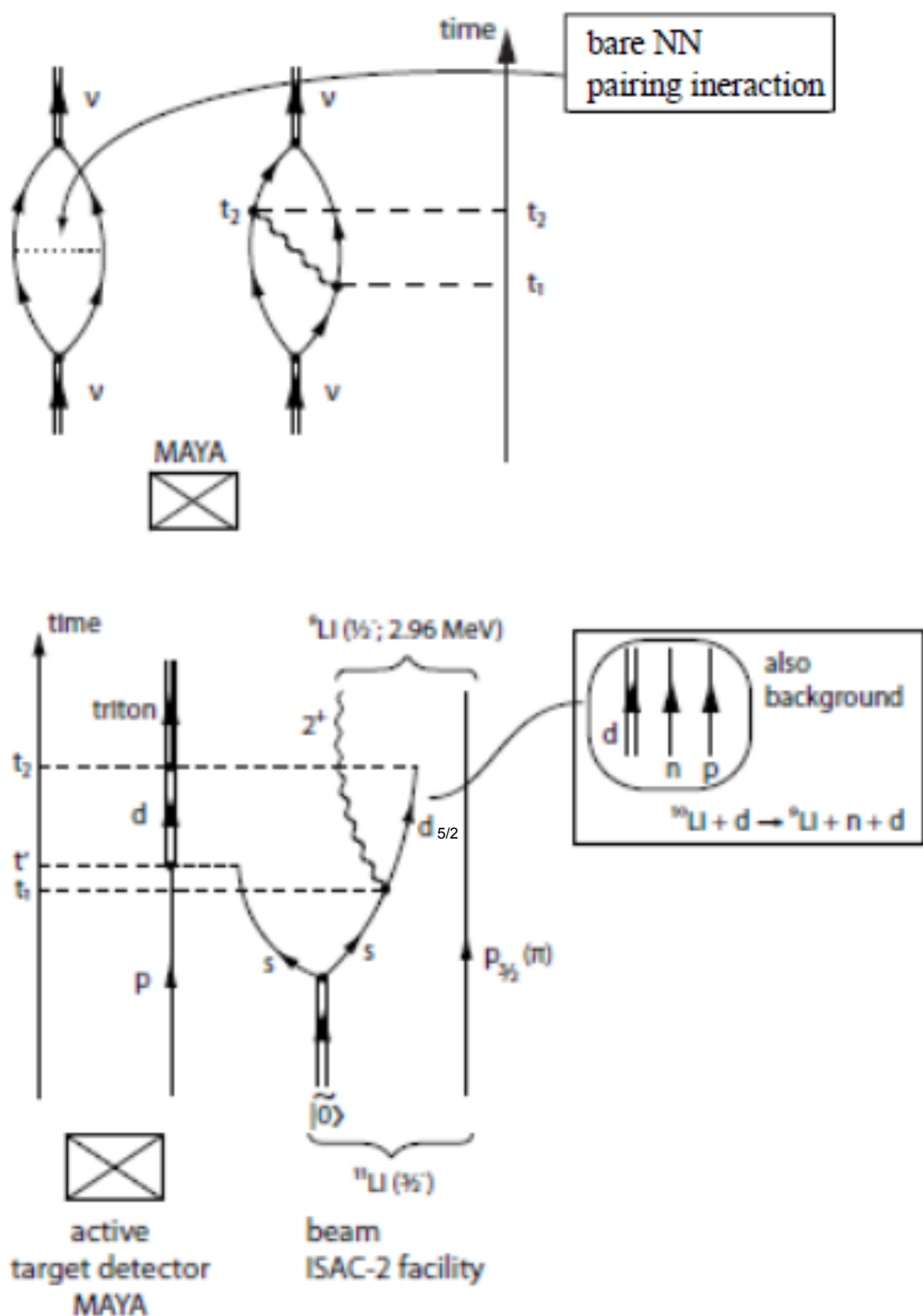


Figure 6.1.2: Schematic representation of the bare nucleon-nucleon and phonon induced pairing correlations (upper part) NFT diagrams, and of the population of the first, excited state of  ${}^9\text{Li}(1/2^-; 2.69 \text{ MeV})$ , in the TRIUMF experiment reported in ref. Tanihata, I. et al. (2008).

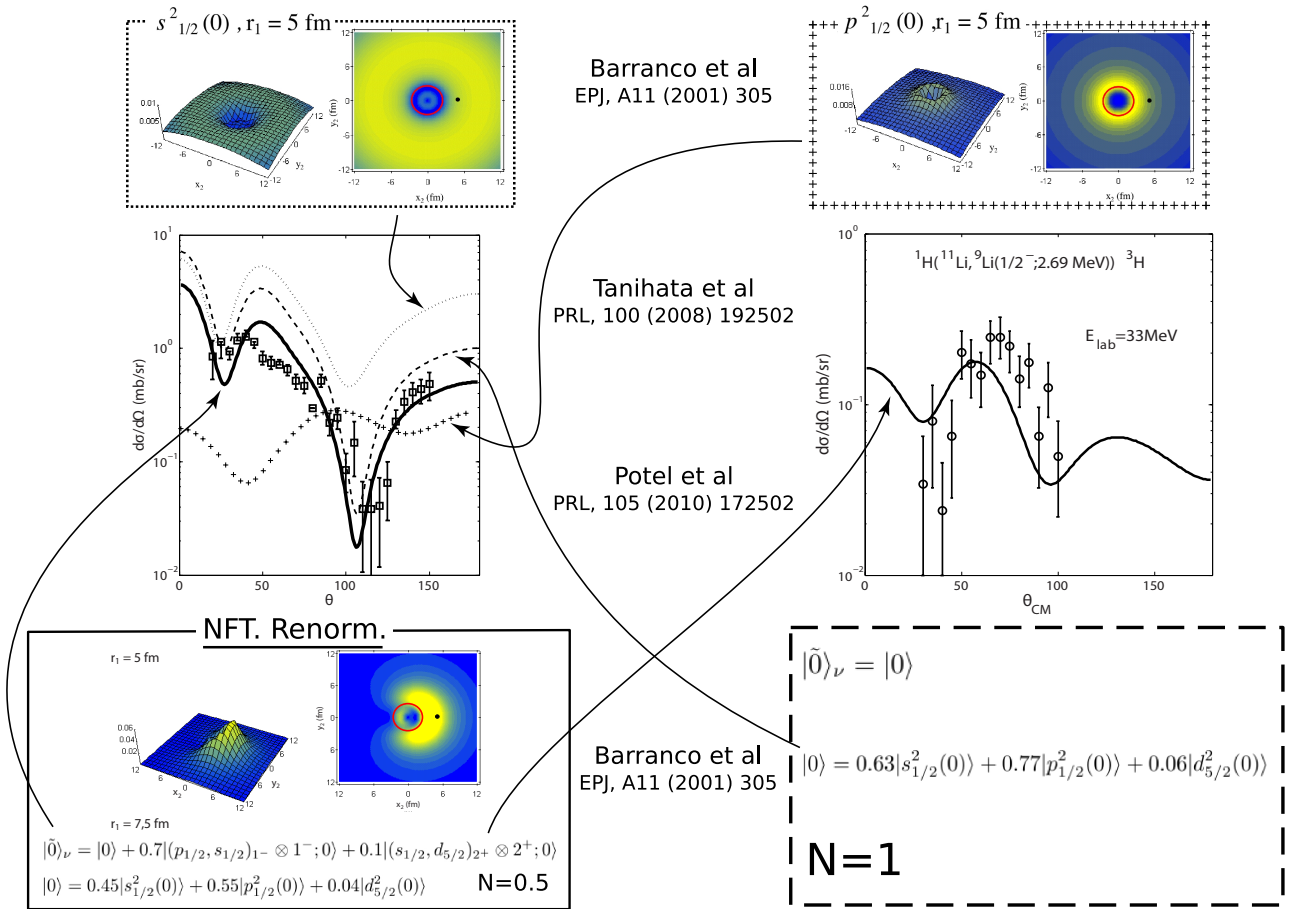


Figure 6.1.3: Absolute, two-nucleon transfer differential cross section associated with the ground state and the first excited state of  ${}^9\text{Li}$ , excited in the reaction  ${}^1\text{H}({}^{11}\text{Li}, {}^9\text{Li}){}^3\text{H}$  (Tanihata, I. et al., 2008) in comparison with the predicted differential cross sections (Potel et al., 2010) calculated making use of spectroscopic amplitudes and Cooper pair wavefunctions calculated in NFT.

isotopes, mean field effects are dominant, while in the case of halo exotic nuclei renormalization effects can be as large as mean field ones.

### 6.1.1 Structure

Within the scenario presented in Chapter 2 (App. 2.F) and Chapter 4 (Sect. 4.2.2) the wavefunction describing the structure of the halo neutrons in the ground state of  $^{11}\text{Li}$  (the  $p_{3/2}$  proton being assumed to act only as a spectator) can be written as

$$|0\rangle_v = |0\rangle + \alpha|(p_{1/2}, s_{1/2})_{1^-} \otimes 1^-; 0\rangle + \beta|(s_{1/2}, d_{5/2})_{2^+} \otimes 2^+; 0\rangle, \quad (6.1.1)$$

with

$$\alpha = 0.7, \quad \text{and} \quad \beta = 0.1, \quad (6.1.2)$$

and

$$|0\rangle = 0.45|s_{1/2}^2(0)\rangle + 0.55|p_{1/2}^2(0)\rangle + 0.04|d_{5/2}^2(0)\rangle, \quad (6.1.3)$$

$|1^-\rangle$  and  $|2^+\rangle$  being the (RPA) states describing the dipole pigmy resonance of  $^{11}\text{Li}$  and the quadrupole vibration of the core. While these states are virtual excitations which, exchanged between the two neutrons bind them to the Fermi surface provided by the  $^9\text{Li}$  core, they can be forced to become real with the help of the specific probe of Cooper pairs in nuclei, namely two-particle transfer reactions (Figs. 6.1.2 and 6.1.3).

$^{11}\text{Li}(p, t)^9\text{Li}$												
	$V$	$W$	$V_{so}$	$W_d$	$r_1$	$a_1$	$r_2$	$a_2$	$r_3$	$a_3$	$r_4$	$a_4$
$p, {}^{11}\text{Li}^d)$	63.62	0.33	5.69	8.9	1.12	0.68	1.12	0.52	0.89	0.59	1.31	0.52
$d, {}^{10}\text{Li}^b)$	90.76	1.6	3.56	10.58	1.15	0.75	1.35	0.64	0.97	1.01	1.4	0.66
$t, {}^9\text{Li}^c)$	152.47	12.59	1.9	12.08	1.04	0.72	1.23	0.72	0.53	0.24	1.03	0.83

Table 6.1.1: Optical potentials (cf. Tanihata, I. et al. (2008)) used in the calculation of the absolute differential cross sections displayed in Fig. 6.1.3.

We are then in presence of a paradigmatic nuclear embodiment of Cooper's model which is at the basis of BCS theory: a single weakly bound neutron pair on top of the Fermi surface of the  $^9\text{Li}$  core. But the analogy goes beyond these aspects, and covers also the very nature of the interaction acting between Cooper pair partners. Due to the the high polarizability of the system under study and of the small overlap of halo and core single particle wavefunctions, most of the Cooper pair correlation energy stems, according to NFT, from the exchange of collective vibrations, the role of the strongly screened bare interaction being, in this case, minor and subcritical (see App. 1F chapter structure in a nutshell). In other words, we are in the presence of a new realization of Cooper's model in which a totally novel Bardeen–Pines–Frölich–like phonon induced interaction is generated by a self induced collective vibration of the nuclear medium. In connection

with (6.1.1), it is revealing that, the two final states excited in the inverse kinematics, two-neutron pick up reaction  ${}^1\text{H}({}^{11}\text{Li}, {}^9\text{Li}){}^3\text{H}$  are, the  $|3/2^-\text{gs}({}^9\text{Li})\rangle$  and the first excited  $|1/2^-, 2.69\text{MeV}\rangle$  Tanihata, I. et al. (2008). In fact, the associated absolute differential cross sections probe, within the NFT scenario, the  $|0\rangle$  and the  $|(s_{1/2}, d_{5/2})_{2+} \otimes 2^+; 0\rangle$  component of the Cooper pair wavefunction respectively, (Fig. 6.1.2 cf. also Figs 4.2.5 and 4.2.6; cf. also Figs. 6.1.3 and 2.F.3 1F3). They were calculated making use of modified formfactors worked out (cf. App. 6.C) making use of the spectroscopic amplitudes given in Eqs. (6.1.1–6.1.3) and of the optical potentials collected in Table 6.1.1 and are compared with the experimental findings in Fig. 6.1.3. Theory reproduces the absolute two-particle differential cross section within experimental errors. But, more important, it provides a general picture of the physics behind the workings of halo pair addition modes.

### 6.1.2 Reaction

Because second order calculations of inelastic, break up and final state interaction channels, which in principle can provide alternative routes for the population of the  $|1/2^-, 2.69\text{MeV}\rangle$  (see Fig. 6.B.1) state to that predicted by the wavefunction (6.1.1) ( $\beta$  component), lead to absolute cross sections which are smaller by few orders of magnitude than that shown in Fig. 6.1.3 (see Figs. 6.B.2, 6.B.3, as well as Table 6.B.1, Potel et al. (2010)), one can posit that quadrupole core polarization effects in  $|\text{gs}({}^{11}\text{Li})\rangle$  is essential to account for the observation of the  $|1/2^-, 2.69\text{ MeV}\rangle$  state, thus providing direct evidence for phonon mediated pairing in nuclei.

The reason why in the case of  ${}^{11}\text{Li}$  evidence for phonon mediated pairing is, arguably, inescapable, is connected with the fact that reaching the limits of stability associated with drip line nuclei, the system also reaches to situations in which medium polarization effects become overwhelming. In fact, one is, in such cases confronted with elementary modes of nuclear excitation in which dynamic fluctuation effects are as important as static, mean field effects. Within this context we refer to parity inversion (cf. Figs. 2.F.3 1F3 and 4.2.4). Nuclear Field Theory within the Bloch–Horowitz (Dyson) set up which allows one to sum to infinite order little convergent processes are specially suited to study these systems (cf. e.g. Barranco, F. et al. (2001) and Gori et al. (2004)). From these studies it emerges a possible new elementary mode of excitation, namely pair addition halo vibration, of which  $|\text{gs}({}^{11}\text{Li})\rangle$  state is a concrete embodiment. They are associated with a novel mechanism for stabilizing Cooper pairs, which arises from a (dynamical) breakup of gauge invariance (cf. App 6.A). Their most distinctive feature, namely that of carrying on top of it a (dipole) pigmy resonance at a relative excitation energy of about 1 MeV, a necessary although not sufficient condition for this new mode to exist, can be instrumental for its characterization. While in the case of Li it constitutes the ground state, in other nuclei it may be an excited state which could be observed in a combined  $L = 0$ , and  $L = 1$ , two-particle transfer reaction to excited states, or in terms of  $E1$  decay of the pigmy resonance built on top of it. Within this context, it is an open question whether one could expect to find a

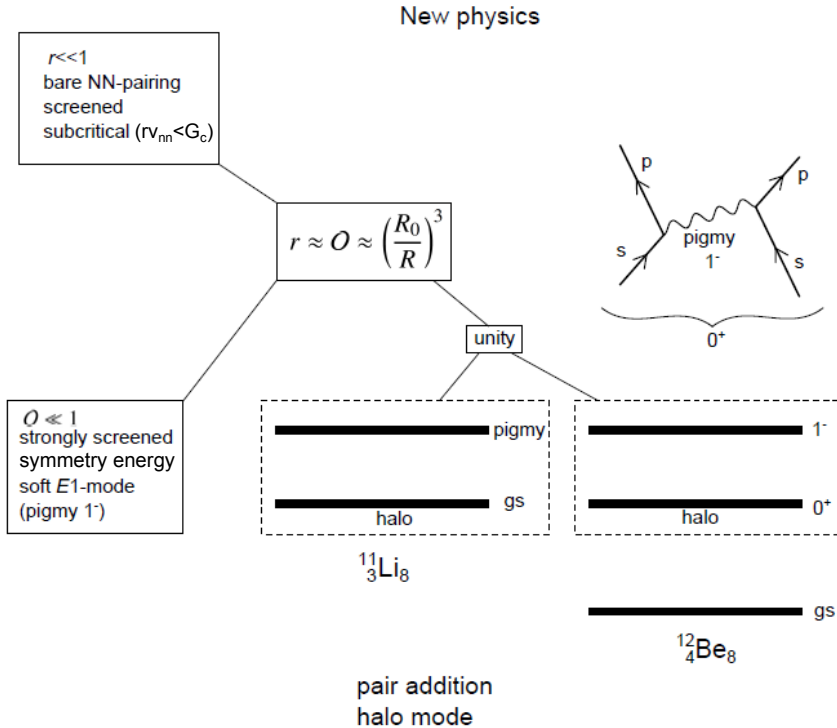


Figure 6.1.4: Schematic representation of a possible realization of halo pair addition mode in terms of the first excited  $0^+$  state of  $^{12}\text{Be}$  (for details see App. 2.F).

realization of such a halo pair addition mode in, for example, the first excited state of  $^{12}\text{Be}$  (see Fig. 6.1.4).

Pairing elementary modes of excitation based on  $s_{1/2}$  and  $p_{1/2}$  states at threshold have been found to lead, within the framework of a bare, short range, pairing interaction scheme to halo anti-pairing effects (cf. Bennaceur, K. et al. (2000), cf. also Hamamoto and Mottelson (2003), Hamamoto, I. and Mottelson (2004)). The fact that the separation energy of the halo neutrons (halo Cooper pair) of  $^{11}\text{Li}(\text{gs})$  is  $\approx 400\text{keV}$ , testifies to the fact that the anti-halo pairing effect is, in this case, overwhelmed by (dynamical) medium polarization effects.

Within this context it is of notice that, again, the interweaving of the different elementary modes of nuclear excitation, pairing and pigmy resonances in the present case, condition reaction studies, let alone the possibility to study (pigmy) giant resonances built on excited states, and to provide a novel test of the Brink-Axel hypothesis which is at the basis of the statistical description of photon decay from hot (compound) nuclei (cf. Brink (1955); cf. also Bortignon, P.F. et al. (1998), Bertsch, G. F. and Broglia (1986) and references therein).

Before concluding this section we provide in Fig. 6.1.5 examples of pairing vibrational states based on  $^9_3\text{Li}_6$ ,  $^{10}_4\text{Be}_6$ ,  $^{48}_{20}\text{Ca}_{28}$  and  $^{208}_{82}\text{Pb}_{126}$ ,  $N = 6$ ,  $N = 28$

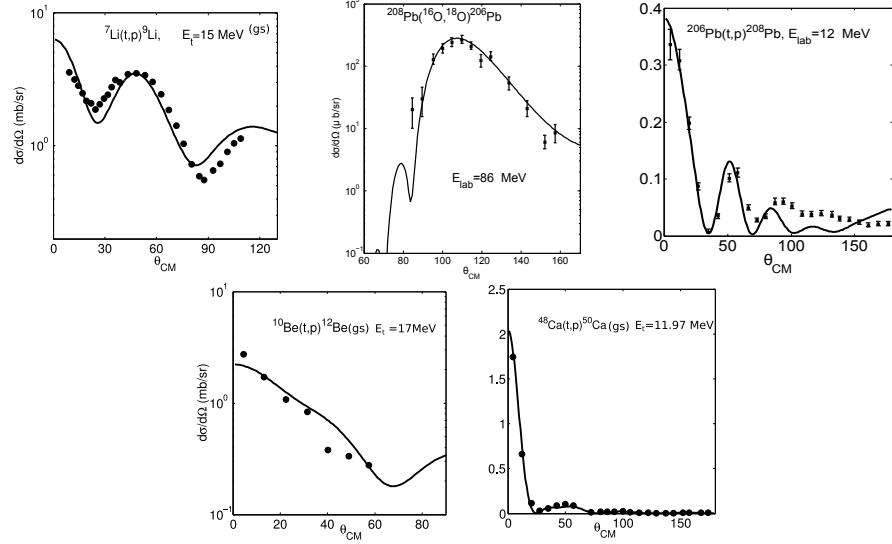


Figure 6.1.5: Absolute two-particle transfer differential cross sections for a number of reactions. Making use of spectroscopic amplitudes calculated as described in App. 2.E 1E in the particular case of  $N = 126$  (Pb),  $N = 48$  (Ca), and  $N = 6$  (Li,Be), of global optical parameters and of the software COOPER, the absolute differential cross sections were calculated and are displayed in comparison with the experimental data (after Potel, G. et al. (2013a)).

and  $N = 126$  neutron closed shell systems. The fact that among the  $(p,t)$  and  $(t,p)$  absolute differential cross sections one also finds the  ${}^{208}\text{Pb}({}^{16}\text{O}, {}^{18}\text{O}){}^{206}\text{Pb(gs)}$  absolute differential cross section is in keeping with the fact that the formalism to treat both light and heavy ions two-nucleon transfer reactions and their connection is well known (cf. Broglia and Winther (2004), Bayman and Chen (1982) and Thompson (1988) and references therein) and rather homogeneous (cf. Potel, G. et al. (2013b)). Thus, it has been implemented in the software COOPER as a standard option (cf. App. 6.D).

## 6.2 Pairing rotational band with two-nucleon transfer: Sn-isotopes

Nuclear superfluidity can be studied at profit in terms of the mean field, (cf. also Sect. 2.D.2) BCS diagonalization of the pairing Hamiltonian, namely,

$$H = H_{sp} + V_p, \quad (6.2.1)$$

where

$$H_{sp} = \sum_{\nu} (\epsilon_{\nu} - \lambda) a_{\nu}^{\dagger} a_{\nu}, \quad (6.2.2)$$

while

$$V_p = -\Delta(P^+ + P) - \frac{\Delta^2}{G}, \quad (6.2.3)$$

and

$$\Delta = G\alpha_0, \quad (6.2.4)$$

is the pairing gap ( $\Delta \approx 12 \text{ MeV}/\sqrt{A}$ ),  $G$  ( $\approx 25 \text{ MeV}/A$ ) being the pairing coupling constant (Bohr, A. and Mottelson, 1975), and

$$P^+ = \sum_{\nu>0} P_\nu^+ = \sum_{\nu>0} a_\nu^+ a_{\bar{\nu}}^+, \quad (6.2.5)$$

$$P = \sum_{\nu>0} a_{\bar{\nu}} a_\nu, \quad (6.2.6)$$

are the pair addition and pair removal operators,  $a_\nu$  and  $a_\nu^+$  being single-particle creation and annihilation operators, ( $\nu\bar{\nu}$ ) labeling pairs of time reversal states.

The BCS ground state wavefunction describing the most favorable configuration of pairs to profit from the pairing interaction, can be written in terms of the product of the occupancy probabilities  $h_\nu$  for individual pairs,

$$|BCS\rangle = \prod_{\nu>0} ((1 - h_\nu)^{1/2} + h_\nu^{1/2} a_\nu^+ a_{\bar{\nu}}^+) |0\rangle, \quad (6.2.7)$$

where  $|0\rangle$  is the fermion vacuum (Schrieffer (1964); Schrieffer, J. R. (1973)).

Superfluidity is tantamount to the existence of a finite average value of the operators (6.2.5), (6.2.6) in this state, that is, to a finite value of the order parameter

$$\alpha_0 = \langle BCS | P^+ | BCS \rangle = \langle BCS | P | BCS \rangle^*, \quad (6.2.8)$$

which is equivalent to Cooper pair condensation. In fact,  $\alpha_0$  gives a measure of the number of correlated pairs in the BCS ground state which in the nuclear case is few units ( $< 10$ ). While the pairing gap (6.2.4) is an important quantity relating theory with experiment,  $\alpha_0$  provides the specific measure of superfluidity. In fact, the matrix elements of the pairing interaction may vanish for specific regions of space, or in the case of specific pairs of time reversal orbits, but this does not necessarily imply a vanishing of the order parameter  $\alpha_0$ , nor the obliteration of superfluidity.

In keeping with the fact that Cooper pair tunneling is proportional to  $|\alpha_0|^2$ , this quantity plays also the role of a ( $L = 0$ ) two-nucleon transfer sum rule, sum rule which is essentially exhausted by the superfluid nuclear  $|BCS\rangle$  ground state (see Fig. 1.1.3 capitulo 1 nuclear structure in a nutshell).

### 6.2.1 Fluctuations

The BCS solution of the pairing Hamiltonian was recasted by Bogoljubov (1958) and Valatin (1958) in terms of quasiparticles,

$$a_\nu^+ = U_\nu a_\nu^+ - V_\nu a_{\bar{\nu}}, \quad (6.2.9)$$

linear transformation inducing the rotation in  $(a^+, a)$ -space which diagonalizes the Hamiltonian (6.2.1).

The variational parameters  $U_\nu, V_\nu$  appearing in the above relation indicate that  $a_\nu^+$  acting on  $|0\rangle$  creates a particle in the state  $|\nu\rangle$  which is empty with a probability  $U_\nu^2 (\equiv (1 - h_\nu) = (1 + (\epsilon_\nu - \lambda)/E_\nu)/2)$ , and annihilates a particle in the time reversal state  $|\bar{\nu}\rangle$  (creates a hole) which is occupied with probability  $V_\nu^2 (\equiv h_\nu = (1 - (\epsilon_\nu - \lambda)/E_\nu)/2)$ . Thus,

$$|BCS\rangle = \Pi_{\nu>0} (U_\nu + V_\nu a_\nu^+ a_{\bar{\nu}}^+) |0\rangle, \quad (6.2.10)$$

is the quasiparticle vacuum, as  $|BCS\rangle \sim \Pi_\nu \alpha_\nu |0\rangle$ , the order parameter being

$$\alpha_0 = \sum_{\nu>0} U_\nu V_\nu. \quad (6.2.11)$$

Making use of these results we collect in Table 6.2.1 the spectroscopic amplitudes associated with the reactions  $^{A+2}\text{Sn}(p,t)^A\text{Sn}$ , for  $A$  in the interval 112–126.

### 6.2.2 Pairing rotations

	$^{112}\text{Sn}$	$^{114}\text{Sn}$	$^{116}\text{Sn}$	$^{118}\text{Sn}$	$^{120}\text{Sn}$	$^{122}\text{Sn}$	$^{124}\text{Sn}$
$1d_{5/2}$	0.664	0.594	0.393	0.471	0.439	0.394	0.352
$0g_{7/2}$	0.958	0.852	0.542	0.255	0.591	0.504	0.439
$2s_{1/2}$	0.446	0.477	0.442	0.487	0.451	0.413	0.364
$1d_{3/2}$	0.542	0.590	0.695	0.706	0.696	0.651	0.582
$0h_{11/2}$	0.686	0.720	1.062	0.969	1.095	1.175	1.222

Table 6.2.1: Two-nucleon transfer spectroscopic amplitudes  $\langle BCS(A)|P_\nu|BCS(A+2)\rangle = \sqrt{(2j_\nu + 1)/2} U_\nu(A) V_\nu(A+2)$ , associated with the reactions connecting the ground states (members of a pairing rotational band) of two superfluid Sn-nuclei  $^{A+2}\text{Sn}(p,t)^A\text{Sn}(\text{gs})$  (Potel, G. et al. (2013a)).

The phase of the ground state BCS wavefunction may be chosen so that  $U_\nu = |U_\nu| = U'_\nu$  is real and  $V_\nu = V'_\nu e^{2i\phi}$  ( $V'_\nu \equiv |V_\nu|$ ). Thus (Schrieffer, J. R., 1973),

$$\begin{aligned} |BCS(\phi)\rangle_{\mathcal{K}} &= \Pi_{\nu>0} (U'_\nu + V'_\nu e^{-2i\phi} a_\nu^+ a_{\bar{\nu}}^+) |0\rangle = \Pi_{\nu>0} (U'_\nu + V'_\nu a_\nu^{' +} a_{\bar{\nu}}^{' +}) |0\rangle \\ &= |BCS(\phi = 0)\rangle_{\mathcal{K}'}, \end{aligned} \quad (6.2.12)$$

where  $a_\nu^{' +} = e^{-i\phi} a_\nu^+$  and  $a_{\bar{\nu}}^{' +} = e^{-i\phi} a_{\bar{\nu}}^+$ . This is in keeping with the fact that  $a_\nu^+$  and  $a_{\bar{\nu}}^+$  are single-particle creation operators which under gauge transformations (rotations in the 2D-gauge space of angle  $\phi$ ) induced by the operator  $G(\phi) = e^{-i\hat{N}(\phi)}$  and connecting the intrinsic and the laboratory frames of reference  $\mathcal{K}'$  and  $\mathcal{K}$  respectively, behave according to  $a_\nu^{' +} = G(\phi) a_\nu^+ G^{-1}(\phi) = e^{-i\phi} a_\nu^+$  and  $a_{\bar{\nu}}^{' +} = G(\phi) a_{\bar{\nu}}^+ G^{-1}(\phi) = e^{-i\phi} a_{\bar{\nu}}^+$ , a consequence of the fact that  $\hat{N}$  is the number operator and that  $[\hat{N}, a_\nu^+] = a_\nu^+$ .

The fact that the mean field ground state  $(|BCS(\phi)\rangle_{\mathcal{K}})$  is a product of operators - one for each pair state - acting on the vacuum, implies that (6.2.12) represents an

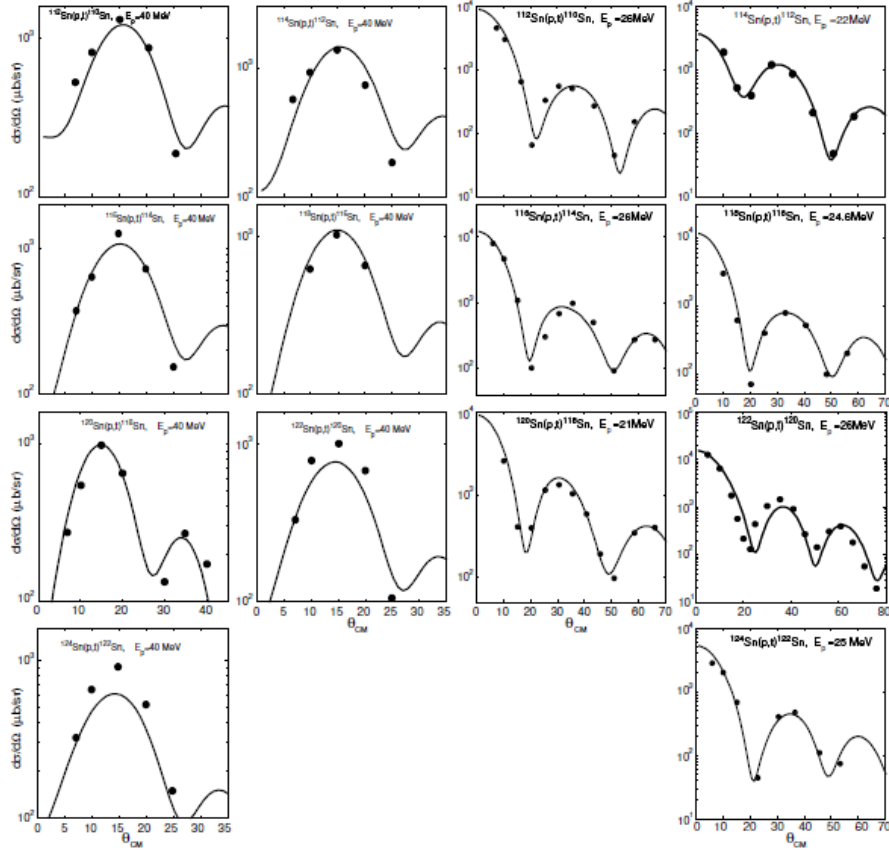


Figure 6.2.1: Predicted (Potel, G. et al. (2013a,b)) absolute differential  $^{A+2}\text{Sn}$  ( $p, t$ ) $^A\text{Sn}(\text{gs})$  cross sections for bombarding energies  $E_p=40$  MeV (in the two left columns) and  $21 \text{ MeV} \leq E_p \leq 26$  MeV (in the two right columns) in comparison with the experimental data (Bassani et al. (1965), Guazzoni, P. et al. (1999), Guazzoni, P. et al. (2004), Guazzoni, P. et al. (2006), Guazzoni, P. et al. (2008), Guazzoni, P. et al. (2011), Guazzoni, P. et al. (2012)).

${}^A\text{Sn}(p,t){}^{A-2}\text{Sn}$												
	$V$	$W$	$V_{so}$	$W_d$	$r_1$	$a_1$	$r_2$	$a_2$	$r_3$	$a_3$	$r_4$	$a_4$
$p, {}^A\text{Sn}^a)$	50	5	3	6	1.35	0.65	1.2	0.5	1.25	0.7	1.3	0.6
$d, {}^{A-1}\text{Sn}^b)$	78.53	12	3.62	10.5	1.1	0.6	1.3	0.5	0.97	0.9	1.3	0.61
$t, {}^{A-2}\text{Sn}^a)$	176	20	8	8	1.14	0.6	1.3	0.5	1.1	0.8	1.3	0.6

Table 6.2.2: Optical potentials used in the calculations of the absolute differential cross sections displayed in Fig. 6.2.1.

ensemble of ground state wavefunctions averaged over systems with ... $N-2, N, N+2$ ... even number of particles. In fact, (6.2.12) can also be written in the form

$$\begin{aligned} |BCS\rangle_{\mathcal{K}} = & (\Pi_{\nu>0} U'_\nu) (1 + \dots + \frac{e^{-(N-2)i\phi}}{\left(\frac{N-2}{2}\right)!} \left( \sum_{\nu>0} c_\nu a_\nu^+ a_\nu^+ \right)^{\frac{N-2}{2}} + \frac{e^{-Ni\phi}}{\left(\frac{N}{2}\right)!} \left( \sum_{\nu>0} c_\nu a_\nu^+ a_\nu^+ \right)^{\frac{N}{2}} \\ & + \frac{e^{-(N+2)i\phi}}{\left(\frac{N+2}{2}\right)!} \left( \sum_{\nu>0} c_\nu a_\nu^+ a_\nu^+ \right)^{\frac{N+2}{2}} + \dots) |0\rangle, \end{aligned} \quad (6.2.13)$$

where  $c_\nu = V'_\nu / U'_\nu$ .

Adjusting the Lagrange multiplier  $\lambda$  (chemical potential, see Eqs. (6.2.9, 6.2.10) and associated text), one can ensure that the mean number of fermions has the desired value  $N_0$ . Summing up, the BCS ground state is a wavepacket in the number of particles. In other words, it is a deformed state in gauge space defining a privileged orientation in this space, and thus an intrinsic coordinate system  $\mathcal{K}'$  (Anderson, 1958; Bohr, 1964; Bès, D. R. and Broglia, 1966). The magnitude of this deformation is measured by  $\alpha_0$ .

### 6.2.3 Pairing vibrations in superfluid nuclei

All the above arguments, point to a static picture of nuclear superfluidity which results from BCS theory. This is quite natural, as one is dealing with a mean field approximation. The situation is radically changed taking into account the interaction acting among the Cooper pairs (quasiparticles) which has been neglected until now, that is the term  $-G(P^+ - \alpha_0)(P - \alpha_0)$  left out in the mean field (BCS) approximation leading to (6.2.3). This interaction can essentially be written as (for details see e.g. Brink, D. and Broglia (2005) Apps. G, I and J and references therein)

$$H_{\text{residual}} = H'_p + H''_p, \quad (6.2.14)$$

where

$$H'_p = -\frac{G}{4} \left( \sum_{\nu>0} (U_\nu^2 - V_\nu^2)(P_\nu^+ + P_\nu^-) \right)^2, \quad (6.2.15)$$

and

$$H_p'' = \frac{G}{4} \left( \sum_{\nu>0} (P^+ - P) \right)^2. \quad (6.2.16)$$

The term  $H_p'$  gives rise to vibrations of the pairing gap which (virtually) change particle number in  $\pm 2$  units. The energy of these pairing vibrations cannot be lower than  $2\Delta$ . They are, as a rule, little collective, corresponding essentially to almost pure two-quasiparticle excitations (see excited  $0^+$  states of Fig. 1.1.3 structure in a nutshell).

The term  $H_p''$  leads to a solution of particular interest, displaying exactly zero energy, thus being degenerate with the ground state. The associated wavefunction is proportional to the particle number operator and thus to the gauge operator inducing an infinitesimal rotation in gauge space. The fluctuations associated with this zero frequency mode diverge, although the Hamiltonian defines a finite inertia. A proper inclusion of these fluctuations (of the orientation angle  $\phi$  in gauge space) restores gauge invariance in the  $|BCS(\phi)\rangle_{\mathcal{K}}$  state leading to states with fixed particle number

$$|N_0\rangle \sim \int_0^{2\pi} d\phi e^{iN_0\phi} |BCS(\phi)\rangle_{\mathcal{K}} \sim \left( \sum_{\nu>0} c_{\nu} a_{\nu}^+ a_{\bar{\nu}}^+ \right)^{N_0/2} |0\rangle. \quad (6.2.17)$$

These are the members of the pairing rotational band, e.g. the ground states of the superfluid Sn-isotope nuclei. These states provide the nuclear embodiment of Schrieffer's ensemble of ground state wavefunctions which is at the basis of the BCS theory of superconductivity. An example of such a rotational band is provided by the ground states of the Sn-isotopes (cf. Fig. 1.1.3 pairing in a nutshell). Making use of COOPER, namely of an implementation of two-nucleon transfer second order DWBA which includes successive and simultaneous transfer, properly corrected from non-orthogonality contributions, of the spectroscopic amplitudes collected in table 6.2.1 (see also Table 1D1 chapter 1 structure in a nutshell), and of global optical parameters from the literature (see Table 6.2.2), the two-nucleon transfer absolute differential cross sections associated with the Sn-isotopes rotational band have been calculated. They are compared with the experimental findings in Fig. 6.2.1 (cf. also Fig. 2.2.1 1.1.5 and Potel, G. et al. (2013a,b)).

### 6.3 BCS correlation (Cooper pair)

The specific probe to quantitative test how much BCS-like correlated are two nucleons (nucleon holes) moving on top of the Fermi surface (in the Fermi sea) and interacting through an attractive pairing force, nuclear embodiment of a Cooper pair and known as pair addition (pair removal) modes (Bohr, A. and Mottelson (1975), Bès, D. R. and Broglia (1966)), is through two-nucleon transfer processes, e.g. through a  $(p, t)$  ( $a(t, p)$ ) reaction, like e.g.  ${}^1\text{H}({}^{11}\text{Li}, {}^9\text{Li(gs)}) {}^3\text{H}$  ( ${}^{206}\text{Pb}(t, p) {}^{208}\text{Pb}$ ).

Let us start discussing the second one. In Fig. 3.A.4 we show the predictions of the pairing vibrational model in comparison with the experimental data (Bjergaard, J. H. et al. (1966)). The calculations were carried out making use of the software COOPER and of the spectroscopic amplitudes collected in Tables 2.E.2 and 2.E.3, and corresponding to the RPA,  $X$ - and  $Y$ - amplitudes associated with  $^{208}\text{Pb}$  pair removal mode, i.e. describing the ground state  $^{206}\text{Pb}$  (two holes interacting via a pairing force of constant matrix element, and allow to move in the single-particle valence states). The global optical parameters for the proton and the triton were taken from the experimental paper, while those of the deuteron channel needed in COOPER to work out the successive transfer amplitude was taken from (An and Cai (2006)). Theory provides an overall account of the experiment findings (RPA  $\sigma = 0.52\text{mb}$  to be compared with the experimental finding  $0.68 \pm 0.24 \text{ mb}$ ).

the large cross section, also for the pair addition mode, that is, associated with the population of the two-phonon ( $2p - 2h$ ) pairing vibrational state of  $^{208}\text{Pb}$  ( $0^+$ ; 4.95 MeV) was interpreted in Bertsch, G. F. et al. (1967) in terms of the angular correlation between the two fermions (holes) displayed in figure 7 of this reference (cf. also Figs. 2.4 and 2.5 Brink, D. and Broglia (2005)). By plotting the modulus square of the two-hole wavefunction as a function of one coordinate leaving the other fixed (both lying on the  $z$ -axis) it was shown that while  $j^2(0)$  displays a symmetric distribution for  $\Omega_{12} = 0^\circ$  and  $180^\circ$ , the correlated state displays an enhancement at  $\Omega = 0^\circ$ .

The fact that in the analysis of Broglia and Riedel (1967) only simultaneous transfer was considered, corroborated the connection between pairing collectivity, closeness of the two nucleons and thus the large cross sections. A further corroboration seems to emerge from the fact that TD (neglect of ground state correlations), let alone the pure two-hole configuration  $|s_{1/2}^{-2}(0)\rangle$  give rise to cross sections which are smaller than that predicted by the full correlated state (Fig. 3.A.4). Now, as can be seen from the inset of this figure, most of the absolute cross section arises from successive transfer, a sobering result. Within this context, let us now comment on the reaction  $^1\text{H}(^{11}\text{Li}, ^9\text{Li(gs)})^3\text{H}$ . As seen from the  $|\Psi(\mathbf{r}_1, \mathbf{r}_2)|^2$  plots of the halo Cooper pair wavefunction displayed in Figs. 2.F.3 and 6.1.3, the correlation between the two pairing interacting neutrons is evident. Similarly the lack of correlation of the pure, angular momentum coupled configurations  $|s_{1/2}^2(0)\rangle$  and  $|p_{1/2}^2(0)\rangle$ . Now, the results reported in Fig. 6.1.3 calculated making use of the NFT results (6.1.1)–(6.1.3) and the optical potentials of Tanihata, I. et al. (2008) (those of An and Cai (2006) for the deuteron channel) reproduced the observations within the experimental findings. Again in this case, most of the absolute two-nucleon transfer differential cross section is connected with successive transfer (cf. Figs. 6.B.2 and 6.B.3). But not only this. While in the present case the absolute cross section associated with the pure  $|p_{1/2}^2(0)\rangle$  configuration is about an order of magnitude smaller than that associated with the full wavefunction (and thus also experiment), as observed in connection with  $^{206}\text{Pb}(t, p)^{208}\text{Pb(gs)}$ , that associated with the  $|s_{1/2}^2(0)\rangle$  pure configuration overpredicts the data by an order of

magnitude. This in spite of the fact that, as seen from the left, top corner of the two-dimensional plot of this configuration, the two nucleons are as far as they can be from each other. This result is due to the fact that the  $p_{1/2}^2(0)$  is a cold configuration (small  $S = 0$  component) while  $s_{1/2}^2(0)$  is a hot one (large  $S = 0$  component) (?). Furthermore the density associated with the two halo neutrons is much lower than that associated with the core nucleons, implies that in average, they're much further away than nucleons in a “normal” ( $R_0 = 1.2A^{1/3}$  fm-like) nucleus, being able thus to lower the relative momentum, without for that fact loosing their coherence, nor the associated conspicuous ability to tunnel as a single entity (absolute  $(p, t)$  cross section). In fact  $\sigma(^{11}\text{Li}(p, t)^9\text{Li(gs)}) \approx 5.7 \pm 0.9$  mb (cf. Fig. 6.B.2), to be compared to  $\sigma(^{206}\text{Pb}(t, p)^{208}\text{Pb(gs)}) \approx 0.68 \pm 0.24$  mb.

Summarizing up, the two halo neutrons of  $^{11}\text{Li}$  are likely to provide a paradigm of nuclear Cooper pairs: delicate (soap bubble like) extended objects with low relative momentum behaving in tunneling processes as an entity, in keeping with their unique emergent property: generalized gauge rigidity, similarly present in collective pairing vibrational (dynamic) as pairing rotational situations (within this context cf. also Apps. 6.G, 6.H and 6.I).

One can conclude this section by stating that its title could, as well having been that of “prejudices revisited”, prejudices that the senior author of this monograph have helped foster for a long time.

## Appendix 6.A Bootstrap particle–phonon mechanism to spontaneously break gauge invariance

In this Appendix we discuss a gedanken experiment, aimed at clarifying the bootstrap pairing mechanism resulting in the binding of the neutron halo of  $^{11}\text{Li}$ .

### 6.A.1 Gedanken eksperiment

Let us assume that one shines a low-energy neutron beam on a  $^9\text{Li}$  target. If these neutrons felt only the associated single-particle mean field, they will go by essentially as fast as they came in. However, part of the time pairs of these neutrons will bound themselves in presence of phonon (bosonic) excitations of quadrupole and of (pygmy) dipole character, produced also by the field the two neutron create themselves. The first of these collective modes is associated with vibrations of the (even)  $^8\text{He}$  core, the second resulting from the sloshing back and forth of the strongly non-local field of two (passing by) neutrons of the beam, together with the neutrons, and against the protons, of the core. Such possibility implies that, for a short time, of the order of the traversal time, the two (unbound) neutrons will move in a gas of virtual bosonic excitations, also made out of dipole pygmy resonances. Consequently, they can get dressed becoming heavier (lighter), as well as getting correlated by exchanging these bosonic collective vibrations. The first phenomenon is associated, as discussed above, with phononic backflow (Pauli prin-

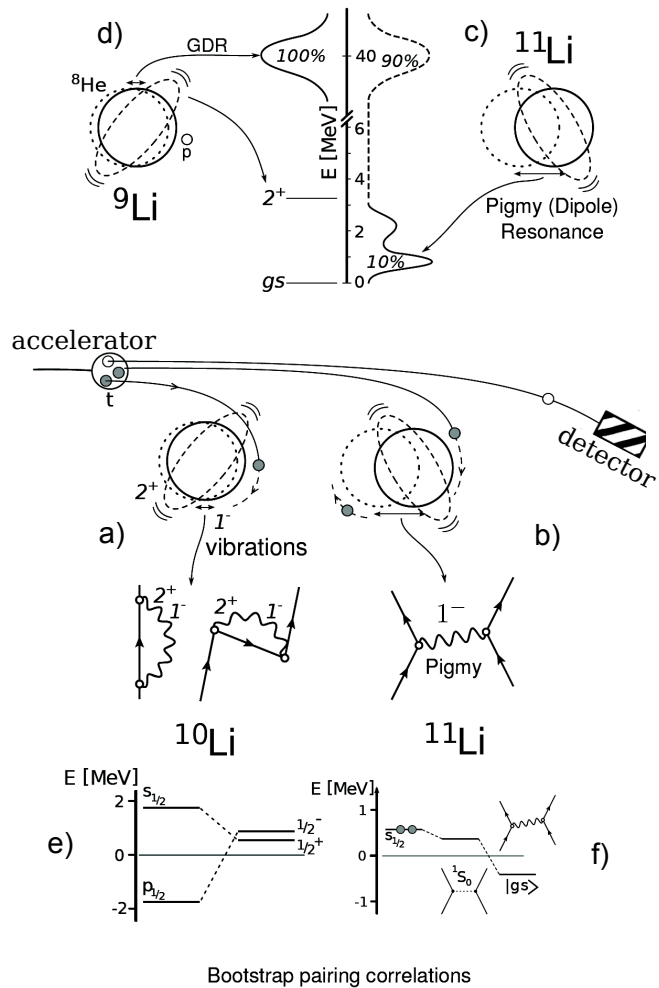


Figure 6.A.1: Schematic representation of the collective quadrupole and dipole response of lithium isotopes, and of a ( $t, p$ ) reaction (in the text one reasons in terms of flux of low energy neutrons) in which two neutrons are transferred to  $^{9}\text{Li}$  (see also Fig. 6.1.3).

ciple upflow) leading to  $^{10}\text{Li}$ -like quasi-bound ( $s$ -wave) and resonant ( $p$ -wave) dressed single-particle states displaying parity inversion. The second phenomenon, mediated by phonon exchange between halo neutrons, contributes in a major way to the glue which binds the neutron halo Cooper pair to the  $^{9}\text{Li}$  core. Within the above scenario, one can posit that the  $^{11}\text{Li}$  dipole pigmy resonance can hardly be viewed but in symbiosis with the  $^{9}\text{Li}$  halo neutron pair addition mode. The above described bootstrap phonon-exchange mechanism can be viewed as a novel microscopic embodiment of the Bardeen–Pines–Frölich-like processes to spontaneously

break gauge invariance<sup>1</sup>.

To conclude, let us comment on Fig. 6.A.1. As said above, (a) the dressing of single-particle levels by collective vibrations and (b) the renormalization of the bare  $NN$ -interaction, in particular of the pairing interaction, through the exchange of these modes between nucleons moving in time reversal states lying close to the Fermi energy, play a central role in nuclear structure. In particular, in the case of the single Cooper pair system  $^{11}\text{Li}$ , most of the glue is provided by the exchange of the pigmy resonance, namely a low-lying isovector dipole vibration. The pigmy resonance (c) is a chunk of the GDR of the core  $^9\text{Li}$  (d) and arises from radial inhomogeneous damping. This mode is intimately related to the spontaneous symmetry breaking of space homogeneity associated with the fact that the center of mass of a finite system like the atomic nucleus, specifies a privileged position in space. While  $^3\text{Li}_6$  is bound,  $^3\text{Li}_7$  is not. (e) through renormalization processes, the  $p_{1/2}$  bound state is shifted to higher energies from that predicted by a standard mean field potential, while the  $s_{1/2}$  continuum state is lowered to an energy close, below that of the  $p_{1/2}$  state. (f) While the screened bare pairing interaction is subcritical, the exchange of vibrations between the halo neutrons is able to, weakly, bind the system.

## Appendix 6.B Table 1 PRL

The  $1/2^-$  (2.69 MeV) first excited state of  $^9\text{Li}$  can in principle, not only be populated through a two-particle transfer process, but also through a break up process in which one (see Fig. 6.B.1(f)), or both neutrons (see Fig. 6.B.1(g)) are forced into the continuum for then eventually one of them to fall into the  $1p_{3/2}$  orbital of  $^9\text{Li}$  and excite the quadrupole vibration of the core (Potel et al. (2010)), in keeping with the fact that the main RPA amplitude of this state is precisely  $X(1p_{3/2}^{-1}, 1p_{1/2})(\approx 1)$  (cf. ref Barranco, F. et al. (2001)). The remaining channel populating the first excited state of  $^9\text{Li}$  is associated with an inelastic process (see Fig. 6.B.1(h)): two-particle transfer to the ground state of  $^9\text{Li}$  and Final State (inelastic scattering) Interaction (FSI) between the outgoing triton and  $^9\text{Li}$  in its ground state, resulting in the inelastic excitation of the  $1/2^-$  state.

Making use of the wavefunctions of Barranco, F. et al. (2001) and of a software developed on purpose to take into account microscopically all the different processes mentioned above, that is 9 different reaction channels (cf. caption to Table 6.B.1) and continuum states up to 50 MeV of excitation energy, the corresponding transfer amplitudes and associated probabilities  $p_l$  were calculated.

In Table 6.B.1 are displayed the probabilities  $p_l = |S_l^{(c)}|^2$  associated with each of the processes discussed above, where the amplitude  $S_l^{(c)}$  is related to the total cross section associated with each of the channels  $c$  by the expression (Satchler,

---

<sup>1</sup>Bootstrapping or booting. The term is often attributed to Rudolf Erich Raspe's story The surprising Adventures of Baron Münchhausen, where the main character pulls himself out of a swamp by his hair. Early 19th century USA: "pull oneself over a fence by one's bootstraps"

$l \backslash c$	<b>1</b>	<b>2</b>	<b>3</b>	<b>4</b>	<b>5</b>
0	$4.35 \times 10^{-3}$	$1.79 \times 10^{-4}$	$4.81 \times 10^{-6}$	$2.90 \times 10^{-11}$	$3.79 \times 10^{-8}$
1	$3.50 \times 10^{-3}$	$9.31 \times 10^{-4}$	$1.47 \times 10^{-5}$	$1.87 \times 10^{-9}$	$1.09 \times 10^{-6}$
2	$7.50 \times 10^{-4}$	$8.00 \times 10^{-5}$	$2.45 \times 10^{-5}$	$1.25 \times 10^{-8}$	$1.21 \times 10^{-6}$
3	$6.12 \times 10^{-4}$	$9.81 \times 10^{-5}$	$1.51 \times 10^{-6}$	$6.50 \times 10^{-10}$	$2.20 \times 10^{-7}$
4	$1.10 \times 10^{-4}$	$1.18 \times 10^{-5}$	$2.21 \times 10^{-7}$	$4.80 \times 10^{-11}$	$1.46 \times 10^{-8}$
5	$3.65 \times 10^{-5}$	$2.16 \times 10^{-7}$	$7.42 \times 10^{-9}$	$6.69 \times 10^{-13}$	$9.63 \times 10^{-10}$
6	$1.35 \times 10^{-5}$	$6.05 \times 10^{-8}$	$2.88 \times 10^{-10}$	$8.04 \times 10^{-15}$	$1.08 \times 10^{-11}$
7	$4.93 \times 10^{-6}$	$7.78 \times 10^{-8}$	$6.01 \times 10^{-11}$	$4.05 \times 10^{-16}$	$5.26 \times 10^{-13}$
8	$2.43 \times 10^{-6}$	$2.62 \times 10^{-8}$	$7.4 \times 10^{-12}$	$1.26 \times 10^{-17}$	$9.70 \times 10^{-11}$

Table 6.B.1: Probabilities  $p_l$  associated with the processes described in the text for each partial wave  $l$ . The different channels are labeled by a channel number  $c$  equal to: **1**, multistep transfer to the  ${}^9\text{Li}$  ground state (Fig. 6.B.1(d)); **2**, multistep transfer (Fig. 6.B.1(e)) to the first excited  ${}^9\text{Li}$  state, **3**, breakup (Fig. 6.B.1(f)), **4**, breakup (Fig. 6.B.1(g)), and **5** inelastic processes (Fig. 6.B.1(h)) involved in the population of the  $1/2^-$  (2.69 MeV) first excited state of  ${}^9\text{Li}$ . Of notice that the probabilities displayed in columns **1** and **2** result from the (coherent) sum of three amplitudes namely those associated with successive, simultaneous and non-orthogonality transfer channels (see also Fig. 6.B.3) after Potel et al. (2010).

1980; Landau and Lifshitz, 1981)

$$\sigma_c = \frac{\pi}{k^2} \sum_l (2l+1) |S_l^{(c)}|^2, \quad (6.B.1)$$

$k$  being the wave number of the relative motion between the reacting nuclei.

In keeping with the small values of  $p_l$ , in what follows we take into account the interference between the contributions associated with the different reaction paths making use of second order perturbation theory, instead of a coupled channel treatment (cf. e.g. Ascuitto and Glendenning (1969) Tamura, T. et al. (1970) Khoa and von Oertzen (2004) Keeley et al. (2007) Thompson (1988)). In particular in the case of the  $1/2^-$  (2.69 MeV) first excited state of  ${}^9\text{Li}$ ,

$$\frac{d\sigma}{d\Omega}(\theta) = \frac{\mu^2}{16\pi^3 \hbar^4} \left| \sum_l (2l+1) P_l(\theta) \sum_{c=2}^5 T_l^{(c)} \right|^2, \quad (6.B.2)$$

where  $\mu$  is the reduced mass and  $T_l^{(c)}$  are the transition matrix elements (in the DWBA Satchler (1980)) associated with the different channels and for each partial wave.

Making use of all the elements discussed above, multistep transfer (see e.g. Bayman and Chen (1982), Igarashi et al. (1991), Bayman and Feng (1973) as well

as Broglia and Winther (2004)), breakup and inelastic channels were calculated, and the results displayed in Figs. 6.B.2 and 6.B.3 and in Table 6.B.1. Theory provides an overall account of the experimental findings. In particular, in connection with the  $1/2^-$  state, this result essentially emerges from cancellations and coherence effects taking place between the three terms contributing to the multistep two-particle transfer cross section (see Fig. 6.B.3), tuned by the nuclear structure amplitudes associated with the process shown in Fig. 6.B.1 (e) as well as Eqs. (6.1.1)–(6.1.3). In fact, and as shown in Figs. 6.B.2 and 6.B.3, the contributions of break up processes and inelastic (Figs. 6.B.1(f),(g) and (h) respectively) to the population of the  $1/2^-$  (2.69 MeV) first excited state of  $^9Li$  are negligible as compared with the process depicted in Fig. 6.B.1(e). In the case of the breakup channel (Figs. 6.B.1(f) and 6.B.1(g)) this is a consequence of the low bombarding energy of the  $^{11}Li$  beam (inverse kinematics), combined with the small overlap between continuum (resonant) neutron  $p_{1/2}$  wavefunctions and bound state wavefunctions. In the case of the inelastic process (Fig. 6.B.1(h)), it is again a consequence of the relative low bombarding energy. In fact, the adiabaticity parameters  $\xi_C, \xi_N$  (see eqs. (IV.12) and (IV.14) of ref. Broglia and Winther (2004)) associated with Coulomb excitation and inelastic excitation in the  $t+^9Li$  channel are larger than 1, implying an adiabatic cutoff. In other words, the quadrupole mode is essentially only polarized during the reaction but not excited. The situation is quite different in the case of the intervening of the virtual processes displayed in Fig. 6.B.1 (b) and (c) leading to the population of the  $1/2^-$  state displayed in Fig. 6.B.1 (e). Being those off-the-energy shell processes, energy is not conserved, and adiabaticity gets profoundly modified.

## Appendix 6.C Modified formfactor associated with the reactions $^1H(^{11}Li, ^9Li(gs))^3H$ and $^1H(^{11}Li, ^9Li(1/2^-; 2.69 \text{ MeV})^3H$ state

## Appendix 6.D Software

In this Appendix we provide a brief description of the numerical methods implemented in the code written to evaluate the differential cross sections. The two-nucleon transfer differential cross section is given by Eq. (5.1.4), so the principal task consist in calculating the transfer amplitudes  $T^{(1)}(\theta)$ ,  $T_{succ}^{(2)}(\theta)$  and  $T_{NO}^{(2)}(\theta)$  described in Eqs. 5.1.5a–5.1.5c, by numerically evaluating the corresponding integrals. The dimensionality of the integrals can be reduced by expanding in partial waves (eigenfunctions of the angular momentum operator) the distorted waves and wavefunctions present in the corresponding integrands. The resulting expressions are Eqs. (5.2.36) and (5.2.37) for  $T^{(1)}(\theta)$ , Eqs. (5.2.128), (5.2.129) and (5.2.130) for  $T_{succ}^{(2)}(\theta)$ , and Eqs. (5.2.154), (5.2.155) and (5.2.156) for  $T_{NO}^{(2)}(\theta)$ . The integrals are computed numerically with the method of Gaussian quadratures.

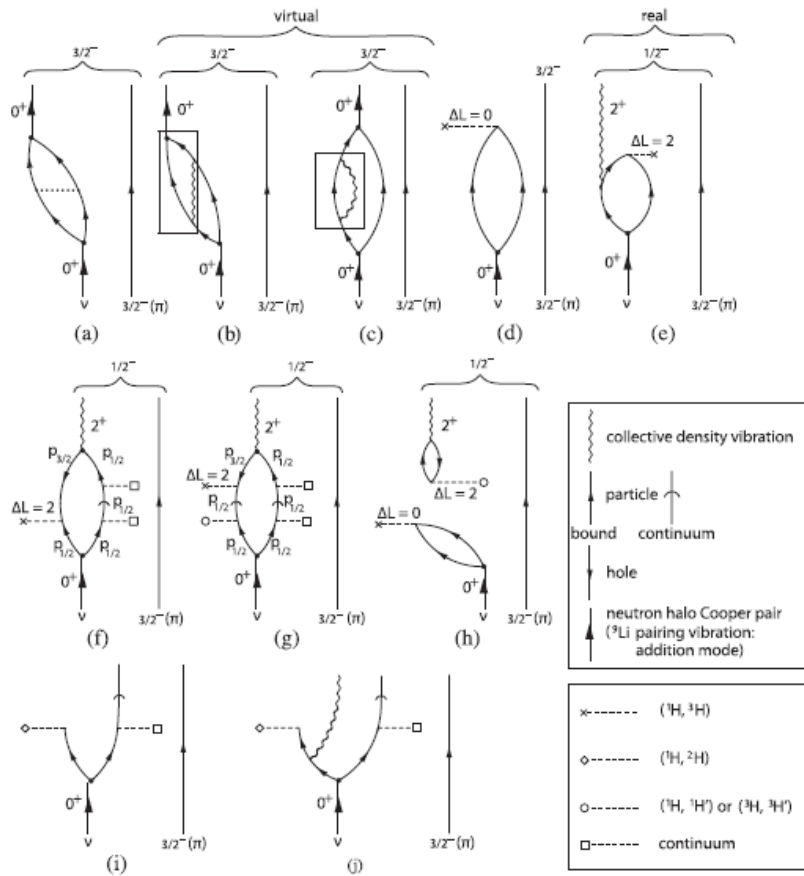


Figure 6.B.1: Representative Nuclear Field Theory–Feynman diagrams associated with correlation process ((a),(b),(c)) and with one- and two-particle pick-up reactions ((i),(j) and (d),(e) respectively) of the halo neutrons of  $^{11}\text{Li}$  (Cooper pair, indicated in terms of a double arrowed line). Also shown are the possible diagrams associated with other channels (breakup and inelastic) populating the  $1/2^-$  (2.69 MeV) state: f) one of the halo neutrons is picked up (the other one going into the continuum, i.e. breaking up from the  $^{9}\text{Li}$  core) together with a neutron from the  $p_{3/2}$  orbital of the  $^{9}\text{Li}$  core leading eventually to the excitation of the  $1/2^-$  final state ( $2^+$  density mode (wavy line) coupled to the  $p_{3/2}(\pi)$ ), g) the proton field acting once breaks the Cooper pair forcing one of the halo neutrons to populate a  $p_{1/2}$  continuum state (the other one follows suit), while acting for the second time picks up one of the neutrons moving in the continuum and another one from those moving in the  $p_{3/2}$  orbital of  $^{9}\text{Li}$  eventually leaving the core in the quadrupole mode of excitation. In (h) the two-step transfer to the  $^{9}\text{Li}$  ground state plus the inelastic final channel process exciting the  $(2^+ \otimes p_{3/2}(\pi))_{1/2^-}$  state is shown. After Potel et al. (2010).

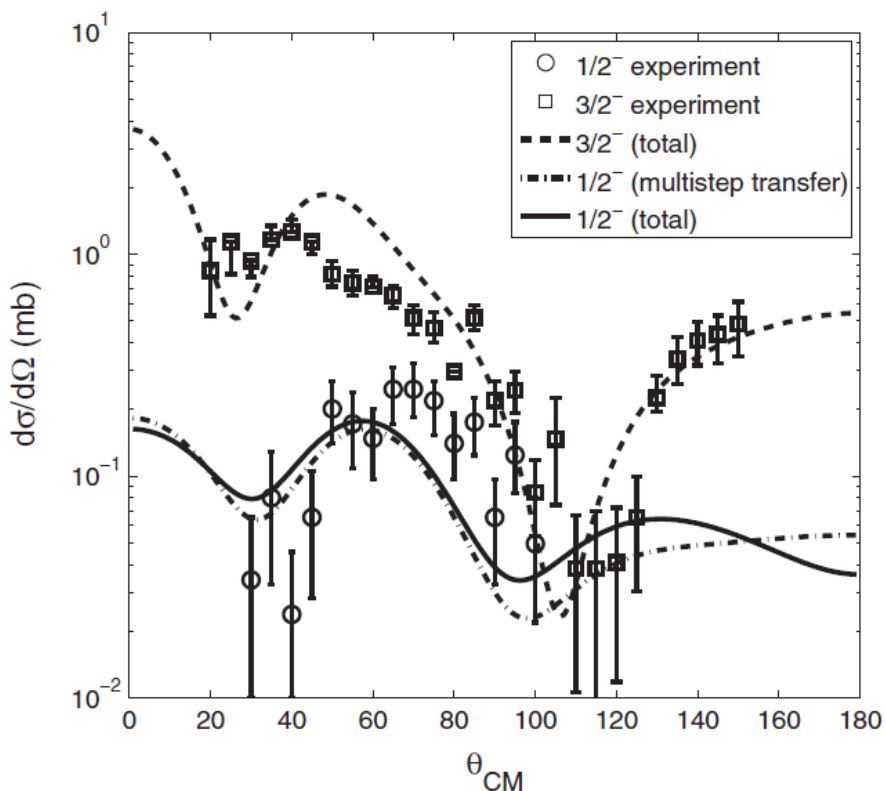


Figure 6.B.2: Experimental (Tanihata, I. et al. (2008)) and theoretical differential cross sections (including multistep transfer as well as breakup and inelastic channels, Potel et al. (2010)). of the  ${}^1\text{H}({}^{11}\text{Li}, {}^9\text{Li}){}^3\text{H}$  reaction populating the ground state ( $3/2^-$ ) and the first excited state ( $1/2^-$ ; 2.69 MeV) of  ${}^9\text{Li}$ . Also shown (dash-dotted curve) is the differential cross section associated with this state but taking into account only multistep transfer. The optical potentials used are from (Tanihata, I. et al., 2008; An and Cai, 2006).

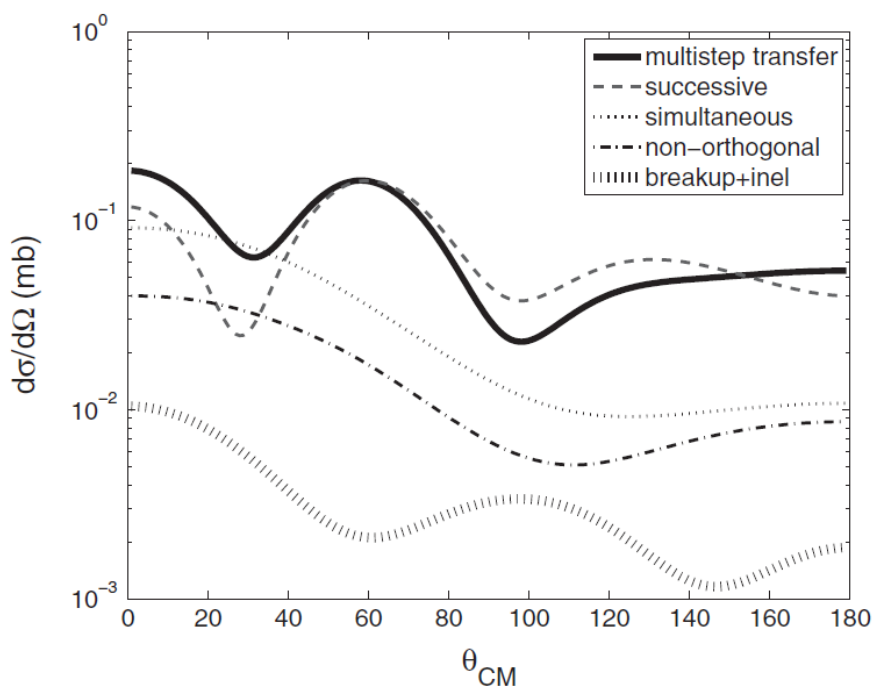


Figure 6.B.3: Successive, simultaneous and non-orthogonality contributions (prior representation) to the  ${}^1\text{H}({}^{11}\text{Li}, {}^9\text{Li}){}^3\text{H}$  differential cross section associated with the population of the  $1/2^-$  state of  ${}^9\text{Li}$ , displayed in Fig. 6.B.2. Also shown is the (coherent) sum of the breakup ( $c = 3$  and  $4$ ) and inelastic ( $c = 5$ ) channel contributions.

## 6.E. ARTICULO BELYAEV PAIRING VIBRATIONAL BAND BASED ON $N = 6.255$

The one-dimensional (radial) functions appearing in the integrands are defined in a spatial grid up to a given maximum radius  $r_{max}$ . The bound state wavefunctions are obtained by numerical integration of the radial Schrödinger equation for a Woods–Saxon potential with a spin–orbit term. The parameters defining the shape of the potential are given as an input, while the depth is adjusted to reproduce the binding energy of the state under consideration. The resulting potential corresponding to the final (initial) nucleon bound state stands also for the interaction potential featured in the integrand in the prior (post) representation. The distorted waves are obtained by integrating the radial Schrödinger equation with positive energy from  $r = 0$  to  $r_{max}$ , and matching the solution with the corresponding Coulomb wave function at a given  $r = r_{match}$ , big enough to lie outside of the range of the nuclear interaction. The Woods–Saxon optical potentials used to obtain the distorted waves consist on a real Coulomb term, a real and imaginary volume terms, an imaginary surface term, and a real and imaginary spin orbit terms. The parameters needed to specify all those terms are given as an input.

## Appendix 6.E Articulo Belyaev Pairing vibrational band based on $N = 6$ .

## Appendix 6.F Simple estimates revisited.

## Appendix 6.G Statistics.

Let us consider two identical particles moving in a one-dimensional harmonic oscillator, let us assume one that one is in the first excited state and the other one is in the ground state. According to the superposition principle

$$\Phi(x_1, x_2) = \lambda\phi_1(x_1)\phi_0(x_2) + \mu\phi_0(x_1)\phi_1(x_2). \quad (6.G.1)$$

Let us calculate the correlation of these particles, that is, the quantity

$$\langle x_1 x_2 \rangle - \langle x_1 \rangle \langle x_2 \rangle. \quad (6.G.2)$$

Let us start with

$$\begin{aligned} \langle x_1 x_2 \rangle &= \int dx_1 dx_2 \left( \lambda^* \phi_1^*(x_1) \phi_0^*(x_2) + \mu^* \phi_0^*(x_1) \phi_1^*(x_2) \right) \\ &\times (x_1 x_2) (\lambda\phi_1(x_1)\phi_0(x_2) + \mu\phi_0(x_1)\phi_1(x_2)) \\ &= |\lambda|^2 \langle \phi_1 | x_1 | \phi_1 \rangle \langle \phi_0 | x_2 | \phi_0 \rangle + \lambda^* \mu \langle \phi_1 | x_1 | \phi_0 \rangle \langle \phi_0 | x_2 | \phi_1 \rangle \\ &+ \lambda \mu^* \langle \phi_0 | x_1 | \phi_1 \rangle \langle \phi_1 | x_2 | \phi_0 \rangle + |\mu|^2 \langle \phi_0 | x_1 | \phi_0 \rangle \langle \phi_1 | x_1 | \phi_1 \rangle \langle \phi_0 | x_1 | \phi_0 \rangle \langle \phi_1 | x_1 | \phi_1 \rangle \end{aligned} \quad (6.G.3)$$

In keeping with the fact that

$$\langle \phi_1 | x | \phi_1 \rangle = \langle \phi_0 | x | \phi_0 \rangle = 0, \quad (6.G.4)$$

and

$$\langle \phi_0 | x | \phi_1 \rangle = \langle \phi_1 | x | \phi_0 \rangle = \sqrt{\frac{\hbar\omega}{2C}}, \quad (6.G.5)$$

one obtains

$$\langle x_1 x_2 \rangle = \left( \frac{\hbar\omega}{2C} \right) \Re(\lambda^* \mu). \quad (6.G.6)$$

From the above results and the fact that  $\langle \phi_1 | \phi_0 \rangle = 0$ ,

$$\langle x_1 \rangle = \langle x_2 \rangle = 0. \quad (6.G.7)$$

From the above results the correlation function between particle 1 and 2 is

$$C = \frac{2C}{\hbar\omega} \langle x_1 x_2 \rangle = 2\Re(\lambda^* \mu) = \begin{cases} 1 & (\lambda = +\mu = \frac{1}{\sqrt{2}}) \\ -1 & (\lambda = -\mu = \frac{-1}{\sqrt{2}}) \end{cases} \quad (6.G.8)$$

Thus bosons are correlated while fermions are anti correlated.

## Appendix 6.H Correlation length and quantality parameter.

The correlation length can be defined as

$$\xi = \frac{\hbar v_F}{2\Delta} \approx \frac{\hbar^2}{m} \frac{k_F}{2\Delta} \quad (6.H.1)$$

where the Fermi momentum in the case of stable nuclei lying along the stability valley is

$$k_F \approx 1.36 \text{ fm}^{-1}. \quad (6.H.2)$$

Thus,

$$\xi = 20 \text{ MeV fm}^2 \times \frac{1.36}{\Delta} \text{ fm}^{-1} \approx \frac{27}{\Delta} \text{ fm}, \quad (6.H.3)$$

and,

$$\xi \approx 27 \text{ fm}, \quad (\Delta \approx 1 \text{ MeV}). \quad (6.H.4)$$

We now write,

$$k_F \approx \frac{a}{\xi} \quad (6.H.5)$$

## Appendix 6.I *k*-mass in $^{11}\text{Li}$ and Pauli principle.

### Bibliography

- H. An and C. Cai. Global deuteron optical model potential for the energy range up to 183 MeV. *Phys. Rev. C*, 73:054605, 2006.
- P. W. Anderson. Random-phase approximation in the theory of superconductivity. *Phys. Rev. Lett.*, 112:1900, 1958.
- R. J. Ascrutto and N. K. Glendenning. Inelastic processes in particle transfer reactions. *Physical Review*, 181:1396, 1969.
- F. Barranco, R. A. Broglia, G. Gori, E. Vigezzi, P. F. Bortignon, and J. Terasaki. Surface vibrations and the pairing interaction in nuclei. *Phys. Rev. Lett.*, 83: 2147, 1999.
- Barranco, F., P. F. Bortignon, R. A. Broglia, G. Colò, and E. Vigezzi. The halo of the exotic nucleus  $^{11}\text{Li}$ : a single Cooper pair. *Europ. Phys. J. A*, 11:385, 2001.
- G. Bassani, N. M. Hintz, C. D. Kavaloski, J. R. Maxwell, and G. M. Reynolds. ( $p, t$ ) Ground-State  $L = 0$  Transitions in the Even Isotopes of Sn and Cd at 40 MeV,  $N = 62$  to 64. *Phys. Rev.*, 139:B830, 1965.
- B. F. Bayman and J. Chen. One-step and two-step contributions to two-nucleon transfer reactions. *Phys. Rev. C*, 26:1509, 1982.
- B. F. Bayman and B. H. Feng. Monte Carlo calculations of two-neutron transfer cross sections. *Nuclear Physics A*, 205:513, 1973.
- Bennaceur, K., J. Dobaczewski, and M. Ploszajczak. Pairing anti-halo effect. *Physics Letters B*, 496:154, 2000.
- Bertsch, G. F. and R. A. Broglia. Giant resonances in hot nuclei. *Physics Today*, 39 (8):44, 1986.
- Bertsch, G. F., R. A. Broglia, and C. Riedel. Qualitative description of nuclear collectivity. *Nucl. Phys. A*, 91:123, 1967.
- Bès, D. R. and R. A. Broglia. Pairing vibrations. *Nucl. Phys.*, 80:289, 1966.
- Bjerregaard, J. H., O. Hansen, Nathan, and S. Hinds. States of  $^{208}\text{Pb}$  from double triton stripping. *Nucl. Phys.*, 89:337, 1966.
- N. Bogoljubov. On a new method in the theory of superconductivity. *Il Nuovo Cimento*, 7:794, 1958.
- A. Bohr. In *Comptes Rendus du Congrès International de Physique Nucléaire*, volume 1, page 487. Centre National de la Recherche Scientifique, 1964.

- Bohr, A. and B. R. Mottelson. *Nuclear Structure, Vol.II.* Benjamin, New York, 1975.
- Bortignon, P.F., A. Bracco, and R. Broglia. *Giant Resonances.* Harwood Academic Publishers, Amsterdam, 1998.
- D. M. Brink. *PhD Thesis.* Oxford University, 1955.
- Brink, D. and R. A. Broglia. *Nuclear Superfluidity.* Cambridge University Press, Cambridge, 2005.
- R. Broglia and A. Winther. *Heavy Ion Reactions.* Westview Press, Boulder, CO., 2004.
- R. A. Broglia and C. Riedel. Pairing vibration and particle-hole states excited in the reaction  $^{206}\text{Pb}(t, p)^{208}\text{Pb}$ . *Nucl. Phys.*, 92:145, 1967.
- G. Gori, F. Barranco, E. Vigezzi, and R. A. Broglia. Parity inversion and breakdown of shell closure in Be isotopes. *Phys. Rev. C*, 69:041302, 2004.
- Guazzoni, P., M. Jaskola, L. Zetta, A. Covello, A. Gargano, Y. Eisermann, G. Graw, R. Hertenberger, A. Metz, F. Nuoffer, and G. Staudt. Level structure of  $^{120}\text{Sn}$ : High resolution ( $p, t$ ) reaction and shell model description. *Phys. Rev. C*, 60: 054603, 1999.
- Guazzoni, P., L. Zetta, A. Covello, A. Gargano, G. Graw, R. Hertenberger, H.-F. Wirth, and M. Jaskola. High-resolution study of the  $^{116}\text{Sn}(p, t)$  reaction and shell model structure of  $^{114}\text{Sn}$ . *Phys. Rev. C*, 69:024619, 2004.
- Guazzoni, P., L. Zetta, A. Covello, A. Gargano, B. F. Bayman, G. Graw, R. Hertenberger, H.-F. Wirth, and M. Jaskola. Spectroscopy of  $^{110}\text{Sn}$  via the high-resolution  $^{112}\text{Sn}(p, t)^{110}\text{Sn}$  reaction. *Phys. Rev. C*, 74:054605, 2006.
- Guazzoni, P., L. Zetta, A. Covello, A. Gargano, B. F. Bayman, T. Faestermann, G. Graw, R. Hertenberger, H.-F. Wirth, and M. Jaskola.  $^{118}\text{Sn}$  levels studied by the  $^{120}\text{Sn}(p, t)$  reaction: High-resolution measurements, shell model, and distorted-wave Born approximation calculations. *Phys. Rev. C*, 78:064608, 2008.
- Guazzoni, P., L. Zetta, A. Covello, A. Gargano, B. F. Bayman, T. Faestermann, G. Graw, R. Hertenberger, H.-F. Wirth, and M. Jaskola. High-resolution measurement of the  $^{118,124}\text{Sn}(p, t)^{116,122}$  reactions: Shell-model and microscopic distorted-wave Born approximation calculations. *Phys. Rev. C*, 83:044614, 2011.
- Guazzoni, P., L. Zetta, A. Covello, A. Gargano, B. F. Bayman, G. Graw, R. Hertenberger, H. F. Wirth, T. Faestermann, and M. Jaskola. High resolution spectroscopy of  $^{112}\text{Sn}$  through the  $^{114}\text{Sn}(p, t)^{112}\text{Sn}$  reaction. *Phys. Rev. C*, 85:054609, 2012.

- I. Hamamoto and B. R. Mottelson. Pair correlation in neutron drip line nuclei. *Phys. Rev. C*, 68:034312, 2003.
- Hamamoto, I. and B. R. Mottelson. Weakly bound  $s_{1/2}$  neutrons in the many-body pair correlation of neutron drip line nuclei. *Phys. Rev. C*, 69:064302, 2004.
- M. Igarashi, K. Kubo, and K. Yagi. Two–nucleon transfer mechanisms. *Phys. Rep.*, 199:1, 1991.
- N. Keeley, R. Raabe, N. Alamanos, and J.-L. Sida. Fusion and direct reactions of halo nuclei at energies around the Coulomb barrier. *Prog. Nucl. Part. Phys.*, 59: 579, 2007.
- D. T. Khoa and W. von Oertzen. Di-neutron elastic transfer in the  ${}^4\text{He}({}^6\text{He}, {}^6\text{He}){}^4\text{He}$  reaction. *Physics Letters B*, 595:193, 2004.
- L. Landau and L. Lifshitz. *Quantum Mechanics, 3rd ed.* Butterworth-Heinemann, 1981.
- G. Potel, F. Barranco, E. Vigezzi, and R. A. Broglia. Evidence for phonon mediated pairing interaction in the halo of the nucleus  ${}^{11}\text{Li}$ . *Phys. Rev. Lett.*, 105:172502, 2010.
- G. Potel, A. Idini, F. Barranco, E. Vigezzi, and R. A. Broglia. Nuclear Field Theory predictions for  ${}^{11}\text{Li}$  and  ${}^{12}\text{Be}$ : shedding light on the origin of pairing in nuclei. *Yad. Fiz.*, *in press*: arXiv:1210.5085 [nucl-th], 2014.
- Potel, G., A. Idini, F. Barranco, E. Vigezzi, and R. A. Broglia. Cooper pair transfer in nuclei. *Rep. Prog. Phys.*, 76:106301, 2013a.
- Potel, G., A. Idini, F. Barranco, E. Vigezzi, and R. A. Broglia. Quantitative study of coherent pairing modes with two–neutron transfer: Sn isotopes. *Phys. Rev. C*, 87:054321, 2013b.
- G. Satchler. *Introduction to Nuclear Reactions*. Mc Millan, New York, 1980.
- J. Schrieffer. *Superconductivity*. Benjamin, New York, 1964.
- Schrieffer, J. R. Macroscopic quantum phenomena from pairing in superconductors. *Physics Today*, 26 (7):23, 1973.
- Tamura, T., D. R. Bès, R. A. Broglia, and S. Landowne. Coupled–channel born–approximation calculation of two-nucleon transfer reactions in deformed nuclei. *Physical Review Letters*, 25:1507, 1970.
- Tanihata, I., M. Alcorta, D. Bandyopadhyay, R. Bieri, L. Buchmann, B. Davids, N. Galinski, D. Howell, W. Mills, S. Mythili, R. Openshaw, E. Padilla-Rodal, G. Ruprecht, G. Sheffer, A. C. Shotter, M. Trinczek, P. Walden, H. Savajols, T. Roger, M. Caamano, W. Mittig, P. Roussel-Chomaz, R. Kanungo, A. Gallant,

- M. Notani, G. Savard, and I. J. Thompson. Measurement of the two-halo neutron transfer reaction  $^1\text{H}(^{11}\text{Li}, ^9\text{Li})^3\text{H}$  at 3A MeV. *Phys. Rev. Lett.*, 100:192502, 2008.
- I. J. Thompson. Coupled reaction channels calculations in nuclear physics. *Computer Physics Reports*, 7(4):167, 1988.
- J. Valatin. Comments on the theory of superconductivity. *Il Nuovo Cimento*, 7: 843, 1958.